

Flavor Physics in the Standard Model and Beyond

Inauguraldissertation
der Philosophisch-naturwissenschaftlichen Fakultät
der Universität Bern

vorgelegt von

Francesco Saturnino

von Beinwil am See AG

Leiter der Arbeit:
Prof. Dr. Christoph Greub
Albert Einstein Center for Fundamental Physics
Institut für theoretische Physik
Universität Bern

Flavor Physics in the Standard Model and Beyond

Inauguraldissertation
der Philosophisch-naturwissenschaftlichen Fakultät
der Universität Bern

vorgelegt von

Francesco Saturnino

von Beinwil am See AG

Leiter der Arbeit:
Prof. Dr. Christoph Greub
Albert Einstein Center for Fundamental Physics
Institut für theoretische Physik
Universität Bern

Von der Philosophisch-naturwissenschaftlichen Fakultät angenommen.

Bern, 12. April 2021

Der Dekan

Prof. Dr. Zoltán Balogh

"Alles Denkbare wird einmal gedacht"
– Friedrich Dürrenmatt

Abstract

This thesis is focused on the flavor anomalies in semi-leptonic b quark decays and on calculations of higher order QCD effects in radiative rare B meson decays. The introduction covers topics and concepts relevant for this thesis and is followed by several papers in which Leptoquarks are introduced as possible extensions of the Standard Model. We analyze several models regarding their potential of resolving one or several of the flavor anomalies. Explanations to the individual anomalies are correlated through loop effects, which we calculate and show their phenomenological importance. Effects arising through Leptoquark interactions with the Standard Model Higgs boson are independent of fermionic couplings needed to explain the flavor anomalies. Due to this independence, such effects can serve as a complementary window to distinguish among different Leptoquark representations in future precision experiments. Additionally, Leptoquarks affect purely leptonic transitions through loop-effects, which we calculate in detail. Future experiments are expected to reach very high precisions in these transitions and will therefore be able to strengthen the case for certain models or put stringent constraints on others. The final part of this thesis consists of two ongoing projects in single and double radiative rare B meson decays. We calculate three-loop contributions of the current-current operator to $b \rightarrow s\gamma$ while retaining full analytic dependence on the charm quark mass. Furthermore, gluon bremsstrahlung corrections to the double differential decay spectrum of $b \rightarrow s\gamma\gamma$ are considered.

Acknowledgements

I would like to express my sincerest gratitude to Christoph Greub. Without his help and guidance, this work would not have been possible. It was a pleasure to profit from his vast experience and knowledge during all of our meetings, both on- and offline! I also thank Andreas Crivellin, who I really enjoyed collaborating with. His seemingly endless enthusiasm and motivation surely helped the productive outcome of this thesis. I thank Ulrich Nierste for being the external referee of my thesis and Thomas Becher for being the chairman at my defence.

A special thanks goes to Dario Müller. Even though cross-checking our results was often painful, I had a lot of fun working with him. Discussing novel ideas like the process $b \rightarrow \gamma\gamma$ and the photon-neutrino coupling was very entertaining. I thank all the people at the institute, especially my fellow PhD students and friends Marcel Balsiger, Samuel Favrod, Greg Jackson, Laetitia Laub and Joachim Monnard, the latter also for running company! I thank my former office mates Matteo Fael and Christoph Wiegand for help concerning programming issues.

I thank my family for their never-ending support and my wonderful wife-to-be for all her support and for bearing with me, especially during the last stages of my PhD.

Contents

1	Introduction	1
1.1	The Standard Model Lagrangian	3
1.1.1	Higgs Mechanism and Gauge Boson Masses	5
1.1.2	Fermion Masses and CKM Matrix	7
1.1.3	Problems of the Standard Model	8
1.2	Effective Field Theory	9
1.2.1	Running of the Couplings	10
1.3	Computational Methods	13
1.3.1	The Heavy Mass Expansion	13
1.3.2	Integration by Parts Relations	14
1.3.3	Master Integrals From Differential Equations	15
1.3.4	Soft Gluon Approximation	16
1.4	The Flavor Anomalies	17
1.4.1	$b \rightarrow s\ell\ell$	17
1.4.2	$b \rightarrow c\ell\nu$	20
1.4.3	Anomalous Magnetic Moment of the Muon	22
1.5	Leptoquarks	23
1.5.1	The Leptoquark Lagrangian	24
1.5.2	Leptoquarks as Solution to the Anomalies	25
1.5.3	Outlook	26
2	Importance of Loop Effects in Explaining the Accumulated Evidence for New Physics in B Decays with a Vector Leptoquark	29
2.1	Introduction	30
2.2	Model and One-Loop Effects	32
2.2.1	W Boxes Contributing to $d_i \rightarrow d_f\nu\bar{\nu}$	33
2.2.2	W Off-Shell Penguins Contributing to $\tau \rightarrow \mu\nu\bar{\nu}$	33
2.2.3	Photon and Gluon Penguins	34
2.2.4	Box Diagrams with LQs	35
2.3	Phenomenology	35
2.4	Conclusions	36
2.5	Appendix	37
2.5.1	$d_k \rightarrow d_j\ell_f^-\ell_i^+$	37
2.5.2	$d_k \rightarrow d_j\nu_i\bar{\nu}_f$	39
2.5.3	$d_k \rightarrow u_j\bar{\nu}\ell^-$	39

3	Explaining the Flavor Anomalies with a Vector Leptoquark (Moriond 2019 Update)	41
3.1	Introduction	42
3.2	The Pati Salam Vector Leptoquark as Combined Solution to the Anomalies . . .	43
4	Correlating Tauonic B Decays to the Neutron EDM via a Scalar Leptoquark	47
4.1	Introduction	48
4.2	Observables and Contributions	49
4.2.1	$b \rightarrow s\nu\nu$	49
4.2.2	$b \rightarrow c(u)\tau\nu$	50
4.2.3	EDMs	51
4.2.4	$D_0 - \bar{D}_0$ Mixing	53
4.2.5	$W \rightarrow \tau\nu$ and $Z \rightarrow \tau\tau$	54
4.3	Phenomenology	55
4.4	Conclusions	55
5	Flavor Phenomenology of the Leptoquark Singlet-Triplet Model	57
5.1	Introduction	58
5.2	Setup	60
5.3	Processes and Observables	62
5.3.1	$ddll$ and $dd\gamma$ Processes	62
5.3.2	$dd\nu\nu$ Processes	66
5.3.3	$dul\nu$ Processes	67
5.3.4	$\Delta F = 2$ Processes	68
5.3.5	$ll\gamma$ Processes	70
5.3.6	Zll and $Z\nu\nu$ Processes	71
5.3.7	$Wl\nu$ Processes	73
5.3.8	$4l$ Processes	74
5.3.9	$ll\nu\nu$ Processes	76
5.4	Phenomenology	77
5.4.1	LHC Bounds	77
5.4.2	$b \rightarrow c\tau\nu$	78
5.4.3	$b \rightarrow c\tau\nu$ and $b \rightarrow sl^+\ell^-$	80
5.4.4	$b \rightarrow c\tau\nu$, $b \rightarrow sl^+\ell^-$ and a_μ	81
5.5	Conclusions	83
5.6	Appendix	85
5.6.1	Loop Functions	85
5.6.2	$ddll$	86
5.6.3	$uv\gamma$ and EDM	86
5.6.4	$dul\nu$	87
5.6.5	$dd\nu\nu$ and $B_s - \bar{B}_s$ Mixing	88
5.6.6	$ll\gamma$, Zll and $Z\nu\nu$	88
5.6.7	$Wl\nu$	90
5.6.8	$\tau \rightarrow 3\mu$, $\tau \rightarrow \mu e^+e^-$ and $\mu \rightarrow 3e$	91
5.6.9	$\tau \rightarrow l\nu\bar{\nu}$ and $\mu \rightarrow e\nu\bar{\nu}$	91

6	Leptoquarks in Oblique Corrections and Higgs Signal Strength: Status and Prospects	93
6.1	Introduction	94
6.2	Setup and Conventions	95
6.3	Oblique Corrections	98
6.4	Higgs Couplings to g , γ and Z	100
6.5	Phenomenological Analysis	102
6.6	Conclusions	103
6.7	Appendix	106
6.7.1	Loop Functions	106
6.7.2	Expanded Matrices	107
6.7.3	Exact Results for the Vacuum Polarization Functions	110
6.7.4	Leading Order SM Amplitudes in Higgs Decays	111
7	Correlating $h \rightarrow \mu^+ \mu^-$ to the Anomalous Magnetic Moment of the Muon via Leptoquarks	113
7.1	Introduction	114
7.2	Setup and Observables	115
7.3	Phenomenology	118
7.4	Conclusions	119
8	Scalar Leptoquarks in Leptonic Processes	121
8.1	Introduction	122
8.2	Setup and Conventions	123
8.2.1	Leptoquark-Higgs Interactions and Electroweak Symmetry Breaking . . .	125
8.2.2	Leptoquark-Fermion Couplings	127
8.2.3	Leptoquark-Higgs Couplings	128
8.3	Self-Energies, Masses and Renormalization	129
8.3.1	Neutrino Masses	130
8.3.2	Renormalization	131
8.4	Calculation of the One-Loop Effects	132
8.4.1	$ll\gamma$	133
8.4.2	Zll and $Z\nu\nu$	135
8.4.3	$Wl\nu$	138
8.4.4	hll	139
8.4.5	$4l$	140
8.4.6	$2l2\nu$	142
8.5	Phenomenology	142
8.5.1	Electroweak Gauge-Boson Couplings to Leptons: Zll , $Z\nu\nu$ and $Wl\nu$. . .	143
8.5.2	Correlating the AMM of the Muon with $Z \rightarrow \ell^+ \ell^-$ and $h \rightarrow \mu^+ \mu^-$. . .	145
8.5.3	Charged Lepton Flavor Violation	147
8.6	Conclusions	148
8.7	Appendix	152
8.7.1	Self-Energies	152
8.7.2	Loop Functions	154
8.7.3	Exact Result for $ll\gamma$	155
8.7.4	Exact Results for Zll , $Z\nu\nu$, $Wl\nu$ and hll	156
8.7.5	Higgs, Z and W Boson Coupling Matrices	161
8.7.6	$4l$	164

8.7.7	$2\ell 2\nu$	164
9	Towards Full m_c Dependence of the \mathcal{O}_2 Contribution at $\mathcal{O}(\alpha_s^2)$ in $b \rightarrow s\gamma$	165
9.1	Current Status	165
9.2	Details about the Calculation	167
9.3	Results for the Matrix Elements	169
9.4	Appendix	173
10	Complete Bremsstrahlung Corrections to the $\mathcal{O}_2 - \mathcal{O}_7$ Interference Contribution for $B \rightarrow X_s \gamma\gamma$	177
10.1	Current Status	177
10.2	Theoretical Framework and Calculation	178
10.3	Appendix	181

Chapter 1

Introduction

What is matter made of? This question is as old as humanity's scientific endeavor and even dates back to the ancient Greeks. On the fundamental level, it was only a bit more than a century ago that the first answers to this question were found.

In 1897, Joseph John Thomson discovered the first elementary particle, the electron [1]. He also determined its mass to be small – much smaller than the ones of the lightest atoms. Since atoms were known to be electrically neutral, the question how mass and charge are distributed within the atom arose. This question was eventually answered by Ernest Rutherford, Hans Geiger and Ernest Marsden through their famous scattering experiment in 1911 [2]. In their experiment they concentrated a beam of α -particles through a thin gold foil. If the charge of the gold particles had been evenly distributed throughout the whole atom, α -particles would have been expected to get deflected only a little. However, the team observed that most of the α -particles were not deflected at all, but some of them rebounded from the foil at unexpectedly large angles. Since the electrons are too light to play a role in the scattering, Rutherford concluded that the atom's mass and therewith its positive charge has to be concentrated within only a very small fraction of the atom's volume. Following Niels Bohr's model of the hydrogen atom in 1913 [3], it was natural to assume that heavier atoms would simply consist of a bunch of protons, bound in the nucleus, surrounded by the electrons. However, the mass fractions of the lightest atoms did not support this assumption. This problem was resolved in 1932 with the discovery of the neutron by James Chadwick [4]. By that time, the work of Max Planck, Albert Einstein [5] and finally the experiments performed by Arthur Hally Compton in 1923 [6] had also established the particle character of the photon. In the twenties, the theory of quantum mechanics emerged, introduced by the work of Werner Heisenberg [7], Erwin Schrödinger [8], Niels Bohr [9] and others. The first step towards a relativistic theory of quantum mechanics and therefore towards quantum field theory (QFT) was achieved by Paul Dirac, who in 1928 came up with his famous equation [10] which led to the prediction of the positron which in turn was discovered by Carl Anderson in 1931 [11]. In the forties, Richard Feynman and Ernst Stückelberg then realized that the Dirac equation actually implied the existence of an anti-particle for every fermion and sure enough, the anti-proton and anti-neutron were discovered at the Berkeley Bevatron in 1955 and 1956, respectively [12].

In 1930, a problem arose in nuclear β decays. The naive picture there was that a nucleus is converted into a lighter nucleus with an increased electric charge under the emission of an electron (today we know that this process is a conversion of a neutron into a proton, however the neutron had not yet been discovered in 1930). In this naive picture the beta decay would simply be a two-body decay in which all energies are kinematically fixed. The experiments on the other hand showed that the emitted electron actually had a continuous energy spectrum. To account for the missing energy and momentum, Wolfgang Pauli suggested a new particle [13],

which today is known as the neutrino. From the electron's energy spectrum in β decays it was clear that this particle, if real, would need to be extremely light or even massless. Experimental data from Pion and Muon decays supported the idea of the neutrino in the forties, and the direct detection was accomplished in 1962 at the Brookhaven National Laboratory (BNL) [14]. Many more particles, known today as mesons and baryons, were found till the 1960s. In fact the number of discovered particles had grown so rapidly that this situation became known as the *particle zoo*. Things seemed to get out of hand, when in 1961 Murray Gell-Mann came up with the eightfold-way [15], allowing for a classification of the mesons and baryons. Gell-Mann [16], André Petermann [17] and George Zweig [18] then independently proposed the quark model in 1964 which finally allowed to explain the composition of the hadrons. In the same year, Oscar Wallace Greenberg introduced the idea of color as a new quantum number [19], which laid the foundation for the $SU(3)$ gauge group of the strong interaction. Experiments performed at the Stanford linear accelerator (SLAC) showed, much like Rutherford's scattering experiment, that protons and neutrons actually have an inner structure, each consisting of three point-like particles [20]. This strongly supported the idea of the quark model and its proof came in 1974 with the discovery of the J/Ψ meson, a bound state consisting of a charm anti-charm pair, at SLAC [21] and BNL [22]. The charm quark had previously been predicted by Sheldon Lee Glashow, John Iliopoulos and Luciano Maiani in 1970 to make sense of the observations in Kaon mixing [23]. The generalization to three quark families was later suggested by Makoto Kobayashi and Toshihide Maskawa [24] on the basis of Nicola Cabibbo's work [25] by introducing the Cabibbo-Kobayashi-Maskawa (CKM) matrix, which was needed to explain the observed charge parity (CP) violation in kaon decays [26]. The other important development towards the completion of the Standard Model (SM) of particle physics was the construction of the theory of weak interactions. While the theory for quantum electrodynamics (QED) based on the work of Feynman [27], Julian Schwinger [28, 29] and Shin'ichirō Tomonaga [30] had been very successful in the forties, the theory for the weak interactions proved to be more challenging since the effective four-fermion theory by Fermi was known to be non-renormalizable. In 1954, Chen-Ning Yang and Robert Laurence Mills [31] constructed the non-abelian gauge group of $SU(2)$. In 1960, Jeffrey Goldstone announced his theorem [32], which was proved the year after by himself, Abdus Salam and Steven Weinberg [33]. The Goldstone theorem motivated Peter Higgs [34] and François Englert together with Robert Brout [35] to come up with the idea of the Higgs-boson, using the mechanism of spontaneously broken gauge symmetries. Finally, in 1967, Weinberg [36] and independently Salam in 1968 [37] established the electroweak theory based on the $SU(2) \times U(1)$ gauge symmetry (it is worth mentioning that this gauge group had already been proposed by Glashow in 1961 [38] and by Salam and John Clive Ward in 1964 [39]). The business of renormalization was then taken care of by Gerardus t'Hooft and Martinus Veltman in 1971 [40]. At this point, the gauge group of the SM – $SU(3) \times SU(2) \times U(1)$ – was established and the SM completed. Today, all particles present in the SM have been observed experimentally, some of them decades after their respective prediction, like the top quark in 1991 [41] by the CDF collaboration or the Higgs-boson in 2012 by ATLAS [42] and CMS [43]. From today's perspective, the chain of events that lead to the establishment of the SM might seem straightforward. This, however, is far away from the truth. To the interested reader, I highly suggest reading "The Making of the Standard Model" by Steven Weinberg [44], which gives a great insight from the point of view of someone who was highly involved in the theoretical advancements of particle physics.

To this day, the SM has been a very successful theory and no particles beyond the ones present in it have been detected so far. Nevertheless, we can confidently say that the SM is not the end of the story since there are still open problems which the SM cannot explain as we will see in Sec. 1.1.3. A natural way of trying to resolve them is to add more particles

to the ones present in the SM. Directly detecting such new particles is however limited by a collider's energy. Another promising way to experimentally look for new particles are precision measurements of observables where new physics (NP), even if much heavier than the scale of the process, can contribute through quantum effects. In order to compare the effects of NP to precision observables, the SM theory predictions need to compete with the experiment's precision. In this thesis, both the aspect of beyond the standard model (BSM) physics as well as precision physics in the SM will be examined within the context of flavor physics. In this introductory chapter we will recall the most important aspects of the SM, give an introduction to effective field theories and explain some computational methods used within this thesis. We will then discuss the flavor anomalies and introduce Leptoquarks (LQs) as BSM candidates. This will set the basis for the following chapters. The chapters 2–8 represent the papers [45–51] in which LQs were studied as possible solutions to the flavor anomalies while extensively studying correlated effects and implications for future experiments. Chapters 9 and 10 on the other hand summarize ongoing work concerning precision calculations in radiative B decays, namely $b \rightarrow s\gamma$ and $b \rightarrow s\gamma\gamma$.

1.1 The Standard Model Lagrangian

The Standard Model of particle physics is a QFT, described by the Lagrangian \mathcal{L}_{SM} . It is built up in accordance with the principles of Poincaré-invariance and local gauge symmetry, meaning it is invariant under local gauge group transformations. As pointed out earlier, the SM gauge group is given by

$$SU(3)_c \times SU(2)_L \times U(1)_Y , \quad (1.1)$$

where c stands for color, Y for the hypercharge and L indicates that $SU(2)_L$ only acts on left-handed fermion fields. The SM Lagrangian can be decomposed as

$$\mathcal{L}_{\text{SM}} = \mathcal{L}_{\text{gauge}} + \mathcal{L}_{\text{fermions}} + \mathcal{L}_{\text{Higgs}} + \mathcal{L}_{\text{Yukawa}} , \quad (1.2)$$

where $\mathcal{L}_{\text{gauge}}$ describes the self-interactions of the SM vector gauge bosons, $\mathcal{L}_{\text{fermions}}$ the interaction between the fundamental SM fermions and the gauge bosons, $\mathcal{L}_{\text{Higgs}}$ the interaction between the scalar Higgs boson and the gauge bosons while also including the Higgs potential and $\mathcal{L}_{\text{Yukawa}}$ finally contains the Yukawa-interaction, describing the interaction between the Higgs boson and the fermions. We will go through the individual parts in the following.

Let us start with $\mathcal{L}_{\text{fermions}}$, which is given by

$$\mathcal{L}_{\text{fermions}} = \sum_{\substack{f=q,\ell \\ h=L,R}} i \bar{\psi}_{h,f} \not{D} \psi_{h,f} , \quad (1.3)$$

where the sum runs over all quarks q and leptons ℓ as well as over the helicities L (left) and R (right). Note that right-handed neutrinos are not present in the SM. The gauge fields, as the name suggests, are introduced to ensure the gauge invariance of the SM Lagrangian through the covariant derivative

$$D_\mu = \partial_\mu + ig_1 \frac{Y}{2} B_\mu + ig_2 T^i W_\mu^i + ig_s \Lambda^a G_\mu^a . \quad (1.4)$$

Here, B_μ is the gauge field of $U(1)_Y$ with its coupling constant g_1 , the W_μ^i are the three gauge fields of $SU(2)_L$ with coupling constant g_2 and the G_μ^a are the eight gauge fields of the strong

1 st gen.	2 nd gen.	3 rd gen.	$SU(3)_c \times SU(2)_L$	T_3	Y	Q
$\begin{pmatrix} u_L \\ d_L \end{pmatrix}$	$\begin{pmatrix} c_L \\ s_L \end{pmatrix}$	$\begin{pmatrix} t_L \\ b_L \end{pmatrix}$	$(3, 2)$	$+1/2$ $-1/2$	$+1/3$	$+2/3$ $-1/3$
u_R d_R	c_R s_R	t_R b_R	$(3, 1)$	0 0	$+4/3$ $-2/3$	$+2/3$ $-1/3$
$\begin{pmatrix} \nu_{eL} \\ e_L \end{pmatrix}$	$\begin{pmatrix} \nu_{\mu L} \\ \mu_L \end{pmatrix}$	$\begin{pmatrix} \nu_{\tau L} \\ \tau_L \end{pmatrix}$	$(1, 2)$	$+1/2$ $-1/2$	-1	0 -1
e_R	μ_R	τ_R	$(1, 1)$	0	-2	-1

Table 1.1: The SM fermion fields and their quantum numbers.

interaction $SU(3)_c$, the gluons, with the strong coupling constant g_s . The T^i and Λ^a are the generators of $SU(2)_L$ and $SU(3)_c$, respectively, given by

$$T^i = \frac{\tau^i}{2}, \quad \Lambda^a = \frac{\lambda^a}{2}, \quad (1.5)$$

where τ^i are the Pauli matrices and λ^a the Gell-Mann matrices. Note that the left-handed fermion fields in Eq. (1.3) are quark- and lepton-doublets under $SU(2)_L$

$$\psi_{q,L} = \begin{pmatrix} U \\ D \end{pmatrix}, \quad \psi_{\ell,L} = \begin{pmatrix} \nu_\ell \\ \ell \end{pmatrix}, \quad (1.6)$$

which both come in three different generations with $U = \{u, c, t\}$, $D = \{d, s, b\}$ and $\ell = \{e, \mu, \tau\}$. The right-handed fermion fields on the other hand are singlets under $SU(2)_L$, meaning they do not transform under this gauge group which effectively amounts to setting $T^i = 0$ in the covariant derivative (1.4). In total there are six right-handed quark singlets, three right-handed charged lepton singlets but no right-handed neutrinos, since they are not contained in the SM. Additionally the quark-fields are triplets under $SU(3)_c$, each entry of the triplets representing one of the three colors red, green and blue. The lepton fields are not charged under $SU(3)_c$, which can again be achieved by setting $\Lambda^a = 0$ in the covariant derivative. Note that the electromagnetic charge Q of the fermion fields is related to the hypercharge Y and the third component of the isospin T_3 via

$$Q = T_3 + \frac{Y}{2}. \quad (1.7)$$

The left-handed fermions are eigenstates of T_3 and their corresponding weak isospin is given by the corresponding eigenvalue, i.e. $\pm 1/2$. The fermion fields and their quantum numbers are summarized in Tab. 1.1.

After having introduced the fermion and gauge fields, we turn to $\mathcal{L}_{\text{gauge}}$. It is given by

$$\mathcal{L}_{\text{gauge}} = -\frac{1}{4}B_{\mu\nu}B^{\mu\nu} - \frac{1}{4}W_{\mu\nu}^i W^{i,\mu\nu} - \frac{1}{4}G_{\mu\nu}^a G^{a,\mu\nu}, \quad (1.8)$$

where

$$B_{\mu\nu} = \partial_\mu B_\nu - \partial_\nu B_\mu, \quad (1.9)$$

$$W_{\mu\nu}^i = \partial_\mu W_\nu^i - \partial_\nu W_\mu^i - g_2 \varepsilon^{ijk} W_\mu^j W_\nu^k, \quad i, j, k = \{1, 2, 3\}, \quad (1.10)$$

$$G_{\mu\nu}^a = \partial_\mu G_\nu^a - \partial_\nu G_\mu^a - g_s f^{abc} G_\mu^b G_\nu^c, \quad a, b, c = \{1, \dots, 8\}. \quad (1.11)$$

Here, ε^{ijk} and f^{abc} are the structure constants of $SU(2)$ and $SU(3)$, respectively, given by the commutation relation of their corresponding generators

$$[T^i, T^j] = i\varepsilon^{ijk}T^k, \quad [\Lambda^a, \Lambda^b] = if^{abc}\Lambda^c. \quad (1.12)$$

In a next step we consider $\mathcal{L}_{\text{Higgs}}$, which takes the form

$$\mathcal{L}_{\text{Higgs}} = (D_\mu\phi)^\dagger (D^\mu\phi) - V(\phi) = (D_\mu\phi)^\dagger (D^\mu\phi) + \mu^2\phi^\dagger\phi - \lambda(\phi^\dagger\phi)^2. \quad (1.13)$$

Here, ϕ is the complex scalar Higgs $SU(2)$ -doublet, which is not charged under $SU(3)_c$. The Higgs self-interaction and its mass term are contained in the Higgs potential $V(\phi)$ and the interaction of the Higgs with the gauge bosons is again obtained through the covariant derivative. We will have a detailed look at these interactions and the parameters of $\mathcal{L}_{\text{Higgs}}$ in Sec. 1.1.1.

Finally, we have

$$\mathcal{L}_{\text{Yukawa}} = -\bar{\ell}'_R Y_\ell \phi^\dagger \ell'_L - \bar{D}'_R Y_D \phi^\dagger Q'_L - \bar{U}'_R Y_U \tilde{\phi}^\dagger Q'_L + h.c., \quad (1.14)$$

where the Y_ℓ , Y_D and Y_U matrices are arbitrary complex 3×3 matrices and

$$\tilde{\phi} = i\tau_2\phi^*. \quad (1.15)$$

The subscripts L and R again indicate the helicities of the fields, which explicitly read

$$\ell_R = \begin{pmatrix} e_R \\ \mu_R \\ \tau_R \end{pmatrix}, \quad \ell_L = \begin{pmatrix} \nu_{eL} \\ e_L \\ \nu_{\mu L} \\ \mu_L \\ \nu_{\tau L} \\ \tau_L \end{pmatrix}, \quad D_R = \begin{pmatrix} d_R \\ s_R \\ b_R \end{pmatrix}, \quad U_R = \begin{pmatrix} u_R \\ c_R \\ t_R \end{pmatrix}, \quad Q_L = \begin{pmatrix} u_L \\ d_L \\ c_L \\ s_L \\ t_L \\ b_L \end{pmatrix}. \quad (1.16)$$

In Sec. 1.1.2 we will see why the fields in Eq. (1.14) are primed. Note that the gauge invariance of $\mathcal{L}_{\text{Yukawa}}$ fixes the hypercharge of the Higgs-doublet to be $y_H = 1$.

1.1.1 Higgs Mechanism and Gauge Boson Masses

So far we have avoided discussing the mass terms in the SM Lagrangian, the reason being that it is simply impossible to write down a fermion or boson mass term by hand which does not violate gauge invariance. In order to arrive at such mass terms, the mechanism of *spontaneous symmetry breaking* (SSB) is needed. SSB describes the fact that even though the Lagrangian itself is gauge invariant, its ground state is not. In the SM this can be achieved through the Higgs doublet, which we have introduced in the previous section. The Higgs potential $V(\phi)$ in Eq. (1.13) is minimized by a field configuration that fulfills

$$\phi^\dagger\phi = \frac{v^2}{2}, \quad v = \sqrt{\frac{\mu^2}{\lambda}}, \quad (1.17)$$

where v is the vacuum expectation value (vev). By choosing a vacuum state

$$\phi_0 = \frac{1}{\sqrt{2}} \begin{pmatrix} 0 \\ v \end{pmatrix} \quad (1.18)$$

it is evident that any ground state explicitly breaks the gauge symmetry: An $SU(2)$ gauge transformation leaves the Lagrangian invariant, but rotates any vacuum configuration into another one. Using gauge transformations, we can always choose the Higgs doublet to have a specific form

$$\phi = \frac{1}{\sqrt{2}} \begin{pmatrix} 0 \\ H \end{pmatrix} = \frac{1}{\sqrt{2}} \begin{pmatrix} 0 \\ v + h \end{pmatrix} . \quad (1.19)$$

This choice of gauge is called *unitary gauge*. We have introduced h as the physical real Higgs-field, which itself has a zero vev. Returning to SSB, there is a subgroup which leaves the vacuum state invariant

$$\left(T_3 + \frac{y_H}{2} \right) \phi_0 = \frac{1}{2} \begin{pmatrix} 1 & 0 \\ 0 & 0 \end{pmatrix} \phi_0 = 0 . \quad (1.20)$$

The subgroup generated by $T_3 + Y/2$ stays unbroken and a massless gauge boson, the photon, remains. As anticipated by Eq. (1.7) this is the gauge group of electromagnetism $U(1)_{\text{em}}$, which means that the gauge group $SU(2)_L \times U(1)_Y$ spontaneously breaks to $U(1)_{\text{em}}$. The masses of the gauge bosons can now be expressed in terms of the vev. Therefore, we first need to rotate the gauge fields into their mass eigenstates. For the Z boson (Z_μ) and the photon (A_μ) this can be done via the Weinberg angle θ_W

$$\begin{pmatrix} Z_\mu \\ A_\mu \end{pmatrix} = \begin{pmatrix} \cos \theta_W & -\sin \theta_W \\ \sin \theta_W & \cos \theta_W \end{pmatrix} \begin{pmatrix} W_\mu^3 \\ B_\mu \end{pmatrix} , \quad (1.21)$$

$$\cos \theta_W = \frac{g_2}{\sqrt{g_1^2 + g_2^2}} , \quad \sin \theta_W = \frac{g_1}{\sqrt{g_1^2 + g_2^2}} , \quad (1.22)$$

where g_1 and g_2 are the gauge couplings introduced in Eq. (1.4). In order for the photon to have the right coupling strength to the fermions, the relation

$$g_2 \sin \theta_W = g_1 \cos \theta_W = e \quad (1.23)$$

must hold, where e is the elementary charge. The charged W bosons (W_μ^\pm) are given by

$$W_\mu^\pm = \frac{1}{\sqrt{2}} \left(W_\mu^1 \mp i W_\mu^2 \right) . \quad (1.24)$$

From the first part of $\mathcal{L}_{\text{Higgs}}$ with only taking ϕ_0 yields the mass terms of the gauge bosons

$$(D_\mu \phi_0)^\dagger (D_\mu \phi_0) = \frac{g_2^2 v^2}{4} W_\mu^- W^{\mu+} + \frac{(g_1^2 + g_2^2) v^2}{8} Z_\mu Z^\mu , \quad (1.25)$$

i.e.

$$m_W^2 = \frac{g_2^2 v^2}{4} = \frac{e^2 v^2}{4 \sin^2 \theta_W} , \quad m_Z^2 = \frac{(g_1^2 + g_2^2) v^2}{4} = \frac{e^2 v^2}{4 \sin^2 \theta_W \cos^2 \theta_W} , \quad (1.26)$$

which in particular implies $m_W/m_Z = \cos \theta_W$. The absence of a term $A_\mu A^\mu$ in Eq. (1.25) explicitly shows that the photon stays massless. Three of the four scalar fields contained in the complex doublet ϕ have therefore been absorbed by the gauge bosons to create the mass terms. The mass term of the Higgs itself is contained in the Higgs potential $V(\phi)$ and reads

$$m_h^2 = 2\mu^2 = 2\lambda v^2 . \quad (1.27)$$

The experimental values for m_W , m_Z , m_h and v read [52]

$$\begin{aligned} m_H &= 125.10 \pm 0.14 \text{ GeV} , & m_W &= 80.379 \pm 0.012 \text{ GeV} , \\ m_Z &= 91.1876 \pm 0.0021 \text{ GeV} , & v &= 246 \text{ GeV} . \end{aligned} \quad (1.28)$$

Up quarks	[GeV]	Down quarks	[MeV]	Leptons	[MeV]
m_t	173.1(9)	m_b	4197(22)	m_τ	1776.86(12)
m_c	1.275(35)	m_s	93.6(8)	m_μ	105.6583745(24)
m_u	0.002270(85)	m_d	4.670(85)	m_e	0.5109989461(31)

Table 1.2: Values for the quark and lepton masses [52–56]. These values are dependent on the renormalization scheme.

1.1.2 Fermion Masses and CKM Matrix

Having worked out the gauge boson mass terms we now want to establish the fermion mass terms. These are encoded in $\mathcal{L}_{\text{Yukawa}}$ given in Eq. (1.14) and arise again through SSB. Taking the part of the Yukawa Lagrangian where the Higgs takes its vev, we find

$$\mathcal{L}_{m_\psi} = -\frac{v}{\sqrt{2}} \bar{\ell}'_R Y_\ell \ell'_L - \frac{v}{\sqrt{2}} \bar{D}'_R Y_D D'_L - \frac{v}{\sqrt{2}} \bar{U}'_R Y_U U'_L + h.c. , \quad (1.29)$$

where $U = (u, c, t)$, $D = (d, s, b)$ and $\ell = (e, \mu, \tau)$. These terms already resemble mass terms. However, in order for them to describe the physical mass terms, the matrices Y need to be diagonalized. This is achieved by a bi-unitary transformation, where the fields are rotated from their weak eigenstates into their mass eigenstates

$$\begin{aligned} \ell'_R &= V_{\ell R} \ell_R , & \ell'_L &= V_{\ell L} \ell_L , \\ D'_R &= V_{DR} D_R , & D'_L &= V_{DL} D_L , & V_i &\in U(3) \\ U'_R &= V_{UR} U_R , & U'_L &= V_{UL} U_L , \end{aligned} \quad (1.30)$$

such that the mass matrices are in diagonal form

$$\begin{aligned} M_\ell &= \text{diag}(m_e, m_\mu, m_\tau) = \frac{v}{\sqrt{2}} V_{\ell R}^\dagger Y_\ell V_{\ell L} , \\ M_d &= \text{diag}(m_d, m_s, m_b) = \frac{v}{\sqrt{2}} V_{DR}^\dagger Y_D V_{DL} , \\ M_u &= \text{diag}(m_u, m_c, m_t) = \frac{v}{\sqrt{2}} V_{UR}^\dagger Y_U V_{UL} . \end{aligned} \quad (1.31)$$

The values for the lepton and quark masses are collected in Tab. 1.2.

Since the field redefinitions in Eq. (1.30) are unitary they drop out everywhere in the Lagrangian where a field and its anti-version appear simultaneously. The only place where this is not the case is in the charged current (CC) interaction where the W^\pm bosons interact with the quarks. This term explicitly reads

$$\begin{aligned} \mathcal{L}_{CC} &= -\frac{g_2}{\sqrt{2}} W_\mu^+ \bar{U}'_L \gamma^\mu D'_L - \frac{g_2}{\sqrt{2}} W_\mu^- \bar{D}'_L \gamma^\mu U'_L \\ &= -\frac{g_2}{\sqrt{2}} W_\mu^+ \bar{U}_L \gamma^\mu V_{UL}^\dagger V_{DL} D_L - \frac{g_2}{\sqrt{2}} W_\mu^- \bar{D}_L \gamma^\mu V_{DL}^\dagger V_{UL} U_L \\ &\equiv -\frac{g_2}{\sqrt{2}} W_\mu^+ \bar{U}_L \gamma^\mu V_{\text{CKM}} D_L - \frac{g_2}{\sqrt{2}} W_\mu^- \bar{D}_L \gamma^\mu V_{\text{CKM}}^\dagger U_L , \end{aligned} \quad (1.32)$$

where V_{CKM} is the Cabibbo-Kobayashi-Maskawa matrix which is usually written as

$$V_{\text{CKM}} = \begin{pmatrix} V_{ud} & V_{us} & V_{ub} \\ V_{cd} & V_{cs} & V_{cb} \\ V_{td} & V_{ts} & V_{tb} \end{pmatrix} . \quad (1.33)$$

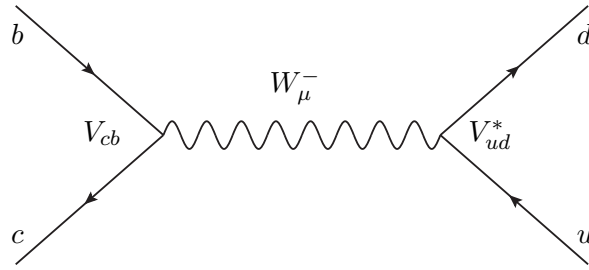


Figure 1.1: FCNC process $b \rightarrow c\bar{u}d$, mediated by the W^- boson. The amplitude is proportional to the CKM matrix elements V_{cb} and V_{ud}^* .

This matrix is unitary but in general not diagonal, i.e. different generations of quarks can interact through the W^\pm bosons in the mass eigenbasis. As a unitary 3×3 matrix, V_{CKM} can be parametrized with three real parameters and six phases. Of these six phases however, five can be rotated away, leaving one physical phase, which is the source of CP violation in the SM. The Wolfenstein [57] parametrization is commonly used to describe the CKM matrix

$$V_{\text{CKM}} = \begin{pmatrix} 1 - \frac{\lambda^2}{2} & \lambda & A\lambda^3(\rho - i\eta) \\ -\lambda & 1 - \frac{\lambda^2}{2} & A\lambda^2 \\ A\lambda^3(1 - \rho - i\eta) & -A\lambda^2 & 1 \end{pmatrix} + \mathcal{O}(\lambda^4), \quad (1.34)$$

where the parameters ρ and η are related to the parameters $\bar{\rho}$ and $\bar{\eta}$ of the generalized Wolfenstein parametrization

$$\rho + i\eta = \frac{(\bar{\rho} + i\bar{\eta})\sqrt{1 - A^2\lambda^4}}{\sqrt{1 - \lambda^2[1 - A^2\lambda^4(\bar{\rho} + i\bar{\eta})]}}. \quad (1.35)$$

The four values, fitted to the SM at 68% C.L., read [58]

$$\begin{aligned} \lambda &= 0.2265_{-0.0023}^{+0.0025}, & A &= 0.801_{-0.020}^{+0.029} \\ \bar{\rho} &= 0.189_{-0.0070}^{+0.088}, & \bar{\eta} &= 0.358_{-0.042}^{+0.046}. \end{aligned} \quad (1.36)$$

Numerically, the CKM matrix is close to the unit matrix. Its small off-diagonal entries however allow for quarks of different generations to interact via the W bosons at tree level. These interactions are the flavor changing charged currents (FCCCs). The amplitude of FCCCs is proportional to the respective entry of the CKM matrix, see e.g. Fig. 1.1.

1.1.3 Problems of the Standard Model

As mentioned in the introduction, the SM is a very successful theory but fails at explaining certain observations.

- The SM only contains three of the four fundamental forces. Gravity is not included.
- Only left-handed neutrinos are contained in the SM. Neutrinos have however been measured to be massive [59] which requires the introduction of right-handed neutrinos or higher order operators to generate a mass term. The source and form of the mass terms is so far unknown. Furthermore, neutrino oscillations have been experimentally confirmed (see Ref. [60] for an overview). Similarly to the CKM matrix in the SM, they are governed by the Pontecorvo–Maki–Nakagawa–Sakata (PMNS) matrix [61, 62].

- The SM is not able to account for the imbalance between matter and anti-matter in the observed universe.
- Dark matter and dark energy constitute to about 95% of the energy content in our universe. The SM does not explain this.

Furthermore there are some issues that are of theoretical nature:

- No mechanism protects the Higgs mass from large loop corrections. This is known as the hierarchy problem.
- A CP violating gluon self-interaction term of the form

$$\frac{\theta}{32\pi^2} \epsilon^{\mu\nu\rho\sigma} G_{\mu\nu}^a G_{\rho\sigma}^a \quad (1.37)$$

is invariant under the SM gauge group. However, the current upper bound for θ is extremely small [63]. What is the reason for this?

- The SM contains 18 free parameters: nine fermion masses (i.e. the Yukawa couplings), four parameters in the CKM matrix, three gauge couplings and two parameters in the Higgs potential. Why do these parameters take their respective value and what is their origin?

Obviously a lot of effort has been put into solving these problems and in fact there are models which can address some of them. However, none of the hypothesized particles have been observed so far.

1.2 Effective Field Theory

Due to the large mass hierarchy in the SM, see Eq. (1.28) and Tab. 1.2, it is possible that a decay process contains very different mass and energy scales at the same time. When the light and heavy scales are clearly separable, it is desirable to construct an equivalent theory in which only the light fields are present. Such theories are called *effective field theories* (EFTs) and the interaction terms are usually written as effective Hamiltonians or effective Lagrangians. As an example, let us consider the process $b \rightarrow c\bar{u}d$, which is mediated by a W^- boson in the SM, see the Feynman diagram in Fig. 1.1. The full amplitude of this decay reads

$$\mathcal{A} = \frac{ig_2^2}{2} V_{cb} V_{ud}^* \bar{u}(p_c) \gamma^\mu P_L u(p_b) \left(g_{\mu\nu} - \frac{k_\mu k_\nu}{m_W^2} \right) \frac{1}{k^2 - m_W^2} \bar{u}(p_d) \gamma^\mu P_L v(p_u) , \quad (1.38)$$

where the components of $k = p_b - p_c$ are of $\mathcal{O}(m_b)$. Having the clear hierarchy $m_W \gg m_b, m_c \gg m_d, m_u \approx 0$ we can expand the amplitude for large m_W which yields at leading order

$$\mathcal{A} = -\frac{ig_2^2}{2m_W^2} V_{cb} V_{ud}^* \bar{u}(p_c) \gamma^\mu P_L u(p_b) \bar{u}(p_d) \gamma_\mu P_L v(p_u) . \quad (1.39)$$

Constructing an EFT which only contains the light fields is obvious in this case and the effective Hamiltonian reads

$$\mathcal{H}_{\text{eff}} = C (\bar{c} \gamma^\mu P_L b) (\bar{d} \gamma_\mu P_L u) . \quad (1.40)$$

All that is left to do is to fix the constant C in such a way that both theories are in fact equivalent. This process is called the *matching* of the EFT onto the full theory and C is called the *Wilson coefficient*. By requiring

$$A = \langle c\bar{u}d | -i\mathcal{H}_{\text{eff}} | b \rangle$$

one finds

$$C = \frac{g_2^2}{2m_W^2} V_{cb} V_{ud}^* = \frac{4G_F}{\sqrt{2}} V_{cb} V_{ud}^* . \quad (1.41)$$

Note that the effective Hamiltonian in Eq. (1.40) exactly describes Fermi's effective four-fermion theory, which is also indicated by the Fermi constant G_F contained in C . This effective Hamiltonian is of mass-dimension six. Had we considered additional terms beyond leading order in m_W , those terms would have been of $\mathcal{O}(k^2/m_W^2)$. In position space, the momentum k corresponds to derivatives of the fields, making the operator of higher dimension. Generally, effective Hamiltonians are of the form

$$\mathcal{H}_{\text{eff}} = \frac{1}{\Lambda^2} \sum_k C_k^{(6)} \mathcal{O}_k^{(6)} + \frac{1}{\Lambda^4} \sum_k C_k^{(8)} \mathcal{O}_k^{(8)} + \dots ,$$

where the superscripts indicate the dimensionality of the effective operators and Λ is a cutoff scale below which the effective theory is valid, in our exemplary case m_W . The Wilson coefficients only depend on the heavy scales that have been integrated out and the renormalization scale μ . The dependence on the light scales arises from the matrix elements of the effective operators.

1.2.1 Running of the Couplings

Including higher orders in QCD, the Wilson coefficients will be of the form

$$C_i(\mu) \approx \mathcal{O}(\alpha_s^0) + \sum_{n=1}^{\infty} \left(\frac{\alpha_s(\mu)}{4\pi} \right)^n \left(a_{n0}(\Lambda) \log^n \left(\frac{\Lambda^2}{\mu^2} \right) + a_{n1}(\Lambda) \log^{n-1} \left(\frac{\Lambda^2}{\mu^2} \right) + \dots + a_{nn}(\Lambda) \right) , \quad (1.42)$$

where the $a_{ni}(\Lambda)$ are functions that depend on the masses of the heavy particles that have been integrated out. The terms $\alpha_s^n \log^n$ are called *leading logarithms* (LL), $\alpha_s^n \log^{n-1}$ are next-to-leading logarithms (NLL) and so on. These logarithms bare one problem: Evaluated at a low scale μ_l , they become too large for a treatment within perturbation theory. Of course, one could simply evaluate the Wilson coefficients at a high scale Λ and the logarithms would disappear. Unfortunately this does not solve the problem either because by doing so, the matrix elements of the effective operators then contain logarithms of the form $\log(\mu^2/\mu_l^2)$ which become large at the high scale. Ideally, one evaluates the Wilson coefficients at the high scale and then evolves them down to the low scale via a differential equation. This can be achieved through *renormalization group equations* (RGEs) which take the form

$$\mu \frac{d\vec{C}(\mu)}{d\mu} = \hat{\gamma}^T \vec{C}(\mu) . \quad (1.43)$$

Here, \vec{C} contains the Wilson coefficients C_i in a certain basis and $\hat{\gamma}$ is the corresponding *anomalous dimension matrix* (ADM) which can be calculated in perturbation theory

$$\hat{\gamma} = \frac{\alpha_s}{4\pi} \hat{\gamma}^0 + \left(\frac{\alpha_s}{4\pi} \right)^2 \hat{\gamma}^1 + \dots . \quad (1.44)$$

The ADM is derived through the renormalization of the Wilson coefficients

$$\hat{\gamma}^T = - \left(\bar{Z}^C \right)^{-1} \mu \frac{d\bar{Z}^C}{d\mu} , \quad (1.45)$$

where \bar{Z}^C is the counter-term matrix, which also governs how the Wilson coefficients mix under renormalization. The renormalization of the Wilson coefficients is equivalent to the renormalization of the effective operators: One only renormalizes either one but not both. The solution of the RGE of Eq. (1.43) can be written as

$$\vec{C}(\mu) = \hat{U}(\mu, \mu_0) \vec{C}(\mu_0) , \quad (1.46)$$

where the evolution matrix \hat{U} reads

$$\hat{U}(\mu, \mu_0) = \exp \left[\int_{g_s(\mu_0)}^{g_s(\mu)} \frac{\hat{\gamma}^T(g')}{\beta(g')} dg' \right] . \quad (1.47)$$

We introduced the β -function $\beta(g)$, which enters the RGE of g_s

$$\mu \frac{dg_s}{d\mu} = \beta(g_s) . \quad (1.48)$$

Like the ADM it can be calculated in perturbation theory

$$\beta(g_s) = -\beta_0 \frac{g_s^3}{16\pi^2} - \beta_1 \frac{g_s^5}{(16\pi^2)^2} - \dots \quad (1.49)$$

and is known today up to five loops, the first two orders reading

$$\beta_0 = \frac{11N_c - 2f}{3} , \quad \beta_1 = \frac{34}{3}N_c^2 - \frac{10}{3}N_c f - 2C_F f . \quad (1.50)$$

Here, N_c is the number of colors, C_F is a color factor and f is the number of active flavors. The RGE of g_s is obviously related to the RGE of α_s , whose solution can be written in terms of the β -function and to leading order is given by

$$\alpha_s(\mu) = \frac{\alpha_s(\mu_0)}{1 - \beta_0 \frac{\alpha_s(\mu_0)}{2\pi} \log \left(\frac{\mu_0}{\mu} \right)} . \quad (1.51)$$

The value of $\alpha_s(m_Z)$, which was measured precisely at LEP [52]

$$\alpha_s(m_Z) = 0.1179 \pm 0.001 , \quad (1.52)$$

can be used as an initial value. Expanding Eq. (1.51) we obtain

$$\alpha_s(\mu) = \alpha_s(\mu_0) \left[1 + \beta_0 \frac{\alpha_s(\mu_0)}{2\pi} \log \left(\frac{\mu_0}{\mu} \right) + \left(\beta_0 \frac{\alpha_s(\mu_0)}{2\pi} \right)^2 \log^2 \left(\frac{\mu_0}{\mu} \right) + \dots \right] \quad (1.53)$$

and see explicitly that the LL terms get resummed to all orders. If one aims at a resummation of the NLL terms as well, one needs to take into account higher orders of the β -function in Eq. (1.51), i.e. β_1 for NLL precision.

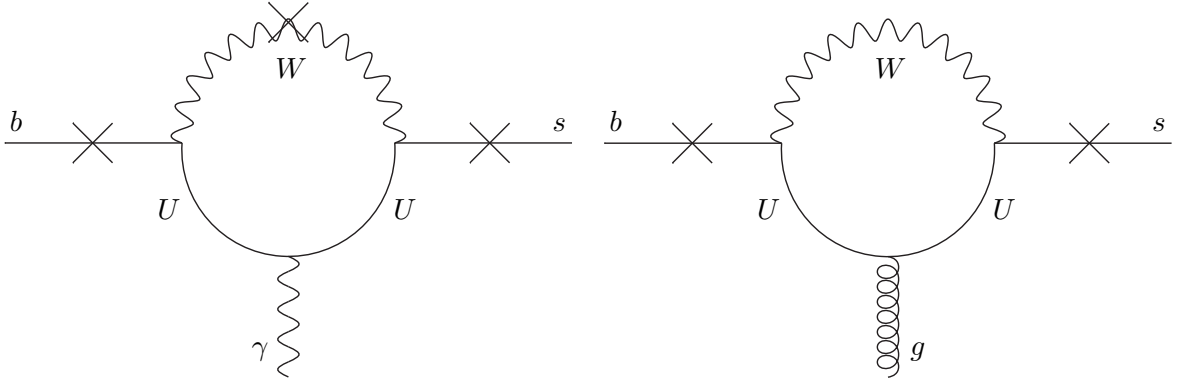


Figure 1.2: SM contribution to $b \rightarrow s\gamma$ (left) and $b \rightarrow sg$ (right). The internal quark can be any up-type quark $U = \{u, c, t\}$ and the crosses indicate other possible places of photon or gluon emissions, respectively. These FCNC are only induced at loop-level.

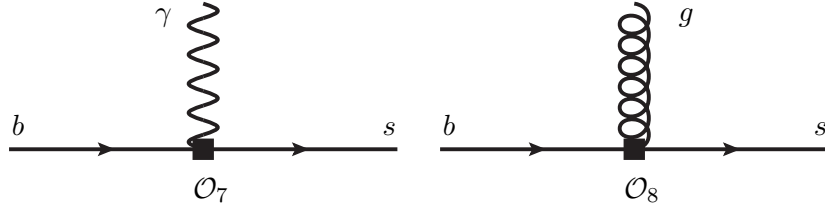


Figure 1.3: Contribution of the operator \mathcal{O}_7 to $b \rightarrow s\gamma$ (left) and \mathcal{O}_8 to $b \rightarrow sg$ (right).

As an example of running operators and mixing among them, let us have a look at a subset of the B physics effective Hamiltonian

$$\begin{aligned} \mathcal{H}_{\text{eff}} &\supset -\frac{4G_F}{\sqrt{2}} V_{tb} V_{ts}^* (C_2 \mathcal{O}_2 + C_7 \mathcal{O}_7 + C_8 \mathcal{O}_8) , \\ \mathcal{O}_2 &= (\bar{s}_\alpha \gamma_\mu P_L c_\alpha) (\bar{c}_\beta \gamma^\mu P_L b_\beta) , \\ \mathcal{O}_7 &= \frac{e}{16\pi^2} m_b (\bar{s}_\alpha \sigma^{\mu\nu} P_R b_\alpha) F_{\mu\nu} , \\ \mathcal{O}_8 &= \frac{g_s}{16\pi^2} m_b (\bar{s}_\alpha \sigma^{\mu\nu} T_{\alpha\beta}^a P_R b_\beta) G_{\mu\nu}^a , \end{aligned} \tag{1.54}$$

where α and β are color indices and $\sigma^{\mu\nu} = i[\gamma^\mu, \gamma^\nu]/2$. To match the operators at $\mathcal{O}(\alpha_s^0)$, one can use the processes $b \rightarrow s\gamma$ and $b \rightarrow sg$ for C_7 and C_8 , respectively. In the SM these processes are loop-suppressed since flavor changing neutral currents (FCNCs) do not occur at tree level as seen in Fig. 1.2. On the EFT side, \mathcal{O}_7 is the only operator contributing to $b \rightarrow s\gamma$ while \mathcal{O}_8 is the only one contributing to $b \rightarrow sg$, see Fig. 1.3. Note that \mathcal{O}_2 is the same operator as in Eq. (1.40) when exchanging the u and c field as well as the d and s field, so we have already discussed the matching of C_2 at lowest order. Even though there are one-loop diagrams involving \mathcal{O}_2 that seemingly contribute to $b \rightarrow s\gamma$ and $b \rightarrow sg$ at $\mathcal{O}(\alpha_s^0)$, see Fig. 1.4, their contribution vanishes.

Next, we want to see how the operators mix and evolve under the RGE. For this purpose, the entries of the ADM $\hat{\gamma}$ have to be calculated. This requires the computation of $\mathcal{O}(\alpha_s)$ diagrams. In Fig. 1.5 we show the EFT diagrams that give rise to the diagonal entries of the ADM. The diagrams giving rise to the off-diagonal entries and therefore inducing the mixing among the operators are shown in Fig. 1.6. Note that the mixing of \mathcal{O}_2 into \mathcal{O}_7 and \mathcal{O}_8 already involves a

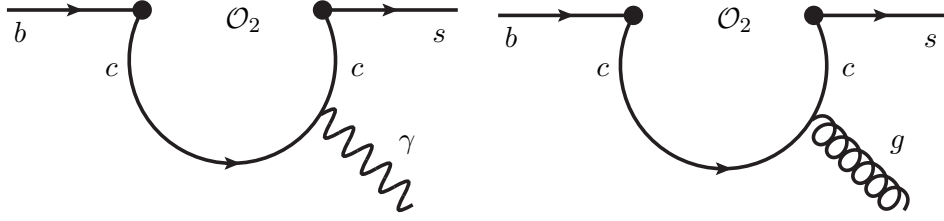


Figure 1.4: Apparent \mathcal{O}_2 contribution to $b \rightarrow s\gamma$ (left) and $b \rightarrow sg$ (right). These contributions vanish.

two-loop diagram. We omit explicitly calculating the entries of the ADM here and instead just give its result

$$\hat{\gamma}^0 = \begin{pmatrix} -2 & \frac{516}{81} & \frac{70}{27} \\ 0 & \frac{32}{3} & 0 \\ 0 & -\frac{32}{9} & \frac{28}{3} \end{pmatrix}. \quad (1.55)$$

To solve the RGE, we need to find the evolution matrix \hat{U}

$$\hat{U}(\mu, \mu_0) = \exp \left[- \int_{g_s(\mu_0)}^{g_s(\mu)} \frac{\hat{\gamma}^{0T}}{\beta_0 g'} dg' \right] = \exp \left[- \frac{\hat{\gamma}^{0T}}{2\beta_0} \log \left(\frac{\alpha_s(\mu)}{\alpha_s(\mu_0)} \right) \right]. \quad (1.56)$$

Abbreviating $\eta = \alpha_s(\mu_0)/\alpha_s(\mu)$ and taking the analytic expression for β_0 from Eq. (1.50), the result reads

$$\hat{U}(\mu, \mu_0) = \begin{pmatrix} \eta^{\frac{3}{2f-33}} & 0 & 0 \\ \frac{280}{459} \eta^{\frac{14}{33-2f}} - \frac{22}{513} \eta^{\frac{16}{33-2f}} - \frac{4946}{8721} \eta^{\frac{3}{2f-33}} & \eta^{\frac{16}{33-2f}} & \frac{8}{3} \left(\eta^{\frac{14}{33-2f}} - \eta^{\frac{16}{33-2f}} \right) \\ \frac{35}{153} \left(\eta^{\frac{14}{33-2f}} - \eta^{\frac{3}{2f-33}} \right) & 0 & \eta^{\frac{14}{33-2f}} \end{pmatrix}. \quad (1.57)$$

1.3 Computational Methods

The computation of loop integrals is unavoidable in any precision calculation. When many different energy scales, propagators, loops or a combination of the three are present, these calculations become very challenging. In this section, we introduce some techniques and tools that are useful in this undertaking.

1.3.1 The Heavy Mass Expansion

The *heavy mass expansion* (HME) is a technique that can be applied if all masses of a given Feynman diagram Γ can be divided into a set $\underline{M} = \{M_1, M_2, \dots\}$ of large masses and a set $\underline{m} = \{m_1, m_2, \dots\}$ of small masses and if all external momenta $\underline{q} = \{q_1, q_2, \dots\}$ are small compared to the scale of the large masses. In the previous section we have seen that those are exactly the requirements for the applicability of an EFT, making the HME an invaluable tool for matching calculations. The dimensionally regularized (unrenormalized) Feynman integral F_Γ associated with the Feynman diagram Γ can then be written as [64]

$$F_\Gamma \stackrel{M \rightarrow \infty}{\sim} \sum_{\gamma} F_{\Gamma \setminus \gamma} \circ \mathcal{T}_{\underline{q}^\gamma, \underline{m}^\gamma} F_\gamma(\underline{q}^\gamma, \underline{m}^\gamma, \underline{M}), \quad (1.58)$$

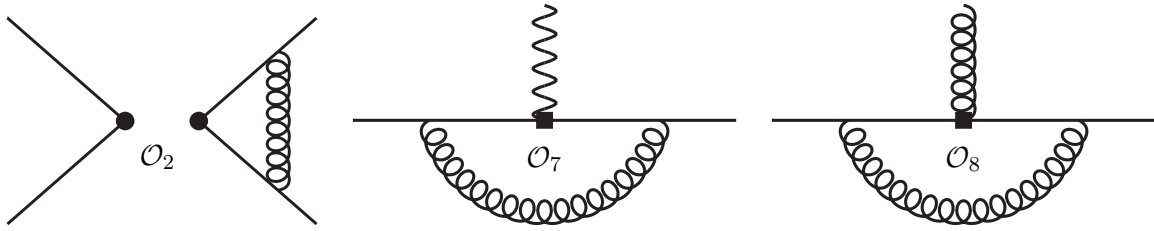


Figure 1.5: Exemplary EFT diagrams giving rise to the diagonal entries of the ADM, i.e. $\mathcal{O}(\alpha_s)$ contributions of the operators \mathcal{O}_2 (left), \mathcal{O}_7 (middle) and \mathcal{O}_8 (right).

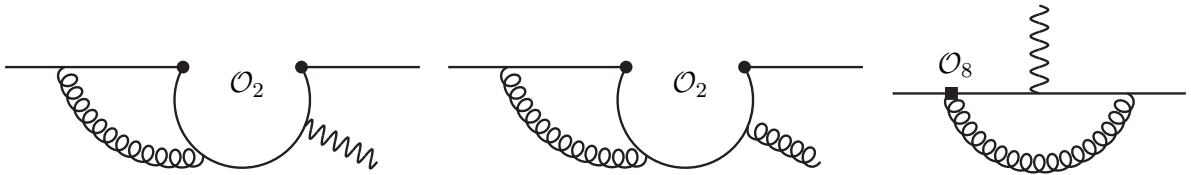


Figure 1.6: Exemplary diagrams showing the mixing among the operators. Left (middle): \mathcal{O}_2 mixing into \mathcal{O}_7 (\mathcal{O}_8). Right: \mathcal{O}_8 mixing into \mathcal{O}_7 . Note that \mathcal{O}_7 does not mix into other operators.

where the sum is taken over all subgraphs γ of Γ and $F_{\Gamma \setminus \gamma}$ denotes the Feynman integral corresponding to the reduced graph $\Gamma \setminus \gamma$, i.e. Γ without γ . A subgraph γ contains all lines with heavy masses \underline{M} and is at the same time one-particle-irreducible with respect to lines with small masses \underline{m} . The operator \mathcal{T} acts directly on the integrand of the subgraph γ and performs a Taylor expansion in the variables \underline{m}^γ , the set of light masses in γ , and in \underline{q}^γ , the set of the external momenta with respect to the subgraph γ . Note that an internal momentum with respect to the whole graph Γ like a loop momentum can be an external momentum with respect to the subgraph γ . To illustrate this procedure, let us have another look at the left-hand side of Fig. 1.2, i.e. the process $b \rightarrow s\gamma$, which we encountered in the previous section. Here, the heavy masses correspond to $\underline{M} = \{m_t, m_W\}$, the light masses to $\underline{m} = \{m_b, m_c, m_u\}$ and the external momenta to $\underline{q} = \{p_b, q\}$, where p_b is the momentum of the b quark and q the momentum of the photon. In case where the top quark runs in the loop, the whole diagram is the only existing subdiagram and one can directly apply the expansion to the whole diagram. For the c and u quark however, also the subdiagram consisting only of the W boson line exists in addition to the full diagram.

1.3.2 Integration by Parts Relations

With increasing amounts of loops and propagators, the number of loop integrals to be calculated in a given process can increase drastically. The different integrals are in general not independent but related through integration by parts (IBP) identities [65]. They arise through vanishing surface terms

$$\int \prod_{i=1}^m d^d l_i \frac{\partial}{\partial l_j^\mu} \left(\frac{k_a^\mu}{(P_1^2 - m_1^2)^{n_1} \dots (P_n^2 - m_n^2)^{n_n}} \right) = 0, \quad (1.59)$$

where P_i are linear combinations of the loop momenta l_i and the external momenta p_k and k_a is one of either the external momenta or the loop momenta. Performing the derivative on the left-hand side of the above equation explicitly yields combinations of different loop integrals. Repeating the procedure for all possibilities of k_a and specific choices of the indices n_k , it is

possible to construct linear equations among the different loop integrals. In the end this allows to express the original loop integrals in terms of a common basis of integrals, called *master integrals* (MIs). Not only are these MIs in general less complex to compute, the procedure using IBP relations often allows for a drastic reduction in number of integrals that need to be calculated.

1.3.3 Master Integrals From Differential Equations

A possible way to calculate MIs is through differential equations [66]. Consider a set of MIs $\vec{f}(\epsilon, m) = \{M_1, \dots, M_n\}$, where m is a particle's mass contained in the MIs. Differentiating the MIs with respect to m and using IBP relations to express the derivatives in terms of the MIs, one finds a system of first order differential equations

$$\frac{\partial}{\partial m} \vec{f}(\epsilon, m) = A(\epsilon, m) \vec{f}(\epsilon, m) , \quad (1.60)$$

where A is an $n \times n$ matrix depending on the dimensional regulator ϵ and the mass term m . These differential equations are usually very difficult to solve. In Ref. [67] it was therefore suggested to move to a *canonical form* (also called ϵ -form) which is related to the original MIs by the basis change $\vec{f} = T\vec{g}$. Obtaining a canonical form in a first step usually requires to perform a variable change $m \rightarrow x(m)$ in the differential equation. Two explicit cases are shown in Chapter 9, Eqs. (9.9) and (9.10). The integrals in canonical form \vec{g} by definition obey

$$\frac{\partial}{\partial x} \vec{g}(\epsilon, x) = \epsilon \tilde{A}(x) \vec{g}(\epsilon, x) . \quad (1.61)$$

The differential equation of this form has the huge advantage compared to the one in Eq. (1.60) that the matrix \tilde{A} only depends on x but not on ϵ . Its solution can therefore be written in terms of Chen iterated integrals [68]. Assuming an expansion in ϵ for the MIs in the canonical basis

$$\vec{g}(\epsilon, x) = \sum_{i=a} \epsilon^i \vec{g}^{(i)}(x) , \quad (1.62)$$

the solution can further be simplified to (see Ref. [69] and references therein)

$$\begin{aligned} \vec{g}^{(a)}(x) &= \vec{g}^{(a)}(x_0) , \\ \vec{g}^{(n)}(x) &= \int_{x_0}^x dx' \tilde{A}(x') \vec{g}^{(n-1)}(x') + \vec{g}^{(n)}(x_0) , \quad n > a \end{aligned} \quad (1.63)$$

where $\vec{g}^{(i)}(x_0)$ denote the MIs in the canonical basis evaluated at a fixed value of $x = x_0$ which can be used to fix the integration constants. Note that the above procedure can be generalized to the case where the MIs depend on several masses m_j . In many applications, including the one in Chapter 9, the matrix \tilde{A} can be brought into the form

$$\tilde{A} = \sum_j \frac{\tilde{A}_j}{x - a_j} , \quad (1.64)$$

where \tilde{A}_j are constant matrices. The solution of the differential equation can then be written in terms of Goncharov polylogarithms (GPLs) [70], defined recursively as

$$G(\{a_1, \dots, a_n\}, x) = \int_0^x \frac{dt}{t - a_1} G(\{a_2, \dots, a_n\}, t) , \quad (1.65)$$

where $G(\{ \}, x) = 1$ and the a_j are called *weights*. When constructing solutions using GPLs, the amount of different combinations of weights usually grows very large. To obtain a result in a compact form, it can therefore be desirable to expand the GPLs around certain values of x . In Chapter 9 the cases $x \approx 0$ and $x \approx 1$, corresponding to $m \rightarrow \infty$ and $m = 0$, respectively, will be of interest. In the case of $x \approx 0$, the expansion is straightforward since one can directly expand the integrand. Let $\mathcal{S}_a^x(f(x))$ be an operator that expands a function $f(x)$ in x around $x = a$. The expansion around $x = 0$ then reads

$$G(\{a_1, \dots, a_n\}, x) \approx \int_0^x dt_1 \mathcal{S}_0^{t_1} \left(\frac{1}{t_1 - a_1} \int_0^{t_1} dt_2 \mathcal{S}_0^{t_2} \left(\frac{1}{t_2 - a_2} \int_0^{t_2} \dots \right) \right) \quad x \ll 1. \quad (1.66)$$

This expression is valid for $a_n \neq 0$. For $x \approx 1$ it is useful to split the integration path. As an example, we consider a GPL of weight two

$$\begin{aligned} G(\{a_1, a_2\}, x) &= \left(\int_0^1 \frac{dt_1}{t_1 - a_1} + \int_1^x \frac{dt_1}{t_1 - a_1} \right) \left(\int_0^{t_1} \frac{dt_2}{t_2 - a_2} \right) \\ &\approx G(\{a_1, a_2\}, 1) + G(\{a_2\}, 1) \int_1^x dt_1 \mathcal{S}_1^{t_1} \left(\frac{1}{t_1 - a_1} \right) \\ &\quad + \int_1^x dt_1 \mathcal{S}_1^{t_1} \left[\left(\frac{1}{t_1 - a_1} \right) \int_1^{t_1} dt_2 \mathcal{S}_1^{t_2} \left(\frac{1}{t_2 - a_2} \right) \right] \quad 1 - x \ll 1. \end{aligned} \quad (1.67)$$

This equation is only true for $a_i \neq 1$. In case where one or several weights are equal to 1, one can apply shuffle relations [71] to remove them. To higher weights one simply extends the above procedure iteratively.

1.3.4 Soft Gluon Approximation

When calculating higher order corrections to decay processes, the inclusion of bremsstrahlung corrections becomes necessary in order to cancel divergences stemming from virtual corrections. The bremsstrahlung corrections induce infrared (IR) divergences, arising from diagrams where a gluon with vanishing momentum k is radiated from an external leg. To calculate these divergences, it is useful to introduce a cutoff energy ΔE . For gluon momenta $|k| < \Delta E$ it is possible to make an approximation for the matrix element, called *soft gluon approximation*. As a starting point let us consider a diagram with an external fermion, given by

$$\mathcal{M}_0 = A(p)u(p) = \longrightarrow \text{---} \bigcirc \quad (1.68)$$

where $u(p)$ is the fermion's spinor with momentum p and $A(p)$ contains the remaining part of the amplitude, depicted by the gray blob. Radiating a gluon with momentum k from the fermion line yields

$$\mathcal{M}_1 = \longrightarrow \text{---} \bigcirc \quad (1.69)$$

$$= A(p - k) \frac{i(\not{p} - \not{k} + m)}{(p - k)^2 - m^2} (-ig_s T^a \not{\epsilon}) u(p),$$

where ε is the gluon's polarization vector. Assuming the gluon momenta k to be soft, i.e. disregarding linear terms in k , one can easily show that the soft matrix element can be written as

$$\mathcal{M}_{1,s} = -ig_s T^a \frac{p \cdot \varepsilon}{p \cdot k} \mathcal{M}_0 . \quad (1.70)$$

We see that the soft matrix element is proportional to the Born amplitude and the IR divergence is encoded in $1/(p \cdot k)$. An analogous expression is obtained for radiation from an outgoing leg that differs only by the global sign. One can proceed to calculate the cross section for the soft matrix element, only integrating over the phase space region where the gluon momentum k is soft, i.e. $|k| < \Delta E$. This allows to obtain analytic expressions for the IR singularities which manifest themselves either as $1/\epsilon_{\text{IR}}$ poles in dimensional regularization or as terms proportional to $\log(\Delta E/m_g)$ when a regulator m_g is used for the gluon mass. Such integrals have been calculated in Ref. [72], see also Ref. [73]. For the contributions of hard gluons with $k > \Delta E$ one proceeds with the full matrix element, where the cutoff ΔE is kept in the phase space integral as lower bound for the gluon momentum to avoid the IR singularities.

1.4 The Flavor Anomalies

In the past few years there have been several hints for physics BSM which appeared in tests of lepton flavor universality (LFU). The SM itself is lepton flavor universal to a very good approximation since the gauge boson couplings to leptons do not depend on flavor. LFU in the SM is only broken by the Yukawa couplings, which however are very small due to the suppression of m_ℓ/m_h . Therefore, experimental evidence for lepton flavor universality violation (LFUV) would be clear evidence of NP. Additionally, it is also interesting to look for lepton flavor violating (LFV) processes such as $\mu \rightarrow e\gamma$ since these are absent in the SM. The collected hints for LFUV have become known as the *flavor anomalies*. They appear in the FCNC $b \rightarrow s\ell\ell$ processes as well as in the FCCC $b \rightarrow c\ell\nu$ processes. Furthermore there is the long standing tension between experiment and theory prediction of the anomalous magnetic moment (AMM) of the muon which can also be seen as a flavor anomaly since it vanishes in the massless limit. We will summarize these anomalies in this section and report on their status and discuss general aspects of NP models that could potentially resolve these anomalies. The latter will also be illustrated from an EFT point of view.

1.4.1 $b \rightarrow s\ell\ell$

Semi-leptonic FCNC b quark decays are suppressed in the SM since they occur only at the loop level and additionally by the small CKM matrix element V_{ts} . This means that even if potential NP interacts weakly with the SM and/or is very heavy, its contribution relative to the SM can still be sizable. It is therefore very intriguing to test LFU in these processes. From a theoretical point of view, the observables

$$R(K^{(*)}) = \frac{\text{Br}[B \rightarrow K^{(*)}\mu\mu]}{\text{Br}[B \rightarrow K^{(*)}ee]} \quad (1.71)$$

are promising for this purpose since many theoretical uncertainties cancel in the ratio and the mass effects of the muon and electron can further be neglected. The predictions for $R(K^{(*)})$ are hence very close to unity except for the low q^2 region (q^2 being the invariant mass of the lepton pair) where QED and mass effects start to play a role [74]. These observables have been

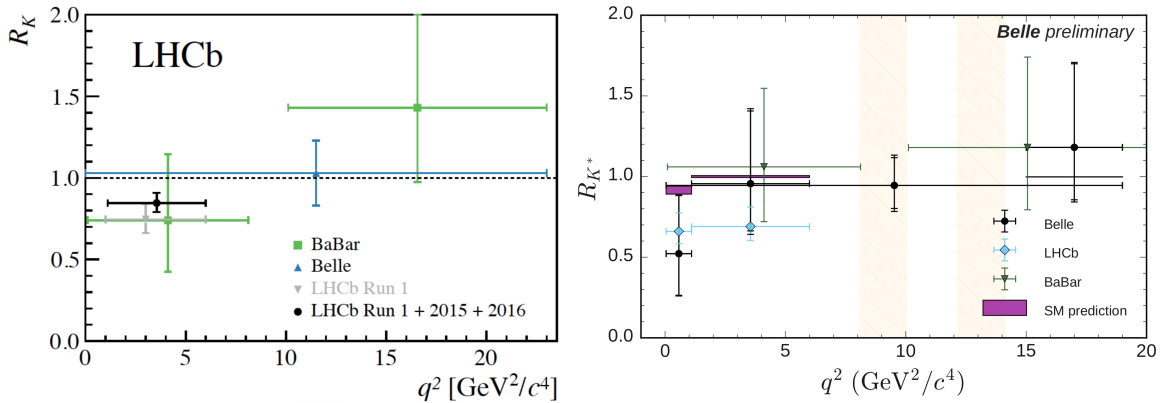


Figure 1.7: Experimental situation for $R(K)$ (left) and $R(K^*)$ (right).

measured at Belle [75], BaBar [76] and LHCb [77], whose most recent results read [78, 79]

$$\begin{aligned} R(K)_{\text{LHCb}} &= 0.846^{+0.060}_{-0.054}(\text{stat})^{+0.016}_{-0.014}(\text{sys}) , \\ R(K^*)_{\text{LHCb}} &= 0.69^{+0.11}_{-0.07}(\text{stat}) \pm 0.05(\text{sys}) . \end{aligned} \quad (1.72)$$

These measurements show a tension to the SM prediction of $\sim 2.5\sigma$. The more recent measurement of $R(K^*)$ by Belle [80], presented at *Rencontres de Moriond EW 2019*, on the other hand agrees with the SM prediction

$$R(K^*)_{\text{Belle}} = 0.96^{+0.45}_{-0.29}(\text{stat}) \pm 0.11(\text{sys}) , \quad (1.73)$$

but is due to its large errors also compatible with the measurement of LHCb. The experimental situation is summarized in Fig. 1.7.

Additionally, another discrepancy between theory prediction and experiment was found in the angular observable P_5' (see Ref. [81] for its precise definition and theory prediction) in the process $B \rightarrow K^* \mu \mu$. It was first measured by LHCb [82, 83] and later also by Belle [84, 85] ATLAS [86] and CMS [87]. Combining the experimental data and the theory predictions yields a discrepancy at the 3σ level [88, 89]. This situation is depicted in Fig. 1.8. Finally there is also a small tension of around 2σ in the decay $B_s \rightarrow \phi \mu \mu$ [88, 89].

Even if none of the mentioned observables is itself proof for NP, the accumulation of tensions between the SM and experiments is intriguing. Of course, if one has a specific NP model at hand which potentially resolves these tensions, other B physics observables that agree with the SM should not be spoiled. In fact, there are many such observables, including $b \rightarrow s \gamma$ transitions and other angular and polarization observables. In order to account for all of them, several groups [88, 90–101] have performed so called *global fits*. In those fits, a certain set of Wilson Coefficients is analyzed regarding how well it fits to the data. Some of these scenarios are able to resolve the anomalies and give overall a much better fit to the data than the SM with a significance of up to 5σ .

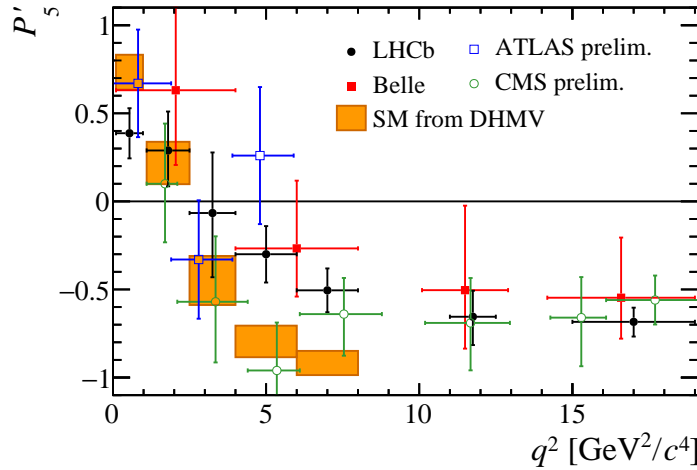


Figure 1.8: Experimental situation for P_5' compared to its SM prediction [102].

Let us now consider a few of these scenarios. We define the effective Hamiltonian as

$$\begin{aligned}
 \mathcal{H}_{\text{eff}} &= -\frac{4G_F}{\sqrt{2}}V_{tb}V_{ts}^* \sum_i C_i \mathcal{O}_i, \\
 \mathcal{O}_7^{(\prime)} &= \frac{e}{16\pi^2}(\bar{s}\sigma_{\mu\nu}P_{R(L)}b)F^{\mu\nu}, \\
 \mathcal{O}_{9\ell}^{(\prime)} &= \frac{e^2}{16\pi^2}(\bar{s}\gamma_\mu P_{L(R)}b)(\bar{\ell}\gamma^\mu\ell), \\
 \mathcal{O}_{10\ell}^{(\prime)} &= \frac{e^2}{16\pi^2}(\bar{s}\gamma_\mu P_{L(R)}b)(\bar{\ell}\gamma^\mu\gamma_5\ell).
 \end{aligned} \tag{1.74}$$

In principle there are also scalar operators which however are tightly constrained by $B_s \rightarrow \mu\mu$ and therefore not considered here. The studied scenarios range from one-dimensional hypotheses, i.e. with one degree of freedom, up to a six-dimensional one, in which every Wilson Coefficient is treated as free parameter. In each case there are scenarios that give a very good fit to the data. The best ones in the 1-D case are $C_{9\mu}$ only, $C_{9\mu} = -C_{10\mu}$ and $C_{9\mu} = -C'_{9\mu}$. Their respective best-fit region and pull, all of them exceeding 5σ with respect to the SM, are given in Tab. 1.3. Among the 2-D fits there are many scenarios that yield a good fit, see e.g. Ref. [98]. In Fig. 1.9 we show two specific scenarios. In the first one, $C_{9\mu}$ and $C_{10\mu}$ are the two independent variables. In the latter, we have a LFUV $C_{9\mu} = -C_{10\mu}$ contribution supported by a LFU contribution in $C_{9\ell}$, i.e.

$$\begin{aligned}
 C_{9e} &= C_{9\tau} = C_{9\ell}^{\text{LFU}}, \\
 C_{9\mu}^{\text{tot}} &= C_{9\mu} + C_{9\ell}^{\text{LFU}}, \\
 C_{10\mu} &= -C_{9\mu}.
 \end{aligned} \tag{1.75}$$

This scenario will be of great importance for the remainder of this thesis. Both previously mentioned 2-D scenarios yield a very good fit to data, see Tab. 1.4. Note that for the second scenario the global fit prefers a sizable LFU effect, even exceeding the LFUV one. Interestingly, this scenario has become favorable with the announcement of the newest measurement by Belle as can be seen in Fig. 1.9. For the pre-Moriond data (dashed lines), the best fit region (red) showed a very good overlap with the $R(K^{(*)})$ (blue) and the remaining $b \rightarrow s\mu\mu$ data (yellow)

Wilson Coefficient	Best fit (1σ)	Pull
$C_{9\mu}$	-0.98 ± 0.17	5.6σ
$C_{9\mu} = -C_{10\mu}$	-0.46 ± 0.10	5.2σ
$C_{9\mu} = -C'_{9\mu}$	-0.99 ± 0.16	5.5σ

Table 1.3: One-dimensional global fit scenarios for $b \rightarrow s\ell\ell$ transitions. Values taken from Ref. [98].

Wilson Coefficient	Best fit	Pull
$(C_{9\mu}, C_{10\mu})$	$(-0.91, 0.18)$	5.4σ
$(C_{9\mu} = -C_{10\mu}, C_{9\ell}^{\text{LFU}})$	$(-0.3, -0.74)$	5.7σ

Table 1.4: Example for 2-D global fit scenarios (see text). Values taken from Ref. [98].

for both scenarios. Now, there is no direct overlap anymore in the first scenario while the fit for the second scenario has even improved.

Of course, the global fits are a priori model-independent. However, the choice of a specific scenario is usually motivated by one or several NP models. For example, the combination $C_{9\mu} = -C_{10\mu}$ is induced by models that only couple to left-handed fermions. Even though a roughly $\mathcal{O}(20\%)$ effect relative to the SM is needed at the level of the amplitude to account for the anomaly, this still amounts to a relatively small effect since, as previously mentioned, this process is already suppressed in the SM. This means that NP should either contribute through loops or be relatively heavy and/or have couplings that are relatively small.

1.4.2 $b \rightarrow c\ell\nu$

Contrary to $b \rightarrow s\ell\ell$ transitions the $b \rightarrow c\ell\nu$ transitions occur already at tree level in the SM. Nevertheless they are still very good candidates to test LFU through the observables

$$R(D^{(*)}) = \frac{\text{Br}[B \rightarrow D^{(*)}\tau\nu]}{\text{Br}[B \rightarrow D^{(*)}\ell\nu]}, \quad (1.76)$$

where $\ell = \{e, \mu\}$. Again, the ratio allows for a good cancellation of theoretical and parametric uncertainties and the SM predictions read [103]

$$\begin{aligned} R(D)_{\text{SM}} &= 0.299 \pm 0.003, \\ R(D^*)_{\text{SM}} &= 0.258 \pm 0.005. \end{aligned} \quad (1.77)$$

These values are not close to one anymore since the mass effect of the tau cannot be neglected. The ratios have been measured at BaBar [104, 105] Belle [106–109] and LHCb [110–112], and their combined value reads [103]

$$R(D) = 0.340 \pm 0.027(\text{stat}) \pm 0.013(\text{sys}), \quad (1.78)$$

$$R(D^*) = 0.295 \pm 0.011(\text{stat}) \pm 0.008(\text{sys}), \quad (1.79)$$

which corresponds to a tension of around 3σ compared to the theory predictions. The different experimental results as well as their combination are shown and compared to the SM prediction in Fig. 1.10. Note that all central values consistently lie above their respective theory prediction.

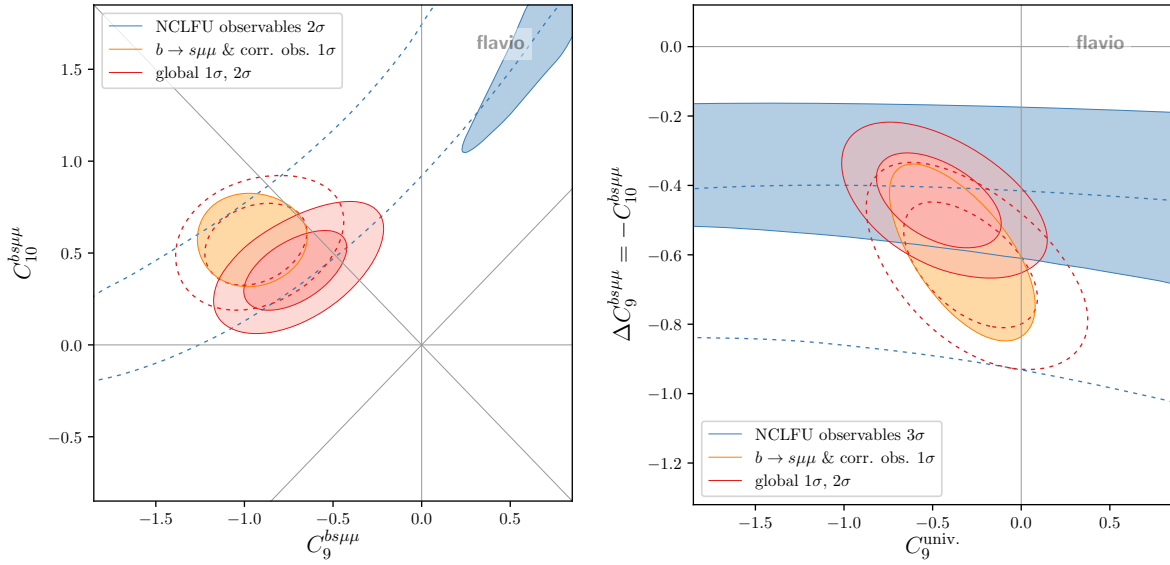


Figure 1.9: The two 2-D global fit scenarios $(C_{9\mu}, C_{10\mu})$ (left) and $(C_{9\mu} = -C_{10\mu}, C_{9\ell}^{\text{LFU}})$ (right). The dashed lines (opaque areas) indicate the pre-(post-)Moriond data. The best fit region for the global fit is shown in red, the data from $R(K^{(*)})$ is shown in blue and the remaining $b \rightarrow s\mu\mu$ data is depicted in yellow. Plots taken from Ref. [97].

Similarly, LHCb also measured the ratio

$$R(J/\psi) = \frac{\text{Br}[B_c \rightarrow J/\psi \tau \nu]}{\text{Br}[B_c \rightarrow J/\psi \mu \nu]} \quad (1.80)$$

to be [113]

$$R(J/\psi) = 0.71 \pm 0.17(\text{stat}) \pm 0.18(\text{sys}) . \quad (1.81)$$

Compared to the SM prediction [114–117]

$$R(J/\psi)_{\text{SM}} = 0.26 \pm 0.02 \quad (1.82)$$

this shows a tension of around 2σ which on its own is not significant but points in the same direction as $R(D^{(*)})$ since the experiment again lies above the SM prediction.

Global fits have also been performed for $b \rightarrow c\tau\nu$ [118–122]. The relevant operators are collected within the effective Hamiltonian, given by

$$\begin{aligned} \mathcal{H}_{\text{eff}} &= 2\sqrt{2}G_F V_{cb} \left[(1 + C_V^L) \mathcal{O}_V^L + C_S^R \mathcal{O}_S^R + C_S^L \mathcal{O}_S^L + C_T \mathcal{O}_T \right] , \\ \mathcal{O}_V^L &= (\bar{c} \gamma^\mu P_L b) (\bar{\tau} \gamma_\mu P_L \nu) , \\ \mathcal{O}_S^R &= (\bar{c} P_R b) (\bar{\tau} P_L \nu) , \\ \mathcal{O}_S^L &= (\bar{c} P_L b) (\bar{\tau} P_L \nu) , \\ \mathcal{O}_T &= (\bar{c} \sigma^{\mu\nu} P_L b) (\bar{\tau} \sigma_{\mu\nu} P_L \nu) . \end{aligned} \quad (1.83)$$

Even though the fits are mainly driven by $R(D^{(*)})$, they also contain polarization observables in $B \rightarrow D_{(L)}^* \tau \nu$. Note that the running of the Wilson coefficients is also taken into account. Among the most prominent scenarios are the 1-D hypothesis of C_V^L only and the 2-D hypothesis

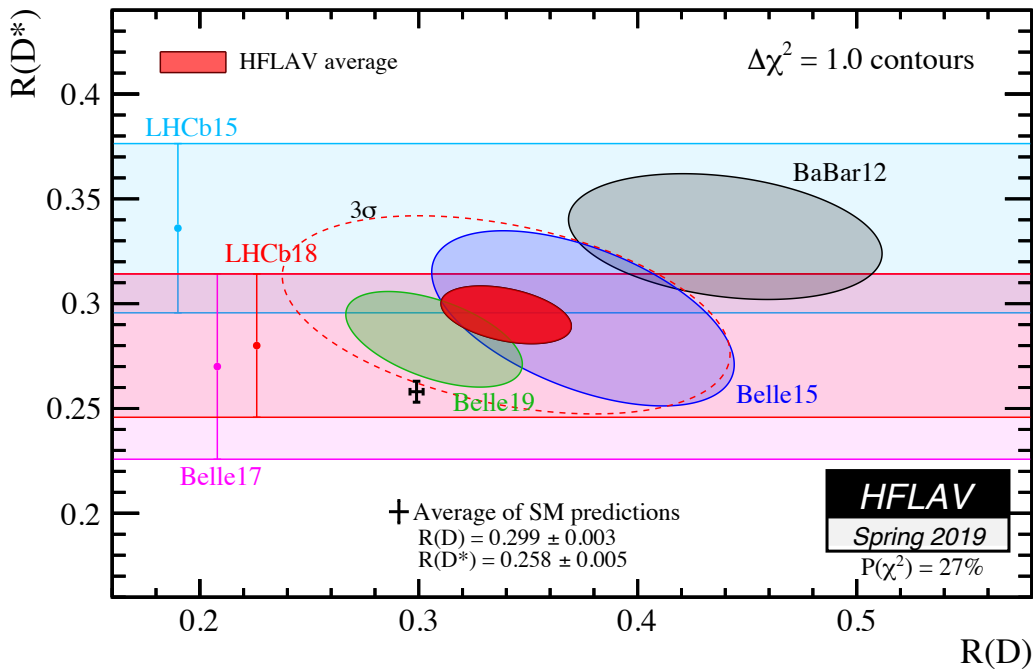


Figure 1.10: Different experimental measurements of $R(D)$ and $R(D^*)$ as well as the SM prediction thereof. The world average is shown in red, the 3σ contour is depicted as dashed line [103].

with C_V and $C_S^L = -4C_T$, where the combination $C_S^L = -4C_T$ is usually induced by Fierz identities. The latter scenario is shown in Fig. 1.11. Both scenarios give a good fit to data and allow to resolve the anomaly in $b \rightarrow c\tau\nu$, however the 1-D hypothesis predicts $R(D) = R(D^*)$ which is not what is currently observed.

Note that an effect of $\mathcal{O}(10\%)$ at the level of the amplitude is needed to resolve the anomaly. Since this process occurs already at tree-level in the SM, the NP contribution needs to be sizable. Therefore, NP should not be heavier than a few TeV and not couple too weakly.

1.4.3 Anomalous Magnetic Moment of the Muon

One of the longest standing anomalies can be found in the anomalous magnetic moment (AMM) of the muon

$$a_\mu \equiv \frac{(g-2)_\mu}{2} . \quad (1.84)$$

Its current experimental value is dominated by the BNL experiment E821 [123]

$$a_\mu^{\text{exp}} = 116592089(63) \times 10^{-11} . \quad (1.85)$$

Compared to its SM prediction, which recently has been reevaluated in a community-wide effort [124]

$$a_\mu^{\text{SM}} = 116591810(43) \times 10^{-11} , \quad (1.86)$$

the difference between theory and experiment yields

$$\delta a_\mu = a_\mu^{\text{exp}} - a_\mu^{\text{SM}} = (279 \pm 76) \times 10^{-11} , \quad (1.87)$$

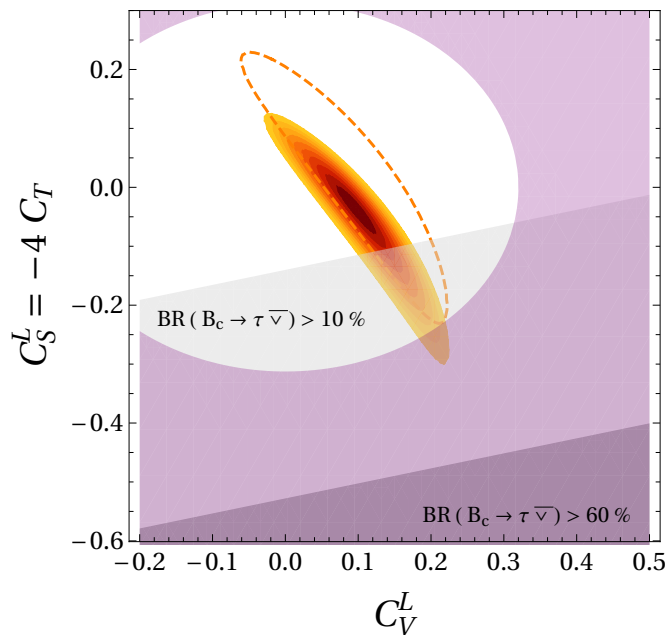


Figure 1.11: Global fit for the 2-D NP hypothesis in $b \rightarrow c\tau\nu$ with C_V^L and $C_S^L = -4C_T$. The Wilson Coefficients are given at the matching scale of 1 TeV, the plot is taken from Ref. [121].

which corresponds to a deviation of 3.7σ . On the theory side, the QED [125] and EW [126–128] contributions are under good control. The main uncertainties stem from hadronic effects, namely the hadronic vacuum polarization [129–135], the hadronic light-by-light scattering [136–142] and higher-order hadronic corrections [143,144]. A lot of effort is currently invested in improving these calculations, prompted by upcoming measurements at Fermilab [145] and J-PARC [146] which aim at reducing the experimental uncertainty by a factor four.

Since the AMM of the muon is proportional to the muon’s mass, it is already LFUV in the SM itself. However, in order to resolve the tension between experiment and theory, an additional source of LFUV in NP is needed since otherwise the AMM of the electron would be spoiled. Hence, δa_μ is another hint for LFUV. Also in this case a rather substantial NP effect is needed to resolve the difference between theory and experiment since it is of the same order as the SM EW contribution.

1.5 Leptoquarks

We have seen that several hints for LFUV exist in semi-leptonic B decays. Since leptoquarks (LQs) directly couple quarks to leptons, they are natural candidates to resolve these anomalies since they can generate FCNCs already at tree-level and also contribute to FCCC at tree-level. We have seen that the latter is a necessary condition to resolve the tension in $b \rightarrow c\tau\nu$. Furthermore, LQs have the advantage that they contribute to other observables like neutral meson mixing only through loops, making these constraints less severe. Such constraints usually exclude models that induce FCNCs at tree level.

In this section, we will briefly introduce the LQ Lagrangian (further details will follow in chapters 2 to 8). We will also preempt some key aspects to solve the anomalies with LQs, which will be relevant for the remainder of this thesis. Finally we conclude this section with an extended outlook to the work performed in Refs. [45–51] which correspond to the chapters 2 to 8

of this thesis.

1.5.1 The Leptoquark Lagrangian

There are in total ten LQ representations: five scalar and five vector ones. They were first classified systematically in Ref. [147]. The representations, their quantum numbers and interaction Lagrangian with the SM fermions read

$$\begin{array}{lll}
 \text{SLQ} & Q_{\text{SM}} & \mathcal{L}_{\text{int}} \\
 \Phi_1 & \left(3, 1, -\frac{2}{3} \right) & \left(\lambda_{fj}^{1R} \bar{u}_f^c \ell_j + \lambda_{fj}^{1L} \bar{Q}_f^c i\tau_2 L_j \right) \Phi_1^\dagger + \text{h.c.} , \\
 \tilde{\Phi}_1 & \left(3, 1, -\frac{8}{3} \right) & \tilde{\lambda}_{fj}^1 \bar{d}_f^c \ell_j \tilde{\Phi}_1^\dagger + \text{h.c.} , \\
 \Phi_2 & \left(\bar{3}, 2, -\frac{7}{3} \right) & \left(\lambda_{fj}^{2RL} \bar{u}_f L_j + \lambda_{fj}^{2LR} \bar{Q}_f i\tau_2 \ell_j \right) \Phi_2^\dagger + \text{h.c.} , \\
 \tilde{\Phi}_2 & \left(\bar{3}, 2, -\frac{1}{3} \right) & \tilde{\lambda}_{fi}^2 \bar{d}_f L_i \tilde{\Phi}_2^\dagger + \text{h.c.} , \\
 \Phi_3 & \left(3, 3 - \frac{2}{3} \right) & \lambda_{fi}^3 \bar{Q}_f^c i\tau_2 (\tau \cdot \Phi_3)^\dagger L_i + \text{h.c.} .
 \end{array} \tag{1.88}$$

$$\begin{array}{lll}
 \text{VLQ} & Q_{\text{SM}} & \mathcal{L}_{\text{int}} \\
 V_1 & \left(\bar{3}, 1, -\frac{4}{3} \right) & \left(\kappa_{fi}^{1R} \bar{d}_f \gamma_\mu \ell_i + \kappa_{fi}^{1L} \bar{Q}_f \gamma_\mu L_i \right) V_1^{\mu\dagger} + \text{h.c.} , \\
 \tilde{V}_1 & \left(\bar{3}, 1, -\frac{10}{3} \right) & \tilde{\kappa}_{fi}^1 \bar{u}_f \gamma_\mu \ell_i \tilde{V}_1^{\mu\dagger} + \text{h.c.} , \\
 V_2 & \left(3, 2, -\frac{5}{3} \right) & \left(\kappa_{fi}^{2RL} \bar{d}_f^c \gamma_\mu L_i + \kappa_{fi}^{2LR} \bar{Q}_f^c \gamma_\mu \ell_i \right) V_2^{\mu\dagger} + \text{h.c.} , \\
 \tilde{V}_2 & \left(3, 2, \frac{1}{3} \right) & \tilde{\kappa}_{fi}^2 \bar{u}_f^c \gamma_\mu L_i \tilde{V}_2^{\mu\dagger} + \text{h.c.} , \\
 V_3 & \left(3, 3, \frac{4}{3} \right) & \kappa_{fi}^3 \bar{Q}_f \gamma_\mu (\tau \cdot V_3^{\mu\dagger})^\dagger L_i + \text{h.c.} .
 \end{array} \tag{1.89}$$

The λ and κ are arbitrary 3×3 coupling matrices with flavor indices f and j . The scalar LQs are denoted by Φ and the vector LQs by V , the (charge-conjugated) quark and lepton doublets are denoted by $Q^{(c)}$ and L , respectively, and the up (down) quark and lepton singlets by $u^{(c)}$ ($d^{(c)}$) and ℓ , respectively. The interaction of LQs and the SM gauge bosons can be introduced through the covariant derivative [148]:

$$\begin{aligned}
 \mathcal{L}_{\text{gauge}}^\Phi &= \sum_{\text{scalars}} (D_\mu \Phi)^\dagger (D_\mu \Phi) , \\
 \mathcal{L}_{\text{gauge}}^V &= \sum_{\text{Vectors}} -\frac{1}{4} F_{\mu\nu}^\dagger F^{\mu\nu} ,
 \end{aligned} \tag{1.90}$$

with

$$F_{\mu\nu} = D_\mu V_\nu - D_\nu V_\mu . \tag{1.91}$$

Furthermore, a mass term for the SLQs can be added in a straightforward way. Additionally the SLQs can also interact with the SM Higgs which actually allows for mixing among the SLQ representations. The Lagrangian for these interactions reads

$$\begin{aligned}
 \mathcal{L}_{H\Phi} = & -A_{\tilde{\Phi}_1}(\tilde{\Phi}_2^\dagger H)\Phi_1 + A_{\tilde{\Phi}_2}(\tilde{\Phi}_2^\dagger(\tau \cdot \Phi_3)H) + Y_{\tilde{\Phi}_2}(\Phi_2^\dagger H)(Hi\tau_2\tilde{\Phi}_2) \\
 & + Y_{\tilde{\Phi}_1}(Hi\tau_2(\tau \cdot \Phi_3)^\dagger H)\tilde{\Phi}_1 + Y_{\tilde{\Phi}_1}(H^\dagger(\tau \cdot \Phi_3)H)\Phi_1^\dagger + \text{h.c.} \\
 & - Y_{\tilde{\Phi}_2}(Hi\tau_2\Phi_2)(Hi\tau_2\tilde{\Phi}_2)^\dagger - Y_{\tilde{\Phi}_2}(Hi\tau_2\tilde{\Phi}_2)(Hi\tau_2\Phi_2)^\dagger \\
 & - iY_{33}\varepsilon_{IJK}H^\dagger\tau_I H\Phi_{3,K}^\dagger\Phi_{3,J} \\
 & - \sum_{k=1}^3(m_k^2 + Y_k H^\dagger H)\Phi_k^\dagger\Phi_k - \sum_{k=1}^2(\tilde{m}_k^2 + Y_{\tilde{k}} H^\dagger H)\tilde{\Phi}_k^\dagger\tilde{\Phi}_k.
 \end{aligned} \tag{1.92}$$

The $m_{\tilde{\Phi}}^2$ represent the bare mass terms of the LQs. When the Higgs acquires the vev, the mass terms are shifted and the mass matrices become off-diagonal. These matrices then need to be diagonalized via a redefinition of the LQ fields, which then also changes the coupling matrices λ of Eq. (1.89). This procedure is performed in detail in Sec. 6.2.

Simply adding a mass term for the VLQs by hand would violate gauge invariance. This means that without any further information about a UV-completion of the model, calculations at loop-level can contain infinities. In cases where the VLQs only contribute to a certain process at tree-level, this is not an issue. Even for certain one-loop processes, calculations turn out to be finite and gauge-invariant, in other cases it is possible to at least calculate the LL contribution, which allows for a good estimate of the true contribution. Several UV complete models for the VLQ singlet V_1 have been proposed, see Refs. [149–157].

1.5.2 Leptoquarks as Solution to the Anomalies

Let us now briefly discuss the requirements for the different LQ representations in order to address the flavor anomalies summarized in Sec. 1.4. We refer to chapters 2 to 8 for detailed analyses. As mentioned earlier, NP needs to contribute to $b \rightarrow c\tau\nu$ already at tree level to be able to account for this anomaly. Additionally, bounds from e.g. $B \rightarrow K^{(*)}\nu\nu$ decays have to be respected. This is an issue for the scalar triplet Φ_3 and vector triplet V_3 : Due to $SU(2)$ invariance, they generate an effect in $b \rightarrow s\nu\nu$ of the same size as in $b \rightarrow c\tau\nu$, violating the bounds by orders of magnitude. The LQs $\tilde{\Phi}_1$, $\tilde{\Phi}_2$, \tilde{V}_1 and \tilde{V}_2 do not generate the desired effect at tree-level. Concerning $b \rightarrow s\ell\ell$ we saw in Sec. 1.4 that certain configurations of Wilson coefficients are preferable in order to address that anomaly. Among the LQs, Φ_3 , V_1 and V_3 give a $C_{9\mu} = -C_{10\mu}$ effect. Finally, there is the AMM of the muon, where also a substantial NP contribution of the order of the SM EW contribution is needed. Due to the nature of the LQs, they contribute to a_μ through diagrams where quarks run in the loop. Through a chirality flip on the internal quark line, these contributions can become proportional to the quark-mass. In case of the top quark, this results in an m_t/m_μ enhanced effect, which numerically is ≈ 1700 . To create this effect however, the LQ needs to couple to left- and right-handed top quarks simultaneously. Only Φ_1 and Φ_2 are able to achieve this. We see that no single LQ can explain all the three anomalies simultaneously, however the VLQ singlet V_1 is able to resolve $b \rightarrow s\ell\ell$ and $b \rightarrow c\tau\nu$ at the same time.

Lepton Flavor Universal Effects

In Sec. 1.4 we mentioned the NP scenario with a $C_{9\mu} = -C_{10\mu}$ effect supported by a LFU effect in $C_{9\ell}$, see Eq. (1.75). This scenario becomes especially interesting for models that aim at

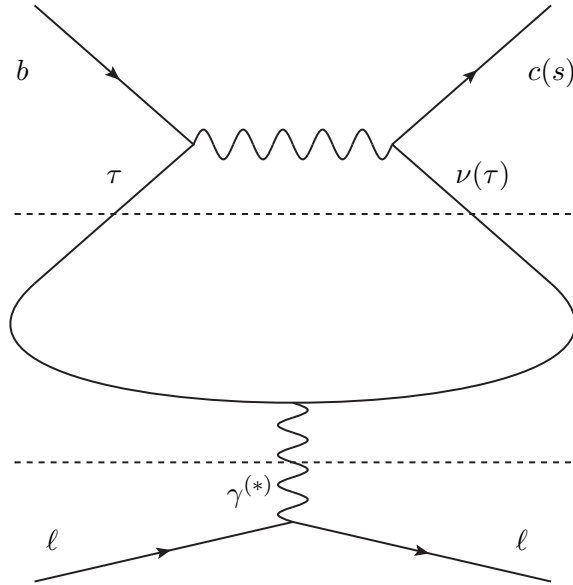


Figure 1.12: V_1 contribution to $b \rightarrow c\tau\nu$ (top part). Due to $SU(2)$ invariance an effect of the same size in $b \rightarrow s\tau\tau$ occurs, which can lead to LFU contributions to $b \rightarrow s\gamma$ (middle part) and $b \rightarrow s\ell\ell$ (bottom part) when closing the loop.

explaining $b \rightarrow c\tau\nu$ and $b \rightarrow s\ell\ell$ simultaneously. Obviously a LFUV effect is necessary both in the CC and NC transitions. However, since the effect in $b \rightarrow c\tau\nu$ needs to be much larger than the one in $b \rightarrow s\mu\mu$, loop effects induced by the tree-level $b \rightarrow c\tau\nu$ contribution can arise which are not only sizable but can in fact even exceed the LFUV tree-level effect in $b \rightarrow s\mu\mu$. In the case of the VLQ singlet V_1 the effect in $b \rightarrow c\tau\nu$ creates an effect of the same size in $b \rightarrow s\tau\tau$ due to $SU(2)$ invariance. Closing the τ -loop then gives an effect in $b \rightarrow s\gamma$ and $b \rightarrow s\ell\ell$. This is illustrated in Fig. 1.12. The model-specific global fit, which also includes the effect in C_7 , is shown in Fig. 1.13.

1.5.3 Outlook

We conclude this section by giving an outlook to the chapters 2 to 8, containing extensive analyses. In chapter 2 we analyze the VLQ singlet V_1 as a favorable candidate to address the CC and NC flavor anomalies simultaneously. We find a very good fit to data without violating any experimental constraints. Chapter 3 contains a proceeding article, which updates the analysis of chapter 2, i.e. it includes also the most recent measurements of Belle. In chapter 4 we investigate how tauonic B decays are correlated to the neutron electric dipole moment (EDM) for the SLQ Φ_1 . Assuming the persistence of the $b \rightarrow c\tau\nu$ anomaly, we show that even small effects relative to the SM in $B \rightarrow \tau\nu$, to be tested at Belle II, generate a sizable neutron EDM, which in turn could be tested at PSI with the n2EDM experiment. In chapter 5 we consider a combination of the scalar singlet and triplet LQs Φ_1 and Φ_3 , respectively. This combination has the distinct advantage that constraining effects in $B \rightarrow K^{(*)}\nu\nu$ can be canceled. In that way, Φ_1 and Φ_3 enter $b \rightarrow c\tau\nu$ while Φ_1 can account for δa_μ and Φ_3 can resolve the tension in $b \rightarrow s\ell\ell$, making a combined explanation of all three anomalies possible. Turning to chapter 6, we investigate SLQ effects in Higgs decays and oblique corrections, taking into account all five scalar representations and mixing among them. The investigated observables can be calculated independently from the couplings to the SM fermions, yielding a complementary window to

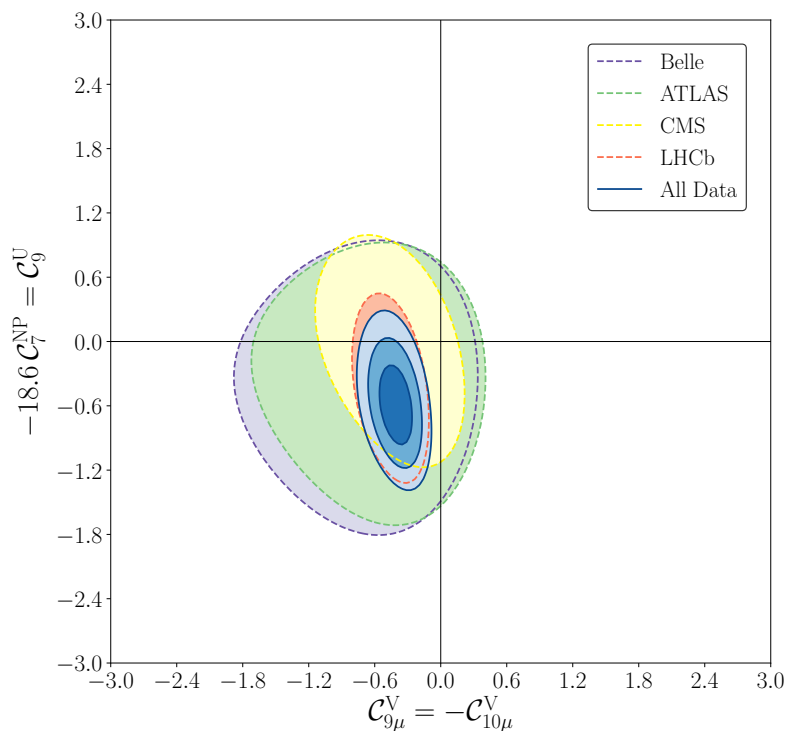


Figure 1.13: Model-specific global fit for the VLQ V_1 in $b \rightarrow s\mu\mu$ transitions. The LFUV effect in $C_{9\mu}^V = -C_{10\mu}^V$ is supported by a LFU effect in $C_{9\ell}$, the effect in C_7 is also included. This fit was used for the plot in Fig. 3.2. Plot courtesy of Bernat Capdevila.

distinguish among the different LQ representations. In chapter 7 we correlate the AMM of the muon to the Higgs decay $h \rightarrow \mu\mu$, prompted by the recent measurement thereof by ATLAS and CMS. This is especially interesting with regard to future experiments. Finally, we extensively investigate loop-effects, which unavoidably are generated when explaining the flavor anomalies, in chapter 8. These loop-effects affect purely leptonic processes like $Z \rightarrow \ell\ell$, $W \rightarrow \ell\nu$ and even LFV decays like $Z \rightarrow \ell\ell'$ or $\ell \rightarrow \ell'\gamma$. In chapters 6 to 8 we also actively analyze the parameter space with regards to future experiments.

Chapter 2

Importance of Loop Effects in Explaining the Accumulated Evidence for New Physics in B Decays with a Vector Leptoquark

published in

Phys. Rev. Lett. **122** (2019) 011805

arXiv: 1807.02068 [hep-ph]

Importance of Loop Effects in Explaining the Accumulated Evidence for New Physics in B Decays with a Vector Leptoquark

Andreas Crivellin

Paul Scherrer Institut, CH-5232 Villigen PSI, Switzerland

Christoph Greub

Albert Einstein Center for Fundamental Physics, Institute for Theoretical Physics, University of Bern, CH-3012 Bern, Switzerland

Dario Müller

*Paul Scherrer Institut, CH-5232 Villigen PSI, Switzerland
Physik-Institut, Universität Zürich, Winterthurerstrasse 190, CH-8057 Zürich, Switzerland*

Francesco Saturnino

Albert Einstein Center for Fundamental Physics, Institute for Theoretical Physics, University of Bern, CH-3012 Bern, Switzerland

In recent years experiments revealed intriguing hints for new physics (NP) in B decays involving $b \rightarrow c\tau\nu$ and $b \rightarrow s\ell^+\ell^-$ transitions at the 4σ and 5σ level, respectively. In addition, there are slight disagreements in $b \rightarrow u\tau\nu$ and $b \rightarrow d\mu^+\mu^-$ observables. While not significant on their own, they point in the same direction. Furthermore, V_{us} extracted from τ decays shows a slight tension ($\approx 2.5\sigma$) with its value determined from CKM unitarity and an analysis of Belle data found an excess in $B_d \rightarrow \tau^+\tau^-$. Concerning NP explanations, the vector leptoquark $SU(2)$ singlet is of special interest since it is the only single particle extension of the Standard Model which can (in principle) address all the anomalies described above. For this purpose, large couplings to τ leptons are necessary and loop effects, which we calculate herein, become important. Including them in our phenomenological analysis, we find that neither the tension in V_{us} nor the excess in $B_d \rightarrow \tau^+\tau^-$ can be fully explained without violating bounds from $K \rightarrow \pi\nu\bar{\nu}$. However, one can account for $b \rightarrow c\tau\nu$ and $b \rightarrow u\tau\nu$ data finding intriguing correlations with $B_q \rightarrow \tau^+\tau^-$ and $K \rightarrow \pi\nu\bar{\nu}$. Furthermore, the explanation of $b \rightarrow c\tau\nu$ predicts a positive shift in C_7 and a negative one in C_9 , being nicely in agreement with the global fit to $b \rightarrow s\ell^+\ell^-$ data. Finally, we point out that one can fully account for $b \rightarrow c\tau\nu$ and $b \rightarrow s\ell^+\ell^-$ without violating bounds from $\tau \rightarrow \phi\mu$, $\Upsilon \rightarrow \tau\mu$ or $b \rightarrow s\tau\mu$ processes.

2.1 Introduction

So far, the LHC has not directly observed any particles beyond the Standard Model (SM). However, intriguing hints for lepton flavor universality (LFU) violating NP have been acquired:

$b \rightarrow s(d)\ell^+\ell^-$:

The ratios

$$R(K^{(*)}) = \frac{\text{Br}[B \rightarrow K^{(*)}\mu^+\mu^-]}{\text{Br}[B \rightarrow K^{(*)}e^+e^-]}, \quad (2.1)$$

[77]([79]) indicate LFU violation with a combined significance of $\approx 4\sigma$ [92,93,158–161]. Taking also into account all other $b \rightarrow s\mu^+\mu^-$ observables, like the angular observable P'_5 [83] in the

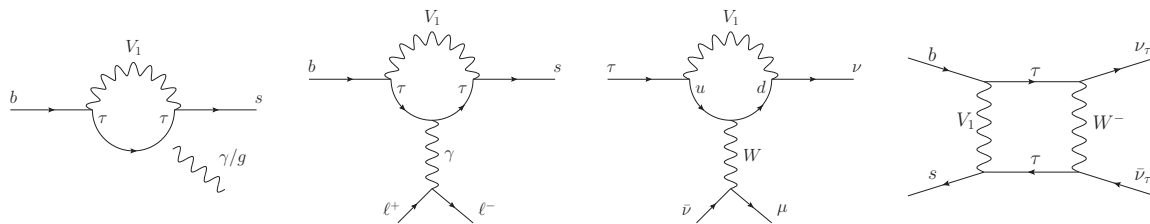


Figure 2.1: Feynman diagrams depicting the one-loop contributions of the vector LQ singlet to $C_{7/8}^{sb}$, $b \rightarrow s\ell^+\ell^-$, $\tau \rightarrow \mu\nu\bar{\nu}$ and $b \rightarrow s\nu\bar{\nu}$ (from left to right).

decay $B \rightarrow K^*\mu^+\mu^-$, the global fit of the Wilson coefficients to all available data even shows compelling evidence [88] for NP ($> 5\sigma$).

Concerning $b \rightarrow d\ell^+\ell^-$ transitions, the theoretical analysis of Ref. [162] shows that the LHCb measurement of $B \rightarrow \pi\mu^+\mu^-$ [163] slightly differs from the theory expectation. Even though this is not significant on its own, the central value is very well in agreement with the expectation from $b \rightarrow s\ell^+\ell^-$ under the assumption of a V_{td}/V_{ts} -like scaling of the NP effect¹. In other words, an effect of the same order and sign as in $b \rightarrow s\ell^+\ell^-$, relative to the SM, is preferred. Furthermore, an (unpublished) analysis of BELLE data found an excess in $B_d \rightarrow \tau^+\tau^-$ [164].

$b \rightarrow c(u)\tau\nu$:

The ratios

$$R(D^{(*)}) = \frac{\text{Br}[B \rightarrow D^{(*)}\tau\nu]}{\text{Br}[B \rightarrow D^{(*)}\ell\nu]} \quad \text{with } \ell = \{e, \mu\}, \quad (2.2)$$

which measure LFU violation in the charged current by comparing τ modes with light leptons ($\ell = e, \mu$), differ in combination from their SM predictions by $\approx 4\sigma$ [103]. Also, the ratio

$$R(J/\psi) = \frac{\text{Br}[B_c \rightarrow J/\psi\tau\nu]}{\text{Br}[B_c \rightarrow J/\psi\mu\nu]} \quad (2.3)$$

[113] exceeds the SM prediction in agreement with the expectations from $R(D^{(*)})$ [165, 166].

Concerning $b \rightarrow u\tau\nu$ transitions, the theory prediction for $B \rightarrow \tau\nu$ crucially depends on V_{ub} . While previous lattice calculations resulted in rather small values of V_{ub} , recent calculations give a larger value (see Ref. [167] for an overview). However, the measurement is still above the SM prediction by more than 1σ , as can be seen from the global fit [58]. In

$$R(\pi) = \frac{\text{Br}[B \rightarrow \pi\tau\nu]}{\text{Br}[B \rightarrow \pi\ell\nu]} \quad (2.4)$$

there is also a small disagreement between theory [168] and experiment [169] which does not depend on V_{ub} . These results are not significant on their own but lie again above the SM predictions like in the case of $b \rightarrow c\tau\nu$.

V_{us}^τ :

V_{us}^τ extracted from τ lepton decays (V_{us}^τ) shows a tension of 2.5σ compared to the value of V_{us} determined from CKM unitarity (V_{us}^{uni}) [103, 170].

The only possible single particle explanation, which can (at least in principle) address all these anomalies is the vector leptoquark (LQ) $SU(2)_L$ singlet V_1 with hypercharge² $-4/3$

¹Here, V refers to the Cabibbo-Kobayashi-Maskawa (CKM) matrix.

²In our conventions, the left-handed lepton doublet has hypercharge -1 .

[171–177] arising in the famous Pati-Salam model [178]: This LQ can explain $b \rightarrow c\tau\nu$ data without violating bounds from $b \rightarrow s\nu\bar{\nu}$ and/or direct searches, provides (at tree level) a left-handed solution to $b \rightarrow s\ell^+\ell^-$ data, and does not lead to proton decay. Therefore, a sizable effect in $b \rightarrow u\tau\nu$ and $b \rightarrow d\ell^+\ell^-$ is straightforward, and also an explanation of V_{us}^τ could be possible. A huge enhancement of $b \rightarrow s\tau^+\tau^-$ rates is predicted as well [179], making an amplification of $B_d \rightarrow \tau^+\tau^-$ possible.

Several attempts to construct a UV completion for this LQ to address the anomalies have been made [149–154, 180–184]. In order to fully account for the $b \rightarrow c\tau\nu$ data (while respecting perturbativity), one needs sizable couplings to third generation leptons and V_1 generates, via $SU(2)_L$ invariance, also large contributions to the operators $d_i d_j \tau \tau$ and $u_i u_j \nu \nu$ at tree level. These operators give rise to couplings of down quarks to neutrinos or light charged leptons at loop level (see Fig. 2.1).

In this article we will calculate these loop effects³, which turn out to be not only numerically important but also give rise to additional correlations among observables. Even though a theory with a massive vector boson without an explicit Higgs sector is not renormalizable, we still identify several phenomenologically important loop effects which are gauge independent and finite and can therefore be calculated reliably (in analogy to flavor observables within the SM).

2.2 Model and One-Loop Effects

We work in a simplified model extending the SM by a vector LQ $SU(2)_L$ singlet with hypercharge $-4/3$, mass M and interactions with fermions determined by

$$\mathcal{L}_{V\mu} = \left(\kappa_{fi}^L \bar{Q}_f \gamma_\mu L_i + \kappa_{fi}^R \bar{d}_f \gamma_\mu e_i \right) V_1^{\mu\dagger} + h.c. . \quad (2.5)$$

Here, Q (L) are quark (lepton) $SU(2)_L$ doublets, d (e) are down quark (charged lepton) singlets and f, i are flavor indices. In the following, we will neglect the right-handed couplings, which are not necessary to explain the anomalies. This then generates the effective four-fermion interactions encoded in

$$\mathcal{L}_{\text{eff}} = -\frac{\kappa_{il}^L \kappa_{jk}^{L*}}{M^2} \bar{Q}_i^\alpha \gamma^\mu Q_j^\beta \bar{L}_k^\beta \gamma_\mu L_l^\alpha , \quad (2.6)$$

where α and β label the $SU(2)$ components. After EW symmetry breaking, we work in the down basis; i.e., no CKM elements appear in flavor changing neutral currents of down quarks. We recall our definitions and the tree-level results in the appendix.

In our setup, one-loop effects involving the LQ and third generation leptons (τ 's and τ neutrinos) can be very important, since we aim for large effects in $b \rightarrow c(u)\tau\nu$ and $b \rightarrow s(d)\tau^+\tau^-$ processes. In principle, a massive vector boson, like our LQ, without a Higgs sector is not renormalizable. However, in flavor physics most effects can still be calculated reliably since they are gauge independent and finite (also in unitary gauge)⁴. This is in analogy to the SM, where the contribution of the W to flavor observables can be correctly calculated in unitary gauge without taking into account the Higgs sector.

We are only interested in effects which are always absent at tree level (like $b \rightarrow s\nu\bar{\nu}$ processes) or are not present at tree level due to a specific coupling structure (like $b \rightarrow s\mu^+\mu^-$ processes in the absence of muon couplings). Furthermore, we neglect tiny dimension-8 effects of the SM Higgs particle. In these cases the loop effects are the leading contributions. We calculate all diagrams at leading order in the external momenta using asymptotic expansion [64].

³Similar loop effects for scalar LQs have been calculated in Refs. [185–187].

⁴In this article we followed two approaches to check the results. First, we calculated the results in unitary gauge. Then, we derived the couplings of the LQ Goldstones to SM fermions by requiring the tree-level amplitude to be gauge independent. Finally, we calculated its contribution in R_ξ gauge.

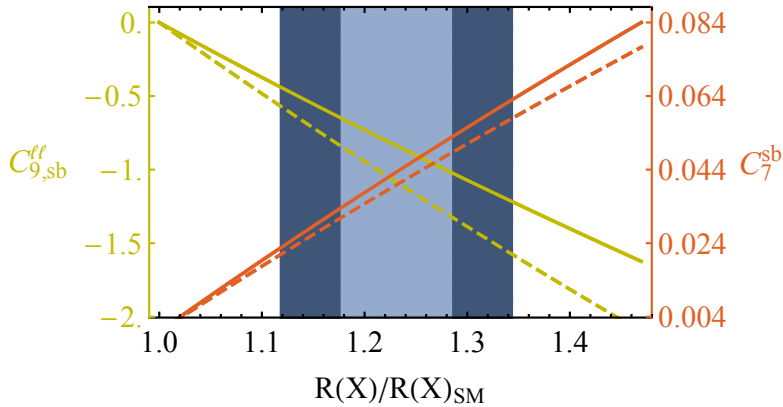


Figure 2.2: $C_{9, sb}^{\ell\ell}$ and $C_7^{sb}(\mu_b)$ as functions of $R(X)/R(X)_{\text{SM}}$ with $X = \{D, D^*, J/\psi\}$. The solid lines correspond to $M = 1$ TeV and the dashed ones to $M = 5$ TeV while the (dark) blue region is preferred by $b \rightarrow c\tau\nu$ data at the 1σ (2σ) level. From the global fit, taking into account only lepton flavor conserving observables we have $-1.29 < C_{9, sb}^{\ell\ell} < -0.87$ [91] and $-0.01 < C_7^{sb}(\mu_b) < 0.05$ [88] at the 1σ level. Therefore, our model predicts just the right sign and size of the effect in $C_{9, sb}^{\ell\ell}$ and $C_7^{sb}(\mu_b)$ necessary to explain $b \rightarrow s\ell^+\ell^-$ data, assuming an explanation of $b \rightarrow c\tau\nu$.

2.2.1 W Boxes Contributing to $d_i \rightarrow d_f\nu\bar{\nu}$

We use the effective Hamiltonian

$$\begin{aligned} \mathcal{H}_{\text{eff}}^{\nu\nu} &= -\frac{4G_F}{\sqrt{2}} V_{tdk} V_{tdj}^* \left(C_{L, jk}^{fi} \mathcal{O}_{L, jk}^{fi} + C_{R, jk}^{fi} \mathcal{O}_{R, jk}^{fi} \right), \\ \mathcal{O}_{L, jk}^{fi} &= \frac{\alpha}{4\pi} \left[\bar{d}_j \gamma^\mu P_L d_k \right] \left[\bar{\nu}_f \gamma_\mu (1 - \gamma_5) \nu_i \right], \\ \mathcal{O}_{R, jk}^{fi} &= \frac{\alpha}{4\pi} \left[\bar{d}_j \gamma^\mu P_R d_k \right] \left[\bar{\nu}_f \gamma_\mu (1 - \gamma_5) \nu_i \right], \end{aligned} \quad (2.7)$$

with $P_{R(L)} = (1 + (-)\gamma_5)/2$ and G_F (α) being the Fermi (electromagnetic fine structure) constant. The result of the box contributions involving a W to $d_i \rightarrow d_f\nu\bar{\nu}$ (an example diagram is shown on the right-hand side of Fig. 2.1) is gauge invariant in R_ξ gauge and the same finite result is obtained in unitary gauge (with $e = \sqrt{4\pi\alpha}$ and m_t (m_W) the top quark (W boson) mass)

$$\begin{aligned} C_{L, fa}^{ij} &= \frac{-m_W^2}{2e^2 V_{3a} V_{3f}^* M^2} \left(6\kappa_{fj}^L \kappa_{ai}^{L*} \log\left(\frac{m_W^2}{M^2}\right) \right. \\ &\quad \left. + 3 \left(V_{3a} V_{3k}^* \kappa_{ki}^{L*} \kappa_{fj}^L + V_{3f}^* V_{3k} \kappa_{kj}^L \kappa_{ai}^{L*} \right) \frac{\log\left(\frac{m_t^2}{m_W^2}\right)}{1 - \frac{m_W^2}{m_t^2}} + V_{3f}^* V_{3k} \kappa_{kj}^L V_{3a} V_{3l}^* \kappa_{li}^{L*} \frac{m_t^2}{m_W^2} \right) \end{aligned} \quad (2.8)$$

2.2.2 W Off-Shell Penguins Contributing to $\tau \rightarrow \mu\nu\bar{\nu}$

Here (see third diagram in Fig. 2.1) we obtain again a finite and gauge independent result for the Wilson coefficient; following the analysis of [188], we use

$$\mathcal{H}_{\text{eff}}^{\tau\mu\nu f\nu_i} = \frac{4G_F}{\sqrt{2}} D_{L, fi}^{\tau\mu} \left[\bar{\nu}_f \gamma^\sigma P_L \nu_i \right] \left[\bar{\mu} \gamma_\sigma P_L \tau \right], \quad (2.9)$$

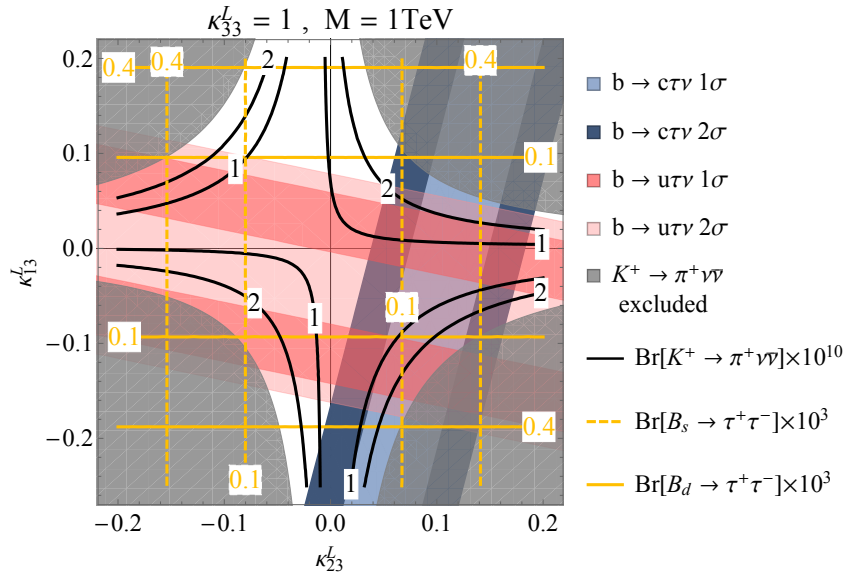


Figure 2.3: Predictions for $B_q \rightarrow \tau^+ \tau^-$ and $K \rightarrow \pi \nu \bar{\nu}$ (contour lines) in the $\kappa_{13}^L - \kappa_{23}^L$ plane for $M = 1 \text{ TeV}$ and $\kappa_{33}^L = 1$. The colored regions are preferred by $b \rightarrow c(u)\tau\nu$ data, where we naively averaged (i.e., we computed the weighted average of the observables and added their errors in quadrature, disregarding correlations) $R(D^{(*)})$ and $R(J/\psi)$ or $R(\pi)$ and $B \rightarrow \tau\nu$, respectively. The gray region is excluded by $K^+ \rightarrow \pi^+ \nu \bar{\nu}$. Here we assumed all couplings κ_{ij}^L to be real.

with

$$D_{L,fi}^{\tau\mu} = N_c \delta_{i2} \frac{V_{3k}^* \kappa_{kf}^{L*} \kappa_{33}^L}{32\pi^2} \frac{m_t^2}{M^2} \left(1 + 2 \log \left(\frac{m_t^2}{M^2} \right) \right). \quad (2.10)$$

We find, in agreement with Ref. [176], that the effect is small.

2.2.3 Photon and Gluon Penguins

We use the standard Hamiltonian (see, for example, Ref. [91]) also defined in the appendix. For on-shell photons and gluons the result of the left-hand diagram in Fig. 2.1 is finite in unitary gauge and the same result is obtained in R_ξ gauge:

$$C_{7(8)}^{sb} = \frac{-\sqrt{2}}{G_F V_{tb} V_{ts}^* M^2} \frac{11}{72} \left(\frac{5}{48} \right) \kappa_{2i}^L \kappa_{3i}^{L*}. \quad (2.11)$$

Taking into account the running from the LQ scale $\mu_{LQ} = M = 1 \text{ TeV}$ down to $\mu_b = 5 \text{ GeV}$ (see, e.g., Refs. [189, 190]), we obtain

$$C_{7(8)}^{sb}(\mu_b) \approx 0.29 \kappa_{2i}^L \kappa_{3i}^{L*}. \quad (2.12)$$

For off-shell photons the full result (second diagram in Fig. 2.1) for the amplitude is gauge dependent and, in general, divergent. However, one can calculate the mixing of $C_{9, sb}^{\tau\tau} = -C_{10, sb}^{\tau\tau}$ into the four-fermion operators $O_{9, sb}^{\ell\ell}$ (containing light leptons as well) within the effective theory (i.e. after integrating out the LQ at tree level). In this way, a gauge independent result is obtained and the leading logarithm of the (unknown) full result is recovered. For off-shell photons we thus calculate the effect in the EFT (below the LQ scale), generating the following mixing into the four-fermion operators with light leptons:

$$C_{9, sb}^{\ell\ell} = \frac{\sqrt{2}}{G_F V_{tb} V_{ts}^* M^2} \frac{1}{6} \log \left(\frac{M^2}{\mu_b^2} \right) \kappa_{2i}^L \kappa_{3i}^{L*}. \quad (2.13)$$

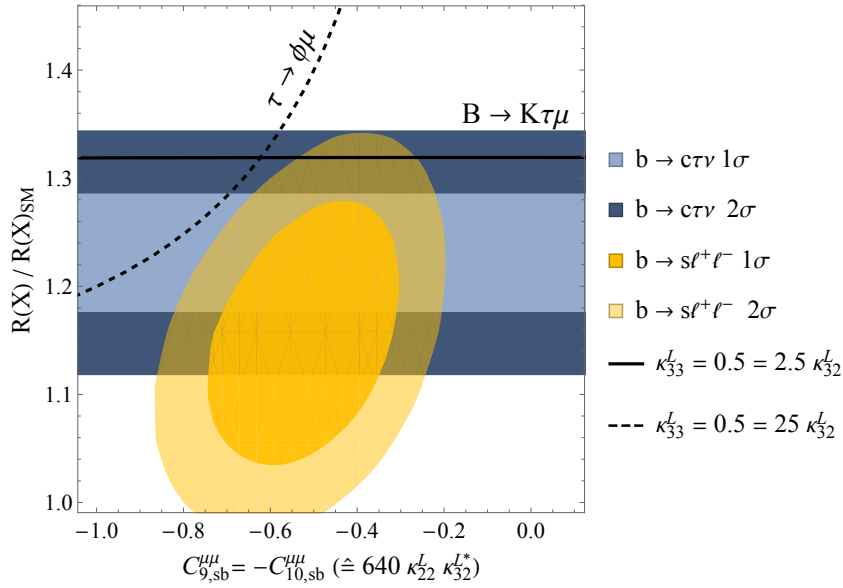


Figure 2.4: Allowed (colored) regions in the $C_{9, sb}^{\mu\mu} = -C_{10, sb}^{\mu\mu} (\cong 640 \kappa_{22}^L \kappa_{32}^{L*}) - R(X)/R(X)_{SM}$ plane for $M = 1$ TeV and $X = D, D^*, J/\psi$ at the 1σ and 2σ level for $\kappa_{33}^L V_{cb} \ll \kappa_{23}^L$. The region above the black dashed (solid) line is excluded by $\tau \rightarrow \phi\mu$ ($B \rightarrow K\tau\mu$) for $\kappa_{33}^L = 0.5 = 25\kappa_{32}^L$ ($\kappa_{33}^L = 0.5 = 2.5\kappa_{32}^L$). The bound from $\tau \rightarrow \phi\mu$ ($B \rightarrow K\tau\mu$) depends on κ_{33}^L and κ_{32}^L and gets stronger if κ_{32}^L gets smaller (larger). That is, for $\kappa_{33}^L = 0.5$ and $2.7 \lesssim \kappa_{33}^L/\kappa_{32}^L \lesssim 27$, the whole 2σ region preferred by $b \rightarrow c\tau\nu$ and $b \rightarrow s\ell^+\ell^-$ data is consistent with $B \rightarrow K\tau\mu$ and $\tau \rightarrow \phi\mu$.

Note that this result is model independent (at leading-log accuracy) in the sense that it does not depend on the model which generates $C_{9, sb}^{\tau\tau} = -C_{10, sb}^{\tau\tau}$. In principle, there are also Z penguins generating $C_{9, sb}^{\ell\ell}$ and $C_{10, sb}^{\ell\ell}$. However, this effect is suppressed by light lepton masses (or small momenta) and is therefore of dimension 8. Further, note that there are no box diagram contributions which generate $\bar{s}b\bar{\mu}\mu$ ($\bar{s}b\bar{e}e$) operators if the couplings of the LQ to muons (electrons) are zero at tree level.

2.2.4 Box Diagrams with LQs

What cannot be calculated consistently are box diagrams involving only LQs [149]. Here, the results are divergent in unitary gauge which corresponds to a gauge dependence in R_ξ gauge. However, these effects are suppressed if $|\kappa^L| < g_2$ and can be further suppressed in the presence of vectorlike fermions by a GIM-like mechanism [151] which, in analogy to the SM, would render the result finite.

2.3 Phenomenology

Assuming $\kappa_{33}^L V_{cb} \ll \kappa_{23}^L$, one is safe from LHC bounds, and the effects in $B_s \rightarrow \tau^+\tau^-$, $C_7^{sb}(\mu_b)$ (Eq. (2.12)) and $C_{9, sb}^{\ell\ell}$ (Eq. (2.13)) directly depend on $R(X)/R(X)_{SM}$ (with $X = D^{(*)}, J/\psi$). In Fig. 2.2 we show these dependences. Intriguingly, the effect generated in $C_7^{sb}(\mu_b)$ and $C_{9, sb}^{\ell\ell}$, within the preferred region from $b \rightarrow c\tau\nu$ data, exactly overlaps with the 1σ ranges of the model independent fit to $b \rightarrow s\mu^+\mu^-$ data excluding LFU violating observables [90,91] (therefore, only

P'_5 etc. but not $R(K^{(*)})$ can be explained).

Let us now include the effect of κ_{13}^L . Here, many correlations arise. First of all, $b \rightarrow c(u)\tau\nu$ is already at tree level correlated to $b \rightarrow s(d)\tau^+\tau^-$. In addition, the W boxes in Eq. (2.8) generate effects in $B \rightarrow K^{(*)}(\pi)\nu\bar{\nu}$ and $K \rightarrow \pi\nu\bar{\nu}$. While the bounds from $B \rightarrow K^{(*)}(\pi)\nu\bar{\nu}$ turn out to be weaker than the ones from $B_q \rightarrow \tau^+\tau^-$, there are striking correlations with $K \rightarrow \pi\nu\bar{\nu}$, as can be seen from Fig. 2.3. Furthermore, we get an effect

$$\delta V_{us}^\tau = \frac{V_{us}^\tau - V_{us}^{\tau(0)}}{V_{us}^{\text{uni}}} \approx -C_{us}^{\tau\tau}, \quad (2.14)$$

where $V_{us}^{\tau(0)}$ is the CKM matrix element extracted from τ decays without NP. However, Eq. (2.8) generates $K \rightarrow \pi\nu\bar{\nu}$, and respecting these bounds, the relative effect in V_{us}^τ can only be at the per-mill level, $|\delta V_{us}^\tau| \approx 0.05\%$, excluding the possibility to account for the discrepancy of $|V_{us}^{\text{uni}}| = 0.22547 \pm 0.00095$ versus $|V_{us}^\tau| = 0.2212 \pm 0.0014$ [103, 170]. The same is true about $B_d \rightarrow \tau^+\tau^-$, where the currently preferred region of analysis using BELLE data [164] of $\text{Br}[B_d \rightarrow \tau^+\tau^-]_{\text{exp}} = (4.39^{+0.80}_{-0.83} \pm 0.45)$ lies outside the plot range.

Now, in addition to the couplings κ_{33}^L and κ_{23}^L , we allow nonvanishing κ_{32}^L and κ_{22}^L . These couplings give rise to tree-level effects in $b \rightarrow s\mu^+\mu^-$. In Fig. 2.4 we show the allowed (colored) regions from $b \rightarrow s\mu^+\mu^-$ and $b \rightarrow c\tau\nu$ as well as the exclusions from $b \rightarrow s\tau\mu$ and $\tau \rightarrow \phi\mu$. Note that a simultaneous explanation of the anomalies is perfectly possible since the colored regions overlap and do not extend to the parameter space excluded by $b \rightarrow s\tau\mu$ and $\tau \rightarrow \phi\mu$. Interestingly, due to the loop effects originating from the $b \rightarrow c\tau\nu$ explanation, we predict a flavor universal effect in $C_{9, sb}^{\ell\ell}$ and C_7^{sb} which is supplemented by a tree-level effect of the form $C_{9, sb}^{\mu\mu} = -C_{10, sb}^{\mu\mu}$ with muons only. This means that the relative NP effect compared to the SM in lepton flavor conserving observables (like P'_5) should be larger than in $R(K^{(*)})$, which is in perfect agreement with the global fit⁵.

2.4 Conclusions

The vector leptoquark $SU(2)$ singlet is a prime NP candidate to explain the current hints for LFU violation. In this article we calculated and studied the important loop effects arising within such a model and performed a phenomenological analysis. We find:

An explanation of $b \rightarrow c\tau\nu$ data generates lepton flavor universal effects in $b \rightarrow sl^+\ell^-$ transitions which nicely agree with the model independent fit (see Fig. 2.2). Therefore, the $C_9 = -C_{10}$ -like tree-level effect, which is in general LFU violating, is supplemented by these effects generating a new pattern for the Wilson coefficients. This can be tested with future data. That is, with more precise measurements of lepton flavour universality violating and lepton flavor universality conserving effects, one can test if in fact there is a lepton flavor universality conserving contribution in addition to the lepton flavor universality violating ones [95]. Similar conclusions hold for the correlations between $b \rightarrow u\tau\nu$ data generating lepton flavor universal effects in $b \rightarrow dl^+\ell^-$ processes.

NP in $b \rightarrow c(u)\tau\nu$ generates important effects in $B_{s(d)} \rightarrow \tau^+\tau^-$ which are even correlated to $b \rightarrow s(d)\nu\bar{\nu}$ processes and $K \rightarrow \pi\nu\bar{\nu}$ via W box contributions (see right-hand diagram in Fig. 2.1). The V_{us}^τ puzzle (like the CP asymmetry in $\tau \rightarrow K_S\pi\nu$ [191]) cannot be solved due to the stringent constraints from $K \rightarrow \pi\nu\bar{\nu}$, and because of $b \rightarrow u\tau\nu$ bounds one cannot fully account for the BELLE excess in $B_d \rightarrow \tau^+\tau^-$ (see Fig. 2.3).

⁵See Ref. [95] for a recent analysis of such scenarios.

$b \rightarrow c\tau\nu$ and $b \rightarrow s\ell^+\ell^-$ data can be simultaneously explained without violating other bounds like $\tau \rightarrow \phi\mu$ (see Fig. 2.4). Furthermore, one could at the same time also account for NP effects in $b \rightarrow d\mu^+\mu^-$ without violating $K_L \rightarrow \mu^+\mu^-$ bounds.

Acknowledgements — We are very grateful to Joaquim Matias and Bernat Capdevilla for providing us with the fit necessary for the $b \rightarrow s\ell^+\ell^-$ region in Fig. 2.4 whose work is supported by an exploratory grant (FPA2014-61478-EXP) and to Aleksey Rusov for providing us with the fit for $C_{9,bd}^{\mu\mu}$. The work of A.C. and D.M. is supported by an Ambizione Grant of the Swiss National Science Foundation (PZ00P2_154834). The work of C.G. and F.S. is supported by the Swiss National Foundation under Grant 200020_175449/1.

2.5 Appendix

In this appendix we recall the tree-level results for the observables and give details on the experimental situation.

2.5.1 $d_k \rightarrow d_j\ell_f^-\ell_i^+$

We define the effective Hamiltonian as

$$\begin{aligned}\mathcal{H}_{\text{eff}}^{\ell\ell} &= -\frac{4G_F}{\sqrt{2}}V_{td_k}V_{td_j}^* \sum_{a=7}^{10} C_{a,d_jd_k}^{fi} \mathcal{O}_{a,d_jd_k}^{fi}, \\ \mathcal{O}_{7(8)}^{jk} &= \frac{e(g_s)}{16\pi^2} m_k [\bar{d}_j \sigma^{\mu\nu} (T^a) P_R d_k] F_{\mu\nu} (G_{\mu\nu}^a), \\ \mathcal{O}_{9(10),jk}^{fi} &= \frac{\alpha}{4\pi} [\bar{d}_j \gamma^\mu P_L d_k] [\bar{\ell}_f \gamma_\mu (\gamma_5) \ell_i],\end{aligned}\tag{2.15}$$

and obtain at tree level

$$C_{9,jk}^{fi} = -C_{10,jk}^{fi} = \frac{-\sqrt{2}}{2G_F V_{td_k} V_{td_j}^*} \frac{\pi}{\alpha} \frac{1}{M^2} \kappa_{ji}^L \kappa_{kf}^{L*}.\tag{2.16}$$

For $b \rightarrow s\mu^+\mu^-$ transitions, the allowed range is [88]

$$-0.37(-0.49) \geq C_{9,sb}^{\mu\mu} = -C_{10,sb}^{\mu\mu} \geq (-0.75) - 0.88,\tag{2.17}$$

at the (1σ) 2σ level, assuming a vanishing effect in electrons. In $b \rightarrow d\mu^+\mu^-$ transitions one finds for the Wilson coefficients

$$C_{9,db}^{\mu\mu} = -C_{10,db}^{\mu\mu} = -1.9 \pm 1.1,\tag{2.18}$$

assuming them to be real [162]. For τ leptons we have experimentally [192]

$$\text{Br} \left[B_s \rightarrow \tau^+ \tau^- \right]_{\text{exp}} \leq 6.8 \times 10^{-3} \quad (95\% \text{ C.L.}),\tag{2.19}$$

and for $B_d \rightarrow \tau^+ \tau^-$ there is a (unpublished) measurement of BELLE [164] and an upper limit of LHCb [192]

$$\begin{aligned}\text{Br} \left[B_d \rightarrow \tau^+ \tau^- \right]_{\text{exp}}^{\text{BELLE}} &= \left(4.39_{-0.83}^{+0.80} \pm 0.45 \right) \times 10^{-3}, \\ \text{Br} \left[B_d \rightarrow \tau^+ \tau^- \right]_{\text{exp}}^{\text{LHCb}} &\leq 2.1 \times 10^{-3} \quad (95\% \text{ C.L.}).\end{aligned}\tag{2.20}$$

Both are compatible at the 2σ level. The SM predictions are given by [193, 194]

$$\begin{aligned}\text{Br}[B_s \rightarrow \tau^+\tau^-]_{\text{SM}} &= (7.73 \pm 0.49) \times 10^{-7}, \\ \text{Br}[B_d \rightarrow \tau^+\tau^-]_{\text{SM}} &= (2.22 \pm 0.19) \times 10^{-8}.\end{aligned}\tag{2.21}$$

In our model, we have

$$\frac{\text{Br}[B_q \rightarrow \tau^+\tau^-]}{\text{Br}[B_q \rightarrow \tau^+\tau^-]_{\text{SM}}} = \left| 1 + \frac{C_{10,qb}^{\tau\tau}}{C_{10,qb}^{\text{SM}}} \right|^2,\tag{2.22}$$

with $q = s, d$ and $C_{10,qb}^{\text{SM}} \approx -4.3$ [195, 196]. For the analysis of $B \rightarrow K^{(*)}\tau\mu$ we will use the results of Ref. [197].

The short distance contribution to the branching ratio of $K_L \rightarrow \mu^+\mu^-$ is given by [198] (with the Hamiltonian defined e.g. in Ref. [199])

$$\text{Br}[K_L \rightarrow \mu^+\mu^-]_{\text{SD}} = a_L \left(\frac{\text{Re}[\lambda_t \tilde{Y}]}{\lambda^5} + \frac{\text{Re}[\lambda_c]}{\lambda} P_c^Y \right)^2$$

with the numerical input

$$\begin{aligned}a_L &= 2.01 \times 10^{-9}, \quad \tilde{Y} = Y_{SM} - s_W^2 C_{10,sd}^{\mu\mu}, \\ Y_{SM} &= 1.018 \left(\frac{m_t}{170 \text{ GeV}} \right)^{1.56}, \quad P_c^Y = 0.115 \pm 0.017, \\ \lambda_i &= V_{is}^* V_{id}, \quad \lambda = |V_{us}|.\end{aligned}\tag{2.23}$$

The upper experimental limit for the short distance contribution is [200]

$$\text{Br}[K_L \rightarrow \mu^+\mu^-]_{\text{SD}} < 2.5 \times 10^{-9}.\tag{2.24}$$

Using Ref. [175] we have

$$\text{Br}[\tau \rightarrow \phi\mu] = \frac{f_\phi^2 m_\tau^3 \tau_\tau}{128\pi} \frac{|\kappa_{22}^L \kappa_{23}^{L*}|^2}{M^4} \left(1 - \frac{m_\phi^2}{m_\tau^2} \right)^2 \left(1 + 2 \frac{m_\phi^2}{m_\tau^2} \right)$$

with the current experimental limit [201]

$$\text{Br}[\tau \rightarrow \phi\mu] < 8.4 \times 10^{-8} \quad (90\% \text{ C.L.}).\tag{2.25}$$

If we consider $\Upsilon(nS) \rightarrow \tau\mu$, we have [177]

$$\text{Br}[\Upsilon(3S) \rightarrow \tau\mu] = 2.6 \times 10^{-7} \frac{|\kappa_{32}^L \kappa_{33}^{L*}|^2}{M^4 (\text{TeV})}.\tag{2.26}$$

Comparing this to the experimental limit $\text{Br}[\Upsilon(3S) \rightarrow \tau\mu] < 3.1 \times 10^{-6}$ (90% C.L.) of Ref. [202], this does not pose relevant constraints on our model.

2.5.2 $d_k \rightarrow d_j \nu_i \bar{\nu}_f$

We use the conventions

$$\begin{aligned} \mathcal{H}_{\text{eff}}^{\nu\nu} &= -\frac{4G_F}{\sqrt{2}} V_{td_k} V_{td_j}^* \left(C_{L,jk}^{fi} \mathcal{O}_{L,jk}^{fi} + C_{R,jk}^{fi} \mathcal{O}_{R,jk}^{fi} \right), \\ \mathcal{O}_{L(R),jk}^{fi} &= \frac{\alpha}{4\pi} \left[\bar{d}_j \gamma^\mu P_{L(R)} d_k \right] \left[\bar{\nu}_f \gamma_\mu (1 - \gamma_5) \nu_i \right]. \end{aligned} \quad (2.27)$$

Note that the LQ does not contribute at tree level.

For $K \rightarrow \pi \nu \bar{\nu}$ we use Ref. [203] with the updated numerical values given in Ref. [204] resulting in

$$\begin{aligned} \text{Br} [K^\pm \rightarrow \pi^\pm \nu \bar{\nu}] &= \frac{1}{3} (1 + \Delta_{EM}) \eta_\pm \times \\ &\sum_{f,i=1}^3 \left[\left(\frac{\text{Im} [\lambda_t \tilde{X}_L^{fi}]}{\lambda^5} \right)^2 + \left(\frac{\text{Re} [\lambda_c]}{\lambda} P_c \delta_{fi} + \frac{\text{Re} [\lambda_t \tilde{X}_L^{fi}]}{\lambda^5} \right)^2 \right], \\ \text{Br} [K_L \rightarrow \pi \nu \bar{\nu}] &= \frac{1}{3} \eta_L \sum_{f,i=1}^3 \left(\frac{\text{Im} [\lambda_t \tilde{X}_L^{fi}]}{\lambda^5} \right)^2, \end{aligned} \quad (2.28)$$

with

$$\begin{aligned} \tilde{X}_L^{fi} &= X_L^{\text{SM},fi} - s_W^2 C_{L,sd}^{fi}, \quad P_c = 0.404 \pm 0.024 \\ \eta_\pm &= (5.173 \pm 0.025) 10^{-11} \left[\frac{\lambda}{0.225} \right]^8, \\ \eta_L &= (2.231 \pm 0.013) 10^{-10} \left[\frac{\lambda}{0.225} \right]^8, \\ \Delta_{EM} &= -0.003, \quad X_L^{\text{SM},fi} = (1.481 \pm 0.005 \pm 0.008) \delta_{fi}. \end{aligned} \quad (2.29)$$

For $B \rightarrow K^{(*)} \nu \bar{\nu}$ we follow Ref. [205], giving $C_{L,sb}^{\text{SM},fi} \approx -1.47/s_W^2 \delta_{fi}$, and the branching ratios normalized by the SM predictions read

$$R_{K^{(*)}}^{\nu\bar{\nu}} = \frac{1}{3} \sum_{f,i=1}^3 \frac{|C_{L,sb}^{fi}|^2}{|C_{L,sb}^{\text{SM},fi}|^2}. \quad (2.30)$$

This has to be compared to the current experimental limits $R_K^{\nu\bar{\nu}} < 3.9$ and $R_{K^*}^{\nu\bar{\nu}} < 2.7$ [206] (both at 90% C.L.). The future BELLE II sensitivity for $B \rightarrow K^{(*)} \nu \bar{\nu}$ is 30% of the SM branching ratio [207].

2.5.3 $d_k \rightarrow u_j \bar{\nu} \ell^-$

We define the effective Hamiltonian as

$$\mathcal{H}_{\text{eff}}^{\ell_f \nu_i} = \frac{4G_F}{\sqrt{2}} V_{jk} C_{jk}^{fi} \left[\bar{u}_j \gamma^\mu P_L d_k \right] \left[\bar{\ell}_f \gamma_\mu P_L \nu_i \right], \quad (2.31)$$

where in the SM $C_{jk, \text{SM}}^{fi} = \delta_{fi}$. The contribution of our model is given by

$$C_{jk}^{fi} = \frac{\sqrt{2}}{4G_F M^2} \frac{V_{jl}}{V_{jk}} \kappa_{li}^L \kappa_{kf}^{L*}. \quad (2.32)$$

With these conventions we have for $b \rightarrow c\tau\nu$ transitions

$$R(X) / R(X)_{\text{SM}} = \sum_{i=1}^3 \left| \delta_{3i} + C_{cb}^{\tau i} \right|^2, \quad (2.33)$$

with $X = \{D, D^*, J/\psi\}$, assuming vanishing contributions to the muon and electron channels. We obtain the analogous expression for $b \rightarrow u\tau\nu$.

Concerning $\tau \rightarrow K(\pi)\nu$ we find that the CKM element V_{us}^τ extracted from these decays is given in terms of the one determined in the absence of NP contributions ($V_{us}^{\tau(0)}$) by

$$V_{us}^\tau = V_{us}^{\tau(0)} / (1 + C_{us}^{\tau\tau}), \quad (2.34)$$

where we neglected LFV effects. This has to be compared to [103,170] $|V_{us}^{\text{uni}}| = 0.22547 \pm 0.00095$ and $|V_{us}^\tau| = 0.2212 \pm 0.0014$.

In Ref. [168] the analysis gives

$$\begin{aligned} R(\pi)_{\text{exp}} &= 1.05 \pm 0.51, \\ R(\pi)_{\text{SM}} &= 0.641 \pm 0.016. \end{aligned} \quad (2.35)$$

For $B \rightarrow \tau\nu$ we use the PDG value [208] and the SM prediction of Ref. [58] at the 2σ level

$$\begin{aligned} \text{Br}[B \rightarrow \tau\nu]_{\text{exp}} &= (1.09 \pm 0.24) \times 10^{-4}, \\ \text{Br}[B \rightarrow \tau\nu]_{\text{SM}} &= (0.851_{-0.077}^{+0.079}) \times 10^{-4}. \end{aligned} \quad (2.36)$$

Chapter 3

Explaining the Flavor Anomalies with a Vector Leptoquark (Moriond 2019 Update)

published in

PoS DIS2019 (2019) 163

arXiv: 1906.01222 [hep-ph]

Explaining the Flavor Anomalies with a Vector Leptoquark (Moriond 2019 Update)

Andreas Crivellin⁶

Paul Scherrer Institut, CH 5232 Villigen PSI, Switzerland

Physik-Institut, Universität Zürich, Winterthurerstrasse 190, CH 8057 Zürich, Switzerland

Francesco Saturnino⁷

*Albert Einstein Center for Fundamental Physics, Institute for Theoretical Physics, University
of Bern, CH-3012 Bern, Switzerland*

Several experiments revealed intriguing hints for lepton flavor universality (LFU) violating new physics (NP) in semi-leptonic B meson decays, mainly in $b \rightarrow c\tau\nu$ and $b \rightarrow s\ell^+\ell^-$ transitions at the $3 - 5\sigma$ level. Leptoquarks (LQ) are prime candidates to address these anomalies as they contribute to semi-leptonic decays already at tree level while effects in other flavor observables, agreeing with the standard model (SM), are loop suppressed.

In these proceedings we review the vector leptoquark $SU(2)_L$ singlet, contained in the famous Pati-Salam model, which is able to address both $b \rightarrow c\tau\nu$ and $b \rightarrow s\mu^+\mu^-$ data simultaneously. Due to the large couplings to tau leptons needed to account for the $b \rightarrow c\tau\nu$ data, sizable loop effects arise which we include in our phenomenological analysis. Updating our result of Ref. [45] with the recent measurements of LHCb [78] and Belle [80,109] we find an even better fit to data than before.

3.1 Introduction

While so far the LHC has not detected any particles beyond the ones present in the Standard Model (SM), intriguing hints for LFU violation in semi-leptonic B -meson decays were accumulated in several (classes of) observables:

$$b \rightarrow s\ell^+\ell^-$$

In these flavor changing neutral current transitions, measurements of the ratios

$$R(K^{(*)}) = \frac{\text{Br}[B \rightarrow K\mu^+\mu^-]}{\text{Br}[B \rightarrow Ke^+e^-]}$$

show sizable deviations from their respective SM prediction. While the newest measurement of $R(K)$ by the LHCb collaboration [78] shows a deviation of 2.5σ from the SM, the Belle result for $R(K^{(*)})$ is consistent with the SM [80]. However, due to the larger errors, this result also agrees with previous LHCb measurement of $R(K^{(*)})$ which deviate from the SM [79] in the same direction as $R(K)$. Taking into account all other $b \rightarrow s\mu^+\mu^-$ observables (like the lepton flavor universal observable P'_5 [83]), the global fit prefers various NP scenarios above the 5σ level [88] compared to the SM, also when the newest measurements are taken into account [97,98,100,209].

⁶I thank the organizers, especially Nazila Mahmoudi, for the invitation to Moriond QCD and the opportunity to present these results. This work is supported by a Professorship Grant (PP00P2_176884) of the Swiss National Science Foundation.

⁷I thank the organizers of the DIS2019 in Turin for giving me the opportunity to present my work, which is supported by the Swiss National Foundation under grant 200020_175449/1. We are very grateful to Joaquim Matias and Bernat Capdevilla for providing us with the fit necessary for the $b \rightarrow s\ell^+\ell^-$ region in Fig. 3.2.

In order to resolve the discrepancy in the neutral current transitions, an effect of $\mathcal{O}(10\%)$ is required at the amplitude level. Since this flavor changing neutral current (FCNC) is suppressed in the SM as it is only induced at one loop level, a small NP contribution is already sufficient. In a global fit one finds a preference for scenarios like $C_9^{\mu\mu} = -C_{10}^{\mu\mu}$ (i.e. a left-handed current coupling to muons only) [98]. Such an effect is naturally obtained at tree-level with the vector LQ $SU(2)$ singlet [45, 149–154, 171–177, 180–184, 210–212]. However, a $C_9^{\mu\mu} = -C_{10}^{\mu\mu}$ effect complemented by a flavor universal effect in C_9 gives an even better fit to data [95, 98]. As we will see, this is exactly the pattern that arises in our model.

$b \rightarrow c\tau\nu$

There are also indications for LFU violation in charged current transitions, namely in the ratios

$$R(D^{(*)}) = \frac{\text{Br}[B \rightarrow D^{(*)}\tau\nu]}{\text{Br}[B \rightarrow D^{(*)}\ell\nu]}$$

where $\ell = \{e, \mu\}$. While the newest measurements from Belle [109] agree with the SM prediction, including previous measurements by BaBar, Belle and LHCb still yield a deviation of 3.1σ [103] from the SM prediction. Furthermore there is also a measurement of the ratio $R(J/\Psi) = \frac{\text{Br}[B_c \rightarrow J/\Psi\tau\nu]}{\text{Br}[B_c \rightarrow J/\Psi\mu\nu]}$ exceeding its SM prediction [113].

Also here a NP effect of $\mathcal{O}(10\%)$ is needed at the amplitude level. However, since $b \rightarrow c\tau\nu$ transitions are mediated at tree level by the exchange of a W boson in the SM, the NP effect needs to be large. This means that NP should contribute at tree level with sizable couplings and at a not too high NP scale. Here, the best single particle solution is the vector LQ $SU(2)$ singlet [45, 149–154, 171–177, 180–184, 210–212] since it does not give a tree-level effect in $b \rightarrow s\nu\nu$ processes and provides a common rescaling of $R(D)$ and $R(D^*)$ with respect to the SM prediction.

3.2 The Pati Salam Vector Leptoquark as Combined Solution to the Anomalies

The vector Leptoquark $SU(2)_L$ singlet with hypercharge $-4/3$, arising in the famous Pati-Salam model [178], is a prime candidate to explain both the anomalies in charged current and neutral current B decays simultaneously [171–177]. It gives a $C_9 = -C_{10}$ effect in $b \rightarrow s\ell^+\ell^-$ at tree level and at the same time a sizable effect in $b \rightarrow c\tau\nu$ without violating bounds from $b \rightarrow s\nu\nu$ and/or direct searches and does not lead to proton decay. Note that this LQ by itself is not UV complete, however several UV complete models for this LQ have been proposed [149–154, 180–184, 213].

For the purpose of our phenomenological analysis, let us consider a model where we simply extend the SM by this LQ. Its interaction with the SM particles is given by the Lagrangian

$$\mathcal{L}_{V_1} = \kappa_{fi}^L \bar{Q}_f \gamma_\mu L_i V_\mu^{1\dagger} + h.c. ,$$

where $Q(L)$ is the quark (lepton) $SU(2)_L$ doublet, κ_{fi}^L represents the couplings of the LQ to the left handed quarks (leptons) and f and i are flavor indices. Note that in principle couplings to right-handed SM particles are also allowed, they are however not relevant for this discussion. After electro-weak symmetry breaking, we work in the down basis, meaning that no CKM matrix elements appear in FCNC processes.

We start by taking κ_{23}^L and κ_{33}^L as the only non-zero couplings, as they are necessary to explain $b \rightarrow c\tau\nu$ data. Here, strong effects in $b \rightarrow s\tau^+\tau^-$ transitions [179] are generated which

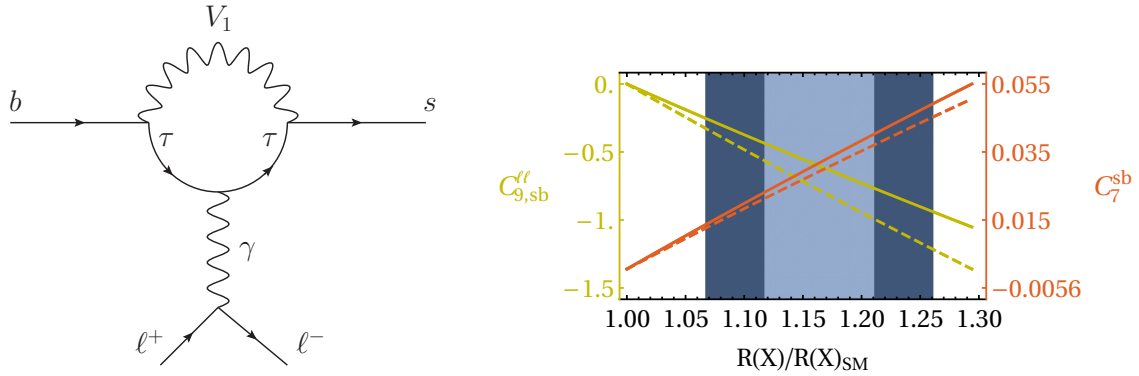


Figure 3.1: Left: Feynman diagram depicting the loop effects induced by the $bc\tau\nu$ operator from $SU(2)$ invariance. Right: $C_{9, sb}^{\ell\ell}$ and $C_7^{sb}(\mu_b)$, generated by these loop effects, as functions of $R(D^{(*)})/R(D^{(*)})_{\text{SM}}$. The solid (dashed) lines correspond to $M = 1$ TeV (5 TeV) while the (dark) blue region is preferred by $b \rightarrow c\tau\nu$ data at the 1σ (2σ) level, taking into account the most recent measurements. From the global fit, taking into account only lepton flavor conserving observables, we have $-1.29 < C_{9, sb}^{\ell\ell} < -0.87$ [91] and $-0.01 < C_7^{sb}(\mu_b) < 0.05$ [88] at the 1σ level. Assuming an explanation of $b \rightarrow c\tau\nu$, our model predicts the right size and sign of the effect in $C_{9, sb}^{\ell\ell}$ and $C_7^{sb}(\mu_b)$ needed to explain $b \rightarrow s\ell^+\ell^-$ data.

at the 1-loop level affect $b \rightarrow s\ell^+\ell^-$ via the Wilson coefficients $C_{9, sb}^{\ell\ell}$ and C_7^{sb} , as is depicted to the left in Fig. 3.1. Due to the correlation with $b \rightarrow c\tau\nu$, these Wilson coefficients can be expressed as functions of $R(D^{(*)})/R(D^{(*)})_{\text{SM}}$. The Wilson coefficients' dependency on these ratios is shown in the right plot of Fig. 3.1, where the RGE evolution of C_7^{sb} from the NP scale down to the b quark scale is also taken into account (see Ref. [47]). Interestingly, assuming an explanation of $b \rightarrow c\tau\nu$ data, the effects generated in $C_{9, sb}^{\ell\ell}$ and C_7^{sb} agree with the 1σ ranges of the model independent fit to $b \rightarrow s\mu^+\mu^-$ data excluding LFU violating observables [90, 91].

Now we also allow κ_{32}^L and κ_{22}^L to be non-zero, generating a tree level effect in $b \rightarrow s\mu^+\mu^-$ which is necessary to account for the LFU violating observables as well. In Fig. 3.2 we show the allowed (colored) regions from $b \rightarrow s\mu^+\mu^-$ and $b \rightarrow c\tau\nu$ as well as the exclusions from $b \rightarrow s\tau\mu$ and $\tau \rightarrow \phi\mu$. A simultaneous explanation of the anomalies is perfectly possible since the colored regions overlap and do not extend to the parameter space excluded by $b \rightarrow s\tau\mu$ and $\tau \rightarrow \phi\mu$. Interestingly, we predict a lepton flavor universal effect in $C_{9, sb}^{\ell\ell}$ and C_7^{sb} in addition to a LFU violating tree-level effect of the form $C_{9, sb}^{\mu\mu} = -C_{10, sb}^{\mu\mu}$ in muonic channels only. This means that the effect of NP compared to the SM is expected to be larger in lepton flavor universal observables like $P5'$ relative to LFU violation observables as $R(K^{(*)})$, which is in perfect agreement with global fit scenarios [98]. In fact, the agreement is even better after the inclusion of the new measurements of BELLE and LHCb.

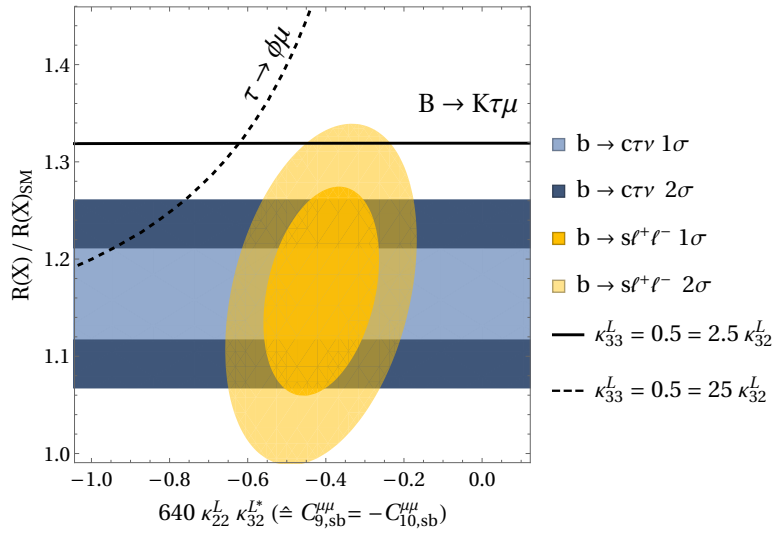


Figure 3.2: Allowed (colored) regions in the $C_{9, sb}^{\mu\mu} = -C_{10, sb}^{\mu\mu}$ ($\equiv 640\kappa_{22}^L\kappa_{32}^{L*}$) - $R(X)/R(X)_{\text{SM}}$ plane for $M = 1$ TeV and $X = \{D, D^*\}$ at the 1σ and 2σ level. The region above the black dashed (solid) line is excluded by $\tau \rightarrow \phi\mu$ ($B \rightarrow K\tau\mu$) for $\kappa_{33}^L = 0.5 = 25\kappa_{32}^L$ ($\kappa_{33}^L = 0.5 = 2.5\kappa_{32}^L$). The bound from $\tau \rightarrow \phi\mu$ ($B \rightarrow K\tau\mu$) depends on κ_{33}^L and κ_{32}^L and gets stronger if κ_{32}^L gets smaller (larger). That is, for $\kappa_{33}^L = 0.5$ and $2.7 \lesssim \kappa_{33}^L/\kappa_{32}^L \lesssim 27$, the whole 2σ region preferred by $b \rightarrow c\tau\nu$ and $b \rightarrow s\ell^+\ell^-$ data is consistent with these bounds. Note that we used the most recent experimental results for both the $b \rightarrow c\tau\nu$ and $b \rightarrow s\ell^+\ell^-$ transitions, therefore updating our analysis in Ref. [47].

Chapter 4

Correlating Tauonic B Decays to the Neutron EDM via a Scalar Leptoquark

published in

Phys. Rev. D **100** (2019) 115014

arXiv: 1905.08257 [hep-ph]

Correlating Tauonic B Decays to the Neutron EDM via a Scalar Leptoquark

Andreas Crivellin

Paul Scherrer Institut, CH 5232 Villigen PSI, Switzerland

Physik-Institut, Universität Zürich, Winterthurerstrasse 190, CH 8057 Zürich, Switzerland

Francesco Saturnino

Albert Einstein Center for Fundamental Physics, Institute for Theoretical Physics, University of Bern, CH-3012 Bern, Switzerland

In this article we investigate the correlations between tauonic B meson decays (e.g. $B \rightarrow \tau\nu$, $B \rightarrow D^{(*)}\tau\nu$, $B \rightarrow \pi\tau\nu$) and electric dipole moments (EDMs), in particular the one of the neutron, in the context of the S_1 scalar leptoquark. We perform the matching of this model on the effective field theory taking into account the leading renormalization group effect for the relevant observables. We find that one can explain the hints for new physics in $b \rightarrow c\tau\nu$ transitions without violating bounds from other observables. Even more interesting, it can also give sizable effects in $B \rightarrow \tau\nu$, to be tested at Belle II, which are correlated to (chromo) electric dipole operators receiving m_τ/m_u enhanced contributions. Therefore, given a deviation from the Standard Model (SM) expectations in $B \rightarrow \tau\nu$, this model predicts a sizable neutron EDM. In fact, even if new physics has CP conserving real couplings, the CKM matrix induces a complex phase and already a 10% change of the $B \rightarrow \tau\nu$ branching ratio (with respect to the SM) will lead to an effect observable with the n2EDM experiment at PSI.

4.1 Introduction

In the past four decades, the Standard Model (SM) of particle physics has been extensively tested and its predictions were very successfully confirmed, both in high energy searches as well as in low energy precision experiments. However, it is well known that the SM cannot be the ultimate theory describing the fundamental constituents of matter and their interactions. For example, it cannot accommodate for the observed matter–antimatter asymmetry in the universe: For satisfying the Sakharov conditions [214] the amount of CP violation within the SM is far too small [215–220]. Therefore, additional sources of CP violation are required and such models in general lead to nonvanishing electric dipole moments of neutral fermions. Thus, EDMs are very promising places to search for physics beyond the SM (see e.g. Ref. [221, 222] for a recent review). However, the effect of new physics (NP) in EDMs decouples with the NP scale which is a priori unknown, unless new particles, or at least deviations from the SM in other precision observables, are found.

In this respect, tauonic B decays are very promising channels for the (indirect) search for NP, especially in the light of the observed tensions between the SM predictions and experiments above the 3σ level [103]. These decays involve both down-type quarks and charged leptons of the third generation (i.e. bottom quarks and tau leptons) which are, due to their mass, very special and distinct from the fermions of the first two generations.⁸ In fact, to explain these anomalies, TeV scale NP with order one couplings to the third generation is required. Note that the tensions in $b \rightarrow c\tau\nu$ transitions are supported by $b \rightarrow u\tau\nu$ data (i.e. $B \rightarrow \pi\tau\nu$ and

⁸In group theory language, the SM possesses a global $U(3)^5$ flavor symmetry which is broken by the third generation Yukawa couplings to $U(2)^5$ [223].

$B \rightarrow \tau\nu$) and the forthcoming measurements of both $b \rightarrow c\tau\nu$ and $b \rightarrow u\tau\nu$ processes by LHCb and BELLE II will be able to confirm (or disprove) the presence of NP in these decays.

Therefore, it is very interesting to investigate the possible impact of models which can give sizable effects in tauonic B decays and EDMs. In this paper we choose the scalar leptoquark S_1 $SU(2)_L$ singlet which couples to SM fermions via the Lagrangian

$$\mathcal{L} = \left(\lambda_{fi}^L \overline{Q}_f^c i\tau_2 L_i + \lambda_{fi}^R \overline{u}_f^c \ell_i \right) \Phi_1^\dagger + \text{h.c.} . \quad (4.1)$$

Here, L (Q^c) is the lepton (charge conjugated quark) $SU(2)_L$ doublet, ℓ (u^c) the charged lepton (charge conjugated up quark) singlet and f, i are flavor indices. This model is theoretically well motivated since S_1 is present within the R -parity violating MSSM in the form of right-handed down squarks [224–228].⁹

This leptoquark (LQ) is a prime candidate for providing the desired correlations between tauonic B decays and EDMs. It possesses couplings to left- and right-handed quarks which is a necessary requirement for generating EDMs at the one-loop level [230, 231]. It also contributes to $b \rightarrow c\tau\nu$ at tree level [212, 232–250] and gives a very good fit to data (including polarization observables) [118, 119, 251, 252] since it generates vector, scalar and tensor operators. Similarly, it contributes to $b \rightarrow u\tau\nu$ transitions, in particular to $B \rightarrow \tau\nu$, where the situation becomes especially interesting. As we will see, in this case the model leads to m_τ/m_u enhanced CP violating effects in (chromo) electric dipole operators (see Fig. 4.1) which are even present for real NP parameters due to the large phase contained in the CKM element V_{ub} .

This paper is structured as follows: In the next section we will calculate the contributions to the relevant observables and discuss their experimental status. Section 4.3 presents our phenomenological analysis before we conclude in Sec. 4.4.

4.2 Observables and Contributions

In this section we discuss our setup, calculate the predictions for the relevant observables and discuss their current experimental situation and future prospects.

After electroweak symmetry breaking, the Lagrangian in Eq. (4.1) decomposes into components

$$\mathcal{L}_{\text{eff}}^{\text{EW}} = \left(\lambda_{fi}^R \overline{u}_f^c P_R \ell_i + V_{fj}^* \lambda_{ji}^L \overline{u}_f^c P_L \ell_i - \lambda_{fi}^L \overline{d}_f^c P_L \nu_i \right) \Phi_1^\dagger + \text{h.c.}$$

Here, we work in the down basis, meaning that the CKM matrix V appears in the couplings to left-handed up-type quarks. We denote the mass of the LQ by M and neglect its couplings to the SM Higgs boson which have a negligible phenomenological impact. The most relevant classes of observables in our model are $b \rightarrow s\nu\nu$ and $b \rightarrow c(u)\tau\nu$ transitions as well as EDMs, $D^0 - \bar{D}^0$ mixing and Z - $\tau\tau$ as well as W - $\tau\nu$ couplings which we consider now in more detail.

4.2.1 $b \rightarrow s\nu\nu$

For $b \rightarrow s\nu\nu$ transitions we follow the conventions of Ref. [205]

$$\begin{aligned} \mathcal{H}_{\text{eff}}^{\nu\nu} &= -\frac{4G_F}{\sqrt{2}} V_{td_k} V_{td_j}^* \left(C_{L,jk}^{fi} \mathcal{O}_{L,jk}^{fi} + C_{R,jk}^{fi} \mathcal{O}_{R,jk}^{fi} \right), \\ \mathcal{O}_{L(R),jk}^{fi} &= \frac{\alpha}{4\pi} \left[\overline{d}_j \gamma^\mu P_{L(R)} d_k \right] \left[\overline{\nu}_f \gamma_\mu (1 - \gamma_5) \nu_i \right], \end{aligned} \quad (4.2)$$

⁹Note that in the minimal R -parity violating MSSM the coupling to charged conjugated fields in Eq. (4.1) is absent. For an analysis of EDM constraints within this setup see Ref. [229].

and obtain, already at tree level, the contribution

$$C_{L,jk}^{fi\text{NP}} = \frac{\sqrt{2}}{4G_F V_{td_k} V_{td_j}^*} \frac{\pi}{\alpha} \frac{\lambda_{jf}^{L*} \lambda_{ki}^L}{M^2}. \quad (4.3)$$

Here the most relevant decays are $B \rightarrow K^{(*)} \nu \nu$ for which $C_{L,sb}^{\text{SM},fi} \approx -1.47/s_W^2 \delta_{fi}$ and branching ratios, normalized by the corresponding SM predictions, read

$$R_{K^{(*)}}^{\nu\bar{\nu}} = \frac{1}{3} \sum_{f,i=1}^3 \frac{|C_{L,sb}^{fi}|^2}{|C_{L,sb}^{\text{SM},ii}|^2}. \quad (4.4)$$

This has to be compared to the current experimental limits $R_K^{\nu\bar{\nu}} < 3.9$ and $R_{K^*}^{\nu\bar{\nu}} < 2.7$ [206] (both at 90% C.L.). The future BELLE II sensitivity for $B \rightarrow K^{(*)} \nu \bar{\nu}$ is 30% of the SM branching ratio [207].

4.2.2 $b \rightarrow c(u)\tau\nu$

For tauonic B decays we define the effective Hamiltonian as

$$\mathcal{H}_{\text{eff}}^{\tau\nu} = \frac{4G_F}{\sqrt{2}} V_{u_f b} \left(C_{VL}^f O_{VL}^f + C_{SL}^f O_{SL}^f + C_{TL}^f O_{TL}^f \right),$$

with the operators given by

$$\begin{aligned} O_{VL}^{u_f} &= \bar{u}_f \gamma^\mu P_L b \bar{\tau} \gamma_\mu P_L \nu_\tau, \\ O_{SL}^{u_f} &= \bar{u}_f P_L b \bar{\tau} P_L \nu_\tau, \\ O_{TL}^{u_f} &= \bar{u}_f \sigma^{\mu\nu} P_L b \bar{\tau} \sigma_{\mu\nu} P_L \nu_\tau. \end{aligned} \quad (4.5)$$

In the SM $C_{VL}^{u_f} = 1$ and our NP matching contributions at tree level are given by

$$\begin{aligned} C_{VL}^{u_f} &= \frac{\sqrt{2}}{8G_F V_{u_f b}} \frac{V_{u_f i} \lambda_{i3}^{L*} \lambda_{33}^L}{M^2}, \\ C_{SL}^{u_f} &= -4C_{TL}^{u_f} = \frac{-\sqrt{2}}{8G_F V_{u_f b}} \frac{\lambda_{f3}^{R*} \lambda_{33}^L}{M^2}. \end{aligned} \quad (4.6)$$

Taking into account the QCD effects of Ref. [253] to the matching, the one-loop EW and two-loop QCD renormalization group equation (RGE) for the scalar and tensor operators [254, 255] can be taken consistently into account. Numerically, this RGE evolution is given by

$$\begin{pmatrix} C_{SL}^{u_f}(m_b) \\ C_T^{u_f}(m_b) \end{pmatrix} \approx \begin{pmatrix} 1.75 & -0.29 \\ 0 & 0.84 \end{pmatrix} \begin{pmatrix} C_{SL}^{u_f}(1 \text{ TeV}) \\ C_T^{u_f}(1 \text{ TeV}) \end{pmatrix},$$

for a matching scale of 1 TeV. Finally, the ratios $R(D^{(*)}) = \frac{\text{Br}[B \rightarrow D^{(*)} \tau \nu]}{\text{Br}[B \rightarrow D^{(*)} \ell \nu]}$ with $\ell = \{\mu, e\}$ in terms of the Wilson coefficients at the b scale are given by [118]

$$\begin{aligned} \frac{R(D)}{R_{\text{SM}}(D)} &\simeq |1 + C_{VL}^c|^2 + 1.54 \Re[(1 + C_{VL}^c) C_{SL}^{c*}] \\ &+ 1.09 |C_{SL}^c|^2 + 1.04 \Re[(1 + C_{VL}^c) C_T^c] + 0.75 |C_T^c|^2, \\ \frac{R(D^*)}{R_{\text{SM}}(D^*)} &\simeq |1 + C_{VL}^c|^2 - 0.13 \Re[(1 + C_{VL}^c) C_{SL}^{c*}] \\ &+ 0.05 |C_{SL}^c|^2 - 5.0 \Re[(1 + C_{VL}^c) C_T^c] + 16.27 |C_T^c|^2. \end{aligned} \quad (4.7)$$

Similarly, for $b \rightarrow u\tau\nu$ transitions we have

$$\frac{\text{Br}[B \rightarrow \tau\nu]}{\text{Br}[B \rightarrow \tau\nu]_{SM}} = \left| 1 + C_{VL}^u - \frac{m_B^2 C_{SL}^u}{m_b m_\tau} \right|^2. \quad (4.8)$$

The corresponding formula for $B \rightarrow \pi\tau\nu$ can be found in Ref. [256]. However, here the effect of scalar and tensor operators is much smaller, making the theoretically very clean $B \rightarrow \tau\nu$ decays the primary place to search for them.

Combining the experimental measurements of $b \rightarrow c\tau\nu$ transitions from LHCb [110–112], Belle [106–109,257] and Babar [104,105], one finds a combined tension of 3.1σ in $R(D^{(*)})$ [103]¹⁰. However, note that here the $B_c \rightarrow J/\Psi\tau\nu$ measurement of LHCb [113], which also lies significantly above the SM prediction, is not included.¹¹ In $b \rightarrow u\tau\nu$ transitions, the theory prediction for $B \rightarrow \tau\nu$ crucially depends on V_{ub} . While previous lattice calculations resulted in rather small values of V_{ub} , recent calculations give a larger value (see Ref. [167] for an overview). However, the measurement is still above the SM prediction by more than 1σ , as can be seen from the global fit [58]. In $R(\pi) = \frac{\text{Br}[B \rightarrow \pi\tau\nu]}{\text{Br}[B \rightarrow \pi\ell\nu]}$ there is also a small disagreement between theory [168] and experiment [169] which does not depend on V_{ub} , once more pointing towards an enhancement. Therefore, even though the $b \rightarrow u\tau\nu$ results are not significant on their own, they point in the same direction as $b \rightarrow c\tau\nu$ (i.e. towards an enhancement with respect to the SM) and thus strengthen the case for NP in tauonic B decays.

4.2.3 EDMs

For EDMs the relevant Hamiltonian in our case is

$$\mathcal{H}_{\text{eff}}^{\text{nEDM}} = C_\gamma^u O_\gamma^u + C_g^u O_g^u + C_T^{u\tau} O_T^{u\tau}, \quad (4.9)$$

with

$$\begin{aligned} O_\gamma^u &= e\bar{u}\sigma^{\mu\nu}P_R u F_{\mu\nu}, \\ O_g^u &= g_s\bar{u}\sigma^{\mu\nu}P_R u T^a G_{\mu\nu}^a, \\ O_T^{u\tau} &= \bar{u}\sigma_{\mu\nu}P_R u \bar{\tau}\sigma^{\mu\nu}P_R \tau. \end{aligned} \quad (4.10)$$

At the high scale we find the matching contributions (depicted in Fig. 4.1)

$$\begin{aligned} C_T^{u\tau} &= -\frac{V_{1j}\lambda_{j3}^{L*}\lambda_{13}^R}{8M^2}, \\ C_\gamma^u &= -\frac{m_\tau V_{ub}}{96\pi^2 M^2}\lambda_{33}^{L*}\lambda_{13}^R \left(4 + 3\log\left(\mu^2/M^2\right)\right), \\ C_g^u &= -\frac{m_\tau V_{ub}}{64\pi^2 M^2}\lambda_{33}^{L*}\lambda_{13}^R. \end{aligned} \quad (4.11)$$

Note that we only get up-quark contributions since we do not have (at the one-loop level) CP violating couplings to down-type quarks. Importantly, note that our effect in C_γ^u and C_g^u is parametrically enhanced by m_τ/m_u , making a sizable effect in EDMs possible. This enhancement of the dipole operators also allows us to safely neglect the effects of charm quarks, four-fermion operators and of the Weinberg operator otherwise relevant for LQs [231].

¹⁰In Ref. [258] it was shown that uncertainties from meson exchanges between initial and final states might be bigger than the estimated SM uncertainty, which could alleviate the tension in $R(D^{(*)})$. On the other hand, recent improvements in form factor calculations [259] lower the SM prediction and increase the tension. These two effects are not included in Ref. [103] but will not change the result significantly.

¹¹See Ref. [165,166] for an analysis including $B_c \rightarrow J/\Psi\tau\nu$ before the latest BELLE update [109].

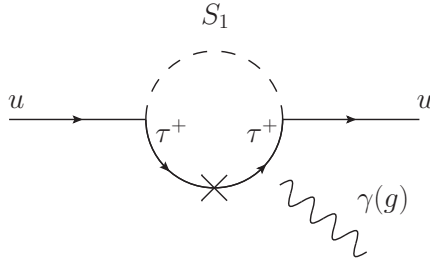


Figure 4.1: Feynman diagram showing the contribution of our model to the dipole operators of Eq. (4.10). The cross denotes the chirality flip by the tau mass which leads to the crucial m_τ/m_u enhancement.

Next, we use the one-loop RGE to evolve these Wilson coefficients of Eq. (4.11) down to the neutron scale. Here, combining and adjusting the results of Ref. [260] and Ref. [189] to our case we obtain¹²

$$\mu \frac{d}{d\mu} \begin{pmatrix} C_T^{u\tau} \\ C_\gamma^u \\ C_g^u \end{pmatrix} = \begin{pmatrix} \frac{C_F \alpha_s}{2\pi} & 0 & 0 \\ -\frac{m_\tau}{2\pi^2} & \frac{\alpha_s C_F}{2\pi} & \frac{4C_F \alpha_s}{3\pi} \\ 0 & 0 & \frac{\alpha_s (10C_F - 12)}{4\pi} \end{pmatrix} \begin{pmatrix} C_T^{u\tau} \\ C_\gamma^u \\ C_g^u \end{pmatrix}.$$

The solution to this differential equation can be written in terms of an evolution matrix in the form

$$\vec{C}(\mu_l) = U(\mu_l, \mu_h) \vec{C}(\mu_h) \quad (4.12)$$

with

$$U(\mu_l, \mu_h) = \begin{pmatrix} \eta^{\frac{4}{3\beta_0}} & 0 & 0 \\ -m_\tau X & \eta^{\frac{4}{3\beta_0}} & \frac{16}{3} \eta^{\frac{14}{3\beta_0}} \left(\eta^{\frac{2}{3\beta_0}} - 1 \right) \\ 0 & 0 & \eta^{\frac{2}{3\beta_0}} \end{pmatrix}, \quad (4.13)$$

$$\beta_0 = \frac{33 - 2f}{3}, \quad \eta = \frac{\alpha_s(\mu_h)}{\alpha_s(\mu_l)}, \quad (4.14)$$

and

$$X = \frac{\eta^{\frac{4}{3\beta_0}} \left(\eta^{\frac{4}{\beta_0}} - 1 \right) \beta_0}{8\pi^2 \log(\eta)} \log \left(\frac{\mu_l}{\mu_h} \right), \quad (4.15)$$

where f is the number of active quark flavors. The final evolution matrix is obtained by running with the appropriate numbers of flavours from the LQ scale down to 1 GeV.

Finally, the effects in the neutron and proton EDMs are given by [262]

$$\begin{aligned} d_n/e &= -(0.44 \pm 0.06) \text{Im} \left[C_\gamma^u \right] - (1.10 \pm 0.56) \text{Im} \left[C_g^u \right], \\ d_p/e &= (1.48 \pm 0.14) \text{Im} \left[C_\gamma^u \right] + (2.6 \pm 1.3) \text{Im} \left[C_g^u \right], \end{aligned}$$

in terms of the Wilson coefficients evaluated at 1 GeV. The neutron and proton EDMs then enter atomic ones, most importantly in mercury and deuteron (see Ref. [262] for details).

¹²For the same RGE in a different operator basis see Ref. [261].

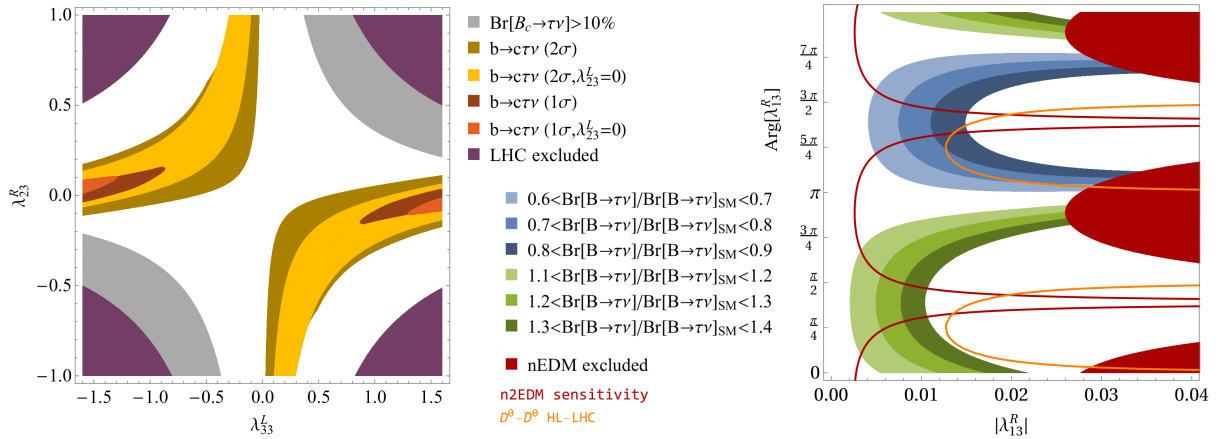


Figure 4.2: Left: preferred regions in the $\lambda_{33}^L - \lambda_{33}^R$ plane from $b \rightarrow c\tau\nu$ data for $M = 1$ TeV. Here, both the case of $\lambda_{23}^L = 0$ and the one taking the maximally allowed value of λ_{23}^L from $B \rightarrow K^*\nu\nu$ are shown. A good fit to data requires $|\lambda_{33}^L| \approx 1$ in both cases. Note that our model is compatible with LHC searches for monotaus and with B_c lifetime constraints which exclude the dark pink and gray regions. Right: The green (blue) regions indicate where $B \rightarrow \tau\nu$ is enhanced (suppressed) by 10%-40% w.r.t. the SM for $M = 1$ TeV, $\lambda_{33}^L = 1$ and $\lambda_{13}^L = 0$. The dark red region is excluded by the neutron EDM and the dark red contour denotes the n2EDM sensitivity. The orange contour shows the HL-LHC sensitivity to CP violation in $D_0 - \bar{D}_0$ mixing which is nicely complementary to EDM searches.

On the experimental side, d_{Hg} [263] gives currently slightly better bounds than the neutron EDM, while the one of the proton and the deuteron is not measured yet. However, d_p and d_D will be very precisely known from future experiments [264, 265] and concerning d_n there will be soon an improvement of one order of magnitude in sensitivity compared to the current limit of $3.6 \times 10^{-26} e cm$ [63, 266] from the n2EDM experiment at PSI [267]. Therefore, we will focus on d_n in our phenomenological analysis.

4.2.4 $D_0 - \bar{D}_0$ Mixing

To describe $D_0 - \bar{D}_0$ mixing we use the effective Hamiltonian

$$\mathcal{H}_{\text{eff}}^{D\bar{D}} = C'_1 Q'_1, \quad Q'_1 = [\bar{u}_\alpha \gamma_\mu P_R c_\alpha] [\bar{u}_\beta \gamma^\mu P_R c_\beta],$$

and find at the high scale

$$C'_1 = \frac{(\lambda_{13}^R \lambda_{23}^{R*})^2}{128\pi^2 M^2}, \quad (4.16)$$

from the one-loop matching. The evolution of C'_1 was calculated in Refs. [268, 269] and yields approximately [270]

$$C'_1(3 \text{ GeV}) \approx 0.8 C'_1(1 \text{ TeV}). \quad (4.17)$$

The matrix element for the D -meson mixing is given by

$$\langle \bar{D}^0 | Q'_1(\mu) | D^0 \rangle = \frac{1}{3} B_1(\mu) m_D f_D^2, \quad (4.18)$$

where $B_1(\mu) = 0.75$ at the scale $\mu = 3 \text{ GeV}$ [271]. The mass difference in the D -meson system is given by

$$\Delta m_D = 2\text{Re} [\langle \bar{D}^0 | \mathcal{H}_{\text{eff}}^{D\bar{D}} | D^0 \rangle] \equiv 2\text{Re} [M_{12}]. \quad (4.19)$$

Further, we write

$$\sin \phi_{12} = -\frac{2\text{Im}[M_{12}]}{\Delta m_D}. \quad (4.20)$$

The averages of the experimental values read [272, 273]

$$\begin{aligned} 0.001 < |M_{12}|[\text{ps}^{-1}] < 0.008, \\ -3.5 < \phi_{12}[\circ] < 3.3, \\ f_D = 212 \text{ MeV}, \end{aligned} \quad (4.21)$$

at 95% C.L. At a high luminosity LHC (HL-LHC) the sensitivity to ϕ_{12} could be improved down to the SM expectation of $\approx 0.17^\circ$ [274].

4.2.5 $W \rightarrow \tau\nu$ and $Z \rightarrow \tau\tau$

Virtual corrections with top quarks and LQs modify couplings of gauge bosons to charged leptons, in particular to the tau. Parametrizing the interactions as

$$-\mathcal{L} = \frac{g_2}{\sqrt{2}} \Lambda_{3i}^W (\bar{\tau} \gamma^\mu P_L \nu_i W_\mu^-) + \frac{g_2}{2c_w} \bar{\tau} \gamma^\mu (\Lambda^V - \Lambda^A \gamma_5) \tau Z_\mu$$

with

$$\begin{aligned} \Lambda_{3i}^W &= \delta_{3i} + \Lambda_{3i}^{\text{LQ}}, \quad \Lambda^{V,A} = \Lambda_{\text{SM}}^{V,A} + \Delta_{\text{LQ}}^{V,A}, \\ \Lambda_{\text{SM}}^V &= -\frac{1}{2} + 2s_w^2, \quad \Lambda_{\text{SM}}^A = -\frac{1}{2}, \end{aligned}$$

the LQ effects at $q^2 = 0$ (the contributions proportional to gauge boson mass are suppressed) are given by

$$\begin{aligned} \Lambda_{3i}^{\text{LQ}} &= \frac{N_c m_t^2}{192\pi^2 M^2} \left[3V_{3h} \lambda_{h3}^{L*} V_{3k}^* \lambda_{ki}^L \left(1 + 2 \log \left(\frac{m_t^2}{M^2} \right) \right) \right], \\ \Delta_{\text{LQ}}^L &= V_{3l} \lambda_{l3}^{L*} V_{3a}^* \lambda_{a3}^L \frac{N_c m_t^2}{32\pi^2 M^2} \left[1 + \log \left(\frac{m_t^2}{M^2} \right) \right], \\ \Delta_{\text{LQ}}^R &= -\lambda_{33}^{R*} \lambda_{33}^R \frac{N_c m_t^2}{32\pi^2 M^2} \left[1 + \log \left(\frac{m_t^2}{M^2} \right) \right], \end{aligned} \quad (4.22)$$

with $\Delta_{\text{LQ}}^V = -\Delta_{\text{LQ}}^L - \Delta_{\text{LQ}}^R$ and $\Delta_{\text{LQ}}^A = \Delta_{\text{LQ}}^R - \Delta_{\text{LQ}}^L$. This leads to $|\Lambda_{33}^W| = \left| 1 + \Lambda_{33}^{\text{LQ}} \right|$. Experimentally, the averaged modification of the W - $\tau\nu$ coupling extracted from $\tau \rightarrow \mu\nu\nu$ and $\tau \rightarrow e\nu\nu$ decays reads (averaging the central value but with unchanged error) [275, 276]

$$|\Lambda_{33}^{W \text{ exp}}| \approx 1.002 \pm 0.0015, \quad (4.23)$$

which provides a better constraint than data of W decays.

Concerning $Z \rightarrow \tau\tau$ the axial vector coupling is much better constrained than the vectorial one [275, 276]

$$\Lambda_{\text{exp}}^A / \Lambda_{\text{SM}}^A = 1.0019 \pm 0.0015, \quad (4.24)$$

with $\Lambda^A / \Lambda_{\text{SM}}^A = 1 + 2\Delta_{\text{LQ}}^L - 2\Delta_{\text{LQ}}^R$.

4.3 Phenomenology

Looking at the phenomenological consequences of our model, note that couplings to muons or electrons are obviously not necessary to obtain the desired effects in tauonic B decays. Even though our S_1 model can in principle account for the anomalous magnetic moment of the muon [238, 277–286] (or electron [286]) via a m_t/m_μ enhanced effect, this is not possible in the presence of large couplings to tau leptons since also here m_t enhanced effects generate too large rates of $\tau \rightarrow \mu(e)\gamma$. Similarly, our model cannot address the $b \rightarrow s\mu^+\mu^-$ anomalies if one aims at a sizable effect in tauonic B decays [287]. Therefore, we will disregard (i.e. set to zero) the couplings to muons and electrons. Couplings to top-quarks affect $\tau \rightarrow \mu\nu\nu$ [288] and $Z \rightarrow \tau^+\tau^-$ [289]. Here we see that $\Delta^L \approx -0.0006|\lambda_{33}^L|^2$ and $\Lambda_{33}^{LQ} \approx -0.0008|\lambda_{33}^L|^2$ (for $M = 1$ TeV) is compatible with experiments for $|\lambda_{33}^L| < 1$. Note that we improve the agreement in $Z \rightarrow \tau\tau$ data while slightly worsening $\tau \rightarrow \ell\nu\nu$ data, which is already a bit away from the SM prediction.

Thus, we are left with $\lambda_{13}^R, \lambda_{23}^R$ and λ_{i3}^L as free parameters for studying the effect in tauonic B decays and the correlations with EDMs. In the following we will set $M = 1$ TeV which is also well compatible with the latest direct search results of CMS for third generation LQs [290, 291].¹³

Let us now turn to $b \rightarrow c\tau\nu$ processes, where effects of the order of 10% compared to the corresponding tree-level SM amplitude are required. Since our model can give (according to Eq. (4.3)) tree-level effects in $B \rightarrow K^{(*)}\nu\nu$ decays (which are loop suppressed in the SM), these contributions must be suppressed. Since the bottom coupling to taus should be sizable, the coupling to strange quarks is tightly bound. We show the preferred regions, according to the updated global fit of Ref. [118], from $b \rightarrow c\tau\nu$ processes in the left plot of Fig. 4.2. These regions are shown for $\lambda_{23}^L = 0$ but also the possible impact of $\lambda_{23}^L \neq 0$, taking its maximally allowed values from $B \rightarrow K^*\nu\nu$, is depicted. Note that our model is not in conflict with the B_c lifetime [296, 297] (in fact, it is even compatible with the 10% limit of Ref. [298]) nor with direct LHC searches for monotaus [295]. So far we worked with real parameters in order to maximize the effect in $R(D^{(*)})$. However, even for complex couplings the effect in nuclear and atomic EDMs would be strongly suppressed since only up and down quarks contribute directly to these observables.

Therefore, let us now turn to $b \rightarrow u\tau\nu$ where couplings to up quarks are obviously needed. Here, even for real couplings an effect in the neutron EDM is generated due to the large phase of V_{ub} . This effect could only be avoided for $\text{Arg}[\lambda_{13}^{R*}\lambda_{33}^L] = \text{Arg}[V_{ub}]$. However, since there is no (obvious) symmetry which could impose this relation, such a configuration would be fine-tuning. This can be seen from the right plot in Fig. 4.2, where we show the predictions for $\text{Br}[B \rightarrow \tau\nu]/\text{Br}[B \rightarrow \tau\nu]_{\text{SM}}$ as a function of the absolute value and the phase of λ_{13}^R for $\lambda_{33}^L = 1$ (as preferred by $b \rightarrow c\tau\nu$ data). The dark red contour lines denote the n2EDM sensitivity, showing that a 10% effect in $B \rightarrow \tau\nu$ with respect to the SM will lead to an observable effect in the neutron EDM within our model. Finally, taking $\lambda_{23}^R = -0.1$, as preferred by $b \rightarrow c\tau\nu$ (see left plot of Fig. 4.2), CP violation in $D^0 - \bar{D}^0$ mixing is generated. Here the red contour denotes the future HL-LHC sensitivity which is complementary to the region covered by EDM searches.

¹³More sophisticated analysis of LHC data can be found in Refs. [292–294]. However, since for t-channel exchange the EFT limits are in general stronger than the ones in the UV complete model, we will use for simplicity the results of Ref. [295] in the following which show that 1 TeV is compatible with data.

4.4 Conclusions

In this article we studied the interplay between tauonic B meson decays and EDMs (in particular the one of the neutron) in a model with a scalar LQ $SU(2)_L$ singlet which can be identified with the right-handed down squark in the R-parity violating MSSM. We found that in order to explain the intriguing tensions in $b \rightarrow c\tau\nu$ data, λ_{33}^L must be sizable and also a coupling to right-handed charm quarks and tau-leptons (λ_{23}^R) is required. In this setup, the model gives a very good fit to data and is compatible with $b \rightarrow s\nu\nu$ observables, LHC searches and B_c lifetime constraints. Extending this analysis to $b \rightarrow u\tau\nu$ transitions, in particular $B \rightarrow \tau\nu$, again right-handed couplings to up quarks (λ_{13}^R) are required to have a sizable effect. This leads to very important m_τ/m_u enhanced effects in (chromo) electric dipole operators generating in turn EDMs of nucleons and atoms. In particular, even for real couplings of the LQ to fermions, the large phase of V_{ub} generates a sizable contribution to the neutron EDM. In fact, this effect should already be observable in the n2EDM experiment at PSI, assuming that, within our model, $B \rightarrow \tau\nu$ is enhanced (or suppressed) by around 10% with respect to the SM.

Acknowledgments — The work of A.C. is supported by a Professorship Grant (PP00P2_176884) of the Swiss National Science Foundation. The work of F.S. is supported by the Swiss National Foundation under Grant No. 200020_175449/1. We thank Dario Müller for collaboration in the early stages of this article and Christoph Greub for useful comments on the manuscript. We are grateful to David Straub and Jason Aebischer for reminding us of the importance of $Z\text{-}\tau\tau$ and $W\text{-}\tau\nu$ couplings.

Chapter 5

Flavor Phenomenology of the Leptoquark Singlet-Triplet Model

published in

JHEP 06 (2020) 020

arXiv: 1912.04224 [hep-ph]

Flavor Phenomenology of the Leptoquark Singlet-Triplet Model

Andreas Crivellin

Paul Scherrer Institut, CH-5232 Villigen PSI, Switzerland

Dario Müller

Paul Scherrer Institut, CH-5232 Villigen PSI, Switzerland

Physik-Institut, Universität Zürich, Winterthurerstrasse 190, CH-8057 Zürich, Switzerland

Francesco Saturnino

Albert Einstein Center for Fundamental Physics, Institute for Theoretical Physics, University of Bern, CH-3012 Bern, Switzerland

In recent years, experiments revealed intriguing hints for new physics (NP) in semi-leptonic B decays. Both in charged current processes, involving $b \rightarrow c\tau\nu$ transitions, and in the neutral currents $b \rightarrow s\ell^+\ell^-$, a preference for NP compared to the standard model (SM) of more than 3σ and 5σ was found, respectively. In addition, there is the long-standing tension between the theory prediction and the measurement of the anomalous magnetic moment (AMM) of the muon (a_μ) of more than 3σ . Since all these observables are related to the violation of lepton flavor universality (LFU), a common NP explanation seems not only plausible but is even desirable. In this context, leptoquarks (LQs) are especially promising since they give tree-level effects in semi-leptonic B decays, but only loop-suppressed effects in other flavor observables that agree well with their SM predictions. Furthermore, LQs can lead to a m_t/m_μ enhanced effect in a_μ , allowing for an explanation even with (multi) TeV particles. However, a single scalar LQ representation cannot provide a common solution to all three anomalies. In this article we therefore consider a model in which we combine two scalar LQs: the $SU(2)_L$ singlet and the $SU(2)_L$ triplet. Within this model we compute all relevant 1-loop effects and perform a comprehensive phenomenological analysis, pointing out various interesting correlations among the observables. Furthermore, we identify benchmark points which are in fact able to explain all three anomalies ($b \rightarrow c\tau\nu$, $b \rightarrow s\ell^+\ell^-$ and a_μ), without violating bounds from other observables, and study their predictions for future measurements.

5.1 Introduction

While the Large Hadron Collider (LHC) at CERN has not directly observed any particles beyond the ones of the SM (see e.g. Refs. [299, 300] for an overview) intriguing indirect hints for NP have been acquired in flavor observables. In particular, measurements of semi-leptonic B meson decays, involving the charged current $b \rightarrow c\tau\nu$ or the flavor changing neutral current $b \rightarrow s\ell^+\ell^-$, point towards the violation of LFU. Furthermore, also the AMM of the muon, which measures LFU violation as it vanishes in the massless limit, points convincingly towards physics beyond the SM. In order to explain these deviations from the SM predictions – also called anomalies – one thus needs NP that couples differently to tau leptons, muons and electrons. As we will see, LQs are prime candidates for such an explanation in terms of physics beyond the SM.

Let us now review these anomalies in more detail. The first anomaly arose in the AMM of the muon $a_\mu = (g - 2)_\mu/2$ in 2006. Here, the E821 experiment at Brookhaven discovered a tantalizing tension between their measurement [55, 123]

$$a_\mu^{\text{exp}} = 116,592,089(63) \times 10^{-11} \quad (5.1)$$

and the SM prediction¹⁴

$$\delta a_\mu = a_\mu^{\text{exp}} - a_\mu^{\text{SM}} = (278 \pm 88) \times 10^{-11} \quad (5.2)$$

of around $3\text{--}4\sigma$ ¹⁵. This discrepancy is of the same order as the electroweak contribution of the SM. Therefore, TeV scale NP needs an enhancement mechanism, called chiral enhancement, to be able to account for the deviation [286]. For LQs this factor can be $m_t/m_\mu \approx 10^3$ which provides the required enhancement, making LQs prime candidates for an explanation in terms of NP [238, 241, 243, 277–286, 309–314]. In fact, there are only two LQ representations (under the SM gauge group), out of the 10 possible ones [147], that can have this enhancement: the scalar LQ $SU(2)_L$ singlet and the scalar LQ $SU(2)_L$ doublet with hypercharge $-2/3$ and $-7/3$, respectively.

In tauonic B decays, BaBar measured in 2012 the ratios

$$R(D^{(*)}) = \frac{\text{Br}[B \rightarrow D^{(*)}\tau\nu]}{\text{Br}[B \rightarrow D^{(*)}\ell\nu]} \quad \text{with } \ell = \{e, \mu\} \quad (5.3)$$

significantly above the SM predictions [104]. This is in agreement with the later LHCb measurements [110–112] of $R(D^*)$, while BELLE found values closer to the SM in its latest analysis [109]. In combination, these deviations from the SM amount to 3.1σ [315]¹⁶. Interestingly, also the ratio

$$R(J/\psi) = \frac{\text{Br}[B_c \rightarrow J/\psi\tau\nu]}{\text{Br}[B_c \rightarrow J/\psi\mu\nu]} \quad (5.4)$$

lies above its SM prediction [113], supporting the assumption of NP in $b \rightarrow c\tau\nu$ [165, 166]. This picture is confirmed by different independent global fits [119–122] which include in addition polarization observables. Interestingly, these hints for NP are accompanied by data on $b \rightarrow u\tau\nu$ transitions.

Once more, LQs are prime candidates for an explanation. Despite the U_1 vector LQ $SU(2)_L$ singlet [45, 149, 151–153, 171–177, 180, 184, 211, 213, 317, 318] and scalar LQ S_2 option [234, 235, 309, 319–325], the scalar LQ Φ_1 [47, 176, 212, 232, 233, 235, 236, 238–242, 244–247, 249, 250, 287, 311] or the combination of Φ_1 and Φ_3 ¹⁷ can explain these data [176, 243, 326, 327].

Finally, the statistically most significant deviations from the SM predictions were observed in observables involving $b \rightarrow s\ell^+\ell^-$ transitions. Here, the LHCb measurements [78, 79] of

$$R(K^{(*)}) = \frac{\text{Br}[B \rightarrow K^{(*)}\mu^+\mu^-]}{\text{Br}[B \rightarrow K^{(*)}e^+e^-]} \quad (5.5)$$

¹⁴The SM prediction of a_μ is currently re-evaluated in a community-wide effort prompted by upcoming improved measurements at Fermilab [145] and J-PARC [146], see also Ref. [301]. With electroweak [126–128] and QED [125] contributions under good control, recent advances in the evaluation of the hadronic part include: hadronic vacuum polarization [129–135], hadronic light-by-light scattering [136–142], and higher-order hadronic corrections [143, 144].

¹⁵During the publication process of this article, the Budapest-Marseilles-Wuppertal collaboration (BMWc) released a lattice QCD calculation from hadronic vacuum polarization (HVP) [302]. These results would render the SM prediction for a_μ compatible with the experiment. However, the BMWc results are in tension with the HVP determined from $e^+e^- \rightarrow \text{hadrons}$ data [130, 133, 303, 304], combined with analyticity and unitarity constraints for the leading 2π [135, 303, 305] and 3π [306] channels, covering almost 80% of the HVP contribution. Furthermore, the HVP also enters the global EW fit [307], whose (indirect) determination disagrees with the BMWc result. Therefore, the BMWc determination of the HVP would lead to a significant tension in EW fit [308] and we therefore use the (conservative) estimate of Eq. (5.2).

¹⁶This tension would even slightly increase by around 0.3σ if the new theory prediction of $R(D^*)$ of Ref. [316] was taken into account.

¹⁷ Φ_1 and Φ_3 are also called S_1 and S_3 , respectively, in the literature.

	Φ_1	Φ_3	Q	L	ℓ	u	d
Y	$-2/3$	$-2/3$	$1/3$	-1	-2	$4/3$	$-2/3$

Table 5.1: Values of the hypercharges for the LQ and fermion fields.

indicate LFU violation with a combined significance of $\approx 4\sigma$ [88, 92, 93, 97, 98, 100, 158–161, 209]. Taking in addition into account all other $b \rightarrow s\mu^+\mu^-$ observables, e.g. the angular observable P'_5 [83] in the decay $B \rightarrow K^*\mu^+\mu^-$, the global fit of the Wilson coefficients even prefers several NP scenarios above the 5σ level [97, 98, 100]. Furthermore, $b \rightarrow d\ell^+\ell^-$ transitions measured in $B \rightarrow \pi\mu^+\mu^-$ [162] deviate slightly from the LHCb measurement [163]. While this is not significant on its own, the central value is very well in agreement with the expectation from $b \rightarrow s\ell^+\ell^-$ assuming a V_{td}/V_{ts} -like scaling [328] of the NP effect as obtained in models possessing an $U(2)$ flavor symmetry in the quark sector (see e.g. Refs. [149, 329–331] for accounts in the context of the flavor anomalies). This means that an effect of the same order and sign as in $b \rightarrow s\ell^+\ell^-$, relative to the SM, is preferred. Once more, LQs are prime candidates for an explanation. In particular the U_1 vector LQ $SU(2)_L$ singlet [45, 46, 149, 151, 171, 172, 174–177, 180, 184, 213, 317, 318, 332], the U_3 vector LQ $SU(2)_L$ triplet [153, 156, 172–175, 177, 180, 317, 332] and the Φ_3 scalar LQ $SU(2)_L$ triplet [173, 175–177, 180, 317, 332, 333] can explain data very well via a purely left-handed current.

From the discussion above it is clear that there are several options for a combined explanation of the flavor anomalies with LQs. Here we will consider the singlet-triplet model introduced in Refs. [243, 326] which was also studied in the context of Dark Matter [334]. Within this model, a combined explanation can be possible since Φ_1 can account for the anomaly in a_μ and affects $b \rightarrow c\tau\nu$ transitions while Φ_3 can explain $b \rightarrow s\ell^+\ell^-$ data and enters $b \rightarrow c\tau\nu$ processes. Furthermore, their combined effects in $b \rightarrow s\nu\bar{\nu}$ processes can be destructive, relieving the bounds. However, in order to perform a complete phenomenological analysis, an inclusion of all relevant loop effects is necessary. We will compute these effects and extend the analysis of Ref. [243], allowing for couplings of Φ_1 to right-handed fermions.

The outline of the article is as follows: In the next section we will define our setup. The conventions for the various observables as well as the results of the matching, taking into account the relevant loop effects, are given in Sec. 5.3 before we perform our phenomenological analysis in Sec. 5.4 and conclude in Sec. 5.5.

5.2 Setup

The scalar LQ singlet-triplet model is obtained by adding a scalar LQ $SU(2)_L$ singlet (Φ_1) and an $SU(2)_L$ triplet (Φ_3), each carrying hypercharge $-2/3$, to the SM particle content. While the couplings to gauge bosons are completely determined by the representations of the LQs under the SM gauge symmetry, their couplings to the SM fermions and the SM Higgs¹⁸ are free parameters of the Lagrangian

$$\begin{aligned} \mathcal{L}_{\text{LQ}} = & \left(\lambda_{fi}^I \overline{Q}_f^c i\tau_2 L_i + \hat{\lambda}_{fi}^I \overline{u}_f^c \ell_i \right) \Phi_1^{I\dagger} + \kappa_{fi}^J \overline{Q}_f^c i\tau_2 \left(\tau \cdot \Phi_3^J \right)^\dagger L_i + \rho_{IJ} \Phi_1^{I\dagger} \left(H^\dagger \left(\tau \cdot \Phi_3^J \right) H \right) \\ & - \sum_{\{I,I'\}=1}^N \left(\left(M_{\Phi_1}^2 \right)_{II'} - \xi_{II'}^{\Phi_1} H^\dagger H \right) \Phi_1^{I\dagger} \Phi_1^{I'} - \sum_{\{J,J'\}=1}^M \left(\left(M_{\Phi_3}^2 \right)_{JJ'} - \xi_{JJ'}^{\Phi_3} H^\dagger H \right) \Phi_3^{J\dagger} \Phi_3^{J'} + \text{h.c.} \end{aligned} \quad (5.6)$$

¹⁸Couplings to the Higgs lead to mixing among different LQ representations. Via this mixing LQs are able to generate Majorana masses for neutrinos [155, 241, 327, 335–339].

Here, Q (L) is the quark (lepton) $SU(2)_L$ doublet and u (ℓ) the quark (charged lepton) singlet. The superscript c denotes charge conjugation, f, i are flavor indices and $I^{(\prime)}, J^{(\prime)}$ denote the number of LQs in a given representation (i.e. $\{I, I'\} = 1, \dots, N$ for Φ_1 and $\{J, J'\} = 1, \dots, M$ for Φ_3)¹⁹. For the hypercharge Y we use the convention $Q_{em} = T_3 + Y/2$, where Q_{em} is the electric charge and T_3 the third component of weak isospin (see Tab. 5.1).

After electroweak symmetry breaking the Higgs acquires its vacuum expectation value $v \approx 174$ GeV. The last term in Eq. (5.6) then leads to a shift in the bi-linear mass terms of the LQs. However, this shift can be absorbed by defining

$$\left(M_{\Phi_{1,3}}^2\right)_{KK'} - v^2 \xi_{KK'}^{\Phi_{1,3}} \equiv \left(\tilde{M}_{\Phi_{1,3}}^2\right)_{KK'} . \quad (5.7)$$

Thus, the terms $\xi_{KK'}^{\Phi_{1,3}}$ have (at leading order in perturbation theory) no impact on the low energy flavor phenomenology of the singlet-triplet model but would only enter processes with an external Higgs (or at higher loop level). Furthermore, by unitary rotations of the LQ fields, we can now diagonalize their bi-linear mass terms via unitary rotations $U_{1,2}$:

$$\begin{aligned} U_1^\dagger \tilde{M}_{\Phi_1}^2 U_1 &= \text{diag}(\hat{m}_1^2, \dots, \hat{m}_N^2) \equiv m_{\Phi_1}^2, \\ U_3^\dagger \tilde{M}_{\Phi_3}^2 U_3 &= \text{diag}(\bar{m}_1^2, \dots, \bar{m}_M^2) \equiv m_{\Phi_3}^2. \end{aligned} \quad (5.8)$$

In turn, these rotations lead to an effect in the couplings to the Higgs which can however be absorbed by the definition

$$U_1^\dagger \rho U_3 \equiv \hat{\rho}. \quad (5.9)$$

The LQ field rotations in Eq. (5.8) have to be applied to their fermionic interactions as well. Here, they can again be absorbed by a redefinition of the couplings

$$\lambda_{fi}^I U_{1,KI}^* \equiv \lambda_{fi}^K, \quad \hat{\lambda}_{fi}^I U_{1,KI}^* \equiv \hat{\lambda}_{fi}^K, \quad \kappa_{fi}^J U_{3,KJ}^* \equiv \kappa_{fi}^K. \quad (5.10)$$

Hence, we are left with diagonal bi-linear mass terms with entries $(m_{\Phi_1}^2)_{II}$ and $(m_{\Phi_3}^2)_{JJ}$ and off-diagonal $\Phi_1 - \Phi_3$ mixing governed by $\hat{\rho}_{IJ}$. While the LQs with $Q_{em} = \{2/3, -4/3\}$ are already in their mass eigenstates, we have to diagonalize the resulting full matrix of the $\Phi_1 - \Phi_3$ system with $Q_{em} = -1/3$

$$W^\dagger \begin{pmatrix} m_{\Phi_1}^2 & v^2 \hat{\rho} \\ v^2 \hat{\rho}^\dagger & m_{\Phi_3}^2 \end{pmatrix} W = \text{diag}(m_1^2, \dots, m_{M+N}^2), \quad (5.11)$$

with a unitary matrix W . Working in the down basis, i.e. in the basis where no CKM elements appear in flavor changing neutral currents of down-type quarks, this leads to the following interaction terms with fermions

$$\begin{aligned} \mathcal{L}_{\text{LQ}} &= \Gamma_{u_f \ell_i}^{L,K} \bar{u}_f^c P_L \ell_i \Phi_K^{-1/3*} + \Gamma_{u_f \ell_i}^{R,K} \bar{u}_f^c P_R \ell_i \Phi_K^{-1/3*} + \Gamma_{d_f \nu_i}^{L,K} \bar{d}_f^c P_L \nu_i \Phi_K^{-1/3*} \\ &+ \Gamma_{u_f \nu_i}^J \bar{u}_f^c P_L \nu_i \Phi_J^{2/3*} + \Gamma_{d_f \ell_i}^J \bar{d}_f^c P_L \ell_i \Phi_J^{-4/3*}, \end{aligned} \quad (5.12)$$

¹⁹In the R-parity violating MSSM this would correspond to the number of generations for the singlet. However, in general N and M do not need to be equal.

where the superscripts of the LQ fields refer to their electric charge and

$$\begin{aligned}
 \Gamma_{u_f \ell_i}^{L,K} &= V_{fj}^* \left(\lambda_{ji}^I W_{IK}^* - \kappa_{ji}^J W_{J+N,K}^* \right), \\
 \Gamma_{u_f \ell_i}^{R,K} &= \hat{\lambda}_{fi}^I W_{IK}^*, \\
 \Gamma_{d_f \nu_i}^{L,K} &= -\lambda_{fi}^I W_{IK}^* - \kappa_{fi}^J W_{J+N,K}^*, \\
 \Gamma_{u_f \nu_i}^J &= \sqrt{2} V_{fj}^* \kappa_{ji}^J, \\
 \Gamma_{d_f \ell_i}^J &= -\sqrt{2} \kappa_{fi}^J.
 \end{aligned} \tag{5.13}$$

Recall that the indices take the numbers $I = \{1, \dots, N\}$, $J = \{1, \dots, M\}$ and $K = \{1, \dots, M + N\}$. In the limit with only one generation of each LQ and without mixing we have

$$\begin{aligned}
 \Gamma_{u_f \ell_i}^{L,K} &= V_{fj}^* (\lambda_{ji} \delta_{1K} - \kappa_{ji} \delta_{2K}), & \Gamma_{u_f \ell_i}^{R,K} &= \hat{\lambda}_{fi} \delta_{1K}, \\
 \Gamma_{d_f \nu_i}^{L,K} &= -\lambda_{fi} \delta_{1K} - \kappa_{fi} \delta_{2K}, & \Gamma_{u_f \nu_i} &= \sqrt{2} V_{fj}^* \kappa_{ji}, & \Gamma_{d_f \ell_i} &= -\sqrt{2} \kappa_{fi},
 \end{aligned} \tag{5.14}$$

where the indices 1 and 2 correspond to Φ_1 and Φ_3 , respectively.

5.3 Processes and Observables

In order to illustrate the phenomenology of our model, we will limit ourselves to the case of one LQ singlet Φ_1 and one LQ triplet Φ_3 without mixing among them. Therefore, we will derive the corresponding expressions for the relevant processes in this simplified limit in this section and denote by M_1 and M_3 the singlet and triplet mass, respectively. In the appendix we will provide the most general expressions for the Wilson coefficients allowing for an arbitrary number of LQs and include mixing among them.

Let us now study the various classes of processes. For each class, we will first define the effective Hamiltonians governing these processes and perform the matching of the model on them. Then we discuss the relation of the Wilson coefficients to observables and review the related available experimental information.

5.3.1 $dd\ell\ell$ and $dd\gamma$ Processes

To describe $d_k \rightarrow d_j \ell_f^- \ell_i^+$ transitions, we use the effective Hamiltonian

$$\begin{aligned}
 \mathcal{H}_{\text{eff}}^{dd\ell\ell} &= -\frac{4G_F}{\sqrt{2}} V_{td_k} V_{td_j}^* \left[\sum_{A=7,8} C_A^{jk} \mathcal{O}_A^{jk} + \sum_{A=9,10} C_{A,jk}^{fi} \mathcal{O}_{A,jk}^{fi} \right], \\
 \mathcal{O}_{7(8)}^{jk} &= \frac{e(g_s)}{16\pi^2} m_k [\bar{d}_j \sigma^{\mu\nu} (T^a) P_R d_k] F_{\mu\nu} (G_{\mu\nu}^a), \\
 \mathcal{O}_{9,jk}^{fi} &= \frac{\alpha}{4\pi} [\bar{d}_j \gamma^\mu P_L d_k] [\bar{\ell}_f \gamma_\mu \ell_i], \\
 \mathcal{O}_{10,jk}^{fi} &= \frac{\alpha}{4\pi} [\bar{d}_j \gamma^\mu P_L d_k] [\bar{\ell}_f \gamma_\mu \gamma_5 \ell_i],
 \end{aligned} \tag{5.15}$$

and define the covariant derivative as

$$D_\mu = \partial_\mu + ieQA_\mu + ig_s G_\mu^a T^a. \tag{5.16}$$

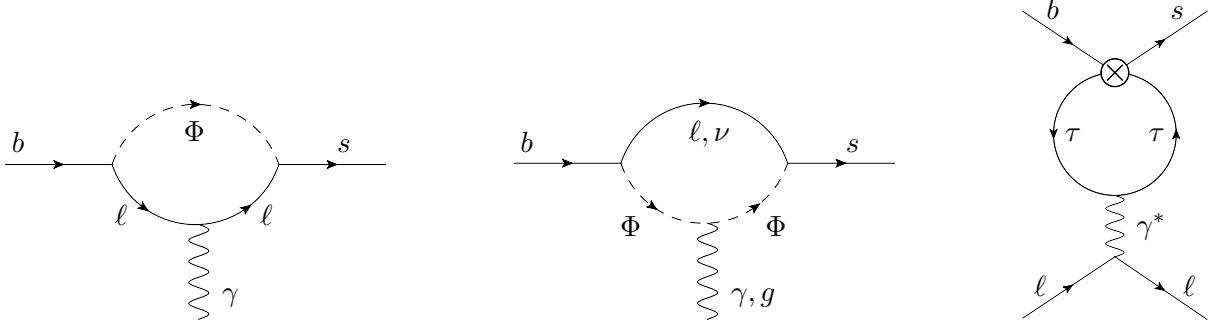


Figure 5.1: Feynman diagrams in our LQ singlet-triplet model generating contributions to $b \rightarrow s\gamma$ and $b \rightarrow s\ell^+\ell^-$ at the 1-loop level. The left two diagrams show the matching contribution to the (chromo) magnetic operator. The diagram on the right, with an off-shell photon, is generating the mixing of $\mathcal{O}_9^{\tau\tau}$ into $\mathcal{O}_9^{\ell\ell}$.

At tree level, the only matching contribution to $C_{9,jk}^{fi}$ and $C_{10,jk}^{fi}$ stems from Φ_3

$$C_{9,jk}^{fi} = -C_{10,jk}^{fi} = \frac{\sqrt{2}}{2G_F V_{td_k} V_{td_j}^*} \frac{\pi}{\alpha} \frac{\kappa_{ki} \kappa_{jf}^*}{M_3^2}. \quad (5.17)$$

As in any model, the Wilson coefficients of the (chromo) magnetic operator can only be generated at the loop level. The left two diagrams in Fig. 5.1 (given for concreteness for $b \rightarrow s$ transitions) with on-shell photon and gluons result in

$$\begin{aligned} C_7^{jk}(\mu_{\text{LQ}}) &= \frac{-\sqrt{2}}{4G_F V_{td_k} V_{td_j}^*} \frac{1}{24} \left(\frac{1}{3} \frac{\lambda_{ki} \lambda_{ji}^*}{M_1^2} + 7 \frac{\kappa_{ki} \kappa_{ji}^*}{M_3^2} \right), \\ C_8^{jk}(\mu_{\text{LQ}}) &= \frac{\sqrt{2}}{4G_F V_{td_k} V_{td_j}^*} \frac{1}{24} \left(\frac{\lambda_{ki} \lambda_{ji}^*}{M_1^2} + 3 \frac{\kappa_{ki} \kappa_{ji}^*}{M_3^2} \right), \end{aligned} \quad (5.18)$$

at the matching scale μ_{LQ} .

Concerning the QCD evolution of these coefficients, O_8 mixes into O_7 at $\mathcal{O}(\alpha_s)$, yielding the relation [189, 190]

$$\begin{pmatrix} C_7(\mu_l) \\ C_8(\mu_l) \end{pmatrix} = \hat{U}^f(\mu_l, \mu_h) \begin{pmatrix} C_7(\mu_h) \\ C_8(\mu_h) \end{pmatrix}, \quad (5.19)$$

with

$$\hat{U}^f(\mu_l, \mu_h) = \begin{pmatrix} \eta^{\frac{16}{33-2f}} & \frac{8}{3} \left(\eta^{\frac{14}{33-2f}} - \eta^{\frac{16}{33-2f}} \right) \\ 0 & \eta^{\frac{14}{33-2f}} \end{pmatrix}. \quad (5.20)$$

Here, f denotes the number of active quark flavors, $\mu_{h(l)}$ refers to the high (low) energy scale and

$$\eta = \frac{\alpha_s(\mu_h)}{\alpha_s(\mu_l)}, \quad (5.21)$$

where α_s needs to be evaluated with the number of active flavors at a given scale as well.

Even though $b \rightarrow s\ell^+\ell^-$ can be induced at tree level in our model, there are still scenarios in which loop effects are phenomenologically important. As pointed out in Ref. [45], the large

couplings to tau leptons, needed to explain $b \rightarrow c\tau\nu$ data, also lead to huge Wilson coefficients $C_{9, sb}^{\tau\tau} = -C_{10, sb}^{\tau\tau}$. In turn, $\mathcal{O}_{9, sb}^{\tau\tau}$ mixes into $\mathcal{O}_{9, sb}^{\ell\ell}$ via the off-shell photon penguin [340], shown in the right diagram of Fig. 5.1. In our UV complete model, we cannot only calculate this mixing, but also the finite part of the effect, contained in the matching contribution

$$C_{9, jk}^{\ell\ell}(\mu_{\text{LQ}}) = \frac{\sqrt{2}}{216G_F V_{td_k} V_{td_j}^*} \left[\frac{\lambda_{kl}\lambda_{jl}^*}{M_1^2} + 3\frac{\kappa_{kl}\kappa_{jl}^*}{M_3^2} \left(19 + 12 \log \left(\frac{\mu_{\text{LQ}}^2}{M_3^2} \right) \right) \right]. \quad (5.22)$$

This means that even if couplings to light leptons are absent at tree level, they are generated via loop effects in the presence of tau couplings. Since we will mainly focus on $b \rightarrow s$ transitions, we shorten our notation in the following and write $C_{7(8)}^{sb} \equiv C_{7(8)}$, $C_{9(10), sb}^{fi} \equiv C_{9(10)}^{fi}$. The logarithm involving μ_{LQ} in Eq. (5.22) originates from the fact that the right-diagram in Fig. 5.1 is divergent. To get rid of this dependence one has to solve the RGE governing the mixing between \mathcal{O}_9^{ii} with different lepton flavors:

$$\mu \frac{\partial C_9^{ii}(\mu)}{\partial \mu} = \gamma C_9^{ff}(\mu) \quad (f \neq i) \quad (5.23)$$

with $\gamma = \frac{2\alpha}{3\pi}$. Here, we do not take into account the running of α and do not consider the running of C_9^{ii} (i.e. just the mixing of \mathcal{O}_9^{ii} into C_9^{jj} with $i \neq j$). This then has the solution

$$C_9^{ii}(\mu) = C_9^{ii}(\mu_{\text{LQ}}) + \gamma \log \left(\frac{\mu}{\mu_{\text{LQ}}} \right) C_9^{ff} \quad (f \neq i). \quad (5.24)$$

For B meson decays, this amounts to replacing the high scale μ_{LQ} in Eq. (5.22) by the low scale of the processes μ_b . In addition, at the B meson scale, $\mathcal{O}_9^{\tau\tau}$ gives a q^2 dependent contribution to $C_{9, \text{eff}}^{\ell\ell}$, which however is numerically small [340] and currently not accessible with the SM independent fit. However, there are intriguing prospects that with improved future data this effect could be distinguished from the q^2 -independent C_9 effect [341].

QCD corrections to the matching of scalar LQs for semi-leptonic processes (both charged and neutral current) can be taken into account by applying the following shifts to the Wilson coefficients of vector (V), scalar (S) and tensor (T) operators [253]

$$\begin{aligned} C_V &\rightarrow C_V \left(1 + \frac{\alpha_s}{4\pi} C_F \left(3l_\mu + \frac{17}{2} \right) \right), \\ C_S &\rightarrow C_S \left(1 + \frac{3\alpha_s}{2\pi} C_F \right), \\ C_T &\rightarrow C_T \left(1 + \frac{\alpha_s}{\pi} C_F (l_\mu + 2) \right), \end{aligned} \quad (5.25)$$

with $l_\mu = \log(\mu^2/M^2)$ (where M can be either M_1 or M_3) and $C_F = 4/3$ as the color factor. Since QCD is insensitive to flavor, electric charge and chirality, these corrections can be applied in a straightforward way to all other semi-leptonic processes, particularly to $b \rightarrow s\nu\bar{\nu}$ and $b \rightarrow c\tau\nu$.

Observables

As mentioned in the introduction, a main motivation for this analysis is the explanation of the hints for NP in $b \rightarrow s\ell^+\ell^-$ data. In order to resolve this discrepancy between SM and

X	$q^2[\text{GeV}^2]$	A_0	A_1	A_2	A_3	A_4	A_5
K	[15, 22]	1.20 ± 0.12	0.15 ± 0.02	-0.42 ± 0.04	0.15 ± 0.01	0.15 ± 0.04	0.02
K^*	[15, 19]	0.98 ± 0.09	0.38 ± 0.03	-0.14 ± 0.01	-0.30 ± 0.03	0.12	0.05
ϕ	[15, 18.8]	0.86 ± 0.06	0.34 ± 0.02	-0.11	-0.28 ± 0.02	0.10	0.05
			A_6	A_7	A_8	A_9	A_{10}
			0.05 ± 0.01	0.02	0.05 ± 0.01	0.04	0.10 ± 0.01
			0.02	0.05 ± 0.01	0.02 ± 0.01	-0.08 ± 0.01	-0.03
			0.01	0.05	0.01 ± 0.02	-0.08	-0.02

Table 5.2: Numerical values for the coefficients given in Eq. (5.31) for the different decay modes involving $b \rightarrow s\tau^+\tau^-$ transitions together with the corresponding q^2 ranges.

experiment, an $\mathcal{O}(20\%)$ effect to $C_{9,10}$ is required compared to the SM contribution which is given by [195, 196]

$$C_9^{\text{SM}}(4.8 \text{ GeV}) = 4.07, \quad C_{10}^{\text{SM}}(4.8 \text{ GeV}) = -4.31. \quad (5.26)$$

In a global fit one finds preference for scenarios like $C_9^{\mu\mu} = -C_{10}^{\mu\mu}$, as generated in our model at tree level. However, a $C_9^{\mu\mu} = -C_{10}^{\mu\mu}$ effect complemented by a LFU one in $C_9^{\ell\ell}$ gives an even better fit to data [95, 98]. As we will see, this is exactly the pattern that arises in our model, taking into account the loop effects discussed above.

For $b \rightarrow s\tau^+\tau^-$ transitions we have on the experimental side [192]

$$\text{Br}[B_s \rightarrow \tau^+\tau^-]_{\text{exp}} \leq 6.8 \times 10^{-3} \quad (95\% \text{ C.L.}). \quad (5.27)$$

For $B_d \rightarrow \tau^+\tau^-$ there is a (unpublished) measurement of BELLE [164] and an upper limit of LHCb [192]

$$\begin{aligned} \text{Br}[B_d \rightarrow \tau^+\tau^-]_{\text{exp}}^{\text{BELLE}} &= (4.39_{-0.83}^{+0.80} \pm 0.45) \times 10^{-3}, \\ \text{Br}[B_d \rightarrow \tau^+\tau^-]_{\text{exp}}^{\text{LHCb}} &\leq 2.1 \times 10^{-3} \quad (95\% \text{ C.L.}). \end{aligned} \quad (5.28)$$

These measurements are compatible at the 2σ level. The SM predictions read [193, 194]

$$\begin{aligned} \text{Br}[B_s \rightarrow \tau^+\tau^-]_{\text{SM}} &= (7.73 \pm 0.49) \times 10^{-7}, \\ \text{Br}[B_d \rightarrow \tau^+\tau^-]_{\text{SM}} &= (2.22 \pm 0.19) \times 10^{-8}. \end{aligned} \quad (5.29)$$

In our model we find

$$\frac{\text{Br}[B_s \rightarrow \tau^+\tau^-]}{\text{Br}[B_s \rightarrow \tau^+\tau^-]_{\text{SM}}} = \left| 1 + \frac{C_{10}^{\tau\tau}}{C_{10}^{\text{SM}}} \right|^2, \quad (5.30)$$

and the analogous expression for $b \rightarrow d$ transitions. Also the branching ratios of semi-leptonic $b \rightarrow s\tau^+\tau^-$ processes can be expressed in terms of NP Wilson coefficients [179]

$$\begin{aligned} \text{Br}[B_{(s)} \rightarrow X\tau^+\tau^-] \times 10^7 &= A_0^X + A_1^X C_9^{\tau\tau} + A_2^X C_{10}^{\tau\tau} + A_3^X C_9^{\prime\tau\tau} + A_4^X C_{10}^{\prime\tau\tau} + A_5^X (C_9^{\tau\tau})^2 \\ &+ A_6^X (C_{10}^{\tau\tau})^2 + A_7^X (C_9^{\prime\tau\tau})^2 + A_8^X (C_{10}^{\prime\tau\tau})^2 + A_9^X C_9^{\tau\tau} C_9^{\prime\tau\tau} + A_{10}^X C_{10}^{\tau\tau} C_{10}^{\prime\tau\tau}. \end{aligned} \quad (5.31)$$

These branching ratios together with the corresponding coefficients are shown in Tab. 5.2.

Turning to $b \rightarrow s\tau\mu$ transitions, we have [197]

$$\text{Br}[B \rightarrow K\tau^\pm\mu^\mp] = 10^{-9} \left[9.6 \left(|C_9^{\mu\tau}|^2 + |C_9^{\tau\mu}|^2 \right) + 10 \left(|C_{10}^{\mu\tau}|^2 + |C_{10}^{\tau\mu}|^2 \right) \right], \quad (5.32)$$

and

$$\begin{aligned} \text{Br}[\bar{B}_s \rightarrow \ell_f^- \ell_i^+] &= \frac{G_F^2 \alpha^2}{64\pi^3} |V_{tb} V_{ts}^*|^2 f_{B_s}^2 \tau_{B_s} m_{B_s} (m_{\ell_i} + m_{\ell_f})^2 \eta(x_i, x_f) \\ &\times \left[|C_{10}^{fi} - C_{10}'^{fi}|^2 (1 - (x_i - x_f)^2) + \left| \frac{m_{\ell_i} - m_{\ell_f}}{m_{\ell_i} + m_{\ell_f}} (C_9^{fi} - C_9'^{fi}) \right|^2 (1 - (x_i + x_f)^2) \right], \end{aligned} \quad (5.33)$$

with $x_k = m_{\ell_k}/m_{B_s}$ and

$$\eta(x, y) = \sqrt{1 - 2(x + y) + (x - y)^2}. \quad (5.34)$$

We neglected the contributions of (pseudo-)scalar operators, since they do not appear in our model. The relevant experimental limits are [342, 343]

$$\begin{aligned} \text{Br}[B \rightarrow K\tau^\pm\mu^\mp]_{\text{exp}} &\leq 4.8 \times 10^{-5}, \\ \text{Br}[B_s \rightarrow \tau^\pm\mu^\mp]_{\text{exp}} &\leq 4.2 \times 10^{-5}. \end{aligned} \quad (5.35)$$

$\bar{d}d\bar{\ell}\ell$ operators contribute to $\tau \rightarrow \phi\mu$ as well. This gives relevant constraints on the parameter space of our model. We use the result of Ref. [175] and obtain

$$\text{Br}[\tau \rightarrow \phi\mu] = \frac{f_\phi^2 m_\tau^3 \tau_\tau |\kappa_{22}\kappa_{23}^*|^2}{128\pi M_3^4} \left(1 - \frac{m_\phi^2}{m_\tau^2} \right)^2 \left(1 + 2 \frac{m_\phi^2}{m_\tau^2} \right), \quad (5.36)$$

which has to be compared to the current experimental limit of [201]

$$\text{Br}[\tau \rightarrow \phi\mu] < 8.4 \times 10^{-8} \quad (90\% \text{ C.L.}). \quad (5.37)$$

5.3.2 $dd\nu\nu$ Processes

To describe $d_k \rightarrow d_j\nu_f\bar{\nu}_i$ processes we use the Hamiltonian

$$\begin{aligned} \mathcal{H}_{\text{eff}}^{dd\nu\nu} &= -\frac{4G_F}{\sqrt{2}} V_{td_k} V_{td_j}^* \left(C_{L,jk}^{fi} \mathcal{O}_{L,jk}^{fi} + C_{R,jk}^{fi} \mathcal{O}_{R,jk}^{fi} \right), \\ \mathcal{O}_{L(R),jk}^{fi} &= \frac{\alpha}{4\pi} \left[\bar{d}_j \gamma^\mu P_{L(R)} d_k \right] \left[\bar{\nu}_f \gamma_\mu (1 - \gamma_5) \nu_i \right]. \end{aligned} \quad (5.38)$$

At tree level we find contributions from Φ_1 and Φ_3 resulting in

$$C_{L,jk}^{fi} = \frac{\sqrt{2}}{4G_F V_{td_k} V_{td_j}^*} \frac{\pi}{\alpha} \left[\frac{\lambda_{ki} \lambda_{jf}^*}{M_1^2} + \frac{\kappa_{ki} \kappa_{jf}^*}{M_3^2} \right]. \quad (5.39)$$

Since these processes are generated at tree level, we do not need to calculate loop effects, which would only amount to numerically small corrections. Again, we simplify the notation for $b \rightarrow s$ transitions, writing $C_{L, sb}^{fi} \equiv C_L^{fi}$. The QCD matching corrections are given in Eq. (5.25) and there is no QCD evolution of these operators.

Observables

For $B \rightarrow K^{(*)}\nu\bar{\nu}$ we follow Ref. [205] and use $C_L^{\text{SM}} \approx -1.47/s_w^2$. The branching ratios normalized to the SM read

$$R_{K^{(*)}}^{\nu\bar{\nu}} = \frac{1}{3} \sum_{f,i=1}^3 \frac{|C_L^{\text{SM}}\delta_{fi} + C_L^{fi}|^2}{|C_L^{\text{SM}}|^2}. \quad (5.40)$$

This has to be compared to the current experimental limits $R_K^{\nu\bar{\nu}} < 3.9$ and $R_{K^*}^{\nu\bar{\nu}} < 2.7$ [206] (both at 90% C.L.). The expected BELLE II sensitivity for $B \rightarrow K^{(*)}\nu\bar{\nu}$ is 30% of the SM branching ratio [207].

5.3.3 $dul\nu$ Processes

For the charged current semi-leptonic processes we define the effective Hamiltonian as

$$\begin{aligned} \mathcal{H}_{\text{eff}}^{dul\nu} = & \frac{4G_F}{\sqrt{2}} V_{jk} (C_{VL,jk}^{fi} [\bar{u}_j \gamma^\mu P_L d_k] [\bar{\ell}_f \gamma_\mu P_L \nu_i] + C_{SL,jk}^{fi} [\bar{u}_j P_L d_k] [\bar{\ell}_f P_L \nu_i] \\ & + C_{TL,jk}^{fi} [\bar{u}_j \sigma^{\mu\nu} P_L d_k] [\bar{\ell}_f \sigma_{\mu\nu} \nu_i]), \end{aligned} \quad (5.41)$$

where in the SM $C_{VL}^{\text{SM}} = 1$. The contribution of our model to the SM Wilson coefficient from Φ_1 and Φ_3 is given by

$$C_{VL,jk}^{fi} = \frac{-\sqrt{2}}{8G_F V_{jk}} \left[-\frac{V_{jl} \lambda_{lf}^* \lambda_{ki}}{M_1^2} + \frac{V_{jl} \kappa_{lf}^* \kappa_{ki}}{M_3^2} \right], \quad (5.42)$$

while scalar and tensor operators are generated by Φ_1 only

$$C_{SL,jk}^{fi} = -4C_{TL,jk}^{fi} = \frac{-\sqrt{2}}{8G_F V_{jk}} \frac{\lambda_{ki} \hat{\lambda}_{jf}^*}{M_1^2}. \quad (5.43)$$

Since we are mainly interested in $b \rightarrow c$ transitions, we abbreviate

$$C_{VL,c b}^{fi} \equiv C_{VL}^{fi}, \quad C_{SL,c b}^{fi} \equiv C_{SL}^{fi}, \quad C_{TL,c b}^{fi} \equiv C_{TL}^{fi}. \quad (5.44)$$

Again, the QCD matching corrections are given in Eq. (5.25). We also include the 2-loop QCD and the 1-loop EW RGE. Using the results of Ref. [255], we have

$$\begin{aligned} C_{VL}^{fi}(\mu_b) &= C_{VL}^{fi}(1 \text{ TeV}), \\ C_{SR}^{fi}(\mu_b) &= 1.737 C_{SR}^{fi}(1 \text{ TeV}), \\ \begin{pmatrix} C_{SL}^{fi}(\mu_b) \\ C_{TL}^{fi}(\mu_b) \end{pmatrix} &= \begin{pmatrix} 1.752 & -0.287 \\ -0.004 & 0.842 \end{pmatrix} \begin{pmatrix} C_{SL}^{fi}(1 \text{ TeV}) \\ C_{TL}^{fi}(1 \text{ TeV}) \end{pmatrix}. \end{aligned} \quad (5.45)$$

Observables

With these conventions, the ratios $R(D^{(*)})$ are given by [118]

$$\begin{aligned} \frac{R(D)}{R(D)_{\text{SM}}} &\simeq |1 + C_{VL}^{\tau\tau}|^2 + 1.54\text{Re}\left[(1 + C_{VL}^{\tau\tau})C_{SL}^{\tau\tau*}\right] + 1.09|C_{SL}^{\tau\tau}|^2 \\ &\quad + 1.04\text{Re}\left[(1 + C_{VL}^{\tau\tau})C_{TL}^{\tau\tau*}\right] + 0.75|C_{TL}^{\tau\tau}|^2, \\ \frac{R(D^*)}{R(D^*)_{\text{SM}}} &\simeq |1 + C_{VL}^{\tau\tau}| - 0.13\text{Re}\left[(1 + C_{VL}^{\tau\tau})C_{SL}^{\tau\tau*}\right] + 0.05|C_{SL}^{\tau\tau}|^2 \\ &\quad - 5.0\text{Re}\left[(1 + C_{VL}^{\tau\tau})C_{TL}^{\tau\tau*}\right] + 16.27|C_{TL}^{\tau\tau}|^2, \end{aligned} \quad (5.46)$$

in terms of the Wilson coefficients given at the B meson scale. Furthermore, the branching ratio of $B_c \rightarrow \tau\nu$ reads [118, 252]

$$\text{Br}[B_c \rightarrow \tau\nu] = 0.02 \left(\frac{f_{B_c}}{0.43 \text{ GeV}} \right)^2 \left| 1 + C_{VL}^{\tau\tau} + 4.3(C_{SR}^{\tau\tau} - C_{SL}^{\tau\tau}) \right|^2. \quad (5.47)$$

In this work we use the most stringent limit of Ref. [298]

$$\text{Br}[B_c \rightarrow \tau\nu] \leq 0.1, \quad (5.48)$$

even though this bound might be too restrictive (see Refs. [121, 298] for theoretical discussions). However, we will see that even this limit does not constrain our model significantly.

A further constraint comes from the determination of the CKM element V_{cb} when comparing electron and muon final states. Here Ref. [344] finds that

$$\frac{\tilde{V}_{cb}^e}{\tilde{V}_{cb}^\mu} = 1.011 \pm 0.012, \quad (5.49)$$

where

$$\tilde{V}_{cb}^\ell = V_{cb} \left[|1 + C_{VL}^{\ell\ell}|^2 + \sum_{\ell \neq \ell'} |C_{VL}^{\ell\ell'}|^2 \right]^{1/2}. \quad (5.50)$$

For observables including first and second generation quarks such as $\tau \rightarrow \pi\nu$, $K \rightarrow \mu\nu/K \rightarrow e\nu$ or D decays, the Wilson coefficients can be applied using appropriate indices. The corresponding formulas and analyses can be found e.g. in Refs. [313, 345].

5.3.4 $\Delta F = 2$ Processes

Dealing with $\Delta F = 2$ processes, concretely $B_s - \bar{B}_s$ mixing, we use the effective Hamiltonian

$$\mathcal{H}_{\text{eff}}^{B\bar{B}} = C_1 [\bar{s}_\alpha \gamma_\mu P_L b_\alpha] [\bar{s}_\beta \gamma^\mu P_L b_\beta]. \quad (5.51)$$

In our model we obtain

$$\begin{aligned} C_1 = \frac{-1}{128\pi^2} &\left(\lambda_{2i}^* \lambda_{3j} \lambda_{2j}^* \lambda_{3i} C_0 \left(0, M_1^2, M_1^2 \right) + 5\kappa_{2i}^* \kappa_{3j} \kappa_{2j}^* \kappa_{3i} C_0 \left(0, M_3^2, M_3^2 \right) \right. \\ &\left. + 2\lambda_{2j}^* \lambda_{3i} \kappa_{2i}^* \kappa_{3j} C_0 \left(0, M_1^2, M_3^2 \right) \right) \end{aligned} \quad (5.52)$$

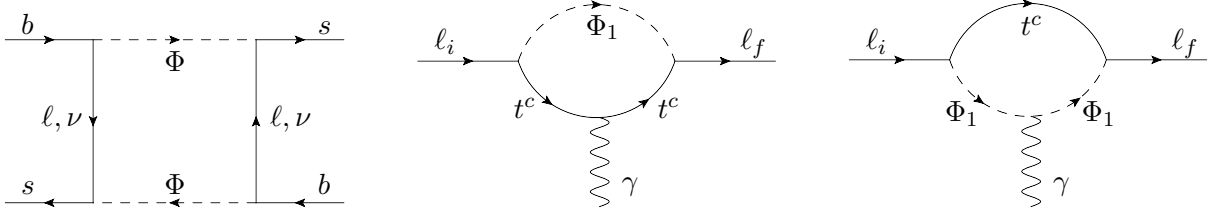


Figure 5.2: Left: LQ boxes contributing to $B_s - \bar{B}_s$ mixing. Middle and right: Loop diagrams induced by Φ_1 , generating effects in $\ell_i \rightarrow \ell_f \gamma$. In case of a top quark, as depicted, a chirally enhanced term can arise.

at the high scale μ_{LQ} . Here the first term originates only from Φ_1 and the second one only from Φ_3 . The last term originates from a box diagram where both LQ representations contribute. One of the corresponding Feynman diagram is shown in Fig. 5.2. The formula for B_d and Kaon mixing follow trivially. We can write the mass difference Δm_{B_s} (including NP) normalized to the SM one as

$$\frac{\Delta m_{B_s}}{\Delta m_{B_s}^{\text{SM}}} = \left| 1 + \frac{C_1}{C_1^{\text{SM}}} \right|, \quad (5.53)$$

with [346]

$$C_1^{\text{SM}} = 2.35 \frac{(V_{tb} V_{ts}^* G_F m_W)^2}{4\pi^2} \quad (5.54)$$

given at the high scale. Since both the SM and LQ contribute to C_1 , the QCD running down to μ_b is the same for both and therefore cancels in Eq. (5.53), neglecting the evolution from μ_{LQ} to the EW scale.

Observables

$B_s - \bar{B}_s$ mixing has been measured to very good precision [347] and the current world average reads [276]

$$\Delta m_{B_s}^{\text{exp}} = (17.757 \pm 0.021) \times 10^{12} \text{ s}^{-1}. \quad (5.55)$$

The theoretical prediction suffers strongly from the uncertainties in QCD effects. While Ref. [348] and Ref. [349] fit well to the measurement (with rather large errors)

$$\Delta m_{B_s}^{\text{SM}} = (18.3 \pm 2.7) \times 10^{12} \text{ s}^{-1}, \quad (5.56)$$

Ref. [350] obtains a larger SM value

$$\Delta m_{B_s}^{\text{SM}} = (20.01 \pm 1.25) \times 10^{12} \text{ s}^{-1}. \quad (5.57)$$

The bounds on the imaginary part of the Wilson coefficient is even more stringent. In our phenomenological analysis we will assume real couplings and allow for NP effects of up to 20% with respect to the SM prediction.

5.3.5 $\ell\ell\gamma$ Processes

In case of charged lepton interactions with on-shell photons we define

$$\mathcal{H}_{\text{eff}}^{\ell\ell\gamma} = C_{\ell_f\ell_i}^L O_{\ell_f\ell_i}^L + C_{\ell_f\ell_i}^R O_{\ell_f\ell_i}^R, \quad (5.58)$$

with

$$O_{\ell_f\ell_i}^{L(R)} = \frac{e}{16\pi^2} [\bar{\ell}_f \sigma^{\mu\nu} P_{L(R)} \ell_i] F_{\mu\nu}. \quad (5.59)$$

We obtain the following matching contribution in case of a top quark in the loop

$$C_{\ell_f\ell_i}^L = -\frac{m_{\ell_f} \lambda_{3f}^* \lambda_{3i} + m_{\ell_i} \hat{\lambda}_{3f}^* \hat{\lambda}_{3i}}{8M_1^2} + \frac{m_t \hat{\lambda}_{3f}^* V_{3k}^* \lambda_{ki}}{4M_1^2} \left(7 + 4 \log \left(\frac{m_t^2}{M_1^2} \right) \right) + \frac{3m_{\ell_f} \kappa_{3f}^* \kappa_{3i}}{8M_3^2} \quad (5.60)$$

from the Feynman diagram given in Fig. 5.2 with $N_c = 3$ already included. Note that we have $C_{\ell_f\ell_i}^R = C_{\ell_i\ell_f}^{L*}$ due to the hermiticity of the Hamiltonian. Here we quoted explicitly the formula for the top quark, which we integrated out together with the LQ at the scale $M \approx M_1 \approx M_3$. In case of light quarks, some comments concerning the use of Eq. (5.60) are in order: in principle, one has to integrate out only the LQ at the scale M but keep the quark as a dynamical degree of freedom. In this way, the matching contribution to $C_{\ell_f\ell_i}^L$ acquires an infrared divergence, which is cancelled by the corresponding UV divergence of the contribution of the tensor operator²⁰, obtained by integrating out the LQ at tree level. This amounts to a replacement of m_t by μ_{LQ} in the logarithm in Eq. (5.60). Now, at the low scale, the solution to the RGE (disregarding QED effects) leads to a replacement of μ_{LQ} by the scale of the processes, or by the quark mass in case this mass is bigger than the scale. Therefore, in the case of light quarks, Eq. (5.60) can be considered as an effective Wilson coefficient at the low scale, which includes the effect of 4-fermion operators (up to QED corrections) and can therefore be used for the numerical evaluation.

Considering $\ell_i \rightarrow \ell_f$ transition with an off-shell photon, we define the amplitude

$$\mathcal{A}(\ell_i \rightarrow \ell_f \gamma^*) = -eq^2 \bar{\ell}_f(p_f) \not{\epsilon}^*(q^2) \left(\hat{\Xi}_{fi}^L P_L + \hat{\Xi}_{fi}^R P_R + \delta_{fi} \right) \ell_i(p_i) \quad (5.61)$$

with

$$\begin{aligned} \hat{\Xi}_{fi}^L &= \frac{-N_c}{576\pi^2} \left(\frac{V_{jk} \lambda_{kf}^* V_{jl}^* \lambda_{li}}{M_1^2} F\left(\frac{m_{u_j}^2}{M_1^2}\right) + \frac{V_{jk} \kappa_{kf}^* V_{jl}^* \kappa_{li}}{M_3^2} F\left(\frac{m_{u_j}^2}{M_3^2}\right) + \frac{2\kappa_{jf}^* \kappa_{ji}}{M_3^2} G\left(\frac{m_{d_j}^2}{M_3^2}\right) \right), \\ \hat{\Xi}_{fi}^R &= \frac{-N_c}{576\pi^2} \frac{\hat{\lambda}_{jf}^* \hat{\lambda}_{ji}}{M_1^2} F\left(\frac{m_{u_j}^2}{M_1^2}\right), \end{aligned} \quad (5.62)$$

where

$$\begin{aligned} F(y) &= \frac{y^3 - 18y^2 + 27y - 10 + 2(y^3 + 6y - 4) \log(y)}{(y-1)^4}, \\ G(y) &= \frac{-17y^3 + 36y^2 - 27y + 8 + (8y^3 - 6y + 4) \log(y)}{(y-1)^4}. \end{aligned} \quad (5.63)$$

²⁰See Sec. 5.6.3 for the matching to the $u\bar{u}\gamma$ and $u\bar{u}\ell\ell$ operators.

Observables

We can now express the branching ratios of flavor changing radiative lepton decays in terms of the Wilson coefficients as

$$\text{Br}[\ell_i \rightarrow \ell_f \gamma] = \frac{\alpha m_{\ell_i}^3}{256\pi^4} \tau_{\ell_i} \left(|C_{\ell_f \ell_i}^L|^2 + |C_{\ell_f \ell_i}^R|^2 \right), \quad (5.64)$$

where τ_{ℓ_i} is the life time of the initial state lepton. The AMM of a charged lepton ℓ_i is given by

$$a_{\ell_i} = -\frac{m_{\ell_i}}{4\pi^2} \text{Re} \left[C_{\ell_i \ell_i}^R \right]. \quad (5.65)$$

The expression for the electric dipole moment of the lepton is quite similar to the one for the AMM, namely

$$d_{\ell_i} = -\frac{e}{8\pi^2} \text{Im} \left[C_{\ell_i \ell_i}^R \right]. \quad (5.66)$$

In case of the AMM of the muon we already discussed the experimental situation in the introduction. In summary, the difference between the experiment and the SM prediction is

$$\delta a_\mu = (278 \pm 88) \times 10^{-11},$$

corresponding to a 3.5σ deviation. Note that in our case the Wilson coefficient is in general complex and could therefore lead to sizable EDMs [286]. The current limits for radiative LFV decays are [351, 352]

$$\begin{aligned} \text{Br}[\mu \rightarrow e \gamma] &< 4.2 \times 10^{-13}, \\ \text{Br}[\tau \rightarrow e \gamma] &< 3.3 \times 10^{-8}, \\ \text{Br}[\tau \rightarrow \mu \gamma] &< 4.4 \times 10^{-8}, \end{aligned} \quad (5.67)$$

representing relevant constraints for our analysis. The off-shell photon penguins contribute to processes like $\tau \rightarrow 3\mu$ which we will consider later.

5.3.6 $Z\ell\ell$ and $Z\nu\nu$ Processes

In this subsection we compute the amplitudes for $Z \rightarrow \ell_i^- \ell_f^+$ and $Z \rightarrow \nu_f \bar{\nu}_i$ processes for massless leptons. At zero momentum transfer (or equivalently vanishing Z mass), these amplitudes are directly related to effective $Z\ell\ell$ and $Z\nu\nu$ couplings, which will enter flavor observables like for example in $\tau \rightarrow 3\mu$. We write the amplitude in an analogous way to the case with the off-shell photon

$$\begin{aligned} \mathcal{A}(Z \rightarrow \ell_f^- \ell_i^+) &= \frac{g}{c_w} \bar{u}(p_f, m_{\ell_f}) \gamma_\mu \left(\Lambda_{\ell_f \ell_i}^L(q^2) P_L + \Lambda_{\ell_f \ell_i}^R(q^2) \right) v(p_i, m_{\ell_i}) \varepsilon^\mu(q), \\ \mathcal{A}(Z \rightarrow \nu_f \bar{\nu}_i) &= \frac{g^2}{c_w} \Sigma_{\nu_f \nu_i}(q^2) \bar{u}(p_f) \gamma_\mu P_L v(p_i) \varepsilon^\mu(q), \end{aligned} \quad (5.68)$$

where ε^μ is the polarization vector of the Z and

$$\Lambda_{\ell_f \ell_i}^{L(R)}(q^2) = \Lambda_{\text{SM}}^{L(R)}(q^2) \delta_{fi} + \Delta_{fi}^{L(R)}(q^2), \quad \Sigma_{\nu_f \nu_i}(q^2) = \Sigma_{\text{SM}}(q^2) \delta_{fi} + \Sigma_{fi}^{\text{LQ}}(q^2). \quad (5.69)$$

At tree-level the SM couplings read

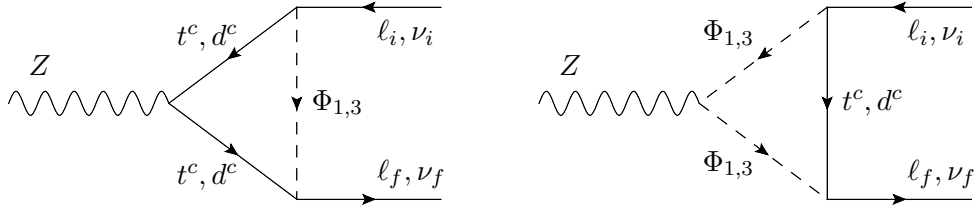


Figure 5.3: Feynman diagrams in our singlet-triplet model contributing to $Z \rightarrow \ell_f^- \ell_i^+$ and $Z \rightarrow \nu_f \bar{\nu}_i$ processes.

$$\Lambda_{\text{SM}}^L = \left(\frac{1}{2} - s_w^2 \right), \quad \Lambda_{\text{SM}}^R = -s_w^2, \quad \Sigma_{\text{SM}} = -\frac{1}{2}, \quad (5.70)$$

with s_w being the Weinberg angle. Beyond tree-level, the SM coefficients receive momentum dependent corrections which are included in the predictions for EW observables. The corresponding Feynman diagrams, generating these amplitudes in our model, are depicted in Fig. 5.3. For the calculation we include the up-type quark masses (which become relevant in case of the top) and the Z mass up to the order m_u^2/M_{LQ}^2 and m_Z^2/M_{LQ}^2 , respectively. In this setup we obtain

$$\begin{aligned} \Delta_{fi}^L(q^2) &= V_{jk} \lambda_{kf}^* V_{jl}^* \lambda_{li} \mathcal{F}_L(m_{u_j}^2, q^2, M_1^2) + V_{jk} \kappa_{kf}^* V_{jl}^* \kappa_{li} \mathcal{F}_L(m_{u_j}^2, q^2, M_3^2) \\ &\quad + 2\kappa_{jf}^* \kappa_{ji} \mathcal{G}_L(q^2, M_3^2), \\ \Delta_{fi}^R(q^2) &= \hat{\lambda}_{jf}^* \hat{\lambda}_{ji} \mathcal{F}_R(m_{u_j}^2, q^2, M_1^2), \\ \Sigma_{fi}^{\text{LQ}}(q^2) &= \lambda_{jf}^* \lambda_{ji} \mathcal{H}_1(q^2, M_1^2) + \kappa_{jf}^* \kappa_{ji} \mathcal{H}_1(q^2, M_3^2) + 2V_{jk} \kappa_{kf}^* V_{jl}^* \kappa_{li} \mathcal{H}_2(m_{u_j}^2, q^2, M_3^2). \end{aligned} \quad (5.71)$$

The corresponding loop functions $\mathcal{F}_{L,R}$, \mathcal{G}_L and $\mathcal{H}_{1,2}$ are given in Eq. (5.117) and Eq. (5.122). In case of Z decays we have $q^2 = m_Z^2$.

For the effective $Z\ell\ell$ and $Z\nu\nu$ couplings (at zero momentum transfer), we define

$$\begin{aligned} \mathcal{L}_{\text{int}}^{Z\ell\ell} &= \frac{g_2}{c_w} [\bar{\ell}_f (\Lambda_{\ell_f \ell_i}^L(0) \gamma_\mu P_L + \Lambda_{\ell_f \ell_i}^R(0) \gamma_\mu P_R) \ell_i] Z^\mu, \\ \mathcal{L}_{\text{int}}^{Z\nu\nu} &= \frac{g_2}{c_w} \Sigma_{\nu_f \nu_i}(0) [\bar{\nu}_f \gamma_\mu P_L \nu_i] Z^\mu. \end{aligned} \quad (5.72)$$

In this case, only the top contribution is relevant and the effective couplings become

$$\begin{aligned} \Lambda_{\ell_f \ell_i}^L(0) &= \Lambda_{\text{SM}}^L(0) \delta_{fi} \\ &\quad + \frac{N_c m_t^2}{32\pi^2} \left(\frac{V_{3k} \lambda_{kf}^* V_{3l}^* \lambda_{li}}{M_1^2} \left(1 + \log \left(\frac{m_t^2}{M_1^2} \right) \right) + \frac{V_{3k} \kappa_{kf}^* V_{3l}^* \kappa_{li}}{M_3^2} \left(1 + \log \left(\frac{m_t^2}{M_3^2} \right) \right) \right), \\ \Lambda_{\ell_f \ell_i}^R(0) &= \Lambda_{\text{SM}}^R(0) \delta_{fi} - \frac{N_c m_t^2}{32\pi^2} \frac{\hat{\lambda}_{3f}^* \hat{\lambda}_{3i}}{M_1^2} \left(1 + \log \left(\frac{m_t^2}{M_1^2} \right) \right), \\ \Sigma_{\nu_f \nu_i}(0) &= \Sigma_{\text{SM}}(0) \delta_{fi} + \frac{N_c m_t^2}{16\pi^2} \frac{V_{3k} \kappa_{kf}^* V_{3l}^* \kappa_{li}}{M_3^2} \left(1 + \log \left(\frac{m_t^2}{M_3^2} \right) \right). \end{aligned} \quad (5.73)$$

Note that $Z \rightarrow \ell_i^- \ell_f^+$ has also been considered in Ref. [289].

Observables

The branching ratio of a Z decaying into a charged lepton pair reads

$$\text{Br} [Z \rightarrow \ell_f^- \ell_i^+] = \frac{G_F m_Z^3}{\sqrt{2} 3\pi} \frac{1}{\Gamma_{\text{tot}}} \left(|\Lambda_{\ell_f \ell_i}^L(m_Z^2)|^2 + |\Lambda_{\ell_f \ell_i}^R(m_Z^2)|^2 \right). \quad (5.74)$$

with $\Gamma_{\text{tot}} \approx 2.5 \text{ GeV}$. The case for a pair of neutrinos in the final state follows trivially. The effective number of active neutrinos, including the corrections in our model, are given by

$$N_\nu = \sum_{f,i} \left| \delta_{fi} + \frac{\Sigma_{fi}^{\text{LQ}}(m_Z^2)}{\Sigma_{\text{SM}}(m_Z^2)} \right|^2. \quad (5.75)$$

At LEP [353] the lepton flavor conserving Z boson couplings were measured precisely. We give the experimental results for each flavor separately

$$\begin{aligned} \Lambda_{\text{exp}}^{Le}(m_Z^2) &= 0.26963 \pm 0.00030, & \Lambda_{\text{exp}}^{Re}(m_Z^2) &= -0.23148 \pm 0.00029, \\ \Lambda_{\text{exp}}^{L\mu}(m_Z^2) &= 0.2689 \pm 0.0011, & \Lambda_{\text{exp}}^{R\mu}(m_Z^2) &= -0.2323 \pm 0.0013, \\ \Lambda_{\text{exp}}^{L\tau}(m_Z^2) &= 0.26930 \pm 0.00058, & \Lambda_{\text{exp}}^{R\tau}(m_Z^2) &= -0.23274 \pm 0.00062, \\ \Sigma_{\text{exp}}^{L\nu}(m_Z^2) &= -0.5003 \pm 0.0012. \end{aligned} \quad (5.76)$$

The SM predictions at the Z pole are

$$\begin{aligned} \Lambda_{\text{SM}}^{Le}(m_Z^2) &= \Lambda_{\text{SM}}^{L\mu}(m_Z^2) = \Lambda_{\text{SM}}^{L\tau}(m_Z^2) = 0.26919 \pm 0.00020, \\ \Lambda_{\text{SM}}^{Re}(m_Z^2) &= \Lambda_{\text{SM}}^{R\mu}(m_Z^2) = \Lambda_{\text{SM}}^{R\tau}(m_Z^2) = -0.23208_{-0.00018}^{+0.00016}, \\ \Sigma_{\text{SM}}^{L\nu}(m_Z^2) &= -0.50199_{-0.00020}^{+0.00017}. \end{aligned} \quad (5.77)$$

Concerning lepton flavor violating Z decays the limits from LEP are [354–356]

$$\begin{aligned} \text{Br} [Z \rightarrow e^\pm \mu^\mp] &\leq 7.5 \times 10^{-7}, \\ \text{Br} [Z \rightarrow e^\pm \tau^\mp] &\leq 9.8 \times 10^{-6}, \\ \text{Br} [Z \rightarrow \mu^\pm \tau^\mp] &\leq 1.2 \times 10^{-5}. \end{aligned} \quad (5.78)$$

From $Z \rightarrow \nu\bar{\nu}$ one can determine the number of active neutrinos to be [353]

$$N_\nu = 2.9840 \pm 0.0082. \quad (5.79)$$

As mentioned before, $Z\ell\ell$ couplings (at zero momentum transfer) contribute to processes like $\tau \rightarrow 3\mu$. Furthermore, $Z\ell\ell$ couplings in Z decays can be measured much more precisely at an FCC-ee which could produce more than 10^{11} Z bosons [357].

5.3.7 $W\ell\nu$ Processes

Computing the amplitude of this process (also considered in Ref. [289]), we obtain

$$\mathcal{A}(W^- \rightarrow \ell_f^- \bar{\nu}_i) = -\frac{g_2}{\sqrt{2}} \Lambda_{\ell_f \nu_i}^W(q^2) \bar{u}(p_{\ell_f}, m_{\ell_f}) \gamma_\mu P_L u(p_{\nu_i}) \varepsilon^\mu(q), \quad (5.80)$$

where

$$\Lambda_{\ell_f \nu_i}^W(q^2) = \Lambda_{\text{SM}}^W(q^2) \delta_{fi} + \Lambda_{fi}^{\text{LQ}}(q^2). \quad (5.81)$$

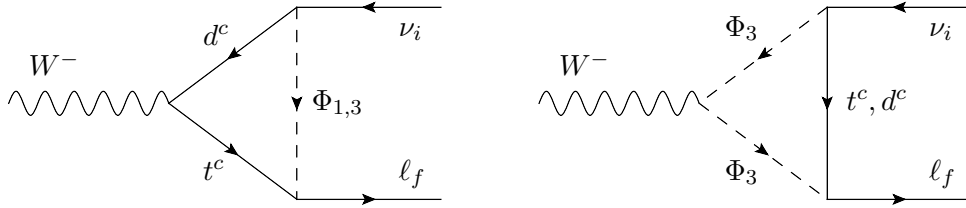


Figure 5.4: Feynman diagrams contributing to $W^- \rightarrow \ell_f^- \bar{\nu}_i$. The right diagram is only present for the triplet since the singlet does not couple to the W boson (at tree-level).

At tree level in the SM we have $\Lambda_{\text{SM}}^W(q^2) = 1$. The Feynman diagrams shown in Fig. 5.4 result in

$$\Lambda_{fi}^{\text{LQ}}(q^2) = \frac{N_c}{288\pi^2} \left[V_{jk} \lambda_{kf}^* V_{jl} \lambda_{li} \mathcal{F}_1(m_{u_j}^2, q^2, M_1^2) + V_{jk} \kappa_{kf}^* V_{jl} \kappa_{li} \mathcal{F}_2(m_{u_j}^2, q^2, M_3^2) + \frac{8\kappa_{jf}^* \kappa_{ji} q^2}{9M_3^2} \right], \quad (5.82)$$

with the loop functions $\mathcal{F}_{1,2}$ given in Eq. (5.129). Again, we set all down-type quark masses to zero but included the up-type quark masses, which are relevant for the top. At the level of effective couplings, we define the Lagrangian

$$\mathcal{L}_{\text{int}}^{W\ell\nu} = -\frac{g}{\sqrt{2}} \Lambda_{\ell_f \nu_i}^W(0) [\bar{\ell}_f \gamma^\mu P_L \nu_i] W_\mu^-. \quad (5.83)$$

The LQ contribution then reads

$$\Lambda_{ji}^{\text{LQ}}(0) = \frac{N_c m_t^2}{64\pi^2} \left[\frac{V_{3l} \lambda_{lj}^* V_{3k}^* \lambda_{ki}}{M_1^2} \left(1 + 2 \log \left(\frac{m_t^2}{M_1^2} \right) \right) - \frac{V_{3l} \kappa_{lj}^* V_{3k}^* \kappa_{ki}}{M_3^2} \left(1 + 2 \log \left(\frac{m_t^2}{M_3^2} \right) \right) \right]. \quad (5.84)$$

Out of this formula one deduces a destructive interference between the contribution of the singlet and the triplet in case of lepton flavor conservation.

Observables

Experimentally, the modification of the $W\tau\nu$ coupling extracted from $\tau \rightarrow \mu\nu\bar{\nu}$ and $\tau \rightarrow e\nu\bar{\nu}$ decays reads [275, 276]

$$|\Lambda_{\tau\nu}^W(0)|_{\text{exp}} \approx 1.002 \pm 0.0015 \quad (5.85)$$

and provides a better constraint than data of W decays. Here we averaged the central values of the muon and tau mode, but did not add the errors in quadrature in order to be conservative. We see that a positive NP effect is preferred which means that the triplet contribution should exceed the one of the singlet.

5.3.8 4ℓ Processes

We define the effective Hamiltonian as

$$\mathcal{H}_{\text{eff}}^{4\ell} = \mathcal{H}_{\text{eff}}^{\ell\ell\gamma} + \sum_{a,b,f,i} \left(C_{abfi}^{VLL} O_{abfi}^{VLL} + C_{abfi}^{VLR} O_{abfi}^{VLR} + C_{abfi}^{SLL} O_{abfi}^{SLL} \right) + L \leftrightarrow R, \quad (5.86)$$

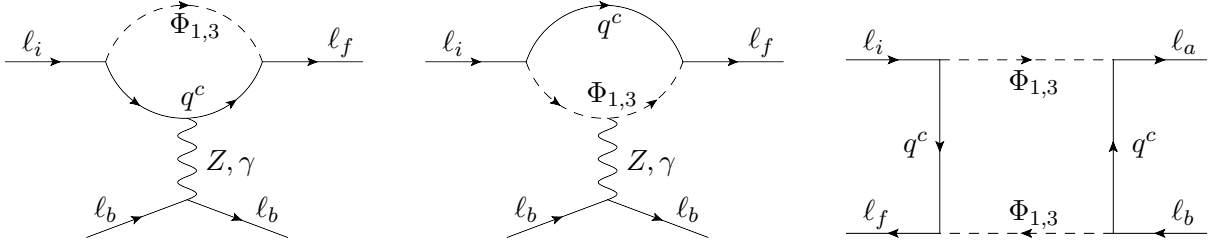


Figure 5.5: Feynman diagrams contributing to $l_i \rightarrow l_f l_a l_b$. Left and centre: Penguin diagrams with Z boson and photon exchange. Right: Box diagram involving two LQs.

with

$$\begin{aligned}
O_{abfi}^{VLL} &= [\bar{l}_a \gamma^\mu P_L l_b] [\bar{l}_f \gamma_\mu P_L l_i] , \\
O_{abfi}^{VLR} &= [\bar{l}_a \gamma^\mu P_L l_b] [\bar{l}_f \gamma_\mu P_R l_i] , \\
O_{abfi}^{SLL} &= [\bar{l}_a P_L l_b] [\bar{l}_f P_L l_i] .
\end{aligned} \tag{5.87}$$

Here we sum over flavor indices. In this way, no distinction for the cases of equal flavors are necessary in the matching and tensor and scalar LR operators do not need to be included since they follow from Fierz identities.

The photon contribution reads

$$\begin{aligned}
C_{abfi}^{VLL} &= -\pi\alpha \left(\Xi_{ab}^L \Xi_{fi}^L + \Xi_{ai}^L \Xi_{fb}^L \right) , \\
C_{abfi}^{VLR} &= -2\pi\alpha \Xi_{ab}^L \Xi_{fi}^R ,
\end{aligned} \tag{5.88}$$

where

$$\Xi_{fi}^{L(R)} = \delta_{fi} + \hat{\Xi}_{fi}^{L(R)} . \tag{5.89}$$

The effective photon off-shell couplings $\hat{\Xi}_{fi}^{L(R)}$ are defined in Eq. (5.62). Using the effective couplings defined in Eq. (5.69), the Z penguins give

$$\begin{aligned}
C_{abfi}^{VLL} &= \frac{2G_F}{\sqrt{2}} \left(\Lambda_{ab}^L(0) \Lambda_{fi}^L(0) + \Lambda_{fb}^L(0) \Lambda_{ai}^L(0) \right) , \\
C_{abfi}^{VLR} &= \frac{4G_F}{\sqrt{2}} \Lambda_{ab}^L(0) \Lambda_{fi}^R(0) .
\end{aligned} \tag{5.90}$$

Note that $C_{abfi}^{VRL(RR)}$ are obtained from $C_{abfi}^{VLR(LL)}$ by interchanging L and R for both the photon and the Z contribution. Finally, we have contributions from box diagrams involving two LQs. Since they turn out to be numerically irrelevant in our model, we omit to list them here analytically. However, in Eq. (5.130) we give the results in full generality, i.e. including LQ mixing with multiple generations. The LQ contributions are depicted in Fig. 5.5.

The expression for the branching ratios, which are in agreement with Ref. [358], read

$$\begin{aligned}
\text{Br} \left[\tau^\mp \rightarrow \mu^\mp e^+ e^- \right] &= \frac{m_\tau^3}{768\pi^3 \Gamma_\tau^{\text{tot}}} \left[\frac{\alpha^2}{\pi^2} |C_{\mu\tau}^L|^2 \left(\log\left(\frac{m_\tau^2}{m_e^2}\right) - 3 \right) + \frac{m_\tau^2}{2} \left(|C_{\mu\tau ee}^{SLL}|^2 + |C_{\mu e e\tau}^{SLL}|^2 \right. \right. \\
&\quad \left. \left. - \text{Re} \left[C_{\mu\tau ee}^{SLL} C_{\mu e e\tau}^{SLL*} \right] + 16 |C_{\mu\tau ee}^{VLL}|^2 + 4 |C_{\mu\tau ee}^{VLR}|^2 + 4 |C_{\mu e e\tau}^{VLR}|^2 \right) \right. \\
&\quad \left. - \frac{2\alpha}{\pi} m_\tau \text{Re} \left[C_{\mu\tau}^{L*} \left(C_{\mu\tau ee}^{VRL} + 2C_{\mu\tau ee}^{VRR} \right) \right] + L \leftrightarrow R \right] \tag{5.91}
\end{aligned}$$

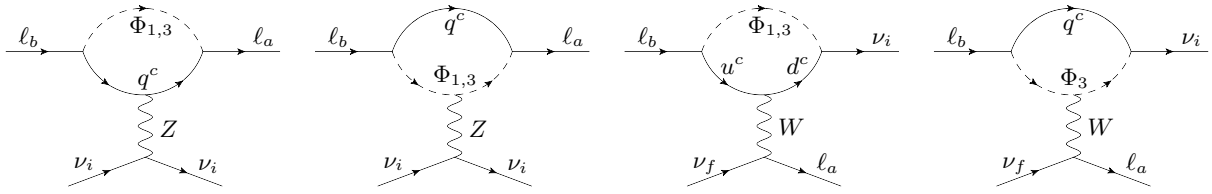


Figure 5.6: Penguin diagrams that contribute to $\ell_b \rightarrow \ell_a \nu_i \bar{\nu}_f$ transitions. In case of the Z boson, lepton flavor is conserved at tree-level vertex ($f = i$). For the W penguins we applied Fierz identities in order to match on the effective operators. The box diagrams look similar to the one in Fig. 5.3 but turn out to be numerically insignificant.

and

$$\begin{aligned} \text{Br} \left[\tau^\mp \rightarrow \mu^\mp \mu^+ \mu^- \right] &= \frac{m_\tau^3}{768\pi^3 \Gamma_\tau^{\text{tot}}} \left[\frac{\alpha^2}{\pi^2} |C_{\mu\tau}^L|^2 \left(\log\left(\frac{m_\tau^2}{m_\mu^2}\right) - \frac{11}{4} \right) \right. \\ &\quad + \frac{m_\tau^2}{4} \left(|C_{\mu\mu\mu\tau}^{SLL}|^2 + 16|C_{\mu\tau\mu\mu}^{VLL}|^2 + 4|C_{\mu\tau\mu\mu}^{VLR}|^2 + 4|C_{\mu\mu\mu\tau}^{VLR}|^2 \right) \\ &\quad \left. - \frac{2\alpha}{\pi} m_\tau \text{Re} \left[C_{\mu\tau}^{L*} (C_{\mu\tau\mu\mu}^{VRL} + 2C_{\mu\tau\mu\mu}^{VRR}) \right] + L \leftrightarrow R \right] \end{aligned} \quad (5.92)$$

with Γ_τ^{tot} as the tau lepton's total decay width. The experimental bounds are [359, 360]

$$\begin{aligned} \text{Br} \left[\tau^\mp \rightarrow \mu^\mp e^+ e^- \right] &< 1.5 \times 10^{-8}, \\ \text{Br} \left[\tau^\mp \rightarrow \mu^\mp \mu^+ \mu^- \right] &< 2.1 \times 10^{-8}, \\ \text{Br} \left[\mu^\mp \rightarrow e^\mp e^+ e^- \right] &< 1.0 \times 10^{-12}. \end{aligned} \quad (5.93)$$

5.3.9 $\ell\nu\nu$ Processes

We define the effective Hamiltonian as

$$\mathcal{H}_{\text{eff}}^{2\ell 2\nu} = \left(D_{\ell_a \ell_b}^{L,fi} O_{\ell_a \ell_b}^{L,fi} + D_{\ell_a \ell_b}^{R,fi} O_{\ell_a \ell_b}^{R,fi} \right), \quad (5.94)$$

with

$$O_{\ell_a \ell_b}^{L(R),fi} = \left[\bar{\ell}_a \gamma_\mu P_{L(R)} \ell_b \right] \left[\bar{\nu}_f \gamma^\mu P_L \nu_i \right]. \quad (5.95)$$

At the 1-loop level, LQs can contribute to these processes through three types of Feynman diagrams: W -penguins, Z -penguins and pure LQ box diagrams, see Fig. 5.6. Again, the boxes are numerically not relevant due to the small couplings to muons. Therefore, we only present these results with full generality in the appendix.

The W penguin given in terms of the modified $W\ell\nu$ couplings of Eq. (5.84) gives

$$D_{\ell_a \ell_b}^{L,fi} = \frac{4G_F}{\sqrt{2}} \Lambda_{\ell_b \nu_f}^{W*}(0) \Lambda_{\ell_a \nu_i}^W(0). \quad (5.96)$$

Finally we also have the Z -penguins, yielding

$$D_{\ell_a \ell_b}^{L,fi} = \frac{8G_F}{\sqrt{2}} \Lambda_{\ell_a \ell_b}^L(0) \Sigma_{\nu_f \nu_i}(0), \quad D_{\ell_a \ell_b}^{R,fi} = \frac{8G_F}{\sqrt{2}} \Lambda_{\ell_a \ell_b}^R(0) \Sigma_{\nu_f \nu_i}(0), \quad (5.97)$$

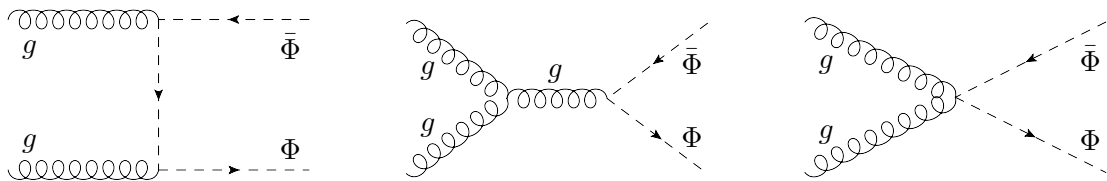


Figure 5.7: Tree-level Feynman diagrams contributing to $gg \rightarrow \Phi\bar{\Phi}$.

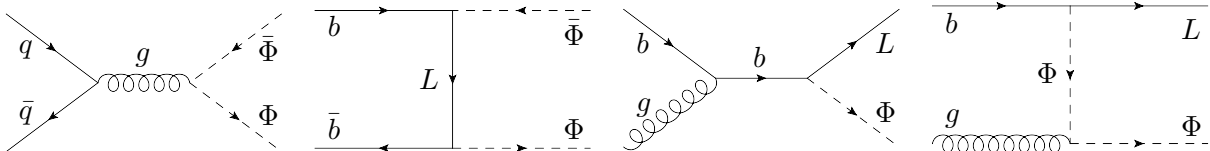


Figure 5.8: Tree-level diagrams contributing to $q\bar{q} \rightarrow \Phi\bar{\Phi}$ and $gg \rightarrow L\Phi$. Except for the left diagram, the cross-sections depend on the couplings of the LQ to SM fermions. L can be either a neutrino or a charged lepton, depending on the specific LQ representation.

where we used the effective $Z\ell\ell$ and $Z\nu\nu$ couplings given in Eq. (5.73).

5.4 Phenomenology

Now we turn to the phenomenological analysis of our singlet-triplet model. We consider the processes discussed above and include the loop effects calculated in the previous section. Our strategy is as follows: First we will discuss the LHC bounds on third-generation LQs. Then we will consider how one can explain $b \rightarrow c\tau\nu$ data taking into account these limits and then study the impacts on other observables like $B_s \rightarrow \tau^+\tau^-$ and $W \rightarrow \tau\nu$. For this purpose, only couplings to tau leptons (but not to muons or electrons) are necessary. In a next step we will include $b \rightarrow s\ell^+\ell^-$ data in our analysis and thus allow for non-zero couplings to left-handed muons, while disregarding couplings to electrons due to the strong constraints from $\mu \rightarrow e\gamma$ [361]. In a final step, we search for benchmark points which can explain $b \rightarrow c\tau\nu$, $b \rightarrow s\ell^+\ell^-$ and a_μ simultaneously. For this purpose we also include couplings to right-handed muons in our analysis.

5.4.1 LHC Bounds

Both Φ_1 and Φ_3 could obviously be produced at the LHC. Since LQs are charged under $SU(3)_c$ they can be pair produced via gluons (depicted in Fig. 5.7), which in general gives the best bound. However, for a third generation LQ, which is the case for our model to a good approximation, also t-channel production from bottom fusion is possible as well as single production via bottom-gluon fusion (see Fig. 5.8). ATLAS and CMS performed searches in these channels. In particular, in Ref. [291] CMS analyzed data taken at a center-of-mass energy of 13 TeV with an integrated luminosity of 35.9 fb^{-1} for the scalar singlet Φ_1 . Assuming $\text{Br}[\Phi_1 \rightarrow t\tau] = 100\%$, LQ masses up to 900 GeV are excluded. ATLAS searched for typical signals of the scalar triplet Φ_3 , using 36.1 fb^{-1} of data at $\sqrt{s} = 13 \text{ TeV}$ [362]. Focusing on NP effects in third generation quarks and leptons, i.e. $\Phi_3 \rightarrow t\nu/b\tau$ and $\Phi_3 \rightarrow t\tau/b\nu$, they find a lower limit on the LQ mass of 800 GeV. This limit can be raised up to 1 TeV if one of the aforementioned decay channels is dominating. Therefore, a third generation scalar LQ with mass above 1 TeV is consistent with LHC searches. We will assume this as a lower limit in the following phenomenological analysis of flavor observables. For more extensive analyses of LQ searches in combination with the flavor

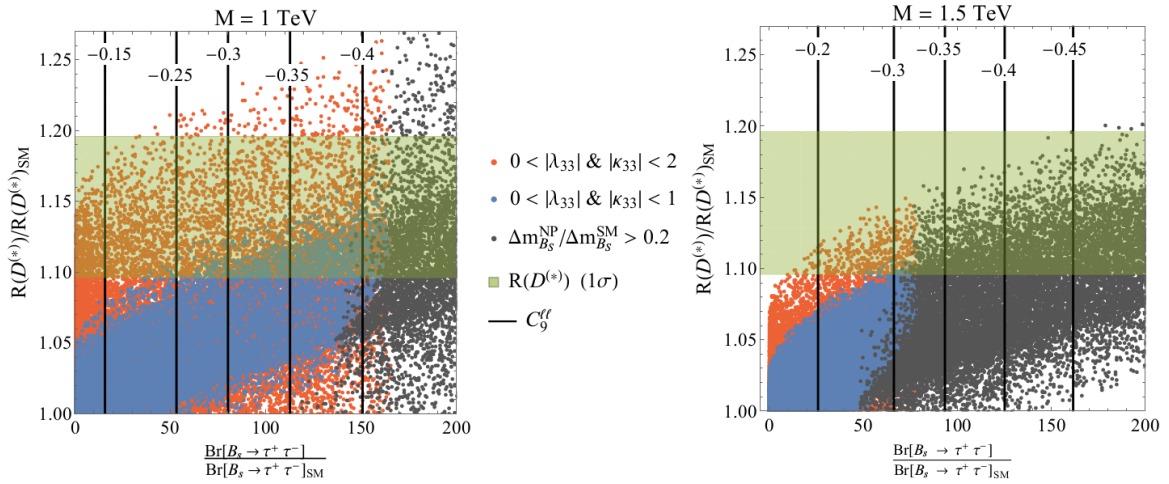


Figure 5.9: Correlation between $\text{Br}[B_s \rightarrow \tau^+ \tau^-]$ and $R(D^{(*)})$, both normalized to their SM values, in the scenario with only left-handed couplings for $M_1 = M_3 \equiv M = 1 \text{ TeV}$ (left plot) and $M_1 = M_3 \equiv M = 1.5 \text{ TeV}$ (right plot). Here we scanned over $\lambda_{23}, \kappa_{23} \in [-1, 1]$ for all points and $\lambda_{33}, \kappa_{33} \in [-1, 1]$ (blue) or $\lambda_{33}, \kappa_{33} \in [-2, 2]$ (red), respectively. The blue points are displayed on top of the red ones, showing only points that are allowed by $R_{K^*}^{\nu\nu}$. The dark gray points are in agreement with $R_{K^*}^{\nu\nu}$, but excluded by $B_s - \bar{B}_s$ mixing. The horizontal contour lines depict the LFU contribution to $C_9^{\ell\ell}$ while the green band represents the region for $R(D^{(*)})$ preferred by data at the 1σ level.

anomalies we refer e.g. to Refs. [212, 274, 363–367].

5.4.2 $b \rightarrow c\tau\nu$

Concerning $b \rightarrow c\tau\nu$ processes one can address the anomalies with couplings to third generation leptons, i.e. the tau lepton and the tau neutrino, while disregarding couplings to muons and electrons. In a first step we consider the simplified case of left-handed couplings only, i.e. $\hat{\lambda} = 0$. Furthermore, we can safely neglect CKM suppressed effects from first-generation quark couplings and are therefore left with the couplings $\lambda_{23,33}$ and $\kappa_{23,33}$, involving second and third generation quarks (i.e. bottom and strange quark in the down-basis). In this case the box contributions to $B_s - \bar{B}_s$ in Eq. (5.52), together with the tree-level effect in $b \rightarrow s\nu\bar{\nu}$ in Eq. (5.39) put an upper limit on the possible contribution to $b \rightarrow c\tau\nu$ processes (see Fig. 5.9). While the relative effect in $b \rightarrow s\nu\bar{\nu}$ compared to $b \rightarrow c\tau\nu$ is independent of the LQ mass, the relative effect in $B_s - \bar{B}_s$ mixing compared to $b \rightarrow c\tau\nu$ amplitudes turns out to have a quadratic scaling with the mass. In fact, assuming real couplings and an exact cancellation in $R_{K^{(*)}}^{\nu\nu}$, Δm_{B_s} can be expressed in terms of the NP effect in $R(D^{(*)})$ as

$$\frac{\Delta m_{B_s}}{\Delta m_{B_s}^{\text{SM}}} = 1 + \frac{1}{4\pi^2} \frac{G_F^2 V_{cb}^2 M^2}{C_1^{\text{SM}}} \left(\sqrt{\frac{R(D^{(*)})}{R(D^{(*)})_{\text{SM}}}} - 1 \right)^2, \quad (5.98)$$

with $M_1 = M_3 = M$. This relation holds once small CKM rotations are neglected which is possible in the case of an anarchic flavor structure, i.e. $V_{cb}\lambda_{33} \ll \lambda_{23}$ and $V_{cb}\kappa_{33} \ll \kappa_{23}$. The tau loops also generate an effect in C_7 as well as a LFU contribution to $C_9^{\ell\ell}$. Both these effects are directly correlated to $b \rightarrow s\tau^+\tau^-$ processes, induced by the tree-level coefficients

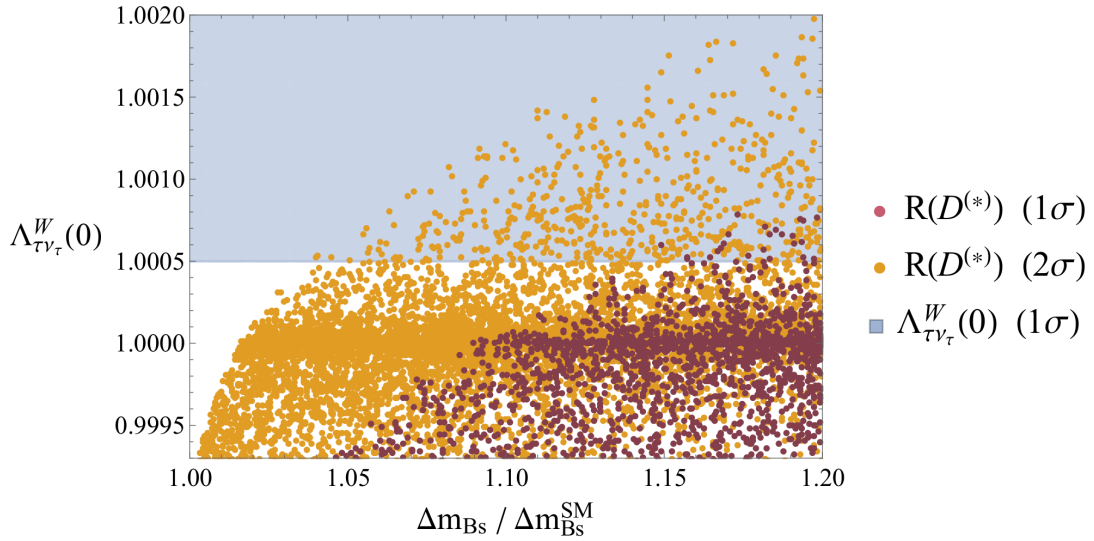


Figure 5.10: Correlations between the NP effect in Δm_{B_s} and the corrections to the effective $W\tau\nu\tau$ coupling $\Lambda_{\tau\nu\tau}^W(0)$, constrained from $\tau \rightarrow \mu\nu\bar{\nu}$ and $\tau \rightarrow e\nu\bar{\nu}$. Like in Fig. 5.9 we only considered the couplings $\lambda_{23,33}$ and $\kappa_{23,33}$, i.e. only couplings to left-handed taus, scanning over λ_{23} and κ_{23} (λ_{33} and κ_{33}) between ± 1 (± 2) and setting $M_1 = M_3 = M = 1$ TeV. The blue region is preferred by $\tau \rightarrow \mu\nu\bar{\nu}$ and $\tau \rightarrow e\nu\bar{\nu}$ data at the 1σ level.

$C_9^{\tau\tau} = -C_{10}^{\tau\tau}$. We find

$$\begin{aligned} C_9^{\ell\ell}(\mu_b) &= \frac{\alpha}{27\pi} \left(14 + 9 \log\left(\frac{\mu_b^2}{M^2}\right) \right) C_9^{\tau\tau}, \\ C_7(\mu_b) &= -\frac{5\alpha}{36\pi} \left(\frac{27}{11} \eta_{23}^{16} - \frac{48}{33} \eta_{23}^{14} \right) C_9^{\tau\tau}, \end{aligned} \quad (5.99)$$

neglecting the different running of C_7 from μ_{LQ} down to m_t . One can also relate these two coefficients, yielding

$$C_9^{\ell\ell}(\mu_b) = -\frac{4}{15} \frac{14 + 9 \log\left(\frac{\mu_b^2}{M^2}\right)}{\frac{27}{11} \eta_{23}^{16} - \frac{48}{33} \eta_{23}^{14}} C_7(\mu_b). \quad (5.100)$$

This situation is illustrated in Fig. 5.9, where we show the correlations between $B_s \rightarrow \tau^+\tau^-$ and $R(D^{(*)})$. Note that for left-handed couplings $R(D)/R(D)_{\text{SM}} = R(D^*)/R(D^*)_{\text{SM}}$ is predicted. The bound from $B_s - \bar{B}_s$ mixing limits the possible effect, both in $B_s \rightarrow \tau^+\tau^-$ and $R(D^{(*)})$, depending on the LQ mass. Heavier LQs lead to larger effects in $B_s - \bar{B}_s$ with respect to $B_s \rightarrow \tau^+\tau^-$ and $R(D^{(*)})$ than lighter LQs. For the same scenario, i.e. only left-handed couplings to tau leptons, we also show corrections to the $W\tau\nu$ coupling in Fig. 5.10. Note that effect of Φ_1 has opposite sign than the one of Φ_3 . Furthermore, if one aims at increasing $R(D^{(*)})$, the effect of Φ_1 (Φ_3) in $W \rightarrow \tau\nu$ is destructive (constructive) such that it increases (decreases) the slight tension in $\tau \rightarrow \mu\nu\bar{\nu}$ data.

Next, let us allow for non-zero right-handed couplings $\hat{\lambda}_{23,33}$ of Φ_1 to quarks and leptons. In this case the left-handed vector current encoded in $C_{VL}^{\tau\tau}$ (originating from Φ_1 and Φ_3 via $\lambda_{23,33}$ and $\kappa_{23,33}$ only) is now complemented by a $C_{SL}^{\tau\tau} = -4C_{TL}^{\tau\tau}$ effect from Φ_1 . This breaks the common rescaling of $R(D)/R(D)_{\text{SM}}$ and $R(D^*)/R(D^*)_{\text{SM}}$, depicted by the green line in Fig. 5.11. The constraint from $B_s - \bar{B}_s$ only limits C_{VL} but not $C_{SL} = -4C_{TL}$. The resulting correlations between $R(D)$ and $R(D^*)$ are shown in Fig. 5.11. One can see that for deviations

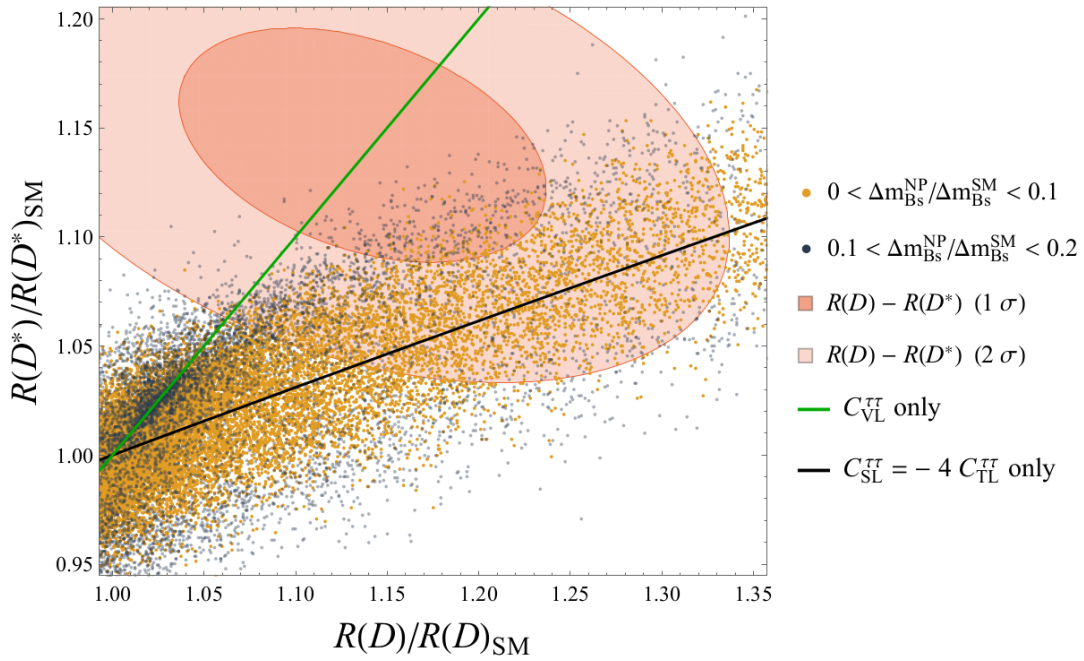


Figure 5.11: Correlation between $R(D)$ and $R(D^*)$, both normalized to their SM values. The (light) red ellipse shows the preferred region at the 1σ (2σ) level. The yellow points yield an effect in $B_s - \bar{B}_s$ mixing of $< 10\%$ with respect to the SM, while for the blue points the NP effect is in the range of 10-20%. Only points allowed by $b \rightarrow s\nu\nu$ are shown. The black (green) solid line depicts the scenario where one generates the vector (scalar and tensor) operator only. We scanned over the couplings $\lambda_{23,33}$, $\kappa_{23,33}$ and $\hat{\lambda}_{23} \in [-1.5, 1.5]$ and the LQ masses $M_1 = M_3 \equiv M \in [1, 2]$ TeV.

of $R(D^*)/R(D^*)_{\text{SM}}$ from unity of more than $\approx 10\%$, our model predicts $R(D)/R(D)_{\text{SM}} > R(D^*)/R(D^*)_{\text{SM}}$.

The size and correlation between C_7 and a LFU effect in $C_9^{\ell\ell}$, induced by the tau loop, is shown in Fig. 5.12. Interestingly, to account for $b \rightarrow c\tau\nu$ data within 1σ , we predict $-0.5 < C_9^{\ell\ell} < -0.2$ (including right-handed couplings) which is in very good agreement with the global fit on $b \rightarrow s\ell^+\ell^-$ data, especially if it is complemented by a $C_9^{\mu\mu} = -C_{10}^{\mu\mu}$ LFUV effect [95, 98].

In the same way, $b \rightarrow d\tau\nu$ data can be addressed. Here, it was shown in Ref. [47] that already a 10% effect with respect to the SM could lead to a neutron EDM observables in the near future.

5.4.3 $b \rightarrow c\tau\nu$ and $b \rightarrow s\ell^+\ell^-$

Let us now turn to the case where we allow for couplings to left-handed muons as well. Here, it is clear that, disregarding for the moment $R(D^*)$ and thus tau couplings, one can explain $b \rightarrow s\ell^+\ell^-$ data with a tree-level $C_9^{\mu\mu} = -C_{10}^{\mu\mu}$ effect from Φ_3 without running into the danger of violating bounds from other flavor observables. However, the situation gets more interesting if one aims at explaining $b \rightarrow s\ell^+\ell^-$ and $b \rightarrow c\tau\nu$ data simultaneously. In this case LFV $\tau - \mu$ effects necessarily arise e.g. in $B \rightarrow K\tau\mu$, $\tau \rightarrow \phi\mu$, $Z \rightarrow \tau\mu$ and $\tau \rightarrow 3\mu$. Note that our model does not possess scalar currents in the down sector, therefore $B_s \rightarrow \tau\mu$ does not receive a chiral enhancement. The correlations between $B \rightarrow K\tau\mu$ and $\tau \rightarrow \phi\mu$ are shown in Fig. 5.13, finding that they are in general anti-correlated despite fine-tuned points.

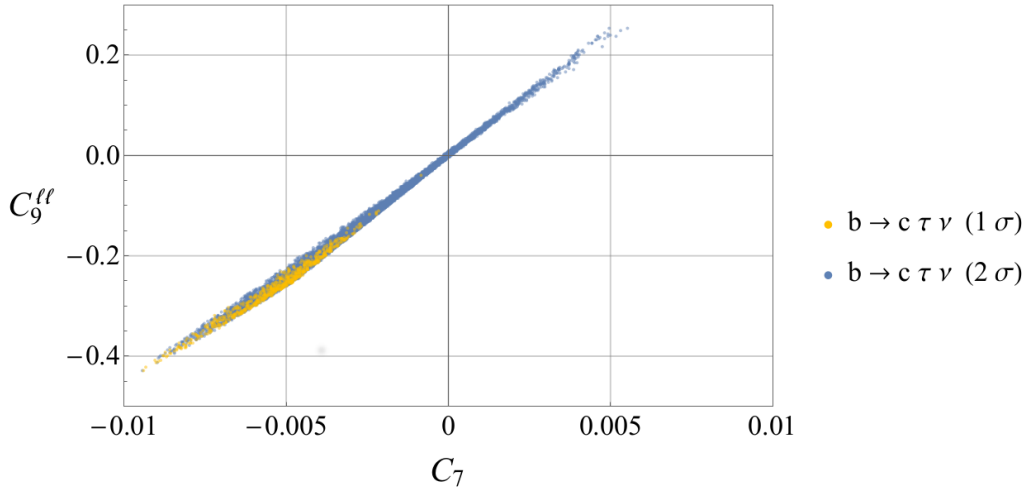


Figure 5.12: Correlations between C_7 and $C_9^{\ell\ell}$, both given at the B meson scale. Here we imposed that the points satisfy $B_s - \bar{B}_s$ mixing (i.e. yield a maximal effect of 20%) and lie within the 1σ (yellow) or 2σ (blue) region preferred by the global fit to $b \rightarrow c\tau\nu$ data. Note that non-zero effects in $C_7(\mu_b)$ and $C_9^{\ell\ell}(\mu_b)$ are mandatory in order to explain $b \rightarrow c\tau\nu$ data at 1σ and that $C_9^{\ell\ell}(\mu_b)$ has the sign preferred by the fit if this is required. Both coefficients include $\mathcal{O}(\alpha_s)$ corrections. Again we scanned over the couplings $\lambda_{23,33}$, $\kappa_{23,33}$ and $\hat{\lambda}_{23} \in [-1.5, 1.5]$ and the LQ masses $M_1 = M_3 \equiv M \in [1, 2]$ TeV.

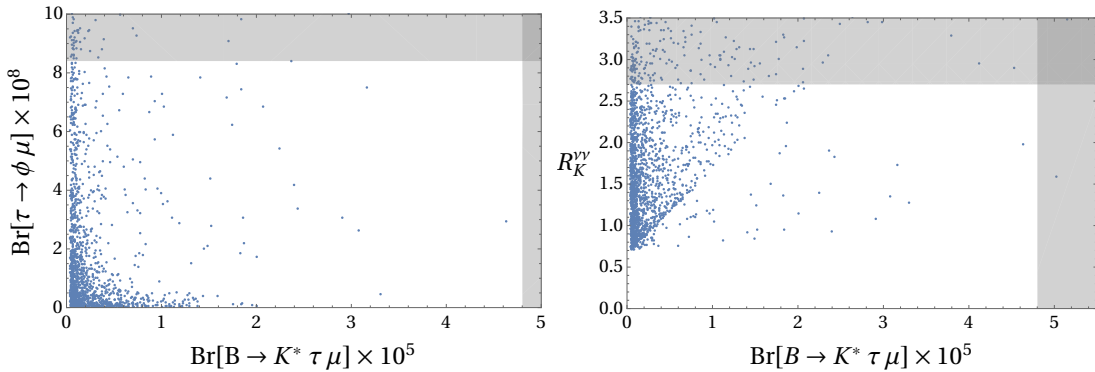


Figure 5.13: Correlations between $\text{Br}[B \rightarrow K^* \tau \mu]$ and $\text{Br}[\tau \rightarrow \phi \mu]$ (left) and between $\text{Br}[B \rightarrow K^* \tau \mu]$ and $R_K^{\nu\nu}$ (right). The blue points lie within the 1σ ranges of both the $b \rightarrow c\tau\nu$ and $b \rightarrow sl^+\ell^-$ fits, give an effect of less than 20% to $B_s - \bar{B}_s$ mixing and do not violate any other constraints. We scanned over the couplings $\{\lambda_{23,33}, \kappa_{23,33}, \hat{\lambda}_{23}\} \in [-1.5, 1.5]$, $\{\lambda_{22,32}, \kappa_{22,32}\} \in [-0.3, 0.3]$ and the LQ masses $M_1 = M_3 \equiv M \in [1, 2]$ TeV.

5.4.4 $b \rightarrow c\tau\nu$, $b \rightarrow sl^+\ell^-$ and a_μ

Finally, we aim at explaining the anomaly in the AMM of the muon in addition to $b \rightarrow c\tau\nu$ and $b \rightarrow sl^+\ell^-$ data. Accounting for δa_μ alone is possible and the only unavoidable effect occurs in $Z \rightarrow \mu^+\mu^-$, which can however only be tested at the FCC-ee [368]. Furthermore, explaining δa_μ together with $b \rightarrow sl^+\ell^-$ data does not pose a problem either since Φ_1 can account for δa_μ while Φ_3 can explain $b \rightarrow sl^+\ell^-$. However, once one wants to account for $b \rightarrow c\tau\nu$ data the situation becomes non-trivial. Scanning over 10 million points²¹ we found approximately

²¹First we individually scanned over two million points for couplings to muons only and over one million points for couplings to taus only. From each of both datasets roughly 3500 points passed all constraints while lying in the 1σ range of the global fits for $b \rightarrow sl^+\ell^-$ or $b \rightarrow c\tau\nu$, respectively. The combination of the two datasets was then used as seed for the final scan over all parameters.

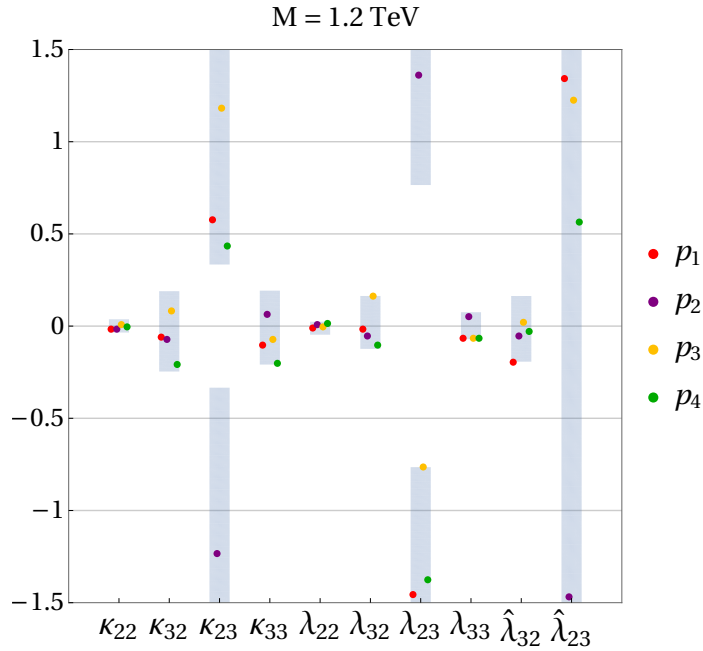


Figure 5.14: Possible ranges for the couplings of the points in parameter space which can explain all three anomalies at the 1σ level. We found these points by performing a parameter scan over the couplings $\{\lambda_{23,33}, \kappa_{23,33}, \hat{\lambda}_{23}\} \in [-1.5, 1.5]$, $\{\lambda_{22,32}, \kappa_{22,32}, \hat{\lambda}_{32}\} \in [-0.3, 0.3]$ and by setting the LQ masses $M_1 = M_3 = 1.2$ TeV. In color we depict the values of the four benchmark points given in Tab. 5.3. We found roughly 350 points that passed all constraints at the 95% C.L. while allowing for an effect in $B_s - \bar{B}_s$ mixing of up to 30%.

350 points which can explain all three anomalies at the same time. The corresponding range for the couplings of these 350 points is shown in Fig. 5.14. Only allowing for an effect of 20% in $B_s - \bar{B}_s$ mixing, the number of points is reduced to 40, where an effect as low as 10% is possible. In addition, we choose (out of these 350 points) four benchmark points, shown in color in Fig. 5.14. The predictions for the various observables for these benchmark points are given in Tab. 5.3. Interestingly, even though in general $\tau \rightarrow \mu\gamma$ represents the most restrictive constraint on our model in case one aims at an explanation of all three anomalies, we still find points that give a relatively small contribution of roughly one order of magnitude below the current experimental bound. The branching ratio of $B_s \rightarrow \tau^-\tau^+$ is enhanced by a factor of roughly 100 with respect to the SM, which also is below the current experimental bound. While the effects in $\Lambda_{\tau\nu}^W$ are small, they are always positive, reducing the slight tension in the effective $W\tau\nu$ coupling. The effects in $B \rightarrow K\tau\mu$ and $\tau \rightarrow \phi\mu$ range from being negligible to close to the current experimental bounds while effects in $\tau \rightarrow \mu ee$ and $\tau \rightarrow 3\mu$ lie roughly two orders of magnitude below the current experimental limit. Furthermore, the effects in $Z \rightarrow \tau^-\tau^+$ would clearly be measurable at an FCC-ee [357].

Update

In Ref. [369] it was pointed out that our benchmark points in Tab. 5.3 are in conflict with $D^0 - \bar{D}^0$ mixing. While this is true under the assumption of a vanishing SM contribution, we point out that with fine-tuning between the SM and the NP contribution our model is not excluded, as the SM effect can currently not be calculated. Furthermore, it was claimed that our points are in tension with $D_s \rightarrow \tau\nu$. While it is true that for points p_1 and p_2 in Tab. 5.3 a very slight tension with the experiment (below the 2σ level) is observed, the points p_3 and p_4 do

	κ_{22}	κ_{32}	κ_{23}	κ_{33}	λ_{22}	λ_{32}	λ_{23}	λ_{33}	$\hat{\lambda}_{32}$	$\hat{\lambda}_{23}$
● p_1	-0.019	-0.059	0.58	-0.11	-0.0082	-0.016	-1.46	-0.064	-0.19	1.34
● p_2	-0.017	-0.070	-1.23	0.066	0.0078	-0.055	1.36	0.052	-0.053	-1.47
● p_3	0.0080	0.081	1.18	-0.073	-0.0017	0.16	-0.76	-0.068	0.023	1.23
● p_4	-0.0032	-0.21	0.44	-0.20	0.014	-0.10	-1.38	-0.068	-0.032	0.57
	$C_9^{\mu\mu} = -C_{10}^{\mu\mu}$	$C_9^{\ell\ell}$	$\frac{R(D)}{R(D)_{\text{SM}}}$	$\frac{R(D^*)}{R(D^*)_{\text{SM}}}$	$\frac{B_s \rightarrow \tau\tau}{B_s \rightarrow \tau\tau}_{\text{SM}}$	$\tau \rightarrow \mu\gamma$ $\times 10^8$	δa_μ $\times 10^{11}$	$V_{cb}^e/V_{cb}^\mu - 1$ $\times 10^6$	$Z \rightarrow \tau\mu$ $\times 10^{10}$	
● p_1	-0.52	-0.21	1.15	1.10	59.88	4.35	207	291	0.117	
● p_2	-0.56	-0.28	1.14	1.10	99.76	0.766	199	448	2.38	
● p_3	-0.31	-0.31	1.14	1.09	112.5	3.62	255	17	0.129	
● p_4	-0.31	-0.31	1.13	1.11	112.5	0.734	230	934	45.6	
	$C_{SL}^{\tau\tau} = -4C_{TL}^{\tau\tau}$	$C_{VL}^{\tau\tau}$	$R_{\nu\nu}^{K^{(*)}}$	$\frac{\Delta m_{B_s}^{\text{NP}}}{\Delta m_{B_s}^{\text{SM}}}$	$B \rightarrow K\tau\mu$ $\times 10^5$	$\tau \rightarrow \phi\mu$ $\times 10^8$	$\tau \rightarrow \mu ee$ $\times 10^{11}$	$ \Lambda_{33}^{\text{LQ}}(0) $ $\times 10^5$	$\frac{\Delta_{33}^L(m_Z^2)}{\Lambda_{\text{SM}}^L \times 10^{-5}}$	
● p_1	0.023	0.040	2.33	0.1	0.512	1.27	44.94	1.11	-3.64	
● p_2	0.020	0.040	0.87	0.16	3.32	4.73	7.783	0.90	-3.02	
● p_3	0.023	0.037	1.08	0.19	4.07	1.00	37.89	0.89	-3.51	
● p_4	0.010	0.047	2.43	0.18	3.69	0.0021	18.60	3.12	-10.04	

Table 5.3: p_1 - p_4 are four benchmark points that can simultaneously explain all three flavor anomalies ($b \rightarrow s\ell^+\ell^-$, $b \rightarrow c\tau\nu$ and δa_μ) at the 1σ level and pass all other constraints at the 95% C.L.. Here we show the values for the fermion couplings, the results for $b \rightarrow s\ell^+\ell^-$, $b \rightarrow c\tau\nu$ and δa_μ as well as the predictions for several flavor observables which can be measured in the future. Note that the effect in $\tau \rightarrow 3\mu$ (not depicted here) is of comparable size as the one in $\tau \rightarrow \mu ee$. The LQ masses were set to $M = M_1 = M_3 = 1.2$ TeV.

not suffer from any tension at all. Nevertheless we decided to extend our analysis and present 4 new benchmark points in Tab. 5.4. In this scenario we neglected the coupling λ_{22} but used the coupling $\hat{\lambda}_{33}$ to tune $\tau \rightarrow \mu\gamma$ as suggested in Ref. [369]. In Fig. 5.15 we show the allowed range for the new benchmark points. Note that these benchmark points are favored compared to the ones in Ref. [369] by τ pair searches (see e.g. Ref. [176]) as our couplings to charm quarks are smaller and the LQ mass bigger.

5.5 Conclusions

Motivated by the intriguing hints for LFU violating NP in $R(D^{(*)})$, $b \rightarrow s\ell^+\ell^-$ processes and a_μ , we studied the flavor phenomenology of the LQ singlet-triplet model. We first defined the most general setup for the model, including an arbitrary number of LQ "generations" as well as mixing among them. With this at hand, we performed the matching of the model on the effective low energy theory and related the Wilson coefficients to flavor observables. Here, we included the potentially relevant loop effects, e.g. in $B_s - \bar{B}_s$ mixing, $b \rightarrow s\gamma$, LFU contributions to $C_9^{\ell\ell}$ and a_μ , as well as in modified Z and W couplings.

Our phenomenological analysis proceeded in three steps: First, we disregarded the anomalies related to muons and considered the possibility of explaining $R(D^{(*)})$ and the resulting implication for other observables. We found that, including only couplings to left-handed fermions, the size of the possible effect depends crucially on the mass of the LQ: the larger (smaller) the mass (couplings) the bigger the relative effect in $B_s - \bar{B}_s$. Together with $b \rightarrow s\nu\bar{\nu}$, this is the limiting factor here. For $M = 1$ TeV and values of κ_{33} up to ± 2 , a 20% effect in $R(D^{(*)})$ is possible, while for $M = 1.5$ TeV and $|\kappa_{33}| < 1$ only a 10% effect with respect to the SM can be generated (see Fig. 5.9). At the same time, an enhancement of $B_s \rightarrow \tau^+\tau^-$ of the order of 10^2 is predicted, which, via loop effects, leads to a LFU $C_9^{\ell\ell} \approx -0.3$. Once couplings to right-handed leptons are included, larger effects in $b \rightarrow c\tau\nu$ processes are possible and $R(D)/R(D)_{\text{SM}} > R(D^*)/R(D^*)_{\text{SM}}$ is predicted, see Figs. 5.11 and 5.12.

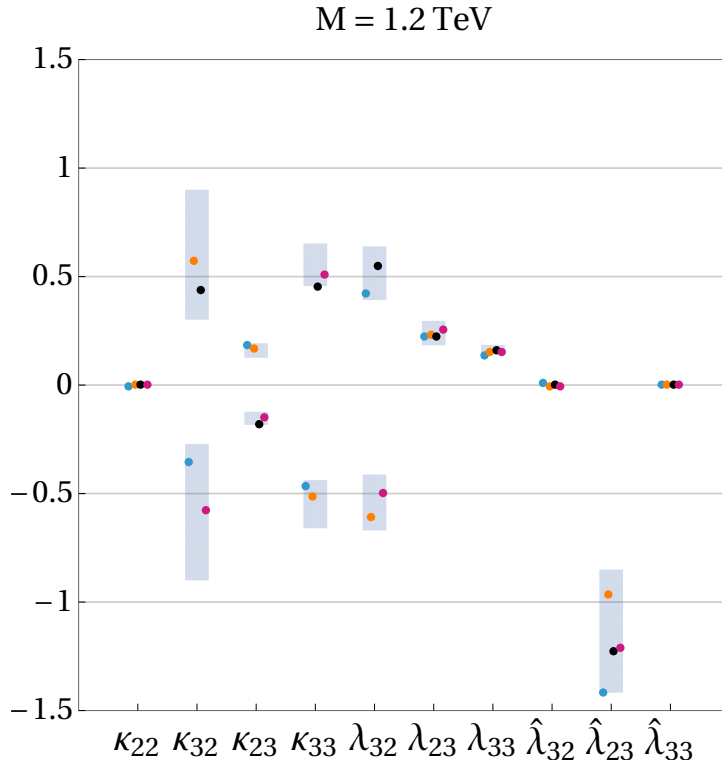


Figure 5.15: Possible ranges for the couplings of the points in parameter space which can explain three anomalies at the 1σ level and are compatible with $D^0 - \bar{D}^0$ mixing. We found these points by performing a parameter scan over the couplings $\{\lambda_{23,33}, \kappa_{23,33}, \hat{\lambda}_{23,33}\} \in [-1.5, 1.5]$, $\{\lambda_{32}, \kappa_{22,32}, \hat{\lambda}_{32}\} \in [-0.3, 0.3]$ and by setting the LQ masses $M_1 = M_3 = 1.2 \text{ TeV}$. In color we depict the values of the four benchmark points given in Tab. 5.4.

In a second step, we aimed at a simultaneous explanation of $b \rightarrow s\ell^+\ell^-$ data together with $R(D^{(*)})$. In this case, effects in lepton flavor violating processes like $B \rightarrow K\tau\mu$ and $\tau \rightarrow \phi\mu$ are predicted as shown in Fig. 5.13. These effects are still compatible with current data but can be tested soon by LHCb and BELLE II.

Finally, including in addition the AMM of the muon in the analysis is challenging since then right-handed couplings to muons are required which, together with the couplings needed to explain $R(D^{(*)})$, lead to chirally enhanced effects in $\tau \rightarrow \mu\gamma$. It is still possible to find a common solution to all three anomalies but only a small region of the parameter space can do this. Nonetheless, we identified four benchmark points which can achieve such a simultaneous explanation to all three anomalies (see Fig. 5.14).

In summary, the LQ singlet-triplet model is a prime candidate for explaining the flavor anomalies and we would like to emphasize that there is no renormalizable model on the market which is more minimal (only two new particles are needed here) and capable to address all three prominent flavor anomalies together.

Acknowledgments — We thank Christoph Greub for useful comments on the manuscript. The work of A.C. and D.M. is supported by a Professorship Grant (PP00P2_176884) of the Swiss National Science Foundation. The work of F.S. is supported by the Swiss National Foundation grant 200020_175449/1.

	κ_{22}	κ_{32}	κ_{23}	κ_{33}	λ_{32}	λ_{23}	λ_{33}	$\hat{\lambda}_{32}$	$\hat{\lambda}_{23}$	$\hat{\lambda}_{33}$
● p_5	-0.0024	-0.36	0.18	-0.47	0.42	0.23	0.14	0.0074	-1.42	0.0032
● p_6	0.0020	0.57	0.16	-0.52	-0.61	0.24	0.16	-0.0058	-0.97	0.003
● p_7	0.0022	0.44	-0.18	0.46	0.55	0.23	0.16	0.0055	-1.23	0.003
● p_8	-0.0017	-0.58	-0.15	0.51	-0.50	0.26	0.15	-0.0064	-1.21	0.003
	$C_9^{\mu\mu} = -C_{10}^{\mu\mu}$	$C_9^{\ell\ell}$	$\frac{R(D)}{R(D)_{\text{SM}}}$	$\frac{R(D^*)}{R(D^*)_{\text{SM}}}$	$\frac{B_s \rightarrow \tau\tau}{B_s \rightarrow \tau\tau _{\text{SM}}}$	$\frac{\tau \rightarrow \mu\gamma}{\times 10^8}$	$\frac{\delta a_\mu}{\times 10^{11}}$	$\frac{V_{cb}^e/V_{cb}^\mu - 1}{\times 10^6}$	$\frac{Z \rightarrow \tau\mu}{\times 10^8}$	
● p_5	-0.41	-0.30	1.21	1.11	107	4.23	210	-304	8.20	
● p_6	-0.54	-0.30	1.17	1.10	108	3.63	238	-224	25.19	
● p_7	-0.45	-0.29	1.21	1.11	105	3.07	202	-959	12.07	
● p_8	-0.48	-0.27	1.20	1.10	93	3.67	217	1194	24.86	
	$C_{SL}^{\tau\tau} = -4C_{TL}^{\tau\tau}$	$C_{VL}^{\tau\tau}$	$R_{\nu\nu}^{K^{(*)}}$	$\frac{\Delta m_{B_s}^{\text{NP}}}{\Delta m_{B_s}^{\text{SM}}}$	$\frac{B \rightarrow K\tau\mu}{\times 10^5}$	$\frac{\tau \rightarrow \phi\mu}{\times 10^{10}}$	$\frac{\tau \rightarrow \mu ee}{\times 10^9}$	$\frac{ \Lambda_{33}^{\text{LQ}}(0) }{\times 10^5}$	$\frac{\Delta_{33}^L(m_Z^2)}{\Lambda_{\text{SM}}^L \times 10^{-5}}$	
● p_5	0.054	0.028	1.34	0.19	1.88	0.21	2.74	13.76	-50.76	
● p_6	0.041	0.029	1.96	0.19	3.90	0.12	7.36	16.78	-62.07	
● p_7	0.052	0.029	1.69	0.19	2.86	0.18	3.85	12.80	-49.77	
● p_8	0.050	0.028	1.46	0.16	3.44	0.08	7.19	16.59	-60.97	

Table 5.4: Four benchmark points (p_5 - p_8) that simultaneously explain $b \rightarrow s\ell^+\ell^-$, $b \rightarrow c\tau\nu$ and δa_μ at the 1σ level and pass all other constraints at the 95% C.L.. Contrary to p_1 - p_4 , they do not yield a big effect in $D^0 - \bar{D}^0$ mixing and therefore do not require fine-tuning with the SM contribution. Again the LQ masses were chosen to be $M = M_1 = M_3 = 1.2$ TeV.

5.6 Appendix

In this appendix we define the loop functions appearing in the calculation of the observables and give the most general expressions for the Wilson coefficients, including multiple LQ generations (N singlets Φ_1 , M triplets Φ_3) and mixing among them. Let us recapitulate the definition of the masses:

- The singlet and triplet representations with electromagnetic charge $Q_{em} = -1/3$ have the masses m_K with $K = \{1, \dots, M + N\}$.
- The LQ with electromagnetic charge $Q_{em} = 2/3$ and $Q_{em} = -4/3$, stemming from the triplet representations, have the same masses \bar{m}_J with $J = \{1, \dots, M\}$.

5.6.1 Loop Functions

Throughout this article we used the loop functions C_0 and $D_{0,2}$, defined as

$$\begin{aligned}
\frac{i}{16\pi^2} C_0(m_0^2, m_1^2, m_2^2) &= \mu^{2\epsilon} \int \frac{d^D \ell}{(2\pi)^D} \frac{1}{(\ell^2 - m_0^2)(\ell^2 - m_1^2)(\ell^2 - m_2^2)}, \\
\frac{i}{16\pi^2} D_0(m_0^2, m_1^2, m_2^2, m_3^2) &= \mu^{2\epsilon} \int \frac{d^D \ell}{(2\pi)^D} \frac{1}{(\ell^2 - m_0^2)(\ell^2 - m_1^2)(\ell^2 - m_2^2)(\ell^2 - m_3^2)}, \\
\frac{i}{16\pi^2} D_2(m_0^2, m_1^2, m_2^2, m_3^2) &= \mu^{2\epsilon} \int \frac{d^D \ell}{(2\pi)^D} \frac{\ell^2}{(\ell^2 - m_0^2)(\ell^2 - m_1^2)(\ell^2 - m_2^2)(\ell^2 - m_3^2)},
\end{aligned} \tag{5.101}$$

with $D = 4 - 2\epsilon$.

5.6.2 $dd\ell\ell$

For $d_k \rightarrow d_j \ell_f^- \ell_i^+$ processes we match on the effective operators defined in Eq. (5.15). The tree-level contribution gives

$$C_{9,jk}^{fi} = -C_{10,jk}^{fi} = \frac{\sqrt{2}}{4G_F V_{td_k} V_{td_j}^*} \pi \sum_{J=1}^M \frac{\Gamma_{d_k \ell_i}^J \Gamma_{d_j \ell_f}^{J*}}{\bar{m}_J^2}, \quad (5.102)$$

while the loop calculations yield

$$\begin{aligned} C_7^{jk}(\mu_{\text{LQ}}) &= \frac{-\sqrt{2}}{4G_F V_{td_k} V_{td_j}^*} \left[\frac{1}{72} \sum_{K=1}^{N+M} \frac{\Gamma_{d_k \nu_i}^{L,K} \Gamma_{d_j \nu_i}^{L,K*}}{m_K^2} + \frac{5}{36} \sum_{J=1}^M \frac{\Gamma_{d_k \ell_i}^J \Gamma_{d_j \ell_i}^{J*}}{\bar{m}_J^2} \right], \\ C_8^{jk}(\mu_{\text{LQ}}) &= \frac{\sqrt{2}}{4G_F V_{td_k} V_{td_j}^*} \frac{1}{24} \left[\sum_{K=1}^{N+M} \frac{\Gamma_{d_k \nu_i}^{L,K} \Gamma_{d_j \nu_i}^{L,K*}}{m_K^2} + \sum_{J=1}^M \frac{\Gamma_{d_k \ell_i}^J \Gamma_{d_j \ell_i}^{J*}}{\bar{m}_J^2} \right], \\ C_{9,jk}^{ii}(\mu_{\text{LQ}}) &= \frac{\sqrt{2}}{216G_F V_{td_k} V_{td_j}^*} \left[\sum_{K=1}^{N+M} \frac{\Gamma_{d_k \nu_i}^{L,K} \Gamma_{d_j \nu_i}^{L,K*}}{m_K^2} + 2 \sum_{J=1}^M \frac{\Gamma_{d_k \ell_i}^J \Gamma_{d_j \ell_i}^{J*}}{\bar{m}_J^2} \left(14 + 9 \log \left(\frac{\mu_{\text{LQ}}^2}{\bar{m}_J^2} \right) \right) \right]. \end{aligned} \quad (5.103)$$

At the low scale of the processes, one has to include the effect of the diagram in the effective theory. This results in a so-called effective Wilson coefficient which also depends on the lepton mass in the loop and q^2

$$C_{9,jk}^{ii \text{ eff}}(\mu) = \frac{\sqrt{2}}{216G_F V_{td_k} V_{td_j}^*} \left[\sum_{K=1}^{N+M} \frac{\Gamma_{d_j \nu_i}^{L,K} \Gamma_{d_k \nu_i}^{L,K*}}{m_K^2} + 2 \sum_{J=1}^M \frac{\Gamma_{d_j \ell_i}^J \Gamma_{d_k \ell_i}^{J*}}{\bar{m}_J^2} \mathcal{F}(q^2, m_{\ell_i}^2, \bar{m}_J^2, \mu^2) \right], \quad (5.104)$$

with

$$\begin{aligned} \mathcal{F}(q^2, m_{\ell}^2, M^2, \mu^2) &= \frac{1}{q^2} \left(9q^2 \log \left(\frac{\mu^2}{M^2} \right) - q^2 - 36m_{\ell}^2 \right) \\ &\quad - \frac{18}{(q^2)^2 \mathcal{X}(m_{\ell}^2, q^2)} \left((q^2)^2 - 2m_{\ell}^2 q^2 - 8m_{\ell}^4 \right) \arctan \left(\frac{1}{\mathcal{X}(m_{\ell}^2, q^2)} \right), \end{aligned} \quad (5.105)$$

where we defined for convenience

$$\mathcal{X}(a, b) = \sqrt{\frac{4a^2}{b^2} - 1}. \quad (5.106)$$

5.6.3 $uu\gamma$ and EDM

We define the effective Hamiltonian as

$$\mathcal{H}_{\text{eff}}^{u\gamma} = C_{\gamma}^{jk} O_{\gamma}^{jk} + C_g^{jk} O_g^{jk} + C_T^{jk\tau} O_T^{jk\tau}, \quad (5.107)$$

with

$$\begin{aligned} O_{\gamma}^{jk} &= e [\bar{u}_j \sigma^{\mu\nu} P_R u_k] F_{\mu\nu}, \\ O_g^{jk} &= g_s [\bar{u}_j \sigma^{\mu\nu} P_R T^a u_k] G_{\mu\nu}^a, \\ O_T^{jk\tau} &= [\bar{u}_j \sigma_{\mu\nu} P_R u_k] [\bar{\tau} \sigma^{\mu\nu} P_R \tau], \end{aligned} \quad (5.108)$$

and obtain in the case of one generation of LQs and no mixing among them

$$\begin{aligned}
 C_\gamma^{jk}(\mu_{\text{LQ}}) &= \frac{1}{1152\pi^2} \left[7 \frac{m_{u_k} V_{kl}^* \lambda_{li} V_{jm} \lambda_{mi}^* + m_{u_j} \hat{\lambda}_{ki} \hat{\lambda}_{ji}^*}{M_1^2} - \frac{12m_{\ell_i} \hat{\lambda}_{ki} V_{jl} \lambda_{li}^*}{M_1^2} \left(4 + 3 \log \left(\frac{\mu_{\text{LQ}}^2}{M_1^2} \right) \right) \right. \\
 &\quad \left. + 3 \frac{m_{u_k} V_{kl}^* \kappa_{li} V_{jm} \kappa_{mi}^*}{M_3^2} \right], \\
 C_g^{jk}(\mu_{\text{LQ}}) &= -\frac{1}{384\pi^2} \left[\frac{m_{u_k} V_{kl}^* \lambda_{li} V_{jm} \lambda_{mi}^* + m_{u_j} \hat{\lambda}_{ki} \hat{\lambda}_{ji}^*}{M_1^2} + \frac{6m_{\ell_i} \hat{\lambda}_{ki} V_{jl} \lambda_{li}^*}{M_1^2} + \frac{3m_{u_k} V_{kl}^* \kappa_{li} V_{jm} \kappa_{mi}^*}{M_3^2} \right], \\
 C_T^{jk\tau}(\mu_{\text{LQ}}) &= \frac{V_{kl} \lambda_{l3}^* \hat{\lambda}_{j3}}{8M_1^2}.
 \end{aligned} \tag{5.109}$$

The contributing diagram is depicted in Fig. 5.1. For the neutron EDM we set $j = k = 1$ and reproduce (setting $m_u = 0$) our result from [47], where also the relevant RGE can be found. In case of LQ mixing, we have

$$\begin{aligned}
 C_7^{jk}(\mu_{\text{LQ}}) &= \frac{\sqrt{2}}{4G_F} \frac{1}{72} \left[2 \sum_{J=1}^M \frac{\Gamma_{u_k \nu_i}^J \Gamma_{u_j \nu_i}^{J*}}{\bar{m}_J^2} - \frac{7}{m_{u_k}} \sum_{K=1}^{M+N} \frac{m_{u_k} \Gamma_{u_k \ell_i}^{L,K} \Gamma_{u_j \ell_i}^{L,K*} + m_{u_j} \Gamma_{u_k \ell_i}^{R,K} \Gamma_{u_j \ell_i}^{R,K*}}{m_K^2} \right. \\
 &\quad \left. + 12 \sum_{K=1}^{M+N} \frac{m_{\ell_i}}{m_{u_k}} \frac{\Gamma_{u_k \ell_i}^{R,K} \Gamma_{u_j \ell_i}^{L,K*}}{m_K^2} \left(4 + 3 \log \left(\frac{\mu_{\text{LQ}}^2}{m_K^2} \right) \right) \right], \\
 C_8^{jk}(\mu_{\text{LQ}}) &= \frac{\sqrt{2}}{4G_F} \frac{1}{24} \left[\sum_{J=1}^M \frac{\Gamma_{u_k \nu_i}^J \Gamma_{u_j \nu_i}^{J*}}{\bar{m}_J^2} + \frac{1}{m_{u_k}} \sum_{K=1}^{M+N} \frac{m_{u_k} \Gamma_{u_k \ell_i}^{L,K} \Gamma_{u_j \ell_i}^{L,K*} + m_{u_j} \Gamma_{u_k \ell_i}^{R,K} \Gamma_{u_j \ell_i}^{R,K*}}{m_K^2} \right. \\
 &\quad \left. + 6 \sum_{K=1}^{M+N} \frac{m_{\ell_i}}{m_{u_k}} \frac{\Gamma_{u_k \ell_i}^{R,K} \Gamma_{u_j \ell_i}^{L,K*}}{m_K^2} \right], \\
 C_T^{jk\tau} &= \frac{\Gamma_{u_k \ell_3}^{L,K*} \Gamma_{u_j \ell_3}^{R,K}}{8m_K^2}.
 \end{aligned} \tag{5.110}$$

5.6.4 $d_{uL}\nu$

For the effective Hamiltonian defined in Eq. (5.41) we find

$$\begin{aligned}
 C_{VL,jk}^{fi} &= \frac{-\sqrt{2}}{8G_F V_{u_j d_k}} \sum_{K=1}^{M+N} \frac{\Gamma_{d_k \nu_i}^K \Gamma_{u_j \ell_f}^{L,K*}}{m_K^2}, \\
 C_{SL,jk}^{fi} &= -4C_{TL,jk}^{fi} = \frac{\sqrt{2}}{8G_F V_{u_j d_k}} \sum_{K=1}^{M+N} \frac{\Gamma_{d_k \nu_i}^K \Gamma_{u_j \ell_f}^{R,K*}}{m_K^2}.
 \end{aligned} \tag{5.111}$$

5.6.5 $dd\nu\nu$ and $B_s - \bar{B}_s$ Mixing

The effective Hamiltonians for $dd\nu\nu$ and $B_s - \bar{B}_s$ mixing are given by Eq. (5.38) and Eq. (5.51), respectively. We find for $b \rightarrow s\nu\bar{\nu}$

$$C_{L,jk}^{fi} = \frac{\sqrt{2}}{4G_F V_{td_k} V_{td_j}^*} \frac{\pi}{\alpha} \sum_{K=1}^{N+M} \frac{\Gamma_{d_k\nu_i}^K \Gamma_{d_j\nu_f}^{K*}}{m_K^2}, \quad (5.112)$$

and for $B_s - \bar{B}_s$ mixing

$$C_1 = \frac{-1}{128\pi^2} \left(\sum_{\{K,P\}=1}^{N+M} \Gamma_{d_2\nu_i}^{K*} \Gamma_{d_3\nu_j}^K \Gamma_{d_2\nu_j}^{P*} \Gamma_{d_3\nu_i}^P C_0(0, m_K^2, m_P^2) + \sum_{\{J,Q\}=1}^M \Gamma_{d_2\ell_i}^{Q*} \Gamma_{d_3\ell_j}^Q \Gamma_{d_2\ell_j}^{J*} \Gamma_{d_3\ell_i}^J C_0(0, \bar{m}_Q^2, \bar{m}_J^2) \right). \quad (5.113)$$

5.6.6 $\ell\ell\gamma$, $Z\ell\ell$ and $Z\nu\nu$

In case of $\ell_i \rightarrow \ell_f\gamma$ transitions and the effective Hamiltonian given by Eq. (5.58) we have

$$C_{\ell_f\ell_i}^L = - \sum_{K=1}^{N+M} \left[\frac{m_{\ell_f} \Gamma_{u_j\ell_i}^{L,K} \Gamma_{u_j\ell_f}^{L,K*} + m_{\ell_i} \Gamma_{u_j\ell_i}^{R,K} \Gamma_{u_j\ell_f}^{R,K*}}{28m_K^2} - \frac{m_{u_j} \Gamma_{u_j\ell_i}^{L,K} \Gamma_{u_j\ell_f}^{R,K*}}{4m_K^2} \left(7 + 4 \log \left(\frac{m_{u_j}^2}{m_K^2} \right) \right) \right] + \sum_{J=1}^M \frac{m_{\ell_f} \Gamma_{d_j\ell_i}^J \Gamma_{d_j\ell_f}^{J*}}{4\bar{m}_J^2}, \quad (5.114)$$

with $N_c = 3$ already included. For the off-shell photon, as given by the amplitude in Eq. (5.61), we obtain

$$\begin{aligned} \tilde{\Xi}_{\ell_f\ell_i}^L &= \frac{-N_c}{576\pi^2} \left[\delta_{fi} + \sum_{K=1}^{N+M} \frac{\Gamma_{u_j\ell_f}^{L,K*} \Gamma_{u_j\ell_i}^{L,K}}{m_K^2} F\left(\frac{m_{u_j}^2}{m_K^2}\right) + \sum_{J=1}^M \frac{\Gamma_{d_j\ell_i}^{J*} \Gamma_{d_j\ell_f}^J}{\bar{m}_J^2} G\left(\frac{m_{d_j}^2}{\bar{m}_J^2}\right) \right], \\ \tilde{\Xi}_{\ell_f\ell_i}^R &= \frac{-N_c}{576\pi^2} \left[\delta_{fi} + \sum_{K=1}^{M+N} \frac{\Gamma_{u_j\ell_f}^{R,K*} \Gamma_{u_j\ell_i}^{R,K}}{m_K^2} F\left(\frac{m_{u_j}^2}{m_K^2}\right) \right], \end{aligned} \quad (5.115)$$

where the loop functions $F(y)$ and $G(y)$ are defined in Eq. (5.63).

For Z decays, where the amplitude is given by Eq. (5.68) and the $\Delta_{fi}^{L(R)}$ are introduced in Eq. (5.69), we find

$$\begin{aligned} \Delta_{fi}^L(q^2) &= \sum_{K=1}^{N+M} \Gamma_{u_j\ell_f}^{L,K*} \Gamma_{u_j\ell_i}^{L,K} \mathcal{F}_L(m_{u_j}^2, q^2, m_K^2) + \sum_{J=1}^M \Gamma_{d_j\ell_f}^{J*} \Gamma_{d_j\ell_i}^J \mathcal{G}_L(q^2, \bar{m}_J^2), \\ \Delta_{fi}^R(q^2) &= \sum_{K=1}^{N+M} \Gamma_{u_j\ell_f}^{R,K*} \Gamma_{u_j\ell_i}^{R,K} \mathcal{F}_R(m_{u_j}^2, q^2, m_K^2), \end{aligned} \quad (5.116)$$

with

$$\begin{aligned}
 \mathcal{F}_L(m_u^2, q^2, M^2) &= \frac{N_c}{864\pi^2 M^2} \left((3q^2(4s_w^2 - 3) + 27m_u^2) \log\left(\frac{m_u^2}{M^2}\right) - s_w^2(5q^2 + 48m_u^2) \right. \\
 &\quad \left. + 3(q^2 + 3m_u^2) + 6\mathcal{X}(m_u^2, q^2) (4s_w^2(q^2 + 2m_u^2) - 3q^2 + 3m_u^2) \arctan\left(\frac{1}{\mathcal{X}(m_u^2, q^2)}\right) \right), \\
 \mathcal{G}_L(q^2, M^2) &= -\frac{N_c q^2}{864\pi^2 M^2} \left((6s_w^2 - 9) \log\left(\frac{q^2}{M^2}\right) + 2s_w^2(1 - 3i\pi) + 9i\pi \right), \\
 \mathcal{F}_R(m_u^2, q^2, M^2) &= \frac{N_c}{864\pi^2 M^2} \left((12s_w^2 q^2 - 27m_u^2) \log\left(\frac{m_u^2}{M^2}\right) - s_w^2(5q^2 + 48m_u^2) + 27m_u^2 \right. \\
 &\quad \left. + 6\mathcal{X}(m_u^2, q^2) (4s_w^2(q^2 + 2m_u^2) - 9m_u^2) \arctan\left(\frac{1}{\mathcal{X}(m_u^2, q^2)}\right) \right),
 \end{aligned} \tag{5.117}$$

again using

$$\mathcal{X}(a^2, b^2) = \sqrt{\frac{4a^2}{b^2} - 1}. \tag{5.118}$$

At the level of the effective couplings ($q^2 = 0$) we have

$$\begin{aligned}
 \Delta_{fi}^L(0) &= \sum_{K=1}^{N+M} \Gamma_{u_3\ell_f}^{L,K*} \Gamma_{u_3\ell_i}^{L,K} \mathcal{F}_L(m_t^2, 0, m_K^2), \\
 \Delta_{fi}^R(0) &= \sum_{K=1}^{N+M} \Gamma_{u_3\ell_f}^{R,K*} \Gamma_{u_3\ell_i}^{R,K} \mathcal{F}_R(m_t^2, 0, m_K^2).
 \end{aligned} \tag{5.119}$$

The functions $\mathcal{F}_{L/R}$ then become

$$\mathcal{F}_L(m_t^2, 0, M^2) = \frac{m_t^2 N_c}{32\pi^2 M^2} \left(1 + \log\left(\frac{m_t^2}{M^2}\right) \right) = -\mathcal{F}_R(m_t^2, 0, M^2). \tag{5.120}$$

The amplitude for $Z \rightarrow \nu\bar{\nu}$ is again given by Eq. (5.68). For the $\Sigma_{fi}^{\text{LQ}}(q^2)$, introduced in Eq. (5.69), we obtain

$$\Sigma_{fi}^{\text{LQ}}(q^2) = \sum_{K=1}^{N+M} \Gamma_{d_j\nu_f}^{L,K*} \Gamma_{d_j\nu_i}^{L,K} \mathcal{H}_1(q^2, m_K^2) + \sum_{J=1}^M \Gamma_{u_j\nu_f}^{J*} \Gamma_{u_j\nu_i}^J \mathcal{H}_2(m_{u_j}^2, q^2, \bar{m}_J^2), \tag{5.121}$$

with

$$\begin{aligned}
 \mathcal{H}_1(q^2, M^2) &= \frac{N_c q^2}{864\pi^2 M^2} \left(3(3 - 2s_w^2) \log\left(\frac{q^2}{M^2}\right) - 3i\pi(3 - 2s_w^2) - 3 + s_w^2 \right), \\
 \mathcal{H}_2(m_u^2, q^2, M^2) &= \frac{N_c}{864\pi^2 M^2} \left(3((4s_w^2 - 3)q^2 + 9m_u^2) \log\left(\frac{m_u^2}{M^2}\right) - 2s_w^2(q^2 + 24m_u^2) \right. \\
 &\quad \left. + 9m_u^2 + 6\mathcal{X}(m_u^2, q^2) (4s_w^2(q^2 + 2m_u^2) - 3q^2 + 3m_u^2) \arctan\left(\frac{1}{\mathcal{X}(m_u^2, q^2)}\right) \right),
 \end{aligned} \tag{5.122}$$

where we again neglected to down-type quark masses, but kept the dependencies on the up-type ones due to the heavy top quark. If we work with effective couplings instead of full amplitudes,

the results are

$$\Sigma_{fi}^{\text{LQ}}(0) = \sum_{J=1}^M \Gamma_{u_3\nu_f}^{J*} \Gamma_{u_3\nu_i}^J \mathcal{H}_2(m_t^2, 0, \bar{m}_J^2), \quad (5.123)$$

with

$$\mathcal{H}_2(m_t^2, 0, M^2) = \frac{N_c m_t^2}{32\pi^2 M^2} \left(1 + \log\left(\frac{m_t^2}{M^2}\right) \right). \quad (5.124)$$

5.6.7 $W\ell\nu$

For the $\Lambda_{fi}^{\text{LQ}}(q^2)$, defined in Eq. (5.80) and Eq. (5.81), we obtain

$$\begin{aligned} \Lambda_{fi}^{\text{LQ}}(q^2) = & \frac{N_c}{64\pi^2} \left\{ \sum_{K=1}^{N+M} \left[V_{u_j d_k}^* \Gamma_{u_j \ell_f}^{L,K*} \Gamma_{d_k \nu_i}^{L,K} \mathcal{F}_W(m_{u_j}^2, q^2, m_K^2) + \Gamma_{u_3 \ell_f}^{L,K*} \Gamma_{u_3 \ell_i}^{L,K} \frac{m_t^2}{m_K^2} \right] \right. \\ & + \sum_{J=1}^M \Gamma_{u_3\nu_f}^{J*} \Gamma_{u_3\nu_i}^J \frac{m_t^2}{\bar{m}_J^2} + 2\sqrt{2} \sum_{K=1}^{N+M} \sum_{J=1}^M W_{J+N,K} \Gamma_{u_3 \ell_j}^{L,K*} \Gamma_{u_3 \nu_i}^J \frac{m_t^2}{m_K^2 - \bar{m}_J^2} \log\left(\frac{m_K^2}{\bar{m}_J^2}\right) \\ & \left. - \frac{2\sqrt{2}}{3} \sum_{K=1}^{N+M} \sum_{J=1}^M q^2 \left(W_{J+N,K} \Gamma_{u_j \ell_f}^{L,K*} \Gamma_{u_j \nu_i}^J - W_{J+N,K}^* \Gamma_{d_k \ell_f}^{L,K*} \Gamma_{d_k \nu_i}^J \right) \mathcal{H}_W(m_K^2, \bar{m}_J^2) \right\} \end{aligned} \quad (5.125)$$

with

$$\begin{aligned} \mathcal{F}_W(m_u^2, q^2, M^2) = & \frac{1}{9M^2} \left[6(2q^2 - 3m_u^2) \log\left(\frac{m_u^2}{M^2}\right) - (4q^2 - 3m_u^2 - \frac{6m_u^4}{q^2}) \right. \\ & \left. + 6\left(2q^2 - 3m_u^2 + \frac{m_u^6}{(q^2)^2}\right) \log\left(1 - \frac{q^2}{m_u^2}\right) \right] \\ \mathcal{H}_W(x^2, y^2) = & \frac{x^2 + y^2}{(x^2 - y^2)^2} - \frac{2x^2 y^2}{(x^2 - y^2)^3} \log\left(\frac{x^2}{y^2}\right). \end{aligned} \quad (5.126)$$

Additionally, there are terms that do not trivially decouple, however, they vanish in the decoupling limit. They read

$$\begin{aligned} \bar{\Lambda}_{fi}^{\text{LQ}}(\mu^2) = & \frac{N_c}{64\pi^2} \left\{ \sum_{K=1}^{N+M} \left[-V_{u_j d_k}^* \Gamma_{u_j \ell_f}^{L,K*} \Gamma_{d_k \nu_i}^{L,K} \left(2\log\left(\frac{\mu^2}{m_K^2}\right) + 1 \right) \right. \right. \\ & \left. \left. - \left(\Gamma_{u_j \ell_f}^{L,K*} \Gamma_{u_j \ell_i}^{L,K} + \Gamma_{d_j \nu_f}^{L,K*} \Gamma_{d_j \nu_i}^{L,K} \right) \left(\log\left(\frac{\mu^2}{m_K^2}\right) + \frac{1}{2} \right) \right] \right. \\ & - \sum_{J=1}^M \left(\Gamma_{u_j \nu_f}^{J*} \Gamma_{u_j \nu_i}^J + \Gamma_{d_j \ell_f}^{J*} \Gamma_{d_j \ell_i}^J \right) \left(\log\left(\frac{\mu^2}{\bar{m}_J^2}\right) + \frac{1}{2} \right) \\ & \left. - \sqrt{2} \sum_{J=1}^M \sum_{K=1}^{N+M} \left[W_{J+N,K} \Gamma_{u_j \ell_f}^{L,K*} \Gamma_{u_j \nu_i}^J \left(2\log\left(\frac{\mu^2}{\bar{m}_J^2}\right) - \frac{2m_K^2}{m_K^2 - \bar{m}_J^2} \log\left(\frac{m_K^2}{\bar{m}_J^2}\right) + 3 \right) \right. \right. \\ & \left. \left. - W_{J+N,K}^* \Gamma_{d_k \ell_f}^{L,K*} \Gamma_{d_k \nu_i}^{L,K} \left(2\log\left(\frac{\mu^2}{m_K^2}\right) - \frac{2\bar{m}_J^2}{m_K^2 - \bar{m}_J^2} \log\left(\frac{m_K^2}{\bar{m}_J^2}\right) + 3 \right) \right] \right\}. \end{aligned} \quad (5.127)$$

Note that the scale dependence μ drops out exactly. If we work at the level of effective couplings, we have

$$\Lambda_{fi}^{\text{LQ}}(0) = \frac{N_c m_t^2}{64\pi^2} \left[\sum_{K=1}^{N+M} \left(\frac{\Gamma_{u_3\ell_f}^{L,K*} \Gamma_{u_3\ell_i}^{L,K}}{m_K^2} - \frac{2V_{u_3 d_k}^* \Gamma_{d_k\nu_i}^{L,K} \Gamma_{u_3\ell_f}^{L,K*}}{m_K^2} \log\left(\frac{m_t^2}{m_K^2}\right) \right) \right. \\ \left. + \sum_{J=1}^M \frac{\Gamma_{u_3\nu_f}^{J*} \Gamma_{u_3\nu_i}^J}{\bar{m}_J^2} + 2\sqrt{2} \sum_{K=1}^{N+M} \sum_{J=1}^M W_{J+N,K} \frac{\Gamma_{u_3\ell_f}^{L,K*} \Gamma_{u_3\nu_i}^J}{m_K^2 - \bar{m}_J^2} \log\left(\frac{m_K^2}{\bar{m}_J^2}\right) \right]. \quad (5.128)$$

In the limit of no LQ mixing, the loop functions used in Eq. (5.82) become

$$\mathcal{F}_1(m_u^2, q^2, M^2) = \mathcal{F}_W(m_u^2, q^2, M^2) + \frac{m_u^2}{M^2} \\ \mathcal{F}_2(m_u^2, q^2, M^2) = \mathcal{F}_W(m_u^2, q^2, M^2) - \frac{m_u^2}{M^2}. \quad (5.129)$$

5.6.8 $\tau \rightarrow 3\mu$, $\tau \rightarrow \mu e^+ e^-$ and $\mu \rightarrow 3e$

The relevant effective Hamiltonian is given in Eq. (5.86). The contributions of the photon and Z penguin diagrams are given by Eq. (5.88) and Eq. (5.90), respectively. Now we use the effective couplings as defined in Eq. (5.115) (photon) and Eq. (5.116) (Z boson).

Finally, we have the box diagrams. Contrary to the vector current operators, the scalar operators $O_{\ell\ell\ell}^S$ are always proportional to m_q^2/M_{LQ}^2 . Therefore, we only consider contributions from the top quark. The box contributions read

$$C_{abfi}^{VLL} = \frac{-N_c}{256\pi^2} \sum_{\{K,P\}=1}^{N+M} \left(\Gamma_{u_k\ell_a}^{L,P*} \Gamma_{u_k\ell_b}^{L,K} \Gamma_{u_j\ell_f}^{L,K*} \Gamma_{u_j\ell_i}^{L,P} + \Gamma_{u_j\ell_a}^{L,K*} \Gamma_{u_k\ell_b}^{L,K} \Gamma_{u_k\ell_f}^{L,P*} \Gamma_{u_j\ell_i}^{L,P} \right) D_2(m_{u_k}^2, m_{u_j}^2, m_K^2, m_P^2) \\ - \frac{N_c}{256\pi^2} \sum_{\{J,Q\}=1}^M \left(\Gamma_{d_k\ell_a}^{Q*} \Gamma_{d_k\ell_b}^J \Gamma_{d_j\ell_f}^{J*} \Gamma_{d_j\ell_i}^Q + \Gamma_{d_j\ell_a}^{J*} \Gamma_{d_k\ell_b}^J \Gamma_{d_k\ell_f}^{Q*} \Gamma_{d_j\ell_i}^Q \right) C_0(0, \bar{m}_J^2, \bar{m}_Q^2), \\ C_{abfi}^{VLR} = \frac{-N_c}{128\pi^2} \sum_{\{K,P\}=1}^{N+M} \left[\Gamma_{u_k\ell_a}^{L,P*} \Gamma_{u_k\ell_b}^{L,K} \Gamma_{u_j\ell_f}^{R,K*} \Gamma_{u_j\ell_i}^{R,P} D_2(m_{u_k}^2, m_{u_j}^2, m_K^2, m_P^2) \right. \\ \left. - 2\Gamma_{u_3\ell_a}^{L,K*} \Gamma_{u_3\ell_b}^{L,K} \Gamma_{u_3\ell_f}^{R,P*} \Gamma_{u_3\ell_i}^{R,P} m_t^2 D_0(m_t^2, m_t^2, m_K^2, m_P^2) \right], \\ C_{abfi}^{SLL} = \frac{-m_t^2 N_c}{64\pi^2} \sum_{\{K,P\}=1}^{N+M} \left(2\Gamma_{u_3\ell_a}^{R,P*} \Gamma_{u_3\ell_b}^{L,K} \Gamma_{u_3\ell_f}^{R,K*} \Gamma_{u_3\ell_i}^{L,P} - \Gamma_{u_3\ell_a}^{R,K*} \Gamma_{u_3\ell_b}^{L,K} \Gamma_{u_3\ell_f}^{R,P*} \Gamma_{u_3\ell_i}^{L,P} \right) D_0(m_t^2, m_t^2, m_K^2, m_P^2). \quad (5.130)$$

Again, $C_{abfi}^{V/S RL(RR)}$ are obtained from $C_{abfi}^{V/S LR(LL)}$ by interchanging L and R .

5.6.9 $\tau \rightarrow \ell\nu\bar{\nu}$ and $\mu \rightarrow e\nu\bar{\nu}$

As it was the case for the previous results, we consider the top as the only non-zero quark mass and in cases where the result is proportional to the quark mass (squared), we directly write the result in terms of the top. The effective Hamiltonian for the process is given in Eq. (5.94). The

box diagrams read

$$\begin{aligned}
 D_{\ell_a \ell_b}^{L,fi} = & -\frac{N_c}{64\pi^2} \left\{ \sum_{\{K,P\}=1}^{N+M} \Gamma_{u_k \ell_a}^{L,P*} \Gamma_{u_k \ell_b}^{L,K} \Gamma_{d_j \nu_f}^{L,K*} \Gamma_{d_j \nu_i}^{L,P} C_0(m_{u_k}^2, m_K^2, m_P^2) \right. \\
 & + \sum_{K=1}^{N+M} \sum_{J=1}^M \left[\Gamma_{u_j \ell_a}^{L,K*} \Gamma_{u_k \ell_b}^{L,K} \Gamma_{u_k \nu_f}^{J*} \Gamma_{u_j \nu_i}^J D_2(m_{u_k}^2, m_{u_j}^2, m_K^2, \bar{m}_J^2) \right. \\
 & \left. \left. + \Gamma_{d_j \ell_a}^{J*} \Gamma_{d_k \ell_b}^J \Gamma_{d_k \nu_f}^{L,K*} \Gamma_{d_j \nu_i}^{L,K} C_0(0, \bar{m}_J^2, m_K^2) \right] \right\}, \quad (5.131)
 \end{aligned}$$

$$\begin{aligned}
 D_{\ell_a \ell_b}^{R,fi} = & -\frac{N_c}{64\pi^2} \left\{ \sum_{\{K,P\}=1}^{N+M} \Gamma_{u_k \ell_a}^{R,P*} \Gamma_{u_k \ell_b}^{R,K} \Gamma_{d_j \nu_f}^{L,K*} \Gamma_{d_j \nu_i}^{L,P} C_0(m_{u_k}^2, m_K^2, m_P^2) \right. \\
 & \left. - 2 \sum_{K=1}^{N+M} \sum_{J=1}^M \Gamma_{u_3 \ell_a}^{R,K*} \Gamma_{u_3 \ell_b}^{R,K} \Gamma_{u_3 \nu_f}^{J*} \Gamma_{u_3 \nu_i}^J m_t^2 D_0(m_t^2, m_t^2, m_K^2, \bar{m}_J^2) \right\}.
 \end{aligned}$$

The contributions of the W and Z penguins are given by Eq. (5.96) and Eq. (5.97), respectively. Now the effective couplings from Eq. (5.125), Eq. (5.116) and Eq. (5.121) have to be used.

Chapter 6

Leptoquarks in Oblique Corrections and Higgs Signal Strength: Status and Prospects

published in

JHEP 11 (2020) 094

arXiv: 2006.10758 [hep-ph]

Leptoquarks in Oblique Corrections and Higgs Signal Strength: Status and Prospects

Andreas Crivellin

Paul Scherrer Institut, CH-5232 Villigen PSI, Switzerland

CERN Theory Division, CH-1211 Geneva 23, Switzerland

Physik-Institut, Universität Zürich, Winterthurerstrasse 190, CH-8057 Zürich, Switzerland

Dario Müller

Paul Scherrer Institut, CH-5232 Villigen PSI, Switzerland

Physik-Institut, Universität Zürich, Winterthurerstrasse 190, CH-8057 Zürich, Switzerland

Francesco Saturnino

Albert Einstein Center for Fundamental Physics, Institute for Theoretical Physics, University of Bern, CH-3012 Bern, Switzerland

Leptoquarks (LQs) are predicted within Grand Unified Theories and are well motivated by the current flavor anomalies. In this article we investigate the impact of scalar LQs on Higgs decays and oblique corrections as complementary observables in the search for them. Taking into account all five LQ representations under the Standard Model gauge group and including the most general mixing among them, we calculate the effects in $h \rightarrow \gamma\gamma$, $h \rightarrow gg$, $h \rightarrow Z\gamma$ and the Peskin-Takeuchi parameters S , T and U . We find that these observables depend on the same Lagrangian parameters, leading to interesting correlations among them. While the current experimental bounds only yield weak constraints on the model, these correlations can be used to distinguish different LQ representations at future colliders (ILC, CLIC, FCC-ee and FCC-hh), whose discovery potential we are going to discuss.

6.1 Introduction

Leptoquarks (LQs) are particles which have a specific interaction vertex, connecting a lepton with a quark. They are predicted in Grand Unified Theories [178, 370–372] and were systematically classified in Ref. [147] into ten possible representations under the Standard Model (SM) gauge group (five scalar and five vector particles). In recent years, LQs experienced a renaissance due to the emergence of the flavor anomalies. In short, hints for new physics (NP) in $R(D^{(*)})$ [104, 105, 109–112], $b \rightarrow sl^+\ell^-$ [78, 79, 83, 84, 373, 374] and a_μ [123] emerged, with a significance of $> 3\sigma$ [103, 119–122], $> 5\sigma$ [88, 92, 97–101, 209] and $> 3\sigma$ [124], respectively. It has been shown that LQs can explain $b \rightarrow sl^+\ell^-$ data [45, 46, 48, 149, 151, 153, 156, 171–177, 180, 184, 213, 253, 317, 318, 332, 333, 361, 375, 376], $R(D^{(*)})$ [45, 47, 48, 149, 151–153, 155, 171–173, 175–177, 180, 184, 211–213, 232, 233, 236, 238–247, 249, 250, 287, 309, 311, 317, 318, 320–327, 375–378] and/or a_μ [48, 238, 241, 243, 277–286, 309–314, 368, 375, 379, 380].

This strong motivation for LQs makes it also interesting to search for their signatures in other observables. Complementary to direct LHC searches [274, 363–367, 381–388], oblique electroweak (EW) parameters (S and T parameters [389, 390]) and the corrections to (effective on-shell) couplings of the SM Higgs to photons ($h\gamma\gamma$), Z and photon ($hZ\gamma$) and gluons (hgg) allow to test LQ interactions with the Higgs, independently of the LQ couplings to fermions. In this context, LQs were briefly discussed in Ref. [391] based on analogous MSSM calculations [392–394], simplified model analysis [395–398], vacuum stability [399], LQ production at hadron

	Φ_1	$\tilde{\Phi}_1$	Φ_2	$\tilde{\Phi}_2$	Φ_3
\mathcal{G}_{SM}	$\left(3, 1, -\frac{2}{3}\right)$	$\left(3, 1, -\frac{8}{3}\right)$	$\left(3, 2, \frac{7}{3}\right)$	$\left(3, 2, \frac{1}{3}\right)$	$\left(3, 3, -\frac{2}{3}\right)$

Table 6.1: LQ representations under the SM gauge group.

colliders [400] and Higgs pair production [401]. In addition, Ref. [402] recently studied LQs in Higgs production and Ref. [403] considered $h \rightarrow \gamma\gamma$, while Ref. [404] performed the matching in the singlet-triplet model [243]. However, none of these analyses considered more than a single LQ representation at a time. The situation is similar concerning the S and T parameter. This was also briefly discussed in Ref. [391], based on simplified model calculations [405] and an analysis discussing only the $SU(2)_L$ doublet LQs [406]. Most importantly, the unavoidable correlations between Higgs couplings to gauge bosons and the oblique parameters were not considered so far. Importantly, these observables can be measured much more precisely at future colliders such as the ILC [407], CLIC [408], and the FCC [357, 409]. Therefore, it is interesting to examine their estimated constraining power and discovery potential.

In this article we will calculate the one-loop effects of LQs in oblique corrections, $h\gamma\gamma$, $hZ\gamma$ and hgg , taking into account all five scalar LQ representations and the complete set of their interactions with the Higgs. In the next section we will define our setup and conventions before we turn to the calculation of the S and T parameters in Sec. 6.3 and to $h\gamma\gamma$, $hZ\gamma$ and hgg in Sec. 6.4. We then perform our phenomenological analysis, examining the current status and future prospects for these observables in Sec. 6.5, before we conclude in Sec. 6.6. An appendix provides useful analytic (perturbative) expressions for LQ couplings and results for the loop functions.

6.2 Setup and Conventions

There are ten possible representations of LQs under the SM gauge group [147]. While for vector LQs a Higgs mechanism is necessary to render the model renormalizable, scalar LQs can simply be added to the SM. Since we are interested in loop effects in this work, we will focus on the latter ones in the following.

The five different scalar LQs transform under the SM gauge group

$$\mathcal{G}_{\text{SM}} = SU(3)_c \times SU(2)_L \times U(1)_Y \quad (6.1)$$

as given in Table 6.1.

We defined the hypercharge Y such that the electromagnetic charge is given by

$$Q = \frac{1}{2}Y + T_3, \quad (6.2)$$

with T_3 representing the third component of weak isospin, e.g. $\pm 1/2$ for $SU(2)_L$ doublets and $1, 0, -1$ for the $SU(2)_L$ triplet. Therefore, we have the following eigenstates with respect to the electric charge

$$\begin{aligned} \Phi_1 &\equiv \Phi_1^{-1/3}, & \tilde{\Phi}_1 &\equiv \tilde{\Phi}_1^{-4/3}, \\ \Phi_2 &\equiv \begin{pmatrix} \Phi_2^{5/3} \\ \Phi_2^{2/3} \end{pmatrix}, & \tilde{\Phi}_2 &\equiv \begin{pmatrix} \tilde{\Phi}_2^{2/3} \\ \tilde{\Phi}_2^{-1/3} \end{pmatrix}, & \tau \cdot \Phi_3 &\equiv \begin{pmatrix} \Phi_3^{-1/3} & \sqrt{2}\Phi_3^{2/3} \\ \sqrt{2}\Phi_3^{-4/3} & -\Phi_3^{-1/3} \end{pmatrix}, \end{aligned} \quad (6.3)$$

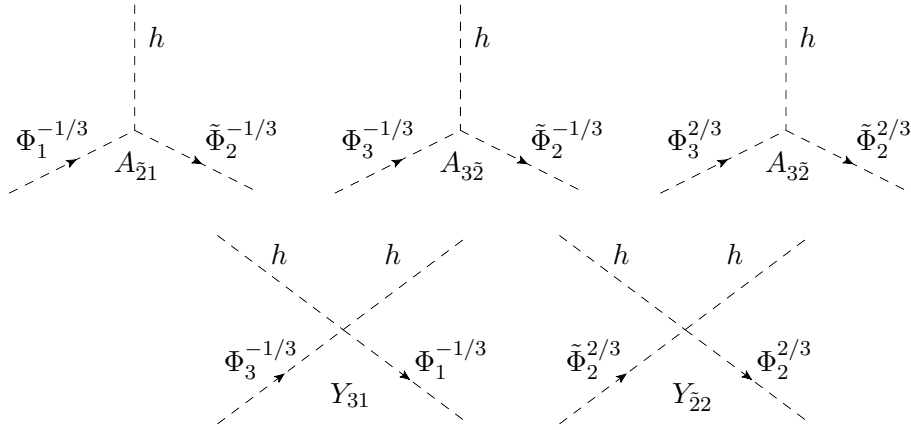


Figure 6.1: Feynman diagrams depicting LQ-Higgs interactions. Here the physical Higgs h can be replaced by its vev, leading to mixing among the LQs.

obtained from the five representations. Note that the upper index refers to the electric charge and the lower one to the $SU(2)_L$ representation from which the field originates.

In addition to the gauge interactions of the LQs, determined by the respective representation under the SM gauge group, LQs can couple to the SM Higgs doublet H (with hypercharge +1) via the Lagrangian [335]²²

$$\begin{aligned}
 \mathcal{L}_{H\Phi} = & -A_{\bar{2}1}(\tilde{\Phi}_2^\dagger H)\Phi_1 + A_{3\bar{2}}(\tilde{\Phi}_2^\dagger(\tau \cdot \Phi_3)H) + Y_{\bar{2}2}(\Phi_2^\dagger H)(Hi\tau_2\tilde{\Phi}_2) \\
 & + Y_{3\bar{1}}(Hi\tau_2(\tau \cdot \Phi_3)^\dagger H)\tilde{\Phi}_1 + Y_{31}(H^\dagger(\tau \cdot \Phi_3)H)\Phi_1^\dagger + \text{h.c.} \\
 & - Y_{22}(Hi\tau_2\Phi_2)(Hi\tau_2\Phi_2)^\dagger - Y_{\bar{2}\bar{2}}(Hi\tau_2\tilde{\Phi}_2)(Hi\tau_2\tilde{\Phi}_2)^\dagger \\
 & - iY_{33}\varepsilon_{IJK}H^\dagger\tau_I H\Phi_{3,K}^\dagger\Phi_{3,J} \\
 & - \sum_{k=1}^3(m_k^2 + Y_k H^\dagger H)\Phi_k^\dagger\Phi_k - \sum_{k=1}^2(\tilde{m}_k^2 + Y_{\bar{k}} H^\dagger H)\tilde{\Phi}_k^\dagger\tilde{\Phi}_k.
 \end{aligned} \tag{6.4}$$

Here m_Φ^2 represent the usual (bare) mass terms of the LQs, present without EW symmetry breaking and ε_{IJK} is the three-dimensional Levi-Civita tensor with $\varepsilon_{123} = 1$. Note that $A_{\bar{2}1}$ and $A_{3\bar{2}}$ have mass dimension one, while the Y couplings are dimensionless. The LQ-Higgs interactions lead to additional contributions to the mass matrices. The mixing among them is depicted in Figure 6.1.

Once the Higgs acquires a vacuum expectation value (vev) with $v \approx 174$ GeV, this generates the following mass matrices in the interaction basis

$$\begin{aligned}
 \mathcal{M}^{-1/3} &= \begin{pmatrix} m_1^2 + v^2 Y_1 & v A_{\bar{2}1}^* & v^2 Y_{31} \\ v A_{\bar{2}1} & \tilde{m}_2^2 + v^2 Y_{\bar{2}} & v A_{3\bar{2}} \\ v^2 Y_{31}^* & v A_{3\bar{2}}^* & m_3^2 + v^2 Y_3 \end{pmatrix}, \\
 \mathcal{M}^{2/3} &= \begin{pmatrix} m_2^2 + v^2 Y_2 & v^2 Y_{\bar{2}2} & 0 \\ v^2 Y_{\bar{2}2}^* & \tilde{m}_2^2 + v^2(Y_{\bar{2}\bar{2}} + Y_{\bar{2}}) & -\sqrt{2}v A_{3\bar{2}} \\ 0 & -\sqrt{2}v A_{3\bar{2}}^* & m_3^2 + v^2(Y_3 + Y_{33}) \end{pmatrix}, \\
 \mathcal{M}^{-4/3} &= \begin{pmatrix} \tilde{m}_1^2 + v^2 Y_{\bar{1}} & \sqrt{2}v^2 Y_{3\bar{1}}^* \\ \sqrt{2}v^2 Y_{3\bar{1}} & m_3^2 + v^2(Y_3 - Y_{33}) \end{pmatrix}, \\
 \mathcal{M}^{5/3} &= m_2^2 + v^2(Y_{22} + Y_2),
 \end{aligned} \tag{6.5}$$

²² $Y_{\bar{2}\bar{2}}$ and Y_{22} were studied in Ref. [406] while the Y_{33} term was considered in Ref. [369].

such that

$$-\Phi_Q^\dagger \mathcal{M}^Q \Phi_Q \subset \mathcal{L}_{H\Phi}. \quad (6.6)$$

This now parametrizes the mass terms in the Lagrangian, where Q is the electric charge and we defined

$$\Phi_{-1/3} \equiv \begin{pmatrix} \Phi_1^{-1/3} \\ \tilde{\Phi}_2^{-1/3} \\ \Phi_3^{-1/3} \end{pmatrix} \quad \Phi_{2/3} \equiv \begin{pmatrix} \Phi_2^{2/3} \\ \tilde{\Phi}_2^{2/3} \\ \Phi_3^{2/3} \end{pmatrix} \quad \Phi_{-4/3} \equiv \begin{pmatrix} \tilde{\Phi}_1^{-4/3} \\ \Phi_3^{-4/3} \end{pmatrix} \quad \Phi_{5/3} \equiv \Phi_2^{5/3}. \quad (6.7)$$

In order to arrive at the physical basis we need to diagonalize the mass matrices in Eq. (6.5). This can be achieved via

$$\hat{\mathcal{M}}^Q = W^Q \mathcal{M}^Q W^{Q\dagger} \quad (6.8)$$

with unitary matrices W^Q . Thus, the interaction eigenstates in Eq. (6.7) are rotated as

$$W^Q \Phi_Q \equiv \hat{\Phi}^Q \quad (6.9)$$

to arrive at the mass eigenstates. The matrices W^Q for $Q = -1/3$ and $Q = 2/3$ too lengthy to be given analytically in full generality, but can of course be computed numerically. However, in order to obtain the explicit dependence on the Lagrangian parameters A and Y , we diagonalize the mass matrices perturbatively up to $\mathcal{O}(v^2)$, which then yields the following expressions

$$\begin{aligned} W^{-1/3} &\approx \begin{pmatrix} 1 - \frac{v^2 |A_{\bar{2}1}|^2}{2(m_1^2 - \tilde{m}_2^2)^2} & \frac{vA_{\bar{2}1}^*}{m_1^2 - \tilde{m}_2^2} & \frac{v^2(Y_{31}(m_1^2 - \tilde{m}_2^2) + A_{\bar{2}1}^* A_{3\bar{2}})}{(m_1^2 - m_3^2)(m_1^2 - \tilde{m}_2^2)} \\ \frac{-vA_{\bar{2}1}}{m_1^2 - \tilde{m}_2^2} & 1 - \frac{v^2}{2} \left(\frac{|A_{\bar{2}1}|^2}{(m_1^2 - \tilde{m}_2^2)^2} + \frac{|A_{3\bar{2}}|^2}{(m_3^2 - \tilde{m}_2^2)^2} \right) & \frac{-vA_{3\bar{2}}}{m_3^2 - \tilde{m}_2^2} \\ \frac{-v^2(Y_{31}^*(m_3^2 - \tilde{m}_2^2) + A_{\bar{2}1} A_{3\bar{2}}^*)}{(m_1^2 - m_3^2)(m_3^2 - \tilde{m}_2^2)} & \frac{vA_{3\bar{2}}^*}{m_3^2 - \tilde{m}_2^2} & 1 - \frac{v^2 |A_{3\bar{2}}|^2}{2(m_3^2 - \tilde{m}_2^2)^2} \end{pmatrix}, \\ W^{2/3} &\approx \begin{pmatrix} 1 & \frac{v^2 Y_{\bar{2}2}}{m_2^2 - \tilde{m}_2^2} & 0 \\ \frac{-v^2 Y_{\bar{2}2}^*}{m_2^2 - \tilde{m}_2^2} & 1 - \frac{v^2 |A_{3\bar{2}}|^2}{(m_3^2 - \tilde{m}_2^2)^2} & \frac{-\sqrt{2}vA_{3\bar{2}}}{\tilde{m}_2^2 - m_3^2} \\ 0 & \frac{\sqrt{2}vA_{3\bar{2}}^*}{\tilde{m}_2^2 - m_3^2} & 1 - \frac{v^2 |A_{3\bar{2}}|^2}{(m_3^2 - \tilde{m}_2^2)^2} \end{pmatrix}, \\ W^{-4/3} &\approx \begin{pmatrix} 1 & \frac{\sqrt{2}v^2 Y_{\bar{3}1}^*}{\tilde{m}_1^2 - m_3^2} \\ \frac{-\sqrt{2}v^2 Y_{\bar{3}1}}{\tilde{m}_1^2 - m_3^2} & 1 \end{pmatrix}. \end{aligned} \quad (6.10)$$

The physical LQ masses then read

$$\begin{aligned} (M_a^{-1/3})^2 &\approx \left(m_1^2 + v^2 \left(Y_1 - \frac{|A_{\bar{2}1}|^2}{\tilde{m}_2^2 - m_1^2} \right), \tilde{m}_2^2 + v^2 \left(Y_{\bar{2}} + \frac{|A_{\bar{2}1}|^2}{\tilde{m}_2^2 - m_1^2} + \frac{|A_{3\bar{2}}|^2}{\tilde{m}_2^2 - m_3^2} \right), \right. \\ &\quad \left. m_3^2 + v^2 \left(Y_3 - \frac{|A_{3\bar{2}}|^2}{\tilde{m}_2^2 - m_3^2} \right) \right)_a, \\ (M_a^{2/3})^2 &\approx \left(m_2^2 + v^2 Y_{\bar{2}}, \tilde{m}_2^2 + v^2 \left(Y_{\bar{2}\bar{2}} + Y_{\bar{2}} + \frac{2|A_{3\bar{2}}|^2}{\tilde{m}_2^2 - m_3^2} \right), \right. \\ &\quad \left. m_3^2 + v^2 \left(Y_3 + Y_{33} - \frac{2|A_{3\bar{2}}|^2}{\tilde{m}_2^2 - m_3^2} \right) \right)_a, \\ (M_a^{-4/3})^2 &\approx \left(\tilde{m}_1^2 + v^2 Y_{\bar{1}}, m_3^2 + v^2 (Y_3 - Y_{33}) \right)_a, \\ (M^{5/3})^2 &\approx m_2^2 + v^2 (Y_{\bar{2}2} + Y_2), \end{aligned} \quad (6.11)$$

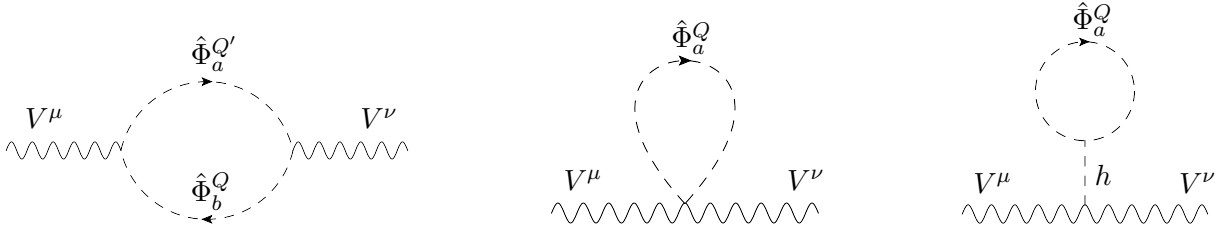


Figure 6.2: The three different topologies of Feynman diagrams that contribute to $\Pi_{VV}(q^2)$ with $V = W, Z, \gamma$. The last diagram only exists for $V = W, Z$ and has no impact on the S , T and U parameters as it is momentum independent.

parameters can be written as

$$\begin{aligned}
 S &= -\frac{4s_w^2 c_w^2}{\alpha m_Z^2} \left(\Pi_{ZZ}(0) - \Pi_{ZZ}(m_Z^2) + \Pi_{\gamma\gamma}(m_Z^2) + \frac{c_w^2 - s_w^2}{c_w s_w} \Pi_{Z\gamma}(m_Z^2) \right), \\
 T &= \frac{\Pi_{WW}(0)}{\alpha m_W^2} - \frac{\Pi_{ZZ}(0)}{\alpha m_Z^2}, \\
 U &= -\frac{4s_w^2 c_w^2}{\alpha} \left(\frac{\Pi_{WW}(0) - \Pi_{WW}(m_W^2)}{c_w^2 m_W^2} - \frac{\Pi_{ZZ}(0) - \Pi_{ZZ}(m_Z^2)}{m_Z^2} \right. \\
 &\quad \left. + \frac{s_w^2}{c_w^2} \frac{\Pi_{\gamma\gamma}(m_Z^2)}{m_Z^2} + 2 \frac{s_w}{c_w} \frac{\Pi_{Z\gamma}(m_Z^2)}{m_Z^2} \right), \tag{6.16}
 \end{aligned}$$

where we used renormalization conditions for the vector fields such that

$$\Pi_{\gamma\gamma}(0) = \Pi_{Z\gamma}(0) = \text{Re}[\Pi_{ZZ}(m_Z^2)] = \text{Re}[\Pi_{WW}(m_W^2)] = 0. \tag{6.17}$$

These conditions are fulfilled automatically for $\Pi_{\gamma\gamma}$ and $\Pi_{Z\gamma}$ because of the Ward identities.

S , T and U can be calculated with the bare (unrenormalized) two-point correlation functions, the corresponding diagrams in our model are shown in Fig. 6.2. Therefore, we used the check that all divergences disappear in the physical observables S , T and U after having summed over all $SU(2)_L$ components in the loop. The complete expressions for these parameters are quite lengthy and therefore given in the appendix. Expanding in addition in q^2/M^2 and in v/M , i.e. perturbatively diagonalizing the LQ mass matrices, we can however obtain relatively compact expressions. Up to leading order in v we find

$$\begin{aligned}
 S &\approx -\frac{N_c v^2}{36\pi} \left(\frac{7Y_{22}}{m_2^2} + \frac{Y_{\tilde{2}\tilde{2}}}{\tilde{m}_2^2} - \frac{8Y_{33}}{m_3^2} - \frac{|A_{\tilde{2}1}|^2}{10\tilde{m}_2^4} \mathcal{K}_1\left(\frac{m_1^2}{\tilde{m}_2^2}\right) + \frac{17|A_{\tilde{3}\tilde{2}}|^2}{10\tilde{m}_2^4} \mathcal{K}_2\left(\frac{m_3^2}{\tilde{m}_2^2}\right) \right), \\
 T &\approx \frac{N_c v^2}{24\pi g_2^2 s_w^2} \left(\frac{Y_{22}^2}{m_2^2} + \frac{Y_{\tilde{2}\tilde{2}}^2}{\tilde{m}_2^2} + \frac{4Y_{33}^2}{m_3^2} + \frac{|A_{\tilde{2}1}|^4}{10\tilde{m}_2^6} \mathcal{K}_3\left(\frac{m_1^2}{\tilde{m}_2^2}\right) + \frac{|A_{\tilde{3}\tilde{2}}|^4}{2\tilde{m}_2^6} \mathcal{K}_4\left(\frac{m_3^2}{\tilde{m}_2^2}\right) + \frac{Y_{\tilde{2}\tilde{2}}|A_{\tilde{2}1}|^2}{2\tilde{m}_2^4} \mathcal{K}_5\left(\frac{m_1^2}{\tilde{m}_2^2}\right) \right. \\
 &\quad - \frac{Y_{\tilde{2}\tilde{2}}|A_{\tilde{3}\tilde{2}}|^2}{2\tilde{m}_2^4} \mathcal{K}_5\left(\frac{m_3^2}{\tilde{m}_2^2}\right) - 2 \frac{Y_{33}|A_{\tilde{3}\tilde{2}}|^2}{\tilde{m}_2^4} \mathcal{K}_6\left(\frac{m_3^2}{\tilde{m}_2^2}\right) + \frac{4|Y_{31}|^2}{m_3^2} \mathcal{K}_7\left(\frac{m_1^2}{m_3^2}\right) - \frac{4|Y_{\tilde{3}\tilde{1}}|^2}{m_3^2} \mathcal{K}_7\left(\frac{\tilde{m}_1^2}{m_3^2}\right) \\
 &\quad \left. - \frac{2|Y_{\tilde{2}\tilde{2}}|^2}{\tilde{m}_2^2} \mathcal{K}_7\left(\frac{m_2^2}{\tilde{m}_2^2}\right) - \frac{2\Re[Y_{31}A_{\tilde{2}1}A_{\tilde{3}\tilde{2}}^*]}{\tilde{m}_2^4} \mathcal{K}_8\left(\frac{m_1^2}{\tilde{m}_2^2}, \frac{m_3^2}{\tilde{m}_2^2}\right) + \frac{|A_{\tilde{2}1}|^2|A_{\tilde{3}\tilde{2}}|^2}{5\tilde{m}_2^6} \mathcal{K}_9\left(\frac{m_1^2}{\tilde{m}_2^2}, \frac{m_3^2}{\tilde{m}_2^2}\right) \right), \tag{6.18} \\
 U &\approx 0,
 \end{aligned}$$

where the loop functions, given in the appendix, are normalized to be unity in case of equal masses. These expressions agree with Refs. [405, 406] for the special cases studied there. Note that U is approximately zero since it only arises at dimension 8.

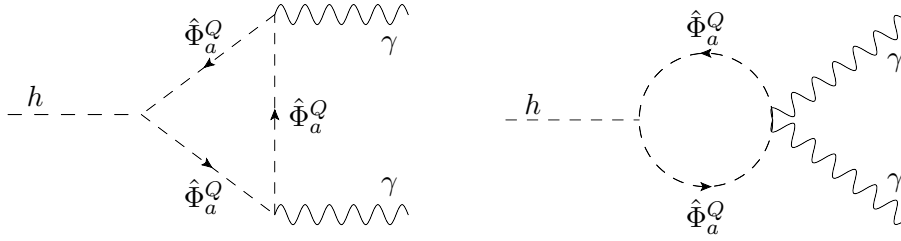


Figure 6.3: The two types of diagrams that induce NP effects in $h \rightarrow \gamma\gamma$. For $h \rightarrow gg$ the photons can simply be replaced by gluons, for $h \rightarrow Z\gamma$ one photon can be replaced by a Z boson. The additional diagrams with reversed charge flow are not depicted.

6.4 Higgs Couplings to g , γ and Z

The Feynman diagrams involving scalar LQs contributing to $h \rightarrow \gamma\gamma$, $h \rightarrow gg$ and $h \rightarrow Z\gamma$ are shown in Fig. 6.3. The amplitude, induced by them, reads

$$\mathcal{A}[h \rightarrow \gamma(p_1)\gamma(p_2)] = \frac{\alpha N_c}{24\pi} \sum_{Q,a} \frac{Q^2 \tilde{\Gamma}_{aa}^Q}{(M_a^Q)^2} (m_h^2 \varepsilon(p_1) \cdot \varepsilon(p_2) - 2(\varepsilon(p_1) \cdot p_2)(\varepsilon(p_2) \cdot p_1)), \quad (6.19)$$

with p_1 and p_2 representing the photon momenta, $\varepsilon_\mu(p_i)$ the corresponding polarization vectors and a running over the number of mass eigenstates with the same electric charge $Q = \{-1/3, 2/3, -4/3, 5/3\}$. Here we used on-shell kinematics and expanded in m_h^2/M^2 .

Similarly, for the decay into a pair of gluons, we obtain

$$\mathcal{A}[h \rightarrow g^A(p_1)g^A(p_2)] = \frac{\alpha_s}{48\pi} \sum_Q \frac{\tilde{\Gamma}_{aa}^Q}{(M_a^Q)^2} (m_h^2 \varepsilon^A(p_1) \cdot \varepsilon^A(p_2) - 2(\varepsilon^A(p_1) \cdot p_2)(\varepsilon^A(p_2) \cdot p_1)),$$

where A labels the 8 gluons (no sum implied). For the Higgs decaying into a Z and a photon we obtain

$$\begin{aligned} \mathcal{A}[h \rightarrow Z(p_Z)\gamma(p_\gamma)] &= \frac{\alpha N_c}{24\pi} \frac{1}{s_w c_w} \sum_Q \left(Q \frac{\tilde{T}_{ab}^Q \tilde{\Gamma}_{ba}^Q}{(M_b^Q)^2} \mathcal{K}_\gamma(x_{ab}^Q) - s_w^2 Q^2 \frac{\tilde{\Gamma}_{aa}^Q}{(M_a^Q)^2} \right) \\ &\times \left((m_h^2 - m_Z^2) \varepsilon(p_Z) \cdot \varepsilon(p_\gamma) - 2(\varepsilon(p_Z) \cdot p_\gamma)(\varepsilon(p_\gamma) \cdot p_Z) \right), \end{aligned} \quad (6.20)$$

with a simultaneous expansion in m_h^2/M^2 and m_Z^2/M^2 and

$$x_{ab}^Q = \frac{(M_a^Q)^2}{(M_b^Q)^2}. \quad (6.21)$$

The relevant observables in this context are the effective on-shell $h\gamma\gamma$, hgg and $hZ\gamma$ couplings, normalized to their SM values

$$\kappa_\gamma = \sqrt{\frac{\Gamma_{h \rightarrow \gamma\gamma}}{\Gamma_{h \rightarrow \gamma\gamma}^{\text{SM}}}}, \quad \kappa_g = \sqrt{\frac{\Gamma_{h \rightarrow gg}}{\Gamma_{h \rightarrow gg}^{\text{SM}}}}, \quad \kappa_{Z\gamma} = \sqrt{\frac{\Gamma_{h \rightarrow Z\gamma}}{\Gamma_{h \rightarrow Z\gamma}^{\text{SM}}}}. \quad (6.22)$$

We then have

$$\begin{aligned}
 \kappa_\gamma &= 1 + \frac{1}{\mathcal{A}_{h \rightarrow \gamma\gamma}^{\text{SM}}} \frac{\alpha N_c}{24\pi} \sum_Q Q^2 \frac{\tilde{\Gamma}_{aa}^Q}{(M_a^Q)^2}, \\
 \kappa_g &= 1 + \frac{1}{\mathcal{A}_{h \rightarrow gg}^{\text{SM}}} \frac{\alpha_s}{48\pi} \sum_Q \frac{\tilde{\Gamma}_{aa}^Q}{(M_a^Q)^2}, \\
 \kappa_{Z\gamma} &= 1 - \frac{1}{\mathcal{A}_{h \rightarrow Z\gamma}^{\text{SM}}} \frac{\alpha N_c}{24\pi} \frac{1}{s_w c_w} \sum_Q \left(Q \frac{\tilde{T}_{ab}^Q \tilde{\Gamma}_{ba}^Q}{(M_b^Q)^2} \mathcal{K}_6(x_{ab}^Q) - s_w^2 Q^2 \frac{\tilde{\Gamma}_{aa}^Q}{(M_a^Q)^2} \right),
 \end{aligned} \tag{6.23}$$

with the LO SM amplitudes (see e.g. Ref. [411] for an overview) given by [391, 412–417]

$$\begin{aligned}
 \mathcal{A}_{h \rightarrow \gamma\gamma}^{\text{SM}} &= \frac{\alpha}{4\pi\sqrt{2}v} \left(A_1(x_W) + \frac{4}{3} A_{1/2}(x_t) \right), \\
 \mathcal{A}_{h \rightarrow gg}^{\text{SM}} &= \frac{\alpha_s}{8\pi\sqrt{2}v} A_{1/2}(x_t), \\
 \mathcal{A}_{h \rightarrow Z\gamma}^{\text{SM}} &= \frac{\alpha}{4\pi s_w \sqrt{2}v} \left(c_w C_1(x_W^{-1}, y_W) + \frac{2}{c_w} \left(1 - \frac{8}{3} s_w^2 \right) C_{1/2}(x_t^{-1}, y_t) \right).
 \end{aligned} \tag{6.24}$$

We defined

$$x_i = \frac{m_h^2}{4m_i^2}, \quad y_i = \frac{4m_i^2}{m_Z^2}, \tag{6.25}$$

while the loop functions are given in the appendix.²⁴

In addition to the expansion of the loop functions, we can also expand the expressions $\tilde{\Gamma}^Q/M^2$ and $\tilde{T}^Q \tilde{\Gamma}^Q \mathcal{K}_6(x_{ab}^Q)/M^2$ in v^2/M^2 up to $\mathcal{O}(v^3)$, using Eq. (6.11). We obtain

$$\begin{aligned}
 \sum_{a=1}^3 \frac{\tilde{\Gamma}_{aa}^{-1/3}}{(M_a^{-1/3})^2} &\approx \sqrt{2}v \left(\frac{Y_1}{m_1^2} + \frac{Y_2}{\tilde{m}_2^2} + \frac{Y_3}{m_3^2} - \frac{|A_{21}|^2}{m_1^2 \tilde{m}_2^2} - \frac{|A_{32}|^2}{m_3^2 \tilde{m}_2^2} \right), \\
 \sum_{a=1}^3 \frac{\tilde{\Gamma}_{aa}^{2/3}}{(M_a^{2/3})^2} &\approx \sqrt{2}v \left(\frac{Y_2}{m_2^2} + \frac{Y_{2\bar{2}} + Y_2}{\tilde{m}_2^2} + \frac{Y_3 + Y_{33}}{m_3^2} - \frac{2|A_{3\bar{2}}|^2}{\tilde{m}_2^2 m_3^2} \right), \\
 \sum_{a=1}^2 \frac{\tilde{\Gamma}_{aa}^{-4/3}}{(M_a^{-4/3})^2} &\approx \sqrt{2}v \left(\frac{Y_{\bar{1}}}{\tilde{m}_1^2} + \frac{Y_3 - Y_{33}}{m_3^2} \right), \\
 \frac{\Gamma^{5/3}}{(M^{5/3})^2} &\approx \sqrt{2}v \frac{Y_{22} + Y_2}{m_2^2},
 \end{aligned} \tag{6.26}$$

$$\begin{aligned}
 \sum_{a,b=1}^3 \frac{\tilde{T}_{ab}^{-1/3} \tilde{\Gamma}_{ba}^{-1/3}}{(M_b^{-1/3})^2} \mathcal{K}_7(x_{ab}^{-1/3}) &\approx \frac{v}{\sqrt{2}} \left(\frac{|A_{21}|^2}{2\tilde{m}_2^4} \mathcal{F}_1 \left(\frac{m_1^2}{\tilde{m}_2^2} \right) + \frac{|A_{32}|^2}{2\tilde{m}_2^4} \mathcal{F}_1 \left(\frac{m_3^2}{\tilde{m}_2^2} \right) - \frac{Y_2}{\tilde{m}_2^2} \right), \\
 \sum_{a,b=1}^3 \frac{\tilde{T}_{ab}^{2/3} \tilde{\Gamma}_{ba}^{2/3}}{(M_b^{2/3})^2} \mathcal{K}_7(x_{ab}^{2/3}) &\approx \frac{v}{\sqrt{2}} \left(\frac{Y_2}{\tilde{m}_2^2} - \frac{Y_2}{m_2^2} + \frac{2(Y_3 + Y_{33})}{m_3^2} + \frac{Y_{2\bar{2}}}{\tilde{m}_2^2} - \frac{3|A_{3\bar{2}}|^2}{\tilde{m}_2^4} \mathcal{F}_2 \left(\frac{m_3^2}{\tilde{m}_2^2} \right) \right), \\
 \sum_{a,b=1}^2 \frac{\tilde{T}_{ab}^{-4/3} \tilde{\Gamma}_{ba}^{-4/3}}{(M_b^{-4/3})^2} \mathcal{K}_7(x_{ab}^{-4/3}) &\approx -\sqrt{2}v \frac{Y_3 - Y_{33}}{m_3^2}, \\
 \frac{\tilde{T}^{5/3} \tilde{\Gamma}^{5/3}}{(M^{5/3})^2} &\approx \frac{v}{\sqrt{2}} \frac{Y_{22} + Y_2}{m_2^2}.
 \end{aligned} \tag{6.27}$$

²⁴Note that we did not include the effects of bottom quarks in the SM prediction which would lead to a 10% destructive interference.

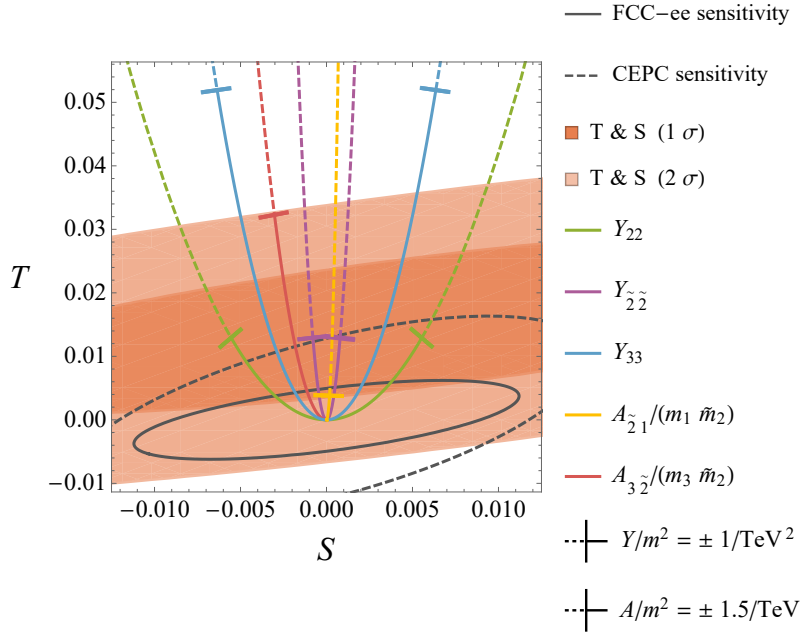


Figure 6.4: Correlations between S and T for four different Lagrangian parameters in Eq. (6.4), assuming that only one of them is non-zero at a time. For simplicity, we assumed all LQ masses to be equal. While Y_{22} and $Y_{\tilde{2}\tilde{2}}$ can yield both positive and negative effects in S , the effect in the T parameter is positive definite. Since our prediction for S and T depends on a single combination of parameters (Y/m^2 or A^2/m^4), we used one degree of freedom to obtain the preferred region in the S - T plane, such that the region within the ellipse labelled by 1σ (2σ) corresponds to 68% C.L. (95% C.L.).

Therefore, we have directly expressed κ_γ , κ_g and $\kappa_{Z\gamma}$ in terms of the Lagrangian parameters. The loop functions \mathcal{F}_1 and \mathcal{F}_2 , given in the appendix, are again normalized to be unity in case of equal masses.

6.5 Phenomenological Analysis

Before we illustrate the effects of LQs in the observables of our interest, let us recall the current experimental situation and the prospects at future colliders. Concerning the oblique corrections, the global fit to electroweak precision measurements (including LEP [353], Tevatron [418] and LHC [419]) of Ref. [420] constrains the S and T parameter to lie within

$$S = [-0.06, 0.07], T = [-0.02, 0.05], \quad (6.28)$$

at 95% C.L. within the 2-dimensional S - T plane, with a correlation factor of 0.72. Here, we can optimistically expect a sensitivity of 0.008 in the future at the FCC-ee [357].

For on-shell Higgs couplings, we used the results of Refs. [421, 422] for the current status, which are

$$\kappa_g = 1.066_{-0.050}^{+0.051}, \quad \kappa_\gamma = 0.999_{-0.053}^{+0.055}. \quad (6.29)$$

Concerning future prospects we expect for κ_γ (κ_g) an accuracy of 7% (2.3%) at the ILC [407], 3.7% (1.5%) at CEPC [423], 2.3% (0.9%) at CLIC [408], 3% (1.4%) at the FCC-ee [357] and 1.45% at the FCC-hh [424]. Finally, concerning $h \rightarrow Z\gamma$, an accuracy of up to 1.8% in $h \rightarrow Z\mu^+\mu^-/h \rightarrow \mu^+\mu^-$ can be achieved at the FCC-ee [357].

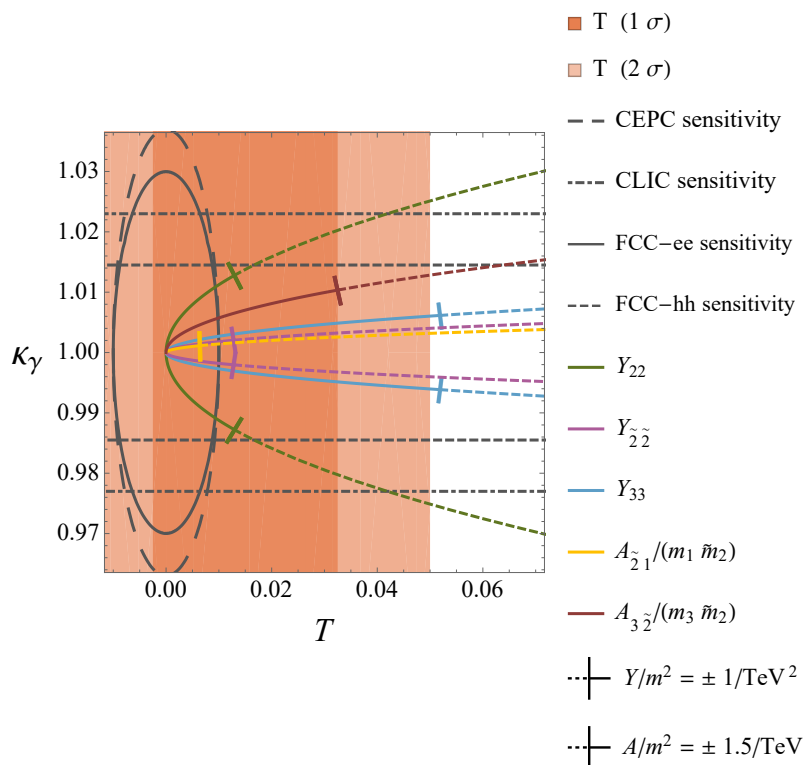


Figure 6.5: Correlations between κ_γ and T for different Lagrangian parameters, assuming that only one of them is non-zero at a time and assuming all LQ masses to be equal.

Let us start by considering the oblique parameters. Here and in the following, we will for definiteness assume a LQ mass of 1 TeV, which is compatible with current LHC limits [291, 362, 425] for a broad range of couplings to fermions. In Fig. 6.4 we show the correlations between S and T for the four cases which contribute to both parameters simultaneously. As one can see, the effect in T is positive definite, as slightly preferred by current data. Note that the A parameters are dimensionful couplings which are naturally expected to be of the same order as the LQ masses and that similarly the dimensionless couplings Y are expected to be of order 1. Therefore, T already now sets relevant limits on these couplings and its future experimental sensitivity allows for stringent constraints or even to discover deviations from the SM within LQ models.

Turning to the effects in Higgs couplings to gauge bosons, we show the correlations between κ_γ and T in Fig. 6.5 and between κ_γ and κ_g in Fig. 6.6. The currently allowed regions (1σ and 2σ , corresponding to 68% and 95% C.L. for one degree of freedom) are shown in color while the future prospects are indicated by dashed and dotted boundaries of the corresponding ellipses. Assuming a value close to the current best fit point in the κ_γ - κ_g plane is confirmed in the future, this would point towards the LQ representation $\tilde{\Phi}_2$. Similarly, one can correlate κ_γ to $\kappa_{Z\gamma}$, see Fig. 6.7, which clearly provides complementary distinguishing power, especially at the FCC-hh. E.g. an anti-correlations between κ_γ to $\kappa_{Z\gamma}$ is not favored by either (single) Lagrangian parameter of coupling LQs to the Higgs.

6.6 Conclusions

LQs are prime candidates to explain the flavor anomalies, i.e. the discrepancies between the SM predictions and experiment in $b \rightarrow c\tau\nu$ and $b \rightarrow s\ell^+\ell^-$ processes and in the anomalous

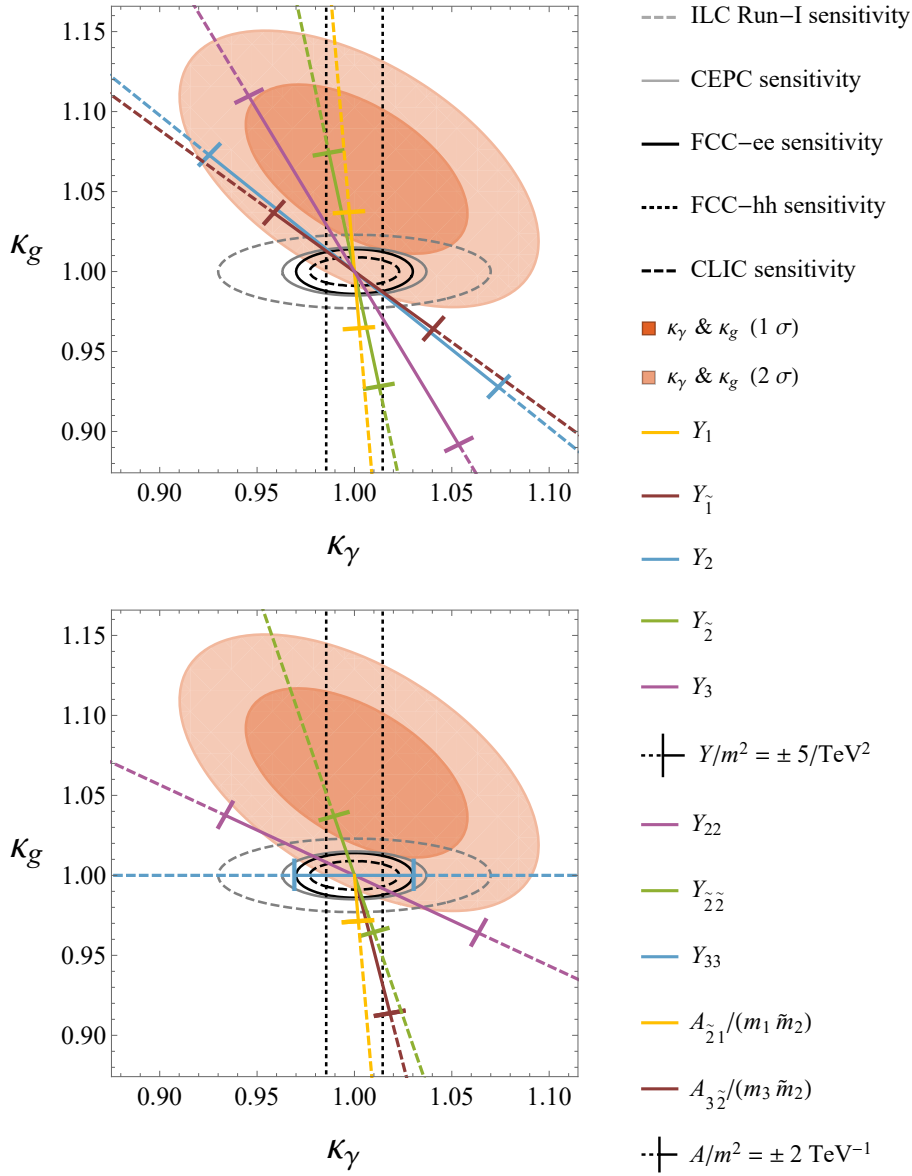


Figure 6.6: Correlations between κ_γ and κ_g for the different Lagrangian parameters. Here we assumed all bi-linear LQ mass terms to be equal. Here we used one degree of freedom in the χ^2 fit for the allowed regions and the future prospects such that the intersection with the LQ line indicates the 68% and 95% CL for the corresponding parameter Y/m^2 or A^2/m^4 .

magnetic moment of the muon. Therefore, it is interesting to study alternative observables which are sensitive to LQs and could therefore as well show deviations from the SM predictions. In this context, parameters sensitive to additional electroweak symmetry breaking effects provide a complementary window. In particular, LQ couplings to the SM Higgs generate loop effects, which contribute to the oblique parameters (S and T) and to effective Higgs couplings, entering on-shell Higgs boson production ($gg \rightarrow h$) and decays ($h \rightarrow \gamma\gamma$, $h \rightarrow Z\gamma$). All these observables have in common that (at the one-loop level) they do not depend on the LQ couplings to fermions but rather only on LQ couplings to Higgses (tri-linear and quadratic ones). Therefore, one

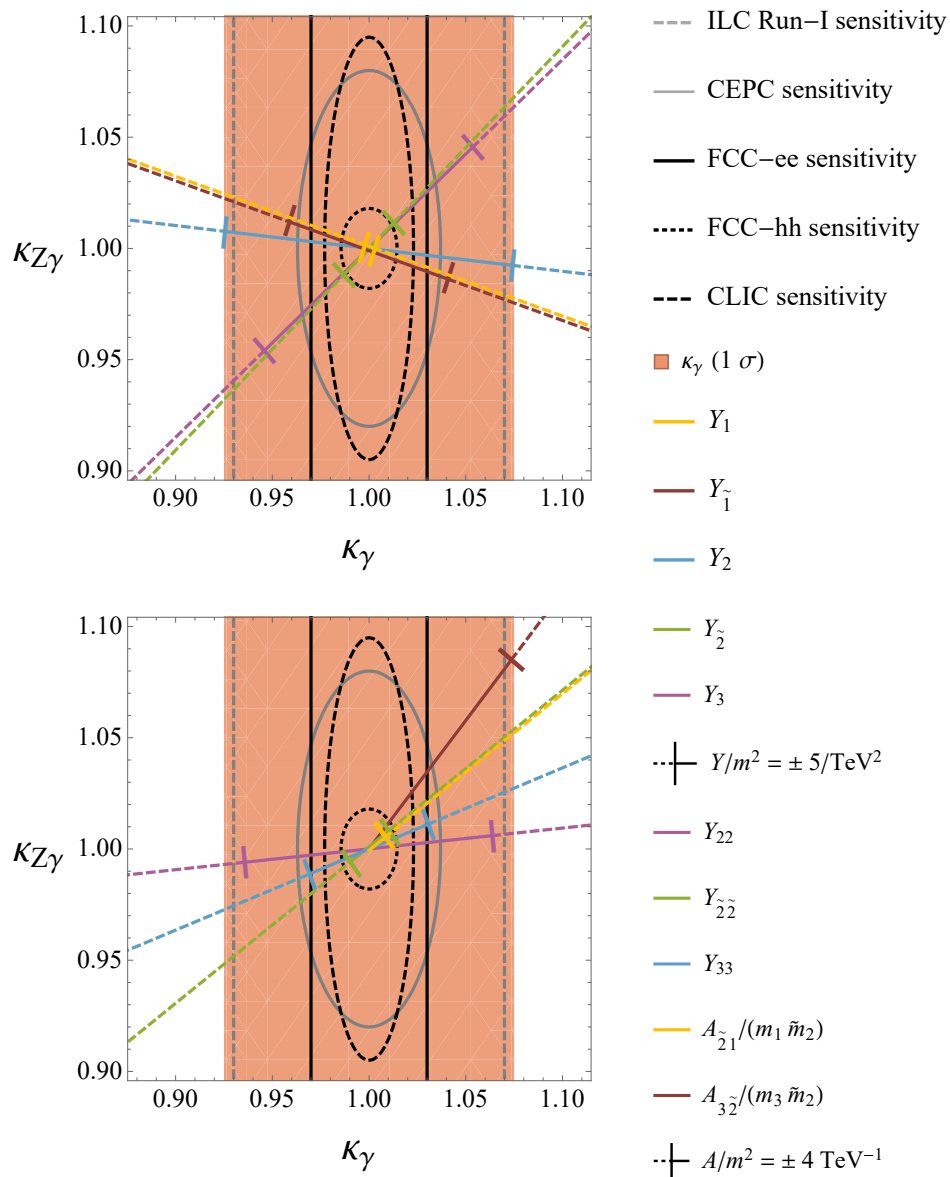


Figure 6.7: Correlations between κ_γ and $\kappa_{Z\gamma}$ for the different Lagrangian parameters coupling LQs to the Higgs. The currently preferred regions are shown as red ellipses and the future sensitivity is indicated by the dashed and dotted lines.

can test this sector of the Lagrangian independently of the fermion couplings entering flavor observables.

Taking into account the most general set of Higgs-LQ interactions, including mixing among different LQ representations, we calculated the one-loop contributions to the oblique parameters S , T and U . Using a perturbative expansion of the mixing matrices we were able to provide simple, analytic expressions for them. Similarly, we calculated the contributions to effective on-shell hgg , $h\gamma\gamma$ and $hZ\gamma$ couplings, expressing the corrections as simple analytic functions of the Lagrangian parameters.

In our phenomenological analysis we correlated the effects in the oblique corrections with

each other, see Fig. 6.4, finding that the contribution to T is positive definite and that T is clearly more sensitive to LQs than S . Similarly, we correlated hgg with $h\gamma\gamma$ in Fig. 6.6 and $h\gamma\gamma$ to $hZ\gamma$ in Fig.6.7. In the future it would be very interesting to include the NLO QCD corrections, in the spirit of Refs. [393,394], as these interesting correlations open the possibility of distinguishing different LQ representations, independently of their couplings to fermions, providing strong motivation for future colliders.

Acknowledgements — We thank Michael Spira for useful discussions. The work of A.C. and D.M. is supported by a Professorship Grant (PP00P2_176884) of the Swiss National Science Foundation. The work of F.S. is supported by the Swiss National Foundation grant 200020_175449/1.

6.7 Appendix

6.7.1 Loop Functions

In this appendix we first present the loop functions, which are used in (6.19) to write the results for the S and T parameters in a compact form

$$\begin{aligned}
 \mathcal{K}_1(y) &= -10 \left(\frac{y^3 + 2y^2 - 19y + 4}{(y-1)^4} - \frac{(4y^3 - 12y^2 - 6y + 2) \log(y)}{(y-1)^5} \right), \\
 \mathcal{K}_2(y) &= \frac{10}{17} \left(\frac{-y^4 + 10y^3 - 45y^2 - 8y + 8}{y(y-1)^4} + \frac{18(3y-1) \log(y)}{(y-1)^5} \right), \\
 \mathcal{K}_3(y) &= 10 \left(\frac{y^2 + 10y + 1}{(y-1)^4} - \frac{6y(y+1) \log(y)}{(y-1)^5} \right), \\
 \mathcal{K}_4(y) &= 2 \left(\frac{(y+4)(y^2 + 10y + 1)}{y(y-1)^4} - \frac{6(y+1)(y+4) \log(y)}{(y-1)^5} \right), \\
 \mathcal{K}_5(y) &= 2 \left(\frac{2y^2 + 5y - 1}{(y-1)^3} - \frac{6y^2 \log(y)}{(y-1)^4} \right), \\
 \mathcal{K}_6(y) &= 2 \left(\frac{y^2 - 5y - 2}{(y-1)^3 y} + \frac{6}{(y-1)^4} \right) \\
 \mathcal{K}_7(x) &= \frac{3(x^2 - 1 - 2x \log(x))}{(x-1)^3}, \\
 \mathcal{K}_8(x, y) &= -3 \left(\frac{4}{(x-1)^2(y-1)} + \frac{8x}{(x-1)(y-x)^2} - \frac{4}{(x-1)^2(y-x)} \right. \\
 &\quad \left. + 4x \log(x) \mathcal{K}_{10}(x, y) + 4y \log(y) \mathcal{K}_{10}(y, x) \right), \\
 \mathcal{K}_9(x, y) &= 10 \left(\frac{12x}{(1-x)^2(x-y)^2} - \frac{2x^2 - 7x - 13}{2(x-1)^3(y-1)} - \frac{6(x+1)}{(x-1)^3(y-x)} \right. \\
 &\quad - \frac{9(x-3)}{2(x-1)^2(y-1)^2} - \frac{3}{(x-1)(y-1)^3} \\
 &\quad \left. + 3x \log(x) \mathcal{K}_{11}(x, y) + 3y \log(y) \mathcal{K}_{11}(y, x) \right),
 \end{aligned}$$

and

$$\begin{aligned}\mathcal{K}_{10}(x, y) &= \frac{2x}{(x-1)(y-x)^3} + \frac{x-2}{(x-1)^2(y-x)^2}, \\ \mathcal{K}_{11}(x, y) &= \frac{4x}{(x-1)^2(y-x)^3} - \frac{4}{(x-1)^3(y-x)^2} + \frac{x}{(x-1)^4(y-x)}.\end{aligned}$$

In $h \rightarrow Z\gamma$ we used the following loop functions for the amplitude

$$\begin{aligned}\mathcal{F}_1(x) &= 2 \left(\frac{x^3 - 6x^2 + 3x + 6x \log(x) + 2}{(x-1)^4} \right), \\ \mathcal{F}_2(x) &= \frac{2}{3} \left(\frac{x^4 - 2x^3 + 9x^2 - 6x^2 \log(x) - 10x + 2}{x(x-1)^4} \right).\end{aligned}$$

6.7.2 Expanded Matrices

Next, we will give the expressions for the coupling matrices, expanded in terms of the vacuum expectation value v . We have the weak isospin matrices T^Q , which read in case of no LQ mixing

$$T^{-1/3} = \begin{pmatrix} 0 & 0 & 0 \\ 0 & -\frac{1}{2} & 0 \\ 0 & 0 & 0 \end{pmatrix}, \quad T^{2/3} = \begin{pmatrix} -\frac{1}{2} & 0 & 0 \\ 0 & \frac{1}{2} & 0 \\ 0 & 0 & 1 \end{pmatrix}, \quad T^{-4/3} = \begin{pmatrix} 0 & 0 \\ 0 & -1 \end{pmatrix}, \quad T^{5/3} = \frac{1}{2}, \quad (6.30)$$

using the basis defined in Eq. (6.7). A unitary redefinition of the LQ fields in order to diagonalize the mass matrices in Eq. (6.5) also affects the T^Q matrices

$$\tilde{T}^Q = W^Q T^Q W^{Q\dagger}. \quad (6.31)$$

Note that the LQ field redefinition has no impact the electromagnetic interaction, since the coupling matrix is proportional to the unit matrix and the W^Q then cancel due to unitarity. If we use the perturbative diagonalization ansatz, we obtain

$$\begin{aligned}\tilde{T}^{-1/3} &\approx \begin{pmatrix} \frac{-v^2 |A_{21}^-|^2}{2(m_1^2 - \tilde{m}_2^2)^2} & \frac{v A_{21}^*}{2(\tilde{m}_2^2 - m_1^2)} & \frac{v^2 A_{32}^- A_{21}^*}{2(m_1^2 - \tilde{m}_2^2)(\tilde{m}_2^2 - m_3^2)} \\ \frac{v A_{21}^-}{2(\tilde{m}_2^2 - m_1^2)} & -\frac{1}{2} + \frac{v^2}{2} \left(\frac{|A_{21}^-|^2}{(m_1^2 - \tilde{m}_2^2)^2} + \frac{|A_{32}^-|^2}{(\tilde{m}_2^2 - m_3^2)^2} \right) & \frac{v A_{32}^-}{2(\tilde{m}_2^2 - m_3^2)} \\ \frac{v^2 A_{21}^- A_{32}^*}{2(m_1^2 - \tilde{m}_2^2)(\tilde{m}_2^2 - m_3^2)} & \frac{v A_{32}^*}{2(\tilde{m}_2^2 - m_3^2)} & \frac{-v^2 |A_{32}^-|^2}{2(\tilde{m}_2^2 - m_3^2)^2} \end{pmatrix}, \\ \tilde{T}^{2/3} &\approx \begin{pmatrix} -\frac{1}{2} & \frac{v^2 Y_{22}^*}{m_2^2 - \tilde{m}_2^2} & 0 \\ \frac{v^2 Y_{22}^*}{m_2^2 - \tilde{m}_2^2} & \frac{1}{2} + \frac{v^2 |A_{32}^-|^2}{(\tilde{m}_2^2 - m_3^2)^2} & \frac{v A_{32}^-}{\sqrt{2}(m_3^2 - \tilde{m}_2^2)} \\ 0 & \frac{v A_{32}^*}{\sqrt{2}(m_3^2 - \tilde{m}_2^2)} & 1 - \frac{v^2 |A_{32}^-|^2}{(\tilde{m}_2^2 - m_3^2)^2} \end{pmatrix}, \\ \tilde{T}^{-4/3} &\approx \begin{pmatrix} 0 & \frac{\sqrt{2} v^2 Y_{31}^*}{m_3^2 - \tilde{m}_1^2} \\ \frac{\sqrt{2} v^2 Y_{31}^*}{m_3^2 - \tilde{m}_1^2} & -1 \end{pmatrix},\end{aligned} \quad (6.32)$$

valid up to $\mathcal{O}(v^2)$. $T^{5/3}$ is not affected, since the LQ with charge $Q = 5/3$ does not mix. There are also interaction matrices for the $ZZ\Phi^Q\Phi^Q$ vertex, which read in case of no LQ mixing

$$\begin{aligned}
 D^{-1/3} &= \begin{pmatrix} \left(\frac{s_w^2}{3}\right)^2 & 0 & 0 \\ 0 & \left(\frac{s_w^2}{3} - \frac{1}{2}\right)^2 & 0 \\ 0 & 0 & \left(\frac{s_w^2}{3}\right)^2 \end{pmatrix} & D^{2/3} &= \begin{pmatrix} \left(\frac{2s_w^2}{3} + \frac{1}{2}\right)^2 & 0 & 0 \\ 0 & \left(\frac{2s_w^2}{3} - \frac{1}{2}\right)^2 & 0 \\ 0 & 0 & \left(\frac{2s_w^2}{3} - 1\right)^2 \end{pmatrix} \\
 D^{-4/3} &= \begin{pmatrix} \left(\frac{4s_w^2}{3}\right)^2 & 0 \\ 0 & \left(\frac{4s_w^2}{3} - 1\right)^2 \end{pmatrix} & D^{5/3} &= \left(\frac{5s_w^2}{3} - \frac{1}{2}\right)^2.
 \end{aligned} \tag{6.33}$$

If we include the LQ mixing, we have

$$\begin{aligned}
 \tilde{D}^{-1/3} &\approx \frac{1}{12} \begin{pmatrix} \frac{4s_w^4}{3} - \frac{(4s_w^2-3)v^2|A_{\tilde{2}1}|^2}{(m_1^2-\tilde{m}_2^2)^2} & \frac{(4s_w^2-3)vA_{\tilde{2}1}^*}{\tilde{m}_2^2-m_1^2} & \frac{(4s_w^2-3)v^2A_{\tilde{2}1}^*A_{\tilde{3}\tilde{2}}}{(m_3^2-\tilde{m}_2^2)(\tilde{m}_2^2-m_1^2)} \\ \frac{(4s_w^2-3)vA_{\tilde{2}1}}{\tilde{m}_2^2-m_1^2} & \tilde{d}_{22} & \frac{(4s_w^2-3)vA_{\tilde{3}\tilde{2}}}{\tilde{m}_2^2-m_3^2} \\ \frac{(4s_w^2-3)v^2A_{\tilde{3}\tilde{2}}^*A_{\tilde{2}1}}{(m_1^2-\tilde{m}_2^2)(\tilde{m}_2^2-m_3^2)} & \frac{(4s_w^2-3)vA_{\tilde{3}\tilde{2}}^*}{\tilde{m}_2^2-m_3^2} & \frac{4s_w^4}{3} - \frac{(4s_w^2-3)v^2|A_{\tilde{3}\tilde{2}}|^2}{(m_3^2-\tilde{m}_2^2)^2} \end{pmatrix}, \\
 \text{with } \tilde{d}_{22} &= \frac{(3-2s_w^2)^2}{3} + \frac{(4s_w^2-3)v^2|A_{\tilde{2}1}|^2}{(m_1^2-\tilde{m}_2^2)^2} + \frac{(4s_w^2-3)v^2|A_{\tilde{3}\tilde{2}}|^2}{(m_3^2-\tilde{m}_2^2)^2}, \\
 \tilde{D}^{2/3} &\approx \frac{1}{12} \begin{pmatrix} \frac{(4s_w^2+3)^2}{3} & \frac{16s_w^2v^2Y_{\tilde{2}2}}{\tilde{m}_2^2-m_2^2} & 0 \\ \frac{16s_w^2v^2Y_{\tilde{2}2}^*}{\tilde{m}_2^2-m_2^2} & \frac{(4s_w^2-3)^2}{3} - \frac{2(8s_w^2-9)v^2|A_{\tilde{3}\tilde{2}}|^2}{(m_3^2-\tilde{m}_2^2)^2} & \frac{\sqrt{2}(8s_w^2-9)vA_{\tilde{3}\tilde{2}}}{\tilde{m}_2^2-m_3^2} \\ 0 & \frac{\sqrt{2}(8s_w^2-9)vA_{\tilde{3}\tilde{2}}^*}{\tilde{m}_2^2-m_3^2} & \frac{4(3-2s_w^2)^2}{3} + \frac{2(8s_w^2-9)v^2|A_{\tilde{3}\tilde{2}}|^2}{(m_3^2-\tilde{m}_2^2)^2} \end{pmatrix}, \\
 \tilde{D}^{-4/3} &\approx \frac{1}{3} \begin{pmatrix} \frac{16s_w^4}{3} & \frac{\sqrt{2}(8s_w^2-3)v^2Y_{\tilde{3}1}^*}{m_3^2-\tilde{m}_1^2} \\ \frac{\sqrt{2}(8s_w^2-3)v^2Y_{\tilde{3}1}}{m_3^2-\tilde{m}_1^2} & \frac{(3-4s_w^2)^2}{3} \end{pmatrix}.
 \end{aligned} \tag{6.34}$$

Analogously to the Z boson, different LQ generations mix under W interactions. Without LQ mixing, the interactions with the W boson can be written in terms of the following matrices

$$B^1 = \begin{pmatrix} 0 & 0 & 0 \\ 0 & 0 & \sqrt{2} \end{pmatrix}, \quad B^2 = \begin{pmatrix} 0 & 0 & 0 \\ 0 & 1 & 0 \\ 0 & 0 & -\sqrt{2} \end{pmatrix}, \quad B^3 = \begin{pmatrix} 1 & 0 & 0 \end{pmatrix}, \tag{6.35}$$

arranging the LQ in their charge eigenstates according to Eq. (6.7). B^1 describes the interaction of LQs with electric charges $Q = -4/3$ and $Q = -1/3$, B^2 the ones with $Q = -1/3$ and $Q = 2/3$, B^3 with $Q = 5/3$ and $Q = 2/3$. If we include LQ mixing, the matrices expanded up to $\mathcal{O}(v^2)$, then read

$$\begin{aligned}
 \tilde{B}^1 &\approx \begin{pmatrix} 0 & 0 & \frac{2v^2Y_{\tilde{3}1}^*}{\tilde{m}_1-m_3^2} \\ \frac{\sqrt{2}v^2}{m_1^2-m_3^2} \left(\frac{A_{\tilde{2}1}^*A_{\tilde{3}\tilde{2}}}{m_1^2-\tilde{m}_2^2} + Y_{\tilde{3}1}^* \right) & \frac{\sqrt{2}vA_{\tilde{3}\tilde{2}}^*}{\tilde{m}_2^2-m_3^2} & \sqrt{2} - \frac{v^2|A_{\tilde{3}\tilde{2}}|^2}{\sqrt{2}(\tilde{m}_2^2-m_3^2)^2} \end{pmatrix}, \\
 \tilde{B}^2 &\approx \begin{pmatrix} 0 & \frac{vA_{\tilde{2}1}^*}{m_1^2-\tilde{m}_2^2} & \frac{\sqrt{2}v^2}{m_1^2-m_3^2} \left(\frac{A_{\tilde{3}\tilde{2}}^*A_{\tilde{2}1}}{m_3^2-\tilde{m}_2^2} - Y_{\tilde{3}1} \right) \\ \frac{v^2Y_{\tilde{2}2}^*}{m_2^2-\tilde{m}_2^2} & 1 - \frac{v^2}{2} \left(\frac{|A_{\tilde{2}1}|^2}{(m_1^2-\tilde{m}_2^2)^2} - \frac{|A_{\tilde{3}\tilde{2}}|^2}{(\tilde{m}_2^2-m_3^2)^2} \right) & 0 \\ 0 & \frac{vA_{\tilde{3}\tilde{2}}^*}{\tilde{m}_2^2-m_3^2} & -\sqrt{2} - \frac{v^2|A_{\tilde{3}\tilde{2}}|^2}{\sqrt{2}(m_3^2-\tilde{m}_2^2)^2} \end{pmatrix}, \\
 \tilde{B}^3 &\approx \begin{pmatrix} 1 & \frac{-v^2Y_{\tilde{2}2}^*}{m_2^2-\tilde{m}_2^2} & 0 \end{pmatrix}.
 \end{aligned} \tag{6.36}$$

We also have interaction matrices for the $W^+W^-\Phi^Q\Phi^Q$ vertex. Without mixing, they read

$$F^{-1/3} = \begin{pmatrix} 0 & 0 & 0 \\ 0 & \frac{1}{2} & 0 \\ 0 & 0 & 2 \end{pmatrix} \quad F^{2/3} = \begin{pmatrix} \frac{1}{2} & 0 & 0 \\ 0 & \frac{1}{2} & 0 \\ 0 & 0 & 1 \end{pmatrix} \quad F^{-4/3} = \begin{pmatrix} 0 & 0 \\ 0 & 1 \end{pmatrix}, \quad F^{5/3} = \frac{1}{2}. \quad (6.37)$$

If we include mixing and expand up to order $\mathcal{O}(v^2)$, we obtain

$$\begin{aligned} \tilde{F}^{-1/3} &\approx \begin{pmatrix} \frac{v^2|A_{21}|^2}{2(m_1^2-\tilde{m}_2^2)^2} & \frac{vA_{21}^*}{2(m_1^2-\tilde{m}_2^2)} & \tilde{f}_{13} \\ \frac{vA_{21}}{2(m_1^2-\tilde{m}_2^2)} & \frac{1}{2} + \frac{v^2}{2} \left(\frac{3|A_{32}|^2}{(\tilde{m}_2^2-\tilde{m}_3^2)^2} - \frac{|A_{21}|^2}{(\tilde{m}_2^2-m_1^2)^2} \right) & \frac{3vA_{32}}{2(\tilde{m}_2^2-\tilde{m}_3^2)}, \\ \tilde{f}_{13}^* & \frac{3vA_{32}^*}{2(\tilde{m}_2^2-\tilde{m}_3^2)} & 2 - \frac{3v^2|A_{32}|^2}{2(\tilde{m}_2^2-\tilde{m}_3^2)^2} \end{pmatrix}, \\ \text{with } \tilde{f}_{13} &= \frac{2v^2Y_{31}}{m_1^2-m_3^2} - \frac{v^2A_{32}A_{21}^*(m_1^2-4\tilde{m}_2^2+3m_3^2)}{2(m_1^2-m_3^2)(m_1^2-\tilde{m}_2^2)(\tilde{m}_2^2-m_3^2)} \\ \tilde{F}^{2/3} &\approx \begin{pmatrix} \frac{1}{2} & 0 & 0 \\ 0 & \frac{1}{2} + \frac{v^2|A_{32}|^2}{(\tilde{m}_2^2-\tilde{m}_3^2)^2} & \frac{vA_{32}}{\sqrt{2}(-m_3^2\tilde{m}_2^2)} \\ 0 & \frac{vA_{32}^*}{\sqrt{2}(m_3^2-\tilde{m}_2^2)} & 1 - \frac{v^2|A_{32}|^2}{(\tilde{m}_2^2-\tilde{m}_3^2)^2} \end{pmatrix}, \\ \tilde{F}^{-4/3} &\approx \begin{pmatrix} 0 & \frac{\sqrt{2}v^2Y_{31}^*}{m_1^2-m_3^2} \\ \frac{\sqrt{2}v^2Y_{31}}{m_1^2-m_3^2} & 1 \end{pmatrix}. \end{aligned} \quad (6.38)$$

Finally we show the Higgs coupling matrices in (6.13) up to $\mathcal{O}(v)$

$$\begin{aligned} \tilde{\Gamma}^{-1/3} &\approx \frac{1}{\sqrt{2}} \begin{pmatrix} 2v\left(Y_1 + \frac{|A_{21}|^2}{m_1^2-\tilde{m}_2^2}\right) & A_{21}^* & v\left(2Y_{31} - \frac{A_{32}A_{21}^*(m_1^2+m_3^2-2\tilde{m}_2^2)}{(m_1^2-\tilde{m}_2^2)(\tilde{m}_2^2-m_3^2)}\right) \\ A_{21} & \tilde{\Gamma}_{22}^{-1/3} & A_{32} \\ v\left(2Y_{31}^* - \frac{A_{21}A_{32}^*(m_1^2+m_3^2-2\tilde{m}_2^2)}{(m_1^2-\tilde{m}_2^2)(\tilde{m}_2^2-m_3^2)}\right) & A_{32}^* & 2v\left(Y_3 + \frac{|A_{32}|^2}{m_3^2-\tilde{m}_2^2}\right) \end{pmatrix}, \\ \text{with } \tilde{\Gamma}_{22}^{-1/3} &= 2v\left(Y_2 - \frac{|A_{21}|^2}{m_1^2-\tilde{m}_2^2} - \frac{|A_{32}|^2}{m_3^2-\tilde{m}_2^2}\right), \\ \tilde{\Gamma}^{2/3} &\approx \frac{1}{\sqrt{2}} \begin{pmatrix} 2vY_2 & 2vY_{22} & 0 \\ 2vY_{22}^* & 2v\left(Y_2 + Y_{22} - \frac{2|A_{32}|^2}{m_3^2-\tilde{m}_2^2}\right) & -\sqrt{2}A_{32} \\ 0 & -\sqrt{2}A_{32}^* & 2v\left(Y_3 + \frac{2|A_{32}|^2}{m_3^2-\tilde{m}_2^2}\right) \end{pmatrix}, \\ \tilde{\Gamma}^{-4/3} &\approx \Gamma^{-4/3}. \end{aligned} \quad (6.39)$$

and

$$\begin{aligned}
 \tilde{\Lambda}^{-1/3} &\approx \frac{1}{2} \begin{pmatrix} Y_1 & v \left(\frac{Y_{31} A_{3\bar{2}}^*}{\tilde{m}_2^2 - \tilde{m}_3^2} + \frac{(Y_2 - Y_1) A_{\bar{2}1}^*}{m_1^2 - \tilde{m}_2^2} \right) & Y_{31} \\ v \left(\frac{Y_{31} A_{3\bar{2}}^*}{\tilde{m}_2^2 - \tilde{m}_3^2} + \frac{(Y_2 - Y_1) A_{\bar{2}1}^*}{m_1^2 - \tilde{m}_2^2} \right) & Y_2 & v \left(\frac{Y_{31} A_{\bar{2}1}^*}{\tilde{m}_2^2 - \tilde{m}_1^2} + \frac{(Y_2 - Y_3) A_{3\bar{2}}^*}{m_3^2 - \tilde{m}_2^2} \right) \\ Y_{31}^* & v \left(\frac{Y_{31} A_{\bar{2}1}^*}{\tilde{m}_2^2 - \tilde{m}_1^2} + \frac{(Y_2 - Y_3) A_{3\bar{2}}^*}{m_3^2 - \tilde{m}_2^2} \right) & Y_3 \end{pmatrix}, \\
 \tilde{\Lambda}^{2/3} &\approx \frac{1}{2} \begin{pmatrix} Y_2 & Y_{\bar{2}2} & \frac{\sqrt{2} v Y_{\bar{2}2} A_{3\bar{2}}}{\tilde{m}_2^2 - \tilde{m}_3^2} \\ Y_{\bar{2}2}^* & Y_2 + Y_{\bar{2}2} & \frac{\sqrt{2} v (Y_3 - Y_2 - Y_{\bar{2}2}) A_{3\bar{2}}}{m_3^2 - \tilde{m}_2^2} \\ \frac{\sqrt{2} v Y_{\bar{2}2}^* A_{3\bar{2}}^*}{\tilde{m}_2^2 - \tilde{m}_3^2} & \frac{\sqrt{2} v (Y_3 - Y_2 - Y_{\bar{2}2}) A_{3\bar{2}}^*}{m_3^2 - \tilde{m}_2^2} & Y_3 \end{pmatrix}, \\
 \tilde{\Lambda}^{-4/3} &\approx \Lambda^{-4/3}.
 \end{aligned} \tag{6.40}$$

6.7.3 Exact Results for the Vacuum Polarization Functions

In this section we give the q^2 -expanded results for the vacuum polarization functions, with the LQ masses and couplings kept unexpanded

$$\begin{aligned}
 \Pi_{\gamma\gamma}(q^2) &= - \sum_Q \frac{N_c e^2 Q^2}{48\pi^2} q^2 \left(\frac{1}{\varepsilon} + \log \left(\frac{\mu^2}{(M_a^Q)^2} \right) + \frac{q^2}{10(M_a^Q)^2} \right), \\
 \Pi_{Z\gamma}(q^2) &= - \sum_Q \frac{N_c g_2 e (\tilde{T}_{aa}^Q - s_w^2 Q)}{48\pi^2 c_w} Q q^2 \left(\frac{1}{\varepsilon} + \log \left(\frac{\mu^2}{(M_a^Q)^2} \right) + \frac{q^2}{10(M_a^Q)^2} \right), \\
 \Pi_{ZZ}(q^2) &= \sum_Q \frac{N_c}{16\pi^2} \left(\frac{g_2 \Gamma_{aa}^Q}{c_w} \frac{m_Z}{m_h^2} - \frac{2g_2^2 \tilde{D}_{aa}^Q}{c_w^2} \right) (M_a^Q)^2 \left(\frac{1}{\varepsilon} + \log \left(\frac{\mu^2}{(M_a^Q)^2} \right) + 1 \right) \\
 &\quad - \sum_Q \frac{N_c g_2^2 (\tilde{T}_{ab}^Q - s_w^2 Q \delta_{ab}) (\tilde{T}_{ba}^Q - s_w^2 Q \delta_{ba})}{32\pi^2 c_w^2} \times F \left((M_a^Q)^2, (M_b^Q)^2 \right), \\
 \Pi_{WW}(q^2) &= \sum_Q \frac{N_c}{16\pi^2} \left(g_2 \Gamma_{aa}^Q \frac{m_W}{m_h^2} - g_2^2 \tilde{F}_{aa}^Q \right) (M_a^Q)^2 \left(\frac{1}{\varepsilon} + \log \left(\frac{\mu^2}{(M_a^Q)^2} \right) + 1 \right) \\
 &\quad - \sum_{a(b)=1}^{2(3)} \frac{N_c g_2^2 |\tilde{B}_{ab}^1|^2}{64\pi^2} (M_a^{-4/3})^2 F \left((M_a^{-4/3})^2, (M_b^{-1/3})^2 \right) \\
 &\quad - \sum_{a,b=1}^3 \frac{N_c g_2^2 |\tilde{B}_{ab}^2|^2}{64\pi^2} (M_a^{-1/3})^2 F \left((M_a^{-1/3})^2, (M_b^{2/3})^2 \right) \\
 &\quad - \sum_{b=1}^3 \frac{N_c g_2^2 |\tilde{B}_b^3|^2}{64\pi^2} (M^{5/3})^2 F \left((M^{5/3})^2, (M_b^{2/3})^2 \right),
 \end{aligned} \tag{6.41}$$

where $Q = \{-1/3, 2/3, -4/3, 5/3\}$ with a and b running from 1 to 3, 3, 2, and 1, respectively. Here we defined

$$F \left((M_a^Q)^2, (M_b^Q)^2 \right) = (M_a^Q)^2 \left(f_0 + \frac{q^2}{(M_a^Q)^2} f_1 + \left(\frac{q^2}{(M_a^Q)^2} \right)^2 f_2 \right), \tag{6.42}$$

with

$$\begin{aligned}
 f_0 &= -2(x_{ba}^Q + 1) \left(\frac{1}{\varepsilon} + \log\left(\frac{\mu^2}{M_a^2}\right) + \frac{3}{2} \right) + \frac{2(x_{ba}^Q)^2 \log(x_{ba}^Q)}{x_{ba}^Q - 1}, \\
 f_1 &= \frac{2}{3} \left(\frac{1}{\varepsilon} + \log\left(\frac{\mu^2}{M_a^2}\right) \right) - \frac{5 - 27x_{ba}^Q + 27(x_{ba}^Q)^2 - 5(x_{ba}^Q)^3 - 6(3 - x_{ba}^Q)(x_{ba}^Q)^2 \log(x_{ba}^Q)}{9(x_{ba}^Q - 1)^3}, \\
 f_2 &= \frac{-1 + 8x_{ba}^Q - 8(x_{ba}^Q)^3 + (x_{ba}^Q)^4 + 12(x_{ba}^Q)^2 \log(x_{ba}^Q)}{6(x_{ba}^Q - 1)^5},
 \end{aligned} \tag{6.43}$$

where again

$$x_{ba}^Q = \frac{(M_b^Q)^2}{(M_a^Q)^2}.$$

6.7.4 Leading Order SM Amplitudes in Higgs Decays

The SM amplitudes for the $h\gamma\gamma$, hgg and $hZ\gamma$ couplings in Eq. (6.24) read

$$\begin{aligned}
 A_1(x) &= \frac{-(2x^2 + 3x + 3(2x - 1)f(x))}{x^2}, \\
 A_{1/2}(x) &= \frac{2(x + (x - 1)f(x))}{x^2}, \\
 C_1(x, y) &= 4\left(3 - \frac{s_w^2}{c_w^2}\right)I_2(x, y) + \left(\left(1 + \frac{2}{x}\right)\frac{s_w^2}{c_w^2} - \left(5 + \frac{2}{x}\right)\right)I_1(x, y), \\
 C_{1/2}(x, y) &= I_1(x, y) - I_2(x, y),
 \end{aligned} \tag{6.44}$$

with

$$\begin{aligned}
 f(x) &= \arcsin^2(\sqrt{x}), \\
 g(x) &= \sqrt{\frac{1}{x} - 1} \arcsin(\sqrt{x}), \\
 I_1(x, y) &= \frac{xy}{2(x - y)} + \frac{x^2y^2(f(x^{-1}) - f(y^{-1}))}{2(x - y)^2} + \frac{x^2y(g(x^{-1}) - g(y^{-1}))}{(x - y)^2}, \\
 I_2(x, y) &= \frac{-xy(f(x^{-1}) - f(y^{-1}))}{2(x - y)}.
 \end{aligned} \tag{6.45}$$

Chapter 7

Correlating $h \rightarrow \mu^+ \mu^-$ to the Anomalous Magnetic Moment of the Muon via Leptoquarks

submitted for publication in

Phys. Rev. Lett.

arXiv: 2008.02643 [hep-ph]

Correlating $h \rightarrow \mu^+\mu^-$ to the Anomalous Magnetic Moment of the Muon via Leptoquarks

Andreas Crivellin

Paul Scherrer Institut, CH-5232 Villigen PSI, Switzerland

CERN Theory Division, CH-1211 Geneva 23, Switzerland

Physik-Institut, Universität Zürich, Winterthurerstrasse 190, CH-8057 Zürich, Switzerland

Dario Müller

Paul Scherrer Institut, CH-5232 Villigen PSI, Switzerland

Physik-Institut, Universität Zürich, Winterthurerstrasse 190, CH-8057 Zürich, Switzerland

Francesco Saturnino

Albert Einstein Center for Fundamental Physics, Institute for Theoretical Physics, University of Bern, CH-3012 Bern, Switzerland

Recently, both ATLAS and CMS measured the decay $h \rightarrow \mu^+\mu^-$, finding a signal strength with respect to the Standard Model expectation of 1.2 ± 0.6 and $1.19^{+0.41+0.17}_{-0.39-0.16}$, respectively. This provides, for the first time, evidence that the Standard Model Higgs couples to second generation fermions. This measurement is particularly interesting in the context of the intriguing hints for lepton flavor universality violation, accumulated within recent years, as new physics explanations could also be tested in the $h \rightarrow \mu^+\mu^-$ decay mode. Leptoquarks are prime candidates to account for the flavor anomalies. In particular, they can provide the necessary chiral enhancement (by a factor m_t/m_μ) to address a_μ with TeV scale new physics. In this letter we point out that such explanations of a_μ also lead to enhanced effects in $h \rightarrow \mu^+\mu^-$ and we examine the correlations between $h \rightarrow \mu^+\mu^-$ and a_μ within leptoquark models. We find that the effect in the branching ratio of $h \rightarrow \mu^+\mu^-$ ranges from several percent up to a factor three, if one aims at accounting for a_μ at the 2σ level. Hence, the new ATLAS and CMS measurements already provide important constraints on the parameter space, rule out specific a_μ explanations and will be very important to test the flavor anomalies in the future.

7.1 Introduction

The Large Hadron Collider (LHC) at CERN confirmed the predictions of the Standard Model (SM) of particle physics by discovering the Brout-Englert-Higgs boson [42, 426] in 2012. However, until now, high energy searches did not discover any particles beyond the ones present in the SM. Therefore, great hopes of finding new physics (NP) rest on low energy precision physics where flavor experiments have accumulated intriguing hints for physics beyond the SM within the recent years, most prominently in $b \rightarrow s\ell^+\ell^-$ data [78, 79, 374], $b \rightarrow c\tau\nu$ transitions [104, 109, 111] and the anomalous magnetic moment (AMM) of the muon ($a_\mu = (g-2)_\mu/2$) [55, 123]. Interestingly, these hints for NP fall into a common pattern: they can be considered as signs of lepton flavor universality violation (LFUV)²⁵, which is respected by the SM gauge interactions and is only broken by the Higgs Yukawa couplings.

Among these anomalies, $a_\mu = (g-2)_\mu/2$, which displays a 3.7σ deviation from the SM prediction [124], is most closely related to Higgs interactions as it is a chirality changing observ-

²⁵Recently, it has been pointed out that also the Cabibbo Angle Anomaly can be interpreted as a sign of LFUV [427, 428].

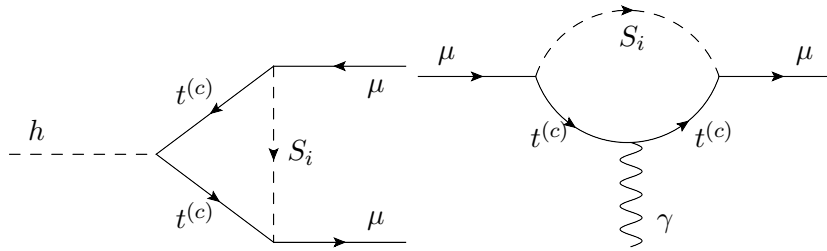


Figure 7.1: Sample Feynman diagrams which contribute to $h \rightarrow \mu^+\mu^-$ (top) and the AMM of the muon (bottom). In addition, we have to include the diagrams where the Higgs and photon couple to the LQ, as well as self-energy diagrams.

able. I.e. it involves a chirality flip and therefore a violation of $SU(2)_L$ is required to obtain a non-zero contribution. Furthermore, the required NP effect to explain a_μ is of the order of the electroweak (EW) SM contribution and TeV scale solutions need an enhancement mechanism, called chiral enhancement, to be able to account for the deviation (see e.g. Ref. [286] for a recent discussion). Obviously, also $h \rightarrow \mu^+\mu^-$ is a chirality changing process and any enhanced effect in a_μ should also result in an enhanced effect here²⁶. Recently, both ATLAS and CMS measured $h \rightarrow \mu^+\mu^-$, finding a signal strength w.r.t. the SM expectation of 1.2 ± 0.6 [433] and $1.19^{+0.41+0.17}_{-0.39-0.16}$ [434], respectively.

The mechanism of chiral enhancement, necessary to explain a_μ , has been well studied (see Ref. [286] for a recent account). Here leptoquarks (LQs) are particularly interesting since they can give rise to an enhancement factor of $m_t/m_\mu \approx 1700$ [48, 238, 241, 243, 277–286, 309–314, 368, 375, 379, 380, 435], allowing for a TeV scale explanation with perturbative couplings that are not in conflict with direct LHC searches. In fact, there are only two LQs, out of the 10 possible representations [147], that can yield this enhancement: the scalar LQ $SU(2)_L$ singlet (S_1) and the scalar LQ $SU(2)_L$ doublet (S_2) with hypercharge $-2/3$ and $-7/3$, respectively. In addition, there is the possibility that S_1 mixes with the $SU(2)_L$ triplet LQ S_3 , where S_1 only couples to right-handed fermions [314].

Furthermore, LQs are also well motivated by the hints for LFUV in semi-leptonic B decays, both in $b \rightarrow s\mu^+\mu^-$ [78, 79, 374] and $b \rightarrow c\tau\nu$ data [104, 109, 111], which deviate from the SM with up to $\approx 6\sigma$ [97, 98, 100, 209] and $\approx 3\sigma$ [119–122, 315], respectively. Here possible solutions include again S_1 [47, 176, 212, 232, 233, 235, 236, 238–242, 244–247, 249, 250, 287, 311], S_2 [234, 235, 309, 319–325] and S_3 [173, 175–177, 180, 317, 332, 333], where S_1 and S_3 together can provide a common explanation of the B anomalies and the AMM of the muon [48, 176, 243, 326, 327]. We take this as a motivation to study these correlations for the LQs which can generate m_t/m_μ enhanced effects by considering three scenarios: 1) S_1 only, 2) S_2 only, 3) $S_1 + S_3$ where S_1 only couples to right-handed fermions. Note that these are the only scenarios which can give rise to the desired m_t/m_μ enhanced effect.

7.2 Setup and Observables

The most precise measurement of the anomalous magnetic moment (AMM) of the muon ($a_\mu = (g - 2)_\mu/2$) has been achieved by the E821 experiment at Brookhaven [55, 123], which differs from the SM prediction by

$$\delta a_\mu = a_\mu^{\text{exp}} - a_\mu^{\text{SM}} = (279 \pm 76) \times 10^{-11}, \quad (7.1)$$

²⁶Correlations between a_μ and $h \rightarrow \mu^+\mu^-$ were considered in the EFT in Ref. [251] and in the context of vector-like leptons (see Ref. [429] for a recent global analysis) in Ref. [286, 430–432].

	\mathcal{G}_{SM}	$\mathcal{L}_{q\ell}$
S_1	$\left(3, 1, -\frac{2}{3}\right)$	$\left(\lambda_{fj}^R \bar{u}_f^c \ell_j + \lambda_{fj}^L \bar{Q}_f^c i\tau_2 L_j\right) S_1^\dagger + \text{h.c.}$
S_2	$\left(3, 2, \frac{7}{3}\right)$	$\gamma_{fj}^{RL} \bar{u}_f S_2^T i\tau_2 L_j + \gamma_{fj}^{LR} \bar{Q}_f \ell_j S_2 + \text{h.c.}$
S_3	$\left(3, 3, -\frac{2}{3}\right)$	$\kappa_{fj} \bar{Q}_f^c i\tau_2 (\tau \cdot S_3)^\dagger L_j + \text{h.c.}$

Table 7.1: Scalar LQ representations together with their couplings to quarks and leptons, generating the desired m_t/m_μ enhanced effect in the AMM of the muon. Here \mathcal{G}_{SM} refers to the SM gauge group $SU(3)_c \times SU(2)_L \times U(1)_Y$, L (Q) is the lepton (quark) $SU(2)_L$ doublet, u (ℓ) the up-type quark (lepton) singlet and c refers to charge conjugation. Furthermore, j and f are flavor indices and τ_k the Pauli matrices.

corresponding to a 3.7σ deviation [124]²⁷. Therefore, it is very interesting to investigate if and how this discrepancy can be explained by physics beyond the SM²⁸.

As we motivated in the introduction, we will focus on the three scalar LQs S_1 , S_2 and S_3 for explaining a_μ . These representations couple to fermions as given in Table 7.1²⁹. Since we are in the following only interested in muon couplings to third generation quarks, we define $\lambda_R \equiv \lambda_{32}^R$, $\lambda_L \equiv \lambda_{32}^L$, $\gamma_{LR} \equiv \gamma_{32}^{LR}$, $\gamma_{RL} \equiv \gamma_{32}^{RL}$, $\kappa = \kappa_{32}$.

In addition to the gauge interactions, which are determined by the representation under the SM gauge group, LQ can couple to the SM Higgs [335]

$$\begin{aligned} \mathcal{L}_H &= Y_{13} S_1^\dagger \left(H^\dagger (\tau \cdot S_3) H \right) + \text{h.c.} \\ &- Y_{22} (H i\tau_2 S_2)^\dagger (H i\tau_2 S_2) - \sum_{k=1}^3 (m_k^2 + Y_k H^\dagger H) S_k^\dagger S_k \end{aligned} \quad (7.2)$$

Here m_k^2 are the $SU(2)_L$ invariant bi-linear masses of the LQs. After $SU(2)_L$ breaking, the term Y_{13} generates off-diagonal elements in the LQ mass matrices and one has to diagonalize them through unitary transformations in order to arrive at the physical basis. Therefore, non-zero values of Y_{13} are necessary to generate m_t/m_μ enhanced effects in scenario 3). Y_1 and $Y_{2,22}$ are phenomenologically relevant for $h \rightarrow \mu^+ \mu^-$ in scenario 1) and 2), respectively, but not necessary for an m_t/m_μ enhancement.

²⁷This result is based on Refs. [128, 130, 133, 135, 139, 142–144, 303, 304, 306, 436–444]. The recent lattice result of the Budapest-Marseilles-Wuppertal collaboration (BMWc) for the hadronic vacuum polarization (HVP) [302] on the other hand is not included. This result would render the SM prediction of a_μ compatible with experiment. However, the BMWc results are in tension with the HVP determined from $e^+e^- \rightarrow \text{hadrons}$ data [130, 133, 135, 303, 304, 306]. Furthermore, the HVP also enters the global EW fit [307], whose (indirect) determination is below the BMWc result [308]. Therefore, the BMWc determination of the HVP would increase tension in EW fit [445, 446] and we opted for using the community consensus of Ref. [124].

²⁸Recently, also a discrepancy of $\approx 2.5\sigma$ in the AMM of the electron has been observed [125, 447–450], which has interestingly opposite sign than in the muon case. While this discrepancy cannot be explained by a single LQ representation or generation [286, 435], multiple LQs could account for both anomalies since the contributions have a free phase. Note that our conclusions for the correlation between a_μ and $h \rightarrow \mu^+ \mu^-$ are independent of a_e .

²⁹Note that “pure” LQs with couplings only to one quark and one lepton do not give rise to proton decays at any perturbative order. In order to generate such an effect, di-quark couplings would be necessary, which can however be avoided (again at any order in perturbation theory) by assigning baryon and/or lepton number to the LQs.

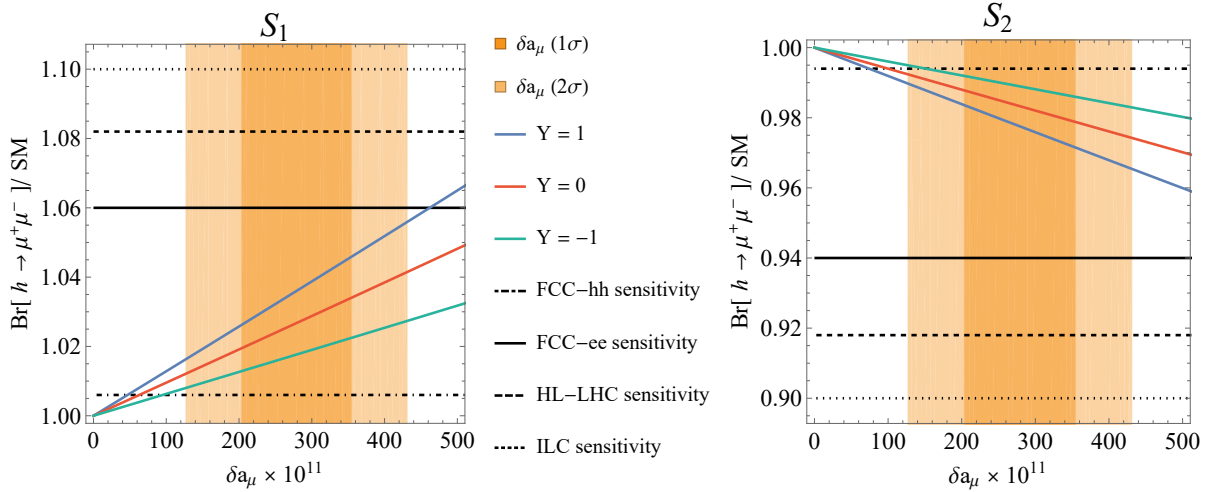


Figure 7.2: Correlations between the $\text{Br}[h \rightarrow \mu^+\mu^-]$, normalized to its SM value, and the NP contribution in the AMM of the muon δa_μ for scenario 1) (left) and scenario 2) (right) with $m_{1,2} = 1.5 \text{ TeV}$. The predictions for different values of the LQ couplings to the Higgs are shown, where for scenario 1) $Y = Y_1$ while in scenario 2) $Y = Y_2 + Y_{22}$. Even though the current ATLAS and CMS results are not yet constraining for these models, sizeable effects are predicted, which can be tested at future colliders. Furthermore, scenario 1) yields a constructive effect in $h \rightarrow \mu^+\mu^-$ while the one in scenario 2) is destructive such that they can be clearly distinguished with increasing experimental precision.

Now we can calculate the effects in a_μ and $h \rightarrow \mu^+\mu^-$ ³⁰ for which sample diagrams are shown in Fig. 7.1. In both cases we have on-shell kinematics. For a_μ the self-energies can simply be taken into account via the Lehmann-Symanzik-Zimmermann formalism and no renormalization is necessary. This is however required for $h \rightarrow \mu^+\mu^-$ in order to express the result in terms of the physical muon mass. Here, the effective Yukawa coupling, which enters $h \rightarrow \mu^+\mu^-$, is given by $Y_\mu^{\text{eff}} = \frac{m_\mu - \Sigma_{\mu\mu}^{LR}}{v} + \Lambda_{\mu\mu}^{LR}$, where $\Lambda_{\mu\mu}^{LR}$ is the genuine vertex correction shown in Fig. 7.1 and $\Sigma_{\mu\mu}^{LR}$ is the chirality changing part of the muon self-energy. In these conventions $-i\Sigma_{\mu\mu}^{LR} P_R$ equals the expression of the Feynman diagram for the self-energy. Note that Y_μ^{eff} is finite without introducing a counter-term. For a_μ we expand in the muon mass and external momenta up to the first non-vanishing order, while in $h \rightarrow \mu^+\mu^-$ external momenta can be set to zero from the outset but we expand in $m_h^2/m_{1,2,3}^2$. The resulting amplitudes can be further simplified by expanding the LQ mixing matrices and mass eigenvalues in $v^2/m_{1,2,3}^2$ and the loop functions in m_h^2/m_t^2 , which gives a very precise numerical approximation, resulting in

$$\frac{\text{Br}[h \rightarrow \mu^+\mu^-]}{\text{Br}[h \rightarrow \mu^+\mu^-]_{\text{SM}}} \approx \left| 1 + \frac{m_t}{m_\mu} \frac{N_c}{8\pi^2} \left[\frac{\lambda_R^* \lambda_L}{m_1^2} \left(\frac{m_t^2}{8} \mathcal{J} \left(\frac{m_h^2}{m_t^2}, \frac{m_t^2}{m_1^2} \right) + v^2 Y_1 \right) + v^2 \lambda_R^* \kappa Y_{13} \frac{\log(m_3^2/m_1^2)}{m_3^2 - m_1^2} \right. \right. \\ \left. \left. + \frac{\gamma_{LR}^* \gamma_{RL}}{m_2^2} \left(\frac{m_t^2}{8} \mathcal{J} \left(\frac{m_h^2}{m_t^2}, \frac{m_t^2}{m_2^2} \right) + v^2 (Y_2 + Y_{22}) \right) \right] \right|^2, \quad (7.3)$$

$$\delta a_\mu \approx \frac{m_\mu}{4\pi^2} \frac{N_c m_t}{12} \text{Re} \left[\frac{\gamma_{LR} \gamma_{RL}^*}{m_2^2} \mathcal{E}_1 \left(\frac{m_t^2}{m_2^2} \right) - \frac{\lambda_R}{m_1^2} \left(\lambda_L^* \mathcal{E}_2 \left(\frac{m_t^2}{m_1^2} \right) + \kappa Y_{13} \frac{v^2}{m_3^2} \mathcal{E}_3 \left(\frac{m_1^2}{m_3^2}, \frac{m_t^2}{m_3^2} \right) \right) \right], \quad (7.4)$$

³⁰Correlations between the related modes $\tau \rightarrow \mu\gamma$ and $h \rightarrow \tau\mu$ were studied in Refs. [451–453] in the context of LQs

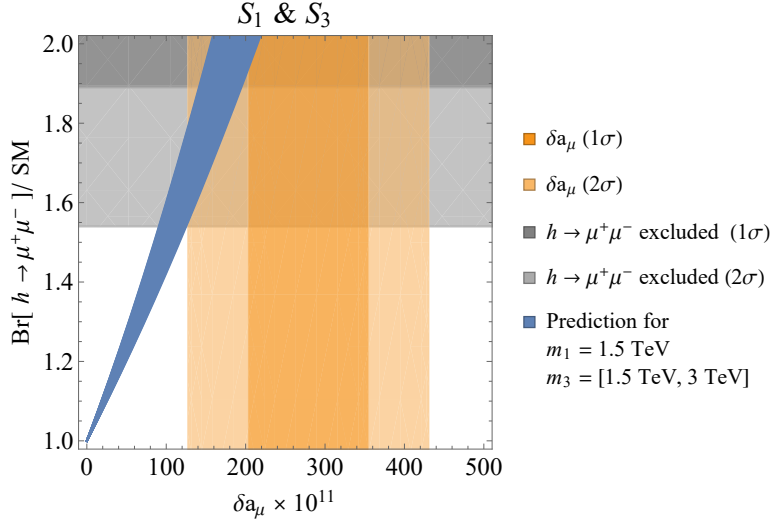


Figure 7.3: Correlations between the NP contribution to the AMM of the muon (δa_μ) and $\text{Br}[h \rightarrow \mu^+ \mu^-]$, normalized to its SM value in scenario 3). This correlation depends to a good approximation only on the ratio m_1/m_3 . As the effect is symmetric in m_1 and m_3 , we fix one mass to 1.5 TeV and obtain the dark-blue band by varying the other mass between 1.5 TeV and 3 TeV. The effect in $h \rightarrow \mu^+ \mu^-$ within the preferred region for a_μ is necessarily constructive and so large that an explanation is already constrained by the ATLAS and CMS measurements of $h \rightarrow \mu^+ \mu^-$.

with the loop functions given by

$$\mathcal{J}(x, y) = 2(x - 4) \log(y) - 8 + \frac{13}{3}x, \quad (7.5)$$

$$\begin{aligned} \mathcal{E}_1(x) &= 1 + 4 \log(x), \quad \mathcal{E}_2(x) = 7 + 4 \log(x), \\ \mathcal{E}_3(x, y) &= \mathcal{E}_2(y) + \frac{4 \log(x)}{x - 1}. \end{aligned} \quad (7.6)$$

We only considered the m_t enhanced effects and neglected small CKM rotations, which in principle appear after EW symmetry breaking. As anticipated, in Eq. (7.4) one can see that scenario 3) only contributes if Y_{13} is non-zero. Furthermore, since in this scenario a_μ has a relative suppression of $v^2/m_{1,3}^2$ with respect to $h \rightarrow \mu^+ \mu^-$, one expects here the largest effects in Higgs decays. In principle also Y_1 , Y_2 and Y_{22} enter in Eq. (7.4). However, their effect is sub-leading as it is suppressed by $v^2/m_{1,2}^2$.

7.3 Phenomenology

Let us now study the correlations between a_μ and $h \rightarrow \mu^+ \mu^-$ in our three scenarios with m_t -enhanced contributions. First, we consider scenario 1) and 2) where S_1 and S_2 give separately rise to m_t -enhanced effects in a_μ and $h \rightarrow \mu^+ \mu^-$. Since both processes involve the same product of couplings to SM fermions, the correlation depends only weakly via a logarithm on $m_t^2/m_{1,2}^2$. However, there is a dependence on Y_1 and $Y_{22} + Y_2$ which breaks the direct correlation but cannot change the sign of the effect for order one couplings. This can be seen in Fig. 7.2, where the correlations are depicted for $m_{1,2} = 1.5$ TeV, respecting LHC bounds [454–456]. The predicted effect is not large enough such that the current ATLAS and CMS measurements are sensitive to it. However, note that it is still sizeable due to the m_t enhancement and therefore detectable

at future colliders where the ILC [407], the HL-LHC [457], the FCC-ee [357], CEPC [423] or the FCC-hh [424] aim at a precision of approximately 10%, 8%, 6% and below 1%, respectively. Furthermore, the effect in $\text{Br}[h \rightarrow \mu^+\mu^-]$ in scenario 1) is necessarily constructive while in scenario 2) it is destructive, such that in the future a LQ explanation of a_μ by S_1 could be clearly distinguished from the one involving S_2 .

In scenario 3), where S_1 only couples to right-handed fermions, the effect in $\text{Br}[h \rightarrow \mu^+\mu^-]$ is even more pronounced due to the relative suppression of the contribution to a_μ by $v^2/m_{1,3}^2$, see Eq. (7.4). Furthermore, in this case the correlation between a_μ and $h \rightarrow \mu^+\mu^-$ depends to a good approximation only on the ratio m_1/m_3 . As the effect is symmetric in m_1 and m_3 we fix one mass to 1.5 TeV and obtain the band shown in Fig. 7.3 by varying the other mass between 1.5 and 3 TeV. The effect in $h \rightarrow \mu^+\mu^-$ within the preferred region for a_μ is necessarily constructive and large enough that an explanation of the central value of a_μ is already disfavored by the ATLAS and CMS measurements of $h \rightarrow \mu^+\mu^-$. Clearly, with more data the LHC will be able to support (disprove) this scenario if it finds a (no) significant enhancement of the $h \rightarrow \mu^+\mu^-$ decay, assuming δa_μ is confirmed. This scenario also leads to sizeable effects in $Z\mu\mu$ [314] which are compatible with LEP data [353], but could be observed at the ILC [407], CLIC [408] or the FCC-ee [357].

7.4 Conclusions

LQs are prime candidates for an explanation of the intriguing hints of LFUV. As LFUV within the SM only originates from the Higgs, chirality changing observables as the AMM of the muon and, of course, $h \rightarrow \mu^+\mu^-$ are especially interesting. In particular, there are three possible LQ scenarios which can address the discrepancy in the AMM of the muon by an m_t/m_μ enhancement. This also leads to enhanced corrections in $h \rightarrow \mu^+\mu^-$, which involve the same coupling structure as the a_μ contribution. This leads to interesting correlations between a_μ and $h \rightarrow \mu^+\mu^-$, which we study in light of the recent ATLAS and CMS measurements.

We find that scenario 3), in which S_1 only couples to right-handed fermions and mixes after EW symmetry breaking with S_3 , predicts large constructive effects in $h \rightarrow \mu^+\mu^-$ such that the current ATLAS and CMS measurements are already excluding part of the parameter space. In case δa_μ is solely explained by S_1 or S_2 the effect in $\text{Br}[h \rightarrow \mu^+\mu^-]$ is of the order of several percent and therefore detectable at future colliders, in particular at the FCC-hh. Furthermore, while the S_1 scenario predicts constructive interference in $h \rightarrow \mu^+\mu^-$ for the currently preferred range of a_μ , the S_2 scenario predicts destructive interference such that they can be clearly distinguished in the future.

Therefore, if the forthcoming measurements of a_μ by the Fermilab experiment [145] and the independent (approved) experiment at J-PARC [146] confirm the a_μ anomaly, this will strengthen the case for LQs and further enhance the importance of precision measurements of $h \rightarrow \mu^+\mu^-$. Furthermore, note that any model with a chirally enhanced effect in a_μ also generates an enhanced effects in $h \rightarrow \mu^+\mu^-$ (similar to the LQ models studied here) making the correlation among these observables particularly interesting.

Acknowledgements — Acknowledgements – A.C. thanks Martin Hoferichter for useful discussions. The work of A.C. and D.M. supported by a Professorship Grant (PP00P2_176884) of the Swiss National Science Foundation and the one of F.S. by the Swiss National Science Foundation grant 200020_175449/1.

Chapter 8

Scalar Leptoquarks in Leptonic Processes

published in

JHEP **02** (2021) 182

arXiv: 2010.06593 [hep-ph]

Scalar Leptoquarks in Leptonic Processes

Andreas Crivellin

Paul Scherrer Institut, CH-5232 Villigen PSI, Switzerland

CERN Theory Division, CH-1211 Geneva 23, Switzerland

Physik-Institut, Universität Zürich, Winterthurerstrasse 190, CH-8057 Zürich, Switzerland

Christoph Greub

Albert Einstein Center for Fundamental Physics, Institute for Theoretical Physics, University of Bern, CH-3012 Bern, Switzerland

Dario Müller

Paul Scherrer Institut, CH-5232 Villigen PSI, Switzerland

Physik-Institut, Universität Zürich, Winterthurerstrasse 190, CH-8057 Zürich, Switzerland

Francesco Saturnino

Albert Einstein Center for Fundamental Physics, Institute for Theoretical Physics, University of Bern, CH-3012 Bern, Switzerland

Leptoquarks are hypothetical new particles, which couple quarks directly to leptons. They experienced a renaissance in recent years as they are prime candidates to explain the so-called *flavor anomalies*, i.e. the deviations between the Standard Model predictions and measurements in $b \rightarrow sl^+\ell^-$ and $b \rightarrow c\tau\nu$ processes and in the anomalous magnetic moment of the muon. At the one-loop level these particles unavoidably generate effects in the purely leptonic processes like $Z \rightarrow \ell^+\ell^-$, $Z \rightarrow \nu\bar{\nu}$, $W \rightarrow \ell\nu$ and $h \rightarrow \ell^+\ell^-$ and can even generate non-zero rates for lepton flavor violating processes such as $\ell \rightarrow \ell'\gamma$, $Z \rightarrow \ell^+\ell'^-$, $h \rightarrow \ell^+\ell'^-$ and $\ell \rightarrow 3\ell'$. In this article we calculate these processes for all five representations of scalar Leptoquarks. We include their most general interaction terms with the Standard Model Higgs boson, which leads to Leptoquark mixing after the former acquires a vacuum expectation value. In our phenomenological analysis we investigate the effects in modified lepton couplings to electroweak gauge bosons, we study the correlations of the anomalous magnetic moment of the muon with $h \rightarrow \mu^+\mu^-$ and $Z \rightarrow \mu^+\mu^-$ as well as the interplay between different lepton flavor violating decays.

8.1 Introduction

Leptoquarks (LQs) are particles with an interaction vertex connecting leptons with quarks. These particles are predicted by Grand Unified Theories [178, 370–372] and were systematically classified for the first time in Ref. [147] into ten possible representations under the Standard Model (SM) gauge group (five representations of scalar particles and five representations of vector particles). Their tree-level effects in low energy precision and flavor observables were studied comprehensively in Ref. [278]. After the disappearance of the HERA excess [458, 459], which could have been interpreted as a LQ, the interest in LQs decreased until in recent years they experienced a renaissance due to the emergence of the *flavor anomalies*.

These flavor anomalies are hints for lepton flavor universality (LFU) violating NP in $R(D^{(*)})$ [104, 105, 109–112], $b \rightarrow sl^+\ell^-$ [78, 79, 83, 84, 373, 374] and in the anomalous magnetic moment (AMM) of the muon (a_μ) [123], with a significance of $> 3\sigma$ [103, 119–122],

	\mathcal{G}_{SM}	$\mathcal{L}_{q\ell\Phi}$
Φ_1	$\left(3, 1, -\frac{2}{3}\right)$	$\left(\lambda_{fj}^{1R} \bar{u}_f^c \ell_j + \lambda_{fj}^{1L} \bar{Q}_f^c i\tau_2 L_j\right) \Phi_1^\dagger + \text{h.c.}$
$\tilde{\Phi}_1$	$\left(3, 1, -\frac{8}{3}\right)$	$\tilde{\lambda}_{fj}^1 \bar{d}_f^c \ell_j \tilde{\Phi}_1^\dagger + \text{h.c.}$
Φ_2	$\left(3, 2, \frac{7}{3}\right)$	$\lambda_{fj}^{2RL} \bar{u}_f \Phi_2^T i\tau_2 L_j + \lambda_{fj}^{2LR} \bar{Q}_f \ell_j \Phi_2 + \text{h.c.}$
$\tilde{\Phi}_2$	$\left(3, 2, \frac{1}{3}\right)$	$\tilde{\lambda}_{fj}^2 \bar{d}_f \tilde{\Phi}_2^T i\tau_2 L_j + \text{h.c.}$
Φ_3	$\left(3, 3, -\frac{2}{3}\right)$	$\lambda_{fj}^3 \bar{Q}_f^c i\tau_2 (\tau \cdot \Phi_3)^\dagger L_j + \text{h.c.}$

Table 8.1: The five different possible scalar representations of LQs under the SM gauge group and their couplings to quarks and leptons. Note that in our conventions all LQs are $SU(3)_c$ triplets. The superscript T refers to transposition in $SU(2)_L$ space, c to charge conjugation and τ to the Pauli matrices. We did not include LQ couplings to two quarks, which are possible for some representations and which would lead to proton decays. Note that such couplings can always be avoided by assigning quark or lepton number to the SM fermions and to the LQs.

$> 5\sigma$ [88, 92, 97–101, 209] and $> 3\sigma$ [124], respectively³¹. In this context, it has been shown that LQs can explain $b \rightarrow s\ell^+\ell^-$ data [45, 46, 48, 149, 151, 153, 156, 171–177, 180, 184, 213, 253, 317, 318, 332, 333, 361, 369, 375, 376, 461], $R(D^{(*)})$ [45, 47, 48, 149, 151–153, 155, 171–173, 175–177, 180, 184, 211–213, 232, 233, 236, 238–247, 249, 250, 287, 309, 311, 317, 318, 320–327, 369, 375–378] and/or a_μ [48, 238, 241, 243, 277–286, 309–314, 368, 369, 375, 379, 380, 435, 461, 462], which makes them prime candidates for extending the SM with new particles.

Therefore, the search for LQ effects in observables other than the flavor anomalies is very well motivated. Complementary to direct LHC searches [274, 363–367, 381–388], oblique electroweak (EW) parameters and Higgs couplings to gauge bosons can be used to test LQs indirectly [391, 402–404, 406], as studied recently in detail in Ref. [49]. In this article we focus on the purely leptonic processes $\ell \rightarrow \ell'\gamma$, a_ℓ , $Z \rightarrow \ell^+\ell'^-$, $Z \rightarrow \nu\bar{\nu}$, $W \rightarrow \ell\nu$, $h \rightarrow \ell^+\ell'^-$, $\ell \rightarrow 3\ell'$ and $\ell \rightarrow \ell'\nu\bar{\nu}$. The correlations between $h \rightarrow \tau\mu$ and $\tau \rightarrow \mu\gamma$ were studied in Refs. [452, 453], between $Z \rightarrow \mu^+\mu^-$ and a_μ in Ref. [368] and between Z and W decays in Ref. [289]. While in the references above no LQ mixing, induced via couplings to the SM Higgs, was considered, this has been done for a_μ in Ref. [314] and for the case of the singlet-triplet model in Refs. [369, 404]. However, a complete calculation of leptonic processes with scalar LQs, including all possible interaction terms with the SM Higgs, is still missing. This is the purpose of this article.

In the next section we define our conventions before we discuss the self-energies, masses and the renormalization in Sec. 8.3. We then present the analytic results of LQ-induced effects in leptonic amplitudes in Sec. 8.4. In Sec. 8.5 we perform our phenomenological analysis, followed by the conclusions. The Appendix contains further helpful results, in particular the generic expressions with exact diagonalization of the LQ mixing matrices.

³¹Also the (apparent) deficit in first row CKM unitarity can be interpreted as a sign of LFU violation [427–429, 460].

8.2 Setup and Conventions

As outlined in the introduction, LQs are prime candidates to explain the accumulated anomalies in semi-leptonic B meson decays. Since vector LQs, as any massive vector particle, are not renormalizable without a Higgs mechanism, and since we are interested in loop processes, we will study only scalar LQs in the following.

The five different representations of scalar LQs transform under the SM gauge group

$$\mathcal{G}_{\text{SM}} = SU(3)_c \times SU(2)_L \times U(1)_Y \quad (8.1)$$

as given in Tab. 8.1. Note that we have two singlets under $SU(2)_L$ (Φ_1 and $\tilde{\Phi}_1$), two doublets (Φ_2 and $\tilde{\Phi}_2$) and one triplet Φ_3 . The fermion fields $Q^{(c)}$ and L are (charge-conjugated) quark and lepton $SU(2)_L$ doublets, while $u^{(c)}$, $d^{(c)}$ and ℓ are the corresponding $SU(2)_L$ singlets of up-quarks, down-quarks and charged leptons, respectively. The indices f and j refer to flavor and τ are the Pauli matrices, for which we use the convention

$$\tau_1 = \begin{pmatrix} 0 & 1 \\ 1 & 0 \end{pmatrix}, \quad \tau_2 = \begin{pmatrix} 0 & -i \\ i & 0 \end{pmatrix}, \quad \tau_3 = \begin{pmatrix} 1 & 0 \\ 0 & -1 \end{pmatrix}. \quad (8.2)$$

We defined the hypercharge Y such that the electromagnetic charge is given by

$$Q = \frac{1}{2}Y + T_3, \quad (8.3)$$

with T_3 representing the third component of the weak isospin ($\pm 1/2$ for $SU(2)_L$ doublets and $1, 0, -1$ for the $SU(2)_L$ triplet). According to this relation, LQs can be decomposed into the electromagnetic charge eigenstates as

$$\Phi_1 \equiv \Phi_1^{-1/3}, \quad (8.4a)$$

$$\tilde{\Phi}_1 \equiv \tilde{\Phi}_1^{-4/3}, \quad (8.4b)$$

$$\Phi_2 \equiv \begin{pmatrix} \Phi_2^{5/3} \\ \Phi_2^{2/3} \end{pmatrix}, \quad (8.4c)$$

$$\tilde{\Phi}_2 \equiv \begin{pmatrix} \tilde{\Phi}_2^{2/3} \\ \tilde{\Phi}_2^{-1/3} \end{pmatrix}, \quad (8.4d)$$

$$\tau \cdot \Phi_3 \equiv \begin{pmatrix} \Phi_3^{-1/3} & \sqrt{2}\Phi_3^{2/3} \\ \sqrt{2}\Phi_3^{-4/3} & -\Phi_3^{-1/3} \end{pmatrix}, \quad (8.4e)$$

where the superscripts refer to the electric charge.

The LQs couple according to their representation under the SM gauge group to gauge bosons, introduced for the first time in Ref. [463], where we use the following definition for the covariant derivative

$$D_\mu \Phi = \left(\partial_\mu - ig_1 \frac{Y}{2} B_\mu - ig_2 T_k W_\mu^k - ig_s \frac{\lambda_a}{2} G_\mu^a \right) \Phi. \quad (8.5)$$

Here, B_μ is the $U(1)_Y$ gauge boson, W_μ the one of $SU(2)_L$ and G_μ of $SU(3)_c$ with the couplings g_1 , g_2 and g_s , respectively. The index k runs from 1 to 3, a from 1 to 8. T_k are the generators of $SU(2)$ and λ_a are the well-known Gell-Mann matrices. For $SU(2)_L$ singlets we have $T_k = 0$,

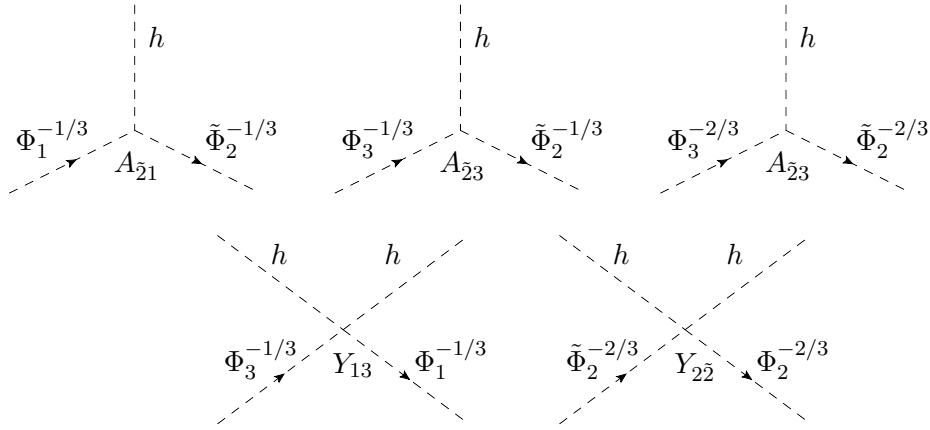


Figure 8.1: Feynman diagrams depicting the LQ-Higgs interactions induced by the terms in the first two lines of Eq. (8.7). If the physical Higgs h is replaced by its vev, mixing among the LQ representations is generated.

for doublets we have $T_k = \tau_k/2$ with the Pauli matrices from Eq. (8.2) while the $SU(2)_L$ triplet Φ_3 is in the adjoint representation of $SU(2)$. We use

$$T_1 = \begin{pmatrix} 0 & 0 & 0 \\ 0 & 0 & -i \\ 0 & i & 0 \end{pmatrix}, \quad T_2 = \begin{pmatrix} 0 & 0 & i \\ 0 & 0 & 0 \\ -i & 0 & 0 \end{pmatrix}, \quad T_3 = \begin{pmatrix} 0 & -i & 0 \\ i & 0 & 0 \\ 0 & 0 & 0 \end{pmatrix}, \quad (8.6)$$

where Φ_3 is defined according to Eq. (8.4e).

8.2.1 Leptoquark-Higgs Interactions and Electroweak Symmetry Breaking

In addition to their couplings to fermions and the gauge interactions, LQs can couple to the SM-like Higgs doublet H (with hypercharge +1) via the Lagrangian [335]

$$\begin{aligned} \mathcal{L}_{H\Phi} = & \left(-A_{\bar{2}1}(\tilde{\Phi}_2^\dagger H)\Phi_1 + A_{\bar{2}3}(\tilde{\Phi}_2^\dagger(\tau \cdot \Phi_3)H) + Y_{2\bar{2}}(\Phi_2^\dagger H)(Hi\tau_2\tilde{\Phi}_2) \right. \\ & + Y_{3\bar{1}}(Hi\tau_2(\tau \cdot \Phi_3)^\dagger H)\tilde{\Phi}_1 + Y_{13}(H^\dagger(\tau \cdot \Phi_3)H)\Phi_1^\dagger + \text{h.c.}) \\ & - Y_{22}(Hi\tau_2\Phi_2)(Hi\tau_2\Phi_2)^\dagger - Y_{\bar{2}\bar{2}}(Hi\tau_2\tilde{\Phi}_2)(Hi\tau_2\tilde{\Phi}_2)^\dagger \\ & - iY_{33}\varepsilon_{IJK}H^\dagger\tau_I H\Phi_{3,K}^\dagger\Phi_{3,J} \\ & \left. - \sum_{k=1}^3 (m_k^2 + Y_k H^\dagger H)\Phi_k^\dagger\Phi_k - \sum_{k=1}^2 (\tilde{m}_k^2 + Y_k H^\dagger H)\tilde{\Phi}_k^\dagger\tilde{\Phi}_k \right). \end{aligned} \quad (8.7)$$

Here m_k^2 and \tilde{m}_k^2 represent the $SU(2)_L$ invariant mass terms of the LQs before EW symmetry breaking and ε_{IJK} is the three-dimensional Levi-Civita tensor with $\varepsilon_{123} = 1$. For simplicity, we omitted the color indices, which are always contracted among the LQs. Note that $A_{\bar{2}1}$ and $A_{\bar{2}3}$ have mass dimension one, while the Y couplings are dimensionless³². The LQ-Higgs interactions depicted in Fig. 8.1 lead to mixing among the LQ representations after EW symmetry breaking.

³²We did not include terms with three or four LQ fields since they do not contribute at the one-loop level to the observables computed in this article.

Once the Higgs acquires its vacuum expectation value (vev) $v \approx 174$ GeV, this generates the mass matrices

$$\mathcal{L}_{\mathcal{M}}^{\text{LQ}} = - \sum_Q \Phi_Q^\dagger \mathcal{M}^Q \Phi_Q \quad (8.8)$$

in the weak basis, with $Q = \{-1/3, 2/3, -4/3, 5/3\}$ and

$$\mathcal{M}^{-1/3} = \begin{pmatrix} m_1^2 + v^2 Y_1 & v A_{21}^* & v^2 Y_{13} \\ v A_{21} & \tilde{m}_2^2 + v^2 Y_2 & v A_{23}^* \\ v^2 Y_{13}^* & v A_{23}^* & m_3^2 + v^2 Y_3 \end{pmatrix}, \quad (8.9a)$$

$$\mathcal{M}^{2/3} = \begin{pmatrix} m_2^2 + v^2 Y_2 & v^2 Y_{2\bar{2}} & 0 \\ v^2 Y_{2\bar{2}}^* & \tilde{m}_2^2 + v^2 (Y_{2\bar{2}} + Y_2) & -\sqrt{2} v A_{23} \\ 0 & -\sqrt{2} v A_{23}^* & m_3^2 + v^2 (Y_3 + Y_{33}) \end{pmatrix}, \quad (8.9b)$$

$$\mathcal{M}^{-4/3} = \begin{pmatrix} \tilde{m}_1^2 + v^2 Y_{\bar{1}} & \sqrt{2} v^2 Y_{3\bar{1}}^* \\ \sqrt{2} v^2 Y_{3\bar{1}} & m_3^2 + v^2 (Y_3 - Y_{33}) \end{pmatrix}, \quad (8.9c)$$

$$\mathcal{M}^{5/3} = m_2^2 + v^2 (Y_{22} + Y_2), \quad (8.9d)$$

where the eigenstates of the electric charge

$$\Phi_{-1/3} \equiv \begin{pmatrix} \Phi_1^{-1/3} \\ \tilde{\Phi}_2^{-1/3} \\ \Phi_3^{-1/3} \end{pmatrix}, \quad (8.10a)$$

$$\Phi_{2/3} \equiv \begin{pmatrix} \Phi_2^{2/3} \\ \tilde{\Phi}_2^{2/3} \\ \Phi_3^{2/3} \end{pmatrix}, \quad (8.10b)$$

$$\Phi_{-4/3} \equiv \begin{pmatrix} \tilde{\Phi}_1^{-4/3} \\ \Phi_3^{-4/3} \end{pmatrix}, \quad (8.10c)$$

$$\Phi_{5/3} \equiv \Phi_2^{5/3}, \quad (8.10d)$$

are assembled from the LQ field components of Eq. (8.4).

To work in the physical basis with mass eigenstates, in which the amplitudes are calculated, we need to diagonalize the mass matrices in Eq. (8.9). This can be achieved by a unitary transformation

$$\hat{\mathcal{M}}^Q = W^Q \mathcal{M}^Q W^{Q\dagger}, \quad (8.11)$$

such that $\hat{\mathcal{M}}^Q$ is diagonal. This means that the interaction eigenstates in (8.10) are written as

$$W^Q \Phi_Q \equiv \hat{\Phi}^Q, \quad (8.12)$$

where $\hat{\Phi}^Q$ are the mass eigenstates. The analytic expressions for the diagonalization matrices $W^{-1/3}$ and $W^{2/3}$ are very lengthy or must be computed numerically. Therefore, we diagonalize the mass matrices perturbatively up to $\mathcal{O}(v^2/m_{\text{LQ}}^2)$, where m are the $SU(2)_L$ invariant mass

terms of the LQs. The analytic expressions for the perturbative W^Q read

$$W^{-1/3} \approx \begin{pmatrix} 1 - \frac{v^2 |A_{\bar{2}1}|^2}{2(m_1^2 - \tilde{m}_2^2)^2} & \frac{vA_{\bar{2}1}^*}{m_1^2 - \tilde{m}_2^2} & \frac{v^2(Y_{13}(m_1^2 - \tilde{m}_2^2) + A_{\bar{2}1}^* A_{\bar{2}3})}{(m_1^2 - m_3^2)(m_1^2 - \tilde{m}_2^2)} \\ \frac{-vA_{\bar{2}1}}{m_1^2 - \tilde{m}_2^2} & 1 - \frac{v^2}{2} \left(\frac{|A_{\bar{2}1}|^2}{(m_1^2 - \tilde{m}_2^2)^2} + \frac{|A_{\bar{2}3}|^2}{(m_3^2 - \tilde{m}_2^2)^2} \right) & \frac{-vA_{\bar{2}3}}{m_3^2 - \tilde{m}_2^2} \\ \frac{-v^2(Y_{13}^*(m_3^2 - \tilde{m}_2^2) + A_{\bar{2}1} A_{\bar{2}3}^*)}{(m_1^2 - m_3^2)(m_3^2 - \tilde{m}_2^2)} & \frac{vA_{\bar{2}3}^*}{m_3^2 - \tilde{m}_2^2} & 1 - \frac{v^2 |A_{\bar{2}3}|^2}{2(m_3^2 - \tilde{m}_2^2)^2} \end{pmatrix}, \quad (8.13a)$$

$$W^{2/3} \approx \begin{pmatrix} 1 & \frac{v^2 Y_{\bar{2}2}}{m_2^2 - \tilde{m}_2^2} & 0 \\ \frac{-v^2 Y_{\bar{2}2}^*}{m_2^2 - \tilde{m}_2^2} & 1 - \frac{v^2 |A_{\bar{2}3}|^2}{(m_3^2 - \tilde{m}_2^2)^2} & \frac{-\sqrt{2}vA_{\bar{2}3}}{\tilde{m}_2^2 - m_3^2} \\ 0 & \frac{\sqrt{2}vA_{\bar{2}3}^*}{\tilde{m}_2^2 - m_3^2} & 1 - \frac{v^2 |A_{\bar{2}3}|^2}{(m_3^2 - \tilde{m}_2^2)^2} \end{pmatrix}, \quad (8.13b)$$

$$W^{-4/3} \approx \begin{pmatrix} 1 & \frac{\sqrt{2}v^2 Y_{\bar{3}1}^*}{\tilde{m}_1^2 - m_3^2} \\ \frac{-\sqrt{2}v^2 Y_{\bar{3}1}}{\tilde{m}_1^2 - m_3^2} & 1 \end{pmatrix}. \quad (8.13c)$$

Then the physical LQ masses are

$$\begin{aligned} (M_a^{-1/3})^2 &\approx \left(m_1^2 + v^2 \left(Y_1 - \frac{|A_{\bar{2}1}|^2}{\tilde{m}_2^2 - m_1^2} \right), \tilde{m}_2^2 + v^2 \left(Y_2 + \frac{|A_{\bar{2}1}|^2}{\tilde{m}_2^2 - m_1^2} + \frac{|A_{\bar{2}3}|^2}{\tilde{m}_2^2 - m_3^2} \right), \right. \\ &\quad \left. m_3^2 + v^2 \left(Y_3 - \frac{|A_{\bar{2}3}|^2}{\tilde{m}_2^2 - m_3^2} \right) \right)_a, \end{aligned} \quad (8.14a)$$

$$\begin{aligned} (M_a^{2/3})^2 &\approx \left(m_2^2 + v^2 Y_2, \tilde{m}_2^2 + v^2 \left(Y_{\bar{2}2} + Y_2 + \frac{2|A_{\bar{2}3}|^2}{\tilde{m}_2^2 - m_3^2} \right), \right. \\ &\quad \left. m_3^2 + v^2 \left(Y_3 + Y_{33} - \frac{2|A_{\bar{2}3}|^2}{\tilde{m}_2^2 - m_3^2} \right) \right)_a, \end{aligned} \quad (8.14b)$$

$$(M_a^{-4/3})^2 \approx (\tilde{m}_1^2 + v^2 Y_{\bar{1}}, m_3^2 + v^2 (Y_3 - Y_{33}))_a, \quad (8.14c)$$

$$(M^{5/3})^2 \approx m_2^2 + v^2 (Y_{22} + Y_2), \quad (8.14d)$$

keeping terms up to order v^2 . The index a runs from 1 to 3 for $Q = -1/3$ and $Q = 2/3$ and from 1 to 2 for $Q = -4/3$, respectively.

8.2.2 Leptoquark-Fermion Couplings

EW symmetry breaking also leads to non-diagonal quark mass matrices in the weak basis, originating from the SM Yukawa couplings. Note that we can work in the basis with a diagonal lepton Yukawa coupling in the approximation of massless neutrinos. We therefore apply the following unitary rotation matrices on the left-handed quark fields

$$u_L \rightarrow U^{uL} u_L, \quad d_L \rightarrow U^{dL} d_L, \quad (8.15)$$

while the right-handed rotations can be absorbed by a redefinition of the LQ-quark-lepton couplings and are therefore unphysical. We now choose to work in the so-called down basis such that

$$U_{ji}^{uL*} = V_{ij}, \quad U_{ij}^{dL} = \delta_{ij}, \quad (8.16)$$

with V_{ij} being the CKM matrix. This means that CKM elements only appear in couplings involving up-type quarks.

We now decompose the LQ-fermion interactions in Tab. 8.1 into their $SU(2)_L$ components and write them in terms of mass eigenstates

$$\begin{aligned}
 \mathcal{L}_{q\ell\Phi} = & [\bar{u}_i^c(\Gamma_{u_i^c\ell_j}^{R,a} P_R + \Gamma_{u_i^c\ell_j}^{L,a} P_L)\ell_j + \Gamma_{d_i^c\nu_j}^{L,a} \bar{d}_i^c P_L \nu_j + \Gamma_{d_i\nu_j}^{L,a*} \bar{\nu}_j P_R d_i] \hat{\Phi}_a^{-1/3\dagger} \\
 & + [\bar{d}_i(\Gamma_{d_i\ell_j}^{R,a} P_R + \Gamma_{d_i\ell_j}^{L,a} P_L)\ell_j + \Gamma_{u_i^c\nu_j}^{L,a*} \bar{\nu}_j P_R u_i^c + \Gamma_{u_i\nu_j}^{L,a} \bar{u}_i P_L \nu_j] \hat{\Phi}_a^{2/3} \\
 & + [\bar{d}_i^c(\Gamma_{d_i^c\ell_j}^{R,a} P_R + \Gamma_{d_i^c\ell_j}^{L,a} P_L)\ell_j] \hat{\Phi}_a^{-4/3\dagger} + [\bar{u}_i(\Gamma_{u_i\ell_j}^R P_R + \Gamma_{u_i\ell_j}^L P_L)\ell_j] \hat{\Phi}_a^{5/3} \\
 & + \text{h.c.},
 \end{aligned} \tag{8.17}$$

with

$$\begin{aligned}
 \Gamma_{u_i^c\ell_j}^{R,a} &= \lambda_{ij}^{1R} W_{a1}^{-1/3}, & \Gamma_{u_i^c\ell_j}^{L,a} &= V_{ik}^* (\lambda_{kj}^{1L} W_{a1}^{-1/3} - \lambda_{kj}^3 W_{a3}^{-1/3}), \\
 \Gamma_{d_i\nu_j}^{L,a*} &= -\tilde{\lambda}_{ij}^{2*} W_{a2}^{-1/3}, & \Gamma_{d_i^c\nu_j}^{L,a} &= -(\lambda_{ij}^{1L} W_{a1}^{-1/3} + \lambda_{ij}^3 W_{a3}^{-1/3}), \\
 \Gamma_{d_i\ell_j}^{R,a} &= \lambda_{ij}^{2LR} W_{a1}^{2/3*}, & \Gamma_{d_i\ell_j}^{L,a} &= \tilde{\lambda}_{ij}^2 W_{a2}^{2/3*}, \\
 \Gamma_{u_i^c\nu_j}^{L,a*} &= \sqrt{2} V_{ik} \lambda_{kj}^{3*} W_{a3}^{2/3*}, & \Gamma_{u_i\nu_j}^{L,a} &= -\lambda_{ij}^{2RL} W_{a1}^{2/3*}, \\
 \Gamma_{d_i^c\ell_j}^{R,a} &= \tilde{\lambda}_{ij}^1 W_{a1}^{-4/3}, & \Gamma_{d_i^c\ell_j}^{L,a} &= -\sqrt{2} \lambda_{ij}^3 W_{a2}^{-4/3}, \\
 \Gamma_{u_i\ell_j}^R &= V_{ik} \lambda_{kj}^{2LR}, & \Gamma_{u_i\ell_j}^L &= \lambda_{ij}^{2RL}.
 \end{aligned} \tag{8.18}$$

Note that the index a runs from 1 to 3 for $Q = -1/3$ and $Q = 2/3$, while for $Q = -4/3$ only from 1 to 2. Due to our choice of basis, the CKM matrix appears in all couplings involving left-handed up-type quarks. Similarly, also the PMNS matrix would enter in all couplings involving neutrinos in case they were taken to be massive. However, all processes that we are interested in can be calculated for massless neutrinos such that the PMNS matrix drops out. Nonetheless, we will return to the PMNS matrix in the next section when we discuss possible contributions to Majorana mass terms and the renormalization of the $W\ell\nu$ vertex.

8.2.3 Leptoquark-Higgs Couplings

Let us finally consider the couplings of the SM Higgs to LQs. The interaction terms are also affected by the LQ rotations induced by EW symmetry breaking. Again, we express Eq. (8.7) in terms of mass eigenstates as

$$\begin{aligned}
 \mathcal{L}_{H\Phi} = & -\tilde{\Gamma}_{ab}^{1/3} h \hat{\Phi}_a^{-1/3\dagger} \hat{\Phi}_b^{-1/3} - \tilde{\Gamma}_{ab}^{2/3} h \hat{\Phi}_a^{2/3\dagger} \hat{\Phi}_b^{2/3} - \tilde{\Gamma}_{cd}^{4/3} h \hat{\Phi}_c^{-4/3\dagger} \hat{\Phi}_d^{-4/3} \\
 & - \Gamma_{ab}^{5/3} h \hat{\Phi}_a^{5/3\dagger} \hat{\Phi}_b^{5/3} - \tilde{\Lambda}_{ab}^{1/3} h^2 \hat{\Phi}_a^{-1/3\dagger} \hat{\Phi}_b^{-1/3} - \tilde{\Lambda}_{ab}^{2/3} h^2 \hat{\Phi}_a^{2/3\dagger} \hat{\Phi}_b^{2/3} \\
 & - \tilde{\Lambda}_{cd}^{4/3} h^2 \hat{\Phi}_c^{-4/3\dagger} \hat{\Phi}_d^{-4/3} - \Lambda^{5/3} h^2 \hat{\Phi}_a^{5/3\dagger} \hat{\Phi}_b^{5/3},
 \end{aligned} \tag{8.19}$$

with h as the physical Higgs field, $a, b = \{1, 2, 3\}$ and $c, d = \{1, 2\}$. The couplings are defined as

$$\begin{aligned}
 \tilde{\Gamma}^{1/3} &= W^{-1/3} \Gamma^{1/3} W^{-1/3\dagger}, & \tilde{\Lambda}^{1/3} &= W^{-1/3} \Lambda^{1/3} W^{-1/3\dagger}, \\
 \tilde{\Gamma}^{2/3} &= W^{2/3} \Gamma^{2/3} W^{2/3\dagger}, & \tilde{\Lambda}^{2/3} &= W^{2/3} \Lambda^{2/3} W^{2/3\dagger}, \\
 \tilde{\Gamma}^{4/3} &= W^{-4/3} \Gamma^{4/3} W^{-4/3\dagger}, & \tilde{\Lambda}^{4/3} &= W^{-4/3} \Lambda^{4/3} W^{-4/3\dagger}, \\
 \Gamma^{5/3} &= \sqrt{2} v (Y_{22} + Y_2), & \Lambda^{5/3} &= \frac{1}{2} (Y_{22} + Y_2),
 \end{aligned} \tag{8.20}$$

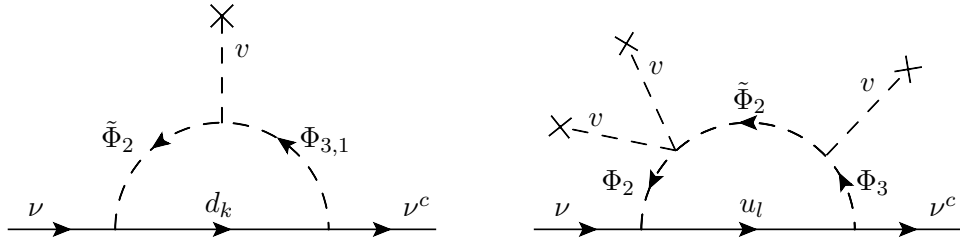


Figure 8.2: One-loop self-energy diagrams generating Majorana-like neutrino masses. On the left-hand side, we have a down-type quark in the loop. In the case of up-type quarks, the leading contribution only occurs at $\mathcal{O}(v^3)$.

divergent and non-decoupling. Furthermore, they are the only relevant ones in the calculation of $Z\ell\ell$, $Z\nu\nu$, $Wl\nu$ and $h\ell\ell$ vertices to be discussed later. The terms linear in p^2/m^2 are only necessary to calculate $\ell \rightarrow \ell'\gamma$. However, as they are finite and do not affect the renormalization of any parameter, they can be included in the calculation of $\ell \rightarrow \ell'\gamma$ in a straightforward way and we do not give the explicit results here. The ones for $\Sigma_{fi}^{\ell,\nu AB} \equiv \Sigma_{fi}^{\ell,\nu AB}(0)$ are given in the Appendix 8.7.1.

8.3.1 Neutrino Masses

The contribution to the Majorana mass term of the neutrinos can be calculated by considering the $\bar{\nu}_f^c \nu_i$ two-point function. We have generically

$$m_{ij}^{\nu\text{LQ}} = \frac{-m_{q_k} N_c (\Gamma_{q_k \nu_i}^L \Gamma_{q_k \nu_j}^L + \Gamma_{q_k \nu_j}^{L*} \Gamma_{q_k \nu_i}^{L*})}{16\pi^2} \mathcal{I}_0\left(\frac{\mu^2}{M^2}, \frac{m_{q_k}^2}{M^2}\right), \quad (8.26)$$

where we neglected the external momenta. An implicit sum over all internal quarks u, d, u^c and d^c as well as over their flavors and the corresponding LQs is understood. The loop function \mathcal{I}_0 is given in the Appendix 8.7.1.

After summation one can expand this expression in terms of v/m_{LQ} . In this way, one recovers the two diagrams shown in Fig. 8.2 and finds

$$\begin{aligned} m_{ij}^{\nu\text{LQ}} \approx & \frac{m_{d_k} N_c v}{16\pi^2 \tilde{m}_2^2} \left((\lambda_{ki}^{1L} \tilde{\lambda}_{kj}^2 A_{\tilde{2}1} + \lambda_{kj}^{1L*} \tilde{\lambda}_{ki}^{2*} A_{\tilde{2}1}^*) \mathcal{H}_1\left(\frac{m_1^2}{\tilde{m}_2^2}\right) \right. \\ & \left. + (\lambda_{ki}^3 \tilde{\lambda}_{kj}^2 A_{\tilde{2}3} + \lambda_{kj}^{3*} \tilde{\lambda}_{ki}^{2*} A_{\tilde{2}3}^*) \mathcal{H}_1\left(\frac{m_3^2}{\tilde{m}_2^2}\right) \right) + \mathcal{O}(m_d v^3/m^4) \\ & + \frac{m_{u_l} N_c v^3}{8\pi^2} \frac{\lambda_{lj}^{2RL} V_{lk}^* \lambda_{ki}^3 A_{\tilde{2}3} Y_{\tilde{2}2} + \lambda_{li}^{2RL*} V_{lk} \lambda_{kj}^{3*} A_{\tilde{2}3}^* Y_{\tilde{2}2}^*}{m_2^2 (\tilde{m}_2^2 - m_3^2)} \left(\mathcal{H}_1\left(\frac{\tilde{m}_2^2}{m_2^2}\right) - \mathcal{H}_1\left(\frac{m_3^2}{m_2^2}\right) \right) \\ & + \mathcal{O}(m_{u_l} v^4/m^5), \end{aligned} \quad (8.27)$$

where the first two lines agree with Ref. [337], originating from down-type quark contributions. The third line, generated by couplings to up-type quarks, was not given previously in the literature. Note that for the latter, the leading contribution only appears at $\mathcal{O}(v^3)$, see Fig. 8.2, while for down-type quarks already a v^1 term exists and higher orders in v do not generate new, independent coupling structures. The loop function \mathcal{H}_1 is given in the Appendix 8.7.2.

8.3.2 Renormalization

With these expressions at hand, we can include the loop effects into the Lagrangian of Eq. (8.22) to obtain

$$\begin{aligned} \mathcal{L}^{\ell\nu} = & \bar{\ell}_f \left(\not{p} \left(\delta_{fi} - \Sigma_{fi}^{\ell LL} P_L - \Sigma_{fi}^{\ell RR} P_R \right) - m_f^{\ell(0)} \delta_{fi} - \Sigma_{fi}^{\ell LR} P_R - \Sigma_{fi}^{\ell RL} P_L \right) \ell_i \\ & + \bar{\nu}_f \not{p} \left(\delta_{fi} - \Sigma_{fi}^{\nu LL} \right) \nu_i - \frac{m_f^{\nu(0)} + m_{fi}^{\nu LQ}}{2} \bar{\nu}_f^c \nu_i. \end{aligned} \quad (8.28)$$

The superscript (0) indicates the bare (unrenormalized) quantities. Now we have to make the kinetic terms canonical again and render the mass matrices diagonal in order to arrive at the physical basis. We start with the kinetic terms, which are made diagonal and correctly normalized once the shifts

$$\ell_{fL} \rightarrow \left(\delta_{fi} + \frac{1}{2} \Sigma_{fi}^{\ell LL} \right) \ell_{iL}, \quad (8.29a)$$

$$\ell_{fR} \rightarrow \left(\delta_{fi} + \frac{1}{2} \Sigma_{fi}^{\ell RR} \right) \ell_{iR}, \quad (8.29b)$$

$$\nu_f \rightarrow \left(\delta_{fi} + \frac{1}{2} \Sigma_{fi}^{\nu LL} \right) \nu_i, \quad (8.29c)$$

have been applied. These shifts enter in all observables with external lepton fields, i.e. they also lead to effects in gauge-boson couplings to leptons. Therefore, we include them in this way in our calculations later on.

In addition, these field redefinitions affect the mass terms for charged leptons, which then read [464]

$$\mathcal{L}_m^\ell = -\bar{\ell}_f \left(m_i^{\ell(0)} \delta_{fi} + \frac{1}{2} \Sigma_{fi}^{\ell LL} m_i^{\ell(0)} + \frac{1}{2} m_f^{\ell(0)} \Sigma_{fi}^{\ell RR} + \Sigma_{fi}^{\ell LR} P_R + \Sigma_{fi}^{\ell RL} P_L \right) \ell_i, \quad (8.30)$$

and for neutrinos we have

$$\mathcal{L}_m^\nu = -\frac{1}{2} \bar{\nu}_f^c \left(m_f^{\nu(0)} \delta_{fi} + \frac{1}{2} m_f^{\nu(0)} \Sigma_{fi}^{\nu LL} + \frac{1}{2} \Sigma_{fi}^{\nu LL*} m_i^{\nu(0)} + m_{fi}^{\nu LQ} \right) \nu_i. \quad (8.31)$$

These matrices can now be diagonalized as

$$\begin{aligned} U_{f'f}^{\ell L*} \left(\left(\delta_{f'j} + \frac{1}{2} \Sigma_{f'j}^{\ell LL} \right) m_j^{(0)} \left(\delta_{ji'} + \frac{1}{2} \Sigma_{ji'}^{\ell RR} \right) + \Sigma_{ji'}^{\ell LR} \right) U_{i'i}^{\ell R} &= m_i^\ell \delta_{fi}, \\ U_{f'f}^\nu \left(m_{f'}^{\nu(0)} \delta_{f'i'} + \frac{1}{2} m_{f'}^{\nu(0)} \Sigma_{f'i'}^{\nu LL} + \frac{1}{2} \Sigma_{f'i'}^{\nu LL*} m_{i'}^{\nu(0)} + m_{f'i'}^{\nu LQ} \right) &U_{i'i}^\nu = m_i^\nu \delta_{fi}, \end{aligned} \quad (8.32)$$

with m_i^ℓ and m_i^ν being the physical masses. The unitary matrix $U^{\ell L}$ is given by

$$U^{\ell L} = \begin{pmatrix} 1 & \frac{\Sigma_{12}^{\ell LR}}{m_2^\ell} + \frac{1}{2} \Sigma_{12}^{\ell LL} & \frac{\Sigma_{13}^{\ell LR}}{m_3^\ell} + \frac{1}{2} \Sigma_{13}^{\ell LL} \\ -\frac{\Sigma_{12}^{\ell LR*}}{m_2^\ell} - \frac{1}{2} \Sigma_{12}^{\ell LL*} & 1 & \frac{\Sigma_{23}^{\ell LR}}{m_3^\ell} + \frac{1}{2} \Sigma_{23}^{\ell LL} \\ -\frac{\Sigma_{13}^{\ell LR*}}{m_3^\ell} - \frac{1}{2} \Sigma_{13}^{\ell LL*} & -\frac{\Sigma_{23}^{\ell LR*}}{m_3^\ell} - \frac{1}{2} \Sigma_{23}^{\ell LL*} & 1 \end{pmatrix}. \quad (8.33)$$

We used the lepton mass hierarchy to simplify $U^{\ell L}$ and the fact that the self-energies are just corrections to a diagonal matrix to get an explicit expression. $U^{\ell R}$ is simply obtained by exchanging L and R .

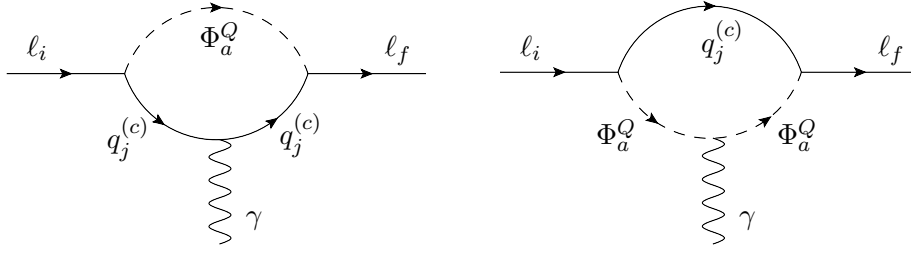


Figure 8.3: The vertex diagrams which contribute to $\ell_i \rightarrow \ell_f \gamma$. Depending on the electric charge of the LQ, we have (charge-conjugated) up- or down-type quarks in the loop.

These unitary rotations (or at leading order the unit matrix plus anti-hermitian corrections) do not have a physical effect in the sense that they cannot be measured in observables. In fact, they correspond to unphysical rotations, in case of $U^{\ell R}$, or they can be absorbed by a renormalization of the PMNS matrix, in case of $U^{\ell L}$ and U^ν . This can also be seen by applying these rotations to gauge bosons vertices, where they drop out for the Z interaction terms and only enter the $W\ell\nu$ vertex in the combination

$$\hat{V}_{fi} = U_{f'f}^{\ell L*} \hat{V}_{f'i}^{(0)} U_{i'i}^\nu, \quad (8.34)$$

where \hat{V} on the left-hand side of the equation is identified with the PMNS matrix, see Eq. 8.23.

Finally, let us consider the $h\ell\ell$ vertex. Here we have

$$-h\bar{\ell}_f U_{f'f}^{\ell L*} \left(\left(\delta_{f'j} + \frac{1}{2} \Sigma_{f'j}^{\ell LL} \right) Y_j^{\ell(0)} \left(\delta_{ji'} + \frac{1}{2} \Sigma_{ji'}^{\ell RR} \right) + \Lambda_{ji'}^{\ell LR} \right) U_{i'i}^{\ell R} P_R \ell_i, \quad (8.35)$$

where $Y_j^{\ell(0)} = m_j^{\ell(0)}/v$ and $\Lambda_{ji'}^{\ell LR}$ represents the genuine vertex correction. Therefore, the effective Yukawa coupling measured in $h \rightarrow \ell^+ \ell'^-$ decays can be expressed in terms of the physical lepton mass and $\Sigma_{fi}^{\ell LR}$ as follows

$$Y_{fi}^{\ell \text{eff}} = \frac{m_i^\ell \delta_{fi} - \Sigma_{fi}^{\ell LR}}{v} + \Lambda_{fi}^{\ell LR}. \quad (8.36)$$

8.4 Calculation of the One-Loop Effects

In this section, we compute the amplitudes governing the various purely leptonic observables. For this we take into account the Higgs-induced mixing among the different LQ representations. We will consider amplitudes involving the following fields:

1. $\ell\ell\gamma$
2. $Z\ell\ell$ and $Z\nu\nu$
3. $W\ell\nu$
4. $h\ell\ell$
5. 4ℓ
6. $2\ell 2\nu$

For our purpose, the gauge bosons and the Higgs can be both on- and off-shell while the leptons are all on-shell. We set all lepton masses to zero, except for $\ell_i \rightarrow \ell_f \gamma$, where we

expand up to the first non-vanishing order. In addition, we expanded the loop integrals in $m_{\text{EW}}/m_{\text{LQ}}$, where $m_{\text{EW}} \approx v$ can denote m_W , m_Z , m_H or m_t . Furthermore, we expanded the mass eigenvalues of the LQs and the mixing matrices in v/m_{LQ} , while the results obtained with exact diagonalization of the LQ mass matrices are given in the Appendix. Note that we do not include Higgs or gauge-boson self-energies in our calculations. Such effects are flavor universal, drop out at leading order if branching ratios are considered and are already included in the oblique parameters [389, 390] as studied in Ref. [49].

8.4.1 $ll\gamma$

In case of an on-shell photon, we define the effective Hamiltonian as

$$\mathcal{H}_{\text{eff}}^{\ell\ell\gamma} = C_{\ell_f\ell_i}^L O_{\ell_f\ell_i}^L + C_{\ell_f\ell_i}^R O_{\ell_f\ell_i}^R, \quad (8.37)$$

with

$$O_{\ell_f\ell_i}^{L(R)} = \frac{e}{16\pi^2} [\bar{\ell}_f \sigma^{\mu\nu} P_{L(R)} \ell_i] F_{\mu\nu}. \quad (8.38)$$

Note that we have $C_{\ell_f\ell_i}^R = C_{\ell_i\ell_f}^{L*}$ due to the hermiticity of the Hamiltonian.

The coefficients are induced by the diagrams in Fig. 8.3 and for a single LQ representation only are given by

$$C_{\ell_f\ell_i}^{L,\Phi_1} \approx \frac{N_c(m_{\ell_f}\lambda_{jf}^{1L*}\lambda_{ji}^{1L} + m_{\ell_i}\lambda_{jf}^{1R*}\lambda_{ji}^{1R})}{24m_1^2} - \frac{N_c m_t}{12m_1^2} \lambda_{3f}^{1R*} V_{3k}^* \lambda_{ki}^{1L} \left(\mathcal{E}_1\left(\frac{m_t^2}{m_1^2}\right) - \frac{v^2 Y_1}{m_1^2} \mathcal{E}_2\left(\frac{m_t^2}{m_1^2}\right) \right), \quad (8.39a)$$

$$C_{\ell_f\ell_i}^{L,\tilde{\Phi}_1} \approx \frac{-m_{\ell_i} \tilde{\lambda}_{jf}^{1*} \tilde{\lambda}_{ji}^{1*}}{12\tilde{m}_1^2}, \quad (8.39b)$$

$$C_{\ell_f\ell_i}^{L,\Phi_2} \approx \frac{-N_c(m_{\ell_f}\lambda_{jf}^{2LR*}\lambda_{ji}^{2LR} + m_{\ell_i}\lambda_{jf}^{2RL*}\lambda_{ji}^{2RL})}{8m_2^2} + \frac{N_c m_t}{12m_2^2} V_{3k}^* \lambda_{kf}^{2LR*} \lambda_{3i}^{2RL} \left(\mathcal{E}_3\left(\frac{m_t^2}{m_2^2}\right) - \frac{v^2(Y_{22} + Y_2)}{m_2^2} \mathcal{E}_4\left(\frac{m_t^2}{m_2^2}\right) \right), \quad (8.39c)$$

$$C_{\ell_f\ell_i}^{L,\tilde{\Phi}_2} \approx 0, \quad (8.39d)$$

$$C_{\ell_f\ell_i}^{L,\Phi_3} \approx \frac{-N_c m_{\ell_f} \lambda_{jf}^{3*} \lambda_{ji}^3}{8m_3^2}, \quad (8.39e)$$

where the quark index j runs from 1 to 3. We expanded the results up to the first non-vanishing order in external momenta and masses. Note that the Wilson coefficients are composed by two parts: a contribution which is proportional to $m_{\ell_{f,i}}$ and a contribution proportional to the quark mass, originating from a chirality flip on the internal quark line. The latter term appears only if a LQ couples simultaneously to left- and right-handed up- or down-type quarks. E.g. for the AMM of the muon this effect dominates in cases where we couple to third generation quarks, i.e. generates a relative enhancement by a factor $m_t/m_\mu \sim 1600$ or $m_b/m_\mu \sim 40$, respectively. Therefore, these terms are the most important ones from the phenomenological point of view. And for our results with m_t and m_b we also include the $\mathcal{O}(v^2/m_{\text{LQ}}^2)$ terms, originating from the Higgs-LQ interaction, while we only present the leading order effects for the $m_{\ell_{f,i}}$ terms.

Turning to the contributions with multiple LQ representations, i.e. the terms involving LQ mixing, we also focus on the terms proportional to $m_{b,t}$ and we find

$$\begin{aligned}
 C_{\ell_f \ell_i}^L &\approx \frac{-N_c m_t v^2}{12 m_1^2} \left[\lambda_{3f}^{1R*} V_{3k}^* \lambda_{ki}^{1L} \frac{|A_{\bar{2}1}|^2}{\tilde{m}_2^4} \mathcal{E}_5 \left(\frac{m_t^2}{\tilde{m}_2^2}, \frac{m_1^2}{\tilde{m}_2^2} \right) \right. \\
 &\quad \left. + \lambda_{3f}^{1R*} V_{3k}^* \lambda_{ki}^3 \left(\frac{Y_{13}}{m_3^2} \mathcal{E}_6 \left(\frac{m_t^2}{m_3^2}, \frac{m_1^2}{m_3^2} \right) + \frac{A_{\bar{2}3} A_{\bar{2}1}^*}{\tilde{m}_2^4} \mathcal{E}_7 \left(\frac{m_t^2}{\tilde{m}_2^2}, \frac{m_1^2}{\tilde{m}_2^2}, \frac{m_3^2}{\tilde{m}_2^2} \right) \right) \right] \\
 &\quad + \frac{N_c m_b v^2}{12} \left[\frac{\lambda_{3f}^{2LR*} \tilde{\lambda}_{3i}^2 Y_{22}^*}{\tilde{m}_2^4} \mathcal{E}_8 \left(\frac{m_b^2}{\tilde{m}_2^2}, \frac{m_2^2}{\tilde{m}_2^2} \right) + \frac{\tilde{\lambda}_{3f}^{1*} \lambda_{3i}^3 Y_{3\bar{1}}^*}{m_3^4} \mathcal{E}_9 \left(\frac{m_b^2}{\tilde{m}_1^2}, \frac{m_1^2}{\tilde{m}_2^2} \right) \right].
 \end{aligned} \tag{8.40}$$

The involved loop functions are given explicitly in the Appendix 8.7.2 and the general analytical results in Appendix 8.7.3. Note that we assumed the quarks of the first two generations to be massless and that we integrated out the bottom and top quark together with the LQs. This means that Eq. (8.39) and Eq. (8.40) should be understood to be at the low scale, such that the mixing of the four-fermion operators into the magnetic one is already included, reproducing the logarithms.

Considering $\ell_i \rightarrow \ell_f \gamma^*$ transitions with a momentum configuration $q^2 = (p_i - p_f)^2$, we define the amplitude

$$\mathcal{A}(\ell_i \rightarrow \ell_f \gamma^*) = -e q^2 \bar{u}(p_f, m_f) \not{e}^*(q) \left(\delta_{fi} + \hat{\Xi}_{fi}^L P_L + \hat{\Xi}_{fi}^R P_R \right) u(p_i, m_i). \tag{8.41}$$

We first give the separate contributions of each LQ representation

$$\Xi_{fi}^{L, \Phi_1} \approx \frac{-N_c \lambda_{kf}^{1L*} V_{jk} V_{jl}^* \lambda_{li}^{1L}}{288 \pi^2 m_1^2} \left(\mathcal{F}_1 \left(\frac{m_{u_j}^2}{m_1^2} \right) - \frac{v^2 Y_1}{m_1^2} \mathcal{F}_2 \left(\frac{m_{u_j}^2}{m_1^2} \right) + \frac{v^2 |A_{\bar{2}1}|^2}{\tilde{m}_2^4} \mathcal{F}_3 \left(\frac{m_{u_j}^2}{m_1^2}, \frac{m_1^2}{\tilde{m}_2^2} \right) \right), \tag{8.42a}$$

$$\Xi_{fi}^{R, \Phi_1} \approx \frac{-N_c \lambda_{jf}^{1R*} \lambda_{ji}^{1R}}{288 \pi^2 m_1^2} \left(\mathcal{F}_1 \left(\frac{m_{u_j}^2}{m_1^2} \right) - \frac{v^2 Y_1}{m_1^2} \mathcal{F}_2 \left(\frac{m_{u_j}^2}{m_1^2} \right) + \frac{v^2 |A_{\bar{2}1}|^2}{\tilde{m}_2^4} \mathcal{F}_3 \left(\frac{m_{u_j}^2}{m_1^2}, \frac{m_1^2}{\tilde{m}_2^2} \right) \right), \tag{8.42b}$$

$$\Xi_{fi}^{R, \Phi_1} \approx \frac{N_c \tilde{\lambda}_{jf}^{1*} \tilde{\lambda}_{ji}^1}{144 \pi^2 \tilde{m}_1^2} \left(\mathcal{F}_4 \left(\frac{m_{d_j}^2}{\tilde{m}_1^2} \right) - \frac{v^2 Y_{\bar{1}}}{\tilde{m}_1^2} \mathcal{F}_8 \left(\frac{m_{d_j}^2}{\tilde{m}_1^2} \right) \right), \tag{8.42c}$$

$$\Xi_{fi}^{L, \Phi_2} \approx \frac{N_c \lambda_{jf}^{2RL*} \lambda_{ji}^{2RL}}{288 \pi^2 m_2^2} \left(\mathcal{F}_5 \left(\frac{m_{u_j}^2}{m_2^2} \right) - \frac{v^2 (Y_2 + Y_{22})}{m_2^2} \mathcal{F}_6 \left(\frac{m_{u_j}^2}{m_2^2} \right) \right), \tag{8.42d}$$

$$\begin{aligned}
 \Xi_{fi}^{R, \Phi_2} &\approx \frac{N_c}{288 \pi^2 m_2^2} \left(V_{jk}^* \lambda_{kf}^{2LR*} V_{jl} \lambda_{li}^{2LR} \left(\mathcal{F}_5 \left(\frac{m_{u_j}^2}{m_2^2} \right) - \frac{v^2 (Y_2 + Y_{22})}{m_2^2} \mathcal{F}_6 \left(\frac{m_{u_j}^2}{m_2^2} \right) \right) \right. \\
 &\quad \left. - 2 \lambda_{jf}^{2LR*} \lambda_{ji}^{2LR} \left(\mathcal{F}_7 \left(\frac{m_{d_j}^2}{m_2^2} \right) - \frac{2v^2 Y_2}{m_2^2} \mathcal{F}_8 \left(\frac{m_{d_j}^2}{m_2^2} \right) \right) \right),
 \end{aligned} \tag{8.42e}$$

$$\Xi_{fi}^{L, \Phi_2} \approx \frac{-N_c \tilde{\lambda}_{jf}^{2*} \tilde{\lambda}_{ji}^2}{144 \pi^2 \tilde{m}_2^2} \left(\mathcal{F}_7 \left(\frac{m_{d_j}^2}{\tilde{m}_2^2} \right) - \frac{v^2 (Y_{\bar{2}} + Y_{\bar{2}\bar{2}})}{\tilde{m}_2^2} \mathcal{F}_4 \left(\frac{m_{d_j}^2}{\tilde{m}_2^2} \right) + \frac{v^2 |A_{\bar{2}3}|^2}{\tilde{m}_2^4} \mathcal{F}_9 \left(\frac{m_{d_j}^2}{\tilde{m}_2^2}, \frac{m_3^2}{\tilde{m}_2^2} \right) \right), \tag{8.42f}$$

$$\begin{aligned}
 \Xi_{fi}^{L, \Phi_3} &\approx \frac{-N_c}{288 \pi^2 m_3^2} \left(\lambda_{kf}^{3*} V_{jk} V_{jl}^* \lambda_{li}^3 \left(\mathcal{F}_1 \left(\frac{m_{u_j}^2}{m_3^2} \right) - \frac{v^2 Y_3}{m_3^2} \mathcal{F}_2 \left(\frac{m_{u_j}^2}{m_3^2} \right) + \frac{v^2 |A_{\bar{2}3}|^2}{\tilde{m}_2^4} \mathcal{F}_3 \left(\frac{m_{u_j}^2}{m_3^2}, \frac{m_3^2}{\tilde{m}_2^2} \right) \right) \right. \\
 &\quad \left. - 4 \lambda_{jf}^{3*} \lambda_{ji}^3 \left(\mathcal{F}_4 \left(\frac{m_{d_j}^2}{m_3^2} \right) - \frac{v^2 (Y_3 - Y_{33})}{m_3^2} \mathcal{F}_8 \left(\frac{m_{d_j}^2}{m_3^2} \right) \right) \right).
 \end{aligned} \tag{8.42g}$$

If we include LQ Higgs interactions, we find a new structure originating from Φ_1 - Φ_3 mixing

$$\begin{aligned}
 \hat{\Xi}_{fi}^L &\approx \frac{N_c v^2 \lambda_{kf}^{3*} V_{jk} V_{jl}^* \lambda_{li}^{1L}}{288 \pi^2} \left(\frac{Y_{13}^*}{m_3^4} \mathcal{F}_{10} \left(\frac{m_{u_j}^2}{m_3^2}, \frac{m_1^2}{m_3^2} \right) + \frac{A_{\bar{2}1} A_{\bar{2}3}^*}{\tilde{m}_2^6} \mathcal{F}_{11} \left(\frac{m_{u_j}^2}{\tilde{m}_2^2}, \frac{m_1^2}{\tilde{m}_2^2}, \frac{m_3^2}{\tilde{m}_2^2} \right) \right) \\
 &\quad + \frac{N_c v^2 \lambda_{kf}^{1L*} V_{jk} V_{jl}^* \lambda_{li}^3}{288 \pi^2} \left(\frac{Y_{13}}{m_3^4} \mathcal{F}_{10} \left(\frac{m_{u_j}^2}{m_3^2}, \frac{m_1^2}{m_3^2} \right) + \frac{A_{\bar{2}3} A_{\bar{2}1}^*}{\tilde{m}_2^6} \mathcal{F}_{11} \left(\frac{m_{u_j}^2}{\tilde{m}_2^2}, \frac{m_1^2}{\tilde{m}_2^2}, \frac{m_3^2}{\tilde{m}_2^2} \right) \right),
 \end{aligned} \tag{8.43}$$

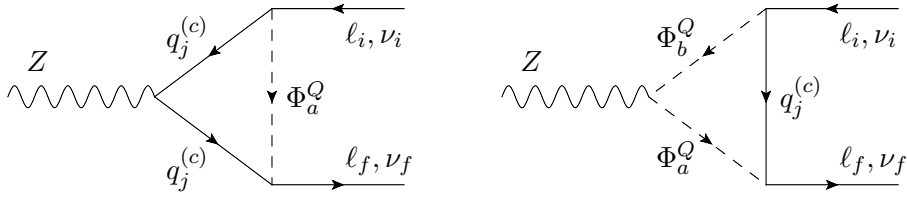


Figure 8.4: Vertex diagrams which contribute to $Z \rightarrow \ell_f^- \ell_i^+$ and $Z \rightarrow \nu_f \bar{\nu}_i$. Note that in case of mixing among LQs, the Z coupling, unlike the photon, can connect different representations with each other.

at $\mathcal{O}(v^2/m_{LQ}^2)$. The quark index j runs from 1 to 3 and the loop functions are given in the Appendix 8.7.2. Note that we again assumed that the quarks can be integrated out at the same scale as the LQs. This means that the expressions should be understood to be at the low scale and include the mixing of two-quark-two-lepton operators into four-fermion ones. Therefore, in case the quark is lighter than the corresponding leptonic process, one has to insert the scale of that process (rather than the quark mass) into the logarithms of the loop functions in Appendix 8.7.2.

8.4.2 $Z\ell\ell$ and $Z\nu\nu$

We now compute the LQ effects on the $Z \rightarrow \ell_f^- \ell_i^+$ and $Z \rightarrow \nu_f \bar{\nu}_i$ amplitudes, depicted in Fig. 8.4

$$\mathcal{A}(Z \rightarrow \ell_f^- \ell_i^+) = \frac{g^2}{c_w} \bar{u}(p_f, m_{\ell_f}) \not{\epsilon}(q) \left(\Lambda_{\ell_f \ell_i}^L(q^2) P_L + \Lambda_{\ell_f \ell_i}^R(q^2) P_R \right) v(p_i, m_{\ell_i}), \quad (8.44a)$$

$$\mathcal{A}(Z \rightarrow \nu_f \bar{\nu}_i) = \frac{g^2}{c_w} \Theta_{\nu_f \nu_i}(q^2) \bar{u}(p_f) \not{\epsilon}(q) P_L v(p_i), \quad (8.44b)$$

with $\epsilon^\mu(q)$ as the polarization vector of the Z boson and $q^2 = (p_f + p_i)^2$. In addition, there is an magnetic form factor for $Z \rightarrow \ell^+ \ell^-$ [465]. However, we do not give the form factor of this amplitude explicitly, since it does not interfere with the SM for $m_\ell = 0$. We perform this calculation for vanishing lepton masses and decompose the form factors as

$$\Lambda_{\ell_f \ell_i}^{L(R)}(q^2) = \Lambda_{\text{SM}}^{L(R)}(q^2) \delta_{fi} + \sum_{\Phi} \Delta_{L(R), fi}^{\Phi}(q^2) + \tilde{\Delta}_{L(R), fi}, \quad (8.45a)$$

$$\Theta_{\nu_f \nu_i}(q^2) = \Theta_{\text{SM}}(q^2) \delta_{fi} + \sum_{\Phi} \Theta_{fi}^{\Phi}(q^2) + \tilde{\Theta}_{fi}. \quad (8.45b)$$

The $\Delta_{L(R), fi}^{\Phi}(q^2)$ and $\Theta_{fi}^{\Phi}(q^2)$ contain the part with no LQ mixing, grouped into $\Phi = \{\Phi_1, \tilde{\Phi}_1, \Phi_2, \tilde{\Phi}_2, \Phi_3\}$, while the $\tilde{\Delta}_{L(R), fi}$ and $\tilde{\Theta}_{fi}$ contain the part induced by LQ mixing. In our conventions, the tree-level SM couplings read

$$\Lambda_{\text{SM}}^L = s_w^2 - \frac{1}{2}, \quad \Lambda_{\text{SM}}^R = s_w^2, \quad \Theta_{\text{SM}} = \frac{1}{2}, \quad (8.46)$$

with s_w (c_w) being the sine (cosine) of the Weinberg angle. Beyond tree-level, also the SM couplings receive momentum dependent corrections, which are included in the predictions for EW observables that we study later in the phenomenological analysis.

In our calculation we only include contributions of $\mathcal{O}(m_{\text{EW}}^2/m_{LQ}^2)$, i.e. effects from the top quark, the Z mass as well as the ones induced by LQ mixing, while setting all other masses to

zero³³. In case where the Z boson has a squared momentum q^2 we find

$$\begin{aligned} \Delta_{L,fi}^{\Phi_1}(q^2) \approx & \frac{-N_c \lambda_{kf}^{1L*} V_{3k} V_{3j}^* \lambda_{ji}^{1L}}{32\pi^2} \left[\mathcal{H}_0\left(\frac{m_t^2}{m_1^2}\right) - \frac{q^2}{18m_1^2} (11 - 10s_w^2 + 2(3 - 4s_w^2) \log\left(\frac{m_t^2}{m_1^2}\right)) \right. \\ & \left. - \frac{q^2}{180m_1^2} \frac{q^2}{m_t^2} (16s_w^2 - 9) \right] \\ & - \sum_{j=1}^2 \frac{N_c \lambda_{kf}^{1L*} V_{jk} V_{jl}^* \lambda_{li}^{1L}}{864\pi^2} \frac{q^2}{m_1^2} \left[3 - 3i\pi(4s_w^2 - 3) - 5s_w^2 + 3(4s_w^2 - 3) \log\left(\frac{q^2}{m_1^2}\right) \right], \end{aligned} \quad (8.47a)$$

$$\begin{aligned} \Delta_{R,fi}^{\Phi_1}(q^2) \approx & \frac{N_c \lambda_{3f}^{1R*} \lambda_{3i}^{1R}}{32\pi^2} \left[\mathcal{H}_0\left(\frac{m_t^2}{m_1^2}\right) - \frac{q^2}{18m_1^2} (3 + 10s_w^2 + 8s_w^2 \log\left(\frac{m_t^2}{m_1^2}\right)) \right. \\ & \left. + \frac{q^2}{180m_1^2} \frac{q^2}{m_t^2} (16s_w^2 - 3) \right] \\ & + \sum_{j=1}^2 \frac{N_c \lambda_{jf}^{1R*} \lambda_{ji}^{1R}}{864\pi^2} \frac{q^2}{m_1^2} \left[5s_w^2 + 12i\pi s_w^2 - 12s_w^2 \log\left(\frac{q^2}{m_1^2}\right) \right], \end{aligned} \quad (8.47b)$$

$$\Delta_{R,fi}^{\tilde{\Phi}_1}(q^2) \approx \sum_{j=1}^3 \frac{N_c \tilde{\lambda}_{jf}^{1*} \tilde{\lambda}_{ji}^1}{432\pi^2} \frac{q^2}{\tilde{m}_1^2} \left[s_w^2 - 3i\pi s_w^2 + 3s_w^2 \log\left(\frac{q^2}{\tilde{m}_1^2}\right) \right], \quad (8.47c)$$

$$\begin{aligned} \Delta_{L,fi}^{\Phi_2}(q^2) \approx & \frac{-N_c \lambda_{3f}^{2RL*} \lambda_{3i}^{2RL}}{32\pi^2} \left[\mathcal{H}_0\left(\frac{m_t^2}{m_2^2}\right) - \frac{q^2}{9m_2^2} (1 + 7s_w^2 + 4s_w^2 \log\left(\frac{m_t^2}{m_2^2}\right)) \right. \\ & \left. + \frac{q^2}{180m_2^2} \frac{q^2}{m_t^2} (16s_w^2 - 3) \right] \\ & - \sum_{j=1}^2 \frac{N_c \lambda_{jf}^{2RL*} \lambda_{ji}^{2RL}}{1728\pi^2} \frac{q^2}{m_2^2} \left[3 - 2s_w^2 + 24i\pi s_w^2 - 24s_w^2 \log\left(\frac{q^2}{m_2^2}\right) \right], \end{aligned} \quad (8.47d)$$

$$\begin{aligned} \Delta_{R,fi}^{\Phi_2}(q^2) \approx & \frac{N_c V_{3k}^* \lambda_{kf}^{2LR*} V_{3j} \lambda_{ji}^{2LR}}{32\pi^2} \left[\mathcal{H}_0\left(\frac{m_t^2}{m_2^2}\right) - \frac{q^2}{9m_2^2} (6 - 7s_w^2 + (3 - 4s_w^2) \log\left(\frac{m_t^2}{m_2^2}\right)) \right. \\ & \left. - \frac{q^2}{180m_2^2} \frac{q^2}{m_t^2} (16s_w^2 - 9) \right] \\ & + \sum_{j=1}^2 \frac{N_c V_{jk}^* \lambda_{kf}^{2LR*} V_{jl} \lambda_{li}^{2LR}}{1728\pi^2} \frac{q^2}{m_2^2} \left[3 + 2s_w^2 - 6i\pi(4s_w^2 - 3) + 6(4s_w^2 - 3) \log\left(\frac{q^2}{m_2^2}\right) \right] \\ & - \sum_{j=1}^3 \frac{N_c \lambda_{jf}^{2LR*} \lambda_{ji}^{2LR}}{1728\pi^2} \frac{q^2}{m_2^2} \left[3 - 6i\pi(2s_w^2 - 3) - 8s_w^2 + 6(2s_w^2 - 3) \log\left(\frac{q^2}{m_2^2}\right) \right], \end{aligned} \quad (8.47e)$$

$$\Delta_{L,fi}^{\tilde{\Phi}_2}(q^2) \approx \sum_{j=1}^3 \frac{-N_c \tilde{\lambda}_{jf}^{2*} \tilde{\lambda}_{ji}^2}{1728\pi^2} \frac{q^2}{\tilde{m}_2^2} \left[3 - 8s_w^2 - 12i\pi s_w^2 + 12s_w^2 \log\left(\frac{q^2}{\tilde{m}_2^2}\right) \right], \quad (8.47f)$$

$$\begin{aligned} \Delta_{L,fi}^{\Phi_3}(q^2) \approx & \frac{-N_c V_{3k} \lambda_{kf}^{3*} V_{3j}^* \lambda_{ji}^3}{32\pi^2} \left[\mathcal{H}_0\left(\frac{m_t^2}{m_3^2}\right) - \frac{q^2}{18m_3^2} (11 - 10s_w^2 + 2(3 - 4s_w^2) \log\left(\frac{m_t^2}{m_3^2}\right)) \right. \\ & \left. - \frac{q^2}{180m_3^2} \frac{q^2}{m_t^2} (16s_w^2 - 9) \right] \\ & - \sum_{j=1}^2 \frac{N_c V_{jk} \lambda_{kf}^{3*} V_{jl}^* \lambda_{li}^3}{864\pi^2} \frac{q^2}{m_3^2} \left[3 - 3i\pi(4s_w^2 - 3) - 5s_w^2 + 3(4s_w^2 - 3) \log\left(\frac{q^2}{m_3^2}\right) \right] \end{aligned}$$

³³Similar results for the diquark contribution to $Z \rightarrow \ell^+ \ell^-$ have been obtained in Ref. [466].

$$- \sum_{j=1}^3 \frac{N_c \lambda_{jf}^{3*} \lambda_{ji}^3}{216\pi^2} \frac{q^2}{m_3^2} \left[3i\pi(2s_w^2 - 3) - 2s_w^2 - 3(2s_w^2 - 3) \log\left(\frac{q^2}{m_3^2}\right) \right], \quad (8.47g)$$

where we expanded the results in q^2/m_{LQ}^2 and m_t^2/m_{LQ}^2 . Finally, the contributions from LQ mixing read

$$\begin{aligned} \tilde{\Delta}_{L,fi} \approx & \sum_{j=1}^3 \frac{-v^2 N_c}{64\pi^2 \tilde{m}_2^4} \left[\lambda_{jf}^{1L*} \lambda_{ji}^{1L} |A_{\bar{2}1}|^2 \mathcal{H}_3\left(\frac{m_1^2}{\tilde{m}_2^2}\right) + \left(\lambda_{jf}^{3*} \lambda_{ji}^3 + 2\tilde{\lambda}_{ji}^{2*} \tilde{\lambda}_{jf}^2\right) |A_{\bar{2}3}|^2 \mathcal{H}_3\left(\frac{m_3^2}{\tilde{m}_2^2}\right) \right. \\ & \left. + \left(\lambda_{jf}^{1L} \lambda_{ji}^{3*} A_{\bar{2}1} A_{\bar{2}3}^* + \lambda_{jf}^3 \lambda_{ji}^{1L*} A_{\bar{2}3} A_{\bar{2}1}^*\right) \mathcal{H}_4\left(\frac{m_1^2}{\tilde{m}_2^2}, \frac{m_3^2}{\tilde{m}_2^2}\right) \right], \end{aligned} \quad (8.48a)$$

$$\tilde{\Delta}_{R,fi} \approx \sum_{j=1}^3 \frac{-v^2 N_c}{64\pi^2 \tilde{m}_2^4} \lambda_{jf}^{1R*} \lambda_{ji}^{1R} |A_{\bar{2}1}|^2 \mathcal{H}_3\left(\frac{m_1^2}{\tilde{m}_2^2}\right), \quad (8.48b)$$

where the \mathcal{H} -functions are given in Appendix 8.7.2.

Now we turn to the $Z \rightarrow \nu_f \bar{\nu}_i$ amplitudes, where we show the contributions again separated by each representation

$$\Theta_{fi}^{\Phi_1}(q^2) \approx \sum_{j=1}^3 \frac{N_c \lambda_{jf}^{1L*} \lambda_{ji}^{1L}}{864\pi^2} \frac{q^2}{m_1^2} \left[3 - s_w^2 + 3i\pi(3 - 2s_w^2) - 3(3 - 2s_w^2) \log\left(\frac{q^2}{m_1^2}\right) \right], \quad (8.49a)$$

$$\begin{aligned} \Theta_{fi}^{\Phi_2}(q^2) \approx & \frac{-N_c \lambda_{3f}^{2RL*} \lambda_{3i}^{2RL}}{32\pi^2} \left[\mathcal{H}_0\left(\frac{m_t^2}{m_2^2}\right) - \frac{2q^2}{9m_2^2} \left(1 + 3s_w^2 + 2s_w^2 \log\left(\frac{m_t^2}{m_2^2}\right)\right) \right. \\ & \left. + \frac{q^2}{180m_2^2} \frac{q^2}{m_t^2} (16s_w^2 - 3) \right] \\ & + \sum_{j=1}^2 \frac{N_c \lambda_{jf}^{2RL*} \lambda_{ji}^{2RL}}{1728\pi^2} \frac{q^2}{m_2^2} \left[3 - 4s_w^2 - 24i\pi s_w^2 + 24s_w^2 \log\left(\frac{q^2}{m_2^2}\right) \right], \end{aligned} \quad (8.49b)$$

$$\Theta_{fi}^{\tilde{\Phi}_2}(q^2) \approx \sum_{j=1}^3 \frac{N_c \tilde{\lambda}_{jf}^{2*} \tilde{\lambda}_{ji}^2}{1728\pi^2} \frac{q^2}{\tilde{m}_2^2} \left[3 + 2s_w^2 + 12i\pi s_w^2 - 12s_w^2 \log\left(\frac{q^2}{\tilde{m}_2^2}\right) \right], \quad (8.49c)$$

$$\begin{aligned} \Theta_{fi}^{\Phi_3}(q^2) \approx & \frac{-N_c V_{3k} \lambda_{ki}^{3*} V_{3j}^* \lambda_{jf}^3}{16\pi^2} \left[\mathcal{H}_0\left(\frac{m_t^2}{m_3^2}\right) - \frac{q^2}{18m_3^2} (13 - 12s_w^2 + (6 - 8s_w^2) \log\left(\frac{m_t^2}{m_3^2}\right)) \right. \\ & \left. - \frac{q^2}{180m_3^2} \frac{q^2}{m_t^2} (16s_w^2 - 9) \right] \\ & + \sum_{j=1}^2 \frac{N_c V_{jk} \lambda_{ki}^{3*} V_{jl}^* \lambda_{lf}^3}{432\pi^2} \frac{q^2}{m_3^2} \left[2s_w^2 - 3i\pi(3 - 4s_w^2) - 3(4s_w^2 - 3) \log\left(\frac{q^2}{m_3^2}\right) \right] \\ & + \sum_{j=1}^3 \frac{N_c \lambda_{jf}^{3*} \lambda_{ji}^3}{864\pi^2} \frac{q^2}{m_3^2} \left[3 - s_w^2 + 3i\pi(3 - 2s_w^2) - 3(3 - 2s_w^2) \log\left(\frac{q^2}{m_3^2}\right) \right]. \end{aligned} \quad (8.49d)$$

Finally, we again have the contributions from LQ mixing

$$\begin{aligned} \tilde{\Theta}_{fi} \approx & \sum_{j=1}^3 \frac{-v^2 N_c}{64\pi^2 \tilde{m}_2^4} \left[\left(\lambda_{jf}^{1L*} \lambda_{ji}^{1L} + \tilde{\lambda}_{ji}^{2*} \tilde{\lambda}_{jf}^2\right) |A_{\bar{2}1}|^2 \mathcal{H}_3\left(\frac{m_1^2}{\tilde{m}_2^2}\right) \right. \\ & \left. + \left(5\lambda_{jf}^{3*} \lambda_{ji}^3 + \tilde{\lambda}_{ji}^{2*} \tilde{\lambda}_{jf}^2\right) |A_{\bar{2}3}|^2 \mathcal{H}_3\left(\frac{m_3^2}{\tilde{m}_2^2}\right) \right. \\ & \left. - \left(\lambda_{jf}^{1L} \lambda_{ji}^{3*} A_{\bar{2}1} A_{\bar{2}3}^* + \lambda_{jf}^3 \lambda_{ji}^{1L*} A_{\bar{2}3} A_{\bar{2}1}^*\right) \mathcal{H}_4\left(\frac{m_1^2}{\tilde{m}_2^2}, \frac{m_3^2}{\tilde{m}_2^2}\right) \right]. \end{aligned} \quad (8.50)$$

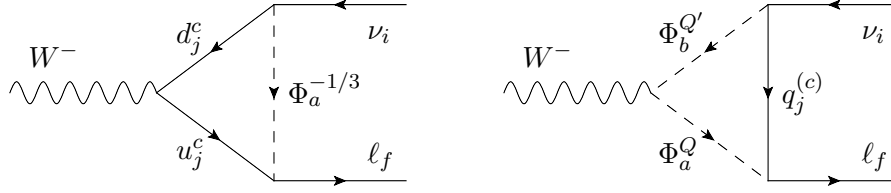


Figure 8.5: Vertex diagrams contributing to $W^- \rightarrow \ell_f^- \bar{\nu}_i$. In the case of massless down-type quarks the diagram on the left-hand side is only present with charge-conjugated quarks, since the W boson couples to purely to left-handed quarks.

In case of zero momentum transfer, i.e. $q^2 = 0$, the form factors correspond to effective $Z\ell\ell$ and $Z\nu\nu$ couplings. We define them for later purposes in an effective Lagrangian

$$\mathcal{L}_{\text{int}}^{Z\ell\ell} = \frac{g^2}{c_w} [\bar{\ell}_f (\Lambda_{\ell_f \ell_i}^L(0) \gamma^\mu P_L + \Lambda_{\ell_f \ell_i}^R(0) \gamma^\mu P_R) \ell_i] Z_\mu, \quad (8.51a)$$

$$\mathcal{L}_{\text{int}}^{Z\nu\nu} = \frac{g^2}{c_w} \Theta_{\nu_f \nu_i}(0) [\bar{\nu}_f \gamma^\mu P_L \nu_i] Z_\mu, \quad (8.51b)$$

where only the $\tilde{\Delta}$, $\tilde{\Theta}$ and the top contributions remain.

8.4.3 $W\ell\nu$

We define the amplitude of this process, also considered for generic new scalars and fermions in Ref. [289], as follows

$$\mathcal{A}(W^- \rightarrow \ell_f^- \bar{\nu}_i) = \frac{g^2}{\sqrt{2}} \Lambda_{\ell_f \nu_i}^W(q^2) \bar{u}(p_{\ell_f}, m_{\ell_f}) \not{\epsilon}(q) P_L v(p_{\nu_i}), \quad (8.52)$$

with

$$\Lambda_{\ell_f \nu_i}^W(q^2) = \Lambda_{\text{SM}}^W(q^2) \delta_{fi} + \sum_{\Phi} \Lambda_{fi}^{\Phi}(q^2) + \tilde{\Lambda}_{fi}. \quad (8.53)$$

The diagrams are shown in Fig. 8.5. The form factors $\Lambda_{fi}^{\Phi}(q^2)$ again contain the parts with no LQ mixing, grouped by representation with $\Phi = \{\Phi_1, \tilde{\Phi}_1, \Phi_2, \tilde{\Phi}_2, \Phi_3\}$, while $\tilde{\Lambda}_{fi}$ contains the part with LQ mixing. In the SM we have at tree-level

$$\Lambda_{\text{SM}}^W = 1. \quad (8.54)$$

The single LQ contributions read

$$\Lambda_{fi}^{\Phi_1}(q^2) \approx \frac{N_c V_{3k} \lambda_{kf}^{1L*} V_{3j}^* \lambda_{ji}^{1L}}{64\pi^2} \left[\frac{m_t^2}{m_1^2} \left(1 + 2 \log\left(\frac{m_t^2}{m_1^2}\right) \right) - \frac{4q^2}{3m_1^2} \left(1 + \log\left(\frac{m_t^2}{m_1^2}\right) \right) + \frac{q^2}{2m_1^2} \frac{q^2}{m_t^2} \right] - \sum_{j=1}^2 \frac{N_c V_{jl} \lambda_{lf}^{1L*} V_{jk}^* \lambda_{ki}^{1L}}{144\pi^2} \frac{q^2}{m_1^2} \left[3 \log\left(\frac{q^2}{m_1^2}\right) + 3i\pi - 1 \right], \quad (8.55a)$$

$$\Lambda_{fi}^{\Phi_2}(q^2) \approx \sum_{j=1}^3 \frac{N_c q^2}{288\pi^2} \frac{\lambda_{jf}^{2RL*} \lambda_{ji}^{2RL}}{m_2^2}, \quad (8.55b)$$

$$\Lambda_{fi}^{\tilde{\Phi}_2}(q^2) \approx \sum_{j=1}^3 \frac{N_c q^2}{288\pi^2} \frac{\tilde{\lambda}_{jf}^{2*} \tilde{\lambda}_{ji}^2}{\tilde{m}_2^2}, \quad (8.55c)$$

$$\begin{aligned}
 \Lambda_{fi}^{\Phi_3}(q^2) &\approx \frac{-N_c V_{3k} \lambda_{kf}^{3*} V_{3j} \lambda_{ji}^3}{64\pi^2} \left[\frac{m_t^2}{m_3^2} \left(1 + 2 \log\left(\frac{m_t^2}{m_3^2}\right) \right) - \frac{4q^2}{9m_3^2} \left(4 + 3 \log\left(\frac{m_t^2}{m_3^2}\right) \right) + \frac{q^2}{2m_3^2} \frac{q^2}{m_t^2} \right] \\
 &+ \sum_{j=1}^2 \frac{N_c}{144\pi^2} V_{jl} \lambda_{lf}^{3*} V_{jk}^* \lambda_{ki}^3 \frac{q^2}{m_3^2} \left(3 \log\left(\frac{q^2}{m_3^2}\right) + 3i\pi + 1 \right) \\
 &- \sum_{j=1}^3 \frac{N_c}{144\pi^2} \frac{q^2}{m_3^2} \lambda_{jf}^{3*} \lambda_{ji}^3.
 \end{aligned} \tag{8.55d}$$

Additionally, we have the $\mathcal{O}(v^2/m_{LQ}^2)$ effects from LQ mixing

$$\begin{aligned}
 \tilde{\Lambda}_{fi} &\approx \sum_{j=1}^3 \frac{v^2 N_c}{64\pi^2} \left[\left(\tilde{\lambda}_{jf}^{2*} \tilde{\lambda}_{ji}^2 - 4 \lambda_{jf}^{3*} \lambda_{ji}^3 \right) \frac{|A_{\tilde{2}3}|^2}{\tilde{m}_2^4} \mathcal{H}_3\left(\frac{m_3^2}{\tilde{m}_2^2}\right) - \tilde{\lambda}_{jf}^{2*} \tilde{\lambda}_{ji}^2 \frac{|A_{\tilde{2}1}|^2}{\tilde{m}_2^4} \mathcal{H}_3\left(\frac{m_1^2}{\tilde{m}_2^2}\right) \right. \\
 &+ 2 \frac{\lambda_{ji}^{1L} \lambda_{jf}^{3*} A_{\tilde{2}3}^* A_{\tilde{2}1} + \lambda_{jf}^{1L*} \lambda_{ji}^3 A_{\tilde{2}3} A_{\tilde{2}1}^*}{\tilde{m}_2^4} \mathcal{H}_4\left(\frac{m_1^2}{\tilde{m}_2^2}, \frac{m_3^2}{\tilde{m}_2^2}\right) \\
 &+ 2 \frac{Y_{13} \lambda_{ji}^{1L*} \lambda_{jf}^3 - Y_{13}^* \lambda_{ji}^{3*} \lambda_{jf}^{1L}}{m_3^2} \mathcal{H}_5\left(\frac{m_1^2}{m_3^2}\right) \\
 &\left. + 2 \frac{\lambda_{ji}^{1L} \lambda_{jf}^{3*} A_{\tilde{2}3}^* A_{\tilde{2}1} - \lambda_{jf}^{1L*} \lambda_{ji}^3 A_{\tilde{2}3} A_{\tilde{2}1}^*}{\tilde{m}_2^4} \mathcal{H}_6\left(\frac{m_1^2}{\tilde{m}_2^2}, \frac{m_3^2}{\tilde{m}_2^2}\right) \right],
 \end{aligned} \tag{8.56}$$

with the loop functions given in the Appendix 8.7.2. Note that the terms in the last two lines in Eq. (8.56) are anti-hermitian in flavor space. Therefore, like the anti-hermitian part of the self-energy contributions, see Eq. (8.33), they are not physical. In fact, we checked that the terms originating from LQ mixing for $Z\ell\ell$, $Z\nu\nu$ and $W\ell\nu$ respect the structure required by the dim-6 operators with manifest $SU(2)_L$ invariance if the anti-hermitian terms are absorbed by the PMNS matrix.

At the level of effective couplings, we have to evaluate the contributions at $q^2 = 0$, which can be treated in the context of an effective Lagrangian

$$\mathcal{L}_{\text{int}}^{W\ell\nu} = \frac{g}{\sqrt{2}} \Lambda_{\ell_f \nu_i}^W(0) [\bar{\ell}_f \gamma^\mu P_L \nu_i] W_\mu^-. \tag{8.57}$$

The effective coupling $\Lambda_{\ell_f \nu_i}^W(0)$ then only receives LQ effects from loop-induced top quarks and from LQ mixing.

8.4.4 $h\ell\ell$

Let us turn next to the Higgs decays $h \rightarrow \ell_f^- \ell_i^+$. We define the amplitude analogously to the leptonic W and Z decays as

$$\mathcal{A}(h \rightarrow \ell_f^- \ell_i^+) = -\frac{m_{fi}}{\sqrt{2}v} \bar{u}(p_f, m_{\ell_f}) \left(\Upsilon_{\ell_f \ell_i}^L(q^2) P_L + \Upsilon_{\ell_f \ell_i}^R(q^2) P_R \right) v(p_i, m_{\ell_i}), \tag{8.58}$$

with

$$\Upsilon_{\ell_f \ell_i}^L(q^2) = \delta_{fi} + \sum_{\Phi} \Upsilon_{L,fi}^{\Phi}(q^2) + \tilde{\Upsilon}_{L,fi}, \tag{8.59a}$$

$$\Upsilon_{\ell_f \ell_i}^R(q^2) = \delta_{fi} + \sum_{\Phi} \Upsilon_{R,fi}^{\Phi}(q^2) + \tilde{\Upsilon}_{R,fi}. \tag{8.59b}$$

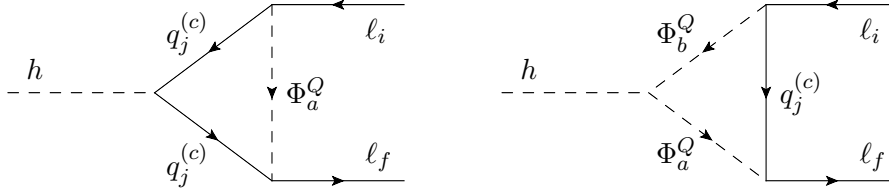


Figure 8.6: Vertex diagrams generating $h \rightarrow \ell_f^- \ell_i^+$ at the 1-loop level.

The sum over Φ refers to the LQ representations $\Phi = \{\Phi_1, \tilde{\Phi}_1, \Phi_2, \tilde{\Phi}_2, \Phi_3\}$, $\tilde{\Upsilon}_{L(R),fi}$ contain the terms which are only generated by LQ mixing and

$$m_{fi} = \max[m_{\ell_f}, m_{\ell_i}], \quad q^2 = (p_f + p_i)^2. \quad (8.60)$$

Note that due to hermicity

$$\Upsilon_{\ell_f \ell_i}^R = \Upsilon_{\ell_i \ell_f}^{L*}. \quad (8.61)$$

If $f \neq i$ we can safely neglect the lighter lepton mass. The corresponding Feynman diagrams are shown in Figure 8.6.

We expand again in v^2/m_{LQ}^2 and set the lepton masses to zero. In the phenomenologically most relevant case of an internal top quark, we additionally use the fact that for Higgs decays $m_t^2 > m_h^2 \equiv q^2$, finding

$$\Upsilon_{L,fi}^{\Phi_1}(q^2) \approx \frac{N_c \lambda_{3f}^{1R*} V_{3k}^* \lambda_{ki}^{1L}}{64\pi^2 m_1^2} \frac{m_t}{m_{fi}} \left(m_t^2 \mathcal{J}_t \left(\frac{q^2}{m_t^2}, \frac{m_t^2}{m_1^2} \right) + 8v^2 Y_1 \right), \quad (8.62a)$$

$$\Upsilon_{L,fi}^{\Phi_2}(q^2) \approx \frac{N_c V_{3k}^* \lambda_{kf}^{2LR*} \lambda_{3i}^{2RL}}{64\pi^2 m_2^2} \frac{m_t}{m_{fi}} \left(m_t^2 \mathcal{J}_t \left(\frac{q^2}{m_t^2}, \frac{m_t^2}{m_2^2} \right) + 8v^2 (Y_{22} + Y_2) \right). \quad (8.62b)$$

The mixing-induced terms read up to $\mathcal{O}(v^2/m_{LQ}^2)$

$$\begin{aligned} \tilde{\Upsilon}_{L,fi} \approx & \sum_{j=1}^3 \frac{-v^2 N_c}{8\pi^2} \left[\frac{m_t}{m_{fi}} \left(\lambda_{3f}^{1R*} V_{3k}^* \lambda_{ki}^{1L} \frac{|A_{21}|^2}{\tilde{m}_2^4} \mathcal{J}_1 \left(\frac{m_1^2}{\tilde{m}_2^2} \right) \right. \right. \\ & \left. \left. - \lambda_{3f}^{1R*} V_{3k}^* \lambda_{ki}^3 \left(\frac{Y_{13}}{m_1^2} \mathcal{H}_1 \left(\frac{m_3^2}{m_1^2} \right) + \frac{A_{23} A_{21}^*}{\tilde{m}_2^4} \mathcal{J}_2 \left(\frac{m_1^2}{\tilde{m}_2^2}, \frac{m_3^2}{\tilde{m}_2^2} \right) \right) \right) \right]. \end{aligned} \quad (8.63)$$

The loop functions that we used in this section can be found in the Appendix 8.7.2. In Appendix 8.7.5 we additionally present the generic results for light quarks, i.e. for the case where $m_{q_j}^2 \ll q^2 \equiv m_h^2$.

8.4.5 4ℓ

To describe processes involving four charged leptons, we define the effective Hamiltonian as

$$\mathcal{H}_{\text{eff}}^{4\ell} = \mathcal{H}_{\text{eff}}^{\ell\ell\gamma} + \sum_{f,i,a,b} \left(C_{fiab}^{VLL} O_{fiab}^{VLL} + C_{fiab}^{VLR} O_{fiab}^{VLR} + C_{fiab}^{SLL} O_{fiab}^{SLL} + L \leftrightarrow R \right), \quad (8.64)$$

with the effective operators

$$\begin{aligned} O_{fiab}^{VLL} &= [\bar{\ell}_f \gamma^\mu P_L \ell_i] [\bar{\ell}_a \gamma_\mu P_L \ell_b], \\ O_{fiab}^{VLR} &= [\bar{\ell}_f \gamma^\mu P_L \ell_i] [\bar{\ell}_a \gamma_\mu P_R \ell_b], \\ O_{fiab}^{SLL} &= [\bar{\ell}_f P_L \ell_i] [\bar{\ell}_a P_L \ell_b]. \end{aligned} \quad (8.65)$$

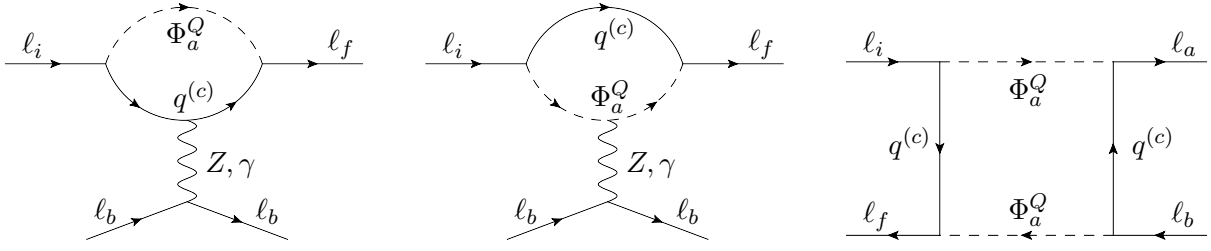


Figure 8.7: Feynman diagrams giving rise to $l_f l_i l_a l_b$ amplitudes. Left and center: Penguin diagrams with off-shell Z boson or photon exchange. Right: Box diagram involving two LQs.

Note that we sum over all flavor indices. Therefore, all other operators can be reduced to the ones in (8.64), using Fierz identities. As an advantage, we do not need to distinguish between decays involving the same or different flavors.

There are two types of diagrams which give a contribution to these operators: penguins and boxes, see Fig 8.7. Starting with the photon penguin, we have

$$\begin{aligned} C_{fiab}^{V LL} &= -\pi\alpha \left(\Xi_{fi}^L \Xi_{ab}^L + \Xi_{fb}^L \Xi_{ai}^L \right), \\ C_{fiab}^{V LR} &= -2\pi\alpha \Xi_{fi}^L \Xi_{ab}^R, \end{aligned} \quad (8.66)$$

with

$$\Xi_{fi}^{L(R)} = \delta_{fi} + \hat{\Xi}_{fi}^{L(R)}. \quad (8.67)$$

The Z boson gives an analogous contribution

$$\begin{aligned} C_{fiab}^{V LL} &= \sqrt{2}G_F (\Lambda_{l_f l_i}^L(0) \Lambda_{l_a l_b}^L(0) + \Lambda_{l_f l_b}^L(0) \Lambda_{l_a l_i}^L(0)), \\ C_{fiab}^{V LR} &= \frac{4G_F}{\sqrt{2}} \Lambda_{l_f l_i}^L(0) \Lambda_{l_a l_b}^R(0). \end{aligned} \quad (8.68)$$

The coefficients $C_{fiab}^{V RL}$ and $C_{fiab}^{V RR}$ are obtained in a straightforward way by simply exchanging $L \leftrightarrow R$.

The box diagrams generate the following contributions

$$\begin{aligned} C_{fiab}^{V LL} &= \frac{N_c}{256\pi^2} \left[\frac{\lambda_{ji}^{1L} \lambda_{kb}^{1L} (\lambda_{jf}^{1L*} \lambda_{ka}^{1L*} + \lambda_{kf}^{1L*} \lambda_{ja}^{1L*})}{m_1^2} + 5 \frac{\lambda_{ji}^3 \lambda_{kb}^3 (\lambda_{jf}^{3*} \lambda_{ka}^{3*} + \lambda_{kf}^{3*} \lambda_{ja}^{3*})}{m_3^2} \right. \\ &\quad + \frac{\lambda_{ji}^3 \lambda_{kb}^{1L} (\lambda_{jf}^{1L*} \lambda_{ka}^{3*} + \lambda_{kf}^{3*} \lambda_{ja}^{1L*}) + \lambda_{ji}^{1L} \lambda_{kb}^3 (\lambda_{jf}^{3*} \lambda_{ka}^{1L*} + \lambda_{kf}^{1L*} \lambda_{ja}^{3*})}{m_3^2} \mathcal{H}_1 \left(\frac{m_1^2}{m_3^2} \right) \\ &\quad \left. + \frac{\lambda_{ji}^{2RL} \lambda_{kb}^{2RL} (\lambda_{jf}^{2RL*} \lambda_{ka}^{2RL*} + \lambda_{kf}^{2RL*} \lambda_{ja}^{2RL*})}{m_2^2} + \frac{\tilde{\lambda}_{ji}^2 \tilde{\lambda}_{kb}^2 (\tilde{\lambda}_{jf}^{2*} \tilde{\lambda}_{ka}^{2*} + \tilde{\lambda}_{kf}^{2*} \tilde{\lambda}_{ja}^{2*})}{\tilde{m}_2^2} \right], \end{aligned} \quad (8.69a)$$

$$C_{fiab}^{V LR} = \frac{N_c}{128\pi^2} \left[\frac{\lambda_{jf}^{1L*} \lambda_{ji}^{1L} \lambda_{ka}^{1R*} \lambda_{kb}^{1R}}{m_1^2} + \frac{\lambda_{jf}^{2RL*} \lambda_{ji}^{2RL} \lambda_{ka}^{2LR*} \lambda_{kb}^{2LR}}{m_2^2} \right], \quad (8.69b)$$

$$\begin{aligned} C_{fiab}^{V RR} &= \frac{N_c}{256\pi^2} \left[\frac{\lambda_{ji}^{1R} \lambda_{kb}^{1R} (\lambda_{jf}^{1R*} \lambda_{ka}^{1R*} + \lambda_{kf}^{1R*} \lambda_{ja}^{1R*})}{m_1^2} \right. \\ &\quad \left. + 2 \frac{\lambda_{ji}^{2LR} \lambda_{kb}^{2LR} (\lambda_{jf}^{2LR*} \lambda_{ka}^{2LR*} + \lambda_{kf}^{2LR*} \lambda_{ja}^{2LR*})}{m_2^2} + \frac{\tilde{\lambda}_{ji}^1 \tilde{\lambda}_{kb}^1 (\tilde{\lambda}_{jf}^{1*} \tilde{\lambda}_{ka}^{1*} + \tilde{\lambda}_{kf}^{1*} \tilde{\lambda}_{ja}^{1*})}{\tilde{m}_1^2} \right], \end{aligned} \quad (8.69c)$$

where the loop function \mathcal{H}_1 is again given in Appendix 8.7.2. The indices j and k run from 1 to 3. Note that we only consider the leading effects in v/m . In scenarios where the λ -couplings

are smaller than the gauge couplings ($e \approx 0.3$ and $g_2 \approx 0.6$), the box contributions are typically less important than the gauge boson penguins.

8.4.6 $2\ell 2\nu$

For these fields we use the effective Hamiltonian

$$\mathcal{H}_{\text{eff}}^{2\ell 2\nu} = D_{\ell_f \ell_i}^{L,ab} O_{\ell_f \ell_i}^{L,ab} + D_{\ell_f \ell_i}^{R,ab} O_{\ell_f \ell_i}^{R,ab} \quad (8.70)$$

with

$$O_{\ell_f \ell_i}^{L(R),ab} = [\bar{\ell}_f \gamma_\mu P_{L(R)} \ell_i] [\bar{\nu}_a \gamma^\mu P_L \nu_b]. \quad (8.71)$$

There are three types of contributions: Z penguins, W penguins and boxes. The Z boson yields

$$D_{\ell_f \ell_i}^{L,ab} = \frac{8G_F}{\sqrt{2}} \Lambda_{\ell_f \ell_i}^L(0) \Theta_{\nu_a \nu_b}(0), \quad D_{\ell_f \ell_i}^{R,ab} = \frac{8G_F}{\sqrt{2}} \Lambda_{\ell_f \ell_i}^R(0) \Theta_{\nu_a \nu_b}(0), \quad (8.72)$$

while we have for the W boson

$$D_{\ell_f \ell_i}^{L,ab} = \frac{4G_F}{\sqrt{2}} \Lambda_{\ell_i \nu_a}^{W*}(0) \Lambda_{\ell_f \nu_b}^W(0). \quad (8.73)$$

The box diagrams yield

$$D_{\ell_f \ell_i}^{L,ab} = \frac{N_c}{64\pi^2} \left[\frac{\lambda_{jf}^{1L*} \lambda_{ji}^{1L} \lambda_{ka}^{1L*} \lambda_{kb}^{1L}}{m_1^2} + \frac{\lambda_{jf}^{3*} \lambda_{ji}^3 \lambda_{ka}^{3*} \lambda_{kb}^3}{m_3^2} - \frac{\lambda_{jf}^{3*} \lambda_{ji}^{1L} \lambda_{ka}^{1L*} \lambda_{kb}^3 + \lambda_{jf}^{1L*} \lambda_{ji}^3 \lambda_{ka}^{3*} \lambda_{kb}^{1L}}{m_3^2} \mathcal{H}_1\left(\frac{m_1^2}{m_3^2}\right) \right], \quad (8.74a)$$

$$D_{\ell_f \ell_i}^{R,ab} = \frac{N_c}{64\pi^2} \left[\frac{\lambda_{jf}^{1R*} \lambda_{ji}^{1R} \lambda_{ka}^{1L*} \lambda_{kb}^{1L}}{m_1^2} + \frac{\lambda_{jf}^{2LR*} \lambda_{ji}^{2LR} \lambda_{ka}^{2RL*} \lambda_{kb}^{2RL}}{m_2^2} \right]. \quad (8.74b)$$

Again the indices j and k run from 1 to 3 and we only considered the leading order LQ effects in v/m_{LQ} .

8.5 Phenomenology

Let us now study the phenomenology of scalar LQs in leptonic processes. Due to the large number of observables and the many free parameters, we will choose some exemplary processes of special interest and use simplifying assumptions for the couplings in order to show the effects and the possible correlations between observables. In particular, we will consider:

- EW gauge-boson couplings to leptons: the effects of scalar LQs in (effective) off-shell $Z\ell\ell$, $Z\nu\nu$ and $W\ell\nu$ couplings and the associated gauge-boson decays.
- Muonic observables: correlations between the AMM of the muon, $Z \rightarrow \ell^+\ell^-$, effective $W\mu\nu$ couplings and $h \rightarrow \mu^+\mu^-$.
- Charged lepton flavor violation: correlations between $\tau \rightarrow \mu\gamma$, $Z \rightarrow \tau\mu$ and $\tau \rightarrow 3\mu$ as well as the analogues in $\mu \rightarrow e$ transitions.

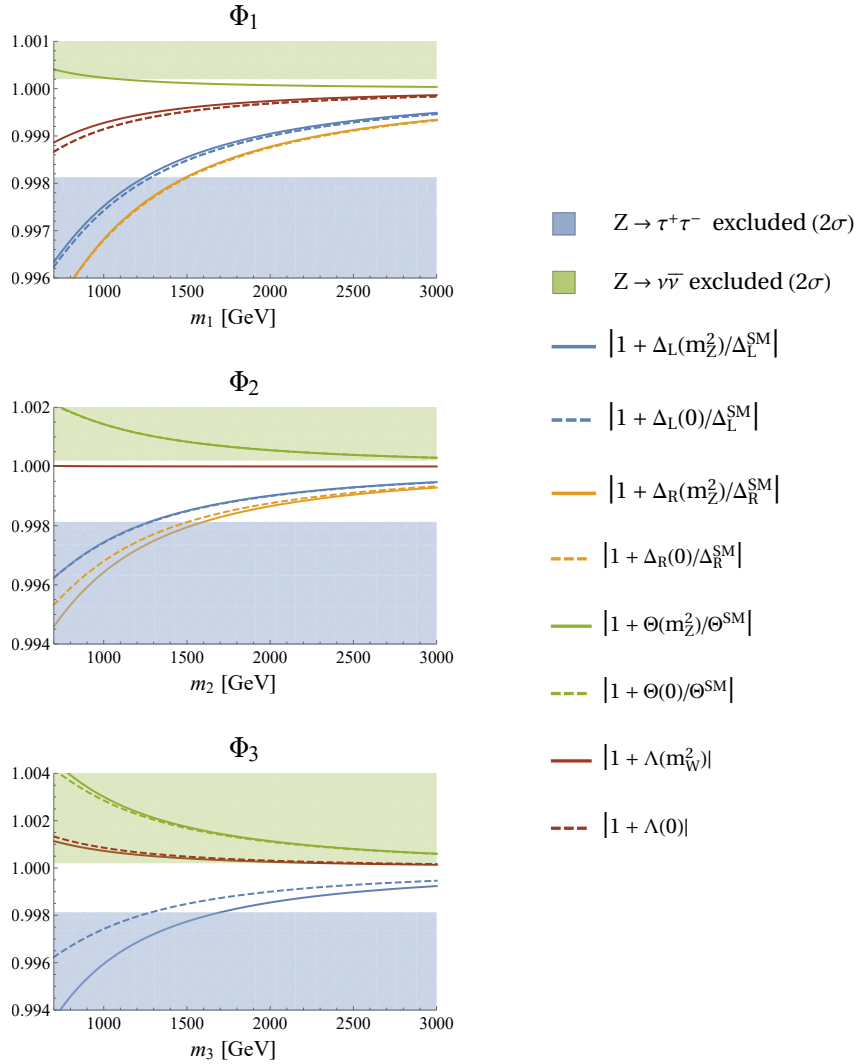


Figure 8.8: LQ effects in $Z\ell\ell$, $Z\nu\nu$ and $Wl\nu$ couplings for the scalar LQ representations which give rise to m_i^2 effects (Φ_1 , Φ_2 and Φ_3) as a function of the LQ mass. We neglected LQ mixing and considered only the couplings of third generation quarks to a single lepton flavor with unit strength, i.e. $\lambda_{3\ell} = 1$. Here, $\Delta_{L,R}$, Θ and Λ stand for the corrections in $Z\ell\ell$, $Z\nu\nu$ and $Wl\nu$ couplings, respectively (see Sec. 8.4.2). The solid (dashed) lines refer to the couplings entering on-shell decays (effective couplings at $q^2 = 0$). The green region is excluded by LEP data [353] from $Z \rightarrow \nu\bar{\nu}$ decays. The blue region is excluded by $Z \rightarrow \tau^+\tau^-$ which is more constraining than $Z \rightarrow \mu^+\mu^-$ (not shown explicitly). Note that we also do not show $Z \rightarrow e^+e^-$ exclusions here for the sake of clarity since couplings to electrons are usually much smaller in setups motivated by the B anomalies, leading to suppressed effects.

8.5.1 Electroweak Gauge-Boson Couplings to Leptons: $Z\ell\ell$, $Z\nu\nu$ and $Wl\nu$

We start our phenomenological analysis by considering the effects of scalar LQs in $Z\ell\ell$, $Z\nu\nu$ and $Wl\nu$ effective couplings (at $q^2 = 0$) and the associated gauge boson decays (at $q^2 = m_Z^2, m_W^2$), calculated in Sec. 8.4.2. While among $Z \rightarrow \ell^+\ell^-$ decays NP effects are strongly bounded by LEP [353] measurements, the effective $Wl\nu$ couplings are best constrained by low-energy observables, testing LFU of the charged current (see Ref. [275] for an overview).

We first focus on the LQ representations which generate an m_i^2/m_{LQ}^2 effect in EW gauge-

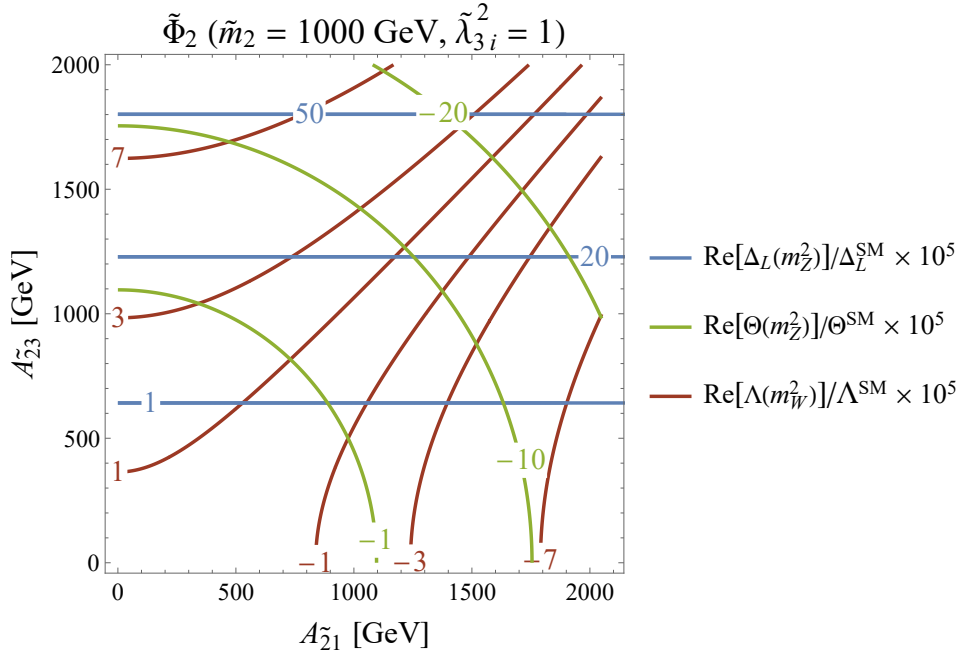


Figure 8.9: Modified $Z\ell\ell$, $Z\nu\nu$ and $W\ell\nu$ couplings in the A_{21} - A_{23} plane (in units of GeV) for $\tilde{m}_2 = m_1 = m_3 = 1$ TeV and $|\tilde{\lambda}_{3\ell}^2| = 1$.

boson couplings to leptons, i.e. Φ_1 , Φ_2 and Φ_3 . In the absence of LQ mixing, we can expect this effect to be dominant and couplings to third generation quarks are well motivated by the flavor anomalies. Note that we nonetheless included the $q^2 = \{m_Z^2, m_W^2\}$ terms which, due to $SU(2)_L$ invariance, can also arise from bottom loops for some of the representations shown in Fig. 8.8. In order to keep the number of free parameters small, we did not include mixing among the LQs and assumed that only couplings to one lepton flavor $\ell = e, \mu, \tau$ at a time exist. This avoids limits from charged lepton flavor violating observables, which we consider later in this article. Furthermore, we normalized the LQ effect to the respective SM coupling and the LQ-quark-lepton coupling to one (i.e. $\lambda_{3\ell} = 1$) while all other couplings are zero. Note that the effect in Fig. 8.8, given for couplings of unit strength, are consistent with $Z \rightarrow \ell^+\ell^-$ bounds for masses around 1.5 TeV or more. Furthermore, $Z \rightarrow \nu\bar{\nu}$ is constrained by the number of neutrino families

$$N_\nu = \sum_{f,i} \left| \delta_{fi} + \frac{\sum_\Phi \Theta_{fi}^\Phi(q^2) + \tilde{\Theta}_{fi}}{\Theta_{\text{SM}}(m_Z^2)} \right|^2, \quad (8.75)$$

where the experimental value lies at [353]

$$N_\nu = 2.9840 \pm 0.0082, \quad (8.76)$$

while the LQ effect is predicted to be constructive. Future colliders are expected to reach a 20 times better precision [409].

Let us now turn to the case of non-vanishing LQ couplings to the SM Higgs. We study as an example the scalar doublet $\tilde{\Phi}_2$ which couples only down-type quarks to leptons such that the v^2/\tilde{m}_2^2 effects from the mixing with Φ_1 (generated by A_{21}) and/or Φ_3 (generated by A_{23}) are expected to be dominant compared to the m_Z^2/\tilde{m}_2^2 effects. In Fig. 8.9 we present the impact of LQs on on-shell Z and W couplings. Again, we set $\tilde{\lambda}_{3\ell}^2 = 1$ and we assume $\tilde{m}_2 = m_1 = m_3 = 1$ TeV, which is compatible with current LHC limits [291, 362, 425]. Note that

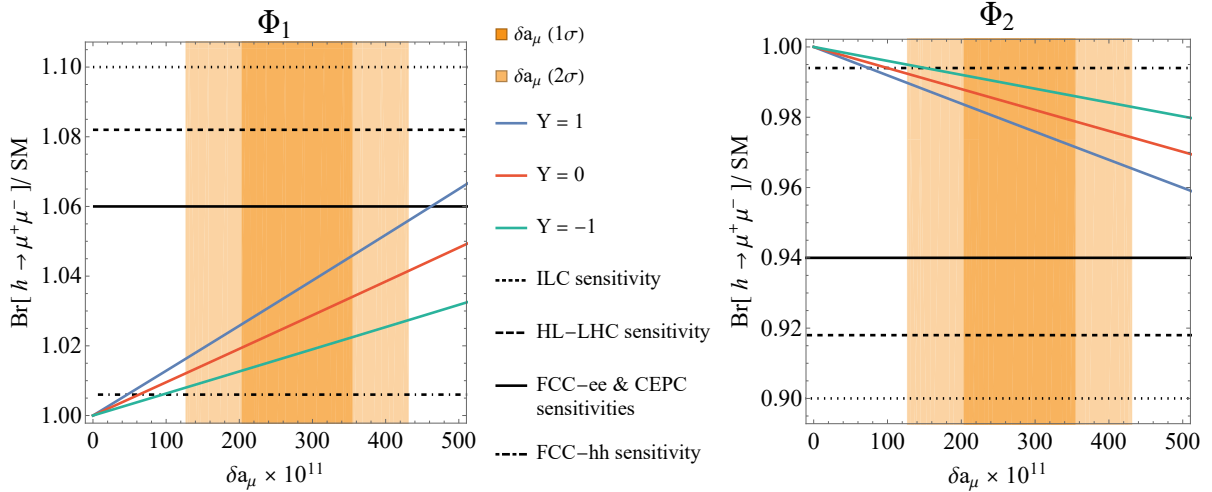


Figure 8.10: Correlations between $\text{Br}[h \rightarrow \mu^+\mu^-]$, normalized to its SM value, and the NP contribution to the AMM of the muon (δa_μ) for scenario Φ_1 (left) and Φ_2 (right) with $m_{1,2} = 1.5 \text{ TeV}$. The predictions for different values of the LQ couplings to the Higgs are shown, where for Φ_1 $Y = Y_1$ while for Φ_2 $Y = Y_1 + Y_{22}$. Even though the current ATLAS and CMS results are not yet constraining this model, sizeable effects are predicted, which can be tested at future colliders. Furthermore, Φ_1 yields a constructive effect in $h \rightarrow \mu^+\mu^-$ while the one of Φ_2 is destructive such that they can be clearly distinguished with increasing experimental precision.

a non-zero A_{51} yields a destructive effect in $Z\ell\ell$ and $W\ell\nu$ couplings while the terms with A_{53} are constructive.

8.5.2 Correlating the AMM of the Muon with $Z \rightarrow \ell^+\ell^-$ and $h \rightarrow \mu^+\mu^-$

In this sub-section, we focus on possible LQ explanations of the long-standing anomaly in the AMM of the muon. The discrepancy between its measurement [123] and the SM prediction [124]³⁴ amounts to

$$\delta a_\mu = (279 \pm 76) \times 10^{-11}, \quad (8.77)$$

corresponding to a 3.7σ tension. Note that this tension is quite large, i.e. of the order of the EW contribution of the SM. Since LQs are colored, the LHC bounds rule out masses significantly below 1 TeV such that an enhancement in a_μ is needed to compensate for the mass suppression. In fact, there are LQ representations that are able to generate m_t/m_μ enhanced contributions, see Eq. (8.39). These NP effects enter the AMM of the muon as

$$a_\mu = \frac{m_\mu}{4\pi^2} \text{Re}[C_{\mu\mu}^R], \quad (8.78)$$

with the Wilson coefficient defined in Eq.(8.37).

First of all, we can expect a direct correlation with $h \rightarrow \mu^+\mu^-$ [50] since both processes are chirality changing and therefore involve the same couplings of LQs to fermions³⁵. We can

³⁴This result is based on Refs. [128, 130, 133, 135, 139, 142–144, 303, 304, 306, 436–444]. The recent lattice result of the Budapest-Marseille-Wuppertal collaboration (BMWc) for the hadronic vacuum polarization (HVP) [302] on the other hand is not included. This result would render the SM prediction of a_μ compatible with experiment. However, the BMWc results are in tension with the HVP determined from $e^+e^- \rightarrow \text{hadrons}$ data [130, 133, 135, 303, 304, 306]. Furthermore, the HVP also enters the global EW fit [307], whose (indirect) determination is below the BMWc result [308]. Therefore, the BMWc determination of the HVP would increase the tension in EW fits [445, 446] and we opted for using the community consensus of Ref. [124].

³⁵Similar results for $\tau \rightarrow \mu\gamma$ were obtained in Refs. [451–453].

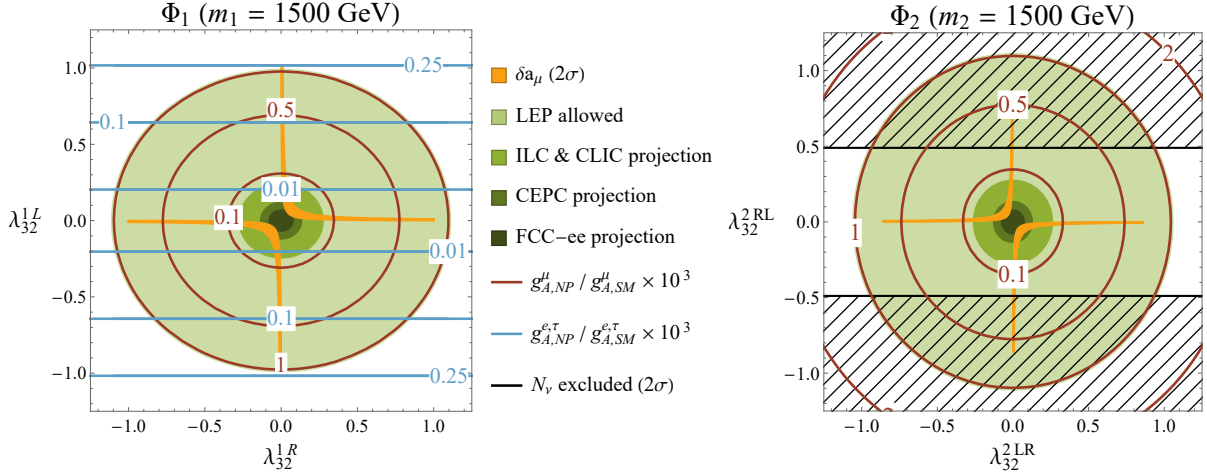


Figure 8.11: Allowed parameter space by LEP [353] (light green) for the couplings to left- and right-handed muons. In addition, we give the expected sensitivities of future collider experiments, see Tab. 8.2. The finite renormalization of g_2 , induced by the effect in the Fermi constant, yields a LFU effect which is depicted by the blue lines in the plot on the left.

express the NP effect in terms of Υ_L^Φ and $\tilde{\Upsilon}_L$, defined in (8.58), as

$$\frac{\text{Br}[h \rightarrow \mu^+ \mu^-]}{\text{Br}[h \rightarrow \mu^+ \mu^-]_{\text{SM}}} = \left| 1 + \sum_{\Phi} \Upsilon_{L,\mu\mu}^\Phi + \tilde{\Upsilon}_{L,\mu\mu} \right|^2. \quad (8.79)$$

The resulting correlations are shown in Fig. 8.10 for Φ_1 and Φ_2 . Note that even though the current CMS and ATLAS measurements [433, 434] are not able to constrain these models yet, a FCC-hh [424] can test them.

The LQ interactions with top quarks and muons also generate effects in $Z\mu\mu$ couplings. Therefore, let us as a next step consider the correlations of a_μ with $Z \rightarrow \ell^+ \ell^-$ where we refine the analysis of Ref. [368] by including the indirect effect, originating from the finite renormalization of the very precisely measured Fermi constant [52]

$$G_F = 1.166\,378\,7(6) \times 10^{-5} \text{ GeV}^{-2}, \quad (8.80)$$

which can be expressed in terms of the SM parameters

$$G_F = \frac{\sqrt{2}g_2^2}{8m_W^2}. \quad (8.81)$$

Since m_W itself is measured in W decays, g_2 can be determined once G_F is measured via the muon lifetime. However, also NP contributions enter such that

$$G_F \rightarrow G_F(1 + \Lambda_{\mu\nu\mu}^{W*}(0))(1 + \Lambda_{e\nu_e}^W(0)), \quad (8.82)$$

resulting in a redefinition of g_2 .

The $SU(2)_L$ singlet Φ_1 with non-zero real couplings λ_{32}^{1L} and λ_{32}^{1R} affects $Z\mu\mu$ as well as $W\mu\nu_\mu$, while the effect on $Z\nu\nu$ is very small, see Fig. 8.11. The modified W coupling by λ_{32}^{1L} then yields a finite, LFU renormalization of g_2 . This has been included in our analysis depicted in Fig. 8.11, leading to the allowed, green region deviating slightly from a circled shape.

The $SU(2)_L$ doublet Φ_2 with non-zero couplings λ_{32}^{2LR} and λ_{32}^{2RL} only yields a negligible contribution to $W\mu\nu_\mu$. However, there is an m_t effect in $Z \rightarrow \nu\bar{\nu}$, affecting N_ν , which has been

ℓ	g_A^ℓ/g_{ASM} LEP [353]	FCC-ee [357]	ILC [467]	CEPC [423]	CLIC [408]
e	0.999681 ± 0.000698227	$\pm 4.1 \times 10^{-6}$	$\pm 4.1 \times 10^{-5}$	$\pm 8.7 \times 10^{-6}$	$\pm 4.4 \times 10^{-5}$
μ	0.99986 ± 0.00107726	$\pm 6.3 \times 10^{-6}$	$\pm 6.3 \times 10^{-5}$	$\pm 1.3 \times 10^{-5}$	$\pm 6.7 \times 10^{-5}$
τ	1.00154 ± 0.00127676	$\pm 7.5 \times 10^{-6}$	$\pm 7.5 \times 10^{-5}$	$\pm 1.6 \times 10^{-5}$	$\pm 8.0 \times 10^{-5}$
LFU	0.99992 ± 0.000518683	$\pm 3.1 \times 10^{-6}$	$\pm 3.0 \times 10^{-5}$	$\pm 6.5 \times 10^{-6}$	$\pm 3.2 \times 10^{-5}$

Table 8.2: Experimental values for $Z\ell\ell$ couplings, extracted from LEP [353] data and normalized to their SM values with $g_A^\ell = \Lambda_{\ell\ell}^L(m_Z^2) - \Lambda_{\ell\ell}^R(m_Z^2)$. We further show various expected sensitivities for future colliders (second to fifth row) under the assumption that the measurements of g_A are improved by the same factor as s_w^2 .

precisely measured, see Eq. (8.76). This then constrains λ_{32}^{2RL} as we show in the plot in the right-hand side of Fig. 8.11. We additionally show in Fig. 8.11 the expected sensitivities of future experiments for $Z\mu\mu$, which are summarized in Tab. 8.2.

8.5.3 Charged Lepton Flavor Violation

Let us now correlate different charged lepton flavor violating observables, i.e. $\ell \rightarrow \ell'\gamma$, $Z \rightarrow \ell\ell'$ and $\ell \rightarrow 3\ell'$. We do not study $\mu \rightarrow e$ conversion in nuclei, which could be dominant in case of couplings to first generation quarks, but rather again assume only couplings to third generation quarks.

The branching ratios for lepton flavor violating radiative lepton decays, as a function of the (effective) Wilson coefficients in Eq. (8.37), are given by

$$\text{Br}[\ell_i \rightarrow \ell_f \gamma] = \frac{\alpha m_{\ell_i}^3}{256\pi^4} \tau_{\ell_i} \left(|C_{\ell_f \ell_i}^L|^2 + |C_{\ell_f \ell_i}^R|^2 \right), \quad (8.83)$$

with τ_{ℓ_i} as the life time of the decaying lepton. Similarly, the branching ratio for $Z \rightarrow \ell^+ \ell'^-$ is given by

$$\text{Br}[Z \rightarrow \ell_i^+ \ell_f^-] = \frac{G_F m_Z^3}{3\sqrt{2}\pi\Gamma_Z^{\text{tot}}} \left(|\Lambda_{\ell_f \ell_i}^L(m_Z^2)|^2 + |\Lambda_{\ell_f \ell_i}^R(m_Z^2)|^2 \right), \quad (8.84)$$

with $\Gamma_Z^{\text{tot}} = 2.495 \text{ GeV}$ [468] being the total Z boson decay width and the $\Lambda_{\ell_f \ell_i}^{L,R}(q^2)$ are defined in (8.44a).

For the three body decays we have

$$\begin{aligned} \text{Br}[\tau^\mp \rightarrow \mu^\mp \mu^+ \mu^-] &= \frac{m_\tau^3}{768\pi^3} \tau_\tau \left[\frac{\alpha^2}{\pi^2} |C_{\mu\tau}^L|^2 \left(\log\left(\frac{m_\tau^2}{m_\mu^2}\right) - \frac{11}{4} \right) \right. \\ &\quad + \frac{m_\tau^2}{4} \left(|C_{\mu\mu\mu\tau}^{SLL}|^2 + 16|C_{\mu\tau\mu\mu}^{VLL}|^2 + 4|C_{\mu\tau\mu\mu}^{VLR}|^2 + 4|C_{\mu\mu\mu\tau}^{VLR}|^2 \right) \\ &\quad \left. - \frac{2\alpha}{\pi} m_\tau \text{Re} \left[C_{\mu\tau}^{L*} (C_{\mu\tau\mu\mu}^{VRL} + 2C_{\mu\tau\mu\mu}^{VRR}) \right] + L \leftrightarrow R \right], \end{aligned} \quad (8.85)$$

with the Wilson coefficients defined in Eq. (8.64). The analogous expression for $\mu \rightarrow 3e$ can be obtained by obvious replacements. These rates have to be compared to the experimental limits given in Tab. 8.3 where we also quote the expected future sensitivities. We do not consider decays like $\tau^\mp \rightarrow \mu^\mp e^\pm e^\mp$ as the experimental constraints are slightly worse.

In our numerical analysis, we again assume that the LQs only couple to third generation quarks but now allow for the possibility that they couple to more than one lepton flavor at

Br [$Z \rightarrow \ell\ell'$]	Ref.	Br [$\ell \rightarrow \ell'\gamma$]	Ref.	Br [$\ell \rightarrow 3\ell$]	Ref.
$Z \rightarrow e^\pm\mu^\mp < 7.5 \times 10^{-7}$	[354]	$\mu \rightarrow e\gamma < 4.2 \times 10^{-13}$	[351]	$\mu \rightarrow 3e < 1.0 \times 10^{-12}$	[469]
$Z \rightarrow e^\pm\tau^\mp < 9.8 \times 10^{-6}$	[356]	$\tau \rightarrow e\gamma < 3.3 \times 10^{-8}$	[352]	$\tau \rightarrow \mu ee < 1.5 \times 10^{-8}$	[359]
$Z \rightarrow \mu^\pm\tau^\mp < 1.2 \times 10^{-5}$	[355]	$\tau \rightarrow \mu\gamma < 4.4 \times 10^{-8}$	[352]	$\tau \rightarrow 3\mu < 2.1 \times 10^{-8}$	[359]
$Z \rightarrow \mu^\pm\tau^\mp < 1.0 \times 10^{-8}$	[467]	$\mu \rightarrow e\gamma < 6.0 \times 10^{-14}$	[470]	$\mu \rightarrow 3e < 5.5 \times 10^{-15}$	[471]
$Z \rightarrow \mu^\pm\tau^\mp < 1.0 \times 10^{-9}$	[357]	$\tau \rightarrow \mu\gamma < 1.0 \times 10^{-9}$	[472]	$\tau \rightarrow 3\mu < 1.0 \times 10^{-9}$	[274]
				$\tau \rightarrow 3\mu < 3.3 \times 10^{-10}$	[472]

Table 8.3: Current experimental limits (top panel) and projected future experimental sensitivities (bottom panel) on lepton flavor violating decays of charged leptons.

the same time. Let us start by examining the correlations between $\tau \rightarrow \mu\gamma$ and $Z \rightarrow \tau\mu$ in Fig. 8.12. One can see that this correlation is very direct under the assumption that only one representation contributes and that for Φ_1 and Φ_2 only either the left- or the right-handed couplings to leptons are non-zero at the same time such that chirality enhanced effects in $\tau \rightarrow \mu\gamma$ are absent. Although currently $\tau \rightarrow \mu\gamma$ is more constraining, even in the absence of chirality enhanced contributions, in the future $Z \rightarrow \tau\mu$ can provide competitive or even superior bounds. The situation for $\tau \rightarrow e$ transitions is very similar and therefore not shown explicitly.

In Fig. 8.13 we show the correlations between $\tau \rightarrow \mu\gamma$ and $\tau \rightarrow 3\mu$. These correlations are not as clear as in the case of $Z \rightarrow \tau\mu$ due to the additional box contributions to $\tau \rightarrow 3\mu$. Therefore, one obtains a cone instead of a straight line. Interestingly, for Φ_1 the effect in $\tau \rightarrow \mu\gamma$ is smallest among the LQ representations due to the electric charge of the LQ. Hence, even though phase space suppressed, $\tau \rightarrow 3\mu$ is more sensitive to this particular LQ than $\tau \rightarrow \mu\gamma$. Again, the situation in $\tau \rightarrow e$ transitions is very similar and therefore not shown explicitly. However, we show our analysis for $\mu \rightarrow e$ transitions in Fig. 8.14. For the $\mu \rightarrow e\gamma$ scenario we do not show $Z \rightarrow \mu e$ since the low energy bounds are so stringent that the former cannot compete, even when taking into account future prospects. The (lower) upper boundary of the cone is obtained for a hierarchic flavor structure, i.e. $\lambda_{33} (\gg) \ll \lambda_{32}$ for $\tau \rightarrow \mu$ and $\lambda_{32} (\gg) \ll \lambda_{31}$ for $\mu \rightarrow e$ transitions, respectively, such that the box contributions are (sub)dominant. The opening angle of the cone is determined by the size of the box contributions to $\ell \rightarrow 3\ell'$. For example, the LQ triplet yields the biggest box contribution, which can easily be seen from Eq. (8.69).

8.6 Conclusions

Leptoquarks are prime candidates to explain the flavor anomalies, i.e. the discrepancies between measurements and the SM predictions in $b \rightarrow s\ell^+\ell^-$, $b \rightarrow c\tau\nu$ and the AMM of the muon. With this motivation in mind, we calculated the one-loop amplitudes generated by scalar LQs for the purely leptonic transitions, involving:

- $\ell\ell\gamma$
- $Z\ell\ell$ and $Z\nu\nu$
- $W\ell\nu$
- $h\ell\ell$
- 4ℓ
- $2\ell 2\nu$

Taking into account the most general set of interactions of the LQs with the SM Higgs doublet, we obtained relatively simple analytic expressions for the amplitudes by expanding the LQ mixing matrices in v/m_{LQ} , corresponding to a mass insertion approximation.

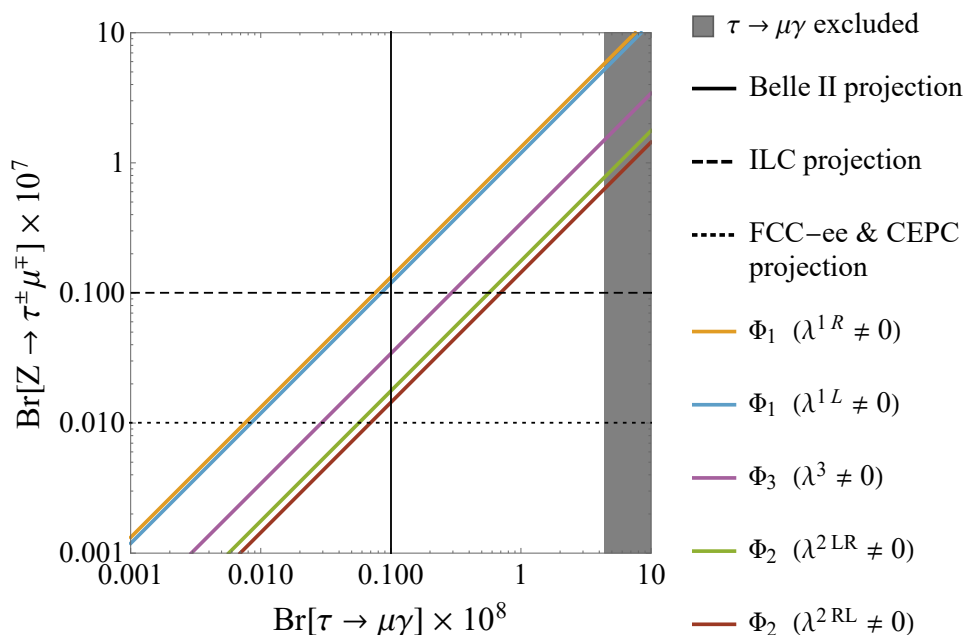


Figure 8.12: Correlations between $\tau \rightarrow \mu\gamma$ and $Z \rightarrow \tau\mu$ for the three LQ representations which generate an m_t^2/m_{LQ}^2 effect in $Z\ell\ell$ couplings. We assume that Φ_1 and Φ_2 couple either to left or to right-handed leptons only such that chirally enhanced effects (which would result in dominant effects in $\tau \rightarrow \mu\gamma$) are absent.

In our phenomenological analysis, we illustrated the results of our calculation by studying:

- LQ effects in effective $Z\ell\ell$, $Z\nu\nu$ and $W\ell\nu$ couplings and the associated gauge boson decays. Here we found for the three representations which generate m_t^2/m_{LQ}^2 enhanced effects (Φ_1 , Φ_2 and Φ_2) that $Z \rightarrow \ell^+\ell^-$ is smaller than within the SM while $Z \rightarrow \nu\nu$ is enhanced. For order one couplings, the effect is at the percent level for TeV scale LQs.
- Correlations between the AMM of the muon, $Z \rightarrow \ell^+\ell^-$, effective $W\mu\nu$ couplings and $h \rightarrow \mu^+\mu^-$. Here we found that, since an explanation of the $(g-2)_\mu$ anomaly requires a m_t/m_μ enhanced effect, also the contribution in $h \rightarrow \mu^+\mu^-$ is pronounced by the same factor. Furthermore, effects scaling like m_t^2/m_{LQ}^2 in $Z \rightarrow \mu^+\mu^-$ are generated which are most relevant in case where the left-handed couplings are much larger than the right handed ones and vice versa.
- Correlations between $\tau \rightarrow \mu\gamma$, $Z \rightarrow \tau\mu$ and $\tau \rightarrow 3\mu$, as well as the analogues in $\mu \rightarrow e$ transitions. Here we observed that $\tau \rightarrow \mu\gamma$ and $Z \rightarrow \tau\mu$ can be directly correlated under the assumption the LQs couple only to left-handed or to right-handed leptons (but not to both of the same time). Furthermore, in this setup $\tau \rightarrow \mu\gamma$ and $\mu \rightarrow e\gamma$ do not receive chirally enhanced effects such that $\tau \rightarrow 3\mu$ and $\mu \rightarrow 3e$ can give competitive bounds, which is in particular the case for Φ_1 .

These interesting correlations can be tested at future precision experiments and high-energy colliders.

Acknowledgments — We thank David Marzocca, Martin Hoferichter, Ulrich Nierste, Adrian Signer and Michael Spira for useful discussions. The work of A.C. and D.M. is supported by a Professorship Grant (PP00P2_176884) of the Swiss National Science Foundation and the one of C.G. and F.S. by the Swiss National Science Foundation grant 200020_175449/1.

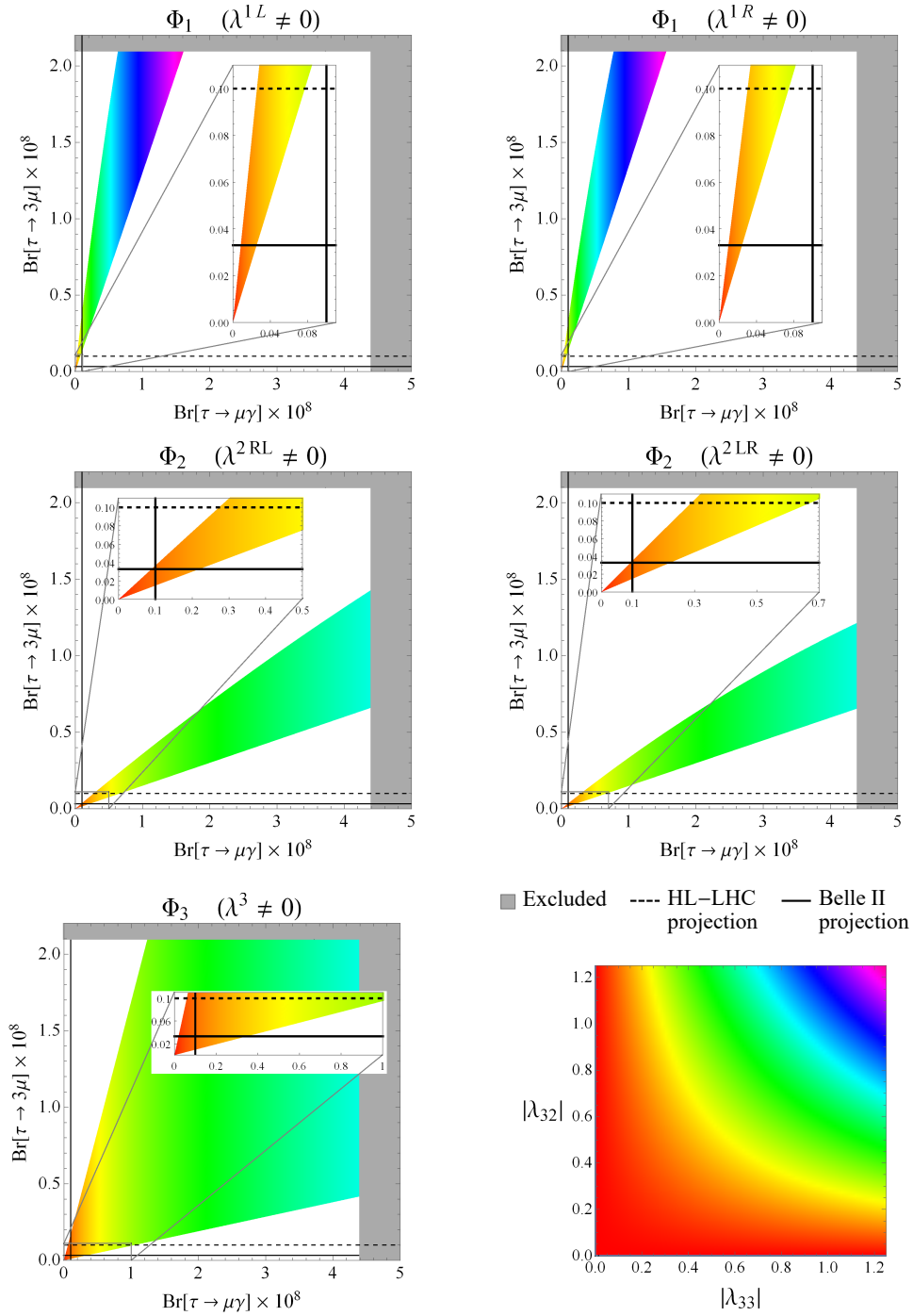


Figure 8.13: The correlations between $\tau \rightarrow \mu\gamma$ and $\tau \rightarrow 3\mu$ for a LQ mass of 1.5 TeV where we scanned λ_{33} and λ_{32} in the range $[-1.5, 1.5]$. The gray regions are currently excluded by experiment. The dashed (solid) lines show the projected sensitivities for the HL-LHC (Belle II), see Tab. 8.3 for the numerical values.

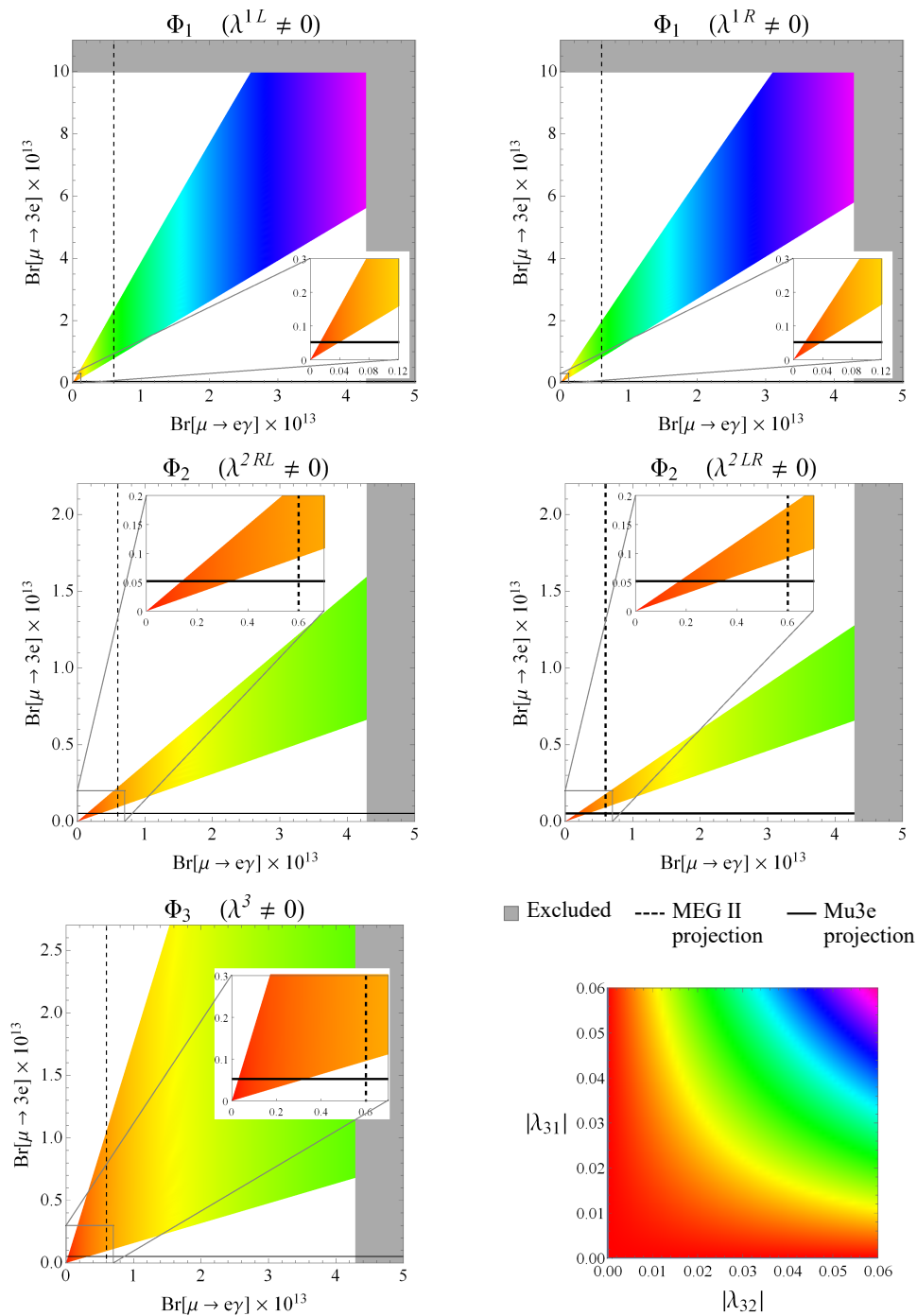


Figure 8.14: The analogue to the plots above for the $\mu \rightarrow e$ transition. The dashed lines depict the expected sensitivity from MEG II [470] and the solid line the one of Mu3e [471]. Note that the color scaling shows the product of two couplings, as can be seen from the legend in the bottom-right.

8.7 Appendix

8.7.1 Self-Energies

Focusing on the non-decoupling, momentum-independent parts of the self-energies, we have generically

$$\Sigma_{fi}^{\ell LR} = \frac{-m_{q_j} N_c}{16\pi^2} \Gamma_{q_j \ell_f}^{L,a*} \Gamma_{q_j \ell_i}^{R,a} \mathcal{I}_0\left(\frac{\mu^2}{M_a^2}, \frac{m_{q_j}^2}{M_a^2}\right), \quad (8.86a)$$

$$\Sigma_{fi}^{\ell LL} = \frac{-N_c}{32\pi^2} \Gamma_{q_j \ell_f}^{L,a*} \Gamma_{q_j \ell_i}^{L,a} \mathcal{I}_1\left(\frac{\mu^2}{M_a^2}, \frac{m_{q_j}^2}{M_a^2}\right), \quad (8.86b)$$

with $\Sigma_{fi}^{\ell RR}$ and $\Sigma_{fi}^{\ell RL}$ obtained by interchanging chiralities and $\Sigma_{fi}^{\nu LL}$ by replacing ℓ with ν . We set all quark masses within the loop equal to zero, except for the top mass. Additionally, one has to sum over all internal quarks u_j, d_j, u_j^c and d_j^c , as well as over their flavors $j = \{1, 2, 3\}$. The loop functions take the simple form

$$\mathcal{I}_0(x, y) = \frac{1}{\varepsilon} + 1 + \log(x) + y \log(y), \quad (8.87a)$$

$$\mathcal{I}_1(x, y) = \frac{1}{\varepsilon} + \frac{1}{2} + \log(x) - y, \quad (8.87b)$$

where the last terms in \mathcal{I}_0 and \mathcal{I}_1 are only relevant for the top quark and can be neglected in all other cases.

Now we expand the expressions in Eq. (8.86) in terms of v/m_{LQ} up to $\mathcal{O}(v^2/m_{\text{LQ}}^2)$

$$\begin{aligned} \Sigma_{\ell, fi}^{LL} \approx & \frac{-N_c}{32\pi^2} \sum_{j=1}^3 \left[V_{jk} \lambda_{kf}^{1L*} V_{jl}^* \lambda_{li}^{1L} \left(\mathcal{I}_1\left(\frac{\mu^2}{m_1^2}, \frac{m_{u_j}^2}{m_1^2}\right) - \frac{v^2 Y_1}{m_1^2} + \frac{v^2 |A_{\bar{2}1}|^2}{\tilde{m}_2^4} \mathcal{I}_4\left(\frac{m_1^2}{\tilde{m}_2^2}\right) \right) \right. \\ & + V_{jk} \lambda_{kf}^{3*} V_{jl}^* \lambda_{li}^3 \left(\mathcal{I}_1\left(\frac{\mu^2}{m_3^2}, \frac{m_{u_j}^2}{m_1^2}\right) + 2\mathcal{I}_1\left(\frac{\mu^2}{m_3^2}, 0\right) - \frac{v^2 (3Y_3 - 2Y_{33})}{m_3^2} + \frac{v^2 |A_{\bar{2}3}|^2}{\tilde{m}_2^4} \mathcal{I}_4\left(\frac{m_3^2}{\tilde{m}_2^2}\right) \right) \\ & + v^2 \left(\frac{\lambda_{jf}^{3*} \lambda_{ji}^{1L} Y_{13}^* + \lambda_{jf}^{1L*} \lambda_{ji}^3 Y_{13}}{m_3^2} \mathcal{H}_1\left(\frac{m_1^2}{m_3^2}\right) \right. \\ & + \frac{\lambda_{jf}^{3*} \lambda_{ji}^{1L} A_{\bar{2}1} A_{\bar{2}3}^* + \lambda_{jf}^{1L*} \lambda_{ji}^3 A_{\bar{2}1}^* A_{\bar{2}3}}{\tilde{m}_2^4} \mathcal{I}_5\left(\frac{m_1^2}{\tilde{m}_2^2}, \frac{m_3^2}{\tilde{m}_2^2}\right) \\ & + \tilde{\lambda}_{jf}^{2*} \tilde{\lambda}_{ji}^2 \left(\mathcal{I}_1\left(\frac{\mu^2}{\tilde{m}_2^2}, 0\right) - \frac{v^2 (Y_{\bar{2}} + Y_{\bar{2}\bar{2}})}{\tilde{m}_2^2} + \frac{2v^2 |A_{\bar{2}3}|^2}{\tilde{m}_2^4} \mathcal{I}_6\left(\frac{m_3^2}{\tilde{m}_2^2}\right) \right) \\ & \left. + \lambda_{jf}^{2RL*} \lambda_{ji}^{2RL} \left(\mathcal{I}_1\left(\frac{\mu^2}{m_2^2}, \frac{m_{u_j}^2}{m_2^2}\right) - \frac{v^2 (Y_2 + Y_{22})}{m_2^2} \right) \right], \quad (8.88a) \end{aligned}$$

$$\begin{aligned} \Sigma_{\ell, fi}^{RR} \approx & \sum_{j=1}^3 \frac{-N_c}{32\pi^2} \left[\lambda_{jf}^{1R*} \lambda_{ji}^{1R} \left(\mathcal{I}_1\left(\frac{\mu^2}{m_1^2}, \frac{m_{u_j}^2}{m_1^2}\right) - \frac{v^2 Y_1}{m_1^2} + \frac{v^2 |A_{\bar{2}1}|^2}{\tilde{m}_2^4} \mathcal{I}_4\left(\frac{m_1^2}{\tilde{m}_2^2}\right) \right) \right. \\ & + V_{jk}^* \lambda_{kf}^{2LR} V_{jl} \lambda_{li}^{2LR} \left(2\mathcal{I}_1\left(\frac{\mu^2}{m_2^2}, \frac{m_{u_j}^2}{m_2^2}\right) - \frac{v^2 (2Y_2 + Y_{22})}{m_2^2} \right) \\ & \left. + \tilde{\lambda}_{jf}^{1*} \tilde{\lambda}_{ji}^1 \left(\mathcal{I}_1\left(\frac{\mu^2}{\tilde{m}_1^2}, 0\right) - \frac{v^2 Y_1}{\tilde{m}_1^2} \right) \right], \quad (8.88b) \end{aligned}$$

$$\Sigma_{fi}^{\ell RL} \approx \sum_{j=1}^3 \frac{-m_{u_j} N_c}{16\pi^2} \left[\lambda_{jf}^{1R*} V_{jk}^* \lambda_{ki}^{1L} \left(\mathcal{I}_0\left(\frac{\mu^2}{m_1^2}, \frac{m_{u_j}^2}{m_1^2}\right) - \frac{v^2 Y_1}{m_1^2} + \frac{v^2 |A_{\bar{2}1}|^2}{\tilde{m}_2^4} \mathcal{I}_4\left(\frac{m_1^2}{\tilde{m}_2^2}\right) \right) \right]$$

$$\begin{aligned}
 & + v^2 \lambda_{jf}^{1R*} V_{jk}^* \lambda_{ki}^3 \left(\frac{Y_{13}}{m_3^2} \mathcal{H}_1 \left(\frac{m_1^2}{m_3^2} \right) + \frac{A_{21}^* A_{23}}{\tilde{m}_2^4} \mathcal{I}_5 \left(\frac{m_1^2}{\tilde{m}_2^2}, \frac{m_3^2}{\tilde{m}_2^2} \right) \right) \\
 & + V_{jk}^* \lambda_{kf}^{2LR*} \lambda_{ji}^{2RL} \left(\mathcal{I}_1 \left(\frac{\mu^2}{m_2^2}, \frac{m_{u_j}^2}{m_2^2} \right) - \frac{v^2 (Y_2 + Y_{22})}{m_2^2} \right) \\
 & + \sum_{j=1}^3 \frac{m_{d_j}}{16\pi^2} \left[\frac{v^2 \lambda_{jf}^{2LR*} \tilde{\lambda}_{ji}^2 Y_{22}^*}{\tilde{m}_2^2} \mathcal{H}_1 \left(\frac{m_2^2}{\tilde{m}_2^2} \right) - \frac{2v^2 \tilde{\lambda}_{jf}^{1*} \lambda_{ji}^3 Y_{31}^*}{m_3^2} \mathcal{H}_1 \left(\frac{\tilde{m}_1^2}{m_3^2} \right) \right], \tag{8.88c}
 \end{aligned}$$

with $\Sigma_{fi}^{\ell LR} = \Sigma_{if}^{\ell RL*}$ and

$$\mathcal{I}_4(x) = \frac{1 - x + x \log(x)}{x(x-1)^2} \tag{8.89a}$$

$$\mathcal{I}_5(x, y) = \frac{\log(x)}{(x-1)(x-y)} + \frac{\log(y)}{(y-1)(y-x)} \tag{8.89b}$$

$$\mathcal{I}_6(x) = \frac{x-1-\log(x)}{(x-1)^2}. \tag{8.89c}$$

For neutrinos we have

$$\begin{aligned}
 \Sigma_{fi}^{\nu LL} & \approx \sum_{j=1}^3 \frac{-N_c}{32\pi^2} \left[\lambda_{jf}^{1L*} \lambda_{ji}^{1L} \left(\mathcal{I}_1 \left(\frac{\mu^2}{m_1^2}, 0 \right) - \frac{v^2 Y_1}{m_1^2} + \frac{v^2 |A_{21}|^2}{\tilde{m}_2^4} \mathcal{I}_4 \left(\frac{m_1^2}{\tilde{m}_2^2} \right) \right) \right. \\
 & + V_{jk} \lambda_{kf}^{3*} V_{jl} \lambda_{li}^3 \left(\mathcal{I}_1 \left(\frac{\mu^2}{m_3^2}, \frac{m_{u_j}^2}{m_3^2} \right) + \mathcal{I}_1 \left(\frac{\mu^2}{m_3^2}, 0 \right) - \frac{v^2 (3Y_3 + 2Y_{33})}{m_3^2} + \frac{5v^2 |A_{23}|^2}{\tilde{m}_2^4} \mathcal{I}_4 \left(\frac{m_3^2}{\tilde{m}_2^2} \right) \right) \\
 & - v^2 \left(\frac{\lambda_{jf}^{1L*} \lambda_{ji}^3 Y_{13} + \lambda_{jf}^{3*} \lambda_{ji}^{1L} Y_{13}^*}{m_3^2} \mathcal{H}_1 \left(\frac{m_1^2}{m_3^2} \right) \right. \\
 & + \frac{\lambda_{jf}^{1L*} \lambda_{ji}^3 A_{21}^* A_{23} + \lambda_{jf}^{3*} \lambda_{ji}^{1L} A_{21} A_{23}^*}{\tilde{m}_2^4} \mathcal{I}_5 \left(\frac{m_1^2}{\tilde{m}_2^2}, \frac{m_3^2}{\tilde{m}_2^2} \right) \left. \right) \\
 & + \tilde{\lambda}_{jf}^{2*} \tilde{\lambda}_{ji}^2 \left(\mathcal{I}_1 \left(\frac{\mu^2}{\tilde{m}_2^2}, 0 \right) - \frac{v^2 Y_2}{\tilde{m}_2^2} + \frac{v^2 |A_{21}|^2}{\tilde{m}_2^4} \mathcal{I}_6 \left(\frac{m_1^2}{\tilde{m}_2^2} \right) + \frac{v^2 |A_{23}|^2}{\tilde{m}_2^4} \mathcal{I}_6 \left(\frac{m_3^2}{\tilde{m}_2^2} \right) \right) \\
 & \left. + \lambda_{jf}^{2RL*} \lambda_{ji}^{2RL} \left(\mathcal{I}_1 \left(\frac{\mu^2}{m_2^2}, \frac{m_{u_j}^2}{m_2^2} \right) - \frac{v^2 Y_2}{m_2^2} \right) \right]. \tag{8.90}
 \end{aligned}$$

8.7.2 Loop Functions

The loop-functions for $\ell\ell\gamma$ with on-shell photons read

$$\mathcal{E}_1(x) = 7 + 4 \log(x) \quad (8.91a)$$

$$\mathcal{E}_2(x) = 11 + 4 \log(x) \quad (8.91b)$$

$$\mathcal{E}_3(x) = 1 + 4 \log(x) \quad (8.91c)$$

$$\mathcal{E}_4(x) = 5 + 4 \log(x) \quad (8.91d)$$

$$\mathcal{E}_5(x, y) = \frac{4}{y} \log(x) + \frac{7y - 11}{y(y - 1)} + 4 \frac{2y - 1}{y(y - 1)^2} \log(y) \quad (8.91e)$$

$$\mathcal{E}_6(x, y) = \mathcal{E}_1(x) + 4 \frac{\log(y)}{y - 1} \quad (8.91f)$$

$$\mathcal{E}_7(x, y, z) = -\frac{1}{z} \mathcal{E}_1(x) + \frac{4}{y - z} \left(\frac{\log(y)}{y - 1} - \frac{x \log(z)}{z(z - 1)} \right) \quad (8.91g)$$

$$\mathcal{E}_8(x, y) = \frac{5}{y} + \frac{2 \log(x)}{y} + \frac{2 \log(y)}{y(y - 1)} \quad (8.91h)$$

$$\mathcal{E}_9(x, y) = -\frac{2}{y} + \frac{4 \log(x)}{y} + \frac{4 \log(y)}{y - 1}, \quad (8.91i)$$

see Eqs. (8.39) and (8.40).

For off-shell photons, the results are given in Eqs. (8.42) and (8.43), we have

$$\mathcal{F}_1(x) = 5 + \log(x) \quad (8.92a)$$

$$\mathcal{F}_2(x) = 9 + 4 \log(x) \quad (8.92b)$$

$$\mathcal{F}_3(x, y) = \frac{4}{y} \log(x) + \frac{5y - 9}{y(y - 1)} + \frac{4(2y - 1) \log(y)}{y(y - 1)^2} \quad (8.92c)$$

$$\mathcal{F}_4(x) = 2 + \log(x) \quad (8.92d)$$

$$\mathcal{F}_5(x) = 7 + 4 \log(x) \quad (8.92e)$$

$$\mathcal{F}_6(x) = 11 + 4 \log(x) \quad (8.92f)$$

$$\mathcal{F}_7(x) = 1 + \log(x) \quad (8.92g)$$

$$\mathcal{F}_8(x) = 3 + \log(x) \quad (8.92h)$$

$$\mathcal{F}_9(x, y) = \frac{2}{y} \log(x) + \frac{2(2y - 1)}{y(y - 1)} - \frac{2 \log(y)}{y(y - 1)^2} \quad (8.92i)$$

$$\mathcal{F}_{10}(x, y) = \frac{4}{y} \log(x) + \frac{5y - 5 + 4 \log(y)}{y(y - 1)}, \quad (8.92j)$$

$$\mathcal{F}_{11}(y, z) = -\frac{4}{yz} \log(x) - \frac{5}{yz} + \frac{4 \log(y)}{y(y - 1)(y - z)} - \frac{4 \log(z)}{z(z - 1)(y - z)}. \quad (8.92k)$$

The \mathcal{H} -functions are defined for the Z and W decays in Sections 8.4.2 and 8.4.3

$$\mathcal{H}_0(x) = x(1 + \log(x)) \quad (8.93a)$$

$$\mathcal{H}_1(x) = \frac{\log(x)}{x-1} \quad (8.93b)$$

$$\mathcal{H}_2(x) = \frac{3(x^2 - 1 - 2x \log(x))}{(x-1)^3} \quad (8.93c)$$

$$\mathcal{H}_3(x) = \frac{2 - 2x + (1+x) \log(x)}{(x-1)^3} \quad (8.93d)$$

$$\mathcal{H}_4(x, y) = \frac{1}{(x-1)(y-1)} + \frac{x \log(x)}{(x-1)^2(x-y)} + \frac{y \log(y)}{(y-1)^2(y-x)} \quad (8.93e)$$

$$\mathcal{H}_5(x) = \frac{2 - 2x + (x+1) \log(x)}{(x-1)^2}, \quad (8.93f)$$

$$\mathcal{H}_6(x, y) = \frac{2 - x - y}{(x-1)(y-1)(x-y)} + \frac{(2x^2 - x - y) \log(x)}{(x-1)^2(x-y)^2} - \frac{(2y^2 - x - y) \log(y)}{(y-1)^2(x-y)^2}. \quad (8.93g)$$

Finally, we have the loop functions used for Higgs decays in Section 8.4.4

$$\mathcal{J}_t(x, y) = 2(x-4) \log(y) - 8 + \frac{13}{3}x - \frac{x^2 y}{5} \quad (8.94a)$$

$$\mathcal{J}_1(x) = \frac{x-1-x \log(x)}{x(x-1)^2} \quad (8.94b)$$

$$\mathcal{J}_2(x, y) = \frac{\log(x)}{(x-1)(x-y)} - \frac{y}{x} \frac{\log(y)}{(y-1)(x-y)} \quad (8.94c)$$

$$\mathcal{J}_3(x) = \frac{x-1-x \log(x)}{(x-1)^2}. \quad (8.94d)$$

8.7.3 Exact Result for $\ell\ell\gamma$

If we expand the amplitudes obtained from the diagrams in Fig. 8.3 up to first non-vanishing order in the external masses and momenta, we obtain [286, 361]

$$\begin{aligned} C_{\ell_f \ell_i}^L = & \frac{-N_c}{4} \sum_q \left[\frac{m_{\ell_f} \Gamma_{q_j \ell_f}^{L, a*} \Gamma_{q_j \ell_i}^{L, a} + m_{\ell_i} \Gamma_{q_j \ell_f}^{R, a*} \Gamma_{q_j \ell_i}^{R, a}}{6M_a^2} (1 + 3Q_q) \right. \\ & \left. + \frac{m_{q_j} \Gamma_{q_j \ell_f}^{R, a*} \Gamma_{q_j \ell_i}^{L, a}}{M_a^2} \left(1 - 2Q_q - 2Q_q \log\left(\frac{\mu_\ell^2}{M_a^2}\right) \right) \right], \end{aligned} \quad (8.95)$$

where q can be, depending on the LQ representations, either a (charge-conjugated) up- or down-type quark and Q_q refers to its electric charge, i.e. $Q_q = \{\pm 1/3, \pm 2/3\}$. The quark flavour index j runs from 1 to 3.

Note that we naively integrated out the internal LQs and quarks at the same scale. Therefore, in the case of light internal quarks, i.e. all except the top quark, the contribution contains both the hard matching part, the mixing within the effective theory and the soft contribution. For this reason, care is required if the internal quarks are lighter than the incoming lepton (e.g. the charm contribution to $\tau \rightarrow \mu\gamma$) since the RGE only contributes from the LQ scale down to

the scale of the process and not to the scale of the internal quark. Therefore, we defined μ_ℓ in Eq. (8.95) as follows

$$\mu_\ell = \begin{cases} m_{q_j} & m_{q_j} > m_{\ell_i} \\ m_{\ell_i} & m_{q_j} \leq m_{\ell_i} \end{cases}. \quad (8.96)$$

Next we give the exact results for off-shell photons, whereof the expanded expressions are given in Eqs. (8.42) and (8.43). They read

$$\widehat{\Xi}_{fi}^L = \sum_q \frac{N_c \Gamma_{q_j \ell_f}^{L,a*} \Gamma_{q_j \ell_i}^{L,a}}{576 \pi^2 M_a^2} \mathcal{F}_{Q_q} \left(\frac{m_{q_j}^2}{M_a^2} \right), \quad (8.97a)$$

$$\widehat{\Xi}_{fi}^R = \sum_q \frac{N_c \Gamma_{q_j \ell_f}^{R,a*} \Gamma_{q_j \ell_i}^{R,a}}{576 \pi^2 M_a^2} \mathcal{F}_{Q_q} \left(\frac{m_{q_j}^2}{M_a^2} \right), \quad (8.97b)$$

with $\widehat{\Xi}_{fi}^{L(R)}$ defined in (8.41) and

$$\mathcal{F}_{Q_q}(y) = 2 + 18Q_q + 12Q_q \log(y). \quad (8.98)$$

Again, j runs from 1 to 3.

8.7.4 Exact Results for $Z\ell\ell$, $Z\nu\nu$, $Wl\nu$ and $h\ell\ell$

In this section we give the exact expressions for the Z and W decays. The \tilde{T}^Q and \tilde{B}^{W_i} matrices, used in this section, are given in Appendix 8.7.5. In this whole section, the M_i stand for the diagonal bilinear mass terms in the charge eigenstates, given in Eq. (8.14). It is implied by the corresponding coupling matrix Γ^i with same index i which of the eigenstates is concerned, e.g. $\Gamma_{u^c \ell}$ corresponds to $M^{-1/3}$. For the Z decays, we use the conventions defined in Eq. (8.44), this time with

$$\Lambda_{\ell_f \ell_i}^{L(R)}(q^2) = \Lambda_{\text{SM}}^{L(R)}(q^2) \delta_{fi} + \sum_Q \Delta_{L(R),fi}^Q(q^2) + \tilde{\Delta}_{L(R),fi}^Q, \quad (8.99a)$$

$$\Theta_{\nu_f \nu_i}(q^2) = \Theta_{\text{SM}}(q^2) \delta_{fi} + \sum_Q \Theta_{fi}^Q(q^2) + \tilde{\Theta}_{fi}^Q, \quad (8.99b)$$

where contrary to Eq. (8.45) we show the results sorted by the charges of the LQs, since we do not distinguish between the cases with and without LQ mixing. Hence, the results cannot be grouped by representation. For $Q = -1/3$ we have for the m_t -enhanced contributions

$$\begin{aligned} \Delta_{L,fi}^{-1/3}(q^2) &= \frac{-N_c \Gamma_{t^c \ell_f}^{L,a*} \Gamma_{t^c \ell_i}^{L,b}}{32 \pi^2} \left[\frac{m_t^2}{M_a^2} \left[\delta_{ab} \left(1 + \log \left(\frac{m_t^2}{M_a^2} \right) \right) + \tilde{T}_{ab}^{-1/3} \mathcal{H}_1 \left(\frac{M_b^2}{M_a^2} \right) \right] \right. \\ &\quad \left. - \frac{q^2}{18 M_a^2} \left[2 \tilde{T}_{ab}^{-1/3} \mathcal{H}_2 \left(\frac{M_b^2}{M_a^2} \right) + \delta_{ab} \left(11 - 10s_w^2 + 2(3 - 4s_w^2) \log \left(\frac{m_t^2}{M_a^2} \right) \right) \right] \right], \quad (8.100a) \end{aligned}$$

$$\begin{aligned} \Delta_{R,fi}^{-1/3}(q^2) &= \frac{N_c \Gamma_{t^c \ell_f}^{R,a*} \Gamma_{t^c \ell_i}^{R,b}}{32 \pi^2} \left[\frac{m_t^2}{M_a^2} \left[\delta_{ab} \left(1 + \log \left(\frac{m_t^2}{M_a^2} \right) \right) - \tilde{T}_{ab}^{-1/3} \mathcal{H}_1 \left(\frac{M_b^2}{M_a^2} \right) \right] \right. \\ &\quad \left. + \frac{q^2}{18 M_a^2} \left[2 \tilde{T}_{ab}^{-1/3} \mathcal{H}_2 \left(\frac{M_b^2}{M_a^2} \right) - \delta_{ab} \left(3 + 10s_w^2 + 8s_w^2 \log \left(\frac{m_t^2}{M_a^2} \right) \right) \right] \right], \quad (8.100b) \end{aligned}$$

and the case with light up-type quarks yields

$$\begin{aligned} \Delta_{L,fi}^{-1/3}(q^2) = & \sum_{j=1}^2 \frac{N_c \Gamma_{u_j^c \ell_f}^{L,a*} \Gamma_{u_j^c \ell_i}^{L,b}}{864\pi^2} \frac{q^2}{M_a^2} \left[3\tilde{T}_{ab}^{-1/3} \mathcal{H}_2\left(\frac{M_b^2}{M_a^2}\right) \right. \\ & \left. - \delta_{ab} \left(3 - 3i\pi(4s_w^2 - 3) - 5s_w^2 + 3(4s_w^2 - 3) \log\left(\frac{q^2}{M_a^2}\right) \right) \right], \end{aligned} \quad (8.100c)$$

$$\begin{aligned} \Delta_{R,fi}^{-1/3}(q^2) = & \sum_{j=1}^2 \frac{N_c \Gamma_{u_j^c \ell_f}^{R,a*} \Gamma_{u_j^c \ell_i}^{R,b}}{864\pi^2} \frac{q^2}{M_a^2} \left[3\tilde{T}_{ab}^{-1/3} \mathcal{H}_2\left(\frac{M_b^2}{M_a^2}\right) \right. \\ & \left. + \delta_{ab} \left(5s_w^2 + 12i\pi s_w^2 - 12s_w^2 \log\left(\frac{q^2}{M_a^2}\right) \right) \right]. \end{aligned} \quad (8.100d)$$

The terms, induced by LQ mixing, read

$$\tilde{\Delta}_{L,fi}^{-1/3} = \sum_{j=1}^3 \frac{N_c \Gamma_{u_j^c \ell_f}^{L,a*} \Gamma_{u_j^c \ell_i}^{L,b}}{64\pi^2} \tilde{T}_{ab}^{-1/3} \left(3 + 2 \log\left(\frac{\mu^2}{M_a^2}\right) - 2\mathcal{H}_1\left(\frac{M_a^2}{M_b^2}\right) \right), \quad (8.101a)$$

$$\tilde{\Delta}_{R,fi}^{-1/3} = \sum_{j=1}^3 \frac{N_c \Gamma_{u_j^c \ell_f}^{R,a*} \Gamma_{u_j^c \ell_i}^{R,b}}{64\pi^2} \tilde{T}_{ab}^{-1/3} \left(3 + 2 \log\left(\frac{\mu^2}{M_a^2}\right) - 2\mathcal{H}_1\left(\frac{M_a^2}{M_b^2}\right) \right). \quad (8.101b)$$

For $Q = 2/3$ we have (massless) down-type quark effects

$$\begin{aligned} \Delta_{L,fi}^{2/3}(q^2) = & \sum_{j=1}^3 \frac{-N_c \Gamma_{d_j \ell_f}^{L,b*} \Gamma_{d_j \ell_i}^{L,a}}{864\pi^2} \frac{q^2}{M_a^2} \left[3\tilde{T}_{ab}^{2/3} \mathcal{H}_2\left(\frac{M_b^2}{M_a^2}\right) \right. \\ & \left. - \delta_{ab} \left(4s_w^2 + 6i\pi s_w^2 - 6s_w^2 \log\left(\frac{q^2}{M_a^2}\right) \right) \right], \end{aligned} \quad (8.102a)$$

$$\begin{aligned} \Delta_{R,fi}^{2/3}(q^2) = & \sum_{j=1}^3 \frac{-N_c \Gamma_{d_j \ell_f}^{R,b*} \Gamma_{d_j \ell_i}^{R,a}}{864\pi^2} \frac{q^2}{M_a^2} \left[3\tilde{T}_{ab}^{2/3} \mathcal{H}_2\left(\frac{M_b^2}{M_a^2}\right) \right. \\ & \left. + \delta_{ab} \left(3 - 3i\pi(2s_w^2 - 3) - 4s_w^2 + 3(2s_w^2 - 3) \log\left(\frac{q^2}{M_a^2}\right) \right) \right], \end{aligned} \quad (8.102b)$$

again with $a, b = \{1, 2, 3\}$ and the mixing terms read

$$\tilde{\Delta}_{L,fi}^{2/3} = \sum_{j=1}^3 \frac{-N_c \Gamma_{d_j \ell_f}^{L,b*} \Gamma_{d_j \ell_i}^{L,a}}{128\pi^2} \left(2(2\tilde{T}_{ab}^{2/3} - \delta_{ab}) \log\left(\frac{\mu^2}{M_a^2}\right) + 6\tilde{T}_{ab}^{2/3} - \delta_{ab} - 4\tilde{T}_{ab}^{2/3} \mathcal{H}_1\left(\frac{M_a^2}{M_b^2}\right) \right), \quad (8.103a)$$

$$\tilde{\Delta}_{R,fi}^{2/3} = \sum_{j=1}^3 \frac{-N_c \Gamma_{d_j \ell_f}^{R,b*} \Gamma_{d_j \ell_i}^{R,a}}{128\pi^2} \left(2(2\tilde{T}_{ab}^{2/3} + \delta_{ab}) \log\left(\frac{\mu^2}{M_a^2}\right) + 6\tilde{T}_{ab}^{2/3} + \delta_{ab} - 4\tilde{T}_{ab}^{2/3} \mathcal{H}_1\left(\frac{M_a^2}{M_b^2}\right) \right). \quad (8.103b)$$

For the LQs with electric charge $Q = -4/3$ we have

$$\begin{aligned} \Delta_{L,fi}^{-4/3}(q^2) &= \sum_{j=1}^3 \frac{N_c \Gamma_{d_j^c \ell_f}^{L,a*} \Gamma_{d_j^c \ell_i}^{L,b}}{864\pi^2} \frac{q^2}{M_a^2} \left[3\tilde{T}_{ab}^{-4/3} \mathcal{H}_2\left(\frac{M_b^2}{M_a}\right) \right. \\ &\quad \left. + \delta_{ab} \left(3 - 3i\pi(2s_w^2 - 3) + 2s_w^2 + 3(2s_w^2 - 3) \log\left(\frac{q^2}{M_a^2}\right) \right) \right], \end{aligned} \quad (8.104a)$$

$$\begin{aligned} \Delta_{R,fi}^{-4/3}(q^2) &= \sum_{j=1}^3 \frac{N_c \Gamma_{d_j^c \ell_f}^{R,a*} \Gamma_{d_j^c \ell_i}^{R,b}}{864\pi^2} \frac{q^2}{M_a^2} \left[3\tilde{T}_{ab}^{-4/3} \mathcal{H}_2\left(\frac{M_b^2}{M_a}\right) \right. \\ &\quad \left. + \delta_{ab} \left(2s_w^2 - 6i\pi s_w^2 + 6s_w^2 \log\left(\frac{q^2}{M_a^2}\right) \right) \right], \end{aligned} \quad (8.104b)$$

with $a, b = \{1, 2\}$ and

$$\begin{aligned} \tilde{\Delta}_{L,fi}^{-4/3} &= \sum_{j=1}^3 \frac{N_c \Gamma_{d_j^c \ell_f}^{L,a*} \Gamma_{d_j^c \ell_i}^{L,b}}{64\pi^2} \left(2(\tilde{T}_{ab}^{-4/3} + \delta_{ab}) \log\left(\frac{\mu^2}{M_a^2}\right) \right. \\ &\quad \left. + 3\tilde{T}_{ab}^{-4/3} + \delta_{ab} - 2\tilde{T}_{ab}^{-4/3} \mathcal{H}_1\left(\frac{M_a^2}{M_b}\right) \right), \end{aligned} \quad (8.105a)$$

$$\tilde{\Delta}_{R,fi}^{-4/3} = \sum_{j=1}^3 \frac{N_c \Gamma_{d_j^c \ell_f}^{R,a*} \Gamma_{d_j^c \ell_i}^{R,b}}{64\pi^2} \tilde{T}_{ab}^{-4/3} \left(2 \log\left(\frac{\mu^2}{M_a^2}\right) + 3 - 2\mathcal{H}_1\left(\frac{M_a^2}{M_b}\right) \right), \quad (8.105b)$$

and for $Q = 5/3$

$$\Delta_{L,fi}^{5/3}(q^2) = \frac{-N_c \Gamma_{t\ell_f}^{L*} \Gamma_{t\ell_i}^L}{32\pi^2} \left[\mathcal{H}_0\left(\frac{m_t^2}{M^2}\right) - \frac{q^2}{9M^2} \left(1 + 7s_w^2 + 4s_w^2 \log\left(\frac{m_t^2}{M^2}\right) \right) \right], \quad (8.106a)$$

$$\Delta_{L,fi}^{5/3}(q^2) = \sum_{j=1}^2 \frac{-N_c \Gamma_{u_j \ell_f}^{L*} \Gamma_{u_j \ell_i}^L}{1728\pi^2} \frac{q^2}{M^2} \left[3 - 2s_w^2 + 24i\pi s_w^2 - 24s_w^2 \log\left(\frac{q^2}{M^2}\right) \right], \quad (8.106b)$$

$$\Delta_{R,fi}^{5/3}(q^2) = \frac{N_c \Gamma_{t\ell_f}^{R*} \Gamma_{t\ell_i}^R}{32\pi^2} \left[\mathcal{H}_0\left(\frac{m_t^2}{M^2}\right) - \frac{q^2}{9M^2} \left(6 - 7s_w^2 + (3 - 4s_w^2) \log\left(\frac{m_t^2}{M^2}\right) \right) \right], \quad (8.106c)$$

$$\Delta_{R,fi}^{5/3}(q^2) = \sum_{j=1}^2 \frac{N_c \Gamma_{u_j \ell_f}^{R*} \Gamma_{u_j \ell_i}^R}{1728\pi^2} \frac{q^2}{M^2} \left[3 + 2s_w^2 - 6i\pi(4s_w^2 - 3) + 6(4s_w^2 - 3) \log\left(\frac{q^2}{M^2}\right) \right], \quad (8.106d)$$

with $M^2 = m_2^2 + v^2(Y_{22} + Y_2)$.

For $Z \rightarrow \nu_i \bar{\nu}_f$ with left-handed neutrinos only, we have for $Q = -1/3$ with (charge-conjugated) down-type quarks

$$\begin{aligned} \Theta_{fi}^{-1/3}(q^2) &= \sum_{j=1}^3 \frac{N_c \Gamma_{d_j^c \nu_f}^{L,a*} \Gamma_{d_j^c \nu_i}^{L,b}}{864\pi^2} \frac{q^2}{M_a^2} \left[3\tilde{T}_{ab}^{-1/3} \mathcal{H}_2\left(\frac{M_b^2}{M_a}\right) \right. \\ &\quad \left. + \delta_{ab} \left(3 - s_w^2 + 3i\pi(3 - 2s_w^2) - 3(3 - 2s_w^2) \log\left(\frac{q^2}{M_a^2}\right) \right) \right] \\ &\quad - \sum_{j=1}^3 \frac{N_c \Gamma_{d_j \nu_f}^{L,a*} \Gamma_{d_j \nu_i}^{L,b}}{864\pi^2} \frac{q^2}{M_a^2} \left[3\tilde{T}_{ab}^{-1/3} \mathcal{H}_2\left(\frac{M_b^2}{M_a}\right) \right. \\ &\quad \left. - \delta_{ab} \left(s_w^2 + 6i\pi s_w^2 - 6s_w^2 \log\left(\frac{q^2}{M_a^2}\right) \right) \right]. \end{aligned} \quad (8.107)$$

The LQ indices run like $a, b = \{1, 2, 3\}$. Analogously to $Z \rightarrow \ell_f^- \ell_i^+$ we have the $\tilde{\Theta}$ terms, originating from the LQ mixing

$$\begin{aligned} \tilde{\Theta}_{fi}^{-1/3} &= \sum_{j=1}^3 \frac{N_c \Gamma_{d_j^c \nu_f}^{L, b*} \Gamma_{d_j^c \nu_i}^{L, a}}{64\pi^2} \tilde{T}_{ab}^{-1/3} \left(3 + 2 \log\left(\frac{\mu^2}{M_a^2}\right) - 2\mathcal{H}_1\left(\frac{M_a^2}{M_b^2}\right) \right) \\ &\quad - \sum_{j=1}^3 \frac{N_c \Gamma_{d_j \nu_f}^{L, a*} \Gamma_{d_j \nu_i}^{L, b}}{128\pi^2} \left(2(2\tilde{T}_{ab}^{-1/3} + \delta_{ab}) \log\left(\frac{\mu^2}{M_a^2}\right) \right. \\ &\quad \left. + 6\tilde{T}_{ab}^{-1/3} + \delta_{ab} - 4\tilde{T}_{ab}^{-1/3} \mathcal{H}_1\left(\frac{M_a^2}{M_b^2}\right) \right). \end{aligned} \quad (8.108)$$

In case of $Q = 2/3$, we have the diagrams which include a heavy top quark

$$\begin{aligned} \Theta_{fi}^{2/3}(q^2) &= \frac{N_c \Gamma_{t \nu_f}^{L, b*} \Gamma_{t \nu_i}^{L, a}}{32\pi^2} \left[\frac{m_t^2}{M_a^2} \left[\tilde{T}_{ab}^{2/3} \mathcal{H}_1\left(\frac{M_b^2}{M_a^2}\right) - \delta_{ab} \left(\frac{1}{2} + \log\left(\frac{m_t^2}{M_a^2}\right) \right) \right] \right. \\ &\quad \left. - \frac{q^2}{18M_a^2} \left[2\tilde{T}_{ab}^{2/3} \mathcal{H}_2\left(\frac{M_b^2}{M_a^2}\right) - \delta_{ab} \left(3 + 12s_w^2 + 8s_w^2 \log\left(\frac{m_t^2}{M_a^2}\right) \right) \right] \right] \\ &\quad - \frac{N_c \Gamma_{t^c \nu_f}^{L, a*} \Gamma_{t^c \nu_i}^{L, b}}{32\pi^2} \left[\frac{m_t^2}{M_a^2} \left[\tilde{T}_{ab}^{2/3} \mathcal{H}_1\left(\frac{M_b^2}{M_a^2}\right) + \delta_{ab} \log\left(\frac{m_t^2}{M_a^2}\right) \right] \right. \\ &\quad \left. - \frac{q^2}{18M_a^2} \left[2\tilde{T}_{ab}^{2/3} \mathcal{H}_2\left(\frac{M_b^2}{M_a^2}\right) + \delta_{ab} \left(11 - 12s_w^2 + (6 - 8s_w^2) \log\left(\frac{m_t^2}{M_a^2}\right) \right) \right] \right], \end{aligned} \quad (8.109)$$

and light up-type quarks

$$\begin{aligned} \Theta_{fi}^{2/3}(q^2) &= \sum_{j=1}^2 \frac{-N_c \Gamma_{u_j \nu_f}^{L, b*} \Gamma_{u_j \nu_i}^{L, a}}{864\pi^2} \frac{q^2}{M_a^2} \left[3\tilde{T}_{ab}^{2/3} \mathcal{H}_2\left(\frac{M_b^2}{M_a^2}\right) \right. \\ &\quad \left. + \delta_{ab} \left(2s_w^2 + 12i\pi s_w^2 - 12s_w^2 \log\left(\frac{q^2}{M_a^2}\right) \right) \right] \\ &\quad + \sum_{j=1}^2 \frac{N_c \Gamma_{u_j^c \nu_f}^{L, a*} \Gamma_{u_j^c \nu_i}^{L, b}}{864\pi^2} \frac{q^2}{M_a^2} \left[3\tilde{T}_{ab}^{2/3} \mathcal{H}_2\left(\frac{M_b^2}{M_a^2}\right) \right. \\ &\quad \left. - \delta_{ab} \left(3 - 2s_w^2 + 3i\pi(3 - 4s_w^2) + 3(4s_w^2 - 3) \log\left(\frac{q^2}{M_a^2}\right) \right) \right]. \end{aligned} \quad (8.110)$$

The LQ indices take the values $a, b = \{1, 2, 3\}$. We finally have

$$\begin{aligned} \tilde{\Theta}_{fi}^{2/3} &= \sum_{j=1}^3 \frac{-N_c \Gamma_{u_j \nu_f}^{L, b*} \Gamma_{u_j \nu_i}^{L, a}}{128\pi^2} \left(2(2\tilde{T}_{ab}^{2/3} + \delta_{ab}) \log\left(\frac{\mu^2}{M_a^2}\right) + 6\tilde{T}_{ab}^{2/3} + \delta_{ab} - 4\tilde{T}_{ab}^{2/3} \mathcal{H}_1\left(\frac{M_a^2}{M_b^2}\right) \right) \\ &\quad + \sum_{j=1}^3 \frac{N_c \Gamma_{u_j^c \nu_f}^{L, a*} \Gamma_{u_j^c \nu_i}^{L, b}}{64\pi^2} \left(2(\tilde{T}_{ab}^{2/3} - \delta_{ab}) \log\left(\frac{\mu^2}{M_a^2}\right) + 3\tilde{T}_{ab}^{2/3} - \delta_{ab} - 2\tilde{T}_{ab}^{2/3} \mathcal{H}_1\left(\frac{M_a^2}{M_b^2}\right) \right). \end{aligned} \quad (8.111)$$

For $W \rightarrow \ell_f^- \bar{\nu}_i$ decays, our definition of the amplitude is given in Eq. (8.52) and contrary to Eq. (8.53), we use

$$\Lambda_{\ell_f \nu_i}^W(q^2) = \Lambda_{\text{SM}}^W(q^2) \delta_{fi} + \Lambda_{fi}^q(q^2) + \tilde{\Lambda}_{fi}^q + \Lambda_{fi}^{q^c}(q^2) + \tilde{\Lambda}_{fi}^{q^c}, \quad (8.112)$$

where we choose to group the results by the fact whether a quark (q) or a charge-conjugated quark (q^c) runs in the loop. Because of obvious reasons, a grouping by representation is again not possible. We have

$$\begin{aligned} \Lambda_{fi}^{q^c}(q^2) = & \frac{N_c}{64\pi^2} \left[\frac{m_t^2}{M_b^2} \Gamma_{t^c\nu_f}^{L,b*} \Gamma_{t^c\nu_i}^{L,b} + \frac{m_t^2}{M_a^2} \left[\Gamma_{t^c\ell_f}^{L,a*} \Gamma_{t^c\ell_i}^{L,a} - 2V_{3k}^* \Gamma_{t^c\ell_f}^{L,a*} \Gamma_{d_k^c\nu_i}^{L,a} \log\left(\frac{m_t^2}{M_a^2}\right) \right. \right. \\ & - 2\tilde{B}_{ab}^{W_2} \Gamma_{t^c\ell_f}^{L,a*} \Gamma_{t^c\nu_i}^{L,b} \mathcal{H}_1\left(\frac{M_b^2}{M_a^2}\right) \left. \right] + \frac{2q^2}{9M_a^2} \left[6V_{3k}^* \Gamma_{t^c\ell_f}^{L,a*} \Gamma_{d_k^c\nu_i}^{L,a} \left(1 + \log\left(\frac{m_t^2}{M_a^2}\right)\right) \right. \\ & \left. \left. + \tilde{B}_{ca}^{W_1} \Gamma_{b^c\ell_f}^{L,c*} \Gamma_{b^c\nu_i}^{L,a} \mathcal{H}_2\left(\frac{M_c^2}{M_a^2}\right) + \tilde{B}_{ab}^{W_2} \Gamma_{t^c\ell_f}^{L,a*} \Gamma_{t^c\nu_i}^{L,b} \mathcal{H}_2\left(\frac{M_b^2}{M_a^2}\right) \right] \right], \end{aligned} \quad (8.113)$$

and its massless case

$$\begin{aligned} \Lambda_{fi}^q(q^2) = & \sum_{j=1}^2 \frac{N_c}{576\pi^2} \frac{q^2}{M_a^2} \left[4V_{jk}^* \Gamma_{u_j^c\ell_f}^{L,a*} \Gamma_{d_k^c\nu_i}^{L,a} \left(\log\left(\frac{q^2}{M_a^2}\right) - 1 + 3i\pi \right) \right. \\ & \left. + 2\tilde{B}_{ca}^{W_1} \Gamma_{d_j^c\ell_f}^{L,c*} \Gamma_{d_j^c\nu_i}^{L,a} \mathcal{H}_2\left(\frac{M_c^2}{M_a^2}\right) + 2\tilde{B}_{ab}^{W_2} \Gamma_{u_j^c\ell_f}^{L,a*} \Gamma_{u_j^c\nu_i}^{L,b} \mathcal{H}_2\left(\frac{M_b^2}{M_a^2}\right) \right]. \end{aligned} \quad (8.114)$$

The LQ indices a and b run from 1 to 3, while $c = \{1, 2\}$. In case of quarks in the loop we have

$$\begin{aligned} \Lambda_{fi}^q(q^2) = & \frac{N_c}{64\pi^2} \left[\frac{m_t^2}{M_b^2} \left(\Gamma_{t\nu_f}^{L,b*} \Gamma_{t\nu_i}^{L,b} - 2\tilde{B}_b^{W_3} \Gamma_{t\ell_f}^{L,*} \Gamma_{t\nu_i}^{L,b} \mathcal{H}_1\left(\frac{M^2}{M_b^2}\right) \right) + \frac{m_t^2}{M^2} \Gamma_{t\ell_f}^{L,*} \Gamma_{t\ell_i}^{L,L} \right. \\ & \left. + \sum_{j=1}^3 \frac{2q^2}{9M_b^2} \left(\tilde{B}_{ab}^{W_2} \Gamma_{d_j\ell_f}^{L,b*} \Gamma_{d_j\nu_i}^{L,a} \mathcal{H}_2\left(\frac{M_a^2}{M_b^2}\right) + \tilde{B}_b^{W_3} \Gamma_{u_j\ell_f}^{L,*} \Gamma_{u_j\nu_i}^{L,b} \mathcal{H}_2\left(\frac{M^2}{M_b^2}\right) \right) \right]. \end{aligned} \quad (8.115)$$

Here, the index b runs from 1 to 3. The $\tilde{\Lambda}$'s read

$$\begin{aligned} \tilde{\Lambda}_{fi}^{q^c} = & \frac{N_c}{64\pi^2} \left[\left(2\tilde{B}_{ca}^{W_1} \Gamma_{d_j^c\ell_f}^{L,c*} \Gamma_{d_j^c\nu_i}^{L,a} + 2\tilde{B}_{ab}^{W_2} \Gamma_{u_j^c\ell_f}^{L,a*} \Gamma_{u_j^c\nu_i}^{L,b} - 2V_{kj}^* \Gamma_{u_k^c\ell_f}^{L,a*} \Gamma_{d_j^c\nu_i}^{L,a} - \Gamma_{d_j^c\nu_f}^{L,a*} \Gamma_{d_j^c\nu_i}^{L,a} \right. \right. \\ & - \Gamma_{u_j^c\ell_f}^{L,a*} \Gamma_{u_j^c\ell_i}^{L,a} \log\left(\frac{\mu^2}{M_a^2}\right) - \Gamma_{u_j^c\nu_f}^{L,b*} \Gamma_{u_j^c\nu_i}^{L,b} \log\left(\frac{\mu^2}{M_b^2}\right) - \Gamma_{d_j^c\ell_f}^{L,c*} \Gamma_{d_j^c\ell_i}^{L,c} \log\left(\frac{\mu^2}{M_c^2}\right) \left. \right) \\ & \left. + 2\tilde{B}_{ca}^{W_1} \Gamma_{d_j^c\ell_f}^{L,c*} \Gamma_{d_j^c\nu_i}^{L,a} \left(1 - \mathcal{H}_1\left(\frac{M_a^2}{M_c^2}\right)\right) + 2\tilde{B}_{ab}^{W_2} \Gamma_{u_j^c\ell_f}^{L,a*} \Gamma_{u_j^c\nu_i}^{L,b} \left(1 - \mathcal{H}_1\left(\frac{M_a^2}{M_b^2}\right)\right) \right], \end{aligned} \quad (8.116a)$$

$$\begin{aligned} \tilde{\Lambda}_{fi}^q = & \frac{-N_c}{64\pi^2} \left[\left(2\tilde{B}_{ab}^{W_2} \Gamma_{d_j\ell_f}^{L,b*} \Gamma_{d_j\nu_i}^{L,a} + \Gamma_{d_j\nu_f}^{L,a*} \Gamma_{d_j\nu_i}^{L,a} \right) \log\left(\frac{\mu^2}{M_a^2}\right) + \Gamma_{u_j\ell_f}^{L,*} \Gamma_{u_j\ell_i}^{L,L} \log\left(\frac{\mu^2}{M^2}\right) \right. \\ & \left. + \left(2\tilde{B}_b^{W_3} \Gamma_{u_j\ell_f}^{L,*} \Gamma_{u_j\nu_i}^{L,b} + \Gamma_{d_j\ell_f}^{L,b*} \Gamma_{d_j\ell_i}^{L,b} + \Gamma_{u_j\nu_f}^{L,b*} \Gamma_{u_j\nu_i}^{L,b} \right) \log\left(\frac{\mu^2}{M_b^2}\right) \right. \\ & \left. + 2\tilde{B}_{ab}^{W_2} \Gamma_{d_j\ell_f}^{L,b*} \Gamma_{d_j\nu_i}^{L,a} \left(1 - \mathcal{H}_1\left(\frac{M_a^2}{M_b^2}\right)\right) + 2\tilde{B}_b^{W_3} \Gamma_{u_j\ell_f}^{L,*} \Gamma_{u_j\nu_i}^{L,b} \left(1 - \mathcal{H}_1\left(\frac{M_b^2}{M^2}\right)\right) \right], \end{aligned} \quad (8.116b)$$

again with $a, b = \{1, 2, 3\}$ and $c = \{1, 2\}$.

Next, we give the results for the Higgs decay into a pair of charged leptons, where our amplitude is defined in Eq. (8.58). Again, we sort the results by the charge eigenstate contributions

$$\Upsilon_{\ell_f\ell_i}^{L(R)}(q^2) = \delta_{fi} + \sum_Q \Upsilon_{L(R),fi}^Q(q^2) + \tilde{\Upsilon}_{L(R),fi}^Q. \quad (8.117)$$

In case of a heavy top quark in the loop, the results read

$$\Upsilon_{L,fi}^{-1/3}(q^2) = \frac{-N_c \Gamma_{t^c \ell_f}^{R,a*} \Gamma_{t^c \ell_i}^{L,b}}{64\pi^2 M_a^2} \frac{m_t}{m_{fi}} \left(m_t^2 \delta_{ab} \mathcal{J}_t \left(\frac{q^2}{m_t^2}, \frac{m_t^2}{M_a^2} \right) - 4v \tilde{\Gamma}_{ab}^{-1/3} \mathcal{H}_1 \left(\frac{M_b^2}{M_a^2} \right) \right), \quad (8.118a)$$

$$\Upsilon_{L,fi}^{5/3}(q^2) = \frac{-N_c \Gamma_{t \ell_f}^{R*} \Gamma_{t \ell_i}^{L}}{64\pi^2 M^2} \frac{m_t}{m_{fi}} \left(m_t^2 \mathcal{J}_t \left(\frac{q^2}{m_t^2}, \frac{m_t^2}{M^2} \right) - 8 \frac{v^2 Y_2}{\sqrt{2}} \right), \quad (8.118b)$$

with $M^2 = m_2^2 + v^2(Y_{22} + Y_2)$.

In all the scenarios where $q^2 \equiv m_h^2 \gg m_{q_j}^2 \gg m_{fi}^2$ the Higgs mass gives the dominant contribution

$$\Upsilon_{L,fi}^Q(q^2) = \sum_j \frac{N_c \Gamma_{q_j \ell_f}^{R,a*} \Gamma_{q_j \ell_i}^{L,b}}{64\pi^2 M_a^2} \frac{m_{q_j}}{m_{fi}} \mathcal{J}_{ab}^Q(q^2), \quad (8.119a)$$

$$\Upsilon_{L,fi}^{5/3}(q^2) = \sum_{j=1}^2 \frac{N_c \Gamma_{u_j \ell_f}^{R*} \Gamma_{u_j \ell_i}^{L}}{64\pi^2 M^2} \frac{m_{u_j}}{m_{fi}} \mathcal{J}^{5/3}(q^2), \quad (8.119b)$$

with

$$\mathcal{J}_{ab}^Q(q^2) = q^2 \delta_{ab} \left(2 \log \left(\frac{q^2}{M_a^2} \right) - 2i\pi - 1 \right) - 4v \tilde{\Gamma}_{ab}^Q \mathcal{H}_1 \left(\frac{M_b^2}{M_a^2} \right), \quad (8.120a)$$

$$\mathcal{J}^{5/3}(q^2) = q^2 \left(2 \log \left(\frac{q^2}{M^2} \right) - 2i\pi - 1 \right) - 8 \frac{Y_2}{\sqrt{2}} v^2. \quad (8.120b)$$

In Eq. (8.119a) the range of j depends on whether we have up- ($j = \{1, 2\}$) or down-type ($j = \{1, 2, 3\}$) quarks in the loop, since we treat the top separately. Finally, we consider as a last scenario $m_{fi} \gg m_{q_j} \sim 0$ and we have

$$\Upsilon_{L,fi}^Q = \frac{v N_c \tilde{\Gamma}_{ab}^Q}{32\pi^2} \left(\frac{m_{\ell_f}}{m_{fi}} \frac{\Gamma_{q_j \ell_f}^{L,a*} \Gamma_{q_j \ell_i}^{L,b}}{M_a^2} \mathcal{J}_3 \left(\frac{M_b^2}{M_a^2} \right) + \frac{m_{\ell_i}}{m_{fi}} \frac{\Gamma_{q_j \ell_f}^{R,a*} \Gamma_{q_j \ell_i}^{R,b}}{M_b^2} \mathcal{J}_3 \left(\frac{M_a^2}{M_b^2} \right) \right), \quad (8.121a)$$

$$\Upsilon_{L,fi}^{5/3} = \frac{-\sqrt{2} v^2 N_c Y_2}{64\pi^2 M^2} \left(\frac{m_{\ell_f}}{m_{fi}} \lambda_{jf}^{2RL*} \lambda_{ji}^{2RL} + \frac{m_{\ell_i}}{m_{fi}} \lambda_{jf}^{2LR*} \lambda_{ji}^{2LR} \right). \quad (8.121b)$$

8.7.5 Higgs, Z and W Boson Coupling Matrices

The Higgs-LQ interaction matrices $\tilde{\Gamma}$, used in Eqs. (8.120a) and (8.118a), and $\tilde{\Lambda}$ expanded up to $\mathcal{O}(v^2/m_{LQ}^2)$ read

$$\tilde{\Gamma}^{-1/3} \approx \frac{1}{\sqrt{2}} \begin{pmatrix} 2v(Y_1 + \frac{|A_{21}|^2}{m_1^2 - \tilde{m}_2^2}) & A_{21}^* & v \left(2Y_{13} - \frac{A_{23} A_{21}^* (m_1^2 + m_3^2 - 2\tilde{m}_2^2)}{(m_1^2 - \tilde{m}_2^2)(\tilde{m}_2^2 - m_3^2)} \right) \\ A_{21} & \tilde{\Gamma}_{22}^{-1/3} & A_{23} \\ v \left(2Y_{13}^* - \frac{A_{21} A_{23}^* (m_1^2 + m_3^2 - 2\tilde{m}_2^2)}{(m_1^2 - \tilde{m}_2^2)(\tilde{m}_2^2 - m_3^2)} \right) & A_{23}^* & 2v \left(Y_3 + \frac{|A_{23}|^2}{m_3 - \tilde{m}_2^2} \right) \end{pmatrix},$$

$$\text{with } \tilde{\Gamma}_{22}^{-1/3} = 2v \left(Y_2 - \frac{|A_{21}|^2}{m_1^2 - \tilde{m}_2^2} - \frac{|A_{23}|^2}{m_3^2 - \tilde{m}_2^2} \right), \quad (8.122a)$$

$$\tilde{\Gamma}^{2/3} \approx \frac{1}{\sqrt{2}} \begin{pmatrix} 2vY_2 & 2vY_{22} & 0 \\ 2vY_{22}^* & 2v(Y_2 + Y_{22} - \frac{2|A_{23}|^2}{m_3^2 - \tilde{m}_2^2}) & -\sqrt{2}A_{23} \\ 0 & -\sqrt{2}A_{23}^* & 2v \left(Y_3 + Y_{33} + \frac{2|A_{23}|^2}{m_3^2 - \tilde{m}_2^2} \right) \end{pmatrix}, \quad (8.122b)$$

$$\tilde{\Gamma}^{-4/3} \approx \Gamma^{-4/3}, \quad (8.122c)$$

and

$$\tilde{\Lambda}^{-1/3} \approx \frac{1}{2} \begin{pmatrix} Y_1 & v \left(\frac{Y_{31} A_{23}^*}{\tilde{m}_2^2 - m_3^2} + \frac{(Y_2 - Y_1) A_{21}^*}{m_1^2 - \tilde{m}_2^2} \right) & Y_{13} \\ v \left(\frac{Y_{31}^* A_{23}}{\tilde{m}_2^2 - m_3^2} + \frac{(Y_2 - Y_1) A_{21}}{m_1^2 - \tilde{m}_2^2} \right) & Y_2 & v \left(\frac{Y_{31} A_{21}^*}{\tilde{m}_2^2 - m_1^2} + \frac{(Y_2 - Y_3) A_{23}^*}{m_3^2 - \tilde{m}_2^2} \right) \\ Y_{13}^* & v \left(\frac{Y_{31}^* A_{21}}{\tilde{m}_2^2 - m_1^2} + \frac{(Y_2 - Y_3) A_{23}}{m_3^2 - \tilde{m}_2^2} \right) & Y_3 \end{pmatrix}, \quad (8.123a)$$

$$\tilde{\Lambda}^{2/3} \approx \frac{1}{2} \begin{pmatrix} Y_2 & Y_{22} & \frac{\sqrt{2} v Y_{22} A_{23}}{\tilde{m}_2^2 - m_3^2} \\ Y_{22}^* & Y_{\bar{2}} + Y_{\bar{2}\bar{2}} & \frac{\sqrt{2} v (Y_3 - Y_2 - Y_{22}) A_{23}}{m_3^2 - \tilde{m}_2^2} \\ \frac{\sqrt{2} v Y_{22}^* A_{23}}{\tilde{m}_2^2 - m_3^2} & \frac{\sqrt{2} v (Y_3 - Y_2 - Y_{22}) A_{23}^*}{m_3^2 - \tilde{m}_2^2} & Y_3 + Y_{33} \end{pmatrix}, \quad (8.123b)$$

$$\tilde{\Lambda}^{-4/3} \approx \Lambda^{-4/3}. \quad (8.123c)$$

Next, we will give the expressions for the weak isospin matrices T^Q , expanded in terms of v . They read in case of no LQ mixing

$$T^{-1/3} = \begin{pmatrix} 0 & 0 & 0 \\ 0 & -\frac{1}{2} & 0 \\ 0 & 0 & 0 \end{pmatrix}, \quad T^{2/3} = \begin{pmatrix} -\frac{1}{2} & 0 & 0 \\ 0 & \frac{1}{2} & 0 \\ 0 & 0 & 1 \end{pmatrix}, \quad T^{-4/3} = \begin{pmatrix} 0 & 0 \\ 0 & -1 \end{pmatrix}, \quad T^{5/3} = \frac{1}{2}, \quad (8.124)$$

using the basis defined in Eq. (8.10). A unitary redefinition of the LQ fields in order to diagonalize the mass matrices in Eq. (8.9) also affects the T^Q matrices

$$\tilde{T}^Q = W^Q T^Q W^{Q\dagger}. \quad (8.125)$$

Note that the LQ field redefinition has no impact the electromagnetic interaction, since the coupling matrix is proportional to the unit matrix and the W^Q then cancel due to unitarity. If we use the perturbative diagonalization ansatz, we obtain

$$\tilde{T}^{-1/3} \approx \begin{pmatrix} \frac{-v^2 |A_{21}|^2}{2(m_1^2 - \tilde{m}_2^2)^2} & \frac{v A_{21}^*}{2(\tilde{m}_2^2 - m_1^2)} & \frac{v^2 A_{23} A_{21}^*}{2(m_1^2 - \tilde{m}_2^2)(\tilde{m}_2^2 - m_3^2)} \\ \frac{v A_{21}}{2(\tilde{m}_2^2 - m_1^2)} & -\frac{1}{2} + \frac{v^2}{2} \left(\frac{|A_{21}|^2}{(m_1^2 - \tilde{m}_2^2)^2} + \frac{|A_{23}|^2}{(\tilde{m}_2^2 - m_3^2)^2} \right) & \frac{v A_{23}}{2(\tilde{m}_2^2 - m_3^2)} \\ \frac{v^2 A_{21} A_{23}^*}{2(m_1^2 - \tilde{m}_2^2)(\tilde{m}_2^2 - m_3^2)} & \frac{v A_{23}^*}{2(\tilde{m}_2^2 - m_3^2)} & \frac{-v^2 |A_{23}|^2}{2(\tilde{m}_2^2 - m_3^2)^2} \end{pmatrix}, \quad (8.126a)$$

$$\tilde{T}^{2/3} \approx \begin{pmatrix} -\frac{1}{2} & \frac{v^2 Y_{22}}{m_2^2 - \tilde{m}_2^2} & 0 \\ \frac{v^2 Y_{22}^*}{m_2^2 - \tilde{m}_2^2} & \frac{1}{2} + \frac{v^2 |A_{23}|^2}{(\tilde{m}_2^2 - m_3^2)^2} & \frac{v A_{23}}{\sqrt{2}(m_3^2 - \tilde{m}_2^2)} \\ 0 & \frac{v A_{23}^*}{\sqrt{2}(m_3^2 - \tilde{m}_2^2)} & 1 - \frac{v^2 |A_{23}|^2}{(\tilde{m}_2^2 - m_3^2)^2} \end{pmatrix}, \quad (8.126b)$$

$$\tilde{T}^{-4/3} \approx \begin{pmatrix} 0 & \frac{\sqrt{2} v^2 Y_{3\bar{1}}^*}{m_3^2 - \tilde{m}_1^2} \\ \frac{\sqrt{2} v^2 Y_{3\bar{1}}}{m_3^2 - \tilde{m}_1^2} & -1 \end{pmatrix}, \quad (8.126c)$$

valid up to $\mathcal{O}(v^2/m_{\text{LQ}}^2)$. $T^{5/3}$ is not affected, since the LQ with charge $Q = 5/3$ does not mix.

Analogously to the isospin coupling of the Z boson, different LQ generations mix under W interactions. Without LQ mixing, the interactions with the W boson can be written in terms of the following matrices

$$B^{W_1} = \begin{pmatrix} 0 & 0 & 0 \\ 0 & 0 & \sqrt{2} \end{pmatrix}, \quad B^{W_2} = \begin{pmatrix} 0 & 0 & 0 \\ 0 & 1 & 0 \\ 0 & 0 & -\sqrt{2} \end{pmatrix}, \quad B^{W_3} = \begin{pmatrix} 1 & 0 & 0 \end{pmatrix}, \quad (8.127)$$

arranging the LQ in their charge eigenstates according to Eq. (8.10). B^{W_1} describes the interaction of LQs with electric charges $Q = -4/3$ and $Q = -1/3$, B^{W_2} the ones with $Q = -1/3$ and $Q = 2/3$, B^{W_3} with $Q = 5/3$ and $Q = 2/3$. If we include LQ mixing, the matrices expanded up to $\mathcal{O}(v^2/m_{\text{LQ}}^2)$, then read

$$\tilde{B}^{W_1} \approx \begin{pmatrix} 0 & 0 & \frac{2v^2 Y_{31}^*}{\tilde{m}_1 - m_3^2} \\ \frac{\sqrt{2}v^2}{m_1^2 - m_3^2} (A_{21}A_{23}^* + Y_{31}^*) & \frac{\sqrt{2}vA_{23}^*}{\tilde{m}_2 - m_3^2} & \sqrt{2} - \frac{v^2|A_{23}|^2}{\sqrt{2}(\tilde{m}_2 - m_3^2)^2} \end{pmatrix}, \quad (8.128a)$$

$$\tilde{B}^{W_2} \approx \begin{pmatrix} 0 & \frac{vA_{21}^*}{m_1^2 - \tilde{m}_2^2} & \frac{\sqrt{2}v^2}{m_1^2 - m_3^2} (A_{23}A_{21}^* - Y_{31}) \\ \frac{v^2 Y_{22}^*}{m_2^2 - \tilde{m}_2^2} & 1 - \frac{v^2}{2} \left(\frac{|A_{21}|^2}{(m_1^2 - \tilde{m}_2^2)^2} - \frac{|A_{23}|^2}{(\tilde{m}_2 - m_3^2)^2} \right) & 0 \\ 0 & \frac{vA_{23}^*}{\tilde{m}_2 - m_3^2} & -\sqrt{2} - \frac{v^2|A_{23}|^2}{\sqrt{2}(m_3^2 - \tilde{m}_2^2)^2} \end{pmatrix}, \quad (8.128b)$$

$$\tilde{B}^{W_3} \approx \begin{pmatrix} 1 & \frac{-v^2 Y_{22}^*}{m_2^2 - \tilde{m}_2^2} & 0 \end{pmatrix}. \quad (8.128c)$$

8.7.6 4ℓ

Besides the penguin diagrams, mediated by the off-shell photon and Z boson, we also have the box diagrams. The matching results on $\ell_i^- \rightarrow \ell_f^- \ell_p^- \ell_r^+$ read

$$\begin{aligned}
 C_{fipr}^{VLL} = & \frac{-N_c}{256\pi^2} \left[\left(\Gamma_{u_j^c \ell_f}^{L,a*} \Gamma_{u_j^c \ell_i}^{L,b} \Gamma_{u_k^c \ell_p}^{L,b*} \Gamma_{u_k^c \ell_r}^{L,a} + \Gamma_{u_j^c \ell_p}^{L,a*} \Gamma_{u_j^c \ell_i}^{L,b} \Gamma_{u_k^c \ell_f}^{L,b*} \Gamma_{u_k^c \ell_r}^{L,a} \right) D_2(m_k^2, m_j^2, M_a^2, M_b^2) \right. \\
 & + \left(\Gamma_{u_j \ell_f}^{L*} \Gamma_{u_j \ell_i}^L \Gamma_{u_k \ell_p}^{L*} \Gamma_{u_k \ell_r}^L + \Gamma_{u_j \ell_p}^{L*} \Gamma_{u_j \ell_i}^L \Gamma_{u_k \ell_f}^{L*} \Gamma_{u_k \ell_r}^L \right) D_2(m_k^2, m_j^2, M^2, M^2) \\
 & + \left(\Gamma_{d_j \ell_f}^{L,a*} \Gamma_{d_j \ell_i}^{L,b} \Gamma_{d_k \ell_p}^{L,b*} \Gamma_{d_k \ell_r}^{L,a} + \Gamma_{d_j \ell_p}^{L,a*} \Gamma_{d_j \ell_i}^{L,b} \Gamma_{d_k \ell_f}^{L,b*} \Gamma_{d_k \ell_r}^{L,a} \right) C_0(0, M_a^2, M_b^2) \\
 & \left. + \left(\Gamma_{d_j^c \ell_f}^{L,a*} \Gamma_{d_j^c \ell_i}^{L,b} \Gamma_{d_k^c \ell_p}^{L,b*} \Gamma_{d_k^c \ell_r}^{L,a} + \Gamma_{d_j^c \ell_p}^{L,a*} \Gamma_{d_j^c \ell_i}^{L,b} \Gamma_{d_k^c \ell_f}^{L,b*} \Gamma_{d_k^c \ell_r}^{L,a} \right) C_0(0, M_a^2, M_b^2) \right], \quad (8.129a)
 \end{aligned}$$

$$\begin{aligned}
 C_{fipr}^{VLR} = & \frac{-N_c}{128\pi^2} \left[\Gamma_{u_j^c \ell_f}^{L,a*} \Gamma_{u_j^c \ell_i}^{L,b} \Gamma_{u_k^c \ell_p}^{R,b*} \Gamma_{u_k^c \ell_r}^{R,a} D_2(m_k^2, m_j^2, M_a^2, M_b^2) \right. \\
 & - 2\Gamma_{t^c \ell_f}^{L,a*} \Gamma_{t^c \ell_i}^{L,a} \Gamma_{t^c \ell_p}^{R,b*} \Gamma_{t^c \ell_r}^{R,b} m_t^2 D_0(m_t^2, m_t^2, M_a^2, M_b^2) \\
 & + \Gamma_{u_j \ell_f}^{L*} \Gamma_{u_j \ell_i}^L \Gamma_{u_k \ell_p}^{R*} \Gamma_{u_k \ell_r}^R D_2(m_k^2, m_j^2, M^2, M^2) \\
 & - 2\Gamma_{t \ell_f}^L \Gamma_{t \ell_i}^L \Gamma_{t \ell_p}^R \Gamma_{t \ell_r}^R m_t^2 D_0(m_t^2, m_t^2, M^2, M^2) \\
 & \left. + \Gamma_{d_j \ell_f}^{L,a*} \Gamma_{d_j \ell_i}^{L,b} \Gamma_{d_k \ell_p}^{R,b*} \Gamma_{d_k \ell_r}^{R,a} C_0(0, M_a^2, M_b^2) + \Gamma_{d_j^c \ell_f}^{L,a*} \Gamma_{d_j^c \ell_i}^{L,b} \Gamma_{d_k^c \ell_p}^{R,b*} \Gamma_{d_k^c \ell_r}^{R,a} C_0(0, M_a^2, M_b^2) \right], \quad (8.129b)
 \end{aligned}$$

$$\begin{aligned}
 C_{fipr}^{SLL} = & \frac{-N_c m_t^2}{64\pi^2} \left[2\Gamma_{t^c \ell_f}^{R,a*} \Gamma_{t^c \ell_i}^{L,b} \Gamma_{t^c \ell_p}^{R,b*} \Gamma_{t^c \ell_r}^{L,a} D_0(m_t^2, m_t^2, M_a^2, M_b^2) \right. \\
 & - \Gamma_{t^c \ell_p}^{R,a*} \Gamma_{t^c \ell_i}^{L,b} \Gamma_{t^c \ell_f}^{R,b*} \Gamma_{t^c \ell_r}^{L,a} D_0(m_t^2, m_t^2, M_a^2, M_b^2) \\
 & \left. + \Gamma_{t \ell_f}^{R*} \Gamma_{t \ell_i}^L \Gamma_{t \ell_p}^R \Gamma_{t \ell_r}^L D_0(m_t^2, m_t^2, M^2, M^2) \right], \quad (8.129c)
 \end{aligned}$$

where C_{fipr}^{VRR} , C_{fipr}^{VRL} and C_{fipr}^{SRR} are obtained by simply exchanging $\Gamma^L \leftrightarrow \Gamma^R$.

8.7.7 $2\ell 2\nu$

Here we show the box contributions, induced by the $Q = -1/3$ and $Q = 2/3$ LQs. We obtain for $\ell_i^- \rightarrow \ell_f^- \nu_p \bar{\nu}_r$

$$\begin{aligned}
 D_{\ell_f \ell_i}^{L,pr} = & \frac{-N_c}{64\pi^2} \left[\Gamma_{u_j^c \ell_f}^{L,b*} \Gamma_{u_j^c \ell_i}^{L,a} \left(\Gamma_{d_k^c \nu_p}^{L,a*} \Gamma_{d_k^c \nu_r}^{L,b} - \Gamma_{d_k \nu_p}^{L,b*} \Gamma_{d_k \nu_r}^{L,a} \right) C_0(m_{u_j}^2, M_a^2, M_b^2) \right. \\
 & \left. + \Gamma_{d_k \ell_f}^{L,b*} \Gamma_{d_k \ell_i}^{L,a} \left(\Gamma_{u_j \nu_p}^{L,a*} \Gamma_{u_j \nu_r}^{L,b} - \Gamma_{u_j^c \nu_p}^{L,b*} \Gamma_{u_j^c \nu_r}^{L,a} \right) C_0(m_{u_j}^2, M_a^2, M_b^2) \right], \quad (8.130a)
 \end{aligned}$$

$$\begin{aligned}
 D_{\ell_f \ell_i}^{R,pr} = & \frac{-N_c}{64\pi^2} \left[\Gamma_{u_j^c \ell_f}^{R,b*} \Gamma_{u_j^c \ell_i}^{R,a} \left(\Gamma_{d_k^c \nu_p}^{L,a*} \Gamma_{d_k^c \nu_r}^{L,b} - \Gamma_{d_k \nu_p}^{L,b*} \Gamma_{d_k \nu_r}^{L,a} \right) C_0(m_{u_j}^2, M_a^2, M_b^2) \right. \\
 & \left. + \Gamma_{d_k \ell_f}^{R,b*} \Gamma_{d_k \ell_i}^{R,a} \left(\Gamma_{u_j \nu_p}^{L,a*} \Gamma_{u_j \nu_r}^{L,b} - \Gamma_{u_j^c \nu_p}^{L,b*} \Gamma_{u_j^c \nu_r}^{L,a} \right) C_0(m_{u_j}^2, M_a^2, M_b^2) \right]. \quad (8.130b)
 \end{aligned}$$

Chapter 9

Towards Full m_c Dependence of the \mathcal{O}_2 Contribution at $\mathcal{O}(\alpha_s^2)$ in $b \rightarrow s\gamma$

Rare inclusive B decays like $\bar{B} \rightarrow X_s\gamma$ offer the unique possibility to access potential NP at scales much higher than currently within direct experimental reach. This is due to the fact that such processes only occur via loops in the SM. If BSM particles contribute at the same order, assuming a NP scale that is not orders of magnitude above the EW scale, the contributions stemming from NP relative to the SM can be expected to be large (see also Sec. 1.4). In order to constrain such NP models, precise SM predictions of the branching ratios of such processes are needed. This is especially true in the light of the recent flavor anomalies, which we have explored in much detail throughout this thesis. Already at the current level of precision, NP in $b \rightarrow s\gamma$ contained in the Wilson coefficient C_7 is highly constrained to the region $-0.01 < C_7^{\text{NP}}(m_b) < 0.05$ [98]. In this chapter we compute a subset of three-loop diagrams induced by the operator \mathcal{O}_2 contributing to $b \rightarrow s\gamma$ at $\mathcal{O}(\alpha_s^2)$ while retaining the full dependence on the charm mass m_c . Such diagrams have so far only been calculated in the limits of $m_c = 0$ [473] and $m_c \gg m_b/2$ [474]. These results were used in Ref. [473] to estimate the contribution at the physical charm mass via interpolation in m_c . The error associated with the interpolation is the largest contribution to the theory prediction uncertainty after nonperturbative effects.

First, we give an overview of the current status of the theoretical calculations. We then describe some technical details about our calculation procedure and, as a preparatory step, present results for the two-loop diagrams shown in Fig. 9.1, which can be compared to the literature [475]. In this step, we give the amplitudes up to $\mathcal{O}(\epsilon)$, where ϵ is the dimensional regulator, which is needed to obtain $\mathcal{O}(\alpha_s^2)$ contributions stemming from counterterm insertions. Finally, we will present our results for the mentioned subset of diagrams.

9.1 Current Status

The CP- and isospin-averaged measurements of $\text{Br}[\bar{B} \rightarrow X_s\gamma]$ by CLEO [476], Belle [477, 478] and BaBar [479–482] lead to the combined result of [483]

$$\text{Br}[\bar{B} \rightarrow X_s\gamma] = (3.43 \pm 0.21 \pm 0.07) \times 10^{-4} \quad (9.1)$$

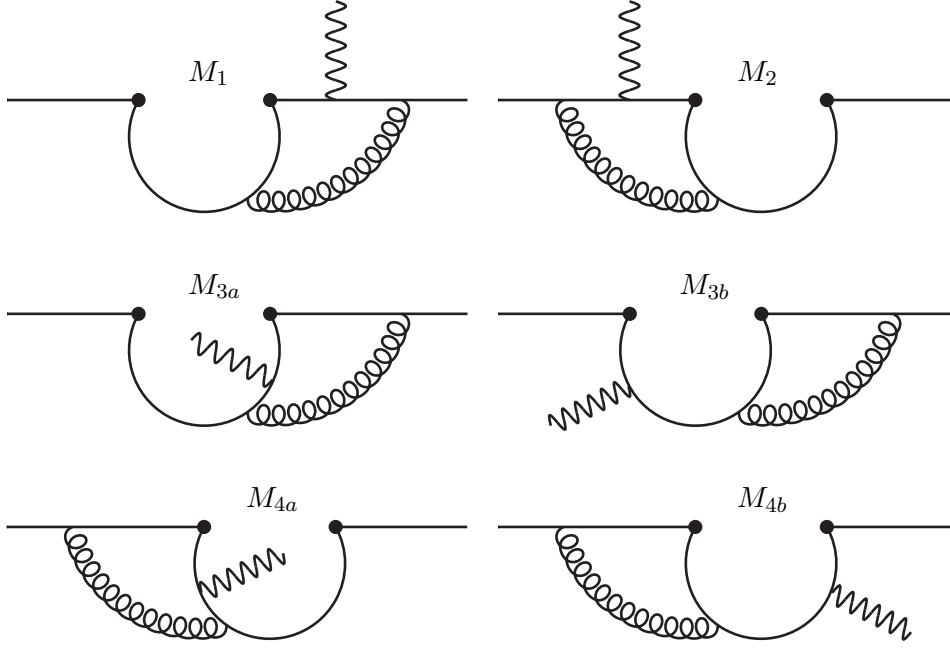


Figure 9.1: The six diagrams M_1 , M_2 , M_{3a} , M_{3b} , M_{4a} and M_{4b} associated with the operator \mathcal{O}_2 at $\mathcal{O}(\alpha_s)$.

for a photon energy of $E_\gamma > E_0 = 1.6 \text{ GeV}$ in the decaying meson rest frame. In the SM, radiative B meson decays can be described by the effective Hamiltonian

$$\begin{aligned}
 \mathcal{H}_{\text{eff}} &= -\frac{4G_F}{\sqrt{2}} V_{tb} V_{ts}^* \sum_{i=1}^8 C_i(\mu) \mathcal{O}_i , \\
 \mathcal{O}_1 &= (\bar{s} \gamma_\mu P_L T^a c) (\bar{c} \gamma^\mu P_L T^a b) , & \mathcal{O}_2 &= (\bar{s} \gamma_\mu P_L c) (\bar{c} \gamma^\mu P_L b) , \\
 \mathcal{O}_3 &= (\bar{s} \gamma_\mu P_L b) \sum_q (\bar{q} \gamma^\mu q) , & \mathcal{O}_4 &= (\bar{s} \gamma_\mu P_L T^a b) \sum_q (\bar{q} \gamma^\mu T^a q) , \\
 \mathcal{O}_5 &= (\bar{s} \gamma_\mu \gamma_\nu \gamma_\rho P_L b) \sum_q (\bar{q} \gamma^\mu \gamma^\nu \gamma^\rho q) , & \mathcal{O}_6 &= (\bar{s} \gamma_\mu \gamma_\nu \gamma_\rho P_L T^a b) \sum_q (\bar{q} \gamma^\mu \gamma^\nu \gamma^\rho T^a q) , \\
 \mathcal{O}_7 &= \frac{e}{16\pi^2} [\bar{s} \sigma^{\mu\nu} (\bar{m}_b(\mu) P_R + \bar{m}_s(\mu) P_L) b] F_{\mu\nu} , & & (9.2) \\
 \mathcal{O}_8 &= \frac{g_s}{16\pi^2} [\bar{s} \sigma^{\mu\nu} (\bar{m}_b(\mu) P_R + \bar{m}_s(\mu) P_L) T^a b] G_{\mu\nu}^a , & &
 \end{aligned}$$

which completes the basis given in Eq. (1.54). The sums in the operators \mathcal{O}_3 - \mathcal{O}_6 run over all active flavors $q = \{u, d, s, c, b\}$. The branching ratio for $\bar{B} \rightarrow X_s \gamma$ can be written as

$$\text{Br}[\bar{B} \rightarrow X_s \gamma] = \text{Br}[b \rightarrow X_s \gamma] + \delta \text{Br}[\bar{B} \rightarrow X_s \gamma] , \quad (9.3)$$

where $\text{Br}[b \rightarrow X_s \gamma]$ represents the contribution calculable in perturbation theory and $\delta \text{Br}[\bar{B} \rightarrow X_s \gamma]$ are nonperturbative contributions. The perturbative part can further be written as

$$\text{Br}[b \rightarrow X_s \gamma]_{E_\gamma > E_0} \sim \sum_{i,j} C_i(\mu) C_j(\mu) G_{ij}(E_0, \mu) , \quad (9.4)$$

where E_0 is the energy cut in the photon spectrum and G_{ij} represent the interference contributions associated with the operators \mathcal{O}_i and \mathcal{O}_j . Several groups have performed involved and laborious calculations, leading to the current SM prediction of [484]

$$\text{Br}[\bar{B} \rightarrow X_s \gamma]_{\text{SM}} = (3.36 \pm 0.23) \times 10^{-4} \quad (9.5)$$

for $E_0 = 1.6$ GeV. The individual contributions to the cited uncertainty are of nonperturbative ($\pm 5\%$), higher-order ($\pm 3\%$), interpolation ($\pm 3\%$) and parametric ($\pm 2\%$) origin. The interpolation uncertainties stem from the G_{27} contribution at $\mathcal{O}(\alpha_s^2)$ as mentioned in this chapter's introduction. Even though the reduction of nonperturbative uncertainties seems unlikely [485], the goal of the community is to reduce the remaining uncertainties to a minimum, which is necessary to compete with the planned measurements at Belle II [486]. The completion of the NNLL calculation is also needed with regards to the strong dependence on the renormalization scheme of the charm mass at NLL, which is induced due to the fact that the current-current operator \mathcal{O}_2 only contributes to the process at $\mathcal{O}(\alpha_s)$. To date, the NNLO calculation is almost completed. The matching of the Wilson coefficients has been completed at $\mathcal{O}(\alpha_s^2)$ in Refs. [487, 488, 488], and the four-loop anomalous dimension matrix allowing for NNLL resummation has been worked out in Ref. [489]. The contributions to G_{77} were computed in Refs. [490–493]. Effects of charm and bottom quark masses in loops on gluon lines were obtained for G_{77} [494], G_{78} [495] and $G_{(1,2)7}$ [496] and a complete calculation of G_{78} is also available [497]. For details on the (N)LO calculations see e.g. Refs. [484, 493, 498, 499]. The challenging calculation of $G_{(1,2)7}$ with full m_c dependence remains an open task which we will partly address in the following.

9.2 Details about the Calculation

In this section we present the calculation, which we performed fully analytic and hence exact in m_c , of the matrix element associated with the operator \mathcal{O}_2 for $b \rightarrow s\gamma$ at $\mathcal{O}(\alpha_s)$ and partially at $\mathcal{O}(\alpha_s^2)$. In the former case we can directly compare our results to the ones obtained as an expansion in m_c/m_b in Ref. [475]. We denote the contributions by

$$M^{\text{NLO}} = M_1 + M_2 + M_{3a} + M_{3b} + M_{4a} + M_{4b} , \quad (9.6)$$

$$M^{\text{NNLO}} = \sum_i^{10} D_i , \quad (9.7)$$

where M^{NLO} is the two-loop result and M^{NNLO} is the result of the subset of diagrams at $\mathcal{O}(\alpha_s^2)$ considered in this work. The diagrams are labeled according to Fig. 9.1 (two-loop) and Fig. 9.2 (three-loop). The consideration of diagrams where the photon is radiated from an external quark line is not necessary. Since only \mathcal{O}_7 contributes to $b \rightarrow s\gamma$ at tree-level, the contribution of \mathcal{O}_2 is necessarily proportional to it at any order

$$\langle s\gamma | \mathcal{O}_2 | b \rangle \sim \langle s\gamma | \mathcal{O}_7 | b \rangle_{\text{tree}} = m_b \frac{e^2}{8\pi^2} \bar{u}(p_s) \not{q} u(p_b) \sim \bar{u}(p_s) (\not{P}_L m_b - 2(p \cdot \varepsilon) P_R) u(p_b) , \quad (9.8)$$

where $p_{b(s)}$ is the b (s) quark momentum and q the photon momentum. Since diagrams with external photons will be proportional to the Dirac structure \not{P}_L , it is sufficient to compute the contributions proportional to $(p \cdot \varepsilon) P_R$ in every diagram to retain the full contribution.

Let us now describe the procedure of the calculation. First, we simplified the Dirac algebra with the algebraic program REDUCE. We then used the Kira program [500] to reduce the scalar integrals contained in the amplitudes to a set of master integrals (MIs), which allowed us to formulate a set of differential equations governing the m_c dependence of the MIs. In a next

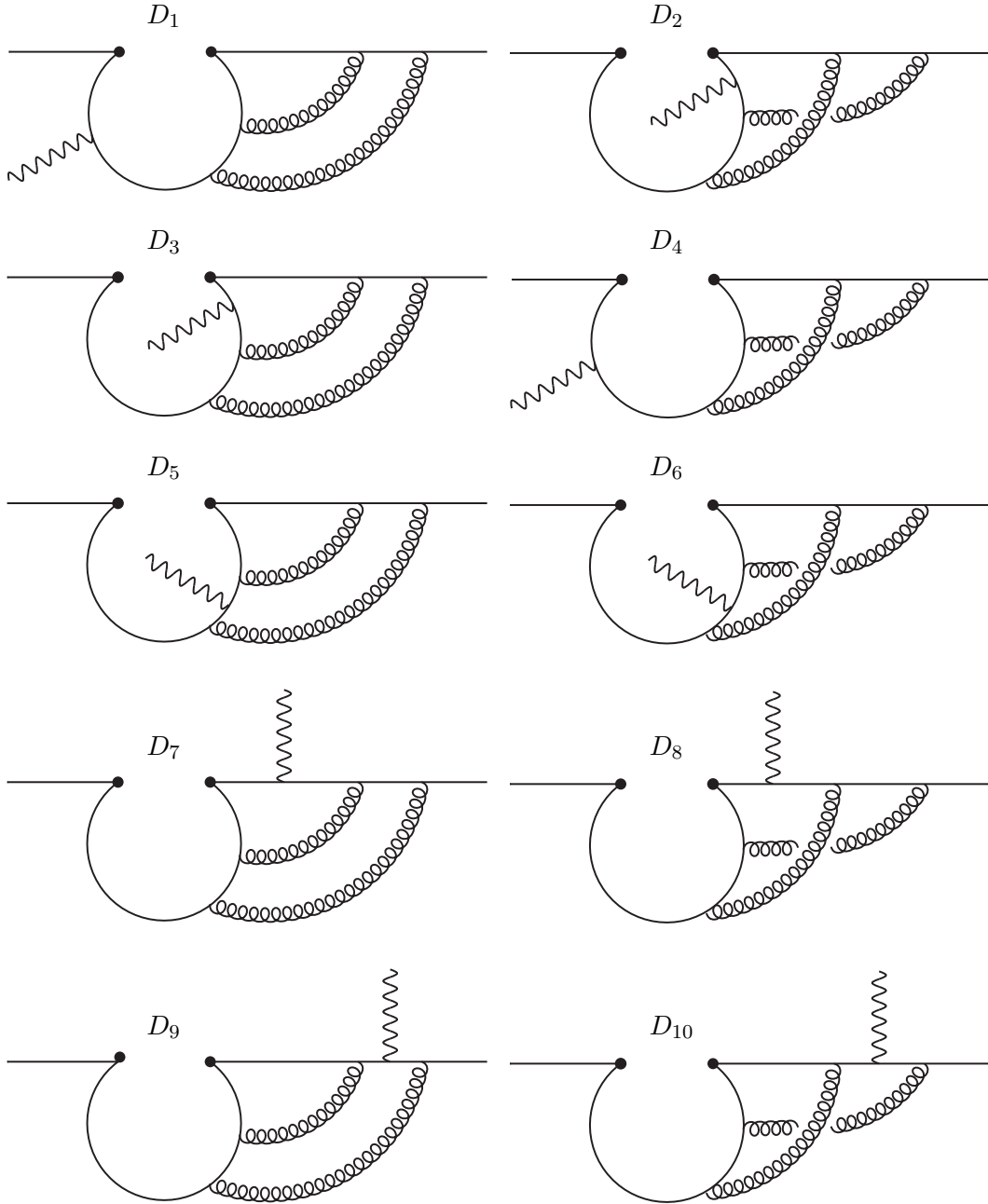


Figure 9.2: The ten diagrams D_1 - D_{10} associated with the operator \mathcal{O}_2 at $\mathcal{O}(\alpha_s^2)$ considered in this work.

step, we used the CANONICA package [501] to perform the basis change to a canonical form (see Sec. 1.3.3). This required the application of a variable change in the differential equations. In the case of the diagrams where the gluon(s) is (are) exchanged between the s and c quark, the substitution reads

$$x = \frac{1}{\sqrt{1-4z}}, \quad (9.9)$$

where $z = m_c^2/m_b^2$. For a gluon exchange between the b and c quark, we used

$$u = \frac{t - 2i}{2 - 2i}, \quad t = \frac{2\sqrt{1 - 4z}}{1 + 2\sqrt{z}}. \quad (9.10)$$

Both variables have the same distinct behavior for extreme values of z

$$\lim_{z \rightarrow \infty} x = \lim_{z \rightarrow \infty} u = 0, \quad \lim_{z \rightarrow 0} x = \lim_{z \rightarrow 0} u = 1. \quad (9.11)$$

Having the canonical basis at hand, the main task was to fix the integration constants arising when iteratively constructing the solution in terms of the Goncharov polylogarithms (GPLs), see Eq. (1.63). Some constants could be fixed right away by calculating the simplest of the MIs by hand. We fixed the remaining constants using information about the solution in the asymptotic limit $z \rightarrow \infty$. This finally allowed us to obtain a fully analytic result for the matrix elements expressed in terms of GPLs and some irrational constants. A numerical result for the matrix elements was then easily obtained with the help of the Ginac library [502] which allows to evaluate the GPLs to arbitrary precision. Finally, to obtain an approximate expression for the matrix elements in terms of powers and logarithms of z , we also deployed an expansion of the GPLs around $x = 1$ and $u = 1$, corresponding to an expansion around $z = 0$, as described in Sec. 1.3.3.

While the steps for the two- and three-loop calculations were in principle the same, the computational challenges increased drastically. In the two-loop case, our problem contained four MIs (eight in the case where the gluon is exchanged between the b and c quark), which in the canonical basis had to be calculated over four powers of ϵ in order to obtain a result up to $\mathcal{O}(\epsilon)$. In the three-loop case, we encountered up to 44 MIs, which on the other hand had to be calculated over ten ϵ powers in the canonical basis to obtain a result at $\mathcal{O}(\epsilon^0)$. We expect the diagrams involving gluons on the b line to be even more involved.

9.3 Results for the Matrix Elements

In this section we present the results of our calculations. The approximate results, obtained after expanding the GPLs as described above, contain irrational constants and constant GPLs. To shorten the notation, we evaluated those constants numerically again using the Ginac library. Our results can be expressed in a compact form

$$M(D)_a = \sum_{m,n=0} a_{mn} z^m L^n, \quad (9.12)$$

with numerical coefficients a_{mn} and $L = \log(z)$. Note that we took into account all occurring powers of L to any given order of z .

Two-Loop Results

For convenience, we directly calculated the sums of the diagrams $3_a + 3_b$ and $4_a + 4_b$. Our results read

$$M_1 = \left\{ \frac{1}{36\epsilon} + \frac{37}{216} + \frac{i\pi}{18} + z \left[-L - \left(\frac{5}{2} + i\pi \right) \right] \right. \\ \left. + z^2 \left[-L^2 + (1 - 6.28319i)L + (7.36960 + i\pi) \right] \right\} \quad (9.13)$$

$$\begin{aligned}
 & + z^3 \left[\frac{2}{3} L^2 - (1.11111 - 4.18879i)L - (7.20937 + 3.49066i) \right] \\
 & + \epsilon \left(0.110471 + 1.076286i + z \left[L^2 + (4.2645 - 15.7080i) \right] \right. \\
 & \quad + z^2 \left[L^3 - \left(\frac{5}{2} - i\pi \right) L^2 + (16.6595 - 9.4248i)L + (0.7522 + 36.6293i) \right] \\
 & \quad + z^3 \left[-\frac{2}{3} L^3 + \left(\frac{2}{3} - 2.09440i \right) L^2 - (9.88409 + 2.79253i)L \right. \\
 & \quad \left. \left. + (16.4092 - 35.0079i) \right] \right) \left. \right\} \times \frac{\alpha_s}{\pi} C_F Q_d \langle s\gamma | \mathcal{O}_7 | b \rangle_{\text{tree}} \times \left(\frac{m_b}{\mu} \right)^{-4\epsilon}, \\
 M_2 = & \left\{ \frac{-5}{36\epsilon} + \frac{13}{216} + 1.144934z - 6.57974z^{3/2} + z^2 \left[\frac{1}{2} (L^2 - 6L + 6) \right] \right. \\
 & \quad + z^3 \left[\frac{4}{3} \left(L^2 + \frac{L}{24} + 3.02206 \right) \right] \\
 & \quad + \epsilon \left(-0.726892 + 7.69509z + z^{3/2} [13.1595L + 7.97361] \right. \\
 & \quad + z^2 \left[-\frac{1}{2} L^3 + \frac{9}{4} L^2 - \frac{19}{4} L - 33.1417 \right] \\
 & \quad + z^{5/2} \left[-\frac{23}{9} (L - 12.8589) \right] \\
 & \quad \left. \left. + z^3 \left[-\frac{4}{3} \left(L^3 - \frac{3L^2}{8} - \frac{61}{8} L + 5.70675 \right) \right] \right) \right\} \\
 & \quad \times \frac{\alpha_s}{\pi} C_F Q_d \langle s\gamma | \mathcal{O}_7 | b \rangle_{\text{tree}} \times \left(\frac{m_b}{\mu} \right)^{-4\epsilon}, \\
 M_3 = & \left\{ -\frac{1}{8\epsilon} - \frac{15}{16} - 0.785398i + z \left[\frac{L^3}{6} + \left(\frac{1}{4} + 1.57080i \right) L^2 \right. \right. \\
 & \quad \left. \left. - (2.93480 - 1.57080i)L - (3.37151 - 1.11547i) \right] \right. \\
 & \quad + z^2 \left[\frac{L^3}{6} - \left(\frac{1}{2} - 1.57080i \right) L^2 - (4.43480 + i\pi)L + (3.78069 - 3.59692i) \right] \\
 & \quad + z^3 \left[L - \frac{17}{12} - i\pi \right] \\
 & \quad + \epsilon \left(-1.98323 - 5.89049i \right. \\
 & \quad + z \left[\left(\frac{1}{4} - 1.57080i \right) L^3 + (1.14493 + 3.92699i)L^2 \right. \\
 & \quad \left. \left. - (6.89222 + 0.91065i)L - (11.89070 - 3.67302i) \right] \right. \\
 & \quad + z^2 \left[\left(\frac{5}{6} - 1.57080i \right) L^3 + (0.39493 + 4.71239i)L^2 \right. \\
 & \quad \left. \left. - (4.8378 + 15.0478i)L + (29.7761 - 1.7791i) \right] \right) \left. \right\}
 \end{aligned} \tag{9.14}$$

$$\begin{aligned}
 & \quad \left. \left. - (2.93480 - 1.57080i)L - (3.37151 - 1.11547i) \right] \right. \\
 & \quad + z^2 \left[\frac{L^3}{6} - \left(\frac{1}{2} - 1.57080i \right) L^2 - (4.43480 + i\pi)L + (3.78069 - 3.59692i) \right] \\
 & \quad + z^3 \left[L - \frac{17}{12} - i\pi \right] \\
 & \quad + \epsilon \left(-1.98323 - 5.89049i \right. \\
 & \quad + z \left[\left(\frac{1}{4} - 1.57080i \right) L^3 + (1.14493 + 3.92699i)L^2 \right. \\
 & \quad \left. \left. - (6.89222 + 0.91065i)L - (11.89070 - 3.67302i) \right] \right. \\
 & \quad + z^2 \left[\left(\frac{5}{6} - 1.57080i \right) L^3 + (0.39493 + 4.71239i)L^2 \right. \\
 & \quad \left. \left. - (4.8378 + 15.0478i)L + (29.7761 - 1.7791i) \right] \right) \left. \right\}
 \end{aligned} \tag{9.15}$$

$$\begin{aligned}
 & \times \frac{\alpha_s}{\pi} C_F Q_u \langle s\gamma | \mathcal{O}_7 | b \rangle_{\text{tree}} \times \left(\frac{m_b}{\mu} \right)^{-4\epsilon}, \\
 M_4 = & \left\{ -\frac{1}{4\epsilon} - \frac{7}{8} + z \left[-\frac{1}{12} L^3 - 1.96740L - 1.024524 \right] \right. \\
 & + z^2 \left[-\frac{1}{12} L^3 + \frac{L^2}{4} - \frac{L}{2} + 4.54905 \right] \\
 & + z^3 \left[-\frac{1}{4} 3L^2 + L - 2.21740 \right] \\
 & + \epsilon \left(-3.70743 + z \left[-\frac{1}{4} L^3 + 1.233701L^2 - 10.54612L - 22.5418 \right] \right. \\
 & + 39.4784z^{3/2} + z^2 \left[-\frac{1}{4} L^3 + \frac{5L^2}{8} + 2.06788L - 5.08920 \right] \\
 & \left. \left. - 21.9325z^{5/2} + z^3 \left[\frac{3L^3}{4} - \frac{3L^2}{8} - 2.39583L + 13.55839 \right] \right) \right\} \\
 & \times \frac{\alpha_s}{\pi} C_F Q_u \langle s\gamma | \mathcal{O}_7 | b \rangle_{\text{tree}} \times \left(\frac{m_b}{\mu} \right)^{-4\epsilon},
 \end{aligned} \tag{9.16}$$

where α_s is the strong coupling constant, $C_F = 4/3$ a color factor and $Q_{d(u)}$ the down (up) quark electric charge. The matrix elements up to $\mathcal{O}(\epsilon^0)$ are in perfect agreement with the ones obtained in Ref. [475].

Three-Loop Results

We present the three-loop results in the same manner as previously the two-loop results. Here, the additional color factor C_A arises. To shorten the notation, we introduced coefficient matrices a_{imn} and f_{imn} which are listed in the Appendix 9.4. Note that in this case we expanded our results up to z^5 since the agreement to our exact result was not satisfactory at lower orders of the expansion.

$$\begin{aligned}
 D_{1+2} = & \left\{ \frac{2C_A - 5C_F}{288\epsilon^3} \right. \\
 & + \frac{1}{\epsilon^2} \left((0.0438683 + 0.0654498i)C_A - (0.145959 + 0.163625i)C_F \right. \\
 & \left. + \sum_{m=1}^5 \sum_{n=1}^3 \left(a_{1mn}^{-2} C_A + f_{1mn}^{-2} C_F \right) z^m L^n \right) \\
 & + \frac{1}{\epsilon} \left((0.0540364 - 1.37563i)C_F - (0.203523 - 0.413449i)C_A \right. \\
 & \left. + \sum_{m=1}^5 \sum_{n=1}^4 \left(a_{1mn}^{-1} C_A + f_{1mn}^{-1} C_F \right) z^m L^n \right) \\
 & \left. + \left((3.34448 - 4.33545i)C_F - (2.00146 - 0.0197299i)C_A \right) \right\}
 \end{aligned} \tag{9.17}$$

$$\begin{aligned}
 & + \sum_{m=1}^5 \sum_{n=1}^5 \left(a_{1mn}^0 C_A + f_{1mn}^0 C_F \right) z^m L^n \Big\} \\
 & \times \frac{\alpha_s^2}{\pi^2} C_F Q_u \langle s\gamma | \mathcal{O}_7 | b \rangle_{\text{tree}} \times \left(\frac{m_b}{\mu} \right)^{-6\epsilon}, \\
 D_{3+4} = & \left\{ \frac{1}{\epsilon^2} \left(0.00509514 C_A - 0.0412139 C_F \right. \right. \\
 & + \sum_{m=1}^5 \sum_{n=1}^3 \left(a_{3mn}^{-2} C_A + f_{3mn}^{-2} C_F \right) z^m L^n \Big) \\
 & + \frac{1}{\epsilon} \left((0.0970453 + 0.0480206i) C_A - (0.418501 + 0.388432i) C_F \right. \\
 & + \sum_{m=1}^5 \sum_{n=1}^4 \left(a_{3mn}^{-1} C_A + f_{3mn}^{-1} C_F \right) z^m L^n \Big) \\
 & + \left((0.799133 + 0.914631i) C_A - (1.16206 + 3.94428i) C_F \right. \\
 & \left. \left. + \sum_{m=1}^5 \sum_{n=1}^5 \left(a_{3mn}^0 C_A + f_{3mn}^0 C_F \right) z^m L^n \right) \right\} \\
 & \times \frac{\alpha_s^2}{\pi^2} C_F Q_u \langle s\gamma | \mathcal{O}_7 | b \rangle_{\text{tree}} \times \left(\frac{m_b}{\mu} \right)^{-6\epsilon},
 \end{aligned} \tag{9.18}$$

$$D_{5+6} = \left\{ \frac{5C_F - 2C_A}{288\epsilon^3} \right. \tag{9.19}$$

$$\begin{aligned}
 & + \frac{1}{\epsilon^2} \left((0.249673 + 0.163625i) C_F - (0.101047 + 0.0654498i) C_A \right. \\
 & \left. + \sum_{m=1}^5 \sum_{n=1}^3 \left(a_{5mn}^{-2} C_A + f_{5mn}^{-2} C_F \right) z^m L^n \right) \\
 & + \frac{1}{\epsilon} \left((1.04676 + 2.35311i) C_F - (0.353214 + 0.952343i) C_A \right. \\
 & \left. + \sum_{m=1}^5 \sum_{n=1}^4 \left(a_{5mn}^{-1} C_A + f_{5mn}^{-1} C_F \right) z^m L^n \right) \\
 & + \left((1.68832 - 5.26685i) C_F - (1.2017 - 14.7102i) C_A \right. \\
 & \left. + \sum_{m=1}^5 \sum_{n=1}^5 \left(a_{5mn}^0 C_A + f_{5mn}^0 C_F \right) z^m L^n \right) \Big\} \\
 & \times \frac{\alpha_s^2}{\pi^2} C_F Q_u \langle s\gamma | \mathcal{O}_7 | b \rangle_{\text{tree}} \times \left(\frac{m_b}{\mu} \right)^{-6\epsilon},
 \end{aligned}$$

$$D_{7+8} = \left\{ -\frac{C_A}{1728\epsilon^3} \right. \tag{9.20}$$

$$\begin{aligned}
& + \frac{1}{\epsilon^2} \left((-0.0078125 - 0.00545415i)C_A \right) \\
& + \frac{1}{\epsilon} \left(0.0241312C_F - (0.032069 + 0.0736311i)C_A \right. \\
& \quad \left. + \sum_{m=1}^5 \sum_{n=1}^4 a_{7mn}^{-1} C_A z^m L^n \right) \\
& + \left((0.153411 + 0.227431i)C_F + (0.0504689 - 0.463735i)C_A \right. \\
& \quad \left. + \sum_{m=1}^5 \sum_{n=1}^5 (a_{7mn}^0 C_A + f_{7mn}^0 C_F) z^m L^n \right) \Big\} \\
& \times \frac{\alpha_s^2}{\pi^2} C_F Q_d \langle s\gamma | \mathcal{O}_7 | b \rangle_{\text{tree}} \times \left(\frac{m_b}{\mu} \right)^{-6\epsilon}, \\
D_{9+10} = & \left\{ -\frac{17C_A}{1728\epsilon^3} \right. \\
& + \frac{1}{\epsilon^2} \left(0.00694444C_F - (0.0752315 + 0.0927206i)C_A \right) \\
& + \frac{1}{\epsilon} \left((0.0706534 - 0.70904i)C_A + (0.0267947 + 0.0654498i)C_F \right. \\
& \quad \left. + \sum_{m=1}^5 \sum_{n=1}^4 (a_{9mn}^{-1} C_A + f_{9mn}^{-1} C_F) z^m L^n \right) \\
& + \left((2.07777 - 2.07946i)C_A - (0.310375 - 0.252534i)C_F \right. \\
& \quad \left. + \sum_{m=1}^5 \sum_{n=1}^5 (a_{9mn}^0 C_A + f_{9mn}^0 C_F) z^m L^n \right) \Big\} \\
& \times \frac{\alpha_s^2}{\pi^2} C_F Q_d \langle s\gamma | \mathcal{O}_7 | b \rangle_{\text{tree}} \times \left(\frac{m_b}{\mu} \right)^{-6\epsilon}.
\end{aligned} \tag{9.21}$$

9.4 Appendix

Here we list the coefficient matrices a_{imn} and f_{imn} encoded in our results explicitly. Note that the coefficients are in principle available to arbitrary precision.

$$a_{1mn}^{-2} = \begin{pmatrix} -0.125 + 0.19635i & 0.03125 & 0 \\ -0.0831085 - 0.883573i & -0.140625 + 0.0981748i & 0.0104167 \\ -0.138889 + 0.1309i & 0.0208333 & 0 \\ -0.0651042 + 0.0981748i & 0.015625 & 0 \\ -0.0611111 + 0.1309i & 0.0208333 & 0 \end{pmatrix}, \tag{9.22}$$

$$f_{1mn}^{-2} = \begin{pmatrix} 0.125 - 0.785398i & -0.125 & 0 \\ 0.894934 + 2.35619i & 0.375 - 0.392699i & -0.0416667 \\ 0.305556 - 0.523599i & -0.0833333 & 0 \\ 0.0729167 - 0.392699i & -0.0625 & 0 \\ -0.00555556 - 0.523599i & -0.0833333 & 0 \end{pmatrix}, \quad (9.23)$$

$$a_{1mn}^{-1} = \begin{pmatrix} -1.90308 - 0.785398i & 0.0625 & -0.03125 & 0 \\ 0.138377 + 1.82692i & 0.621042 + 2.79798i & 0.4375 - 0.261799i & -0.0286458 \\ -6.74501 - 16.4715i & -2.41319 + 2.94524i & 0.291667 & 0 \\ -4.00269 + 2.81434i & 0.545573 + 0.245437i & 0.0104167 & 0 \\ -3.35865 + 2.40637i & 0.474653 + 0.327249i & 0.0138889 & 0 \end{pmatrix}, \quad (9.24)$$

$$f_{1mn}^{-1} = \begin{pmatrix} 6.71795 + 4.77501i & 1.39493 + 0.392699i & 0.166667 - 0.261799i & -0.0208333 \\ -10.1678 - 11.3271i & -3.5564 - 4.61421i & -0.864583 + 0.916298i & 0.104167 \\ 32.4592 + 53.7125i & 8.09028 - 11.781i & -1.16667 & 0 \\ 11.8572 - 14.1917i & -2.36806 - 0.490874i & 0.0104167 & 0 \\ 7.8209 - 10.4982i & -1.6625 - 0.654498i & 0.0138889 & 0 \end{pmatrix}, \quad (9.25)$$

$$a_{1mn}^0 = \begin{pmatrix} 0.586291 - 5.60236i & 1.65456 + 0.785398i & 0.0208333 - 0.19635i & 0.0078125 & 0 \\ -9.00333 - 9.97666i & -5.86453 + 12.1779i & 0.739608 - 2.97536i & -0.564897 + 0.302706i & 0.0364583 \\ 88.2687 - 0.509204i & -0.655595 - 3.56227i & 2.03523 - 2.68344i & -0.432292 & 0 \\ -36.2101 - 53.9965i & -3.51506 + 7.69036i & 0.270399 - 0.343612i & -0.0351563 & 0 \\ -49.106 - 19.273i & 0.736926 + 7.23003i & 0.292477 - 0.458149i & -0.046875 & 0 \end{pmatrix}, \quad (9.26)$$

$$f_{1mn}^0 = \begin{pmatrix} -2.92857 + 19.2604i & -2.89921 - 1.48828i & -1.55285 - 0.916298i & -0.197917 + 0.392699i & 0.0375 \\ 34.7211 + 1.01355i & 16.7987 - 27.6265i & 0.350983 + 5.25306i & 1.06646 - 1.01447i & -0.127083 \\ -284.672 + 34.5018i & -1.6631 + 10.0603i & -7.02285 + 11.1265i & 1.76042 & 0 \\ 148.011 + 172.287i & 12.1019 - 26.1527i & -0.406829 + 0.785398i & 0.0546875 & 0 \\ 170.688 + 42.6231i & -1.65786 - 23.6624i & -0.848148 + 1.0472i & 0.0729167 & 0 \end{pmatrix}, \quad (9.27)$$

$$a_{3mn}^{-2} = \begin{pmatrix} 0.125 + 0.19635i & 0.03125 & 0 \\ -0.458109 - 0.0981748i & -0.015625 + 0.0981748i & 0.0104167 \\ 0.0277778 + 0.1309i & 0.0208333 & 0 \\ 0.0598958 + 0.0981748i & 0.015625 & 0 \\ 0.105556 + 0.1309i & 0.0208333 & 0 \end{pmatrix}, \quad (9.28)$$

$$f_{3mn}^{-2} = \begin{pmatrix} -0.5 - 0.785398i & -0.125 & 0 \\ 1.83243 + 0.392699i & 0.0625 - 0.392699i & -0.0416667 \\ -0.111111 - 0.523599i & -0.0833333 & 0 \\ -0.239583 - 0.392699i & -0.0625 & 0 \\ -0.422222 - 0.523599i & -0.0833333 & 0 \end{pmatrix}, \quad (9.29)$$

$$a_{3mn}^{-1} = \begin{pmatrix} -2.40518 + 0.557736i & -0.509967 + 0.392699i & 0.0104167 + 0.1309i & 0.0104167 \\ 3.47161 - 3.38703i & 0.250909 - 0.343612i & -0.0208333 - 0.229074i & -0.0260417 \\ -7.03021 + 1.63625i & 0.21875 + 0.981748i & 0.0833333 & 0 \\ -0.0748058 + 2.86616i & 0.366319 - 0.0490874i & -0.0208333 & 0 \\ 0.47593 + 3.16777i & 0.345833 - 0.0654498i & -0.0277778 & 0 \end{pmatrix}, \quad (9.30)$$

$$f_{3mn}^{-1} = \begin{pmatrix} 5.93899 - 4.25707i & 0.894934 - 0.785398i & 0.0416667 - 0.261799i & -0.0208333 \\ -12.6171 + 5.23881i & -3.14857 + 1.37445i & 0.0833333 + 1.1781i & 0.125 \\ 28.0375 - 4.97419i & -0.625 - 3.92699i & -0.333333 & 0 \\ 0.722834 - 10.592i & -1.32639 + 0.19635i & 0.0833333 & 0 \\ -1.1308 - 11.6021i & -1.21319 + 0.261799i & 0.111111 & 0 \end{pmatrix}, \quad (9.31)$$

$$a_{3mn}^0 = \begin{pmatrix} -2.62273 - 1.5548i & 0.173252 - 0.253265i & 0.483095 - 0.0654498i & -0.0130208 - 0.19635i & -0.01875 \\ 8.75567 - 0.999793i & -1.65725 + 4.12201i & 0.220719 - 0.346221i & -0.0119264 + 0.261799i & 0.0322917 \\ -19.371 - 12.6559i & 9.55915 + 2.68653i & 0.134838 - 2.48709i & -0.260417 - 0.0163625i & -0.00104167 \\ -17.9008 + 7.68761i & -0.309202 - 2.65345i & -0.647859 + 0.474511i & 0.0533854 & 0 \\ -14.2314 + 18.384i & 1.04685 - 2.47155i & -0.608073 + 0.305433i & 0.0451389 & 0 \end{pmatrix}, \quad (9.32)$$

$$f_{3mn}^0 = \begin{pmatrix} 12.0371 - 3.45954i & -2.46812 + 2.07733i & -0.674523 + 0.523599i & 0.0104167 + 0.392699i & 0.0375 \\ -8.69495 + 9.45469i & 8.79664 - 2.8529i & 3.32564 + 0.365193i & -0.0334389 - 1.58716i & -0.176042 \\ 42.8319 + 48.9221i & -32.5338 - 2.03444i & 0.180674 + 8.08669i & 0.893519 + 0.0545415i & 0.00347222 \\ 67.871 - 24.3428i & 0.594441 + 8.57121i & 2.23582 - 1.5708i & -0.1875 & 0 \\ 56.0738 - 59.3654i & -3.77677 + 7.8142i & 2.0423 - 1.00356i & -0.163194 & 0 \end{pmatrix}, \quad (9.33)$$

$$a_{5mn}^{-2} = \begin{pmatrix} -0.392699i & -0.0625 & 0 \\ 0.541217 + 0.981748i & 0.15625 - 0.19635i & -0.0208333 \\ 0.111111 - 0.261799i & -0.0416667 & 0 \\ 0.00520833 - 0.19635i & -0.03125 & 0 \\ -0.0444444 - 0.261799i & -0.0416667 & 0 \end{pmatrix}, \quad (9.34)$$

$$f_{5mn}^{-2} = \begin{pmatrix} 0.375 + 1.5708i & 0.25 & 0 \\ -2.72737 - 2.74889i & -0.4375 + 0.785398i & 0.0833333 \\ -0.194444 + 1.0472i & 0.166667 & 0 \\ 0.166667 + 0.785398i & 0.125 & 0 \\ 0.427778 + 1.0472i & 0.166667 & 0 \end{pmatrix}, \quad (9.35)$$

$$a_{5mn}^{-1} = \begin{pmatrix} 1 & +0.785398i & 0.145833 & 0 \\ -5.1927 - 4.16534i & -2.19442 - 1.66897i & -0.333333 + 0.621774i & 0.0651042 \\ 14.2336 + 15.6207i & 2.31944 - 3.92699i & -0.375 & 0 \\ 4.56707 - 5.24417i & -0.842448 - 0.19635i & 0.0104167 & 0 \\ 3.60946 - 5.03964i & -0.735417 - 0.261799i & 0.0138889 & 0 \end{pmatrix}, \quad (9.36)$$

$$f_{5mn}^{-1} = \begin{pmatrix} -10.4558 - 1.69605i & -2.47737 - 0.785398i & -0.333333 + 0.523599i & 0.0416667 \\ 26.111 + 8.4445i & 7.07997 + 2.06167i & 0.65625 - 2.0944i & -0.229167 \\ -61.2467 - 48.7383i & -7.46528 + 15.708i & 1.5 & 0 \\ -12.9967 + 24.7837i & 3.69444 + 0.294524i & -0.09375 & 0 \\ -7.20051 + 22.1002i & 2.87569 + 0.392699i & -0.125 & 0 \end{pmatrix}, \quad (9.37)$$

$$a_{5mn}^0 = \begin{pmatrix} -4.06365 + 0.287461i & -3.71603 + 3.84447i & 0.682067 - 0.261799i & -0.130208 - 0.0654498i & -0.00416667 \\ 25.1275 - 20.6835i & 4.44577 - 14.0329i & 0.328536 + 1.88167i & 0.39974 - 0.695405i & -0.0833333 \\ -57.4362 + 58.1576i & -4.72635 - 8.64175i & -3.3049 + 5.90139i & 0.750868 + 0.0163625i & 0.00104167 \\ 55.3826 + 21.4733i & -4.15271 - 5.49233i & 0.259693 + 0.916298i & 0.0651042 & 0 \\ 63.0421 + 29.5963i & 3.75148 - 5.13345i & 0.190741 - 0.501782i & -0.0503472 & 0 \end{pmatrix}, \quad (9.38)$$

$$f_{5mn}^0 = \begin{pmatrix} 7.61581 - 31.9124i & 4.025 - 11.0582i & 0.755745 + 1.309i & 0.354167 - 0.654498i & -0.0666667 \\ -20.2979 + 96.5113i & -17.6377 + 33.0546i & -1.58512 - 1.96349i & -0.648438 + 2.07803i & 0.269792 \\ 144.62 - 285.148i & 5.75246 + 29.3679i & 10.8098 - 20.0204i & -2.71817 - 0.0545415i & -0.00347222 \\ -208.708 + 69.8459i & 43.976 + 12.0788i & -2.41291 - 6.02139i & -0.408854 & 0 \\ -202.565 - 142.899i & -36.4801 + 9.22952i & -1.89641 + 5.45415i & 0.527778 & 0 \end{pmatrix}, \quad (9.39)$$

$$a_{7mn}^{-1} = \begin{pmatrix} -0.0443832 & 0 & 0 & 0 \\ 0.599504 + 0.956145i & 0.152175 & 0 & 0 \\ -2.18369 - 1.39626i & -0.222222 + 0.523599i & 0.0555556 & 0 \\ -0.0868056 + 0.785398i & 0.125 & 0 & 0 \\ 0.178125 + 0.523599i & 0.0833333 & 0 & 0 \end{pmatrix}, \quad (9.40)$$

$$a_{7mn}^0 = \begin{pmatrix} -0.196903 & 0.0665749 & 0 & 0 & 0 \\ -3.79152 + 0.92215i & -0.752492 + 0.519332i & -0.0970723 & 0 & 0 \\ 8.18238 - 1.52317i & 0.154474 - 1.32061i & 0.082101 - 0.1309i & -0.0520833 & 0 \\ -6.73632 - 3.25977i & -0.3886 + 0.981748i & -0.0208333 & 0 & 0 \\ -4.72912 + 1.86718i & 0.0299841 + 0.368155i & -0.0442708 & 0 & 0 \end{pmatrix}, \quad (9.41)$$

$$f_{7mn}^0 = \begin{pmatrix} -0.57954 + 1.19252i & 0.189795 & 0 & 0 & 0 \\ -1.86758 - 7.93934i & 0.586965 + 0.500821i & 0.0531387 - 0.589049i & -0.046875 & 0 \\ 3.78214 + 5.78728i & 1.675 - 0.922478i & -0.097878 - 0.239983i & -0.0190972 & 0 \\ 1.4128 - 1.21173i & -0.192853 - 0.490874i & -0.0520833 & 0 & 0 \\ 0.136517 - 1.4353i & -0.228435 - 0.0818123i & -0.00868056 & 0 & 0 \end{pmatrix}, \quad (9.42)$$

$$a_{9mn}^{-1} = \begin{pmatrix} -0.4375 & 0 & 0 & 0 \\ 0.198715 - 3.19851i & -0.509058 & 0 & 0 \\ -0.576689 + 2.61799i & 0.416667 & 0 & 0 \\ 0.697917 & 0 & 0 & 0 \\ 0.500463 & 0 & 0 & 0 \end{pmatrix}, \quad (9.43)$$

$$f_{9mn}^{-1} = \begin{pmatrix} 0.75 & 0 & 0 & 0 \\ -0.75 + 4.71239i & 0.75 & 0 & 0 \\ 0.833333 - 3.14159i & -0.5 & 0 & 0 \\ -0.75 & 0 & 0 & 0 \\ -0.5 & 0 & 0 & 0 \end{pmatrix}, \quad (9.44)$$

$$a_{9mn}^0 = \begin{pmatrix} -0.790823 - 1.88819i & 0.355736 & 0 & 0 & 0 \\ 21.8428 - 9.06134i & -1.74023 - 0.772597i & 0.427083 & 0 & 0 \\ -31.3912 - 8.40017i & 1.58427 + 5.0458i & 0.118709 - 0.654498i & -0.0520833 & 0 \\ 9.63742 + 23.1565i & 2.6386 - 4.51604i & -0.479167 & 0 & 0 \\ 14.2629 + 7.03331i & 0.368692 - 3.50157i & -0.371528 & 0 & 0 \end{pmatrix}, \quad (9.45)$$

$$f_{9mn}^0 = \begin{pmatrix} 1.75712 + 2.35619i & -0.75 & 0 & 0 & 0 \\ -25.2637 + 23.5864i & 3.02834 - 1.79275i & -0.940217 + 0.589049i & 0.046875 & 0 \\ 21.9485 - 5.32201i & -2.85095 - 0.550144i & 0.441628 + 0.239983i & 0.0190972 & 0 \\ -7.86975 - 15.318i & -1.31293 + 3.04342i & 0.322917 & 0 & 0 \\ -12.2499 - 4.25566i & 0.072691 + 2.78162i & 0.295139 & 0 & 0 \end{pmatrix}. \quad (9.46)$$

Chapter 10

Complete Bremsstrahlung Corrections to the $\mathcal{O}_2 - \mathcal{O}_7$ Interference Contribution for $B \rightarrow X_s \gamma \gamma$

We have encountered FCNCs many times during this thesis and have emphasized the necessity for precise SM predictions of the single radiative decay $\bar{B} \rightarrow X_s \gamma$ in the previous chapter. Even though its branching ratio is much larger than the one of the double radiative decay $\bar{B} \rightarrow X_s \gamma \gamma$, the latter has some distinct advantages. The current-current operators $\mathcal{O}_{1,2}$ already contribute at LO to this process, leading to interesting interference patterns with the dipole operator \mathcal{O}_7 . Therefore, potential NP contributions to \mathcal{O}_2 should be clearly visible not only at the level of the branching ratio but also in the (double) differential decay width. A precise determination of $\text{Br}[\bar{B} \rightarrow X_s \gamma \gamma]$ is also desirable with regards to the planned experiments at Belle II [486, 503].

In this chapter, we calculate bremsstrahlung corrections to the $\mathcal{O}_2 - \mathcal{O}_7$ interference contribution³⁶ associated with the double differential decay with $d\Gamma/ds_1 ds_2$ of this process, where $s_i = (p_b - q_i)^2/m_b^2$. Here, p_b corresponds to the momentum of the b quark and q_i are the momenta of the individual photons. We will first give an overview of the current status of the calculation, proceed with some details about our calculation and then present our results.

10.1 Current Status

The LL results for the branching ratio of $\bar{B} \rightarrow X_s \gamma \gamma$ have been known for a long time [504–507] and are summarized in Ref. [508]. Concerning NLL contributions, the numerically dominant self-interference contribution of the dipole operator \mathcal{O}_7 has been worked out in Refs. [509, 510] in a certain approximation and was completed in Ref. [508]. The self-interference of the chromomagnetic dipole operator \mathcal{O}_8 was computed in Ref. [511]. A relevant contribution that has not yet been calculated is the $\mathcal{O}_2 - \mathcal{O}_7$ interference contribution at $\mathcal{O}(\alpha_s)$, which is the task of this chapter. One of the main challenges of this endeavor is the treatment of singularities stemming from collinear photon or gluon emissions. In principle this requires nonperturbative methods such as fragmentation functions, which however suffer from experimental uncertainties. Therefore, following the argumentation of Refs. [508, 510, 512], we will use the strange quark mass m_s as a regulator and interpret it to be a constituent mass and vary it in the typical range

³⁶Even though not explicitly mentioned in this chapter, we also include the $\mathcal{O}_1 - \mathcal{O}_7$ interference contribution in our numerical analysis, which can be obtained from the $\mathcal{O}_2 - \mathcal{O}_7$ contribution in a straightforward manner.

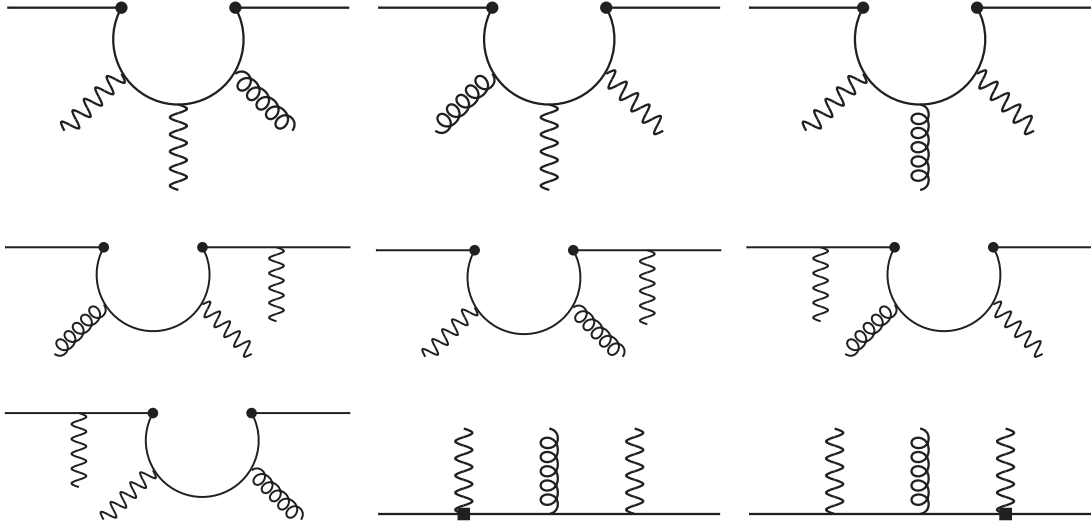


Figure 10.1: Diagrams associated with the operator \mathcal{O}_2 and \mathcal{O}_7 contributing to $b \rightarrow s \gamma \gamma g$. Diagrams not shown explicitly here are obtained by an exchange of the photon momenta.

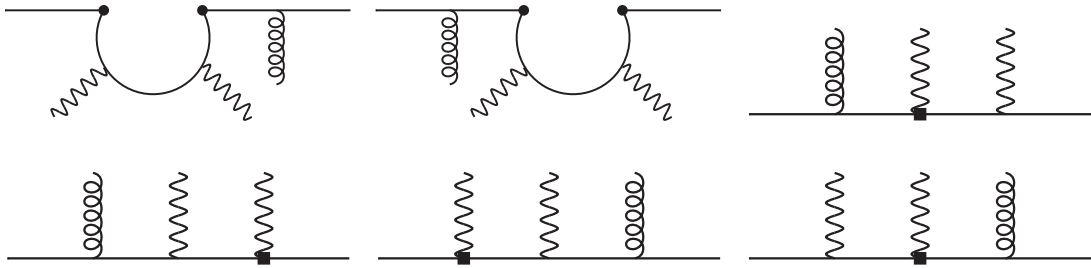


Figure 10.2: Diagrams associated with the operator \mathcal{O}_2 and \mathcal{O}_7 contributing to $b \rightarrow s \gamma \gamma g$. Interferences among these diagrams give rise to the IR singularities. Diagrams not shown explicitly here are obtained by an exchange of the photon momenta.

of 400-600 MeV [513]. This method has been employed previously [508, 510–512, 514] and is expected to give comparable results as the one using fragmentation functions.

10.2 Theoretical Framework and Calculation

The $b \rightarrow s \gamma \gamma$ transitions can be described by the same effective Hamiltonian as $b \rightarrow s \gamma$, given in Eq. (9.3). In the previous chapter we saw that the Wilson coefficients for a NLL calculation are available to sufficient precision. This is not true for the matrix elements $\langle s \gamma \gamma | \mathcal{O}_i | b \rangle$ and $\langle s \gamma \gamma g | \mathcal{O}_i | b \rangle$ which to NLL precision have so far only been worked out for the self-interference contributions of \mathcal{O}_7 and \mathcal{O}_8 . In this work we focus on the four particle final state $b \rightarrow s \gamma \gamma g$, i.e. on bremsstrahlung corrections to $b \rightarrow s \gamma \gamma$. To be more precise, we want to work out its contribution to the double differential decay width $d\Gamma/ds_1 ds_2$ of the branching ratio of $\bar{B} \rightarrow X_s \gamma \gamma$, where

$$s_1 = \frac{(p_b - q_1)^2}{m_b^2}, \quad s_2 = \frac{(p_b - q_2)^2}{m_b^2}, \quad (10.1)$$

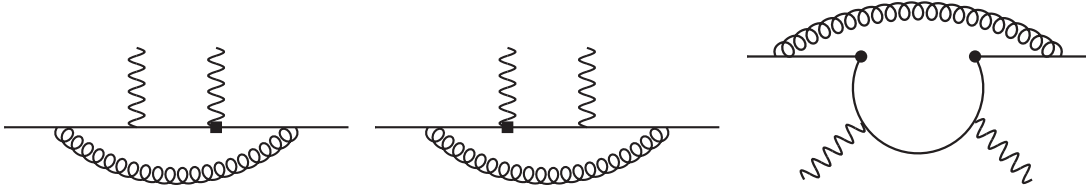


Figure 10.3: Virtual corrections associated with the operator \mathcal{O}_7 and \mathcal{O}_2 . These diagrams in addition to counterterm insertions cancel the IR singularities. Diagrams not shown explicitly here are obtained by an exchange of the photon momenta.

with p_b being the b quark momentum and q_i the momenta of the photons. Furthermore we write the normalized total squared hadronic mass as

$$s_3 = \frac{(p_s + k)^2}{m_b^2}, \quad (10.2)$$

where p_s and k are the momenta of the strange quark and the gluon, respectively. Writing $x_4 = m_s^2/m_b^2$ we see that $s_i > x_4 > 0$ which avoids collinear singularities for the photons and the gluon.

In total there are 18 diagrams associated with the operator \mathcal{O}_2 and 12 diagrams associated with \mathcal{O}_7 that contribute to $b \rightarrow s\gamma\gamma g$, leading to a total of 196 interference terms, see Figs. 10.1 and 10.2. The infrared singularities arise from interference terms of diagrams where the gluon is radiated from an external leg as depicted in Fig. 10.2. Note that interferences with only one radiation from an external leg are IR finite. We write the bremsstrahlung corrections to the double differential spectrum as

$$\frac{d\Gamma_{(1,2)7}^{\text{brems}}}{ds_1 ds_2} = \frac{d\Gamma_{(1,2)7}^{\text{hard}}}{ds_1 ds_2} + \frac{d\Gamma_{(1,2)7}^{\text{soft}}}{ds_1 ds_2}, \quad (10.3)$$

where $d\Gamma_{(1,2)7}^{\text{soft}}/ds_1 ds_2$ contains the IR singularities. We worked this part out analytically, using the soft gluon approximation described in Sec. 1.3.4, and obtain

$$\frac{d\Gamma_{(1,2)7}^{\text{soft}}}{ds_1 ds_2} = \frac{d\Gamma_{(1,2)7}^{\text{LO}}}{ds_1 ds_2} (I_{11}(\mu, \omega, \epsilon) + I_{22}(\mu, \omega, \epsilon) - 2I_{12}(\mu, \omega, \epsilon)), \quad (10.4)$$

where $d\Gamma_{(1,2)7}^{\text{LO}}/ds_1 ds_2$ is the leading order contribution of the $\mathcal{O}_{1,2} - \mathcal{O}_7$ interference contribution whose analytical form can be found e.g. in Ref. [508]. After the application of the approximation, the gluon is excluded from the phase space and the soft function is automatically in double differential form. The functions $I(\mu, \omega, \epsilon)$ explicitly contain the $1/\epsilon_{\text{IR}}$ poles and are given in Appendix 10.3. One easily verifies that the IR singularities are canceled by the UV divergences arising from the virtual corrections depicted in Fig. 10.3 and counterterm insertions on the LO contribution. In the soft gluon approximation, a cut is applied on the gluon momentum, which we restrict to be smaller than some energy ω , i.e. $|k| < \omega$. The finite part of the soft expression is dependent on this cutoff, which also appears in the hard part. There, the gluon energy is required to be larger than this cutoff, i.e. $|k| > \omega$ and therefore, IR singularities are avoided. In principle, one only needs to apply this cutoff to the interferences that are susceptible to those IR divergences. For computational convenience however, we applied this cutoff to all interferences and made sure that our numerical simulation remained unchanged for different small values of ω . This also ensures the validity of the soft gluon approximation. Concerning the hard

contribution, we used the phase space formulas derived in Ref. [515] and adopted to our case in Ref. [508], which we give explicitly in the Appendix 10.3. In that way the phase space is described by five dimensionless variables (including s_1 , s_2 and s_3), three of which we integrated numerically to obtain the double differential spectrum. We used the CUBA library [516] for the Monte-Carlo integration of the phase space and the Fortran library Collier [517] to numerically calculate the one-loop integrals, where we also did some crosschecks with LoopTools [518]. Our results for the bremsstrahlung corrections only are shown in Fig. 10.4 for different values of the renormalization scale μ and the constituent mass m_s . The results contain the complete bremsstrahlung corrections as defined in Eqs. (10.3) and (10.4) where we only removed the IR singularities, since these will eventually cancel once virtual corrections are also taken into account. We find a sizable m_s dependence in the region where the contribution is the largest. The effects on the complete double differential spectrum are shown in Fig. 10.5 and the relative effect is shown in Fig. 10.6. While the effect of the bremsstrahlung corrections calculated in this work are small for $\mu = m_b/2$, this changes for larger values of μ , where the corrections reach up to 15% in a certain region of the spectrum. We emphasize that while our calculations without the inclusion of $\mathcal{O}(\alpha_s)$ virtual corrections are not very meaningful by themselves, the large relative effect of the bremsstrahlung contributions on the complete double differential spectrum should provide enough argumentation for the necessity of a completion of the NLL calculation.

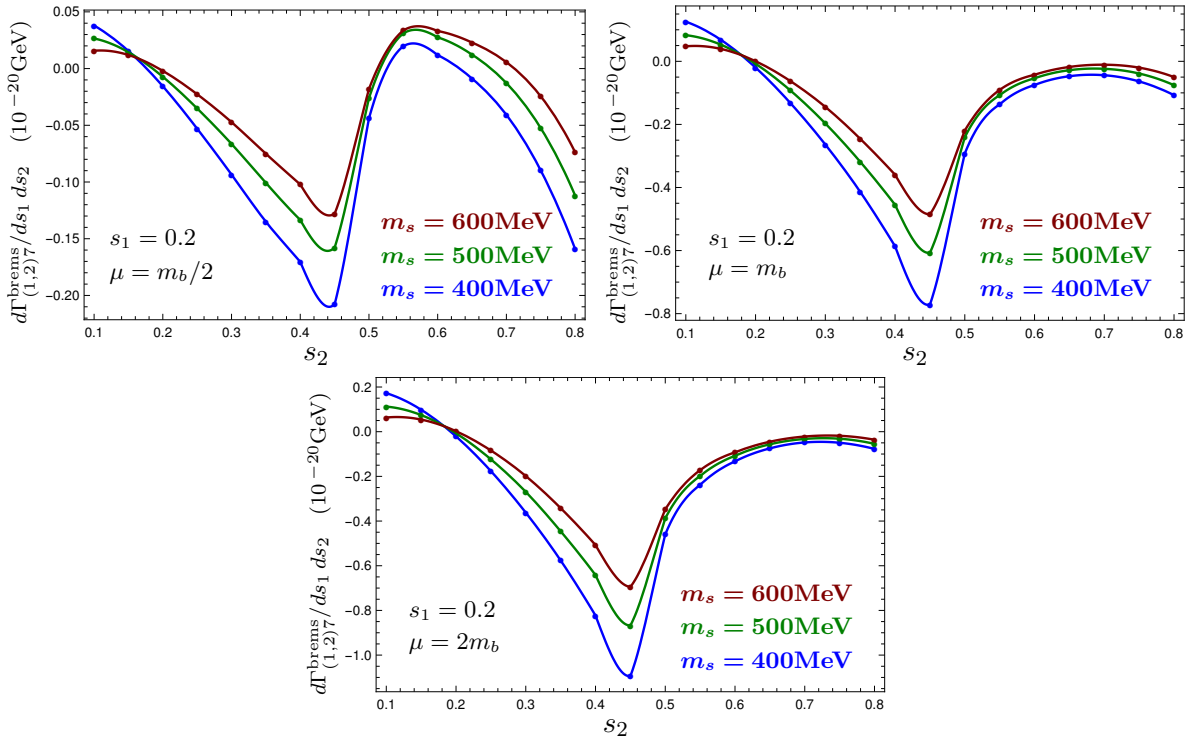


Figure 10.4: Overall contribution of the $\mathcal{O}(\alpha_s)$ bremsstrahlung corrections for the $\mathcal{O}_{1,2} - \mathcal{O}_7$ interference contribution to the double differential spectrum $d\Gamma[B \rightarrow X_s \gamma \gamma]/ds_1 ds_2$ for different values of the constituent mass m_s and renormalization scale μ for s_1 fixed at $s_1 = 0.2$. The points are exact data points while the lines are interpolated functions.

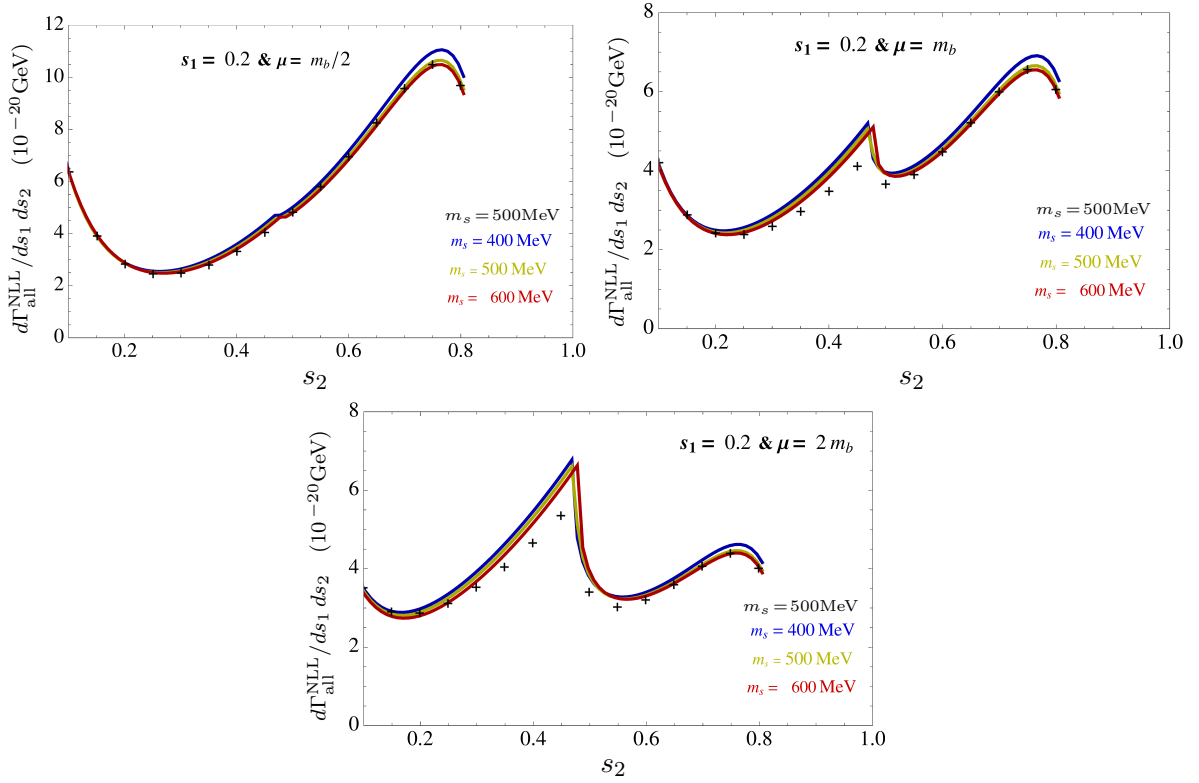


Figure 10.5: NLL spectrum for exact m_s based on all operator contributions available. The colored lines are taken from Ref. [508] and do not include the corrections calculated in this work; the black crosses represent the complete double differential spectrum when our bremsstrahlung corrections are added. For simplicity, we only show the data points for $m_s = 500$ MeV.

10.3 Appendix

Soft Functions

The analytic form of the functions introduced in Eq. 10.4 reads

$$\begin{aligned}
 I_{11} &= -\frac{1}{4\pi^2\epsilon} + \frac{1}{4\pi^2} \left[\log\left(\frac{4\omega^2}{\mu^2}\right) + \frac{p_s^0}{p_s} \log\left(\frac{p_s^0 - p_s}{p_s^0 + p_s}\right) \right], \\
 I_{22} &= -\frac{1}{4\pi^2\epsilon} + \frac{1}{4\pi^2} \left[\log\left(\frac{4\omega^2}{\mu^2}\right) - 2 \right], \\
 I_{12} &= \frac{1}{8\pi^2} \left(\frac{1}{\epsilon} \log\left(\frac{p_s^0 - p_s}{p_s^0 + p_s}\right) - \log\left(\frac{4\omega^2}{\mu^2}\right) \log\left(\frac{p_s^0 - p_s}{p_s^0 + p_s}\right) + \text{Li}_2\left(\frac{2p_s}{p_s - p_s^0}\right) - \text{Li}_2\left(\frac{2p_s}{p_s + p_s^0}\right) \right),
 \end{aligned} \tag{10.5}$$

where $p_s = |\vec{p}_s|$ with \vec{p}_s the three-momentum of the strange quark and p_s^0 is its energy. In the rest frame of the b quark, we can write

$$p_s^0 = \frac{m_b}{2}(s_1 + s_2), \tag{10.6}$$

and as usual $p_s = \sqrt{p_s^{02} - m_s^2}$.

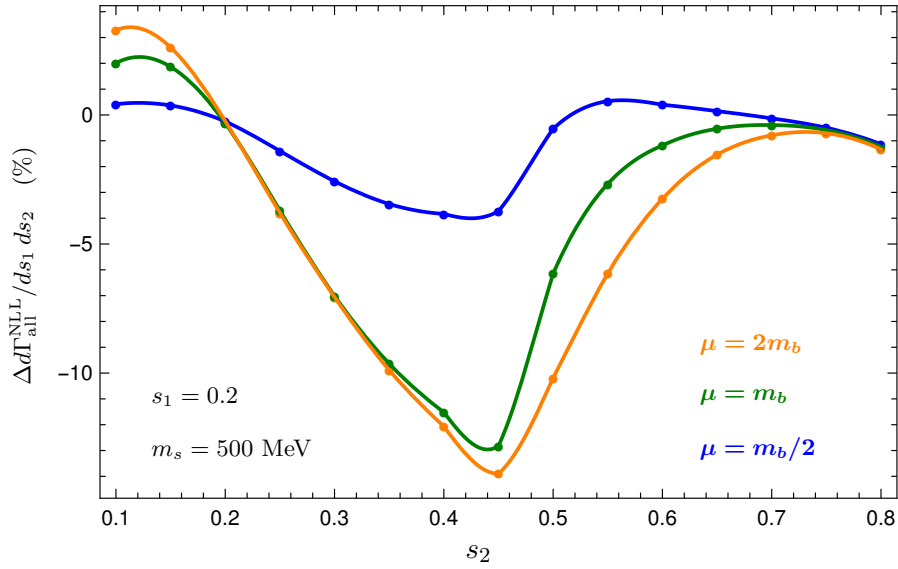


Figure 10.6: Relative effect of the bremsstrahlung corrections calculated in this work on the complete NLL double differential spectrum in % for s_1 fixed at $s_1 = 0.2$ and $m_s = 500$ MeV for different values of the renormalization scale μ . The data points are exact values while the lines represent interpolated functions.

Phase Space Formula for the Four Particle Final State

The differential decay width Γ of a particle with mass M decaying into n final states can always be written as

$$d\Gamma = \frac{1}{2m} \overline{|M|^2} D\Phi(1 \rightarrow n), \quad (10.7)$$

where $\overline{|M|^2}$ is the squared matrix element, summed and averaged over spins and colors of the initial and final state particles and m is the mass of the decaying particle. Derived in Ref. [515] and adopted to our case in Ref. [508], the four particle phase space can be written in terms of five dimensionless quantities λ_i which all run independently in the interval $[0, 1]$

$$\begin{aligned} d\Phi(1 \rightarrow 4) = & (4\pi)^{\frac{-3d}{2}} m_b^{3d-8} \frac{2^{2d-7} \Gamma\left(\frac{d-2}{2}\right)}{(d-3)\Gamma(d-3)^2} (1-x_4)^{3d-7} [(1-\lambda_1)(1-\lambda_2)\lambda_2]^{d-3} \\ & \times \lambda_1^{2d-5} [\lambda_1(1-x_4) + x_4](\lambda_1\lambda_2(1-x_4) + x_4)^{\frac{2-d}{2}} \\ & \times [(1-\lambda_3)\lambda_3(1-\lambda_4)\lambda_4]^{\frac{d-4}{2}} [(1-\lambda_5)\lambda_5]^{\frac{d-5}{2}} d\lambda_1 d\lambda_2 d\lambda_3 d\lambda_4 d\lambda_5, \end{aligned} \quad (10.8)$$

where $x_4 = m_s^2/m_b^2$ and $d = 4 - 2\epsilon$. All scalar products in our application can be expressed in terms of the variables $s_{ij} = (p_i + p_j)^2/m_b^2$ and $s_{ijk} = (p_i + p_j + p_k)^2/m_b^2$ with $p_1 = q_1$, $p_2 = q_2$, $p_3 = k$ and $p_4 = p_s$, which relates to the variables s_1 , s_2 and s_3 of the main text as $s_{234} = s_1$,

$s_{134} = s_2$ and $s_{34} = s_3$. The parameters λ_i are related to s_{ij} and s_{ijk} via

$$\begin{aligned}
 s_{234} &= \lambda_1(1 - x_4) + x_4 , \\
 s_{34} &= \lambda_1\lambda_2(1 - x_4) + x_4 , \\
 s_{23} &= \frac{\lambda_1^2(1 - \lambda_2)\lambda_2\lambda_4(1 - x_4)^2}{\lambda_1\lambda_2(1 - x_4) + x_4} , \\
 s_{134} &= \frac{\lambda_1(1 - x_4) [\lambda_2(1 - (1 - \lambda_1)\lambda_3(1 - x_4)) + \lambda_3(1 - \lambda_1)(1 - x_4)] + x_4}{\lambda_1(1 - x_4) + x_4} , \\
 s_{13} &= (s_{13}^+ - s_{13}^-)\lambda_5 + s_{13}^- ,
 \end{aligned} \tag{10.9}$$

where

$$\begin{aligned}
 s^\pm &= \frac{(1 - \lambda_1)\lambda_1\lambda_2(1 - x_4)^2}{(\lambda_1 + x_4 - \lambda_1x_4)(\lambda_1\lambda_2 + x_4 - \lambda_1\lambda_2x_4)} \left\{ x_4 [(1 - \lambda_3)(1 - \lambda_4) + \lambda_3\lambda_4] \right. \\
 &\quad \left. + (1 - x_4)\lambda_1 [\lambda_2(1 - \lambda_3)(1 - \lambda_4) + \lambda_3\lambda_4] \right. \\
 &\quad \left. \mp 2\sqrt{(1 - \lambda_3)\lambda_3(1 - \lambda_4)\lambda_4(\lambda_1 + x_4 - \lambda_1x_4)(\lambda_1\lambda_2 + x_4 - \lambda_1\lambda_2x_4)} \right\} .
 \end{aligned} \tag{10.10}$$

Bibliography

- [1] J. Thomson, *Cathode rays*, *Phil. Mag. Ser. 5* **44** (1897) 293.
- [2] E. Rutherford, *The scattering of alpha and beta particles by matter and the structure of the atom*, *Phil. Mag. Ser. 6* **21** (1911) 669.
- [3] N. Bohr, *On the Constitution of Atoms and Molecules*, *Phil. Mag. Ser. 6* **26** (1913) 1.
- [4] J. Chadwick, *Possible Existence of a Neutron*, *Nature* **129** (1932) 312.
- [5] A. Einstein, *Concerning an heuristic point of view toward the emission and transformation of light*, *Annalen Phys.* **17** (1905) 132.
- [6] A. H. Compton, *A Quantum Theory of the Scattering of X-rays by Light Elements*, *Phys. Rev.* **21** (1923) 483.
- [7] W. Heisenberg, *A quantum-theoretical reinterpretation of kinematic and mechanical relations*, *Z. Phys.* **33** (1925) 879.
- [8] E. Schrödinger, *Quantisierung als Eigenwertproblem*, *Annalen Phys.* **386** (1926) 109.
- [9] N. Bohr, *The Quantum Postulate and the Recent Development of Atomic Theory*, *Nature* **121** (1928) 580.
- [10] P. A. Dirac, *The quantum theory of the electron*, *Proc. Roy. Soc. Lond. A* **117** (1928) 610.
- [11] C. D. Anderson, *The Apparent Existence of Easily Deflectable Positives*, *Science* **76** (1932) 238.
- [12] O. Chamberlain, E. Segre, C. Wiegand and T. Ypsilantis, *Observation of Anti-protons*, *Phys. Rev.* **100** (1955) 947.
- [13] W. Pauli, *Dear radioactive ladies and gentlemen*, *Phys. Today* **31N9** (1978) 27.
- [14] G. Danby, J. Gaillard, K. Goulianos, L. Lederman, N. Mistry, M. Schwartz et al., *High-energy neutrino interaction in matter*, in *11th International Conference on High-energy Physics*, pp. 809–817, 1962.
- [15] M. Gell-Mann and Y. Ne'eman, *The Eightfold way: a review with a collection of reprints*, .
- [16] M. Gell-Mann, *A Schematic Model of Baryons and Mesons*, *Phys. Lett.* **8** (1964) 214.
- [17] A. Petermann, *Propriétés de l'étrangeté et une formule de masse pour les mésons vectoriels*, *Nucl. Phys.* **63** (1965) 349.

- [18] G. Zweig, *An $SU(3)$ model for strong interaction symmetry and its breaking. Version 2*, pp. 22–101. 2, 1964.
- [19] O. Greenberg, *Spin and Unitary Spin Independence in a Paraquark Model of Baryons and Mesons*, *Phys. Rev. Lett.* **13** (1964) 598.
- [20] M. Breidenbach, J. I. Friedman, H. W. Kendall, E. D. Bloom, D. Coward, H. DeStaebler et al., *Observed behavior of highly inelastic electron-proton scattering*, *Phys. Rev. Lett.* **23** (1969) 935.
- [21] SLAC-SP-017 collaboration, *Discovery of a Narrow Resonance in e^+e^- Annihilation*, *Phys. Rev. Lett.* **33** (1974) 1406.
- [22] J. Aubert et al., *Experimental observation of a heavy Particle J*, *Adv. Exp. Phys.* **5** (1976) 128.
- [23] S. Glashow, J. Iliopoulos and L. Maiani, *Weak Interactions with Lepton-Hadron Symmetry*, *Phys. Rev. D* **2** (1970) 1285.
- [24] M. Kobayashi and T. Maskawa, *CP Violation in the Renormalizable Theory of Weak Interaction*, *Prog. Theor. Phys.* **49** (1973) 652.
- [25] N. Cabibbo, *Unitary Symmetry and Leptonic Decays*, *Phys. Rev. Lett.* **10** (1963) 531.
- [26] J. H. Christenson, J. W. Cronin, V. L. Fitch and R. Turlay, *Evidence for the 2π Decay of the K_2^0 Meson*, *Phys. Rev. Lett.* **13** (1964) 138.
- [27] R. Feynman, *Space-time approach to nonrelativistic quantum mechanics*, *Rev. Mod. Phys.* **20** (1948) 367.
- [28] J. S. Schwinger, *Quantum electrodynamics. I A covariant formulation*, *Phys. Rev.* **74** (1948) 1439.
- [29] J. S. Schwinger, *On Quantum electrodynamics and the magnetic moment of the electron*, *Phys. Rev.* **73** (1948) 416.
- [30] S. Tomonaga, *On a relativistically invariant formulation of the quantum theory of wave fields*, *Prog. Theor. Phys.* **1** (1946) 27.
- [31] C.-N. Yang and R. L. Mills, *Conservation of Isotopic Spin and Isotopic Gauge Invariance*, *Phys. Rev.* **96** (1954) 191.
- [32] J. Goldstone, *Field Theories with Superconductor Solutions*, *Nuovo Cim.* **19** (1961) 154.
- [33] J. Goldstone, A. Salam and S. Weinberg, *Broken Symmetries*, *Phys. Rev.* **127** (1962) 965.
- [34] P. W. Higgs, *Broken Symmetries and the Masses of Gauge Bosons*, *Phys. Rev. Lett.* **13** (1964) 508.
- [35] F. Englert and R. Brout, *Broken Symmetry and the Mass of Gauge Vector Mesons*, *Phys. Rev. Lett.* **13** (1964) 321.
- [36] S. Weinberg, *A Model of Leptons*, *Phys. Rev. Lett.* **19** (1967) 1264.
- [37] A. Salam, *Weak and Electromagnetic Interactions*, *Conf. Proc. C* **680519** (1968) 367.

-
- [38] S. Glashow, *Partial Symmetries of Weak Interactions*, *Nucl. Phys.* **22** (1961) 579.
- [39] A. Salam and J. C. Ward, *Electromagnetic and weak interactions*, *Phys. Lett.* **13** (1964) 168.
- [40] G. 't Hooft, *Renormalizable Lagrangians for Massive Yang-Mills Fields*, *Nucl. Phys. B* **35** (1971) 167.
- [41] CDF collaboration, *Observation of top quark production in $\bar{p}p$ collisions*, *Phys. Rev. Lett.* **74** (1995) 2626 [[hep-ex/9503002](#)].
- [42] ATLAS collaboration, *Observation of a new particle in the search for the Standard Model Higgs boson with the ATLAS detector at the LHC*, *Phys. Lett. B* **716** (2012) 1 [[1207.7214](#)].
- [43] CMS collaboration, *Observation of a New Boson at a Mass of 125 GeV with the CMS Experiment at the LHC*, *Phys. Lett. B* **716** (2012) 30 [[1207.7235](#)].
- [44] S. Weinberg, *The Making of the standard model*, *Eur. Phys. J. C* **34** (2004) 5 [[hep-ph/0401010](#)].
- [45] A. Crivellin, C. Greub, D. Müller and F. Saturnino, *Importance of Loop Effects in Explaining the Accumulated Evidence for New Physics in B Decays with a Vector Leptoquark*, *Phys. Rev. Lett.* **122** (2019) 011805 [[1807.02068](#)].
- [46] A. Crivellin and F. Saturnino, *Explaining the Flavor Anomalies with a Vector Leptoquark (Moriond 2019 update)*, *PoS DIS2019* (2019) 163 [[1906.01222](#)].
- [47] A. Crivellin and F. Saturnino, *Correlating tauonic B decays with the neutron electric dipole moment via a scalar leptoquark*, *Phys. Rev.* **D100** (2019) 115014 [[1905.08257](#)].
- [48] A. Crivellin, D. Mueller and F. Saturnino, *Flavor Phenomenology of the Leptoquark Singlet-Triplet Model*, *JHEP* **06** (2020) 020 [[1912.04224](#)].
- [49] A. Crivellin, D. Müller and F. Saturnino, *Leptoquarks in oblique corrections and Higgs signal strength: status and prospects*, *JHEP* **11** (2020) 094 [[2006.10758](#)].
- [50] A. Crivellin, D. Müller and F. Saturnino, *Correlating $h \rightarrow \mu^+ \mu^-$ to the Anomalous Magnetic Moment of the Muon via Leptoquarks*, [2008.02643](#).
- [51] A. Crivellin, C. Greub, D. Müller and F. Saturnino, *Scalar Leptoquarks in Leptonic Processes*, *JHEP* **02** (2021) 182 [[2010.06593](#)].
- [52] PARTICLE DATA GROUP collaboration, *Review of Particle Physics*, *PTEP* **2020** (2020) 083C01.
- [53] B. Chakraborty, C. T. H. Davies, B. Galloway, P. Knecht, J. Koponen, G. C. Donald et al., *High-precision quark masses and QCD coupling from $n_f = 4$ lattice QCD*, *Phys. Rev. D* **91** (2015) 054508 [[1408.4169](#)].
- [54] Y. Kiyo, G. Mishima and Y. Sumino, *Determination of m_c and m_b from quarkonium 1S energy levels in perturbative QCD*, *Phys. Lett. B* **752** (2016) 122 [[1510.07072](#)].
- [55] P. J. Mohr, D. B. Newell and B. N. Taylor, *CODATA Recommended Values of the Fundamental Physical Constants: 2014*, *Rev. Mod. Phys.* **88** (2016) 035009 [[1507.07956](#)].

- [56] Z. Fodor, C. Hoelbling, S. Krieg, L. Lellouch, T. Lippert, A. Portelli et al., *Up and down quark masses and corrections to Dashen's theorem from lattice QCD and quenched QED*, *Phys. Rev. Lett.* **117** (2016) 082001 [1604.07112].
- [57] L. Wolfenstein, *Parametrization of the Kobayashi-Maskawa Matrix*, *Phys. Rev. Lett.* **51** (1983) 1945.
- [58] CKMFITTER GROUP collaboration, *CP violation and the CKM matrix: Assessing the impact of the asymmetric B factories*, *Eur. Phys. J. C* **41** (2005) 1 [hep-ph/0406184].
- [59] E. Giusarma, M. Gerbino, O. Mena, S. Vagnozzi, S. Ho and K. Freese, *Improvement of cosmological neutrino mass bounds*, *Phys. Rev. D* **94** (2016) 083522 [1605.04320].
- [60] I. Esteban, M. C. Gonzalez-Garcia, A. Hernandez-Cabezudo, M. Maltoni and T. Schwetz, *Global analysis of three-flavour neutrino oscillations: synergies and tensions in the determination of θ_{23} , δ_{CP} , and the mass ordering*, *JHEP* **01** (2019) 106 [1811.05487].
- [61] B. Pontecorvo, *Inverse beta processes and nonconservation of lepton charge*, *Sov. Phys. JETP* **7** (1958) 172.
- [62] Z. Maki, M. Nakagawa and S. Sakata, *Remarks on the unified model of elementary particles*, *Prog. Theor. Phys.* **28** (1962) 870.
- [63] J. M. Pendlebury et al., *Revised experimental upper limit on the electric dipole moment of the neutron*, *Phys. Rev.* **D92** (2015) 092003 [1509.04411].
- [64] V. A. Smirnov, *Asymptotic expansions in momenta and masses and calculation of Feynman diagrams*, *Mod. Phys. Lett.* **A10** (1995) 1485 [hep-th/9412063].
- [65] K. G. Chetyrkin and F. V. Tkachov, *Integration by Parts: The Algorithm to Calculate beta Functions in 4 Loops*, *Nucl. Phys. B* **192** (1981) 159.
- [66] A. V. Kotikov, *Differential equations method: New technique for massive Feynman diagrams calculation*, *Phys. Lett. B* **254** (1991) 158.
- [67] J. M. Henn, *Multiloop integrals in dimensional regularization made simple*, *Phys. Rev. Lett.* **110** (2013) 251601 [1304.1806].
- [68] K.-T. Chen, *Iterated path integrals*, *Bull. Am. Math. Soc.* **83** (1977) 831.
- [69] J. M. Henn, *Lectures on differential equations for Feynman integrals*, *J. Phys. A* **48** (2015) 153001 [1412.2296].
- [70] A. B. Goncharov, *Multiple polylogarithms, cyclotomy and modular complexes*, 2011.
- [71] H. Frellesvig, D. Tommasini and C. Wever, *On the reduction of generalized polylogarithms to Li_n and $Li_{2,2}$ and on the evaluation thereof*, *JHEP* **03** (2016) 189 [1601.02649].
- [72] G. 't Hooft and M. J. G. Veltman, *Scalar One Loop Integrals*, *Nucl. Phys. B* **153** (1979) 365.
- [73] A. Denner, *Techniques for calculation of electroweak radiative corrections at the one loop level and results for W physics at LEP-200*, *Fortsch. Phys.* **41** (1993) 307 [0709.1075].

-
- [74] M. Bordone, G. Isidori and A. Pattori, *On the Standard Model predictions for R_K and R_{K^*}* , *Eur. Phys. J. C* **76** (2016) 440 [1605.07633].
- [75] BELLE collaboration, *Measurement of the Differential Branching Fraction and Forward-Backward Asymmetry for $B \rightarrow K^{(*)}\ell^+\ell^-$* , *Phys. Rev. Lett.* **103** (2009) 171801 [0904.0770].
- [76] BABAR collaboration, *Measurement of Branching Fractions and Rate Asymmetries in the Rare Decays $B \rightarrow K^{(*)}l^+l^-$* , *Phys. Rev. D* **86** (2012) 032012 [1204.3933].
- [77] LHCb collaboration, *Test of lepton universality using $B^+ \rightarrow K^+\ell^+\ell^-$ decays*, *Phys. Rev. Lett.* **113** (2014) 151601 [1406.6482].
- [78] LHCb collaboration, *Search for lepton-universality violation in $B^+ \rightarrow K^+\ell^+\ell^-$ decays*, *Phys. Rev. Lett.* **122** (2019) 191801 [1903.09252].
- [79] LHCb collaboration, *Test of lepton universality with $B^0 \rightarrow K^{*0}\ell^+\ell^-$ decays*, *JHEP* **08** (2017) 055 [1705.05802].
- [80] BELLE collaboration, *Test of lepton flavor universality in $B \rightarrow K^*\ell^+\ell^-$ decays at Belle*, 1904.02440.
- [81] S. Descotes-Genon, T. Hurth, J. Matias and J. Virto, *Optimizing the basis of $B \rightarrow K^*ll$ observables in the full kinematic range*, *JHEP* **05** (2013) 137 [1303.5794].
- [82] LHCb collaboration, *Measurement of Form-Factor-Independent Observables in the Decay $B^0 \rightarrow K^{*0}\mu^+\mu^-$* , *Phys. Rev. Lett.* **111** (2013) 191801 [1308.1707].
- [83] LHCb collaboration, *Angular analysis of the $B^0 \rightarrow K^{*0}\mu^+\mu^-$ decay using 3 fb^{-1} of integrated luminosity*, *JHEP* **02** (2016) 104 [1512.04442].
- [84] BELLE collaboration, *Angular analysis of $B^0 \rightarrow K^*(892)^0\ell^+\ell^-$* , in *Proceedings, LHCSki 2016 - A First Discussion of 13 TeV Results: Obergurgl, Austria, April 10-15, 2016*, 2016, 1604.04042.
- [85] BELLE collaboration, *Lepton-Flavor-Dependent Angular Analysis of $B \rightarrow K^*\ell^+\ell^-$* , *Phys. Rev. Lett.* **118** (2017) 111801 [1612.05014].
- [86] ATLAS collaboration, *Angular analysis of $B_d^0 \rightarrow K^*\mu^+\mu^-$ decays in pp collisions at $\sqrt{s} = 8\text{ TeV}$ with the ATLAS detector*, *JHEP* **10** (2018) 047 [1805.04000].
- [87] CMS collaboration, *Measurement of the P_1 and P'_5 angular parameters of the decay $B^0 \rightarrow K^{*0}\mu^+\mu^-$ in proton-proton collisions at $\sqrt{s} = 8\text{ TeV}$* , .
- [88] B. Capdevila, A. Crivellin, S. Descotes-Genon, J. Matias and J. Virto, *Patterns of New Physics in $b \rightarrow s\ell^+\ell^-$ transitions in the light of recent data*, *JHEP* **01** (2018) 093 [1704.05340].
- [89] J. Aebischer, J. Kumar, P. Stangl and D. M. Straub, *A Global Likelihood for Precision Constraints and Flavour Anomalies*, *Eur. Phys. J. C* **79** (2019) 509 [1810.07698].
- [90] W. Altmannshofer and D. M. Straub, *New physics in $b \rightarrow s$ transitions after LHC run 1*, *Eur. Phys. J. C* **75** (2015) 382 [1411.3161].

- [91] S. Descotes-Genon, L. Hofer, J. Matias and J. Virto, *Global analysis of $b \rightarrow s\ell\ell$ anomalies*, *JHEP* **06** (2016) 092 [1510.04239].
- [92] W. Altmannshofer, P. Stangl and D. M. Straub, *Interpreting Hints for Lepton Flavor Universality Violation*, *Phys. Rev.* **D96** (2017) 055008 [1704.05435].
- [93] L.-S. Geng, B. Grinstein, S. Jäger, J. Martin Camalich, X.-L. Ren and R.-X. Shi, *Towards the discovery of new physics with lepton-universality ratios of $b \rightarrow s\ell\ell$ decays*, *Phys. Rev.* **D96** (2017) 093006 [1704.05446].
- [94] W. Altmannshofer, C. Niehoff, P. Stangl and D. M. Straub, *Status of the $B \rightarrow K^*\mu^+\mu^-$ anomaly after Moriond 2017*, *Eur. Phys. J. C* **77** (2017) 377 [1703.09189].
- [95] M. Algueró, B. Capdevila, S. Descotes-Genon, P. Masjuan and J. Matias, *Are we overlooking lepton flavour universal new physics in $b \rightarrow s\ell\ell$?*, *Phys. Rev.* **D99** (2019) 075017 [1809.08447].
- [96] T. Hurth, A. Arbey, F. Mahmoudi and S. Neshatpour, *New global fits to $b \rightarrow s$ data with all relevant parameters*, *Nucl. Part. Phys. Proc.* **303-305** (2018) 2 [1812.07602].
- [97] J. Aebischer, W. Altmannshofer, D. Guadagnoli, M. Reboud, P. Stangl and D. M. Straub, *B -decay discrepancies after Moriond 2019*, *Eur. Phys. J.* **C80** (2020) 252 [1903.10434].
- [98] M. Algueró, B. Capdevila, A. Crivellin, S. Descotes-Genon, P. Masjuan, J. Matias et al., *Emerging patterns of New Physics with and without Lepton Flavour Universal contributions*, *Eur. Phys. J.* **C79** (2019) 714 [1903.09578].
- [99] A. K. Alok, A. Dighe, S. Gangal and D. Kumar, *Continuing search for new physics in $b \rightarrow s\mu\mu$ decays: two operators at a time*, *JHEP* **06** (2019) 089 [1903.09617].
- [100] M. Ciuchini, A. M. Coutinho, M. Fedele, E. Franco, A. Paul, L. Silvestrini et al., *New Physics in $b \rightarrow s\ell^+\ell^-$ confronts new data on Lepton Universality*, *Eur. Phys. J.* **C79** (2019) 719 [1903.09632].
- [101] D. Kumar, K. Kowalska and E. M. Sessolo, *Global Bayesian Analysis of new physics in $b \rightarrow s\mu\mu$ transitions after Moriond-2019*, in *17th Conference on Flavor Physics and CP Violation (FPCP 2019) Victoria, BC, Canada, May 6-10, 2019*, 2019, 1906.08596.
- [102] T. Blake, M. Gersabeck, L. Hofer, S. Jäger, Z. Liu and R. Zwicky, *Round table: Flavour anomalies in $b \rightarrow sl+l-$ processes*, *EPJ Web Conf.* **137** (2017) 01001 [1703.10005].
- [103] HFLAV collaboration, *Averages of b -hadron, c -hadron, and τ -lepton properties as of summer 2016*, *Eur. Phys. J.* **C77** (2017) 895 [1612.07233].
- [104] BABAR collaboration, *Evidence for an excess of $\bar{B} \rightarrow D^{(*)}\tau^-\bar{\nu}_\tau$ decays*, *Phys. Rev. Lett.* **109** (2012) 101802 [1205.5442].
- [105] BABAR collaboration, *Measurement of an Excess of $\bar{B} \rightarrow D^{(*)}\tau^-\bar{\nu}_\tau$ Decays and Implications for Charged Higgs Bosons*, *Phys. Rev.* **D88** (2013) 072012 [1303.0571].
- [106] BELLE collaboration, *Measurement of the branching ratio of $\bar{B} \rightarrow D^{(*)}\tau^-\bar{\nu}_\tau$ relative to $\bar{B} \rightarrow D^{(*)}\ell^-\bar{\nu}_\ell$ decays with hadronic tagging at Belle*, *Phys. Rev.* **D92** (2015) 072014 [1507.03233].

-
- [107] BELLE collaboration, *Measurement of the branching ratio of $\bar{B}^0 \rightarrow D^{*+}\tau^-\bar{\nu}_\tau$ relative to $\bar{B}^0 \rightarrow D^{*+}\ell^-\bar{\nu}_\ell$ decays with a semileptonic tagging method*, *Phys. Rev.* **D94** (2016) 072007 [1607.07923].
- [108] BELLE collaboration, *Measurement of the τ lepton polarization and $R(D^*)$ in the decay $\bar{B} \rightarrow D^*\tau^-\bar{\nu}_\tau$ with one-prong hadronic τ decays at Belle*, *Phys. Rev.* **D97** (2018) 012004 [1709.00129].
- [109] BELLE collaboration, *Measurement of $\mathcal{R}(D)$ and $\mathcal{R}(D^*)$ with a semileptonic tagging method*, 1904.08794.
- [110] LHCb collaboration, *Measurement of the ratio of branching fractions $\mathcal{B}(\bar{B}^0 \rightarrow D^{*+}\tau^-\bar{\nu}_\tau)/\mathcal{B}(\bar{B}^0 \rightarrow D^{*+}\mu^-\bar{\nu}_\mu)$* , *Phys. Rev. Lett.* **115** (2015) 111803 [1506.08614].
- [111] LHCb collaboration, *Measurement of the ratio of the $B^0 \rightarrow D^{*-}\tau^+\nu_\tau$ and $B^0 \rightarrow D^{*-}\mu^+\nu_\mu$ branching fractions using three-prong τ -lepton decays*, *Phys. Rev. Lett.* **120** (2018) 171802 [1708.08856].
- [112] LHCb collaboration, *Test of Lepton Flavor Universality by the measurement of the $B^0 \rightarrow D^{*-}\tau^+\nu_\tau$ branching fraction using three-prong τ decays*, *Phys. Rev.* **D97** (2018) 072013 [1711.02505].
- [113] LHCb collaboration, *Measurement of the ratio of branching fractions $\mathcal{B}(B_c^+ \rightarrow J/\psi\tau^+\nu_\tau)/\mathcal{B}(B_c^+ \rightarrow J/\psi\mu^+\nu_\mu)$* , *Phys. Rev. Lett.* **120** (2018) 121801 [1711.05623].
- [114] A. Y. Anisimov, I. M. Narodetsky, C. Semay and B. Silvestre-Brac, *The B_c meson lifetime in the light front constituent quark model*, *Phys. Lett. B* **452** (1999) 129 [hep-ph/9812514].
- [115] V. V. Kiselev, *Exclusive decays and lifetime of B_c meson in QCD sum rules*, hep-ph/0211021.
- [116] M. A. Ivanov, J. G. Korner and P. Santorelli, *Exclusive semileptonic and nonleptonic decays of the B_c meson*, *Phys. Rev. D* **73** (2006) 054024 [hep-ph/0602050].
- [117] E. Hernandez, J. Nieves and J. M. Verde-Velasco, *Study of exclusive semileptonic and non-leptonic decays of B_c - in a nonrelativistic quark model*, *Phys. Rev. D* **74** (2006) 074008 [hep-ph/0607150].
- [118] M. Blanke, A. Crivellin, S. de Boer, M. Moscati, U. Nierste, I. Nišandžić et al., *Impact of polarization observables and $B_c \rightarrow \tau\nu$ on new physics explanations of the $b \rightarrow c\tau\nu$ anomaly*, *Phys. Rev.* **D99** (2019) 075006 [1811.09603].
- [119] C. Murgui, A. Peñuelas, M. Jung and A. Pich, *Global fit to $b \rightarrow c\tau\nu$ transitions*, 1904.09311.
- [120] R.-X. Shi, L.-S. Geng, B. Grinstein, S. Jäger and J. Martin Camalich, *Revisiting the new-physics interpretation of the $b \rightarrow c\tau\nu$ data*, *JHEP* **12** (2019) 065 [1905.08498].
- [121] M. Blanke, A. Crivellin, T. Kitahara, M. Moscati, U. Nierste and I. Nišandžić, *Addendum to “Impact of polarization observables and $B_c \rightarrow \tau\nu$ on new physics explanations of the $b \rightarrow c\tau\nu$ anomaly”*, *Phys. Rev.* **D100** (2019) 035035 [1905.08253].

- [122] S. Kumbhakar, A. K. Alok, D. Kumar and S. U. Sankar, *A global fit to $b \rightarrow c\tau\bar{\nu}$ anomalies after Moriond 2019*, in *2019 European Physical Society Conference on High Energy Physics (EPS-HEP2019) Ghent, Belgium, July 10-17, 2019*, 2019, 1909.02840.
- [123] MUON G-2 collaboration, *Final Report of the Muon E821 Anomalous Magnetic Moment Measurement at BNL*, *Phys. Rev.* **D73** (2006) 072003 [[hep-ex/0602035](#)].
- [124] T. Aoyama et al., *The anomalous magnetic moment of the muon in the Standard Model*, 2006.04822.
- [125] T. Aoyama, T. Kinoshita and M. Nio, *Revised and Improved Value of the QED Tenth-Order Electron Anomalous Magnetic Moment*, *Phys. Rev.* **D97** (2018) 036001 [[1712.06060](#)].
- [126] A. Czarnecki, B. Krause and W. J. Marciano, *Electroweak Fermion loop contributions to the muon anomalous magnetic moment*, *Phys. Rev.* **D52** (1995) R2619 [[hep-ph/9506256](#)].
- [127] A. Czarnecki, B. Krause and W. J. Marciano, *Electroweak corrections to the muon anomalous magnetic moment*, *Phys. Rev. Lett.* **76** (1996) 3267 [[hep-ph/9512369](#)].
- [128] C. Gnendiger, D. Stöckinger and H. Stöckinger-Kim, *The electroweak contributions to $(g - 2)_\mu$ after the Higgs boson mass measurement*, *Phys. Rev.* **D88** (2013) 053005 [[1306.5546](#)].
- [129] M. Della Morte, A. Francis, V. Gülpers, G. Herdoíza, G. von Hippel, H. Horch et al., *The hadronic vacuum polarization contribution to the muon $g - 2$ from lattice QCD*, *JHEP* **10** (2017) 020 [[1705.01775](#)].
- [130] M. Davier, A. Hoecker, B. Malaescu and Z. Zhang, *Reevaluation of the hadronic vacuum polarisation contributions to the Standard Model predictions of the muon $g - 2$ and $\alpha(m_Z^2)$ using newest hadronic cross-section data*, *Eur. Phys. J. C* **77** (2017) 827 [[1706.09436](#)].
- [131] BUDAPEST-MARSEILLE-WUPPERTAL collaboration, *Hadronic vacuum polarization contribution to the anomalous magnetic moments of leptons from first principles*, *Phys. Rev. Lett.* **121** (2018) 022002 [[1711.04980](#)].
- [132] RBC, UKQCD collaboration, *Calculation of the hadronic vacuum polarization contribution to the muon anomalous magnetic moment*, *Phys. Rev. Lett.* **121** (2018) 022003 [[1801.07224](#)].
- [133] A. Keshavarzi, D. Nomura and T. Teubner, *Muon $g - 2$ and $\alpha(M_Z^2)$: a new data-based analysis*, *Phys. Rev.* **D97** (2018) 114025 [[1802.02995](#)].
- [134] D. Giusti, F. Sanfilippo and S. Simula, *Light-quark contribution to the leading hadronic vacuum polarization term of the muon $g - 2$ from twisted-mass fermions*, *Phys. Rev.* **D98** (2018) 114504 [[1808.00887](#)].
- [135] G. Colangelo, M. Hoferichter and P. Stoffer, *Two-pion contribution to hadronic vacuum polarization*, *JHEP* **02** (2019) 006 [[1810.00007](#)].
- [136] A. Gérardin, H. B. Meyer and A. Nyffeler, *Lattice calculation of the pion transition form factor $\pi^0 \rightarrow \gamma^*\gamma^*$* , *Phys. Rev.* **D94** (2016) 074507 [[1607.08174](#)].

-
- [137] T. Blum, N. Christ, M. Hayakawa, T. Izubuchi, L. Jin, C. Jung et al., *Connected and Leading Disconnected Hadronic Light-by-Light Contribution to the Muon Anomalous Magnetic Moment with a Physical Pion Mass*, *Phys. Rev. Lett.* **118** (2017) 022005 [1610.04603].
- [138] G. Colangelo, M. Hoferichter, M. Procura and P. Stoffer, *Rescattering effects in the hadronic-light-by-light contribution to the anomalous magnetic moment of the muon*, *Phys. Rev. Lett.* **118** (2017) 232001 [1701.06554].
- [139] G. Colangelo, M. Hoferichter, M. Procura and P. Stoffer, *Dispersion relation for hadronic light-by-light scattering: two-pion contributions*, *JHEP* **04** (2017) 161 [1702.07347].
- [140] T. Blum, N. Christ, M. Hayakawa, T. Izubuchi, L. Jin, C. Jung et al., *Using infinite volume, continuum QED and lattice QCD for the hadronic light-by-light contribution to the muon anomalous magnetic moment*, *Phys. Rev.* **D96** (2017) 034515 [1705.01067].
- [141] M. Hoferichter, B.-L. Hoid, B. Kubis, S. Leupold and S. P. Schneider, *Pion-pole contribution to hadronic light-by-light scattering in the anomalous magnetic moment of the muon*, *Phys. Rev. Lett.* **121** (2018) 112002 [1805.01471].
- [142] G. Colangelo, F. Hagelstein, M. Hoferichter, L. Laub and P. Stoffer, *Longitudinal short-distance constraints for the hadronic light-by-light contribution to $(g - 2)_\mu$ with large- N_c Regge models*, 1910.13432.
- [143] A. Kurz, T. Liu, P. Marquard and M. Steinhauser, *Hadronic contribution to the muon anomalous magnetic moment to next-to-next-to-leading order*, *Phys. Lett.* **B734** (2014) 144 [1403.6400].
- [144] G. Colangelo, M. Hoferichter, A. Nyffeler, M. Passera and P. Stoffer, *Remarks on higher-order hadronic corrections to the muon $g-2$* , *Phys. Lett.* **B735** (2014) 90 [1403.7512].
- [145] MUON G-2 collaboration, *Muon ($g-2$) Technical Design Report*, 1501.06858.
- [146] J-PARC G-'2/EDM collaboration, *A novel precision measurement of muon $g-2$ and EDM at J-PARC*, *AIP Conf. Proc.* **1467** (2012) 45.
- [147] W. Buchmuller, R. Ruckl and D. Wyler, *Leptoquarks in Lepton - Quark Collisions*, *Phys. Lett.* **B191** (1987) 442.
- [148] J. Blumlein, E. Boos and A. Kryukov, *Leptoquark pair production in hadronic interactions*, *Z. Phys. C* **76** (1997) 137 [hep-ph/9610408].
- [149] R. Barbieri, C. W. Murphy and F. Senia, *B-decay Anomalies in a Composite Leptoquark Model*, *Eur. Phys. J.* **C77** (2017) 8 [1611.04930].
- [150] L. Di Luzio, A. Greljo and M. Nardecchia, *Gauge leptoquark as the origin of B-physics anomalies*, *Phys. Rev.* **D96** (2017) 115011 [1708.08450].
- [151] L. Calibbi, A. Crivellin and T. Li, *A model of vector leptoquarks in view of the B-physics anomalies*, 1709.00692.
- [152] M. Bordone, C. Cornella, J. Fuentes-Martin and G. Isidori, *A three-site gauge model for flavor hierarchies and flavor anomalies*, *Phys. Lett.* **B779** (2018) 317 [1712.01368].

- [153] M. Blanke and A. Crivellin, *B Meson Anomalies in a Pati-Salam Model within the Randall-Sundrum Background*, 1801.07256.
- [154] S. Matsuzaki, K. Nishiwaki and K. Yamamoto, *Simultaneous interpretation of K and B anomalies in terms of chiral-flavorful vectors*, 1806.02312.
- [155] J. Heeck and D. Teresi, *Pati-Salam explanations of the B-meson anomalies*, *JHEP* **12** (2018) 103 [1808.07492].
- [156] J. Fuentes-Martín, G. Isidori, M. König and N. Selimovic, *Vector Leptoquarks Beyond Tree Level*, *Phys. Rev.* **D101** (2020) 035024 [1910.13474].
- [157] J. Fuentes-Martin, G. Isidori, J. Pagès and B. A. Stefanek, *Flavor Non-universal Pati-Salam Unification and Neutrino Masses*, 2012.10492.
- [158] G. D'Amico, M. Nardecchia, P. Panci, F. Sannino, A. Strumia, R. Torre et al., *Flavour anomalies after the R_{K^*} measurement*, *JHEP* **09** (2017) 010 [1704.05438].
- [159] M. Ciuchini, A. M. Coutinho, M. Fedele, E. Franco, A. Paul, L. Silvestrini et al., *On Flavourful Easter eggs for New Physics hunger and Lepton Flavour Universality violation*, *Eur. Phys. J.* **C77** (2017) 688 [1704.05447].
- [160] G. Hiller and I. Nisandzic, *R_K and R_{K^*} beyond the standard model*, *Phys. Rev.* **D96** (2017) 035003 [1704.05444].
- [161] T. Hurth, F. Mahmoudi, D. Martinez Santos and S. Neshatpour, *Lepton nonuniversality in exclusive $b \rightarrow s \ell \ell$ decays*, *Phys. Rev.* **D96** (2017) 095034 [1705.06274].
- [162] C. Hambrock, A. Khodjamirian and A. Rusov, *Hadronic effects and observables in $B \rightarrow \pi \ell^+ \ell^-$ decay at large recoil*, *Phys. Rev.* **D92** (2015) 074020 [1506.07760].
- [163] LHCb collaboration, *First measurement of the differential branching fraction and CP asymmetry of the $B^\pm \rightarrow \pi^\pm \mu^+ \mu^-$ decay*, *JHEP* **10** (2015) 034 [1509.00414].
- [164] M. Ziegler, *Search for the Decay $B^0 \rightarrow \tau^+ \tau^-$ with the Belle Experiment*, Ph.D. thesis, KIT, Karlsruhe, 2016.
- [165] R. Watanabe, *New Physics effect on $B_c \rightarrow J/\psi \tau \bar{\nu}$ in relation to the $R_{D^{(*)}}$ anomaly*, *Phys. Lett.* **B776** (2018) 5 [1709.08644].
- [166] B. Chauhan and B. Kindra, *Invoking Chiral Vector Leptoquark to explain LFU violation in B Decays*, 1709.09989.
- [167] G. Ricciardi, *Semileptonic and leptonic B decays, circa 2016*, *Mod. Phys. Lett.* **A32** (2017) 1730005 [1610.04387].
- [168] F. U. Bernlochner, *$B \rightarrow \pi \tau \bar{\nu}_\tau$ decay in the context of type II 2HDM*, *Phys. Rev.* **D92** (2015) 115019 [1509.06938].
- [169] BELLE collaboration, *Search for $B^0 \rightarrow \pi^- \tau^+ \nu_\tau$ with hadronic tagging at Belle*, *Phys. Rev.* **D93** (2016) 032007 [1509.06521].
- [170] A. Lusiani, *HFAG 2016 and PDG 2016 lepton averages and $|V_{us}|$ determination from data*, *Nucl. Part. Phys. Proc.* **287-288** (2017) 29.

-
- [171] R. Alonso, B. Grinstein and J. Martin Camalich, *Lepton universality violation and lepton flavor conservation in B-meson decays*, *JHEP* **10** (2015) 184 [1505.05164].
- [172] L. Calibbi, A. Crivellin and T. Ota, *Effective Field Theory Approach to $b \rightarrow s\ell\ell'$, $B \rightarrow K^{(*)}\nu\bar{\nu}$ and $B \rightarrow D^{(*)}\tau\nu$ with Third Generation Couplings*, *Phys. Rev. Lett.* **115** (2015) 181801 [1506.02661].
- [173] S. Fajfer and N. Košnik, *Vector leptoquark resolution of R_K and $R_{D^{(*)}}$ puzzles*, *Phys. Lett.* **B755** (2016) 270 [1511.06024].
- [174] G. Hiller, D. Loose and K. Schönwald, *Leptoquark Flavor Patterns & B Decay Anomalies*, *JHEP* **12** (2016) 027 [1609.08895].
- [175] B. Bhattacharya, A. Datta, J.-P. Guévin, D. London and R. Watanabe, *Simultaneous Explanation of the R_K and $R_{D^{(*)}}$ Puzzles: a Model Analysis*, *JHEP* **01** (2017) 015 [1609.09078].
- [176] D. Buttazzo, A. Greljo, G. Isidori and D. Marzocca, *B-physics anomalies: a guide to combined explanations*, *JHEP* **11** (2017) 044 [1706.07808].
- [177] J. Kumar, D. London and R. Watanabe, *Combined Explanations of the $b \rightarrow s\mu^+\mu^-$ and $b \rightarrow c\tau^-\bar{\nu}$ Anomalies: a General Model Analysis*, 1806.07403.
- [178] J. C. Pati and A. Salam, *Lepton Number as the Fourth Color*, *Phys. Rev.* **D10** (1974) 275.
- [179] B. Capdevila, A. Crivellin, S. Descotes-Genon, L. Hofer and J. Matias, *Searching for New Physics with $b \rightarrow s\tau^+\tau^-$ processes*, *Phys. Rev. Lett.* **120** (2018) 181802 [1712.01919].
- [180] R. Barbieri, G. Isidori, A. Pattori and F. Senia, *Anomalies in B-decays and $U(2)$ flavour symmetry*, *Eur. Phys. J.* **C76** (2016) 67 [1512.01560].
- [181] N. Assad, B. Fornal and B. Grinstein, *Baryon Number and Lepton Universality Violation in Leptoquark and Diquark Models*, *Phys. Lett.* **B777** (2018) 324 [1708.06350].
- [182] R. Barbieri and A. Tesi, *B-decay anomalies in Pati-Salam $SU(4)$* , *Eur. Phys. J.* **C78** (2018) 193 [1712.06844].
- [183] A. Greljo and B. A. Stefanek, *Third family quark-lepton unification at the TeV scale*, *Phys. Lett.* **B782** (2018) 131 [1802.04274].
- [184] M. Bordone, C. Cornella, J. Fuentes-Martín and G. Isidori, *Low-energy signatures of the PS^3 model: from B-physics anomalies to LFV*, 1805.09328.
- [185] C. Bobeth and A. J. Buras, *Leptoquarks meet ϵ'/ϵ and rare Kaon processes*, *JHEP* **02** (2018) 101 [1712.01295].
- [186] S. Fajfer, N. Košnik and L. Vale Silva, *Footprints of leptoquarks: from $R_{K^{(*)}}$ to $K \rightarrow \pi\nu\bar{\nu}$* , *Eur. Phys. J.* **C78** (2018) 275 [1802.00786].
- [187] K. Earl and T. Gregoire, *Contributions to $b \rightarrow s\ell\ell$ Anomalies from R-Parity Violating Interactions*, 1806.01343.

- [188] F. Feruglio, P. Paradisi and A. Pattori, *On the Importance of Electroweak Corrections for B Anomalies*, *JHEP* **09** (2017) 061 [1705.00929].
- [189] F. Borzumati and C. Greub, *2HDMs predictions for $\bar{B} \rightarrow X_s \gamma$ in NLO QCD*, *Phys. Rev.* **D58** (1998) 074004 [hep-ph/9802391].
- [190] F. Borzumati, C. Greub, T. Hurth and D. Wyler, *Gluino contribution to radiative B decays: Organization of QCD corrections and leading order results*, *Phys. Rev.* **D62** (2000) 075005 [hep-ph/9911245].
- [191] V. Cirigliano, A. Crivellin and M. Hoferichter, *No-go theorem for nonstandard explanations of the $\tau \rightarrow K_S \pi \nu_\tau$ CP asymmetry*, *Phys. Rev. Lett.* **120** (2018) 141803 [1712.06595].
- [192] LHCb collaboration, *Search for the decays $B_s^0 \rightarrow \tau^+ \tau^-$ and $B^0 \rightarrow \tau^+ \tau^-$* , *Phys. Rev. Lett.* **118** (2017) 251802 [1703.02508].
- [193] C. Bobeth, M. Gorbahn, T. Hermann, M. Misiak, E. Stamou and M. Steinhauser, *$B_{s,d} \rightarrow l^+ l^-$ in the Standard Model with Reduced Theoretical Uncertainty*, *Phys. Rev. Lett.* **112** (2014) 101801 [1311.0903].
- [194] C. Bobeth, *Updated $B_q \rightarrow \bar{\ell} \ell$ in the standard model at higher orders*, in *Proceedings, 49th Rencontres de Moriond on Electroweak Interactions and Unified Theories: La Thuile, Italy, March 15-22, 2014*, pp. 75–80, 2014, 1405.4907, <https://inspirehep.net/record/1297237/files/arXiv:1405.4907.pdf>.
- [195] C. Bobeth, M. Misiak and J. Urban, *Photonic penguins at two loops and m_t dependence of $BR[B \rightarrow X_s l^+ l^-]$* , *Nucl. Phys.* **B574** (2000) 291 [hep-ph/9910220].
- [196] T. Huber, E. Lunghi, M. Misiak and D. Wyler, *Electromagnetic logarithms in $\bar{B} \rightarrow X_s l^+ l^-$* , *Nucl. Phys.* **B740** (2006) 105 [hep-ph/0512066].
- [197] A. Crivellin, L. Hofer, J. Matias, U. Nierste, S. Pokorski and J. Rosiek, *Lepton-flavour violating B decays in generic Z' models*, *Phys. Rev.* **D92** (2015) 054013 [1504.07928].
- [198] A. J. Buras, D. Buttazzo and R. Knegjens, *$K \rightarrow \pi \nu \bar{\nu}$ and ε/ε' in simplified new physics models*, *JHEP* **11** (2015) 166 [1507.08672].
- [199] M. Blanke, A. J. Buras, B. Duling, K. Gemmler and S. Gori, *Rare K and B Decays in a Warped Extra Dimension with Custodial Protection*, *JHEP* **03** (2009) 108 [0812.3803].
- [200] G. Isidori and R. Unterdorfer, *On the short distance constraints from $K_{L,S} \rightarrow \mu^+ \mu^-$* , *JHEP* **01** (2004) 009 [hep-ph/0311084].
- [201] BELLE collaboration, *Search for Lepton-Flavor-Violating tau Decays into a Lepton and a Vector Meson*, *Phys. Lett.* **B699** (2011) 251 [1101.0755].
- [202] BABAR collaboration, *Search for Charged Lepton Flavor Violation in Narrow Upsilon Decays*, *Phys. Rev. Lett.* **104** (2010) 151802 [1001.1883].
- [203] A. J. Buras, T. Ewerth, S. Jager and J. Rosiek, *$K^+ \rightarrow \pi^+ \nu \bar{\nu}$ and $K_L \rightarrow \pi^0 \nu \bar{\nu}$ decays in the general MSSM*, *Nucl. Phys.* **B714** (2005) 103 [hep-ph/0408142].

-
- [204] A. J. Buras, D. Buttazzo, J. Girrbach-Noe and R. Knegjens, $K^+ \rightarrow \pi^+ \nu \bar{\nu}$ and $K_L \rightarrow \pi^0 \nu \bar{\nu}$ in the Standard Model: status and perspectives, *JHEP* **11** (2015) 033 [1503.02693].
- [205] A. J. Buras, J. Girrbach-Noe, C. Niehoff and D. M. Straub, $B \rightarrow K^{(*)} \nu \bar{\nu}$ decays in the Standard Model and beyond, *JHEP* **02** (2015) 184 [1409.4557].
- [206] BELLE collaboration, Search for $B \rightarrow h \nu \bar{\nu}$ decays with semileptonic tagging at Belle, *Phys. Rev.* **D96** (2017) 091101 [1702.03224].
- [207] BELLE-II collaboration, *Belle II Technical Design Report*, 1011.0352.
- [208] PARTICLE DATA GROUP collaboration, *Review of Particle Physics*, *Chin. Phys.* **C40** (2016) 100001.
- [209] A. Arbey, T. Hurth, F. Mahmoudi, D. M. Santos and S. Neshatpour, Update on the $b \rightarrow s$ anomalies, *Phys. Rev.* **D100** (2019) 015045 [1904.08399].
- [210] L. Di Luzio, J. Fuentes-Martin, A. Greljo, M. Nardecchia and S. Renner, Maximal Flavour Violation: a Cabibbo mechanism for leptiquarks, *JHEP* **11** (2018) 081 [1808.00942].
- [211] A. Biswas, D. Kumar Ghosh, N. Ghosh, A. Shaw and A. K. Swain, Collider signature of U_1 Leptoquark and constraints from $b \rightarrow c$ observables, *J. Phys.* **G47** (2020) 045005 [1808.04169].
- [212] A. Angelescu, D. Bečirević, D. A. Faroughy and O. Sumensari, Closing the window on single leptoquark solutions to the B -physics anomalies, *JHEP* **10** (2018) 183 [1808.08179].
- [213] C. Cornella, J. Fuentes-Martin and G. Isidori, Revisiting the vector leptoquark explanation of the B -physics anomalies, *JHEP* **07** (2019) 168 [1903.11517].
- [214] A. D. Sakharov, Violation of CP Invariance, C asymmetry, and baryon asymmetry of the universe, *Pisma Zh. Eksp. Teor. Fiz.* **5** (1967) 32.
- [215] A. G. Cohen, D. B. Kaplan and A. E. Nelson, Progress in electroweak baryogenesis, *Ann. Rev. Nucl. Part. Sci.* **43** (1993) 27 [hep-ph/9302210].
- [216] M. B. Gavela, P. Hernandez, J. Orloff and O. Pene, Standard model CP violation and baryon asymmetry, *Mod. Phys. Lett.* **A9** (1994) 795 [hep-ph/9312215].
- [217] P. Huet and E. Sather, Electroweak baryogenesis and standard model CP violation, *Phys. Rev.* **D51** (1995) 379 [hep-ph/9404302].
- [218] M. B. Gavela, M. Lozano, J. Orloff and O. Pene, Standard model CP violation and baryon asymmetry. Part 1: Zero temperature, *Nucl. Phys.* **B430** (1994) 345 [hep-ph/9406288].
- [219] M. B. Gavela, P. Hernandez, J. Orloff, O. Pene and C. Quimbay, Standard model CP violation and baryon asymmetry. Part 2: Finite temperature, *Nucl. Phys.* **B430** (1994) 382 [hep-ph/9406289].
- [220] A. Riotto and M. Trodden, Recent progress in baryogenesis, *Ann. Rev. Nucl. Part. Sci.* **49** (1999) 35 [hep-ph/9901362].

- [221] T. Chupp, P. Fierlinger, M. Ramsey-Musolf and J. Singh, *Electric dipole moments of atoms, molecules, nuclei, and particles*, *Rev. Mod. Phys.* **91** (2019) 015001 [1710.02504].
- [222] N. Yamanaka, B. K. Sahoo, N. Yoshinaga, T. Sato, K. Asahi and B. P. Das, *Probing exotic phenomena at the interface of nuclear and particle physics with the electric dipole moments of diamagnetic atoms: A unique window to hadronic and semi-leptonic CP violation*, *Eur. Phys. J.* **A53** (2017) 54 [1703.01570].
- [223] R. Barbieri, G. R. Dvali and L. J. Hall, *Predictions from a $U(2)$ flavor symmetry in supersymmetric theories*, *Phys. Lett.* **B377** (1996) 76 [hep-ph/9512388].
- [224] L. J. Hall and M. Suzuki, *Explicit R-Parity Breaking in Supersymmetric Models*, *Nucl. Phys.* **B231** (1984) 419.
- [225] G. G. Ross and J. W. F. Valle, *Supersymmetric Models Without R-Parity*, *Phys. Lett.* **151B** (1985) 375.
- [226] V. D. Barger, G. F. Giudice and T. Han, *Some New Aspects of Supersymmetry R-Parity Violating Interactions*, *Phys. Rev.* **D40** (1989) 2987.
- [227] H. K. Dreiner, *An Introduction to explicit R-parity violation*, hep-ph/9707435.
- [228] R. Barbier et al., *R-parity violating supersymmetry*, *Phys. Rept.* **420** (2005) 1 [hep-ph/0406039].
- [229] N. Yamanaka, T. Sato and T. Kubota, *Linear programming analysis of the R-parity violation within EDM-constraints*, *JHEP* **12** (2014) 110 [1406.3713].
- [230] K. Fuyuto, M. Ramsey-Musolf and T. Shen, *Electric Dipole Moments from CP-Violating Scalar Leptoquark Interactions*, *Phys. Lett.* **B788** (2019) 52 [1804.01137].
- [231] W. Dekens, J. de Vries, M. Jung and K. K. Vos, *The phenomenology of electric dipole moments in models of scalar leptoquarks*, *JHEP* **01** (2019) 069 [1809.09114].
- [232] S. Fajfer, J. F. Kamenik, I. Nisandzic and J. Zupan, *Implications of Lepton Flavor Universality Violations in B Decays*, *Phys. Rev. Lett.* **109** (2012) 161801 [1206.1872].
- [233] N. G. Deshpande and A. Menon, *Hints of R-parity violation in B decays into $\tau\nu$* , *JHEP* **01** (2013) 025 [1208.4134].
- [234] M. Tanaka and R. Watanabe, *New physics in the weak interaction of $\bar{B} \rightarrow D^{(*)}\tau\bar{\nu}$* , *Phys. Rev.* **D87** (2013) 034028 [1212.1878].
- [235] Y. Sakaki, M. Tanaka, A. Tayduganov and R. Watanabe, *Testing leptoquark models in $\bar{B} \rightarrow D^{(*)}\tau\bar{\nu}$* , *Phys. Rev.* **D88** (2013) 094012 [1309.0301].
- [236] M. Freytsis, Z. Ligeti and J. T. Ruderman, *Flavor models for $\bar{B} \rightarrow D^{(*)}\tau\bar{\nu}$* , *Phys. Rev.* **D92** (2015) 054018 [1506.08896].
- [237] C. Hati, G. Kumar and N. Mahajan, *$\bar{B} \rightarrow D^{(*)}\tau\bar{\nu}$ excesses in ALRSM constrained from B, D decays and $D^0 - \bar{D}^0$ mixing*, *JHEP* **01** (2016) 117 [1511.03290].
- [238] M. Bauer and M. Neubert, *Minimal Leptoquark Explanation for the $R_{D^{(*)}}$, R_K , and $(g-2)_g$ Anomalies*, *Phys. Rev. Lett.* **116** (2016) 141802 [1511.01900].

-
- [239] X.-Q. Li, Y.-D. Yang and X. Zhang, *Revisiting the one leptoquark solution to the $R(D^0)$ anomalies and its phenomenological implications*, *JHEP* **08** (2016) 054 [1605.09308].
- [240] J. Zhu, H.-M. Gan, R.-M. Wang, Y.-Y. Fan, Q. Chang and Y.-G. Xu, *Probing the R -parity violating supersymmetric effects in the exclusive $b \rightarrow c\ell^-\bar{\nu}_\ell$ decays*, *Phys. Rev.* **D93** (2016) 094023 [1602.06491].
- [241] O. Popov and G. A. White, *One Leptoquark to unify them? Neutrino masses and unification in the light of $(g-2)_\mu$, $R_{D^{(*)}}$ and R_K anomalies*, *Nucl. Phys.* **B923** (2017) 324 [1611.04566].
- [242] N. G. Deshpande and X.-G. He, *Consequences of R -parity violating interactions for anomalies in $\bar{B} \rightarrow D^{(*)}\tau\bar{\nu}$ and $b \rightarrow s\mu^+\mu^-$* , *Eur. Phys. J.* **C77** (2017) 134 [1608.04817].
- [243] A. Crivellin, D. Müller and T. Ota, *Simultaneous explanation of $R(D^0)$ and $b \rightarrow s\mu^+\mu^-$: the last scalar leptoquarks standing*, *JHEP* **09** (2017) 040 [1703.09226].
- [244] W. Altmannshofer, P. S. Bhupal Dev and A. Soni, *$R_{D^{(*)}}$ anomaly: A possible hint for natural supersymmetry with R -parity violation*, *Phys. Rev.* **D96** (2017) 095010 [1704.06659].
- [245] S. Kamali, A. Rashed and A. Datta, *New physics in inclusive $B \rightarrow X_c\ell\bar{\nu}$ decay in light of $R(D^{(*)})$ measurements*, *Phys. Rev.* **D97** (2018) 095034 [1801.08259].
- [246] A. Azatov, D. Bardhan, D. Ghosh, F. Sgarlata and E. Venturini, *Anatomy of $b \rightarrow c\tau\nu$ anomalies*, *JHEP* **11** (2018) 187 [1805.03209].
- [247] J. Zhu, B. Wei, J.-H. Sheng, R.-M. Wang, Y. Gao and G.-R. Lu, *Probing the R -parity violating supersymmetric effects in $B_c \rightarrow J/\psi\ell^-\bar{\nu}_\ell, \eta_c\ell^-\bar{\nu}_\ell$ and $\Lambda_b \rightarrow \Lambda_c\ell^-\bar{\nu}_\ell$ decays*, *Nucl. Phys.* **B934** (2018) 380 [1801.00917].
- [248] Q.-Y. Hu, X.-Q. Li, Y. Muramatsu and Y.-D. Yang, *R -parity violating solutions to the $R_{D^{(*)}}$ anomaly and their GUT-scale unifications*, *Phys. Rev.* **D99** (2019) 015008 [1808.01419].
- [249] T. J. Kim, P. Ko, J. Li, J. Park and P. Wu, *Correlation between $R_{D^{(*)}}$ and top quark FCNC decays in leptoquark models*, 1812.08484.
- [250] H. Yan, Y.-D. Yang and X.-B. Yuan, *Phenomenology of $b \rightarrow c\tau\bar{\nu}$ decays in a scalar leptoquark model*, 1905.01795.
- [251] F. Feruglio, P. Paradisi and O. Sumensari, *Implications of scalar and tensor explanations of $R_{D^{(*)}}$* , *JHEP* **11** (2018) 191 [1806.10155].
- [252] S. Iguro, T. Kitahara, Y. Omura, R. Watanabe and K. Yamamoto, *D^* polarization vs. $R_{D^{(*)}}$ anomalies in the leptoquark models*, *JHEP* **02** (2019) 194 [1811.08899].
- [253] J. Aebischer, A. Crivellin and C. Greub, *QCD improved matching for semileptonic B decays with leptoquarks*, *Phys. Rev.* **D99** (2019) 055002 [1811.08907].
- [254] J. A. Gracey, *Three loop \overline{MS} -bar tensor current anomalous dimension in QCD*, *Phys. Lett.* **B488** (2000) 175 [hep-ph/0007171].

- [255] M. González-Alonso, J. Martin Camalich and K. Mimouni, *Renormalization-group evolution of new physics contributions to (semi)leptonic meson decays*, *Phys. Lett.* **B772** (2017) 777 [1706.00410].
- [256] M. Tanaka and R. Watanabe, *New physics contributions in $B \rightarrow \pi\tau\bar{\nu}$ and $B \rightarrow \tau\bar{\nu}$* , *PTEP* **2017** (2017) 013B05 [1608.05207].
- [257] BELLE collaboration, *Measurement of the τ lepton polarization and $R(D^*)$ in the decay $\bar{B} \rightarrow D^*\tau^-\bar{\nu}_\tau$* , *Phys. Rev. Lett.* **118** (2017) 211801 [1612.00529].
- [258] N. Ikeno, L. Dai and E. Oset, *Meson exchange between initial and final state and the R_D ratio in the $\bar{B} \rightarrow D\bar{\nu}\ell(\bar{\nu}_\tau\tau)$ reactions*, 1907.11128.
- [259] M. Bordone, M. Jung and D. van Dyk, *Theory determination of $\bar{B} \rightarrow D^{(*)}\ell^-\bar{\nu}$ form factors at $\mathcal{O}(1/m_c^2)$* , 1908.09398.
- [260] A. Crivellin, S. Davidson, G. M. Pruna and A. Signer, *Renormalisation-group improved analysis of $\mu \rightarrow e$ processes in a systematic effective-field-theory approach*, *JHEP* **05** (2017) 117 [1702.03020].
- [261] J. Hisano, K. Tsumura and M. J. S. Yang, *QCD Corrections to Neutron Electric Dipole Moment from Dimension-six Four-Quark Operators*, *Phys. Lett.* **B713** (2012) 473 [1205.2212].
- [262] V. Cirigliano, W. Dekens, J. de Vries and E. Mereghetti, *Constraining the top-Higgs sector of the Standard Model Effective Field Theory*, *Phys. Rev.* **D94** (2016) 034031 [1605.04311].
- [263] B. Graner, Y. Chen, E. G. Lindahl and B. R. Heckel, *Reduced Limit on the Permanent Electric Dipole Moment of Hg199*, *Phys. Rev. Lett.* **116** (2016) 161601 [1601.04339].
- [264] JEDI collaboration, *Measurement of Permanent Electric Dipole Moments of Charged Hadrons in Storage Rings*, *Hyperfine Interact.* **214** (2013) 111 [1301.2937].
- [265] JEDI collaboration, *New method for a continuous determination of the spin tune in storage rings and implications for precision experiments*, *Phys. Rev. Lett.* **115** (2015) 094801 [1504.00635].
- [266] C. A. Baker et al., *An Improved experimental limit on the electric dipole moment of the neutron*, *Phys. Rev. Lett.* **97** (2006) 131801 [hep-ex/0602020].
- [267] C. Abel et al., *The $n2EDM$ experiment at the Paul Scherrer Institute*, in *International Workshop on Particle Physics at Neutron Sources 2018 (PPNS 2018) Grenoble, France, May 24-26, 2018*, 2018, 1811.02340.
- [268] A. J. Buras, M. Misiak and J. Urban, *Two loop QCD anomalous dimensions of flavor changing four quark operators within and beyond the standard model*, *Nucl. Phys.* **B586** (2000) 397 [hep-ph/0005183].
- [269] M. Ciuchini, E. Franco, V. Lubicz, G. Martinelli, I. Scimemi and L. Silvestrini, *Next-to-leading order QCD corrections to $\Delta F = 2$ effective Hamiltonians*, *Nucl. Phys.* **B523** (1998) 501 [hep-ph/9711402].
- [270] E. Golowich, J. Hewett, S. Pakvasa and A. A. Petrov, *Implications of $D^0 - \bar{D}^0$ Mixing for New Physics*, *Phys. Rev.* **D76** (2007) 095009 [0705.3650].

-
- [271] N. Carrasco et al., $D^0-\bar{D}^0$ mixing in the standard model and beyond from $N_f = 2$ twisted mass QCD, *Phys. Rev.* **D90** (2014) 014502 [1403.7302].
- [272] UTFIT collaboration, *The UFit collaboration average of D meson mixing data: Winter 2014*, *JHEP* **03** (2014) 123 [1402.1664].
- [273] A. Bazavov et al., *B- and D-meson leptonic decay constants from four-flavor lattice QCD*, *Phys. Rev.* **D98** (2018) 074512 [1712.09262].
- [274] A. Cerri et al., *Opportunities in Flavour Physics at the HL-LHC and HE-LHC*, 1812.07638.
- [275] A. Pich, *Precision Tau Physics*, *Prog. Part. Nucl. Phys.* **75** (2014) 41 [1310.7922].
- [276] PARTICLE DATA GROUP collaboration, *Review of Particle Physics*, *Phys. Rev.* **D98** (2018) 030001.
- [277] A. Djouadi, T. Kohler, M. Spira and J. Tutas, *(e b), (e t) TYPE LEPTOQUARKS AT e p COLLIDERS*, *Z. Phys.* **C46** (1990) 679.
- [278] S. Davidson, D. C. Bailey and B. A. Campbell, *Model independent constraints on leptoquarks from rare processes*, *Z. Phys.* **C61** (1994) 613 [hep-ph/9309310].
- [279] G. Couture and H. Konig, *Bounds on second generation scalar leptoquarks from the anomalous magnetic moment of the muon*, *Phys. Rev.* **D53** (1996) 555 [hep-ph/9507263].
- [280] D. Chakraverty, D. Choudhury and A. Datta, *A Nonsupersymmetric resolution of the anomalous muon magnetic moment*, *Phys. Lett.* **B506** (2001) 103 [hep-ph/0102180].
- [281] K.-m. Cheung, *Muon anomalous magnetic moment and leptoquark solutions*, *Phys. Rev.* **D64** (2001) 033001 [hep-ph/0102238].
- [282] U. Mahanta, *Implications of BNL measurement of delta a(mu) on a class of scalar leptoquark interactions*, *Eur. Phys. J.* **C21** (2001) 171 [hep-ph/0102176].
- [283] F. S. Queiroz, K. Sinha and A. Strumia, *Leptoquarks, Dark Matter, and Anomalous LHC Events*, *Phys. Rev.* **D91** (2015) 035006 [1409.6301].
- [284] D. Das, C. Hati, G. Kumar and N. Mahajan, *Towards a unified explanation of $R_{D^{(*)}}$, R_K and $(g-2)_\mu$ anomalies in a left-right model with leptoquarks*, *Phys. Rev.* **D94** (2016) 055034 [1605.06313].
- [285] C. Biggio, M. Bordone, L. Di Luzio and G. Ridolfi, *Massive vectors and loop observables: the $g-2$ case*, *JHEP* **10** (2016) 002 [1607.07621].
- [286] A. Crivellin, M. Hoferichter and P. Schmidt-Wellenburg, *Combined explanations of $(g-2)_{\mu,e}$ and implications for a large muon EDM*, *Phys. Rev.* **D98** (2018) 113002 [1807.11484].
- [287] D. Bečirević, N. Košnik, O. Sumensari and R. Zukanovich Funchal, *Palatable Leptoquark Scenarios for Lepton Flavor Violation in Exclusive $b \rightarrow s\ell_1\ell_2$ modes*, *JHEP* **11** (2016) 035 [1608.07583].

- [288] F. Feruglio, P. Paradisi and A. Pattori, *Revisiting Lepton Flavor Universality in B Decays*, *Phys. Rev. Lett.* **118** (2017) 011801 [1606.00524].
- [289] P. Arnan, D. Becirevic, F. Mescia and O. Sumensari, *Probing low energy scalar leptoquarks by the leptonic W and Z couplings*, *JHEP* **02** (2019) 109 [1901.06315].
- [290] CMS collaboration, *Leptoquark searches in CMS*, in *53rd Rencontres de Moriond on Electroweak Interactions and Unified Theories (Moriond EW 2018) La Thuile, Italy, March 10-17, 2018*, 2019, 1901.03570.
- [291] CMS collaboration, *Search for leptoquarks coupled to third-generation quarks in proton-proton collisions at $\sqrt{s} = 13$ TeV*, *Phys. Rev. Lett.* **121** (2018) 241802 [1809.05558].
- [292] N. Raj, *Anticipating nonresonant new physics in dilepton angular spectra at the LHC*, *Phys. Rev.* **D95** (2017) 015011 [1610.03795].
- [293] S. Bansal, R. M. Capdevilla, A. Delgado, C. Kolda, A. Martin and N. Raj, *Hunting leptoquarks in monolepton searches*, *Phys. Rev.* **D98** (2018) 015037 [1806.02370].
- [294] T. Mandal, S. Mitra and S. Raz, *$R_{D^{(*)}}$ motivated \mathcal{S}_1 leptoquark scenarios: Impact of interference on the exclusion limits from LHC data*, *Phys. Rev.* **D99** (2019) 055028 [1811.03561].
- [295] A. Greljo, J. Martin Camalich and J. D. Ruiz-Álvarez, *Mono- τ Signatures at the LHC Constrain Explanations of B-decay Anomalies*, *Phys. Rev. Lett.* **122** (2019) 131803 [1811.07920].
- [296] A. Celis, M. Jung, X.-Q. Li and A. Pich, *Scalar contributions to $b \rightarrow c(u)\tau\nu$ transitions*, *Phys. Lett.* **B771** (2017) 168 [1612.07757].
- [297] R. Alonso, B. Grinstein and J. Martin Camalich, *Lifetime of B_c^- Constrains Explanations for Anomalies in $B \rightarrow D^{(*)}\tau\nu$* , *Phys. Rev. Lett.* **118** (2017) 081802 [1611.06676].
- [298] A. G. Akeroyd and C.-H. Chen, *Constraint on the branching ratio of $B_c \rightarrow \tau\bar{\nu}$ from LEP1 and consequences for $R(D^{(*)})$ anomaly*, *Phys. Rev.* **D96** (2017) 075011 [1708.04072].
- [299] CMS collaboration, *Highlights and Perspectives from the CMS Experiment*, in *5th Large Hadron Collider Physics Conference (LHCP 2017) Shanghai, China, May 15-20, 2017*, 2017, 1709.03006, <http://lss.fnal.gov/archive/preprint/fermilab-conf-17-366-cms.shtml>.
- [300] ATLAS collaboration, *ATLAS results and prospects with focus on beyond the Standard Model*, *Nucl. Part. Phys. Proc.* **303-305** (2018) 43.
- [301] T. P. Gorringer and D. W. Hertzog, *Precision Muon Physics*, *Prog. Part. Nucl. Phys.* **84** (2015) 73 [1506.01465].
- [302] S. Borsanyi et al., *Leading-order hadronic vacuum polarization contribution to the muon magnetic moment from lattice QCD*, 2002.12347.
- [303] M. Davier, A. Hoecker, B. Malaescu and Z. Zhang, *A new evaluation of the hadronic vacuum polarisation contributions to the muon anomalous magnetic moment and to $\alpha(m_Z^2)$* , *Eur. Phys. J. C* **80** (2020) 241 [1908.00921].

-
- [304] A. Keshavarzi, D. Nomura and T. Teubner, $g - 2$ of charged leptons, $\alpha(M_Z^2)$, and the hyperfine splitting of muonium, *Phys. Rev. D* **101** (2020) 014029 [1911.00367].
- [305] B. Ananthanarayan, I. Caprini and D. Das, Pion electromagnetic form factor at high precision with implications to $a_\mu^{\pi\pi}$ and the onset of perturbative QCD, *Phys. Rev. D* **98** (2018) 114015 [1810.09265].
- [306] M. Hoferichter, B.-L. Hoid and B. Kubis, Three-pion contribution to hadronic vacuum polarization, *JHEP* **08** (2019) 137 [1907.01556].
- [307] M. Passera, W. Marciano and A. Sirlin, The Muon $g-2$ and the bounds on the Higgs boson mass, *Phys. Rev. D* **78** (2008) 013009 [0804.1142].
- [308] J. Haller, A. Hoecker, R. Kogler, K. Mönig, T. Peiffer and J. Stelzer, Update of the global electroweak fit and constraints on two-Higgs-doublet models, *Eur. Phys. J. C* **78** (2018) 675 [1803.01853].
- [309] C.-H. Chen, T. Nomura and H. Okada, Explanation of $B \rightarrow K^{(*)}\ell^+\ell^-$ and muon $g - 2$, and implications at the LHC, *Phys. Rev.* **D94** (2016) 115005 [1607.04857].
- [310] C.-H. Chen, T. Nomura and H. Okada, Excesses of muon $g - 2$, $R_{D^{(*)}}$, and R_K in a leptoquark model, *Phys. Lett.* **B774** (2017) 456 [1703.03251].
- [311] Y. Cai, J. Gargalionis, M. A. Schmidt and R. R. Volkas, Reconsidering the One Leptoquark solution: flavor anomalies and neutrino mass, *JHEP* **10** (2017) 047 [1704.05849].
- [312] K. Kowalska, E. M. Sessolo and Y. Yamamoto, Constraints on charmphilic solutions to the muon $g-2$ with leptoquarks, *Phys. Rev.* **D99** (2019) 055007 [1812.06851].
- [313] R. Mandal and A. Pich, Constraints on scalar leptoquarks from lepton and kaon physics, *JHEP* **12** (2019) 089 [1908.11155].
- [314] I. Doršner, S. Fajfer and O. Sumensari, Muon $g - 2$ and scalar leptoquark mixing, 1910.03877.
- [315] HFLAV collaboration, Averages of b -hadron, c -hadron, and τ -lepton properties as of 2018, 1909.12524.
- [316] P. Gambino, M. Jung and S. Schacht, The V_{cb} puzzle: An update, *Phys. Lett.* **B795** (2019) 386 [1905.08209].
- [317] I. de Medeiros Varzielas and J. Talbert, Simplified Models of Flavourful Leptoquarks, *Eur. Phys. J.* **C79** (2019) 536 [1901.10484].
- [318] M. Bordone, O. Catà and T. Feldmann, Effective Theory Approach to New Physics with Flavour: General Framework and a Leptoquark Example, *JHEP* **01** (2020) 067 [1910.02641].
- [319] I. Doršner, S. Fajfer, N. Košnik and I. Nišandžić, Minimally flavored colored scalar in $\bar{B} \rightarrow D^{(*)}\tau\bar{\nu}$ and the mass matrices constraints, *JHEP* **11** (2013) 084 [1306.6493].
- [320] S. Sahoo and R. Mohanta, Scalar leptoquarks and the rare B meson decays, *Phys. Rev.* **D91** (2015) 094019 [1501.05193].

- [321] U. K. Dey, D. Kar, M. Mitra, M. Spannowsky and A. C. Vincent, *Searching for Leptoquarks at IceCube and the LHC*, *Phys. Rev.* **D98** (2018) 035014 [1709.02009].
- [322] D. Bečirević and O. Sumensari, *A leptoquark model to accommodate $R_K^{\text{exp}} < R_K^{\text{SM}}$ and $R_{K^*}^{\text{exp}} < R_{K^*}^{\text{SM}}$* , *JHEP* **08** (2017) 104 [1704.05835].
- [323] B. Chauhan, B. Kindra and A. Narang, *Discrepancies in simultaneous explanation of flavor anomalies and IceCube PeV events using leptoquarks*, *Phys. Rev.* **D97** (2018) 095007 [1706.04598].
- [324] D. Becirevic, I. Dorsner, S. Fajfer, N. Kosnik, D. A. Faroughy and O. Sumensari, *Scalar leptoquarks from grand unified theories to accommodate the B-physics anomalies*, *Phys. Rev.* **D98** (2018) 055003 [1806.05689].
- [325] O. Popov, M. A. Schmidt and G. White, *R_2 as a single leptoquark solution to $R_{D^{(*)}}$ and $R_{K^{(*)}}$* , *Phys. Rev.* **D100** (2019) 035028 [1905.06339].
- [326] D. Marzocca, *Addressing the B-physics anomalies in a fundamental Composite Higgs Model*, *JHEP* **07** (2018) 121 [1803.10972].
- [327] I. Bigaran, J. Gargalionis and R. R. Volkas, *A near-minimal leptoquark model for reconciling flavour anomalies and generating radiative neutrino masses*, *JHEP* **10** (2019) 106 [1906.01870].
- [328] A. V. Rusoy, *Probing New Physics in $b \rightarrow d$ Transitions*, 1911.12819.
- [329] A. Crivellin, G. D'Ambrosio and J. Heeck, *Addressing the LHC flavor anomalies with horizontal gauge symmetries*, *Phys. Rev.* **D91** (2015) 075006 [1503.03477].
- [330] J. Fuentes-Martín, G. Isidori, J. Pagès and K. Yamamoto, *With or without $U(2)$? Probing non-standard flavor and helicity structures in semileptonic B decays*, *Phys. Lett.* **B800** (2020) 135080 [1909.02519].
- [331] L. Calibbi, A. Crivellin, F. Kirk, C. A. Manzari and L. Vernazza, *Z' models with less-minimal flavour violation*, 1910.00014.
- [332] J. Bernigaud, I. de Medeiros Varzielas and J. Talbert, *Finite Family Groups for Fermionic and Leptoquark Mixing Patterns*, *JHEP* **01** (2020) 194 [1906.11270].
- [333] I. de Medeiros Varzielas and G. Hiller, *Clues for flavor from rare lepton and quark decays*, *JHEP* **06** (2015) 072 [1503.01084].
- [334] S.-M. Choi, Y.-J. Kang, H. M. Lee and T.-G. Ro, *Lepto-Quark Portal Dark Matter*, *JHEP* **10** (2018) 104 [1807.06547].
- [335] M. Hirsch, H. V. Klapdor-Kleingrothaus and S. G. Kovalenko, *New low-energy leptoquark interactions*, *Phys. Lett.* **B378** (1996) 17 [hep-ph/9602305].
- [336] F. F. Deppisch, S. Kulkarni, H. Päs and E. Schumacher, *Leptoquark patterns unifying neutrino masses, flavor anomalies, and the diphoton excess*, *Phys. Rev.* **D94** (2016) 013003 [1603.07672].
- [337] I. Doršner, S. Fajfer and N. Košnik, *Leptoquark mechanism of neutrino masses within the grand unification framework*, *Eur. Phys. J.* **C77** (2017) 417 [1701.08322].

-
- [338] O. Catà and T. Mannel, *Linking lepton number violation with B anomalies*, 1903.01799.
- [339] K. S. Babu, P. S. B. Dev, S. Jana and A. Thapa, *Non-Standard Interactions in Radiative Neutrino Mass Models*, 1907.09498.
- [340] C. Bobeth, U. Haisch, A. Lenz, B. Pecjak and G. Tetlalmatzi-Xolocotzi, *On new physics in $\Delta\Gamma_d$* , *JHEP* **06** (2014) 040 [1404.2531].
- [341] C. Cornella, G. Isidori, M. König, S. Liechti, P. Owen and N. Serra, *Hunting for $B^+ \rightarrow K^+\tau^+\tau^-$ imprints on the $B^+ \rightarrow K^+\mu^+\mu^-$ dimuon spectrum*, 2001.04470.
- [342] BABAR collaboration, *A search for the decay modes $B^{+-} \rightarrow h^{+-}\tau^{+-}l$* , *Phys. Rev.* **D86** (2012) 012004 [1204.2852].
- [343] LHCb collaboration, *Search for the lepton-flavour-violating decays $B_s^0 \rightarrow \tau^\pm\mu^\mp$ and $B^0 \rightarrow \tau^\pm\mu^\mp$* , 1905.06614.
- [344] M. Jung and D. M. Straub, *Constraining new physics in $b \rightarrow c\ell\nu$ transitions*, 1801.01112.
- [345] S. de Boer and G. Hiller, *Flavor and new physics opportunities with rare charm decays into leptons*, *Phys. Rev.* **D93** (2016) 074001 [1510.00311].
- [346] A. Lenz, U. Nierste, J. Charles, S. Descotes-Genon, A. Jantsch, C. Kaufhold et al., *Anatomy of New Physics in $B - \bar{B}$ mixing*, *Phys. Rev.* **D83** (2011) 036004 [1008.1593].
- [347] UTFIT collaboration, *First Evidence of New Physics in $b \leftrightarrow s$ Transitions*, *PMC Phys.* **A3** (2009) 6 [0803.0659].
- [348] T. Jubb, M. Kirk, A. Lenz and G. Tetlalmatzi-Xolocotzi, *On the ultimate precision of meson mixing observables*, *Nucl. Phys.* **B915** (2017) 431 [1603.07770].
- [349] UTFIT collaboration, *Constraints on new physics from the quark mixing unitarity triangle*, *Phys. Rev. Lett.* **97** (2006) 151803 [hep-ph/0605213].
- [350] L. Di Luzio, M. Kirk and A. Lenz, *Updated B_s -mixing constraints on new physics models for $b \rightarrow s\ell^+\ell^-$ anomalies*, *Phys. Rev.* **D97** (2018) 095035 [1712.06572].
- [351] MEG collaboration, *Search for the lepton flavour violating decay $\mu^+ \rightarrow e^+\gamma$ with the full dataset of the MEG experiment*, *Eur. Phys. J.* **C76** (2016) 434 [1605.05081].
- [352] BABAR collaboration, *Searches for Lepton Flavor Violation in the Decays $\tau^\pm \rightarrow e^\pm\gamma$ and $\tau^\pm \rightarrow \mu^\pm\gamma$* , *Phys. Rev. Lett.* **104** (2010) 021802 [0908.2381].
- [353] ALEPH, DELPHI, L3, OPAL, SLD, LEP ELECTROWEAK WORKING GROUP, SLD ELECTROWEAK GROUP, SLD HEAVY FLAVOUR GROUP collaboration, *Precision electroweak measurements on the Z resonance*, *Phys. Rept.* **427** (2006) 257 [hep-ex/0509008].
- [354] ATLAS collaboration, *Search for the lepton flavor violating decay $Z \rightarrow e\mu$ in pp collisions at \sqrt{s} TeV with the ATLAS detector*, *Phys. Rev.* **D90** (2014) 072010 [1408.5774].
- [355] OPAL collaboration, *A Search for lepton flavor violating $Z0$ decays*, *Z. Phys.* **C67** (1995) 555.

- [356] DELPHI collaboration, *Search for lepton flavor number violating $Z0$ decays*, *Z. Phys.* **C73** (1997) 243.
- [357] FCC collaboration, *FCC-ee: The Lepton Collider*, *Eur. Phys. J. ST* **228** (2019) 261.
- [358] A. Crivellin, M. Ghezzi, L. Panizzi, G. M. Pruna and A. Signer, *Low- and high-energy phenomenology of a doubly charged scalar*, *Phys. Rev.* **D99** (2019) 035004 [1807.10224].
- [359] K. Hayasaka et al., *Search for Lepton Flavor Violating Tau Decays into Three Leptons with 719 Million Produced Tau+Tau- Pairs*, *Phys. Lett.* **B687** (2010) 139 [1001.3221].
- [360] U. Bellgardt, G. Otter, R. Eichler, L. Felawka, C. Niebuhr, H. Walter et al., *Search for the decay $\mu^+ \rightarrow e^+e^+e^-$* , *Nuclear Physics B* **299** (1988) 1 .
- [361] A. Crivellin, D. Müller, A. Signer and Y. Ulrich, *Correlating lepton flavor universality violation in B decays with $\mu \rightarrow e\gamma$ using leptoquarks*, *Phys. Rev.* **D97** (2018) 015019 [1706.08511].
- [362] ATLAS collaboration, *Searches for third-generation scalar leptoquarks in $\sqrt{s} = 13$ TeV pp collisions with the ATLAS detector*, *JHEP* **06** (2019) 144 [1902.08103].
- [363] D. A. Faroughy, A. Greljo and J. F. Kamenik, *Confronting lepton flavor universality violation in B decays with high- p_T tau lepton searches at LHC*, *Phys. Lett.* **B764** (2017) 126 [1609.07138].
- [364] A. Greljo and D. Marzocca, *High- p_T dilepton tails and flavor physics*, *Eur. Phys. J.* **C77** (2017) 548 [1704.09015].
- [365] I. Doršner, S. Fajfer, D. A. Faroughy and N. Košnik, *The role of the S_3 GUT leptoquark in flavor universality and collider searches*, 1706.07779.
- [366] G. Hiller, D. Loose and I. Nišandžić, *Flavorful leptoquarks at hadron colliders*, *Phys. Rev.* **D97** (2018) 075004 [1801.09399].
- [367] M. Schmaltz and Y.-M. Zhong, *The leptoquark Hunter's guide: large coupling*, *JHEP* **01** (2019) 132 [1810.10017].
- [368] E. Coluccio Leskow, G. D'Ambrosio, A. Crivellin and D. Müller, *$(g - 2)\mu$, lepton flavor violation, and Z decays with leptoquarks: Correlations and future prospects*, *Phys. Rev.* **D95** (2017) 055018 [1612.06858].
- [369] V. Gherardi, D. Marzocca and E. Venturini, *Low-energy phenomenology of scalar leptoquarks at one-loop accuracy*, 2008.09548.
- [370] H. Georgi and S. L. Glashow, *Unity of All Elementary Particle Forces*, *Phys. Rev. Lett.* **32** (1974) 438.
- [371] H. Georgi, H. R. Quinn and S. Weinberg, *Hierarchy of Interactions in Unified Gauge Theories*, *Phys. Rev. Lett.* **33** (1974) 451.
- [372] H. Fritzsch and P. Minkowski, *Unified Interactions of Leptons and Hadrons*, *Annals Phys.* **93** (1975) 193.
- [373] CMS, LHCb collaboration, *Observation of the rare $B_s^0 \rightarrow \mu^+\mu^-$ decay from the combined analysis of CMS and LHCb data*, *Nature* **522** (2015) 68 [1411.4413].

-
- [374] LHCb collaboration, *Measurement of CP-averaged observables in the $B^0 \rightarrow K^{*0} \mu^+ \mu^-$ decay*, 2003.04831.
- [375] S. Saad, *Combined explanations of $(g - 2)_\mu$, $R_{D^{(*)}}$, $R_{K^{(*)}}$ anomalies in a two-loop radiative neutrino mass model*, 2005.04352.
- [376] S. Saad and A. Thapa, *A Common Origin of Neutrino Masses and $R_{D^{(*)}}$, $R_{K^{(*)}}$ Anomalies*, 2004.07880.
- [377] P. S. B. Dev, R. Mohanta, S. Patra and S. Sahoo, *Unified explanation of flavor anomalies, radiative neutrino mass and ANITA anomalous events in a vector leptoquark model*, 2004.09464.
- [378] W. Altmannshofer, P. S. B. Dev, A. Soni and Y. Sui, *Addressing $R_{D^{(*)}}$, $R_{K^{(*)}}$, muon $g - 2$ and ANITA anomalies in a minimal R-parity violating supersymmetric framework*, 2002.12910.
- [379] L. Delle Rose, C. Marzo and L. Marzola, *Simplified leptoquark models for precision $l_i \rightarrow l_f \gamma$ experiments: two-loop structure of $O(\alpha_S Y^2)$ corrections*, 2005.12389.
- [380] I. Bigaran and R. R. Volkas, *Getting chirality right: top-philic scalar leptoquark solution to the $(g - 2)_{e,\mu}$ puzzle*, 2002.12544.
- [381] M. Kramer, T. Plehn, M. Spira and P. M. Zerwas, *Pair production of scalar leptoquarks at the Tevatron*, *Phys. Rev. Lett.* **79** (1997) 341 [[hep-ph/9704322](#)].
- [382] M. Kramer, T. Plehn, M. Spira and P. M. Zerwas, *Pair production of scalar leptoquarks at the CERN LHC*, *Phys. Rev.* **D71** (2005) 057503 [[hep-ph/0411038](#)].
- [383] P. Bandyopadhyay and R. Mandal, *Revisiting scalar leptoquark at the LHC*, *Eur. Phys. J. C* **78** (2018) 491 [[1801.04253](#)].
- [384] T. Faber, M. Hudec, H. Kolesova, Y. Liu, M. Malinsky, W. Porod et al., *Collider phenomenology of a unified leptoquark model*, *Phys. Rev.* **D101** (2020) 095024 [[1812.07592](#)].
- [385] K. Chandak, T. Mandal and S. Mitra, *Hunting for scalar leptoquarks with boosted tops and light leptons*, *Phys. Rev.* **D100** (2019) 075019 [[1907.11194](#)].
- [386] B. C. Allanach, T. Corbett and M. Madigan, *Sensitivity of Future Hadron Colliders to Leptoquark Pair Production in the Di-Muon Di-Jets Channel*, *Eur. Phys. J. C* **80** (2020) 170 [[1911.04455](#)].
- [387] L. Buonocore, U. Haisch, P. Nason, F. Tramontano and G. Zanderighi, *Resonant single leptoquark production at hadron colliders*, 2005.06475.
- [388] C. Borschensky, B. Fuks, A. Kulesza and D. Schwartländer, *Precision predictions for scalar leptoquark pair-production at hadron colliders*, 2002.08971.
- [389] M. E. Peskin and T. Takeuchi, *Estimation of oblique electroweak corrections*, *Phys. Rev.* **D46** (1992) 381.
- [390] G. Altarelli and R. Barbieri, *Vacuum polarization effects of new physics on electroweak processes*, *Phys. Lett.* **B253** (1991) 161.

- [391] I. Dorsner, S. Fajfer, A. Greljo, J. F. Kamenik and N. Kosnik, *Physics of leptoquarks in precision experiments and at particle colliders*, *Phys. Rept.* **641** (2016) 1 [1603.04993].
- [392] A. Djouadi, *The Anatomy of electro-weak symmetry breaking. II. The Higgs bosons in the minimal supersymmetric model*, *Phys. Rept.* **459** (2008) 1 [hep-ph/0503173].
- [393] M. Muhlleitner and M. Spira, *Higgs Boson Production via Gluon Fusion: Squark Loops at NLO QCD*, *Nucl. Phys.* **B790** (2008) 1 [hep-ph/0612254].
- [394] R. Bonciani, G. Degrassi and A. Vicini, *Scalar particle contribution to Higgs production via gluon fusion at NLO*, *JHEP* **11** (2007) 095 [0709.4227].
- [395] M. Carena, I. Low and C. E. M. Wagner, *Implications of a Modified Higgs to Diphoton Decay Width*, *JHEP* **08** (2012) 060 [1206.1082].
- [396] W.-F. Chang, J. N. Ng and J. M. S. Wu, *Constraints on New Scalars from the LHC 125 GeV Higgs Signal*, *Phys. Rev.* **D86** (2012) 033003 [1206.5047].
- [397] S. Gori and I. Low, *Precision Higgs Measurements: Constraints from New Oblique Corrections*, *JHEP* **09** (2013) 151 [1307.0496].
- [398] C.-S. Chen, C.-Q. Geng, D. Huang and L.-H. Tsai, *New Scalar Contributions to $h \rightarrow Z\gamma$* , *Phys. Rev.* **D87** (2013) 075019 [1301.4694].
- [399] P. Bandyopadhyay and R. Mandal, *Vacuum stability in an extended standard model with a leptoquark*, *Phys. Rev. D* **95** (2017) 035007 [1609.03561].
- [400] P. Agrawal and U. Mahanta, *Leptoquark contribution to the Higgs boson production at the CERN LHC collider*, *Phys. Rev.* **D61** (2000) 077701 [hep-ph/9911497].
- [401] T. Enkhbat, *Scalar leptoquarks and Higgs pair production at the LHC*, *JHEP* **01** (2014) 158 [1311.4445].
- [402] A. Bhaskar, D. Das, B. De and S. Mitra, *Enhancement of Higgs Production Through Leptoquarks at the LHC*, 2002.12571.
- [403] J. Zhang, C.-X. Yue, C.-H. Li and S. Yang, *Constraints on scalar and vector leptoquarks from the LHC Higgs data*, 1905.04074.
- [404] V. Gherardi, D. Marzocca and E. Venturini, *Matching scalar leptoquarks to the SMEFT at one loop*, 2003.12525.
- [405] C. D. Froggatt, R. G. Moorhouse and I. G. Knowles, *Leading radiative corrections in two scalar doublet models*, *Phys. Rev.* **D45** (1992) 2471.
- [406] E. Keith and E. Ma, *S, T, and leptoquarks at HERA*, *Phys. Rev. Lett.* **79** (1997) 4318 [hep-ph/9707214].
- [407] H. Abramowicz et al., *The International Linear Collider Technical Design Report - Volume 4: Detectors*, 1306.6329.
- [408] M. Aicheler, P. Burrows, M. Draper, T. Garvey, P. Lebrun, K. Peach et al., *A Multi-TeV Linear Collider Based on CLIC Technology*, .
- [409] FCC collaboration, *FCC Physics Opportunities*, *Eur. Phys. J.* **C79** (2019) 474.

-
- [410] M. E. Peskin and T. Takeuchi, *A New constraint on a strongly interacting Higgs sector*, *Phys. Rev. Lett.* **65** (1990) 964.
- [411] M. Spira, *Higgs Boson Production and Decay at Hadron Colliders*, *Prog. Part. Nucl. Phys.* **95** (2017) 98 [1612.07651].
- [412] J. R. Ellis, M. K. Gaillard and D. V. Nanopoulos, *A Phenomenological Profile of the Higgs Boson*, *Nucl. Phys.* **B106** (1976) 292.
- [413] R. N. Cahn, M. S. Chanowitz and N. Fleishon, *Higgs Particle Production by $Z \rightarrow H\gamma$* , *Phys. Lett.* **82B** (1979) 113.
- [414] L. Bergstrom and G. Hulth, *Induced Higgs Couplings to Neutral Bosons in e^+e^- Collisions*, *Nucl. Phys.* **B259** (1985) 137.
- [415] T. Inami, T. Kubota and Y. Okada, *Effective Gauge Theory and the Effect of Heavy Quarks in Higgs Boson Decays*, *Z. Phys. C* **18** (1983) 69.
- [416] A. Djouadi, M. Spira and P. M. Zerwas, *Production of Higgs bosons in proton colliders: QCD corrections*, *Phys. Lett.* **B264** (1991) 440.
- [417] M. Spira, A. Djouadi, D. Graudenz and P. M. Zerwas, *Higgs boson production at the LHC*, *Nucl. Phys.* **B453** (1995) 17 [hep-ph/9504378].
- [418] CDF, D0 collaboration, *Combination of CDF and D0 W-Boson Mass Measurements*, *Phys. Rev.* **D88** (2013) 052018 [1307.7627].
- [419] ATLAS collaboration, *Measurement of W^\pm -boson and Z-boson production cross-sections in pp collisions at $\sqrt{s} = 2.76$ TeV with the ATLAS detector*, *Eur. Phys. J.* **C79** (2019) 901 [1907.03567].
- [420] J. Ellis, C. W. Murphy, V. Sanz and T. You, *Updated Global SMEFT Fit to Higgs, Diboson and Electroweak Data*, *JHEP* **06** (2018) 146 [1803.03252].
- [421] J. Bernon and B. Dumont, *Lilith: a tool for constraining new physics from Higgs measurements*, *Eur. Phys. J.* **C75** (2015) 440 [1502.04138].
- [422] S. Kraml, T. Q. Loc, D. T. Nhung and L. D. Ninh, *Constraining new physics from Higgs measurements with Lilith: update to LHC Run 2 results*, *SciPost Phys.* **7** (2019) 052 [1908.03952].
- [423] F. An et al., *Precision Higgs physics at the CEPC*, *Chin. Phys. C* **43** (2019) 043002 [1810.09037].
- [424] FCC collaboration, *FCC-hh: The Hadron Collider*, *Eur. Phys. J. ST* **228** (2019) 755.
- [425] ATLAS collaboration, *Searches for scalar leptoquarks and differential cross-section measurements in dilepton-dijet events in proton-proton collisions at a centre-of-mass energy of $\sqrt{s} = 13$ TeV with the ATLAS experiment*, *Eur. Phys. J.* **C79** (2019) 733 [1902.00377].
- [426] CMS collaboration, *Observation of a New Boson at a Mass of 125 GeV with the CMS Experiment at the LHC*, *Phys. Lett. B* **716** (2012) 30 [1207.7235].

- [427] A. M. Coutinho, A. Crivellin and C. A. Manzari, *Global Fit to Modified Neutrino Couplings and the Cabibbo-Angle Anomaly*, *Phys. Rev. Lett.* **125** (2020) 071802 [1912.08823].
- [428] A. Crivellin and M. Hoferichter, *β Decays as Sensitive Probes of Lepton Flavor Universality*, *Phys. Rev. Lett.* **125** (2020) 111801 [2002.07184].
- [429] A. Crivellin, F. Kirk, C. A. Manzari and M. Montull, *Global Electroweak Fit and Vector-Like Leptons in Light of the Cabibbo Angle Anomaly*, 2008.01113.
- [430] K. Kannike, M. Raidal, D. M. Straub and A. Strumia, *Anthropic solution to the magnetic muon anomaly: the charged see-saw*, *JHEP* **02** (2012) 106 [1111.2551].
- [431] R. Dermisek and A. Raval, *Explanation of the Muon $g-2$ Anomaly with Vectorlike Leptons and its Implications for Higgs Decays*, *Phys. Rev. D* **88** (2013) 013017 [1305.3522].
- [432] R. Dermisek, A. Raval and S. Shin, *Effects of vectorlike leptons on $h \rightarrow 4\ell$ and the connection to the muon $g-2$ anomaly*, *Phys. Rev. D* **90** (2014) 034023 [1406.7018].
- [433] ATLAS collaboration, *A search for the dimuon decay of the Standard Model Higgs boson with the ATLAS detector*, 2007.07830.
- [434] CMS collaboration, *Measurement of Higgs boson decay to a pair of muons in proton-proton collisions at $\sqrt{s} = 13$ TeV*, .
- [435] I. Doršner, S. Fajfer and S. Saad, *$\mu \rightarrow e\gamma$ selecting scalar leptoquark solutions for the $(g-2)_{e,\mu}$ puzzles*, *Phys. Rev. D* **102** (2020) 075007 [2006.11624].
- [436] T. Aoyama, M. Hayakawa, T. Kinoshita and M. Nio, *Complete Tenth-Order QED Contribution to the Muon $g-2$* , *Phys. Rev. Lett.* **109** (2012) 111808 [1205.5370].
- [437] T. Aoyama, T. Kinoshita and M. Nio, *Theory of the Anomalous Magnetic Moment of the Electron*, *Atoms* **7** (2019) 28.
- [438] A. Czarnecki, W. J. Marciano and A. Vainshtein, *Refinements in electroweak contributions to the muon anomalous magnetic moment*, *Phys. Rev. D* **67** (2003) 073006 [hep-ph/0212229].
- [439] K. Melnikov and A. Vainshtein, *Hadronic light-by-light scattering contribution to the muon anomalous magnetic moment revisited*, *Phys. Rev. D* **70** (2004) 113006 [hep-ph/0312226].
- [440] P. Masjuan and P. Sanchez-Puertas, *Pseudoscalar-pole contribution to the $(g_\mu - 2)$: a rational approach*, *Phys. Rev. D* **95** (2017) 054026 [1701.05829].
- [441] M. Hoferichter, B.-L. Hoid, B. Kubis, S. Leupold and S. P. Schneider, *Dispersion relation for hadronic light-by-light scattering: pion pole*, *JHEP* **10** (2018) 141 [1808.04823].
- [442] A. Gérardin, H. B. Meyer and A. Nyffeler, *Lattice calculation of the pion transition form factor with $N_f = 2 + 1$ Wilson quarks*, *Phys. Rev. D* **100** (2019) 034520 [1903.09471].
- [443] J. Bijnens, N. Hermansson-Truedsson and A. Rodríguez-Sánchez, *Short-distance constraints for the HLbL contribution to the muon anomalous magnetic moment*, *Phys. Lett. B* **798** (2019) 134994 [1908.03331].

-
- [444] T. Blum, N. Christ, M. Hayakawa, T. Izubuchi, L. Jin, C. Jung et al., *Hadronic Light-by-Light Scattering Contribution to the Muon Anomalous Magnetic Moment from Lattice QCD*, *Phys. Rev. Lett.* **124** (2020) 132002 [1911.08123].
- [445] A. Crivellin, M. Hoferichter, C. A. Manzari and M. Montull, *Hadronic Vacuum Polarization: $(g - 2)_\mu$ versus Global Electroweak Fits*, *Phys. Rev. Lett.* **125** (2020) 091801 [2003.04886].
- [446] A. Keshavarzi, W. J. Marciano, M. Passera and A. Sirlin, *Muon $g - 2$ and $\Delta\alpha$ connection*, *Phys. Rev. D* **102** (2020) 033002 [2006.12666].
- [447] D. Hanneke, S. Fogwell and G. Gabrielse, *New Measurement of the Electron Magnetic Moment and the Fine Structure Constant*, *Phys. Rev. Lett.* **100** (2008) 120801 [0801.1134].
- [448] A. Crivellin and M. Hoferichter, *Combined explanations of $(g - 2)_\mu$, $(g - 2)_e$ and implications for a large muon EDM*, in *An Alpine LHC Physics Summit 2019*, pp. 29–34, 2019, 1905.03789.
- [449] R. H. Parker, C. Yu, W. Zhong, B. Estey and H. Müller, *Measurement of the fine-structure constant as a test of the Standard Model*, *Science* **360** (2018) 191 [1812.04130].
- [450] S. Laporta, *High-precision calculation of the 4-loop contribution to the electron $g-2$ in QED*, *Phys. Lett. B* **772** (2017) 232 [1704.06996].
- [451] I. Doršner, S. Fajfer, A. Greljo, J. F. Kamenik, N. Košnik and I. Nišandžić, *New Physics Models Facing Lepton Flavor Violating Higgs Decays at the Percent Level*, *JHEP* **06** (2015) 108 [1502.07784].
- [452] K. Cheung, W.-Y. Keung and P.-Y. Tseng, *Leptoquark induced rare decay amplitudes $h \rightarrow \tau^\mp \mu^\pm$ and $\tau \rightarrow \mu \gamma$* , *Phys. Rev. D* **93** (2016) 015010 [1508.01897].
- [453] S. Baek and K. Nishiwaki, *Leptoquark explanation of $h \rightarrow \mu \tau$ and muon $(g - 2)$* , *Phys. Rev. D* **93** (2016) 015002 [1509.07410].
- [454] CMS collaboration, *Search for pair production of second-generation leptoquarks at $\sqrt{s} = 13$ TeV*, *Phys. Rev. D* **99** (2019) 032014 [1808.05082].
- [455] B. Diaz, M. Schmaltz and Y.-M. Zhong, *The leptoquark Hunter’s guide: Pair production*, *JHEP* **10** (2017) 097 [1706.05033].
- [456] ATLAS collaboration, *Search for scalar leptoquarks in pp collisions at $\sqrt{s} = 13$ TeV with the ATLAS experiment*, *New J. Phys.* **18** (2016) 093016 [1605.06035].
- [457] *High-Luminosity Large Hadron Collider (HL-LHC): Technical Design Report V. 0.1*, .
- [458] H1 collaboration, *Observation of events at very high Q^2 in ep collisions at HERA*, *Z. Phys. C* **74** (1997) 191 [hep-ex/9702012].
- [459] ZEUS collaboration, *Comparison of ZEUS data with standard model predictions for $e^+p \rightarrow e^+X$ scattering at high x and Q^2* , *Z. Phys. C* **74** (1997) 207 [hep-ex/9702015].
- [460] M. Kirk, *The Cabibbo anomaly versus electroweak precision tests – an exploration of extensions of the Standard Model*, 2008.03261.

- [461] M. Bordone, O. Cata, T. Feldmann and R. Mandal, *Constraining flavour patterns of scalar leptoquarks in the effective field theory*, 2010.03297.
- [462] K. Babu, P. B. Dev, S. Jana and A. Thapa, *Unified Framework for B-Anomalies, Muon $g - 2$, and Neutrino Masses*, 2009.01771.
- [463] J. Blumlein and R. Ruckl, *Production of scalar and vector leptoquarks in $e^+ e^-$ annihilation*, *Phys. Lett. B* **304** (1993) 337.
- [464] A. Crivellin and J. Girrbach, *Constraining the MSSM sfermion mass matrices with light fermion masses*, *Phys. Rev. D* **81** (2010) 076001 [1002.0227].
- [465] W. Bernreuther, A. Brandenburg and P. Overmann, *CP violation beyond the standard model and tau pair production in $e^+ e^-$ collisions*, *Phys. Lett. B* **391** (1997) 413 [hep-ph/9608364].
- [466] A. Djouadi and M. Spira, *Measuring Static Quark Properties at LEP*, *Phys. Lett. B* **228** (1989) 443.
- [467] *The International Linear Collider Technical Design Report - Volume 2: Physics*, 1306.6352.
- [468] OPAL collaboration, *Precise determination of the Z resonance parameters at LEP: 'Zedometry'*, *Eur. Phys. J. C* **19** (2001) 587 [hep-ex/0012018].
- [469] SINDRUM collaboration, *Search for the Decay $\mu^\pm \rightarrow e^\pm e^\pm e^\mp$* , *Nucl. Phys. B* **299** (1988) 1.
- [470] MEG II collaboration, *The design of the MEG II experiment*, *Eur. Phys. J. C* **78** (2018) 380 [1801.04688].
- [471] MU3E collaboration, *The Mu3e Experiment*, *Nucl. Phys. B Proc. Suppl.* **248-250** (2014) 35.
- [472] BELLE-II collaboration, *The Belle II Physics Book*, *PTEP* **2019** (2019) 123C01 [1808.10567].
- [473] M. Czakon, P. Fiedler, T. Huber, M. Misiak, T. Schutzmeier and M. Steinhauser, *The $(Q_7, Q_{1,2})$ contribution to $\bar{B} \rightarrow X_s \gamma$ at $\mathcal{O}(\alpha_s^2)$* , *JHEP* **04** (2015) 168 [1503.01791].
- [474] M. Misiak and M. Steinhauser, *Large- m_c Asymptotic Behaviour of $\mathcal{O}(\alpha_s^2)$ Corrections to $B \rightarrow X_s \gamma$* , *Nucl. Phys. B* **840** (2010) 271 [1005.1173].
- [475] C. Greub, T. Hurth and D. Wyler, *Virtual $\mathcal{O}(\alpha_s)$ corrections to the inclusive decay $b \rightarrow s \gamma$* , *Phys. Rev. D* **54** (1996) 3350 [hep-ph/9603404].
- [476] CLEO collaboration, *Branching fraction and photon energy spectrum for $b \rightarrow s \gamma$* , *Phys. Rev. Lett.* **87** (2001) 251807 [hep-ex/0108032].
- [477] BELLE collaboration, *A Measurement of the branching fraction for the inclusive $B \rightarrow X_s \gamma$ decays with BELLE*, *Phys. Lett. B* **511** (2001) 151 [hep-ex/0103042].
- [478] BELLE collaboration, *Measurement of Inclusive Radiative B-meson Decays with a Photon Energy Threshold of 1.7-GeV*, *Phys. Rev. Lett.* **103** (2009) 241801 [0907.1384].

-
- [479] BABAR collaboration, *Measurement of the $B \rightarrow X_s \gamma$ branching fraction and photon energy spectrum using the recoil method*, *Phys. Rev. D* **77** (2008) 051103 [0711.4889].
- [480] BABAR collaboration, *Precision Measurement of the $B \rightarrow X_s \gamma$ Photon Energy Spectrum, Branching Fraction, and Direct CP Asymmetry $A_{CP}(B \rightarrow X_{s+d} \gamma)$* , *Phys. Rev. Lett.* **109** (2012) 191801 [1207.2690].
- [481] BABAR collaboration, *Measurement of $B(B \rightarrow X_s \gamma)$, the $B \rightarrow X_s \gamma$ photon energy spectrum, and the direct CP asymmetry in $B \rightarrow X_{s+d} \gamma$ decays*, *Phys. Rev. D* **86** (2012) 112008 [1207.5772].
- [482] BABAR collaboration, *Exclusive Measurements of $b \rightarrow s \gamma$ Transition Rate and Photon Energy Spectrum*, *Phys. Rev. D* **86** (2012) 052012 [1207.2520].
- [483] HEAVY FLAVOR AVERAGING GROUP (HFAG) collaboration, *Averages of b-hadron, c-hadron, and τ -lepton properties as of summer 2014*, 1412.7515.
- [484] M. Misiak et al., *Updated NNLO QCD predictions for the weak radiative B-meson decays*, *Phys. Rev. Lett.* **114** (2015) 221801 [1503.01789].
- [485] M. Benzke, S. J. Lee, M. Neubert and G. Paz, *Factorization at Subleading Power and Irreducible Uncertainties in $\bar{B} \rightarrow X_s \gamma$ Decay*, *JHEP* **08** (2010) 099 [1003.5012].
- [486] T. Aushev et al., *Physics at Super B Factory*, 1002.5012.
- [487] M. Misiak and M. Steinhauser, *Three loop matching of the dipole operators for $b \rightarrow s \gamma$ and $b \rightarrow sg$* , *Nucl. Phys. B* **683** (2004) 277 [hep-ph/0401041].
- [488] M. Gorbahn, U. Haisch and M. Misiak, *Three-loop mixing of dipole operators*, *Phys. Rev. Lett.* **95** (2005) 102004 [hep-ph/0504194].
- [489] M. Czakon, U. Haisch and M. Misiak, *Four-Loop Anomalous Dimensions for Radiative Flavour-Changing Decays*, *JHEP* **03** (2007) 008 [hep-ph/0612329].
- [490] K. Melnikov and A. Mitov, *The Photon energy spectrum in $B \rightarrow X_s \gamma$ in perturbative QCD through $O(\alpha_s^2)$* , *Phys. Lett. B* **620** (2005) 69 [hep-ph/0505097].
- [491] I. R. Blokland, A. Czarnecki, M. Misiak, M. Slusarczyk and F. Tkachov, *The Electromagnetic dipole operator effect on $\bar{B} \rightarrow X_s \gamma$ at $O(\alpha_s^2)$* , *Phys. Rev. D* **72** (2005) 033014 [hep-ph/0506055].
- [492] H. M. Asatrian, T. Ewerth, A. Ferroglia, P. Gambino and C. Greub, *Magnetic dipole operator contributions to the photon energy spectrum in $\bar{B} \rightarrow X_s \gamma$ at $O(\alpha_s^2)$* , *Nucl. Phys. B* **762** (2007) 212 [hep-ph/0607316].
- [493] M. Misiak et al., *Estimate of $\mathcal{B}(\bar{B} \rightarrow X_s \gamma)$ at $O(\alpha_s^2)$* , *Phys. Rev. Lett.* **98** (2007) 022002 [hep-ph/0609232].
- [494] H. M. Asatrian, T. Ewerth, H. Gabrielyan and C. Greub, *Charm quark mass dependence of the electromagnetic dipole operator contribution to $\bar{B} \rightarrow X_s \gamma$ at $O(\alpha_s^2)$* , *Phys. Lett. B* **647** (2007) 173 [hep-ph/0611123].
- [495] T. Ewerth, *Fermionic corrections to the interference of the electro- and chromomagnetic dipole operators in $\bar{B} \rightarrow X_s \gamma$ at $O(\alpha_s^2)$* , *Phys. Lett. B* **669** (2008) 167 [0805.3911].

- [496] R. Boughezal, M. Czakon and T. Schutzmeier, *NNLO fermionic corrections to the charm quark mass dependent matrix elements in $\bar{B} \rightarrow X_s \gamma$* , *JHEP* **09** (2007) 072 [0707.3090].
- [497] H. M. Asatrian, T. Ewerth, A. Ferroglia, C. Greub and G. Ossola, *Complete $(\mathcal{O}_7, \mathcal{O}_8)$ contribution to $B \rightarrow X_s \gamma$ at order α_s^2* , *Phys. Rev. D* **82** (2010) 074006 [1005.5587].
- [498] A. J. Buras and M. Misiak, *$\bar{B} \rightarrow X_s \gamma$ after completion of the NLO QCD calculations*, *Acta Phys. Polon. B* **33** (2002) 2597 [hep-ph/0207131].
- [499] T. Hurth, *Present status of inclusive rare B decays*, *Rev. Mod. Phys.* **75** (2003) 1159 [hep-ph/0212304].
- [500] P. Maierhöfer, J. Usovitsch and P. Uwer, *Kira—A Feynman integral reduction program*, *Comput. Phys. Commun.* **230** (2018) 99 [1705.05610].
- [501] C. Meyer, *Algorithmic transformation of multi-loop master integrals to a canonical basis with CANONICA*, *Comput. Phys. Commun.* **222** (2018) 295 [1705.06252].
- [502] C. W. Bauer, A. Frink and R. Kreckel, *Introduction to the GiNaC framework for symbolic computation within the C++ programming language*, *J. Symb. Comput.* **33** (2002) 1 [cs/0004015].
- [503] I. Heredia de la Cruz, *The Belle II experiment: fundamental physics at the flavor frontier*, *J. Phys. Conf. Ser.* **761** (2016) 012017 [1609.01806].
- [504] H. Simma and D. Wyler, *Hadronic Rare B Decays: The Case $b \rightarrow s g g$* , *Nucl. Phys. B* **344** (1990) 283.
- [505] L. Reina, G. Ricciardi and A. Soni, *The $B \rightarrow X_s \gamma \gamma$ rare decay*, *Phys. Lett. B* **396** (1997) 231 [hep-ph/9612387].
- [506] L. Reina, G. Ricciardi and A. Soni, *QCD corrections to $b \rightarrow s \gamma \gamma$ induced decays: $B \rightarrow X_s \gamma \gamma$ and $B_s \rightarrow \gamma \gamma$* , *Phys. Rev. D* **56** (1997) 5805 [hep-ph/9706253].
- [507] J.-j. Cao, Z.-j. Xiao and G.-r. Lu, *The $B \rightarrow X_s \gamma \gamma$ decay in the standard model and the general two Higgs doublet model*, *Phys. Rev. D* **64** (2001) 014012 [hep-ph/0103154].
- [508] H. M. Asatrian, C. Greub and A. Kokulu, *Improved analysis of the $(\mathcal{O}_7, \mathcal{O}_7)$ contribution to $\bar{B} \rightarrow X_s \gamma \gamma$ at $O(\alpha_s)$* , *Phys. Rev. D* **95** (2017) 053006 [1611.08449].
- [509] H. M. Asatrian, C. Greub, A. Kokulu and A. Yeghiazaryan, *NLL QCD contribution of the Electromagnetic Dipole operator to $\bar{B} \rightarrow X_s \gamma \gamma$* , *Phys. Rev. D* **85** (2012) 014020 [1110.1251].
- [510] H. M. Asatrian and C. Greub, *Next-to-leading logarithmic QCD contribution of the electromagnetic dipole operator to $\bar{B} \rightarrow X_s \gamma \gamma$ with a massive strange quark*, *Phys. Rev. D* **89** (2014) 094028 [1403.4502].
- [511] H. M. Asatrian, C. Greub and A. Kokulu, *$(\mathcal{O}_8, \mathcal{O}_8)$ contribution to $\bar{B} \rightarrow X_s \gamma \gamma$ at $O(\alpha_s)$* , *Phys. Rev. D* **93** (2016) 014037 [1511.00153].
- [512] H. M. Asatrian and C. Greub, *Tree-level contribution to $\bar{B} \rightarrow X_d \gamma$ using fragmentation functions*, *Phys. Rev. D* **88** (2013) 074014 [1305.6464].

-
- [513] M. Karliner and H. J. Lipkin, *The Constituent quark model revisited: Quark masses, new predictions for hadron masses and KN pentaquark*, [hep-ph/0307243](#).
- [514] M. Kaminski, M. Misiak and M. Poradzinski, *Tree-level contributions to $B \rightarrow X_s \gamma$* , *Phys. Rev. D* **86** (2012) 094004 [[1209.0965](#)].
- [515] H. M. Asatrian, A. Hovhannisyan and A. Yeghiazaryan, *The phase space analysis for three and four massive particles in final states*, *Phys. Rev. D* **86** (2012) 114023 [[1210.7939](#)].
- [516] T. Hahn, *CUBA: A Library for multidimensional numerical integration*, *Comput. Phys. Commun.* **168** (2005) 78 [[hep-ph/0404043](#)].
- [517] A. Denner, S. Dittmaier and L. Hofer, *Collier: a fortran-based Complex One-Loop Library in Extended Regularizations*, *Comput. Phys. Commun.* **212** (2017) 220 [[1604.06792](#)].
- [518] T. Hahn, *Loop calculations with FeynArts, FormCalc, and LoopTools*, *Acta Phys. Polon. B* **30** (1999) 3469 [[hep-ph/9910227](#)].

Erklärung

gemäss Art. 18 PromR Phil.-nat. 2019

Name/Vorname: Saturnino Francesco

Matrikelnummer: 12-113-437

Studiengang: Theoretische Physik
Bachelor Master Dissertation

Titel der Arbeit: Flavor Physics in the Standard Model and Beyond

Leiter der Arbeit: Prof. Dr. Christoph Greub

Ich erkläre hiermit, dass ich diese Arbeit selbständig verfasst und keine anderen als die angegebenen Quellen benutzt habe. Alle Stellen, die wörtlich oder sinngemäss aus Quellen entnommen wurden, habe ich als solche gekennzeichnet. Mir ist bekannt, dass andernfalls der Senat gemäss Artikel 36 Absatz 1 Buchstabe r des Gesetzes über die Universität vom 5. September 1996 und Artikel 69 des Universitätsstatuts vom 7. Juni 2011 zum Entzug des Dokortitels berechtigt ist.

Für die Zwecke der Begutachtung und der Überprüfung der Einhaltung der Selbständigkeitserklärung bzw. der Reglemente betreffend Plagiate erteile ich der Universität Bern das Recht, die dazu erforderlichen Personendaten zu bearbeiten und Nutzungshandlungen vorzunehmen, insbesondere die Doktorarbeit zu vervielfältigen und dauerhaft in einer Datenbank zu speichern sowie diese zur Überprüfung von Arbeiten Dritter zu verwenden oder hierzu zur Verfügung zu stellen.